may my heart always be open to little
birds who are the secrets of living
whatever they sing is better than to know
and if men should not hear them men are old

-e e cummings

STRUCTURED CATALYTIC SYSTEMS FOR WATER PURIFICATION

João Monteiro de Oliveira Restivo

Candidato ao grau de Doutor, pelo Programa Doutoral em Engenharia do Ambiente

FACULDADE DE ENGENHARIA DA UNIVERSIDADE DO PORTO

Departamento de Engenharia Química – Laboratório de Catálise e Materiais

ORIENTAÇÃO

Professor Manuel Fernando Ribeiro Pereira

Professor José Joaquim de Melo Órfão

Submetida

31/09/2014

Defendida

19/12/2014

ABSTRACT

The emergence of new concerns in water quality related with the appearance of new pollutants, or with the discovery of health related hazards of known substances, creates the need for novel water treatment technologies. In fact, many of the pollutants of concern have been observed to be resistant to current conventional water treatment methods.

Several interesting alternatives have been the focus of the scientific community in order to achieve efficient and sustainable treatment technologies that could be applied in real cases. Among these, the catalytic oxidation (with ozone) and reduction (with hydrogen) of organic and inorganic pollutants, respectively, have been shown to be alternatives with very interesting potentials. In the former case, the application of carbon nanomaterials as catalysts has been observed to be a promising alternative due to the high efficiency achieved. In the latter, the development of supported metallic catalysts using different materials and active phases has shown room for development of very active catalysts.

The application of macrostructured catalysts in multiphase reactions has been shown to be an interesting solution for real applications with low pressure drop, no filtration steps, no sludge formation and improved efficiency due to lower mass transfer resistances between the phases.

The goal of this work is the development and application of macrostructured catalytic system to be applied to novel water treatment catalytic technologies for the abatement of recalcitrant emerging pollutants.

First, the catalytic ozonation using carbon based structured catalysts was considered. Different configurations of macrostructured catalysts were tested in two-phase and three-phase flow. The behaviour of the flow in three-phase flow operation was determinant when choosing the most interesting configuration, i.e. honeycomb monoliths, which were selected for further testing. The mechanisms of catalytic ozonation of selected

emerging organic micropollutants were observed in detail. It was found that the application of a catalyst improves the mineralization degree, while the degradation pathway of the pollutants is changed with the predominance of surface or bulk reactions. The changes in the distribution of the accumulated products were shown to affect the potential toxicity of the resulting effluent. The influence of the operation conditions of the structured catalysts in multiphase flow was assessed. It was observed that when the experimental conditions were varied, the changes in the hydrodynamic regime affected the efficiency of the catalytic system due to the variations in the mass transfer between the phases. Modification of the carbon surface with the introduction of heteroatoms was studied, and it was shown that it is possible to enhance the performance of the catalytic system when applied to catalytic ozonation. The behaviour of the catalysts was related to the electronic density of the carbon surface, which could be altered through the introduction of different elements, such as nitrogen, oxygen or sulphur. The stability of the catalysts was assessed, and it was observed that despite a small initial deactivation due to the introduction of acidic functionalities on their surface, the catalysts remained stable during long term experiments.

Afterwards, the catalytic reduction of bromate under hydrogen using metallic catalysts supported on different materials, including structured catalysts, was evaluated. The activity of different metals supported on activated carbon was assessed, and palladium and platinum were found to be the most active for the reduction of bromate, the selected pollutant. A simplified mechanism for the reduction of bromate over supported monometallic catalysts was proposed, comprising the dissociative chemisorption of hydrogen and adsorption of bromate on the surface of the metal and subsequent reduction of the metal to its metallic form. The addition of a second metal to the supported metallic catalyst was studied, and it was found that, in most cases, it resulted in decreased activity. Nevertheless, in the case of the Pd-Cu system, the activity was increased in a specific weight ratio range due to the exposure of the more active

coordination sites of palladium. The performance of the most active metals supported on different materials was assessed, and it was found that using multiwalled carbon nanotubes and titanium dioxide as supports resulted in much more active catalysts for this reaction, due to the electronic interaction between the support and the metal. Finally, several structured catalysts were prepared using the most active metal-support combinations using honeycomb monoliths macrostructures. The preparation method was observed to influence the activity of the prepared catalyst due to several factors such as: amount of metal impregnated, layering of the different materials, exposure of the active phases and close contact between active phases. These catalysts were observed to be very active in the continuous catalytic reduction of bromate. Some leaching was observed in repeated experiments, but this was not observed in long term.

Structured catalysts were developed and applied to the continuous catalytic ozonation of emerging organic micropollutants and to the continuous catalytic reduction of bromate. Promising results were obtained regarding their application in real cases, and some progress was made in the understanding of the related fundamental science.

RESUMO

O aparecimento de novas preocupações quanto à qualidade de água relacionadas com o aparecimento de novos poluentes, ou com a descoberta de efeitos nocivos de poluentes anteriormente conhecidos, dá azo à necessidade de desenvolvimento de novas tecnologias para o tratamento de águas. De facto, muitos dos poluentes de cariz mais preocupante têm-se mostrado resistentes aos tratamentos convencionais.

Várias alternativas de interesse têm sido foco da comunidade científica com vista ao desenvolvimento de tecnologias que se revelem eficazes e sustentáveis para a aplicação em casos reais. Entre outras, a oxidação catalítica (com ozono) e a redução catalítica (com hidrogénio) têm mostrado ser duas tecnologias com potencial de aplicação interessante. No primeiro caso, a aplicação de nanomateriais de carbono como catalisador revela-se uma opção aliciante devido às altas eficiências atingidas na remoção de poluentes orgânicos emergentes. No segundo caso, a aplicação como catalisador de metais suportados em diferentes materiais mostra ser um possível caminho para atingir excelentes desempenhos, ainda com espaço para desenvolvimento.

A aplicação de catalisadores macroestruturados em reacções multifásicas já é conhecida como uma tecnologia atraente, especialmente devido às baixas perdas de carga, não formação de lamas, não ser necessário filtração e as altas eficiências passíveis de serem alcançadas devido à diminuição das resistências à transferência de massa entre as fases.

Assim, o objectivo deste trabalho foi o desenvolvimento e a aplicação de sistemas catalíticos macroestruturados a novas tecnologias catalíticas de tratamento de água para a mitigação de poluição causada por poluentes emergentes.

A abordagem inicial considerou o processo de ozonização catalítica utilizando catalisadores estruturados à base de nanomateriais de carbono. Diferentes configurações de macroestruturas foram testadas em sistemas com fluxo com duas ou três fases. O comportamento dos

diferentes sistemas catalíticos em sistema de fluxo com três fases foi determinante na decisão sobre o tipo de estrutura que foi, posteriormente, estudado na aplicação às reacções de ozonização e redução catalíticas, de modo a ser possível o aproveitamento das propriedades mais interessantes dos escoamentos multifásicos. O mecanismo da reacção de ozonização catalítica de poluentes orgânicos emergentes foi estudado em detalhe. Observou-se que a presença de um catalisador melhora o grau de mineralização obtido, enquanto que a sequência de degradação dos poluentes se altera em função da predominância das reacções de oxidação ocorrerem na superfície do catalisador ou no seio da solução. As mudanças na distribuição dos produtos acumulados mostraram-se como um factor determinante no potencial tóxico dos efluentes resultantes. A influência das condições de operação dos sistemas estruturados catalíticos em regime contínuo com fluxo de três fases foi avaliada. Foi demonstrado que o desempenho catalítico do sistema é alterado com as modificações provocadas no regime de escoamento dentro dos canais dos catalisadores macroestruturados pela modificação das condições de operação. O efeito da introdução de modificações na superfície dos catalisadores de carbono, consistindo na introdução de diferentes elementos, foi estudado, tendo sido demonstrado que é possível aumentar a actividade catalítica através deste método. Este fenómeno foi atribuído às modificações na densidade electrónica da superfície do catalisador. A estabilidade dos catalisadores estruturados à base de carbono foi testada na ozonização catalítica, e foi demonstrado (em testes de longa duração) que após um período inicial de desactivação relacionado com a introdução de grupos oxigenados ácidos na superfície do catalisador, o catalisador se mantinha estável.

Numa segunda fase, a aplicação de catalisadores metálicos suportados em diferentes materiais, incluindo suportes macroestruturados, foi avaliada. A actividade de diversos catalisadores metálicos foi examinada, sendo que o paládio e a platina foram os metais mais activos na redução do poluente seleccionado, o bromato. Um mecanismo simplificado para a

redução dos bromatos foi sugerido, consistindo na quimissorção dissociativa do hidrogénio na superfície metálica, reacção com o bromato adsorvido, e subsequente redução do metal à sua forma metálica original. A adição de um segundo metal ao sistema catalítico foi estudada, e foi demonstrado que na generalidade dos casos este processo prejudica a actividade dos catalisadores preparados. Contudo, no caso do par Pd-Cu, foi observado um efeito benéfico quando comparado com o catalisador monometálico devido à exposição dos locais com coordenação mais interessante para a reacção da superfície das partículas de paládio, sendo que este fenómeno foi observado apenas numa gama de valores de proporções mássicas. Os metais com melhor performance nestes sistemas foram testados utilizando diferentes materiais como suporte, tendo-se demonstrado que a actividade destes é largamente melhorada quando suportados em nanotubos de carbono ou em dióxido de titânio. Este fenómeno foi associado às interacções electrónicas existentes entre o material de suporte e as partículas metálicas. Por fim, os metais e suportes mais interessantes foram aplicados sobre a forma de catalisadores estruturados à redução de bromato em contínuo na presença de hidrogénio. Os métodos de preparação demonstraram ser um factor com larga influência na actividade catalítica, devido a causas como a quantidade de metal impregnada, a disposição das camadas de material depositado, a exposição dos materiais aos reagentes e o contacto entre as fases activas na superfície destes catalisadores. Estes sistemas catalíticos demonstraram ser altamente activos na redução de bromatos. Alguma lixiviação foi observada em alguns casos, mas verificou-se que este fenómeno apenas ocorria durante os períodos iniciais de utilização, sendo o catalisador estável após sucessivas reutilizações.

Catalisadores estruturados foram desenvolvidos e aplicados à ozonização catalítica de poluentes orgânicos emergentes e à redução de bromato, em contínuo. Resultados promissores foram alcançados para

ambas as reacções, tendo-se alcançado um progresso significativo na compreensão da ciência por detrás dos sistemas estudados.

ACKNOWLEDGEMENTS

The author would like to thank funding received from FCT and FEDER under Programme COMPETE (Project PEst-C/EQB/LA0020/2013), from QREN, ON2 and FEDER (Project NORTE-07-0162-FEDER-000050, Project NORTE-07-0124-FEDER-0000015) and from projects MONACAT and FREECATS, financed by the European Union 7th FP (2007-2013) grant nº. 226347 and 280658.

The author would like to thank FCT for the scholarship received (SFRH/BD/85751/2012), and MONACAT and FREECATS, financed by the European Union 7th FP (2007-2013) grant nº. 226347 and 280658, for the research grants received.

The author would like to acknowledge Prof. J.L Figueiredo for access to the laboratorial space and to the available equipment in the Laboratory of Catalysis and Materials; the Department of Chemical Engineering at the Faculty of Engineering of the University of Porto for access to the facilities, in particular Prof, Rui Boaventura, Dr. Vítor Vilar, Prof. Luís Melo and Prof. J.L. Faria, and the laboratory technicians for assistance; Prof. Carlos Sá and the laboratory technicians at CEMUP for access to materials characterization techniques and assistance.

The European project partners for the collaboration, in particular Prof. Garcia-Bordejé in Zaragoza, Prof. Alexei Lapkin and Dr. Xiaolei Fan in Warwick, Cambridge and also Manchester, and Dr. Salim Derrouiche in Veolia.

-

Aos meus orientadores, Prof. Fernando Pereira e Prof. José Órfão, pela oportunidade oferecida, pela disponibilidade, pelo aconselhamento e por todo o apoio, essencial na elaboração deste trabalho e nos meus primeiros passos no mundo da investigação científica.

A todos os colegas com quem partilhei espaço nestes anos, incluindo os que vieram e os que ficaram; em especial àqueles que acompanharam esta aventura desde o início ao fim e que certamente assim continuarão a fazer, com todo o apoio e carinho com o qual me continuam a surpreender.

Aos meus mais antigos amigos, por toda a amizade e apoio nos bons e maus momentos, pela força e inspiração, mas também pela perspectiva de que, quando tudo corre mal, continua a haver motivos para sorrir.

Aos meus pais e irmão, pelo amor e apoio em todas as etapas que conduziram a este ponto, mas também naquelas que virão.

À Joana, pela paciência, compreensão e amor, mas em especial por saber que continuarei a ter muito mais por que lhe agradecer.

TABLE OF CONTENTS

LIST OF TABLES

PART I

PART II

PART III

LIST OF FIGURES

PART I

PART II

PART III

ABBREVIATION LIST

AC – activated carbon

ATZ – atrazine

Ca – capillary number

CF – carbon felt

CNF – carbon nanofibers

COZ – catalytic ozonation

Cpsi – channels per square inch

CX – carbon xerogel

DEA – desethyl atrazine

DEIA – desethyl desisopropyl atrazine

DIA – desisopropyl atrazine

HM – honeycomb monolith

MTLC – metolachlor

MWCNT – multiwalled carbon nanotubes

NLP – nonylphenol

Re – Reynolds number

SMF – sintered metal fibers

TOC- Total organic carbon

UOC – unidentified organic compound

We –Webber number

Part I

Introduction and state of the art

INTRODUCTION

The emergence of new challenges in maintaining water quality suitable for human use and consumption, and the integrity of aquatic ecosystems, is the main driving force in the development of new technologies to be applied in water management.

New concerns about water quality are generally related to the appearance of unknown harmful products or the discovery of health related hazards of known products. Many times, the compounds of interest are found to be resistant to the current conventional water treatment technologies. Therefore, the scientific community has focused in the development of new technologies to achieve efficient removal of the pollutants of concern. In fact, the regulating and legislative authorities, besides issuing new recommendations and regulations on the maximum levels of concentration of these emerging pollutants, have funded the scientific research in order to promote the creation or the development of new treatment alternatives.

The work here presented concerns the study of the application of novel technologies based in the application of catalysts to enhance the complete removal of emerging pollutants. Specifically, it is focused in the development and application of macrostructured catalysts to catalytic ozonation of emerging organic pollutants, and to catalytic reduction of inorganic pollutants. The transference of state of the art catalysts from powder to structured form envisions their real life application through the development of environmental catalytic systems with low-pressure drop, no sludge formation, no need for filtration and high efficiency.

MOTIVATION

The motivation behind the research here presented is related to concerns regarding the degradation of water quality. The work of the regulating entities has driven the scientific community to develop new technologies

that can answer to new regulations, and thus, to the new challenges that arise with the emergence of harmful pollutants resistant to conventional treatments.

While several alternatives have been considered (and still are) to be potential solutions to mitigate the concerning pollution found in water, catalytic technologies are a particularly interesting subsector due to their potential to correspond to the demands efficiently and sustainably.

Several advanced oxidation processes are known to be able to enhance the efficiency of the traditional oxidants used in water treatment. In particular, the catalytic ozonation process has been shown to promote the mineralization of several pollutants that are recalcitrant during conventional water treatment. On the other hand, catalytic reduction has been shown to be an interesting alternative for the removal of several resistant inorganic pollutants through conversion into safe compounds.

Considering catalytic ozonation, novel carbon materials have been recently found to act as good catalysts for this reaction. In particular, carbon nanomaterials have been observed to have high potential to be applied as catalysts for the reaction. On the other hand, the application of heterogeneous catalysts containing a metallic phase supported on different materials, such as carbon or metallic oxides, to the catalytic reduction process has been shown to be able to greatly increase the removal of inorganic pollutants when compared with that obtained with traditional methods.

The development of macrostructured heterogeneous catalysts has been proposed mainly for industrial reactions, aiming at the reduction of pressure drop in gas or liquid phase applications, avoiding sludge formation and filtration. Their application in three-phase reactions has been observed to be able to enhance the reaction rates obtained in classical systems through the improvement of the mass transfer between the phases. This improvement is attributed to the development of interesting hydrodynamic regimes inside the channels of macrostructures,

such as honeycomb catalysts, which correspond to three-phase flow formed inside capillary channels. The regime formed has been named Taylor flow, and is characterized by the formation of a bubble train inside the channels, where there is formation of a thin liquid film around the gas bubbles, and the recirculation of the fluids inside the bubbles is promoted. The environmental application of such structures to three-phase systems has not yet been studied in detail.

Thus, the work here presented aimed at the development and application of structured catalysts for water purification, taking advantage of the known potential of novel catalysts when applied to oxidation and reduction reactions. For this end, macrostructured catalysts containing active materials for the studied reactions were developed and applied to the mitigation of the pollutants of concern, and several considerations regarding the fundamental science behind them were studied.

OBJECTIVES

The main purpose of the work here presented is the development of novel structured catalysts to be applied in different catalytic processes for the purification of water. For this purpose, several individual goals were identified and pursued. After the presentation of the state of the art concerning the application of structured catalysts in water purification, since two different catalytic reactions were studied, the work here presented is divided in two parts: one pertaining to the catalytic ozonation process, and the second to the catalytic reduction under hydrogen,

The first part (catalytic ozonation) consists in five chapters, which correspond to the following points:

- evaluation of different types of macrostructures to be used as support for the catalysts;
- application of the selected structured catalysts to the catalytic ozonation of emerging organic micropollutants;

- evaluation of the influence of the operation conditions on the performance of the structured catalysts;
- evaluation of the possibility of enhancing the catalytic properties of the carbon catalysts by doping with heteroatoms such as oxygen, nitrogen or sulphur;
- assessment of the stability of the structured catalysts in the catalytic ozonation reaction.

The second part (catalytic reduction under hydrogen) consists in four chapters, which correspond to the following objectives:

- assessment of the activity of several different metals supported on activated carbon;
- exploration of the enhancement of the activity by application of bimetallic supported catalysts;
- evaluation of the activity of the most active metal phases using different supporting materials:
- preparation and testing of structured catalysts using the most active metal/support combinations.

Finally, the main conclusions are presented in the end.

1. STATE OF THE ART

1.1 DESCRIPTION

In this introductory chapter the state of the art regarding the development and application of structured catalysts for the removal of emerging pollutants from water and wastewater is presented in detail.

The identification of the problematic of the emergence of organic and inorganic pollutants that are not targeted by current conventional water treatment technologies is initially presented. Subsequently, novel treatment technologies which present potential to eventually become solutions for this problem are described, with emphasis on those that were studied in the present work: catalytic ozonation and catalytic reduction under hydrogen. Finally, the development and application of different materials as catalysts for these reactions is discussed, focusing in the case of the application of structured catalysts.

1.2 WATER TREATMENT

Access to fresh water is, without any doubt, one of the most important current concerns of mankind. Its essential character for the livelihood of people is wholly recognized, and the development of sustainable practices regarding its use is a worldwide priority [1, 2].

Attention to the quality of water, in either fresh or wastewater streams, has been an important issue since the late 1800s, ever since the link between disease and sanitation was established with the development of germ theory [3]. Further ahead, the impracticability of disposing untreated wastewater, especially for large settlements with massive wastewater production rates, lead to the need for the development of intensive water treatment methodologies [3].

With new developments in the effluent characterization technologies available, and discoveries about the harmful effects of water contaminants, the regulations for water and wastewater quality become stricter [4]. While, ideally, the production of less harmful wastewater streams and reduced consumption of fresh water is the ultimate goal in terms of assuring the sustainability of the water resources, the purification of fresh water and wastewater is, and will be, a necessity, either considering its consumption, reutilization or disposal. These driving forces lead to the effort of the scientific community to develop novel treatment technologies which will help create a more sustainable future regarding water consumption, reutilization and wastewater disposal.

1.2.1 TYPICAL POLLUTANTS

The current national and European regulations for surface, groundwater and wastewater quality primarily target a series of pollutants which have been identified in these streams and are considered harmful for the ecosystem and human health. Current national law follows the goals proposed by the European Union for its member states in the Water Framework Directive of 2000 [5]. Generally, this directive concerns different classes of characteristics which ought to be monitored and controlled through the necessary methods, depending on the type of water concerned. The types of waters are classified by several means: their geographical location, their source (i.e. ground or surface water, fresh water or wastewater), dimensions and intended use.

The indicative list of pollutants that is presented in this document includes the following classes as those critical for the maintenance of appropriate water quality: organohalogen compounds, organophosphorous compounds, organotin compounds, compounds with carcinogenic or mutagenic properties, persistent hydrocarbons, persistent organic toxic substances, cyanides, metals, arsenic, biocides and plant protection compounds, materials in suspension, eutrophicating susbstances (nitrates and phosphates) and substances that may alter the oxygen balance [6].

The directive also presents values that are required to be met by 2016 by the signing member states, both for fresh water sources as for the wastewater being disposed into the environment, regarding the classes of pollutants listed above, as well as several physical and chemical parameters such as turbidity, oxygen balance, temperature, density and pH, as well as other biological parameters.

The indications of the Water Framework Directive were transposed to the national law of Portugal, and, together with previous legislation still standing, may be found in the following documents:

- DL n^{o} 348/98, November 9th, reclassification or areas sensible to eutrophication, updated by DL n^{o} 172/2001, May 26th and by DL n^{o} 140/2004, June 22nd;
- DL n^{o} 236/98, August 1st, goals for water quality in function of its utilization;
- DL n^{o} 58/2005, December 29th, transposes the information of the Water Framework Directive related to the definition of good environmental practices to guarantee adequate water quality;
- DL n^{o} 77/2006, March 30th, sets the standards for water characterization;
- DL n^{o} 226-A/2007, May 31st, where the control and responsibility over the water resources are determined.

Furthermore, the Plano Estratégico de Abastecimento de Água e Saneamento de Águas Residuais (General Strategies for Water Supply and Wastewater Disposal) delineates the general strategies for the management of the fresh water supply system, and for the disposal of wastewater.

The sources of the contaminants that are found in surface, ground and wastewater, both point and nonpoint, are represented in Figure 1.1 [7].

Figure 1.1 – Point and non-point water sources of water pollution (from U.S. Environmental Protection Agency).

While efforts are made in order to minimize the production of wastewater effluents that are not suitable for direct discharge into the environment, currently the operation of water and wastewater plants is a necessity to guarantee the adequate disposal of wastewater, and to guarantee that water with adequate quality is supplied.

1.2.2 CONVENTIONAL WATER TREATMENT SOLUTIONS

Water treatment technologies may be divided in three categories: physical, chemical and biological [3, 5]. The extent and type of technology that is used depends mostly on the nature of the influent that reaches the water treatment plant, and of the goal, e.g. suitable for disposal, water consumption, reutilization in an industrial process, among others.

Physical processes include technologies such as filtration, flotation, sedimentation, mixing, flocculation and screening. These processes were the first that were historically applied to wastewater treatment, mostly for the removal of suspended solids, although removal of other pollutants may occur as a side effect. Biological processes include technologies such as aerobic and anaerobic digestion, using different types of suspended or fixed biological reactors. In this case, the removal of biodegradable organics and excess nutrients is achieved by the development of adequate conditions for the growth and contact of a microorganic population that fulfils this need. Finally, chemical processes include oxidation using chlorine or ozone, disinfection using chemical oxidants or UV radiation, coagulation, adsorption, ion exchange and chemical precipitation. The application of chemical processes aims at the removal of organic compounds not converted by biological means, as well as the removal of pathogens.

The implementation of a water or wastewater treatment plant must take into consideration several factors in order to determine what technologies should be employed. Some examples include flow rate, properties of the influent, objectives for water quality of the effluent (which depends of its final use: disposal, reutilization, consumption and applicable

legislation/regulations), land availability, cost and variability of the flow, among others. In general, a typical water treatment plant might be divided in segments in the following manner: preliminary, primary, secondary and tertiary treatments.

Preliminary treatment is constituted by a series of operations that aim at the removal of elements that may disrupt the operation of the processes ahead. This may include screening for the removal of debris and coarse suspended matter or flotation for the removal of large quantities of oil or grease. Primary water treatment typically includes physical operations such as sedimentation and filtration, and is generally used as a precursor to the secondary treatment. This aims at the removal of suspended solids and biodegradable organics, usually consisting of biological processes coupled with sedimentation, and adequate processes for the treatment of generated activated sludges, if necessary. Finally, advanced or tertiary water treatment technologies is generally applied when a high quality of water is mandatory, and includes processes such as chemical oxidation and coagulation, ion exchange, adsorption, reverse osmosis and disinfection. Examples of classic water and wastewater treatment plants process flow designs are presented in Figures 1.2 [8] and 1.3 [3], respectively.

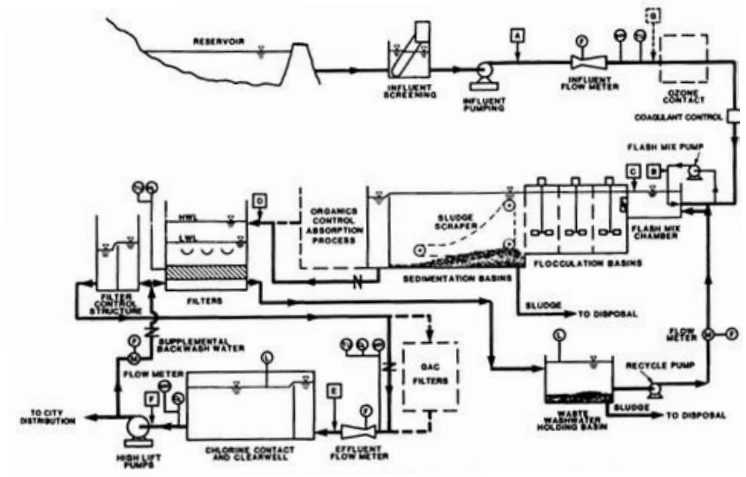

Figure 1.2 – Water treatment plant: example of a flow diagram.

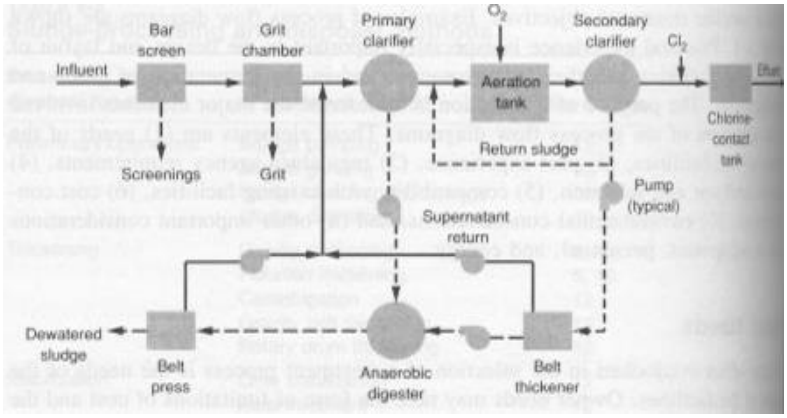

Figure 1.3 – Wastewater treatment plant: example of a flow diagram.

Nevertheless, new challenges for water and wastewater treatment have been developing in recent years, either due to the discovery of new pollutants or of previously unknown harmful effects of already known pollutants found at very low concentrations. These new challenges are described further ahead, together with the current proposals for the treatment of these emerging contaminants, and specifically the methods that are being studied in the present work.

1.3 EMERGING POLLUTANTS

Emerging water pollutants may be defined as contaminants that are not commonly monitored in water and lack regulation, but have been recently recurrently detected, and which present a suspected or confirmed harmful character [9]. These may include chemical substances that were not previously known or went undetected due to low concentrations or lack of adequate analytical methods, or those that were not considered harmful, either by their chemical characteristics or due to the concentrations at which they were found. Thus, factors such as changes in human behaviour, demographic changes, landscape changes, novel uses of water resources, new technologies, microbial adaptations, climate changes and new methods for detection or analysis are listed as causes for the emergence of these type of pollutants [9]. In fact, in recent years a growing interest in these pollutants has been rising, regarding their

occurrence [10-29], their fate [11, 13, 24, 30-41] and their harmful effects [22, 24, 30, 33, 34, 42-66].

While reference to emerging pollutants are found outside the official legislation, major health and environmental organizations have published compilations listing those emerging pollutants which are considered priority in terms of risk assessment, monitoring and remediation [67, 68].

The emerging pollutants of concern might be divided in different ways, considering their chemical nature, their use, their source, or their harmful potential. However, these classifications generally do not aim at the listing of the complete lot of emerging pollutants, but rather their grouping under convenient umbrella terms. The most common categories found in the literature are listed in Table 1.1.

In the present work the emerging pollutants were divided into two classes: organic and inorganic. Microbiological contamination is not generally addressed by catalytic technologies, and thus was not discussed here.

Table 1.1 – Classification of emerging pollutants.

Classification factors	Categories
Nature [67]	Organic Inorganic Microbiologic
Use [12-14, 31, 69-71]	Pharmaceuticals Life-style Industrials Hormones Pesticides PPCP (Pharmaceuticals and personal care products)
Source [13, 14]	Industries Hospitals Domestic wastewater Farming Cattle Atmospheric deposition
Harmful effect [1, 9, 68, 72-75]	EDC (Endocrine disruptive compound) Carcinogenic Mutagenic Acutely toxic Chronically toxic

1.3.1 ORGANIC MICROPOLLUTANTS

The list of emerging organic micropollutants is extremely long and constantly growing. In this work, we have opted to present a concise description of their origins, harmful effects and fate during water treatment and in the environment.

These compounds may be grouped relatively to their origin or nature [74]. The classes obtained pertain to natural compounds [76-83], hormones [84], surfactants [85-88], pharmaceuticals and personal care products (PPCPs) [89-99], industrial chemicals [100-103], combustion by-products [74] and pesticides [104-114]. Such a wide variety of sources explains why these compounds are considered ubiquitous in natural waters and the environment [74].

The category of pharmaceutical and personal care products includes a variety of products which are commonly used in hospitals and households. Regarding pharmaceuticals, this includes antibiotics, steroids, hormones, analgesics, and other therapeutic drugs [9, 12, 14, 21, 23, 27, 33, 34, 56, 59, 64, 69, 71, 115-128].

Since these products are designed to interact with biological systems and are bioaccumulating, their potential to cause a harmful effect is rather large [117].

The pharmaceutical products may occur in the environment, or in wastewater, from different sources. Among these, the most important ones include the direct disposal of surplus production by industries, excretion of substances, from human households or medical institutions, aqua cultures, landfill leachates, soil runoff from manure used as fertilizer, waste from fish farming and livestock production [13, 117, 118, 123].

Personal care products refer to products which are used by the general population, which may include fragrances, cosmetics, personal hygiene products and caffeine or other stimulants, and which generally enter the environment through their disposal to wastewater treatment facilities,

either from households or from specialized industries [23, 58, 64, 69, 71, 122, 126, 129].

The fate of PPCPs is related to their origin. While those that originate in the industry, households, hospitals or landfill leachates will be disposed into the appropriate channels for wastewater treatment, others may end up directly on the soil or in water [25, 27, 33, 69, 117, 118, 120, 124, 130]. Nevertheless, even though a part of these contaminants is directed onto the appropriate wastewater treatment facilities, their removal may not be complete due to inefficient technologies, which are not prepared to handle compounds of refractory nature. It has been observed that some of these compounds are not removed during water and wastewater treatment, or that they are being metabolized onto different products, which are not necessarily less dangerous than their parent compounds [14, 26, 27, 71, 115-117, 119, 121, 123, 125, 126, 131-135].

Industrial chemicals regarded as emerging organic pollutants include those that are used for several applications: phthalates used as plasticizers [116, 136], polychlorobiphenyls used as coolants and plasticizers [116], polycyclic aromatic hydrocarbons originating from combustion processes [116], bisphenol A used as an antioxidant and a polymerization inhibitor [69, 116], nonylphenol used as a surfactant [69], galaxolide used in the manufacture of soaps and detergents [69], tris(2-chloroethyl) phosphate used as a plasticizer, flame retardant and viscosity regulator [69], perfluorooctane sulfonate and perfluorooctanoic acid used as surfactants [137], perfluorinated compounds used in cleaning agents, flame retardants, paper coatings and packaged food containers [137], alkylphosphates used in agriculture [137], and polybrominated diphenyl ethers as flame retardants [138], among several others [67].

Furthermore, the release of these chemicals might also occur as a side effect of the utilization of the industrially prepared products, such as during operation, cleaning or disposal [35, 51, 56, 64, 69, 120, 137]. Several chemical compounds which are used in industrial processes are discharged into the environment, either due to lack of regulation or due to

their resistance to the conventional water treatments used [35, 51, 56, 59, 64, 69, 120, 139-141].

Pesticides and herbicides include a variety of chemical products which are used in agriculture to control the uprising of biological plagues, either fauna or flora, which may render entire crops useless.

Compounds used as pesticides and herbicides include atrazine, triphenyltin hydroxide, alachlor, metolachlor, acetochlor, triethylamine, oxyfluorfen, acrolein, bensulide, clethodim, dimethipin, diuron and molinate[67]. Several metabolites of these pesticides are also considered as emerging organic pollutants, since they are commonly detected in water, due to their degradation due to natural biological action, or other physicochemical processes, or during water treatment; furthermore, it has been observed that these metabolites might be more harmful to the environment and human health than the original contaminants [64, 67, 124, 142, 143].

The main source of pesticides and herbicides in the environment is the run-off from agricultural sites to the soil and groundwater, or to surface waters [64, 120, 124, 144, 145].

Generally, pesticides and herbicides that are subjected to water treatment might be removed by oxidizing technologies, such as ozonation, but the formation of by-products which may be more harmful than the parent compound occurs regularly [37, 64, 115, 120, 124, 146, 147].

1.3.1.1 HARMFUL EFFECTS

Regarding the harmful effect of the organic substances of importance to this study, many of them can be grouped into a class known as Endocrine Disrupting Compounds (EDC). A type of EDCs that that are found in aqueous streams and has been often cited as the most important is the PPCP class [12].

EDCs are defined by the Environmental Protection Agency (EPA) as “exogenous agents that interfere with the synthesis, secretion, transport,

binding, action, or elimination of natural hormones in the body that are responsible for the maintenance of homeostasis, reproduction, development and/or behaviour." [148]. This type of interference with the endocrinal system, which is one of the three major regulatory systems in the bodies of humans and other animals, the other two being the nervous and the immune systems is particularly harmful.

Although considered an emerging contaminant by the water industry, natural and synthetic EDCs' disrupting activity has been known for several decades. Reports of disturbances on animals' endocrine system can be found as early as 1930 [71]. Concerns related to the environmental presence of these compounds began around 1970 [148]. Some harmful effects found on animals and humans are listed on Table 1.2.

There is some controversy related to these associated effects. For example, the decline in sperm count as an effect of exposure to EDCs has been refuted later on, suggesting these compounds might not be directly responsible for past suspicions [149]. Moreover, some might argue that the minute concentrations found in water are not relevant when compared to those found in food supplies or naturally formed estrogens, especially since the human contact with these compounds in water is limited to the amounts consumed, and not directly as in the case of fishes or other aquatic fauna [71].

Attention should also be paid to disinfection by-products, which may also disturb the endocrine system's normal function, and thus their formation must be monitored when oxidative removal of EDCs is planned or studied. It has been stated that EDCs must not only refer to substances that actuate similarly to natural hormones, but to all the substances that disturb the endocrine system normal function [148].

Public interest in the presence of EDCs in the environment has increased as a result of the discovery of trace concentrations (at micro or nano gram level) in wastewater treatment plants' effluents, which have been shown to

have a possible impact, directly of by accumulation, in human health and in the ecosystems [150, 151].

Other compounds, such as pesticides and herbicides, generally present chronic or acute toxicity to the exposed populations, at different levels of concentration. The toxic effects of pesticides have been known since the mid 1900's, when the harmful effect of DDT was made popular [152]. The toxicity of insecticides aldrin, dieldrin, and endrin were observed to result in high mortality rates at lower concentrations than DDT or strobane. Furthermore, the reproduction of pheasant population was shown to be hurt by the inclusion of these insecticides in their diet [153]. The use of organochlorine and organophosphate pesticides have been observed to be detrimental to the neurodevelopment of exposed in utero animals and children [154]. Organochlorine pesticides have also been observed to be inhibitors of the ATPase activity in fishes [155]. Aldrin and dieldrin, and other polychlorinated pesticides, were also observed to exhibit toxicity in animal populations, and were also shown to hurt the reproducibility of the studied species [156]. Exposure of algae and plants to pesticides including triazines, sulfonylureas, phenoxyalkanes, pyridines, substituted ureas, amine derivatives and imidazolinone showed that many of these compounds are harmful to phytopopulations on different levels [157]. The negative effect of the exposure of humans to pesticides due to their use in food crops has also been reported [158].

Table 1.2 – Harmful effects of EDCs found in the environment.

Associated Effect	Reference
Feminization of gulls	[159-161]
Sexual abnormalities in alligators	[104, 105]
Cancers related to hormones	[109]
Infertility, abortion, birth defects, ovarian failure and growth retardation.	[162]
Decline on sex ratios	[149, 163]
Interference with the immune system and two-way interaction with the reproductive system	[42]
Influence on the degree of estrogenic and androgenic bioactivity in rodents	[164]
Influence on the metamorphosis of amphibians	[106-108, 165]
Reproductive disorder and population decay on marine gastropods	[100]
Reproductive anomalies and masculinization of fishes	[101-103, 166-170]
Unfavourable reproductive effects in humans	[171, 172]
Decrease in human sperm count	[173-175]
Increase in breast , prostate and testicular cancer	[148, 173, 176-179]

1.3.1.2 REMOVAL ALTERNATIVES

According to Nakada et al. [134], an aromatic ring is consistently found in the structure of recalcitrant organic pollutants throughout the different categories, suggesting that their hydrophobicity might be of importance when regarding their handling. The reports on the polarity and hydrophobicity of EDCs seem to vary from compound to compound. However, the trend seen indicates that the removal rates in conventional treatments are highly dependent of their nature [71, 72, 74, 75, 134]. In general, they seem to be considerably resistant to conventional water and wastewater treatments [74].

Conventional wastewater treatment techniques present only a limited capacity for the removal of EDCs and other refractory emerging organic pollutants, being that, at best, the processes aim at the removal of carbon, nitrogen and phosphorous. The removal of these substances is merely a side effect. Comparing influent with effluent at wastewater treatment plants it is noticeable that a percentage of these pollutants remain in the water, either as unbroken molecules or as a metabolites of the original molecule. The extent of the removal that is noticeable depends on the compound studied, and the mechanisms by which EDCs are eliminated in conventional treatment schemes are not well identified, although processes like bio and chemical degradation, adsorption, removal with activated sludge, coagulation and volatilization have been suggested [72, 74, 180].

The application of advanced water treatments, in-situ or at urban treatment plants, is a subject of attention from the scientific community. There is a need to develop techniques that allow the removal of substances refractory to conventional treatments, or that can be associated with existing treatments, facilitating their action towards these substances.

Several methods have been proposed for the dedicated removal of EDCs and emerging toxic compounds. These seem to be focused for

application in wastewater treatment plants. Physical methods proposed are based in rejection by membranes. Biological methods proposed are similar to those found for biodegradation of organic matter in conventional treatment. Chemical methods proposed include adsorption to activated carbon, advanced oxidation and reduction processes [75, 134]. The chemical methods will be subject of detailed attention as they are related with the goals established for this work.

1.3.1.3 SELECTED ORGANIC POLLUTANTS

Three emerging organic pollutants were selected for this work: atrazine, metolachlor and nonylphenol.

Atrazine (ATZ) is a triazine herbicide used to control weeds in various crops [181]. Its molecular formulation is presented in Figure 1.4.

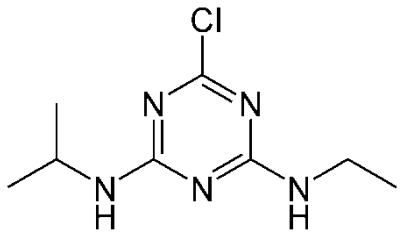

Figure 1.4 – Molecular formulation of the herbicide Atrazine.

Atrazine is widely used worldwide in agricultural and forestry applications, with an estimated use of 70000-90000 tons per year [182]. Due to its carcinogenic potential [183], and the exposure of humans by contact with contaminated groundwater [184] due to its resistance to microbial degradation, slow hydrolysis, low vapour pressure and aqueous solubility, the control of atrazine and its metabolites in water is very important. Furthermore, it has been detected in natural waters and has been shown to affect the reproduction of aquatic flora and fauna [185]. Due to its low biodegradability, it is often resistant to conventional water treatments [186], including oxidative treatments [187, 188].

Metolachlor (MTLC) is a chloroacetanilide and is one of the most common herbicides used to control weeds in several food crops around the world,

with between 77-99 million lb applied to crops in 2001 together with other chloroacetanilide pesticides [189, 190]. Its molecular formulation is presented in Figure 1.5.

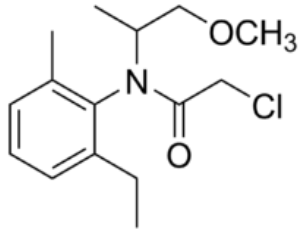

Figure 1.5 – Molecular formulation of the herbicide Metolachlor.

While metolachlor is partially degraded in soil in between 15-50 days [191] through hydrolytic reactions and microbial degradation [192], it is rather stable in water [193]. Due to high mobility in water and slow biodegradation, it is commonly found in natural waters [194, 195], including surface waters [196] and ground water [197]; moreover, it has been detected in fresh water used for consumption (prior to treatment) [198], and in drinking water [199]. It is listed as a possible carcinogen and is included in EPA's third Contaminants Candidate List [67]. The metabolites of metolachlor are also included in this list [67], since they have been shown to be as (or more) toxic than the original pollutant [45].

Nonylphenol (NLP) is a surfactant that is widely used in detergents, plastics, pesticides applications, and as a stabilizer [200]. Its molecular structure is represented in Figure 1.6.

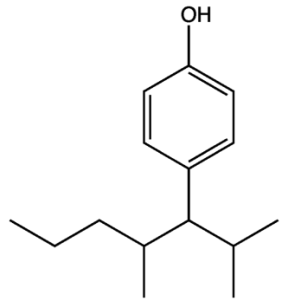

Figure 1.6 – Molecular formulation of the surfactant nonylphenol.

Nonylphenol and corresponding metabolites are refractory to conventional water treatment technologies [201, 202] and are toxic to aquatic

population [203, 204], presenting activity as endocrine disrupting compound [205], possibly related to the observed decline of human and wildlife reproductive health [206]. Its presence has been detected in sewage sludge and sediments, wastewater, landfill leachates, surface water and conventionally treated drinking water [207].

1.3.2 INORGANIC POLLUTANTS

There are several inorganic chemical compounds which are listed by environmental organizations as water pollutants, with a large portion of them being already included in regulations and legislation [9]. These include some nitrogen, bromine, chlorine or fluorine containing inorganic chemicals, as well as metallic compounds such as lead, mercury, arsenic, cadmium, aluminium, and copper, among others.

Many of these inorganic compounds are naturally present in water due to leaching from rocks and sediments [208, 209] and from degradation of plants and animal tissues [210]. Nevertheless, anthropogenic activity has introduced very large amounts of these compounds into water. Such processes include combustion [211], use of flame retardants [212], use of artificial fertilizers [213], various construction and mining activities [214], among others.

1.3.2.1 HARMFUL EFFECTS

Several health risks have been associated with the inorganic contaminants occurring at concentrations larger than the background levels. The presence of high levels of fluoride in drinking water has been observed to lead to dental and skeletal problems in the general population [215-217]. High nitrate concentrations have been linked to infantile methemoglobinaemia (blue baby syndrome) [218], while the chronic exposure to high concentrations of nitrates might lead to cancer in adults [219]. Similarly, long term consumption of water with high boron content has been linked with cardiac-vascular, nervous and alimentary system problems in adults [220]. Furthermore, some inorganic contaminants have

been show to act as EDCs. The reproductive levels of animal populations have been shown to be affected by the exposure to high levels of fluorine, while boron is known to be toxic to animal reproductive systems [221]. High concentrations of nitrate in natural systems are also known to lead to eutrophication, which may lead to the death of fish due to an overgrowth of the algae population [3].

1.3.2.2 REMOVAL ALTERNATIVES

The removal of inorganic contaminants during water and wastewater treatment might be possible by biological methods, adsorption, membrane filtration or coagulation; however, these methods present drawbacks such as low efficiency and sludge generation [222-224]. Thus, the development of efficient methods that lead to the conversion of these inorganic pollutants to non-hazardous products.

1.3.2.3 SELECTED INORGANIC POLLUTANTS

Bromate was selected as model pollutant for the development of a catalytic process for its removal from water. The molecular formulation of bromate is presented in Figure 1.7.

Bromates removal from drinking water has been subject to recent attention, since they were classified by the International Agency for Research on Cancer in Group 2B (possibly carcinogenic for humans) [225]. In fact, it is estimated that 3.9 μg/L correspond to a cancer risk of 10^{-5} for life-time exposures [226]. Additionally, other source of information indicates that life-time exposures to 5, 0.5 and 0.05 μg/L lead to cancer risks of 10^{-4}, 10^{-5}, and 10^{-6}, respectively [227]. The main risks are associated with the kidneys, both as targets for cancer and for toxic action of bromate. The peritoneum and the thyroid are also considered as cancer targets, and there is also the possibility that exposure to bromate may result in low sperm counts [228].

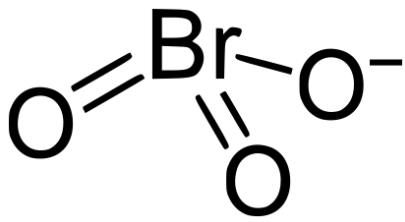

Figure 1.7 – Molecular formulation of bromate anion.

As a consequence of the mentioned classification, the World Health Organization (WHO) and the United States Environmental Protection Agency (USEPA) have established a provisional guideline for bromates in drinking water of 0.01 mg/L [226, 227]. Bromate ions are very stable in water, and their presence is mainly due to the ozonation of bromide containing water during the respective treatment for human consumption. Bromide has various natural and anthropogenic sources, such as seawater intrusion, pesticide run-off, industrial wastes and impurities from road de-icing salts [229].

The alternatives for bromate removal from drinking water are biological treatment, photocatalysis, electrochemical reduction and catalytic reduction [224]. The catalytic route presents advantages in terms of efficiency and rate of removal, without producing secondary waste streams with the accumulated remnants [224].

1.4 NOVEL TREATMENT TECHNOLOGIES

Since the focus of the scientific community on the problematic of emerging pollutants has been rising in recent years, several technologies have been developed towards this common objective, such as photocatalysis [230], catalytic ozonation [231], catalytic reduction [232, 233], filtration by membranes [18, 234-236], electrofenton [237], electroxidation [238] and other electronic methods [239], phytoremediation [240], as well as combinative processes [241], among others.

In this work two catalytic technologies were studied for the removal of emerging pollutants from water using structured catalysts: the catalytic

ozonation of organic pollutants, and the catalytic reduction of bromate under hydrogen.

1.4.1 CATALYTIC OZONATION

Catalytic ozonation may be defined as an advanced oxidation process (AOP) that uses a catalyst to initiate the decomposition of molecular ozone into highly reactive compounds, which will oxidize the concerned recalcitrant pollutants. The definition of AOP is very wide and gathers technologies that, although similar in goals, present diverse mechanisms and applications. Hence, these are currently defined as aqueous phase oxidation processes that rely on the higher reactivity of intermediate species towards the degradation of pollutants recalcitrant to typical oxidants [242]. Usually these processes use a combination of oxidation reactants (O_3 and H_2O_2), catalysts or irradiation technologies (ultraviolet, ultrasound) as means to produce the desired intermediates [243, 244]. The compounds whose formation these reactions aim at is normally the hydroxyl radical, which presents very high typical reaction rates with organic molecules, in the range of 10^6 to 10^9 M^{-1} s^{-1} [245, 246]. Additionally, the hydroxyl radical presents lower selectivity towards pollutants compared to more common oxidants, and thus is more efficient on their complete mineralization, attacking not only the parent compound, but also the intermediates formed [243-245]. However, low selectivity can become a disadvantage when we are aiming at the removal of one specific class of pollutant in the presence of other organic compounds, as is commonly found in real water matrices. The removal efficiency may be reduced due to the consumption of radicals in the degradation of these other compounds [72]. Several AOPs have been applied to the removal of EDCs and other emerging organic micropollutants, including catalytic ozonation [25, 55, 58, 75, 131, 147, 187, 188, 231, 242, 246-264].

1.4.1.1 OZONE IN WATER

Although ozonation alone is technically an AOP since ozone spontaneous ly decomposes in aqueous phase to produce hydroxyl

radicals, the concentrations achieved at pH below 10 are very low and do not play an important part on the degradation of pollutants [265]. Besides, the control of pH during water treatment is not desirable, due to engineering concerns.

Single ozonation is used in water and wastewater treatment as a disinfection technique, particle remover or chemical oxidizer of organic solutes and, more rarely, of inorganic solutes [243, 266, 267]. For the removal of organic micropollutants in drinking water and refractory chemical oxygen demand (COD), single ozonation proves to be a limited solution. Thus, for these situations, the application of an AOP that promotes the formation of more active compounds is regarded as a possible solution. The use of ozone is not as widespread as the use of chlorines because it leaves no residuals in the treated water and has an higher cost associated to the need for in-situ generation of ozone, as it is an highly unstable compound [267]. However, problems encountered with chlorines and chloramines by-products have increased the world wide interest in the use of ozone for these processes. On the other hand, it is possible that the discovery of the formation of bromates as a by-product of ozonation will have a refraining effect on the development of new technologies [231]. In aqueous solution containing organic contaminants, it is suggested that ozone may react with substances following two distinct routes, a direct and an indirect one [243, 268, 269]. The direct reaction route consists of the straight oxidation of the pollutant.

The indirect reaction route combines several steps and intermediates, where the substances found in aqueous solution can act either as promoters or as inhibitors [269-272]. The main steps identified are the initiation step, the chain reaction step and the termination step. The first one, as the name suggests, consists on the initiation of a chain reaction triggered by species as the OH^- ion, at values higher than pH 10 [243, 270, 271]. This reaction creates two radicals, one superoxide anion $O_2^{\bullet-}$, and one hydroperoxide $HO_2^{\bullet}$.Afterwards, the chain reaction step, also known as the propagation step, takes place. Here, several different

radicals play a part. The superoxide anion formed on the first step reacts with the aqueous ozone to form the hydroxyl radical $OH^{\bullet}$. The hydroxyl radical can then react with either aqueous ozone or the organic solute. In the former case, the formation of the hydroperoxide radical closes a cycle and allows the reaction to start again. This is also where the reaction cycle in pure water ends. Staehelin and Hoigné [269] state that it's much more probable, when in presence or organic solutes, that the hydroxyl radicals react with these, and not with ozone. When the hydroxyl radical reacts with the functional groups in the organic molecules present in aqueous solution, organic radicals can be formed. These also convert hydroxyl radicals into superoxide radicals, promoting the chain reaction, and thus are regarded as promoters. In the presence of oxygen, the organic radicals may further react, eliminating the $O_2^{\bullet-}/HO_2^{\bullet}$ radicals and forming hydroxyl or hydroperoxil radicals which will allow the chain reaction to proceed. As mentioned above, an organic solute can also act as a scavenger for the hydroxyl radical, behaving as an inhibitor. In this case, the propagation step is not continued due to the lack of formation of $O_2^{\bullet-}/HO_2^{\bullet}$ radicals. An inorganic solute such as CO_3^{2-} or HCO_3^{-} may also terminate the reaction. When this situation occurs, the termination step is reached.. An alternative termination step may occur when two radicals react to produce oxygen and water.

1.4.1.2 MECHANISM OF CATALYTIC OZONATION

The use of a catalyst in the ozonation of water or wastewater aims at the decomposition of ozone in aqueous phase into more active and less selective intermediate radicals towards the degradation of solutes which are not mineralized by molecular ozone, independently of the pH of operation.

A variety of different heterogeneous catalysts have been applied to the catalytic ozonation process, generally based on metal oxides or carbon materials [231].

Metal or metallic oxides which have been experimented as catalysts for the ozonation process include iron [273], ceria [274-277], cobalt [278], manganese [188, 278-281] and alumina [282-285].

Several studies using carbon materials have been carried out, including activated carbon [275, 277, 286-297], carbon xerogels [276] and carbon nanomaterials [274, 275, 293, 298, 299], such as carbon nanotubes (see Figure 1.8).

In the current study the focus is on the application of carbon nanomaterials to the catalytic ozonation process, since it is expected that their mesoporosity and low tortuosity will facilitate the diffusion of the reactants and the catalytic performance [300]. Furthermore, it has been suggested that the modification of the textural and chemical properties of carbon nanomaterials might enhance their catalytic activity in liquid phase oxidation [301-303].

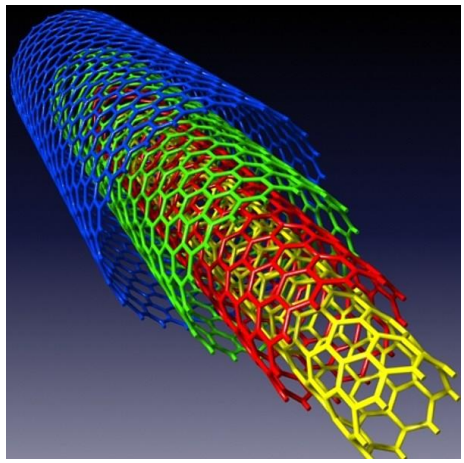

Figure 1.8 – Schematic representation of a multiwalled carbon nanotube.

The mechanism of catalytic ozonation in the presence of carbon materials has been described as a combination of bulk and surface reactions [291, 304, 305]. A similar mechanism should occur when nanocarbon materials (NCM) are used as catalyst [306]. The mechanism for the formation of highly-reactive radicals and how they react with the organic pollutants has been described in the literature [243, 291, 305, 307]:

In aqueous solution ozone decomposes into hydroxyl radicals, process that is initiated by the presence of OH^- (equation 1).

$$O_3 \xrightarrow{OH^-} OH^{\cdot} \quad (1)$$

In the presence of carbon materials, the organic pollutant can be adsorbed (eq. 2). Dissolved ozone either reacts with the surface of the catalyst to yield free radical species released to the solution (eq. 3), which will react with the organic pollutant in the bulk (eq. 4), or ozone is adsorbed on the surface of the catalyst, yielding active surface groups (eq. 5), which will in turn react with the adsorbed pollutant (eq. 6).

$$NCM + Organic \rightarrow NCM - Organic \quad (2)$$

$$O_3 \xrightarrow{NCM} OH^{\cdot} \quad (3)$$

$$OH^{\cdot} + Organic \rightarrow Product \quad (4)$$

$$O_3 + NCM \rightarrow NCM - O \quad (5)$$

$$NCM - O + NCM - Organic \rightarrow Product \quad (6)$$

It is also possible that the adsorbed pollutants react with aqueous species (eq. 7 and 8).

$$NCM - Organic + O_3 \rightarrow Product \quad (7)$$

$$NCM - Organic + OH^{\cdot} \rightarrow Product \quad (8)$$

Some different general reaction mechanisms between ozone and organic compounds are presented by von Gunten [308]. The reaction begins with an electrophilic addition of ozone to the compound, forming an intermediate which then decomposes following one of the five different pathways: oxygen atom transfer, electron transfer, formation of an oxyl radical, ozone insertion or ring formation.

Von Sonntag et al. [309] reported some considerations about the reaction of hydroxyl radicals with organic matter. Two pathways are presented, the first consisting on the addition to a carbon double bound and the second on the abstraction of a carbon bound hydrogen atom. Legube and Leitner [231] refer three main mechanisms for the reaction of OH radicals with organic matter: H abstraction, OH addition and electron transfer.

Ikehata and El-Din [254] also consider the same three main pathways for the oxidation of organic compounds by hydroxyl radicals. Focusing on hydrogen abstraction, which plays a major role in most cases, the generation of the organic radicals and their interactions with oxygenated species are studied. Particularly, the reaction with hydrogen peroxide and molecular oxygen, which yields hydroxyl and peroxyl radicals, respectively, is observed. These reactions will either lead to the mineralization of the organic matter or will contribute to the known aqueous ozone decomposition chain.

Buffle et al [310] argue that pharmaceutical compounds with high reactivity to ozone will be oxidized by it, and those with low reactivity will be target of hydroxyl radicals. The ozone's oxidation of organic matter is reported by Rivera-Utrilla et al. [311, 312] as being due to the interaction with its aromatic rings. This idea is confirmed and further developed by von Gunten et al. [308]. Observation of experimental data taken from literature stating rate constants for the oxidation of pharmaceutical compounds suggests that oxidation of organic micropollutants by molecular ozone is only an efficient process when an unprotonated and uncomplexated amino group, an activated aromatic system, a double bond or a sulfidic group are present. Moreover, increase of the number of aromatic rings and electron donating groups will lead to enhanced reactivity, while electron withdrawing groups decrease reactivity. Compounds which consist of saturated ring systems are difficult to oxidize with molecular ozone. Halogenation leads to low electron density at the carbon centre, which results in low reactivity with ozone and hydroxyl

radicals. Several works present results agreeing with these conclusions [291, 313-316].

Beltrán et al. [305] while developing a mechanism for the decomposition of ozone in the catalytic ozonation process made some considerations about whether the degradation of organic pollutants occurred on the catalyst surface or in the liquid bulk. It was suggested that the interaction may occur between adsorbed compounds or in the liquid bulk. However, it seems that the reaction which would lead to the total mineralization of the pollutants, the hydroxyl radicals being the main oxidizer, would predominately occur on the liquid bulk, since intermediate organic compounds formed during ozonation seem to have low affinity to the activated carbon's surface. The reactions between ozone compounds and organic matter taking place on the catalyst's surface generally yield hydrogen peroxide or hydroxyl radicals and saturated carboxylic acids. Liu et al. [306] studied the degradation of oxalic acid by catalytic ozonation when using MWCNT as a catalyst. The degradation of oxalic acid by oxygenated radicals is suggested to take place both on the carbon's surface and on the liquid bulk. Faria et al. [316] state that the reaction of ozone, or a highly reactive oxygenated radical, with organic compounds on the catalytic ozonation process, might occur either in the solution bulk or on the catalyst's surface after adsorption. The study of the ozonation of aniline suggests that aromatic compounds with unshared electron pairs are highly prone to electrophilic attack by molecular ozone. The less selective hydroxyl radical is shown to also be able to react with organic compounds, in this case aniline, albeit with a different reaction path and thus different intermediate products. Both mechanisms are favored at basic pH values since the electrophilic nature of the molecules is enhanced. These ideas were confirmed by the work of Oliviero et al. [317].

1.4.2 CATALYTIC REDUCTION

The heterogeneous catalytic reduction of water pollutants (e.g. nitrates) using metallic catalysts has already been demonstrated to be an efficient process, using different supports for the metal phase, such as: activated carbon cloths [318], activated carbon [319-323], multi-walled carbon nanotubes [324, 325], titanium oxide [326-328], cerium oxide [329-331] and carbon-coated monolithic supports [332-334].

The mechanism for catalytic reduction of nitrate ion over metallic catalysts under hydrogen of is proposed to occur through the dissociation of hydrogen on the surface of the catalyst, and reaction with the adsorbed reactants ; however, a bimetallic system might be necessary for complete reduction to be achieved [335, 336].

Nevertheless, few systems have been tested in the reduction of bromate ion, which was the selected pollutant for the assessment of the catalytic activity of developed structured catalysts applied to the reduction under hydrogen. The reduction of bromate to hypobromide and subsequently to bromide in the presence of activated carbon, through the formation of surface oxides, has been reported [228, 229, 337, 338]. The adsorption and reduction of bromate is proposed to be influenced by the particle size, the pore volume and the presence of surface oxygenated groups, particularly carboxylic groups. The influence of the surface oxygen content on the activated carbon capacity for bromate reduction has also been reported, as well as the influence of pH and of some organic and inorganic species usually present in water [229]. However, the reaction rates for these systems are not satisfactory, and it is not always clear whether actual conversion of bromate or just adsorption is taking place.

A silicon-based structured microreactor was recently used to test the catalytic activity of Ru supported on carbon nanofibers for the reduction of bromate [224]. Although redox reactions involving oxidation of water are possible, they are too slow and bromate is too stable in water. Thus, methanol was used as a proton donor. Turn-over frequencies of 0.032 s^{-1}

were achieved for this system, but deactivation was observed. It was proposed that RuO_2 is responsible for the reduction of bromate, being oxidized to RuO_3. The latter is then reduced to the former species by the alcohol present in solution. However, hydroxylation occurs simultaneously, which leads to deactivation of the catalyst.

A different reaction mechanism is proposed in two other studies. Mills and Meadows [339] applied a ruthenium oxide heterogeneous catalyst to the reduction of bromate in water, with and without the addition of an organic alcohol to the solution. The influence of the initial bromate concentration, loading of the catalyst and the presence of other anions in solution were evaluated. It was also observed that the presence of an alcohol in the solution led to faster reduction of bromate into bromide ion. It was suggested that the Ru heterogeneous catalyst used is capable of promoting the hydrolysis of water, thus leaving hydrogen available for reaction with bromate ions on the surface of the catalyst, which ultimately lead to the reduction of bromate into bromide coupled with the release of oxygen. Nevertheless, they observed that the addition of an alcohol increased the reaction rate due to its faster oxidation relatively to water. Chen et al. [340] used palladium supported on alumina as heterogeneous catalyst for bromate reduction in the presence of hydrogen. Other supports were also tested, including silica and activated carbon. Adsorption of bromate is stated as essential for initiation of the reaction, acting as the controlling step. The influence of pH was also tested, since negatively charged surfaces may cause repelling of bromate anions and consequent decrease of the bromate reduction rate. Metallic palladium supported on alumina showed the best activity, which correlates with the hydrogen adsorption capacity of the metal. A mechanism similar to the one proposed by Mills and Meadows [339] was considered, in which the slow oxidation of water over the catalyst was overcome by the introduction of oxygen into the reaction system. Thus, they propose that hydrogen is adsorbed and dissociated on the surface of palladium, and then reacts with adsorbed bromate.

Finally, the reduction of bromate has also been tested using Pd supported on macro structures, such as honeycomb monoliths, sintered metal filters or carbon felts, which were previously covered with carbon nanofibers [341], where the influence of the type of macro structure used as support for the carbon nanofibers was assessed. A life cycle assessment of the application of these type of catalysts to the reduction of bromate in water was also performed [342]. Similarly, other mono and bimetallic catalysts were also tested, using the same types of structured carbon nanofibers supports [343]. Furthermore, the N-doping of the carbon nanofibers on a structured support did not influence the activity of supported Pd or Ru catalysts [344].

1.5 STRUCTURED CATALYSTS

Structured catalysts consist in catalytic materials that present structural organization at different levels. The most typical example for a structured catalyst consists in the macrostructured monoliths used in automobile catalytic converters, as pictured in Figure 1.9 [345].

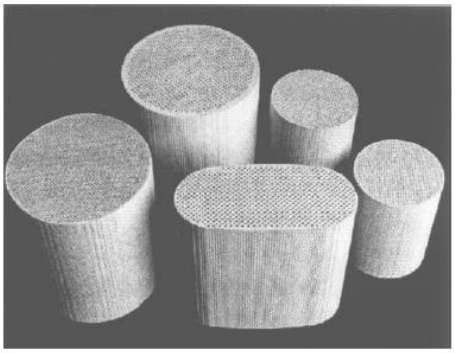

Figure 1.9 – Monoliths used as support for structured catalysts typically used in automobile catalytic converters.

Structured catalysts might also include ordered structures at different levels, such as nano [343, 346-350] or microstructured catalysts [351, 352]. The use of macrostructured catalysts present several advantages, such as low pressure drop, possibility of increased mass transfer and ease of handling [353].

While several applications of structured catalysts for gas-phase reactions are current industry standards or alternatives, such as the application of monoliths in automobile catalytic converters, and other reactions [345, 354-364], their application as catalysts in three-phase system is still under exploration. The use of a macrostructured reactor of the honeycomb monolith type as seen in Figure 1.9 is expected to present advantages in the decrease of mass transfer resistances between the phases. The first studies regarding the multiphase flow inside capillary channels date as far back as 1935 [365]. From 1960 onward, several studies were carried out to detail the characteristics of the flow that form inside capillary channels [366-369]. Several different hydrodynamic regimes were identified for three-phase flow, as presented in Figure 1.10.

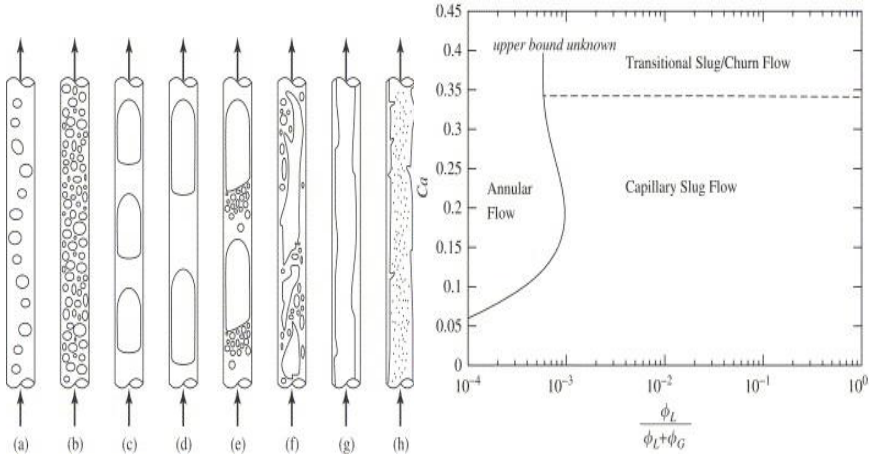

Figure 1.10 - Sketch of observed flow patterns in capillary channels. (a,b): bubbly flow, (c,d) segmented flow (a.k.a. bubble train flow, Taylor flow, capillary slug flow), (e) transitional slug/churn flow, (f) churn flow, (g) film flow (downflow only), (h) annular flow [370].

The hydrodynamic regime of interest for the enhancement of mass transfer is the Taylor flow regime, which is characterized by the formation of a segmented flow, with well-defined gas bubbles and liquid slugs passing through the channel, occupying most of the horizontal section. The influence of the operation conditions on the hydrodynamic characteristics of the regime, and subsequent effect on the mass transfer

has been subject of attention in recent years [370-391]. The hydrodynamic characteristics that define Taylor flow are depicted in Figure 1.11. The enhancement of mass transfer between the phases has been suggested to be due mostly to factors such as liquid slug and gas bubble lengths [371-374, 379-381, 388, 389, 392], recirculation vortexes formed inside the liquid slugs [373, 374, 381-383, 387] and formation of a thin liquid film around the gas bubbles inside the channel [353, 379, 381, 391, 393]. These parameters are widely influenced by the operation conditions at which the catalytic reactors are being operated.

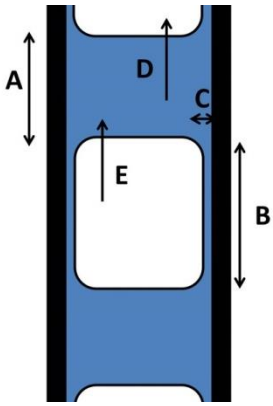

Figure 1.11 – Hydraulic parameters of interest in Taylor flow: A) liquid slug length; B) gas bubble length; C) film thickness; D) liquid slug velocity; E) gas bubble velocity.

The application of structured reactors to three-phase environmental catalysis is a field that is still under exploration. Some studies have been published in catalytic ozonation [394, 395] and catalytic reduction [333, 334, 341-344, 396].

Regarding the preparation of structured catalysts, different types may be developed for environmental applications, containing various active phases such as metal oxides [364, 397, 398] or carbon materials of varying natures [399-402]. Furthermore, carbon on monolith supports may be further loaded with a metallic phase [355, 403-405]. Examples of a

metal oxide structured catalyst may be found in Figure 1.12, and of a carbon structured catalysts in Figure 1.13.

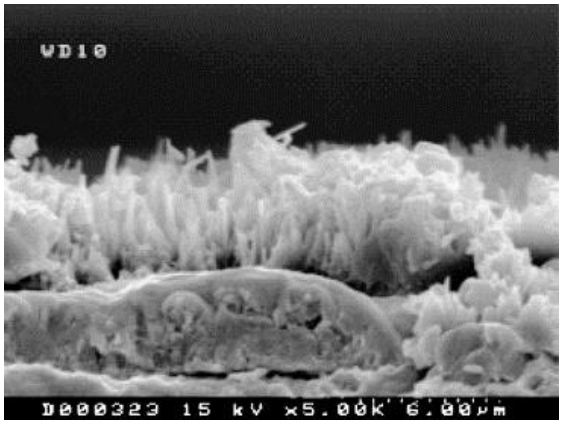

Figure 1.12 – Alumina whiskers loaded on a honeycomb monolith wall [406].

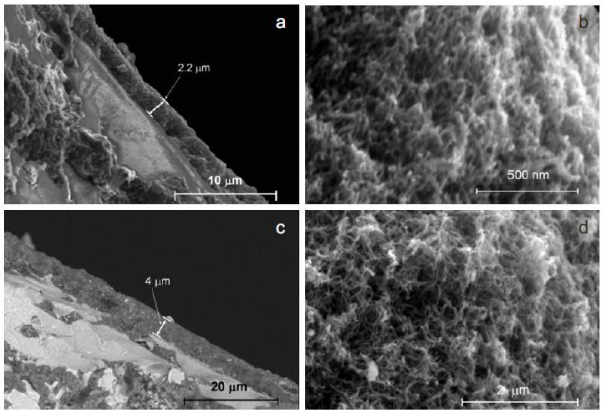

Figure 1.13 – Carbon nanofibers layer on a honeycomb monolith wall [402].

Thus, due to the advantages presented in terms of operation and performance, the use of structured catalysts containing carbon (for catalytic ozonation) or a metallic phase (for catalytic reduction) is an interesting alternative aiming at the large scale application of novel catalytic processes for the removal of emerging pollutants in water.

REFERENCES

[1] World Health Organization, Water quality and health strategy 2013-2020, World Health Organization, 2013.
[2] United Nations Environment Programme, Healthy waters for sustainable development, UNEP Operational strategy for freshwater (2012–2016), United Nations Environment Programme, 2012.
[3] L. Metcalf, H.P. Eddy, G. Tchobanoglous, Wastewater engineering: treatment, disposal, and reuse, McGraw-Hill, 1972.
[4] Water Treatment, American Water Works Association, 2003.
[5] C. Binnie, M. Kimber, G. Smethurst, Basic Water Treatment, Thomas Telford, 2002.
[6] Water framework directive, European Parlamient and the Council of the European Union, 2000.
[7] Consider The Source: An Interactive Guide to Protecting America's Drinking Water, 2002.
[8] S. Kawamura, Integrated Design and Operation of Water Treatment Facilities, Wiley, 2000.
[9] I. Xagoraraki, D. Kuo, Water Pollution: Emerging Contaminants Associated with Drinking Water, in: H.K. Heggenhougen (Ed.) International Encyclopedia of Public Health, Academic Press, Oxford, 2008, pp. 539-550.
[10] L. Boithias, S. Sauvage, L. Taghavi, G. Merlina, J.-L. Probst, S. Pérez, J. Miguel, Journal of Hazardous Materials, 196 (2011) 210-219.
[11] M. Clara, G. Windhofer, P. Weilgony, O. Gans, M. Denner, A. Chovanec, M. Zessner, Chemosphere, 87 (2012) 1265-1272.
[12] S.D. Kim, J. Cho, I.S. Kim, B.J. Vanderford, S.A. Snyder, Water Research, 41 (2007) 1013-1021.
[13] S. Mompelat, B. Le Bot, O. Thomas, Environment International, 35 (2009) 803-814.
[14] M.F. Rahman, E.K. Yanful, S.Y. Jasim, Desalination, 248 (2009) 578-585.
[15] A.J. Watkinson, E.J. Murby, D.W. Kolpin, S.D. Costanzo, Science of the Total Environment, 407 (2009) 2711-2723.
[16] G.G. Ying, Journal of Environmental Monitoring, 11 (2009) 1498-1505.
[17] D. Zaruk, M. Alaee, E. Sverko, M. Comba, Analytica Chimica Acta, 376 (1998) 113-117.
[18] S. Lyko, T. Wintgens, T. Melin, Desalination, 178 (2005) 95-105.
[19] N. Martí, D. Aguado, L. Segovia-Martínez, A. Bouzas, A. Seco, Marine Pollution Bulletin, 62 (2011) 615-625.
[20] L. Qasemian, D. Guiral, M. Belghazi, E. Ferré, R. Gros, A.-M. Farnet, Chemosphere, 84 (2011) 1321-1328.
[21] E. Vulliet, C. Cren-Olivé, Environmental Pollution, 159 (2011) 2929-2934.
[22] M. Gust, M. Gélinas, M. Fortier, M. Fournier, F. Gagné, Environmental Pollution, 169 (2012) 50-58.

[23] Q. Bu, B. Wang, J. Huang, S. Deng, G. Yu, Journal of Hazardous Materials, 262 (2013) 189-211.
[24] A.Z. Aris, A.S. Shamsuddin, S.M. Praveena, Environment International, 69 (2014) 104-119.
[25] A. Ziylan, N.H. Ince, Journal of Hazardous Materials, 187 (2011) 24-36.
[26] P. Verlicchi, M. Al Aukidy, E. Zambello, Science of the Total Environment, 429 (2012) 123-155.
[27] E. Aydin, I. Talinli, Chemosphere, 90 (2013) 2004-2012.
[28] S.W. Krasner, W.A. Mitch, D.L. McCurry, D. Hanigan, P. Westerhoff, Water Research, 47 (2013) 4433-4450.
[29] S. Marin, A.J. Ramos, G. Cano-Sancho, V. Sanchis, Food and Chemical Toxicology, 60 (2013) 218-237.
[30] A. Soares, B. Guieysse, B. Jefferson, E. Cartmell, J.N. Lester, Environment International, 34 (2008) 1033-1049.
[31] P. Westerhoff, Y. Yoon, S. Snyder, E. Wert, Environmental Science & Technology, 39 (2005) 6649-6663.
[32] J. Aldekoa, C. Medici, V. Osorio, S. Pérez, R. Marcé, D. Barceló, F. Francés, Journal of Hazardous Materials, 263, Part 1 (2013) 207-213.
[33] M.l. Farré, S. Pérez, L. Kantiani, D. Barceló, TRAC Trends in Analytical Chemistry, 27 (2008) 991-1007.
[34] A.J.M. Horvat, S. Babić, D.M. Pavlović, D. Ašperger, S. Pelko, M. Kaštelan-Macan, M. Petrović, A.D. Mance, TRAC Trends in Analytical Chemistry, 31 (2012) 61-84.
[35] S.-K. Kim, J.S. Khim, K.-T. Lee, J.P. Giesy, K. Kannan, D.-S. Lee, C.-H. Koh, Chapter 2 Emission, Contamination and Exposure, Fate and Transport, and National Management Strategy of Persistent Organic Pollutants in South Korea, in: S.T.G.J.J.P.G. An Li, K.S.L. Paul (Eds.) Developments in Environmental Science, Elsevier2007, pp. 31-157.
[36] R. Lohmann, K. Breivik, J. Dachs, D. Muir, Environmental Pollution, 150 (2007) 150-165.
[37] R. Mailler, J. Gasperi, G. Chebbo, V. Rocher, Waste Management, 34 (2014) 1217-1226.
[38] S. Manzetti, R. Ghisi, Marine Pollution Bulletin, 79 (2014) 7-15.
[39] J. Robles-Molina, B. Gilbert-López, J.F. García-Reyes, A. Molina-Díaz, Science of the Total Environment, 479–480 (2014) 247-257.
[40] H. Sun, C. Kwan, A. Suvorova, H.M. Ang, M.O. Tadé, S. Wang, Applied Catalysis B: Environmental, 154-155 (2014) 134-141.
[41] O. Zuloaga, P. Navarro, E. Bizkarguenaga, A. Iparraguirre, A. Vallejo, M. Olivares, A. Prieto, Analytica Chimica Acta, 736 (2012) 7-29.
[42] S. Ansar Ahmed, Toxicology, 150 (2000) 191-206.
[43] C.C. Chou, S.S. Que Hee, Ecotoxicology and Environmental Safety, 23 (1992) 355-363.
[44] R. Goto, T. Kubota, Y. Ibuki, K. Kaji, A. Goto, Toxicology, 202 (2004) 237-247.
[45] Y.-J. Lin, M. Karuppiah, A. Shaw, G. Gupta, Ecotoxicology and Environmental Safety, 43 (1999) 35-37.
[46] T. Olmez-Hanci, I. Arslan-Alaton, B. Genc, Journal of Hazardous Materials, 263, Part 2 (2013) 283-290.

[47] O. Osano, W. Admiraal, H.J.C. Klamer, D. Pastor, E.A.J. Bleeker, Environmental Pollution, 119 (2002) 195-202.
[48] G.W. Stratton, Archives of Environmental Contamination and Toxicology, 13 (1984) 35-42.
[49] S. Webb, T. Ternes, M. Gibert, K. Olejniczak, Toxicology Letters, 142 (2003) 157-167.
[50] P. Brezovšek, T. Eleršek, M. Filipič, Water Research, 52 (2014) 168-177.
[51] J. Cristale, A. García Vázquez, C. Barata, S. Lacorte, Environment International, 59 (2013) 232-243.
[52] R.F. Dantas, M. Canterino, R. Marotta, C. Sans, S. Esplugas, R. Andreozzi, Water Research, 41 (2007) 2525-2532.
[53] R. Fabbri, M. Montagna, T. Balbi, E. Raffo, F. Palumbo, L. Canesi, Marine Environmental Research, 99 (2014) 1-8.
[54] A.R. Flegal, J.A. Davis, M.S. Connor, C.H. Conaway, Environmental Research, 105 (2007) 0-4.
[55] Y. Gao, T. An, H. Fang, Y. Ji, G. Li, Journal of Hazardous Materials, 278 (2014) 417-425.
[56] M. Gavrilescu, K. Demnerová, J. Aamand, S. Agathos, F. Fava, New Biotechnology, in press in press.
[57] O. Herrero, J.M. Pérez Martín, P. Fernández Freire, L. Carvajal López, A. Peropadre, M.J. Hazen, Mutation Research/Genetic Toxicology and Environmental Mutagenesis, 743 (2012) 20-24.
[58] J.-Q. Jiang, Z. Zhou, V.K. Sharma, Microchemical Journal, 110 (2013) 292-300.
[59] M. Kuzmanović, A. Ginebreda, M. Petrović, D. Barceló, Science of the Total Environment, in press.
[60] D. Lin, Q. Zhou, X. Xie, Y. Liu, Chemosphere, 81 (2010) 1328-1333.
[61] E. Nieto, J. Blasco, E. González-Ortegón, P. Drake, M. Hampel, Journal of Hazardous Materials, 263, Part 1 (2013) 256-265.
[62] R. Rosal, I. Rodea-Palomares, K. Boltes, F. Fernández-Piñas, F. Leganés, A. Petre, Chemosphere, 81 (2010) 288-293.
[63] K. Stamatelatou, C. Pakou, G. Lyberatos, 6.37 - Occurrence, Toxicity, and Biodegradation of Selected Emerging Priority Pollutants in Municipal Sewage Sludge, in: M. Moo-Young (Ed.) Comprehensive Biotechnology (Second Edition), Academic Press, Burlington, 2011, pp. 473-484.
[64] M. Stuart, D. Lapworth, E. Crane, A. Hart, Science of the Total Environment, 416 (2012) 1-21.
[65] S. Villa, M. Vighi, A. Finizio, Chemosphere, 108 (2014) 239-244.
[66] P.C. von der Ohe, V. Dulio, J. Slobodnik, E. De Deckere, R. Kühne, R.-U. Ebert, A. Ginebreda, W. De Cooman, G. Schüürmann, W. Brack, Science of the Total Environment, 409 (2011) 2064-2077.
[67] United States Environmental Protection Agency, Contaminate Candidate List and Regulatory Determinations, United States Environmental Protection Agency, California, 2012.
[68] World Health Organization, Guidelines for drinking-water quality, third edition, incorporating first and second addenda, World Health Organization, 2006.

[69] D.J. Lapworth, N. Baran, M.E. Stuart, R.S. Ward, Environmental Pollution, 163 (2012) 287-303.
[70] B.J. Vanderford, R.A. Pearson, D.J. Rexing, S.A. Snyder, Analytical Chemistry, 75 (2003) 6265-6274.
[71] S. Snyder, P. Westerhoff, D. Sedlak, Y. Yoon, Environmental engineering science, 20 (2003) 449-469.
[72] M. Auriol, Y. Filali-Meknassi, R.D. Tyagi, C.D. Adams, R.Y. Surampalli, Process Biochemistry, 41 (2006) 525-539.
[73] C. Bizarro, O. Ros, A. Vallejo, A. Prieto, N. Etxebarria, M.P. Cajaraville, M. Ortiz-Zarragoitia, Marine Environmental Research, 96 (2014) 19-28.
[74] H.-S. Chang, K.-H. Choo, B. Lee, S.-J. Choi, Journal of Hazardous Materials, 172 (2009) 1-12.
[75] Z.-h. Liu, Y. Kanjo, S. Mizutani, Science of the Total Environment, 407 (2009) 731-748.
[76] B.S. Walker, J.C. Janney, Endocrinology, 14 (1930) 389-392.
[77] E. Levin, J.F. Burns, V.K. Collins, Endocrinology, 49 (1951) 289-301.
[78] E.O. Brookbanks, M.R. Coup, New Zealand Veterinary Journal, 17 (1969) 159-160.
[79] M. Metzler, E. Pfeiffer, Environmental Health Perspectives, 103 (1995) 21-22.
[80] S.H. Safe, K. Gaido, Environmental Toxicology and Chemistry, 17 (1998) 119-126.
[81] A.J. Millington, C.M. Francis, N.R. McKeown, Aust. J. Agric. Res., 15 (1964) 527-536.
[82] N.R. Adams, Pure and Applied Chemistry, 70 (1998) 1855-1862.
[83] K.D.R. Setchell, S.J. Gosselin, M.B. Welsh, Gastroenterology, 93 (1987) 225-233.
[84] C. Desbrow, E.J. Routledge, G.C. Brighty, J.P. Sumpter, M. Waldock, Environmental Science and Technology, 32 (1998) 1549-1558.
[85] G.C. Mueller, U.H. Kim, Endocrinology, 102 (1978) 1429-1435.
[86] R. White, S. Jobling, S.A. Hoare, J.P. Sumpter, M.G. Parker, Endocrinology, 135 (1994) 175-182.
[87] E.J. Routledge, J.P. Sumpter, Journal of Biological Chemistry, 272 (1997) 3280-3288.
[88] J.P. Giesy, S.L. Pierens, E.M. Snyder, S. Miles-Richardson, V.J. Kramer, S.A. Snyder, K.M. Nichols, D.A. Villeneuve, Environmental Toxicology and Chemistry, 19 (2000) 1368-1377.
[89] S.A. Snyder, D.L. Villeneuve, E.M. Snyder, J.P. Giesy, Environmental Science and Technology, 35 (2001) 3620-3625.
[90] S.A. Snyder, T.L. Keith, D.A. Verbrugge, E.M. Snyder, T.S. Gross, K. Kannan, J.P. Giesy, Environmental Science and Technology, 33 (1999) 2814-2820.
[91] L.D. Arcand-Hoy, A.C. Nimrod, W.H. Benson, International Journal of Toxicology, 17 (1998) 139-158.
[92] V.J. Kramer, S. Miles-Richardson, S.L. Pierens, J.P. Giesy, Aquatic Toxicology, 40 (1998) 335-360.
[93] G.H. Panter, R.S. Thompson, J.P. Sumpter, Aquatic Toxicology, 42 (1998) 243-253.

[94] E. Stumm-Zollinger, G.M. Fair, Journal of the Water Pollution Control Federation, 37 (1965) 1506-1510.
[95] H.H. Tabak, R.L. Bunch, Dev Ind Microbiol, 11 (1970) 367-376.
[96] C. Hignite, D.L. Azarnoff, Life Sciences, 20 (1977) 337-341.
[97] B. Halling-SÃ¸rensen, S. Nors Nielsen, P.F. Lanzky, F. Ingerslev, H.C. Holten LÃ¼tzhÃ¸ft, S.E. JÃ¸rgensen, Chemosphere, 36 (1998) 357-393.
[98] C.G. Daughton, T.A. Ternes, Environmental Health Perspectives, 107 (1999) 907-938.
[99] D.W. Kolpin, E.T. Furlong, M.T. Meyer, E.M. Thurman, S.D. Zaugg, L.B. Barber, H.T. Buxton, Environmental Science and Technology, 36 (2002) 1202-1211.
[100] P.E. Gibbs, G.W. Bryan, P.L. Pascoe, Marine Environmental Research, 32 (1991) 79-87.
[101] K.R. Munkittrick, M.R. Servos, J.H. Carey, G.J. Van Der Kraak, Environmental impacts of pulp and paper wastewater: Evidence for a reduction in environmental effects at North American pulp mills since 1992, Water Science and Technology, 1997, pp. 329-338.
[102] S.A. Bortone, R.P. Cody, Bulletin of Environmental Contamination and Toxicology, 63 (1999) 150-156.
[103] D.G.J. Larsson, H. HaÌˆllman, L. FoÌˆrlin, Environmental Toxicology and Chemistry, 19 (2000) 2911-2917.
[104] L.J. Guillette Jr, T.S. Gross, G.R. Masson, J.M. Matter, H.F. Percival, A.R. Woodward, Environmental Health Perspectives, 102 (1994) 680-688.
[105] L.J. Guillette Jr, D.B. Pickford, D.A. Crain, A.A. Rooney, H.F. Percival, General and Comparative Endocrinology, 101 (1996) 32-42.
[106] M. Ouellet, J. Bonin, J. Rodrigue, J.L. DesGranges, S. Lair, Journal of Wildlife Diseases, 33 (1997) 95-104.
[107] D.W. Sparling, Journal of the Iowa Academy of Sciences, 107 (2000) 90-91.
[108] T.B. Hayes, A. Collins, M. Lee, M. Mendoza, N. Noriega, A.A. Stuart, A. Vonk, Proceedings of the National Academy of Sciences of the United States of America, 99 (2002) 5476-5480.
[109] S. Ejaz, W. Akram, C.W. Lim, J.J. Lee, I. Husain, Experimental Oncology, 26 (2004) 98-105.
[110] J. Bitman, H.C. Cecil, Journal of Agricultural and Food Chemistry, 18 (1970) 1108-1112.
[111] J. Bitman, H.C. Cecil, S.J. Harris, G.F. Fries, Science, 162 (1968) 371-372.
[112] A.L. Fisher, H.H. Keasling, F.W. Schueler, Proc. Soc. Exp. Biol. Med., 81 (1952) 439-441.
[113] R.M. Welch, W. Levin, A.H. Conney, Toxicology and Applied Pharmacology, 14 (1969) 358-367.
[114] T.R. Wrenn, J.R. Wood, G.F. Fries, J. Bitman, Bulletin of Environmental Contamination and Toxicology, 5 (1970) 61-66.
[115] R. Broséus, S. Vincent, K. Aboulfadl, A. Daneshvar, S. Sauvé, B. Barbeau, M. Prévost, Water Research, 43 (2009) 4707-4717.

[116] T. Deblonde, C. Cossu-Leguille, P. Hartemann, International Journal of Hygiene and Environmental Health, 214 (2011) 442-448.
[117] B. Halling-Sørensen, S. Nors Nielsen, P.F. Lanzky, F. Ingerslev, H.C. Holten Lützhøft, S.E. Jørgensen, Chemosphere, 36 (1998) 357-393.
[118] T. Heberer, Toxicology Letters, 131 (2002) 5-17.
[119] O.A. Jones, J.N. Lester, N. Voulvoulis, Trends in Biotechnology, 23 (2005) 163-167.
[120] A. Jurado, E. Vàzquez-Suñé, J. Carrera, M. López de Alda, E. Pujades, D. Barceló, Science of the Total Environment, 440 (2012) 82-94.
[121] M. Kotchen, J. Kallaos, K. Wheeler, C. Wong, M. Zahller, Journal of Environmental Management, 90 (2009) 1476-1482.
[122] A. Kumar, I. Xagoraraki, Science of the Total Environment, 408 (2010) 5972-5989.
[123] A. Nikolaou, S. Meric, D. Fatta, Analytical and Bioanalytical Chemistry, 387 (2007) 1225-1234.
[124] A. Pal, Y. He, M. Jekel, M. Reinhard, K.Y.-H. Gin, Environment International, 71 (2014) 46-62.
[125] R. Rodil, J.B. Quintana, E. Concha-Graña, P. López-Mahía, S. Muniategui-Lorenzo, D. Prada-Rodríguez, Chemosphere, 86 (2012) 1040-1049.
[126] R. Rosal, A. Rodríguez, J.A. Perdigón-Melón, A. Petre, E. García-Calvo, M.J. Gómez, A. Agüera, A.R. Fernández-Alba, Water Research, 44 (2010) 578-588.
[127] T.A. Ternes, A. Joss, UK: IWA Publishing, in press(2006).
[128] P. Verlicchi, A. Galletti, M. Petrovic, D. Barceló, Journal of Hydrology, 389 (2010) 416-428.
[129] J.-W. Kim, H.-S. Jang, J.-G. Kim, H. Ishibashi, M. Hirano, K. Nasu, N. Ichikawa, Y. Takao, R. Shinohara, K. Arizono, Journal of Health Science, 55 (2009) 249-258.
[130] A. Pal, K.Y.-H. Gin, A.Y.-C. Lin, M. Reinhard, Science of the Total Environment, 408 (2010) 6062-6069.
[131] S. Esplugas, D.M. Bila, L.G.T. Krause, M. Dezotti, Journal of Hazardous Materials, 149 (2007) 631-642.
[132] F. Javier Benitez, J.L. Acero, F.J. Real, G. Roldán, Chemosphere, 77 (2009) 53-59.
[133] K.H. Langford, K.V. Thomas, Environment International, 35 (2009) 766-770.
[134] N. Nakada, H. Shinohara, A. Murata, K. Kiri, S. Managaki, N. Sato, H. Takada, Water Research, 41 (2007) 4373-4382.
[135] C. Zwiener, Water Research, 34 (2000) 1881.
[136] F. Zeng, K. Cui, Z. Xie, L. Wu, M. Liu, G. Sun, Y. Lin, D. Luo, Z. Zeng, Environmental Pollution, 156 (2008) 425-434.
[137] T. Eggen, M. Moeder, A. Arukwe, Science of the Total Environment, 408 (2010) 5147-5157.
[138] Occurrence of Contaminants of Emerging Concern in Wastewater From Nine Publicly Owned Treatment Works in: U.S.E.P. Agency (Ed.), 2009.

[139] N. De Castro-Català, I. Muñoz, L. Armendáriz, B. Campos, D. Barceló, J. López-Doval, S. Pérez, M. Petrovic, Y. Picó, J.L. Riera, Science of the Total Environment, in press.
[140] H. Nakata, R.-I. Shinohara, Y. Nakazawa, T. Isobe, A. Sudaryanto, A. Subramanian, S. Tanabe, M.P. Zakaria, G.J. Zheng, P.K.S. Lam, E.Y. Kim, B.-Y. Min, S.-U. We, P.H. Viet, T.S. Tana, M. Prudente, D. Frank, G. Lauenstein, K. Kannan, Marine Pollution Bulletin, 64 (2012) 2211-2218.
[141] A.D. Syakti, M.M. Ahmed, N.V. Hidayati, E. Hilmi, I. Sulystyo, A. Piram, P. Doumenq, IERI Procedia, 5 (2013) 216-222.
[142] S.J. Trumble, E.M. Robinson, S.R. Noren, S. Usenko, J. Davis, S.B. Kanatous, Science of the Total Environment, 439 (2012) 275-283.
[143] K.A. Hostetler, E.M. Thurman, Science of the Total Environment, 248 (2000) 147-155.
[144] R.D. Wauchope, Journal of Environment Quality, 7 (1978) 459-472.
[145] J.E. Barbash, E.A. Resek, Pesticides in ground water: distribution, trends, and governing factors, Ann Arbor Press, 1996.
[146] M.-C. Lu, J.-N. Chen, Water Science and Technology, 36 (1997) 117-122.
[147] J.J. Pignatello, Y. Sun, Water Research, 29 (1995) 1837-1844.
[148] Environmental Protection Agency, Special report on environmental endocrine disruption: An effects and assessment and analysis., Environmental Protection Agency, Washington D.C., 1997.
[149] S.H. Safe, Environmental Health Perspectives, 108 (2000) 487.
[150] C.G. Daughton, Pharmaceuticals in the Environment, 219th National Meeting of the American Chemical Society, U.S. Environmental Protection Agency, San Francisco, California, 2000.
[151] C. Daughton, T. Ternes, Environmental health perspectives. Supplements, in press(1999) 907.
[152] R. Carson, Silent Spring, Houghton Mifflin, 2002.
[153] J.B. DeWitt, Journal of Agricultural and Food Chemistry, 4 (1956) 863-866.
[154] B. Eskenazi, L.G. Rosas, A.R. Marks, A. Bradman, K. Harley, N. Holland, C. Johnson, L. Fenster, D.B. Barr, Basic & Clinical Pharmacology & Toxicology, 102 (2008) 228-236.
[155] P.W. Davis, G.A. Wedemeyer, Comparative Biochemistry and Physiology Part B: Comparative Biochemistry, 40 (1971) 823-827.
[156] J.F. Treon, F.P. Cleveland, Journal of Agricultural and Food Chemistry, 3 (1955) 402-408.
[157] H.G. Peterson, C. Boutin, P.A. Martin, K.E. Freemark, N.J. Ruecker, M.J. Moody, Aquatic Toxicology, 28 (1994) 275-292.
[158] M.A. Green, M.A. Heumann, H.M. Wehr, L.R. Foster, L.P. Williams, J.A. Polder, C.L. Morgan, S.L. Wagner, L.A. Wanke, J.M. Witt, American Journal of Public Health, 77 (1987) 1431-1434.
[159] D.M. Fry, C.K. Toone, Science, 231 (1981) 919-924.
[160] D.M. Fry, C.K. Toone, S.M. Speich, R.J. Peard, Stud. Avian Biol., 10 (1987) 26-43.
[161] D.M. Fry, Environmental Health Perspectives, 103 (1995) 165-171.
[162] P. Pocar, T.A.L. Brevini, B. Fischer, F. Gandolfi, Reproduction, 125 (2003) 313-325.

[163] C.A. Mackenzie, A. Lockridge, M. Keith, Environmental Health Perspectives, 113 (2005) 1295-1298.
[164] F.W. Schueler, Science, 103 (1946) 221-223.
[165] A. Sluczewski, P. Roth, Gynecol. Obstet., 47 (1948) 164-176.
[166] H.E. Bevans, S.L. Goodbred, J.F. Miesner, S.A. Watkins, T.S. Gross, N.D. Denslow, T. Schoeb, Synthetic Organic Compounds and Carp Endocrinology and Histology in Las Vegas Wash and Las Vegas and Callville Bays of Lake Mead, Nevada, 1992 and 1995, in press(1996).
[167] L.C. Folmar, N.D. Denslow, V. Rao, M. Chow, D.A. Crain, J. Enblom, J. Marcino, L.J. Guillette Jr, Environmental Health Perspectives, 104 (1996) 1096-1101.
[168] J.E. Harries, D.A. Sheahan, S. Jobling, P. Matthiessen, P. Neall, E.J. Routledge, R. Rycroft, J.P. Sumpter, T. Tylor, Environmental Toxicology and Chemistry, 15 (1996) 1993-2002.
[169] S. Jobling, M. Nolan, C.R. Tyler, G. Brighty, J.P. Sumpter, Environmental Science and Technology, 32 (1998) 2498-2506.
[170] C.E. Purdom, P.A. Hardiman, V.J. Bye, N.C. Eno, C.R. Tyler, J.P. Sumpter, Chem. Ecol., 8 (1994) 275-285.
[171] W.B. Gill, G.F.B. Schumacher, M. Bibbo, Journal of Urology, 122 (1979) 36-39.
[172] A.L. Herbst, H. Ulfelder, D.C. Poskanzer, New England Journal of Medicine, 284 (1971) 878-881.
[173] E. Carlsen, A. Giwercman, N. Keiding, N.E. Skakkebaek, Environmental Health Perspectives, 103 (1995) 137-139.
[174] R.M. Sharpe, N.E. Skakkebaek, Lancet, 341 (1993) 1392-1395.
[175] R. Stone, Science, 265 (1994) 308-310.
[176] U.G. Ahlborg, L. Lipworth, L. Titus-Ernstoff, C.C. Hsieh, A. Hanberg, J. Baron, D. Trichopoulos, H.O. Adami, Critical Reviews in Toxicology, 25 (1995) 463-531.
[177] J. Ashby, Environmental Toxicology and Pharmacology, 3 (1997) 87-90.
[178] B.E. Gillesby, T.R. Zacharewski, Environmental Toxicology and Chemistry, 17 (1998) 3-14.
[179] V. Krishnan, S. Safe, Toxicology and Applied Pharmacology, 120 (1993) 55-61.
[180] T.A. Ternes, Water research, 32 (1998) 3245-3260.
[181] C.S. Castro, M.C. Guerreiro, M. Gonçalves, L.C.A. Oliveira, A.S. Anastácio, Journal of Hazardous Materials, 164 (2009) 609-614.
[182] N. Ta, J. Hong, T. Liu, C. Sun, Journal of Hazardous Materials, 138 (2006) 187-194.
[183] Pesticide Transformation Products, American Chemical Society, 1991.
[184] S. Nélieu, L. Kerhoas, J. Einhorn, Environmental Science & Technology, 34 (1999) 430-437.
[185] Y.M. Vera, R.J.d. Carvalho, M.L. Torem, B.A. Calfa, Chemical Engineering Journal, 155 (2009) 691-697.
[186] K.H. Chan, W. Chu, Applied Catalysis B: Environmental, 58 (2005) 157-163.
[187] J. Ma, N.J.D. Graham, Water Research, 33 (1999) 785-793.

[188] J. Ma, N.J.D. Graham, Water Research, 34 (2000) 3822-3828.
[189] V.A. Sakkas, I.M. Arabatzis, I.K. Konstantinou, A.D. Dimou, T.A. Albanis, P. Falaras, Applied Catalysis B, 49 (2004) 195-205.
[190] M.L. Hladik, A.L. Roberts, E.J. Bouwer, Water Research, 39 (2005) 5033-5044.
[191] C. Yanze Kontchou, N. Gschwind, Ecotoxicology and Environmental Safety, 40 (1998) 29-33.
[192] H. Sabik, S. Cooper, P. Lafrance, J. Fournier, Talanta, 42 (1995) 717-724.
[193] J. Kochany, R.J. Maguire, Journal of Agricultural and Food Chemistry, 42 (1994) 406-412.
[194] C. Aguilar, I. Ferrer, F. Borrull, R.M. Marcé, D. Barceló, Analytica Chimica Acta, 386 (1999) 237-248.
[195] T.A. Albanis, D.G. Hela, T.M. Sakellarides, I.K. Konstantinou, Journal of Chromatography A, 823 (1998) 59-71.
[196] W. Battaglin, E. Furlong, M. Burkhardt, C. Peter, Science of the Total Environment, 248 (2000) 123-133.
[197] J.E. Barbash, G.P. Thelin, D.W. Kolpin, R.J. Gilliom, Journal of Environmental Quality, 30 (2001) 831-845.
[198] D.W. Kolpin, J.E. Barbash, R.J. Gilliom, Environmental Science & Technology, 32 (1998) 558-566.
[199] R.H. Coupe, J.D. Blomquist, Journal (American Water Works Association), in press(2004) 56-68.
[200] H. Kuramitz, J. Saitoh, T. Hattori, S. Tanaka, Water Research, 36 (2002) 3323-3329.
[201] M. Ahel, T. Conrad, W. Giger, Environmental Science & Technology, 21 (1987) 697-703.
[202] W. Giger, P.H. Brunner, C. Schaffner, Science, 225 (1984) 623-625.
[203] E. Argese, A. Marcomini, C. Bettiol, G. Perin, P. Miana, Environmental Toxicology and Chemistry, 13 (1994) 737-742.
[204] D. McLeese, V. Zitko, D. Sergeant, L. Burridge, C. Metcalfe, Chemosphere, 10 (1981) 723-730.
[205] R. White, S. Jobling, S. Hoare, J. Sumpter, M. Parker, Endocrinology, 135 (1994) 175-182.
[206] B.V. Chang, C.H. Yu, S.Y. Yuan, Chemosphere, 55 (2004) 493-500.
[207] J. Kim, G.V. Korshin, A.B. Velichenko, Water Research, 39 (2005) 2527-2534.
[208] R. Bassett, P. Buszka, G. Davidson, D. Chong-Diaz, Environmental Science & Technology, 29 (1995) 2915-2922.
[209] A. Favre-Réguillon, G. Lebuzit, D. Murat, J. Foos, C. Mansour, M. Draye, Water Research, 42 (2008) 1160-1166.
[210] T. Harter, L. Rollins, Watersheds, Groundwater and Drinking Water: A Practical Guide, UCANR Publications, 2008.
[211] J.O. Nriagu, J.M. Pacyna, Nature, 333 (1988) 134-139.
[212] R.J. Law, C.R. Allchin, J. De Boer, A. Covaci, D. Herzke, P. Lepom, S. Morris, J. Tronczynski, C.A. De Wit, Chemosphere, 64 (2006) 187-208.
[213] K.S. Ritter, Paul Sibley, Ken Hall, Patricia Keen, Gevan Mattu, Beth Linton, Len, Journal of Toxicology and Environmental Health Part A, 65 (2002) 1-142.

[214] C.B. Braungardt, E.P. Achterberg, F. Elbaz-Poulichet, N.H. Morley, Applied Geochemistry, 18 (2003) 1757-1771.
[215] D. Browne, H. Whelton, D. O'Mullane, Journal of Dentistry, 33 (2005) 177-186.
[216] M.N. Tamer, B. Kale Köroğlu, Ç. Arslan, M. Akdoğan, M. Köroğlu, H. Çam, M. Yildiz, Science of the Total Environment, 373 (2007) 43-48.
[217] M. Zeni, R. Riveros, K. Melo, R. Primieri, S. Lorenzini, Desalination, 185 (2005) 241-244.
[218] A.M. Fan, V.E. Steinberg, Regulatory Toxicology and Pharmacology, 23 (1996) 35-43.
[219] A. El Midaoui, F. Elhannouni, M. Taky, L. Chay, M.A. Menkouchi Sahli, L. Echihabi, M. Hafsi, Separation and Purification Technology, 29 (2002) 235-244.
[220] L. Melnyk, V. Goncharuk, I. Butnyk, E. Tsapiuk, Desalination, 185 (2005) 147-157.
[221] D. Ortiz-Pérez, M. Rodríguez-Martínez, F. Martínez, V.c.H. Borja-Aburto, J. Castelo, J.I. Grimaldo, E. de la Cruz, L. Carrizales, F. Díaz-Barriga, Environmental Research, 93 (2003) 20-30.
[222] K.-S. Ng, Z. Ujang, P. Le-Clech, Reviews in Environmental Science and Biotechnology, 3 (2004) 43-53.
[223] D.B. Thakur, R.M. Tiggelaar, J.G.E. Gardeniers, L. Lefferts, K. Seshan, Chemical Engineering Journal, 227 (2013) 128-136.
[224] D.B. Thakur, R.M. Tiggelaar, Y. Weber, J.G.E. Gardeniers, L. Lefferts, K. Seshan, Applied Catalysis B: Environmental, 102 (2011) 243-250.
[225] International Agency for Cancer Research, Agents Classified by the IARC Monographs, Volumes 1–106, International Agency for Cancer Research, Lyon, 2012.
[226] World Health Organization, Bromate in drinking-water;Background document for preparation of WHO guidelines for drinking-water quality., World Health Organization, Geneva, 2003.
[227] United States Environmental Protection Agency, Public health goals for chemicals in drinking water - Bromate, United States Environmental Protection Agency, California, 2009.
[228] W.J. Huang, Y.L. Cheng, Separation and Purification Technology, 59 (2008) 101-107.
[229] M.J. Kirisits, V.L. Snoeyink, J.C. Kruithof, Water Research, 34 (2000) 4250-4260.
[230] M.N. Chong, B. Jin, C.W. Chow, C. Saint, Water Research, 44 (2010) 2997-3027.
[231] B. Legube, N. Karpel Vel Leitner, Catalysis Today, 53 (1999) 61.
[232] A. Pintar, Catalysis Today, 53 (1999) 35.
[233] F. Epron, F. Gauthard, C. Pinéda, J. Barbier, Journal of Catalysis, 198 (2001) 309-318.
[234] O.M. Ilinich, Separation and Purification Technology, 21 (2000) 55.
[235] O.M. Ilinitch, Catalysis Today, 56 (2000) 137.
[236] K. Daub, V.K. Wunder, R. Dittmeyer, Catalysis Today, 67 (2001) 257-272.

[237] A. Ozcan, Y. Sahin, A.S. Koparal, M.A. Oturan, Applied catalysis. B, Environmental, 89 (2009) 620-626.
[238] G. Pérez, A. Fernández-Alba, A. Urtiaga, I. Ortiz, Water Research, 44 (2010) 2763-2772.
[239] G. Chen, Separation and Purification Technology, 38 (2004) 11-41.
[240] P. Schröder, J. Navarro-Aviñó, H. Azaizeh, A.G. Goldhirsh, S. DiGregorio, T. Komives, G. Langergraber, A. Lenz, E. Maestri, A.R. Memon, Environmental Science and Pollution Research-International, 14 (2007) 490-497.
[241] J.P. Scott, D.F. Ollis, Environmental Progress, 14 (1995) 88-103.
[242] M. Klavarioti, D. Mantzavinos, D. Kassinos, Environment International, 35 (2009) 402-417.
[243] C. Gottschalk, J.A. Libra, A. Saupe, Ozonation of water and waste water a practical guide to understanding ozone and its application, Wiley-VCH, 2000.
[244] B. Kasprzyk-Hordern, Ziólek, M., Nawrocki, J., Applied Catalysis B, 46 (2003) 639.
[245] W.H. Glaze, Kang, J.W, Douglas, C.H., Ozone: science and engineering, 9 (1987) 335.
[246] R. Andreozzi, V. Caprio, I. Amedeo, R. Marotta, Catalysis Today, 53 (1999) 51.
[247] V. Camel, A. Bermond, Water Research, 32 (1998) 3208-3222.
[248] S.A. Carr, R.B. Baird, Water Research, 34 (2000) 4036-4048.
[249] W.J. Cooper, S.P. Mezyk, J.R. Peller, S.K. Cole, W.H. Song, B.J. Mincher, B.M. Peake, Ozone: science and engineering, 30 (2008) 58-64.
[250] S. Derrouiche, D. Bourdin, P. Roche, B. Houssais, C. Machinal, M. Coste, J. Restivo, J.J.M. Orfao, M.F.R. Pereira, Y. Marco, E. Garcia-Bordeje, Water Sci Technol, 68 (2013) 1377-1383.
[251] E. Felis, J. Wiszniowski, K. Miksch, Archiwum ochrony środowiska, 35 (2009) 15-25.
[252] M. Hammad Khan, J.Y. Jung, Chemosphere, 72 (2008) 690-696.
[253] K. Ikehata, Ozone: science and engineering, 30 (2008) 21-26.
[254] K. Ikehata, M.G. El-Din, Ozone Science and Engineering, 27 (2005) 83-114.
[255] K. Ikehata, M.G. El-Din, Ozone Science and Engineering, 27 (2005) 173-202.
[256] J.A. Khan, X. He, H.M. Khan, N.S. Shah, D.D. Dionysiou, Chemical Engineering Journal, 218 (2013) 376-383.
[257] K.-H. Kim, S.-K. Ihm, Journal of Hazardous Materials, 186 (2011) 16-34.
[258] S.J. Masten, M.J. Galbraith, S.H.R. Davies, Ozone Science and Engineering, 18 (1996) 535-547.
[259] S.A.S. Melo, A.G. Trovo, I.R. Bautitz, R.F.P. Nogueira, Quimica Nova, 32 (2009) 188-197.
[260] M. Nakonechny, K. Ikehata, M. El-Din, Ozone: science and engineering, 30 (2008) 249-255.
[261] Z. Qiang, C. Liu, B. Dong, Y. Zhang, Chemosphere, 78 (2010) 517-526.

[262] J. Radjenovic, A. Bagastyo, R.A. Rozendal, Y. Mu, J. Keller, K. Rabaey, Water Research, 45 (2011) 1579-1586.
[263] M. Trapido, Y. Veressinina, R. Munter, Environmental Technology, 16 (1995) 729-740.
[264] A.G. Trovó, S.A.S. Melo, R.F.P. Nogueira, Journal of Photochemistry and Photobiology A: Chemistry, 198 (2008) 215-220.
[265] F.J. Beltrán, Applied Catalysis B, Environmental, 63 (2006) 249.
[266] N.P. Cheremisinoff, Handbook of water and wastewater treatment technologies, Butterworth Heinemann, 2002.
[267] F.L. Burton, G. Tchobanoglous, Wastewater Engineering: treatment, disposal and reuse, Tata McGraw-Hill Publishing Company, 2000.
[268] F.J. Beltrán, Ozone reaction kinetics for water and wastewater systems, Lewis Publishers, 2004.
[269] J. Staehelin, Environmental Science & Technology, 19 (1985) 1206.
[270] J. Staehelin, Environmental Science & Technology, 16 (1982) 676.
[271] J. Staehelin, The Journal of physical chemistry, 88 (1984) 5999.
[272] H. Tomiyasu, H. Fukutomi, G. Gordon, Inorganic Chemistry, 24 (2002) 2962-2966.
[273] F.J. Beltrán, F.J. Rivas, R. Montero-de-Espinosa, Water Research, 39 (2005) 3553-3564.
[274] A.G. Gonçalves, J.J.M. Órfão, M.F.R. Pereira, Journal of Environmental Chemical Engineering, 1 (2013) 260-269.
[275] A.G. Gonçalves, J.J.M. Órfão, M.F.R. Pereira, Chemical Engineering Journal, 250 (2014) 366-376.
[276] C.A. Orge, J.J.M. Órfão, M.F.R. Pereira, Applied Catalysis B: Environmental, 126 (2012) 22-28.
[277] L. Li, Journal of Hazardous Materials, 170 (2009) 411.
[278] A. Lv, C. Hu, Y. Nie, J. Qu, Applied Catalysis B: Environmental, 100 (2010) 62-67.
[279] M. Sui, S. Xing, L. Sheng, S. Huang, H. Guo, Journal of Hazardous Materials, 227–228 (2012) 227-236.
[280] S.-p. Tong, W.-p. Liu, W.-h. Leng, Q.-q. Zhang, Chemosphere, 50 (2003) 1359-1364.
[281] L. Zhao, Applied catalysis. B, Environmental, 83 (2008) 256.
[282] Z.L. Chen, F. Qi, B.B. Xu, J.M. Shen, Y. Ben, M.M. Ye, Chinese Journal of Environmental Science, 28 (2007) 563-568.
[283] C.A. Guzman-Perez, J. Soltan, J. Robertson, Journal of Environmental Science and Health. Part B: Pesticides, Food Contaminants, and Agricultural Wastes, 47 (2012) 544-552.
[284] A. Ikhlaq, D.R. Brown, B. Kasprzyk-Hordern, Applied Catalysis B: Environmental, 123–124 (2012) 94-106.
[285] X. Wang, J. Guan, R.M. Stuetz, Water Sci Technol, 66 (2012) 1781-1786.
[286] P.M. Alvárez, Applied catalysis. B, Environmental, 92 (2009) 393.
[287] F.J. Beltran, P. Pocostales, P. Alvarez, A. Oropesa, Journal of Hazardous Materials, 163 (2009) 768-776.
[288] F.J. Beltrán, F.J. Rivas, L.A. Fernández, P.M. Álvarez, R. Montero-de-Espinosa, Industrial & engineering chemistry research, 41 (2002) 6510-6517.

[289] F.J. Beltrán, F.J. Rivas, R. Montero-de-Espinosa, Journal of Chemical Technology and Biotechnology, 78 (2003) 1225-1233.
[290] H. Cao, L. Xing, G. Wu, Y. Xie, S. Shi, Y. Zhang, D. Minakata, J.C. Crittenden, Applied Catalysis B: Environmental, 146 (2014) 169-176.
[291] P.C.C. Faria, J.J.M. Órfão, P. M.F.R., Applied Catalysis B, Environmental, 79 (2008) 237.
[292] P.C.C. Faria, J.J.M. Órfão, M.F.R. Pereira, Applied Catalysis B: Environmental, 83 (2008) 150-159.
[293] A.G. Gonçalves, J.J.M. Órfão, M.F.R. Pereira, Journal of Hazardous Materials, 239–240 (2012) 167-174.
[294] C.A. Guzman-Perez, J. Soltan, J. Robertson, Separation and Purification Technology, 79 (2011) 8-14.
[295] X. Li, Journal of Hazardous Materials, 163 (2009) 115.
[296] J. Ma, Ozone: science and engineering, 26 (2004) 3.
[297] J.P. Pocostales, P.M. Alvarez, F.J. Beltrán, Chemical Engineering Journal, 164 (2010) 70-76.
[298] X. Fan, J. Restivo, J.J.M. Órfão, M.F.R. Pereira, A.A. Lapkin, Chemical Engineering Journal, 241 (2014) 66-76.
[299] S. Zhang, D. Wang, X. Quan, L. Zhou, X. Zhang, Separation and Purification Technology, 116 (2013) 351-359.
[300] J.K. Chinthaginjala, Seshan, K., Lefferts, L., Industrial & engineering chemistry research, 46 (2007) 3968.
[301] A.G. Gonçalves, J.L. Figueiredo, J.J.M. Órfão, M.F.R. Pereira, Carbon, 48 (2010) 4369-4381.
[302] J.L. Figueiredo, M.F.R. Pereira, Catalysis Today, 150 (2010) 2-7.
[303] R.P. Rocha, J.P.S. Sousa, A.M.T. Silva, M.F.R. Pereira, J.L. Figueiredo, Applied Catalysis B: Environmental, 104 (2011) 330-336.
[304] P.C.C. Faria, Catalytic ozonation of effluents from the textile industry, PhD thesis, University of Porto, 2008.
[305] F.J. Beltrán, J.P. Pocostales, P.M. Alvarez, J. Jaramillo, Journal of Hazardous Materials, 169 (2009) 532-538.
[306] Z.Q. Liu, Applied catalysis. B, Environmental, 92 (2009) 301.
[307] U. Jans, J. Hoigne, Ozone: science and engineering, 20 (1998) 67-90.
[308] U. Von Gunten, Water Research, 37 (2003) 1443.
[309] C. Von Sonntag, R. Mertens, M. Schuchmann, H.-P. Schuchmann, P. Dowideit, X. Pan, X. Fang, Water Science and Technology, 35 (1997) 9-15.
[310] M.O. Buffle, J. Schumacher, E. Salhi, M. Jekel, U. Von Gunten, Water Research, 40 (2006) 1884.
[311] J. Rivera-Utrilla, M. Sánchez-Polo, J.D. Méndez-Días, M.A. Ferro-García, I. Bautista-Toledo, Journal of Colloid and Interface Science, 325 (2008) 432.
[312] J. Rivera-Utrilla, M. Sánchez-Polo, G. Prados-Joya, M.A. Ferro-García, I. Bautista-Toledo, Journal of Hazardous Materials, In Press, Corrected Proof (2009).
[313] F.J. Beltrán, J.P. Pocostales, P. Álvarez, F. López-Piñeiro, Applied catalysis. B, Environmental, 92 (2009) 262.

[314] F.J. Beltran, I. Giraldez, J.F. Garcia-Araya, Industrial & engineering chemistry research, 47 (2008) 1058-1065.
[315] M. Sanchez-Polo, U. Von Gunten, J. Rivera-Utrilla, Water Research, 39 (2005) 3189.
[316] P.C.C. Faria, J.J.M. Órfão, M.F.R. Pereira, Chemosphere, 67 (2007) 809-815.
[317] L. Oliviero, Applied catalysis. B, Environmental, 40 (2003) 163.
[318] U. Matatov-Meytal, M. Sheintuch, Catalysis Today, 102-103 (2005) 121-127.
[319] Y. Yoshinaga, T. Akita, M. Ikko, O. Toshio, Journal of Catalysis, 207 (2002) 37-45.
[320] O.S.G.P. Soares, J.J.M. Órfão, M.F.R. Pereira, Catalysis Letters, 126 (2008) 253-260.
[321] O.S.G.P. Soares, J.J.M. Órfão, M.F.R. Pereira, Applied Catalysis B: Environmental, 91 (2009) 441-448.
[322] O.S.G.P. Soares, J.J.M. Órfão, J. Ruiz-Martínez, J. Silvestre-Albero, A. Sepúlveda-Escribano, M.F.R. Pereira, Chemical Engineering Journal, 165 (2010) 78-88.
[323] N. Barrabes, J. Just, A. Dafinov, F. Medina, J.L.G. Fierro, J.E. Sueiras, P. Salagre, Y. Cesteros, Applied Catalysis B: Environmental, 62 (2006) 77-85.
[324] O.S.G.P. Soares, J.J.M. Órfão, M.F.R. Pereira, Industrial and Engineering Chemistry Research, 49 (2010) 7183-7192.
[325] O.S.G.P. Soares, J.J.M. Órfão, E. Gallegos-Suarez, E. Castillejos, I. Rodríguez-Ramos, M.F.R. Pereira, Environmental Technology, 33 (2012) 2353-2358.
[326] O.S.G.P. Soares, J.J.M. Órfão, M.F.R. Pereira, Desalination, 279 (2011) 367-374.
[327] W. Gao, N. Guan, J. Chen, X. Guan, R. Jin, H. Zeng, L. Zhiguang, F. Zhang, Applied Catalysis B: Environmental, 46 (2003) 341-351.
[328] W. Gao, J. Chen, X. Guan, R. Jin, F. Zhang, N. Guan, Catalysis Today, 93–95 (2004) 333-339.
[329] F. Epron, F. Gauthard, J. Barbier, Journal of Catalysis, 206 (2002) 363-367.
[330] N. Barrabés, A. Dafinov, F. Medina, J.E. Sueiras, Catalysis Today, 149 (2010) 341-347.
[331] A. Devadas, S. Vasudevan, F. Epron, Journal of Hazardous Materials, 185 (2011) 1412-1417.
[332] A.E. Palomares, J.G. Prato, F. Márquez, A. Corma, Applied Catalysis B: Environmental, 41 (2003) 3-13.
[333] A.E. Palomares, C. Franch, A. Corma, Catalysis Today, 172 (2011) 90-94.
[334] T. Yuranova, C. Franch, A.E. Palomares, E. Garcia-Bordejé, L. Kiwi-Minsker, Applied Catalysis B: Environmental, 123–124 (2012) 221-228.
[335] J. Sá, J.A. Anderson, Applied Catalysis B: Environmental, 77 (2008) 409-417.
[336] O.S.G.P. Soares, J.J.M. Órfão, M.F.R. Pereira, Applied Catalysis B: Environmental, 102 (2011) 424-432.

[337] M. Asami, T. Aizawa, T. Morioka, W. Nishijima, T. Akihisa, Y. Magara, Water Research, 33 (1999) 2797-2804.
[338] M. L. Bao, O. Griffini, D. Santianni, K. Barbieri, D. Burrini, F. Pantani, Water Research, 33 (1999) 2959-2970.
[339] A. Mills, G. Meadows, Water Research, 29 (1995) 2181-2185.
[340] H. Chen, Z. Xu, H. Wan, J. Zheng, D. Yin, S. Zheng, Applied Catalysis B: Environmental, 96 (2010) 307-313.
[341] A.E. Palomares, C. Franch, T. Yuranova, L. Kiwi-Minsker, E. García-Bordeje, S. Derrouiche, Applied Catalysis B: Environmental, 146 (2014) 186-191.
[342] P. Yaseneva, C.F. Marti, E. Palomares, X. Fan, T. Morgan, P.S. Perez, M. Ronning, F. Huang, T. Yuranova, L. Kiwi-Minsker, Chemical Engineering Journal, 248 (2014) 230-241.
[343] T. Yuranova, L. Kiwi-Minsker, C. Franch, A.E. Palomares, S. Armenise, E. García-Bordejé, Industrial & engineering chemistry research, 52 (2013) 13930-13937.
[344] Y. Marco, E. García-Bordejé, C. Franch, A.E. Palomares, T. Yuranova, L. Kiwi-Minsker, Chemical Engineering Journal, 230 (2013) 605-611.
[345] J.L. Williams, Catalysis Today, 69 (2001) 3.
[346] K.S. Suslick, T. Hyeon, M. Fang, A.A. Cichowlas, Materials Science and Engineering: A, 204 (1995) 186-192.
[347] M.-J. Ledoux, C. Pham-Huu, Catalysis Today, 102-103 (2005) 2-14.
[348] A.J. Lachawiec, Langmuir, 21 (2005) 11418.
[349] J.P. Tessonnier, Carbon, 47 (2009) 1779.
[350] E.J. Biddinger, Topics in Catalysis, 52 (2009) 1566.
[351] P. Pfeifer, M. Fichtner, K. Schubert, M.A. Liauw, G. Emig, Microstructured Catalysts for Methanol-Steam Reforming, in: W. Ehrfeld (Ed.) Microreaction Technology: Industrial Prospects, Springer Berlin Heidelberg2000, pp. 372-382.
[352] M.N. Kashid, L. Kiwi-Minsker, Industrial & engineering chemistry research, 48 (2009) 6465-6485.
[353] T.A. Nijhuis, M.T. Kreutzer, A.C.J. Romijn, F. Kapteijn, J.A. Moulijn, Chemical Engineering Science, 56 (2001) 823-829.
[354] R.M. Machado, R.B. Broekhuis, A.F. Nordquist, B.P. Roy, S.R. Carney, Catalysis Today, 105 (2005) 305.
[355] E. García-Bordejé, M.J. Lázaro, R. Moliner, P.M. Álvarez, V. Gómez-Serrano, J.L.G. Fierro, Carbon, 44 (2006) 407-417.
[356] H. Mei, C. Li, S. Ji, H. Liu, Chemical Engineering Science, 62 (2007) 4294.
[357] S. Salomons, R.E. Hayes, M. Votsmeier, A. Drochner, H. Vogel, S. Malmberg, J. Gieshoff, Applied Catalysis B: Environmental, 70 (2007) 305-313.
[358] J. Requies, M.C. Alvarez-Galvan, V.L. Barrio, P.L. Arias, J.F. Cambra, M.B. Güemez, A. Manrique Carrera, V.A. de la Peña O'Shea, J.L.G. Fierro, Applied Catalysis B: Environmental, 79 (2008) 122-131.
[359] J.-H. Ryu, K.-Y. Lee, H.-J. Kim, J.-I. Yang, H. Jung, Applied Catalysis B: Environmental, 80 (2008) 306-312.

[360] S. Araki, N. Hino, T. Mori, S. Hikazudani, International Journal of Hydrogen Energy, 34 (2009) 4727-4734.
[361] L. Bobrova, N. Vernikovskaya, V. Sadykov, Catalysis Today, 144 (2009) 185-200.
[362] W. Liu, Catalysis Today, 140 (2009) 142.
[363] A. Boyano, C. Herrera, M.A. Larrubia, L.J. Alemany, R. Moliner, M.J. Lázaro, Chemical Engineering Journal, 160 (2010) 623-633.
[364] H. Chen, J. Wang, H. Li, D. Wu, M. Yao, Y. Li, Applied Catalysis A: General, 427–428 (2012) 73-78.
[365] F. Fairbrother, A.E. Stubbs, Journal of the Chemical Society, in press(1935) 527-529.
[366] G.I. Taylor, Journal of Fluid Mechanics, 9 (1960) 218-224.
[367] R.N. Marchessault, S.G. Mason, Industrial & Engineering Chemistry, 52 (1960) 79-84.
[368] F.P. Bretherton, Journal of Fluid Mechanics, 10 (1961) 166-188.
[369] E.I. Shen, K.S. Udell, Journal of Applied Mechanics, 52 (1985) 253-256.
[370] M.T. Kreutzer, F. Kapteijn, J.A. Moulijn, J.J. Heiszwolf, Chemical Engineering Science, 60 (2005) 5895-5916.
[371] G. Berčič, A. Pintar, Chemical Engineering Science, 52 (1997) 3709-3719.
[372] M.T. Kreutzer, P. Du, J.J. Heiszwolf, F. Kapteijn, J.A. Moulijn, Chemical Engineering Science, 56 (2001) 6015-6023.
[373] A.N. Tsoligkas, M.J.H. Simmons, J. Wood, C.G. Frost, Catalysis Today, 128 (2007) 36-46.
[374] A.N. Tsoligkas, M.J.H. Simmons, J. Wood, Chemical Engineering Science, 62 (2007) 4365-4378.
[375] J.M. van Baten, R. Krishna, Chemical Engineering Science, 59 (2004) 2535-2545.
[376] J.M. van Baten, R. Krishna, Chemical Engineering Science, 60 (2005) 1117-1126.
[377] J. J. Heiszwolf, L. B. Engelvaart, M. G. van den Eijnden, M. T. Kreutzer, F. Kapteijn, J. A. Moulijn, Chemical Engineering Science, 56 (2001) 805-812.
[378] J.J. Heiszwolf, M.T. Kreutzer, M.G. van den Eijnden, F. Kapteijn, J.A. Moulijn, Catalysis Today, 69 (2001) 51-55.
[379] M.T. Kreutzer, Hydrodynamics of Taylor Flow in Capillaries and Monolith Reactors Delft University Press, 2003.
[380] M.T. Kreutzer, Chemical Engineering Science, 60 (2005) 5895.
[381] M.T. Kreutzer, Catalysis Today, 105 (2005) 421.
[382] R.S. Abiev, I.V. Lavretsov, Chemical Engineering Science, 74 (2012) 59-68.
[383] R.S. Abiev, Chemical Engineering Journal, 227 (2013) 66-79.
[384] H. Liu, C.O. Vandu, R. Krishna, Industrial & engineering chemistry research, 44 (2004) 4884-4897.
[385] C.O. Vandu, H. Liu, R. Krishna, Chemical Engineering Science, 60 (2005) 6430-6437.
[386] C.O. Vandu, J. Ellenberger, R. Krishna, Chemical Engineering and Processing: Process Intensification, 44 (2005) 363-374.

[387] S. Kececi, M. Wörner, A. Onea, H.S. Soyhan, Catalysis Today, 147, Supplement (2009) S125-S131.
[388] A. Onea, M. Wörner, D.G. Cacuci, Chemical Engineering Science, 64 (2009) 1416-1435.
[389] N. Shao, A. Gavriilidis, P. Angeli, Chemical Engineering Journal, 160 (2010) 873-881.
[390] J.A. Howard, P.A. Walsh, International Journal of Multiphase Flow, 55 (2013) 32-42.
[391] Y. Han, N. Shikazono, International Journal of Heat and fluid flow, 30 (2009) 842-853.
[392] H. Ganapathy, E. Al-Hajri, M.M. Ohadi, Chemical Engineering Science, 94 (2013) 156-165.
[393] T.A. Nijhuis, M.T. Kreutzer, A.C.J. Romijn, F. Kapteijn, J.A. Moulijn, Catalysis Today, 66 (2001) 157-165.
[394] L. Zhao, Applied catalysis. B, Environmental, 89 (2009) 326.
[395] L. Zhao, S.U.N. Zhizhong, M.A. Jun, Environmental Science & Technology, 43 (2009) 4157-4163.
[396] A. Devard, M.A. Ulla, F.A. Marchesini, Catalysis Communications, 34 (2013) 26-29.
[397] T. Valdés-Solís, G. Marbán, A.B. Fuertes, Catalysis Today, 69 (2001) 259-264.
[398] L.A. Isupova, E.F. Sutormina, V.P. Zakharov, N.A. Rudina, N.A. Kulikovskaya, L.M. Plyasova, Catalysis Today, 147 (2009) S319-S323.
[399] J.L. Williams, Catalysis Today, 69 (2001) 3-9.
[400] N. Jarrah, J.G. van Ommen, L. Lefferts, Catalysis Today, 79-80 (2003) 29-33.
[401] N.A. Jarrah, Journal of materials chemistry, 14 (2004) 1590.
[402] E. Garcia-Bordeje, I. Kvande, D. Chen, M. Ronning, Advanced Materials, 18 (2006) 1589.
[403] A.F. Pérez-Cadenas, F. Kapteijn, J.A. Moulijn, F.J. Maldonado-Hódar, F. Carrasco-Marín, C. Moreno-Castilla, Carbon, 44 (2006) 2463-2468.
[404] S. Morales-Torres, A.F. Pérez-Cadenas, F. Kapteijn, F. Carrasco-Marín, F.J. Maldonado-Hódar, J.A. Moulijn, Applied Catalysis B: Environmental, 89 (2009) 411-419.
[405] F. Al Badran, S. Awdry, S.T. Kolaczkowski, Catalysis Today, 216 (2013) 229-239.
[406] P. Avila, M. Montes, E.E. Miró, Chemical Engineering Journal, 109 (2005) 11-36.

Part II

Ozonation

1. MATERIALS AND METHODS

1.1 DESCRIPTION

In this chapter the materials and methods used in the study of the application of structured catalysts to the ozonation reaction are described.

The description includes the characterization of the materials that were commercially acquired, those that were obtained through collaboration with foreign research groups through the European project MONACAT, and those that were prepared in our laboratory by other collaborators and that were made available for the study of the ozonation reaction. The characterization techniques that were used in the course of this work to further characterize these materials, either pre- or post-reaction are described.

Furthermore, the experimental installations and procedures are detailed, as well as the analytical techniques used to assess the performance of the catalysts in the ozonation process, both in semi-batch and in continuous reaction.

1.2 CATALYSTS

1.2.1 POWDER CATALYSTS

In the development of the work here presented, several powder catalysts were used; namely multiwalled carbon nanotubes (MWCNT), activated carbon (AC) and carbon xerogels (CX).

The pristine MWCNT and AC were acquired from the manufacturers, respectively Nanocyl and Norit. Carbon xerogels samples were prepared in the LCM laboratory.

The modified MWCNT were prepared in the LCM laboratory and kindly made available by Raquel P. Rocha in order to be used in the ozonation

reaction. The preparation methods are described in detail in the literature [1, 2]. In general, the treatments applied aimed at the inclusion of different elements on the surface of the MWCNT; the treatment with nitric acid (CNT-N) was carried out to introduce acidic oxygen-containing functionalities, the treatment with sulphuric acid (CNT-S) was carried out to introduce sulphur-containing functionalities, the treatment with nitric and sulphuric acid was carried out to introduce a mixture acidic O- and S- containing functionalities (CNT-NS) and finally the treatment with urea was carried out to introduce basic nitrogen-containing surface functionalities (CNT-NUT). The original sample is identified as CNT-O, in the context of these samples.

Characterization of the textural and chemical properties of the pristine MWCNT were carried out according to the techniques described in section *Characterization techniques.* The characterization of the modified MWCNT was obtained from the related literature [1, 2].

The textural characterization of the MWCNT, obtained through the adsorption isotherms of nitrogen at 77K are presented in Table 1.1

Table 1.1 – Textural characterization of the pristine and modified MWCNT samples.

Sample	S_{BET} (m^2 g^{-1})
CNT-O	326
CNT-N	400
CNT-NS	394
CNT-S	293
CNT-NUT	386

The characterization of the chemical properties of the MWCNT is presented in Table 1.2, obtained by TPD analyses and evaluation of the pH_{pzc}.

Furthermore, XPS analyses of the N- and S- containing MWCNT were carried out. The deconvolution of the XPS N1s and S2p peaks allowed the identification and relative quantification of the species present on the surface of the MWCNT. The results were confirmed by elemental analysis. In the case of the CNT-S sample, only one species was identified at 169 eV, corresponding to sulphonic groups. In the case of the CNT-NUT sample, pyridinic groups (N6) were identified at 389.7 eV, and pyrrolic (N5) groups were identified at 400.2 eV. The amount of nitrogen was calculated to be 0.91% by elemental analysis and 0.69% by XPS. The difference in the relative amounts is likely linked to the reduced penetration of the XPS when compared with the elemental analysis, in which the sample is thoroughly analysed.

Table 1.2 – Chemical characterization of the pristine and modified MWCNT samples.

Sample	CO (μmol g^{-1})	CO_2 (μmol g^{-1})	SO_2 (μmol g^{-1})	pH_{pzc}
CNT-O	187	33	-	6.8
CNT-N	1852	1233	-	2.2
CNT-NS	2035	1397	203	4.8
CNT-S	381	195	579	2.5
CNT-NUT	703	76	-	6.7

The carbon xerogel used in the work here presented were prepared in the LCM laboratory, and kindly made available for testing in the ozonation reaction, by Dr. Juliana P. S. Sousa. The detailed preparation methods are described in the literature [3]. In brief, a gel was prepared using resorcinol and formaldehyde, together with a nitrogen precursor either urea or melamine. Before gelation, the pH of the solution was adjusted to the desired value (5.3, 6.0, or 6.9). Afterwards, the gels were carbonized at different temperatures under nitrogen flow (500, 700 or 900 °C). The

materials prepared with urea were named CXU, and those prepared with melamine were named CXM, followed by the pH of the solution prior to gelation, and the carbonization temperature.

The carbon xerogel samples selected for the present work were CXM_6.9_700, CXM_6.9_900, and CXU_6.9_700, since they have relatively similar textural properties and different types and amounts of nitrogen surface groups. In addition, a carbon xerogel sample without nitrogen was prepared from resorcinol and formaldehyde at pH=6.9, and carbonized at 500 ºC (CX_6.9_500).

Analyses of the carbon xerogels samples used in this work, which were selected among a variety of samples due to their similar textural properties, while maintaining a wide range of nitrogen content, were obtained in the related literature [3]. The textural and chemical properties of the carbon surface are presented in Table 1.3.

Table 1.3 – Chemical characterization of the undoped and N-doped carbon xerogels.

Sample	S_{BET} ($m^2\ g^{-1}$)	V_{micro} ($cm^3\ g^{-1}$)	S_{meso} ($m^2\ g^{-1}$)	N_{EA} (% wt.)	CO (µmol g^{-1})	CO_2 (µmol g^{-1})	pH_{pzc}
CXM_6.9_700	287	0.10	35	4.0	454	489	7.1
CXM_6.9_900	331	0.07	156	3.6	395	169	7.6
CXU_6.9_700	461	0.12	122	2.9	1292	579	7.4
CX_6.9_500	486	0.10	174	-	1226	444	7.0

N_{EA}: Total nitrogen content determined by elemental analysis; CO: amount of CO released during TPD; CO_2: amount of CO_2 released during TPD; pH_{PZC}: pH at the point of zero charge.

XPS analysis revealed the presence of three nitrogen functionalities on the surface of the selected nitrogen-doped carbon xerogel samples: pyridine-like N atoms (N6, BE=398.7±0.3 eV), pyrrole-like N atoms (N5, BE= 400.3±0.3 eV), and quaternary nitrogen (NQ, BE=401.4±0.5 eV). Due to the

difficulty in distinguishing clearly the N5 and NQ components [4], the total amount of nitrogen was considered.

The carbon nanofibers used in the work here presented were prepared, and made available, by the group of Prof. Enrique Garcia-Bordejé, at Instituto de Carboquímica, part of the Consejo Superior de Investigación Científica, in the context of the European Commission financed project MONACAT.

The characterization of these materials has been made available by the CSIC group. The superficial surface area was found to be ~200 $m^2 g^{-1}$, with the contribution of micropores ~ 90 $m^2 g^{-1}$. The nitrogen on the surface of the carbon was found to be on the form of pyridinic (N6) and pyrrolic (N5) groups, and as quaternary nitrogen (NQ).

1.2.2 STRUCTURED CATALYSTS

The structured catalysts used in this section were prepared and made available by different groups, in the context of the European Commission financed project MONACAT: the group of L. Kiwi-Minsker at the Ecole Polytechnique Federále de Lausanne (sintered metal fibres); the group of M. Ronning at the Norwegian University of Sciente and Technology (carbon felts); the groups of E. Garcia-Bordejé at the Instituto de Carboquímica, part of the Consejo Superior de Investigación Científica (honeycomb cordierite monoliths).

Carbon nanofibers (CNF) were grown on three different macroscopic structures: sintered metal fibers (SMF), carbon felt (CF) and honeycomb ceramic monoliths (HM). CNF growth was carried out directly on calcined SMF, while a metal catalyst was deposited previously to CNF growth on CF by direct impregnation of a $NiNO_3$ solution and, on HM, by previously washcoating an alumina sol, calcining and impregnation of the $NiNO_3$ solution. The growth was carried out by decomposition of ethane:hydrogen mixtures at temperatures in the range 873-948 K. Different post-treatments were selected to prepare CNFs with different surface chemical properties in order to study how the surface chemistry affects the performance of the

catalysts in the ozonation of organic pollutants. Nitrogen-containing groups were introduced on CNF grown on monoliths by in-situ doping by growing CNFs at 873 K with a 200 cm^3 min^{-1} gas mixture of C_2H_6 and NH_3 in a ratio (50:50).

The CNF/structured catalysts were characterized by SEM, TEM and N_2 adsorption, and the observation presented here were obtained from the related literature [5-10].

Figure 1.1 presents photographs of the three types of structured catalysts used, as received from the project partners.

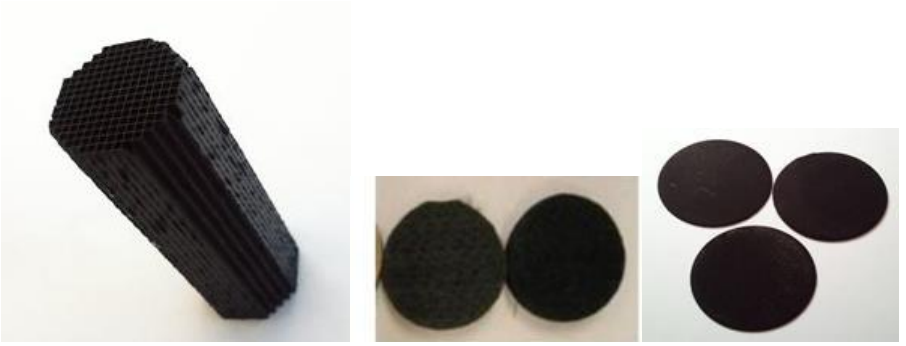

Figure 1.1 – Photographs of the different types of CNF covered structures used as catalysts in the ozonation experiments (HM, CF, SMF).

Figure 1.2 shows microscopy images of CNFs grown on sintered metal fibers, ceramic monoliths and carbon felts, respectively. The CNFs are entangled forming a uniform layer in terms of thickness and coverage. The CNFs showed neither blistering in ultrasound nor leaching in corrosion tests. Therefore, the materials are suitable for water treatment. Table 1 summarizes the characteristics of the prepared samples. The CNF layer has a surface area of around between 12 (for SMF) and 200 m^2 g^{-1} (for HM) and all the pores are in the range of mesoporosity with an average diameter of ca. 20 nm. The mesoporosity and low tortuosity of CNF aggregates favours the diffusion of pollutants to all the catalytic surface area of CNF [11]. The diffusion is more sluggish for inside micropores, as occurs in the case of commercial activated carbons.

TEM images in Figure 1.3 clearly show the presence of CNFs on the cordierite monoliths. Similar images were obtained for the other supports.

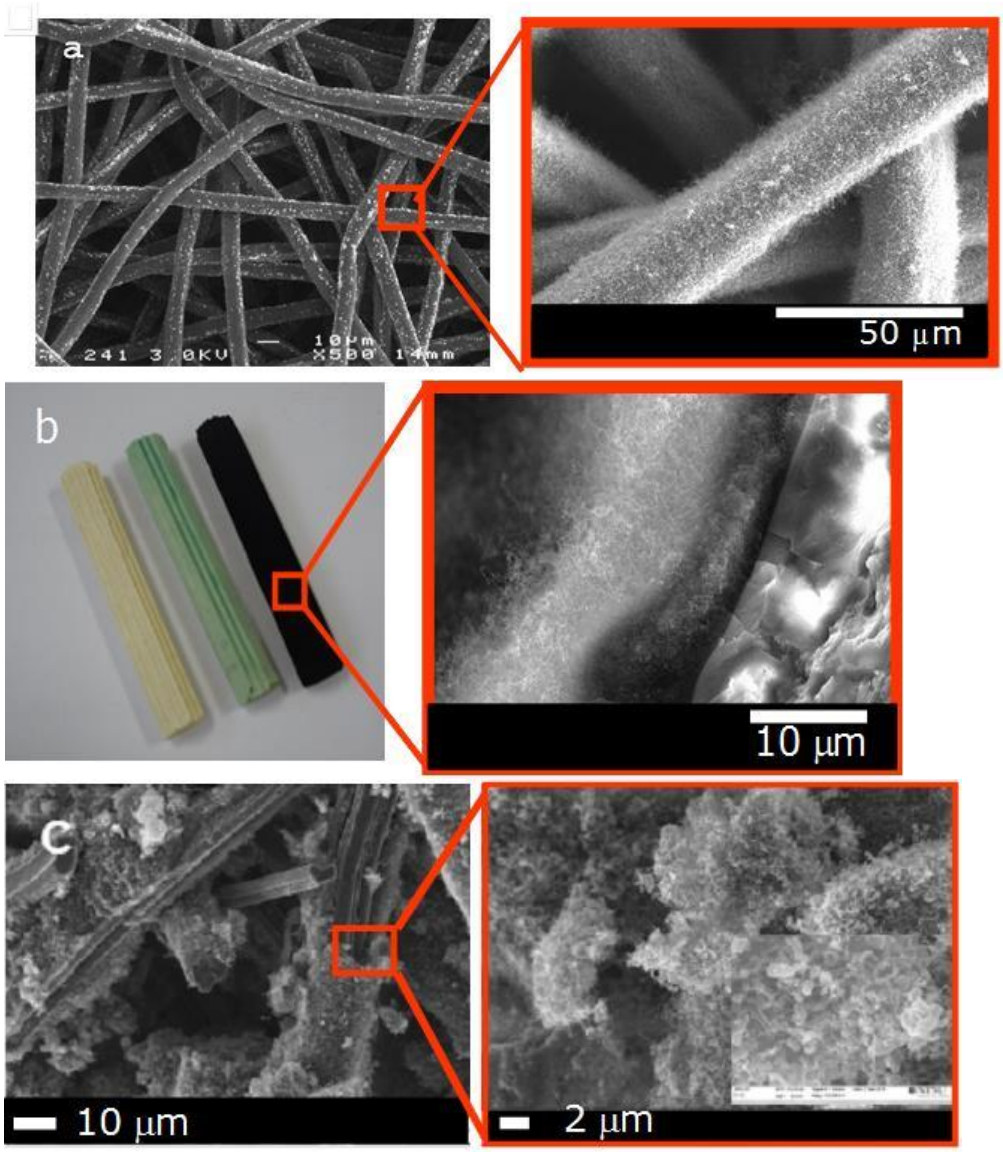

Figure 1.2 - Layer of entangled carbon nanofibers grown on three different macroscopic supports: (a) Inconel sintered metal fibers, (b) cordierite monoliths (c) carbon felt, observed by SEM.

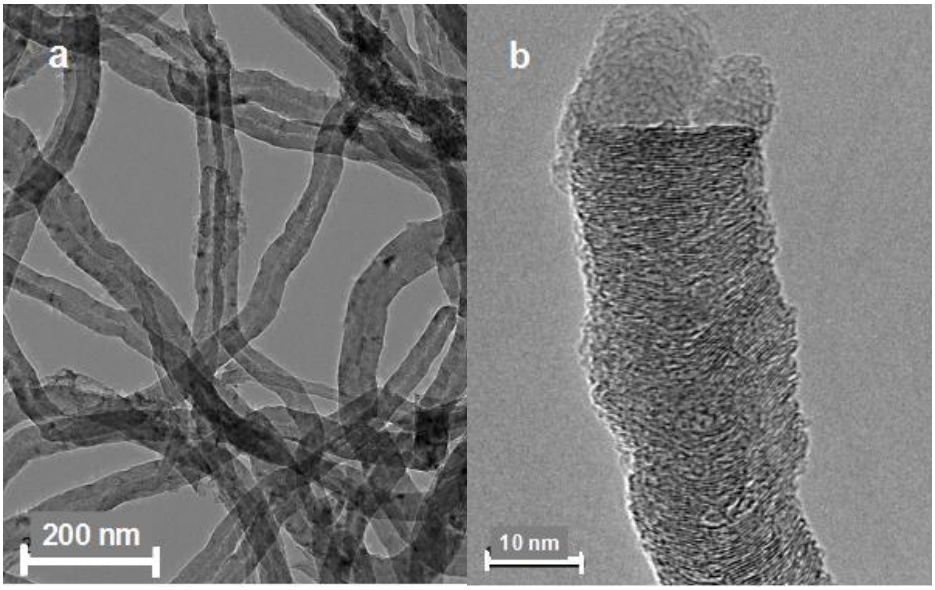

Figure 1.3 - TEM images at two different magnifications of the CNFs grown on cordierite monoliths. (a) image of a entanglement of CNFs; (b) high magnification image of a representative CNF showing the stacked graphitic planes.

Textural characterization of the CNF layers on the different structured supports is presented in Table 1.4. CNF loading was calculated by weight difference and by thermogravimetric analysis.

In the case of the N-CNF covered monoliths, XPS analyses of the N1s peak are found in the literature [8]. In these analyses, four different nitrogen surface functionalities were detected: pyrrol (N5), pyridine (N6), quaternary nitrogen (NQ) and nitrogen oxide (N-Ox). A N/C ratio of 12.8% was measured by elemental analysis.

Table 1.4 - Characteristics of the received structured catalysts.

Name[1]	% CNF	BET[1] (m^2 g^{-1})
HM_Cordierite[2]	-	~1
HM_Alumina[2]	-	~20
HM_CNF_400cpsi_10mm	5 – 23	~200
HM_CNF_400cpsi_22mm	10 – 15	~200
HM_CNF_64cpsi_22mm	11.4	~200
HM_N-CNF_64 cpsi_22mm	7.9	~200
SMFinconel3.5_CNF	3.5	- 16
SMFssNi3_CNF	3.0	- 12
NTNU_CF	-	- 1
NTNU_CF_CNF	40-100	~100

[1]BET surface area obtained considering just the CNF contribution

[2]Bare cordierite sample and alumina washcoated sample.

1.3 CHEMICALS

The synthetic water samples doped with atrazine were prepared using atrazine Pestanal analytical standard (Sigma-Aldrich) and ultrapure water (MilliQ). Atrazine degradation intermediates were purchased from Sigma-Aldrich as Pestanal analytical standards. Metolachlor and 2-ethyl-6-methylaniline were acquired from Sigma-Aldrich (PESTANAL Analytical Standard). Solutions were subject to a brief period in an ultrasound bath to achieve better dissolution. tert-Butanol (t-BuOH) was purchased from Sigma-Aldrich (>99.5%). Oxalic (≥99%), oxamic (≥99%) and pyruvic acids (≥98%) were also acquired from Sigma-Aldrich.

1.4 CHARACTERIZATION TECHNIQUES

The characterization of the original materials prepared outside of the LCM laboratory was carried out by the project partners. The detailed description of the techniques may be found in the appropriate literature [5-10, 12-16]. The characterization of the original materials prepared in the LCM laboratory were characterized by the person responsible for the preparation, and the techniques may be found in the appropriate literature [1-3, 17].

The characterization of the post-reaction or commercial acquired materials was carried out in the context of the work here presented, and the materials and methods used are here described.

Temperature programmed desorption (TPD) experiments were carried out using an Altamira AMI-300 apparatus. Approximately 100 mg sample was placed inside a U-shaped quartz cell through which 25 cm^3 (STP) min^{-1} of helium were constantly flushed. Temperature was increased at 5 K min^{-1} up to 1350 K. The released CO and CO_2 were measured in the exhaust using a Dymaxion Dycor mass spectrometer. Calibration of CO and CO_2 was made at 623 K by injecting 58 µL of each gas in order to obtain ten peaks of known concentration in the mass spectrometer.

XPS analyses of the carbon materials were performed using a Kratos AXIS Ultra HSA, with VISION software for data acquisition and CASAXPS software for data analysis. The analysis was carried out with a monochromatic Al Kα X-ray source (1486.7 eV), operating at 15 kV (90 W), in FAT mode (Fixed Analyser Transmission), with a pass energy of 40 eV for regions ROI and 80 eV for survey. Data acquisition was performed with a pressure lower than $1x10^{-6}$ Pa. The modelling of the spectra was performed using the XPSPEAK41 program, in which an adjustment of the peaks was performed using peak fitting with Gaussian-Lorentzian peak shape and Shirley type background subtraction.

Isotherms of N^2 adsorption at -196 ºC on the carbon materials for calculation of the specific surface area were made using a Quantachrome

NOVA 4200e apparatus. Specific surface areas were calculated using the BET method, taking into account the nitrogen adsorption for pressures below $p/p_0 = 0.30$.

Contact angles with water were measured after 0.25, 0.5, 3, 28 and 100 h of contact with water and ozone, and compared with the original material. A Dataphysics OCA 20 apparatus was used. The pieces were dried in an oven at 110 ^{o}C for 16 h after contact with water and after measurement of the contact angles.

Thermogravimetric (TG) analysis was performed using a STA 490 PC/4/H Luxx Netzsch thermal analyzer, by heating the sample in air flow from 50 ^{o}C to 900 ^{o}C at 5 K min^{-1}.

1.5 ANALYTICAL METHODS

Concentration of atrazine and its degradation intermediates was followed using a Hitachi Elite LaChrom HPLC equipped with a UV DAD. Separation was achieved using a Lichrocart C18-RP Purospher Star (250 mm × 4.6 mm, 5 µm) column and a H2O:methanol mobile phase. The mobile phase flow was 1 mL min^{-1} and the composition was gradually changed from 50:50 to 30:70 v/v in 21 min. ATZ concentration was calibrated and measured at 222 nm and ATZ intermediates at 215 nm.

The concentration of metolachlor and degradation products was followed by HPLC, using a Hitachi Elite LaChrom apparatus equipped with a diode array detector. The separation of MTLC was achieved using a Lichrocart C18-RP Puroshper Star (250 mm × 4.6 mm, 5 µm) column and an isocratic 60%ACN-40%H2O mobile phase at 1 mL/min. Quantification of metolachlor was made at 198 nm.

Concentration of nonylphenol was followed by HPLC, using a Hitachi Elite LaChrom apparatus equipped with a diode array detector. The separation of nonylphenol was achieved using a Lichrocart C18-RP Puroshper Star (250 mm × 4.6 mm, 5 µm) column and a gradient mobile phase consisting of 70% acetonitrile in milliQ ultrapure water to 90% acetonitrile in 14 minutes

and to 100% acetonitrile in 20 minutes, at flow rate 1 mL min^{-1}. Detection of nonylphenol was made at 196 nm.

Likewise, the formation and concentration of organic acids, including in the experiments using oxalic acid, typical end-of-chain degradation products, was followed using a Hitachi Elite LaChrom HPLC equipped with an UV-Vis detector. Separation of the organic acids was achieved using an Alltech OA-1000 chromatography column using an isocratic 5mM H_2SO_4 mobile phase at 0.5 mL min^{-1}. Quantification of the organic acids was made at 200 nm.

The release of ionic compounds into the solution was followed using a liquid chromatography system equipped with a conductivity detector to measure both anions and cations. The separation was achieved witha Dionex ICS-2100 Ion Chromatography System using a Dionex IonPac AS11-HC column (250 mm × 4 mm), under an isocratic elution with a solution of NaOH 30 mM at a flow rate of 1.5 mL min^{-1}, and a Dionex DX-120 Ion Cromatography System using an IonPac CS12A column (250 mm × 4 mm) working with a solution of methanesulfonic acid 20 mM as the mobile phase at a flow rate of 1.0 mL/min, for anions and cations respectively. The system was equipped with a conductivity detector, which performance was improved by electrolyte suppression using ASRS 300 or CSRS ULTRA II self-regeneration suppressors for anions and cations, respectively.

Acute toxicity analyses were performed using an Azure Environment Microtox apparatus and procedure ISO/DIS 11348-3. The microorganisms used were the luminescent bacteria *Vibrio Fischeri* from Hach Lange, which is used as representative of aquatic environments [18, 19]. The bacteria were exposed to samples after activation and 15 minutes incubation at 15 ^{o}C, and the decrease in activity as function of the luminescence was measured after 30 minutes. The standard index used to evaluate acute toxicity, the EC_{50}, was not calculated because, at the concentrations used in this study, a large number of the samples did not reach 50% of inhibition of the luminescent activity. Instead, the inhibition of activity measured is presented.

Total organic carbon, measured with a Shimadzu TOC-5000A apparatus, was used to assess the mineralization of MTLC.

Finally, dissolved ozone concentration was measured using the indigo method [20].

1.6 CATALYSTS EVALUATION

1.6.1 SEMI-BATCH OZONATION

Semi-batch ozonation experiments were carried out to assess the performance of the catalysts in the ozonation procedure, in powder form. Ozonation and adsorption experiments of were performed in semi-batch stirred tank reactor shown schematically in Fig. 1.4 (made available by Dr. Alexandra Gonçalves), which already existed in the LCM laboratory.

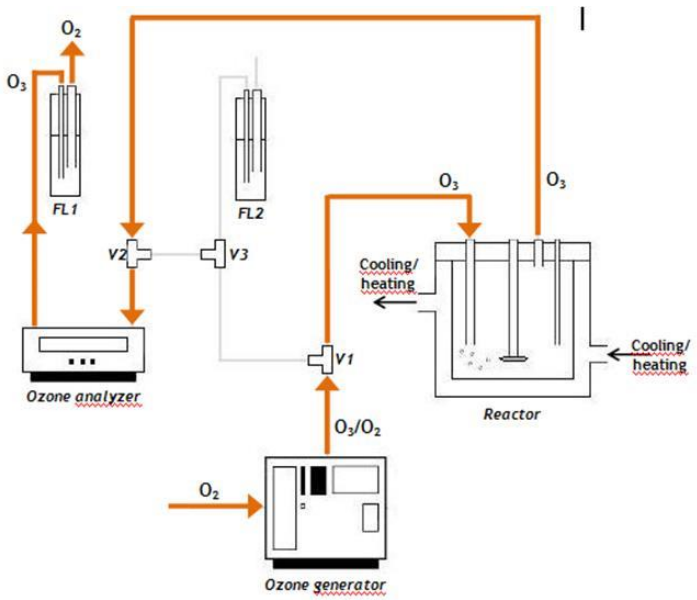

Figure 1.4 – Scheme of the experimental set-up used in semi-batch ozonation experiments.

The mass of catalyst, when applicable, was of 100 mg in a 700 mL solution of the pollutant. Initial pollutant concentration was 10 mg L^{-1} in the case of atrazine, 20 mg L^{-1} in the case of metolachlor and 6 mg L^{-1} in the case of

nonylphenol, under reaction conditions. Ozone was produced from pure oxygen at 50 $g(O_3)$ m^{-3}(STP) using a BMT 802X ozone generator and continuously fed to the reactor through a glass diffusor at 150 cm^3(STP) min^{-1}. The solution was constantly stirred using a magnetic stirrer at 200 rpm. Ozone in the gas phase was analysed using a BMT 964 gas phase analyser. For adsorption experiments the ozone generator was turned off and pure oxygen was fed into the reactor to maintain identical hydraulic conditions. Temperature in the reactor was controlled using a Julabo thermostatic bath. Experiments using a radical scavenger were performed using a tenfold concentration of *t*-BuOH in relation to that of the pollutant.

1.6.2 CONTINUOUS OZONATION

A new system was set up during the development of the work here presented, in order to test the structured catalysts in the continuous ozonation process, as represented in Figure 1.5.

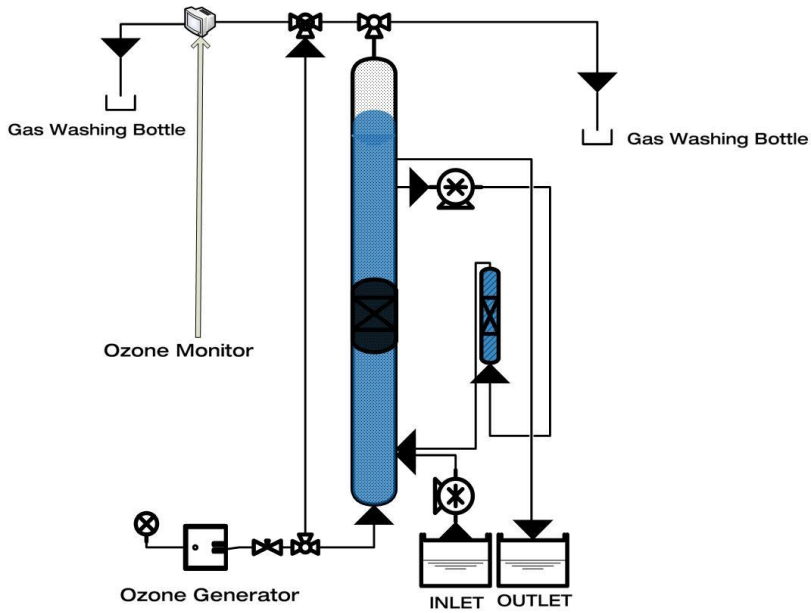

Figure 1.5 – Scheme of the experimental set-up newly designed and set up in the LCM laboratory for assessment of the performance of structured catalysts in the continuous ozonation process.

The system was designed to allow the use of the structured catalysts in a three-phase (gas-liquid-solid in contact inside a bubble column) or a two-phase configuration (gas-liquid in contact in a bubble column; liquid-solid in contact in the internal loop). To this end, the system consists on a bubble column type reactor, to which an internal loop was coupled. Inside the loop, a smaller column allows the placement of the catalyst, when needed. Thus, besides allowing the testing of the catalyst in the two configurations mentioned above, it is also possible to carry out reactions in semi-batch mode (closed loop), and also to change the liquid flow rate going through the bubble column and the catalyst (by changing the loop flow rate) without altering the residence time of the system.

Standard experiments were carried out as follows: ozone was fed through a diffuser in the bottom of the column, and the solution was introduced near the bottom using a peristaltic pump. The monolith was placed inside the column and both gas and liquid phases go through the channels, co-currently in upflow. Biphasic experiments were carried out by placing the monolithic catalyst inside the reactor's internal loop. Liquid phase was pumped at 12 cm^3 min^{-1} and the gas phase at 15 cm^3 min^{-1}. Ozone was generated from pure oxygen at 50 g O_3 m^{-3} using a BMT 802N ozone generator. The internal recirculation loop was kept at 60 cm^3 min^{-1} using a peristaltic pump. These conditions were selected in order to obtain the best homogeneous distribution through the channels of the monolith. For large bubble sizes (2-3 mm diameter) it was found that the bubbles coalesced beneath the monolith, eventually breaking through the channel that offered a smaller pressure drop. However, for bubble sizes with diameters inferior to the channel diameter, a bubbly flow develops inside the channels of the monolith, putting away any advantage in using a three-phase system [21]. Thus, a bubble size with approximately the diameter of the monolith channels was chosen as a compromise between the two situations. The mean superficial liquid velocity (~0.30 cm s^{-1}) and the bubble rise velocity (~10 cm s^{-1} [22]) used should place the hydrodynamic regime as Taylor flow

[21, 23, 24]. The bubble column has a diameter of 22 mm and the liquid column has a height of 60 cm, leaving free head room inside the column.

In section *Operation conditions,* the experiments where the influence of the flow rates on the conversion of dissolved ozone and in the removal of oxalic acid was assessed, were carried out using a slightly different configuration. To allow for a larger range of liquid flow rates, and to avoid the interference of the internal loop in the concentration of dissolved ozone, experiments were performed using the system as a classic bubble column type reactor; i.e. the internal loop was not used in those cases. However, when the influence of the flow rates was assessed in the ozonation of emerging organic micropollutants, the standard reaction conditions were again applied.

REFERENCES

[1] R.P. Rocha, A.M.T. Silva, S.M.M. Romero, M.F.R. Pereira, J.L. Figueiredo, Applied Catalysis B: Environmental, 147 (2014) 314-321.
[2] R.P. Rocha, J.P.S. Sousa, A.M.T. Silva, M.F.R. Pereira, J.L. Figueiredo, Applied Catalysis B: Environmental, 104 (2011) 330-336.
[3] J.P.S. Sousa, M.F.R. Pereira, J.L. Figueiredo, Applied Catalysis B: Environmental, 125 (2012) 398-408.
[4] A.B. Ayusheev, O.P. Taran, I.A. Seryak, O.Y. Podyacheva, C. Descorme, M. Besson, L.S. Kibis, A.I. Boronin, A.I. Romanenko, Z.R. Ismagilov, V. Parmon, Applied Catalysis B: Environmental, 146 (2014) 177-185.
[5] E. Garcia-Bordeje, I. Kvande, D. Chen, M. Ronning, Advanced Materials, 18 (2006) 1589.
[6] E. García-Bordejé, I. Kvande, D. Chen, M. Rønning, Carbon, 45 (2007) 1828-1838.
[7] J. Restivo, J.J.M. Órfão, M.F.R. Pereira, E. Vanhaecke, M. Rönning, T. Iouranova, L. Kiwi-Minsker, S. Armenise, E. Garcia-Bordejé, Water Science and Technology, 65 (2012) 1854.
[8] L. Roldán, S. Armenise, Y. Marco, E. García-Bordejé, Physical Chemistry Chemical Physics, 14 (2012) 3568-3575.
[9] P. Li, T. Li, J.-H. Zhou, Z.-J. Sui, Y.-C. Dai, W.-K. Yuan, D. Chen, Microporous and Mesoporous Materials, 95 (2006) 1-7.
[10] T. Yuranova, C. Franch, A.E. Palomares, E. Garcia-Bordejé, L. Kiwi-Minsker, Applied Catalysis B: Environmental, 123–124 (2012) 221-228.
[11] J.K. Chinthaginjala, Seshan, K., Lefferts, L., Industrial & engineering chemistry research, 46 (2007) 3968.
[12] S. Armenise, M. Nebra, E. García-Bordejé, A. Monzón, Functionalization of carbon nanofibers coated on cordierite monoliths by oxidative treatment, in: M.D.S.H.P.A.J.J.A.M. E.M. Gaigneaux, P. Ruiz (Eds.) Studies in Surface Science and Catalysis, Elsevier2010, pp. 483-486.
[13] P.A.R. Cebollada, E. Garcia-Bordejé, Chemical Engineering Journal, 149 (2009) 447-454.
[14] L. Martínez-Latorre, S. Armenise, E. Garcia-Bordejé, Carbon, 48 (2010) 2047-2056.
[15] L. Martínez-Latorre, P. Ruiz-Cebollada, A. Monzón, E. García-Bordejé, Catalysis Today, 147, Supplement (2009) S87-S93.
[16] P. Tribolet, L. Kiwi-Minsker, Catalysis Today, 105 (2005) 337.
[17] R.P. Rocha, J. Restivo, J.P.S. Sousa, J.J.M. Órfão, M.F.R. Pereira, J.L. Figueiredo, in press, Catalysis today, in press(2014).
[18] V.A. Sakkas, I.M. Arabatzis, I.K. Konstantinou, A.D. Dimou, T.A. Albanis, P. Falaras, Applied Catalysis B, 49 (2004) 195-205.
[19] Y.-J. Lin, M. Karuppiah, A. Shaw, G. Gupta, Ecotoxicology and Environmental Safety, 43 (1999) 35-37.
[20] H. Bader, J. Hoigné, Water Research, 15 (1981) 449-456.
[21] H. Liu, C.O. Vandu, R. Krishna, Industrial & engineering chemistry research, 44 (2004) 4884-4897.

[22] M.A.R. Talaia, World Academy of Science, Engineering and Technology, 28 (2007).
[23] R. Gupta, D.F. Fletcher, B.S. Haynes, Chemical Engineering Science, 64 (2009) 2941-2950.
[24] K.A. Triplett, S.M. Ghiaasiaan, S.I. Abdel-Khalik, D.L. Sadowski, International Journal of Multiphase Flow, 25 (1999) 377-394.

2. COMPARISON OF DIFFERENT STRUCTURES

2.1 DESCRIPTION

In this chapter, different structured catalysts were tested in the ozonation reaction. The different catalysts were firstly ground to controlled particle size and tested in the semi-batch ozonation of oxalic acid in a completely stirred tank reactor. Afterwards, these catalysts, in their integral form, were tested in a newly designed experimental set-up, which consists of a bubble column reactor using an internal loop. In this setup, both semi-batch and continuous ozonation experiments were performed.

It was found that the performance of the structured catalysts is comparable to that of activated carbon or multiwalled carbon nanotubes, which are two of the most studied carbon-based catalysts for the ozonation reaction. It was observed that different structures, and different CNF layers, achieve considerably varied performances in this reaction.

The use of the structured catalysts in a three-phase setup, in order to achieve hydrodynamic regimes that can enhance the mass transfer between the phases, was found to be much more easily applied when using a honeycomb-like monolithic structure. The use of carbon felts and sintered metal fibres, due to high pressure drop, resulted in bypass of the gas phase through the sides of the catalyst. Thus, the honeycomb structures were selected as supports for further testing in the ozonation reaction.

The structured catalysts used in this section were prepared and made available by different groups, in the context of the European Commission financed project MONACAT: the group of L. Kiwi-Minsker at the Ecole Polytechnique Federále de Lausanne; the group of M. Ronning at the Norwegian University of Sciente and Technology; the groups of E. Garcia-Bordejé at the Instituto de Carboquímica, part of the Consejo Superior de Investigación Científica.

Part of the work described in this section has been published in the following reference:

J. Restivo, J.J.M. Órfão, M.F.R. Pereira, E. Vanhaecke, M. Rönning, T. Iouranova, L. Kiwi-Minsker, S. Armenise, E. Garcia-Bordejé, Water Sci. Technol., 65 (2012) 1854.

2.2 SEMI-BATCH OZONATION OF OXALIC ACID

The evaluation of the catalytic activity of the carbon nanofibers (CNF) covered structured catalysts were made, on a first approach, through the ozonation of oxalic acid in semi-batch operation using the catalyst in powder form. These experiments were conducted using a slurry reactor. For this end, the structured catalysts were ground to controlled particle size 0.1-0.3 mm when possible, or finely grounded in the case of the carbon felts and activated carbon fibres. The loadings of the different structured catalysts were calculated in order to obtain 100 mg of the carbon catalyst in solution. When the bare supports, prior to CNF growth, were used in the ozonation experiments, the selected amount was equivalent to what was used in the corresponding experiments with the CNF-covered structured catalysts. Oxalic acid was selected as a model compound due to its known refractory behaviour to oxidation by dissolved molecular ozonation, and the natural pH of a 1 mM solution (3.0) does not promote the homogeneous decomposition of ozone; besides, it is well known that several catalysts enhance its ozonation in the liquid phase [1-9]. Experiments were performed in semi-batch since the activity of several carbon materials in this system is well-known in the ozonation of oxalic acid [7, 10-20]. Thus, the comparison between the structured catalysts and catalysts in powder form was possible.

The dimensionless oxalic acid concentration during semi-batch experiments using particulated activated carbon fibres (ACF) samples is presented in Figure 2.1.

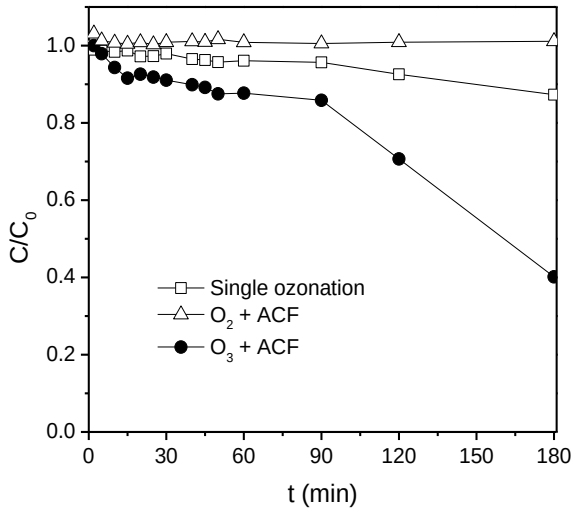

Figure 2.1 – Dimensionless oxalic acid concentration during semi-batch ozonation experiments using sample ACF in a slurry reactor.

While non-catalytic ozonation removed approximately 10% of oxalic acid from solution after 180 min, the presence of the catalyst largely improved the degradation achieved. In fact, after 180 min, more than 60% of oxalic acid was removed from solution. It should be noticed that adsorption had a negligible contribution to the removal of oxalic acid.

Similar experiments were carried out using grounded CF samples. Since the support structure of the CF catalysts is constituted in itself of carbon, the activity of the support prior to the growth of the CNF layer was assessed. The dimensionless oxalic acid concentration during ozonation experiments using CF samples is presented in Figure 2.2.

It is clear that, as was observed with sample ACF, the adsorption of oxalic acid is not contributing to the removal of oxalic acid during the catalytic experiments. It is observable that the CF support has some catalytic activity in the ozonation reaction. However, this contribution may be considered negligible when compared with the remarkable activity of the CNF covered catalyst, which removed approximately 95% of oxalic acid, while the CF support only achieved removals of less than 20%.

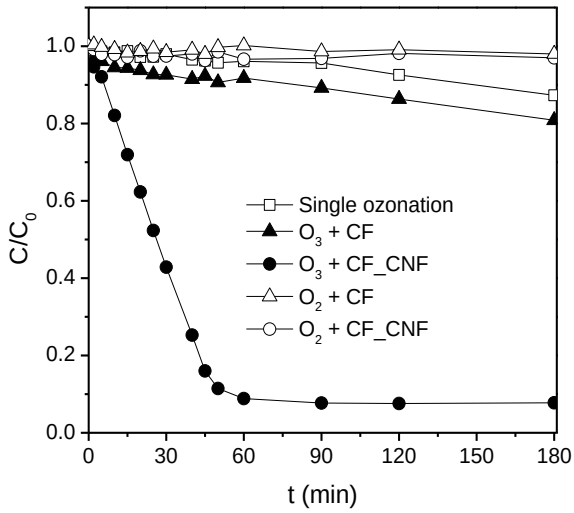

Figure 2.2 – Dimensionless oxalic acid concentration during semi-batch ozonation experiments using samples CF in a slurry reactor.

The honeycomb-like monolithic supports were also tested in the ozonation of oxalic acid in the slurry semi-batch reactor. In this case, possible activity of the support could arise due to the contribution of the alumina and/or nickel layers, which are laid upon the catalyst in the CNF growth process. In the experiment in slurry reactor, the activity of the support with the alumina washcoat was evaluated. The dimensionless oxalic acid concentration during ozonation experiments using HM samples is presented in Figure 2.3.

In the case of the HM structured catalysts, it is clear that the alumina washcoat presented significant catalytic activity in the ozonation process. It is known that such metallic oxides are potential catalysts for this reaction [21-24]. However, the catalytic activity of the HM catalyst post CNF growth is noticeable higher than that of the support. It should be taken into consideration that, for both the HM and CF structured catalysts, the growth of the CNF layer upon the support might reduce accessibility of the reactants to the surface of the support. Thus, even though they might show activity when used independently, this may not represent an actual

contribution to the oxalic acid removal achieved when the CNF-covered catalysts were used.

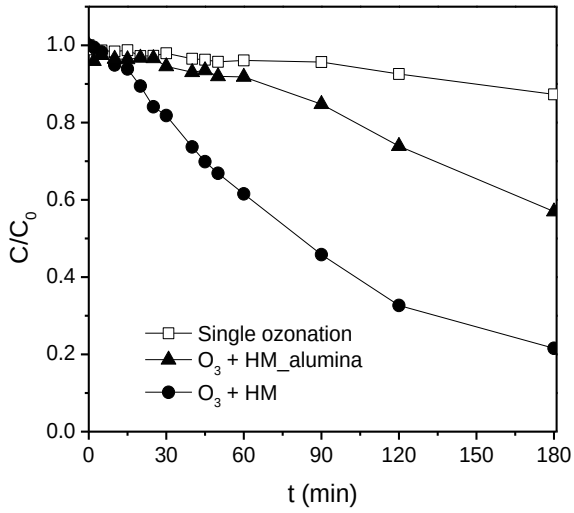

Figure 2.3 – Dimensionless oxalic acid concentration during semi-batch ozonation experiments using samples CF in a slurry reactor.

Due to difficulties in grounding the samples SMF, these were not tested in the slurry semi-batch reactor, and their activity will be discussed later.

The dissolved ozone concentration was also followed in the experiments performed in the slurry semi-batch reactor. The measured concentrations during catalytic and non-catalytic experiments are presented in Figure 2.4.

The presence of a catalyst in the reaction system clearly leads to a lower dissolved ozone concentration, which can be attributed to the conversion of ozone into other species, which are responsible for the increase in the removal of oxalic acid [7, 15]. In fact, the activity of the tested catalysts roughly follows their ability to convert dissolved ozone. When the three different structured catalysts are compared, differences in their activity are clear. The activity decreases in the order CF>HM>ACF. The lower activity of sample ACF is attributed to its microporosity, since this sample results from the carbonization of textile fibres, and not from the growth of carbon nanomaterials on a structured support. Regarding samples CF and HM, it would be expected that the catalyst with larger superficial area would

perform better in this reaction. However, sample HM, with S_{BET} of ~200 m^2 g^{-1}, showed worse performance than sample CF, with with S_{BET} of ~100 m^2 g^{-1}. Thus, the better performance of CF can only be attributed to differences between the CNF layers. Such differences may be related to the structure type of the CNF, density and thickness of the layer, or their distribution across the support [25].

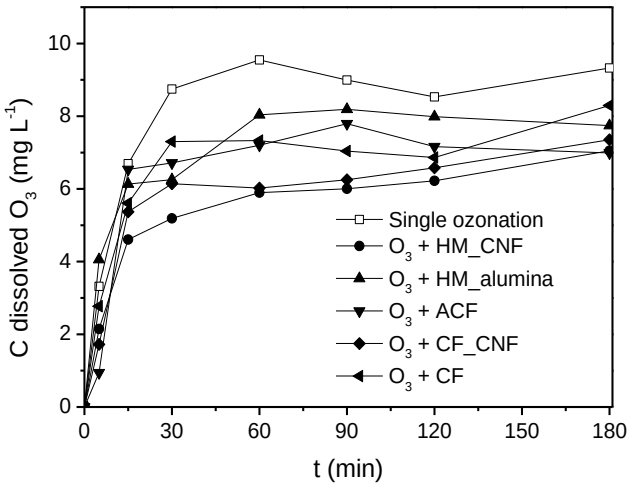

Figure 2.4 – Dissolved ozone concentration during ozonation experiments carried out in a slurry semi-batch reactor.

The performances of the grounded structured catalysts are somewhat comparable to those obtained with other carbon materials in similar systems. The ozonation of oxalic acid using pristine activated carbon (AC) achieved removals close to 90% in 180 min [7], while multiwalled carbon nanotubes (MWCNT) was able to achieve complete removal in approximately 60 min [15].

On a second phase, the catalysts were used in their integral structured form as catalysts for the ozonation of oxalic acid. For this end, a newly prepared experimental set-up was used, which consisted on a bubble column with an internal recirculation loop (detailed in *Methods and materials* section). The performance of the structured catalysts in the catalytic ozonation of oxalic acid, using a two-phase closed loop system (semi-batch) is presented in Figure 2.5. For comparison purposes,

activated carbon and multiwalled carbon nanotubes were also used in this system, as a packed bed.

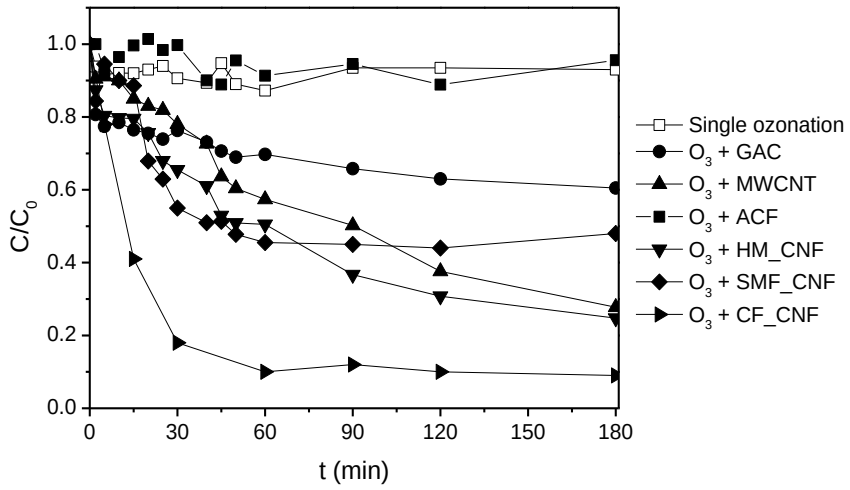

Figure 2.5 – Dimensionless oxalic acid concentration during semi-batch ozonation experiments using integral structured catalysts in bubble column reactor in two-phase configuration.

The presence of carbon-based catalysts in the system clearly improved the removal of oxalic acid when compared with the single ozonation process. All the catalysts constituted by carbon nanomaterials performed better than the conventional activated carbon counterpart, which can be attributed to the higher mesoporosity and higher amount of delocalized π-electrons on the surface of the former [15]. The best performing catalyst, similarly to what was observed with the grounded catalysts, was the CF_CNF sample. The SMF_CNF, in the first 45 min, was the second most efficient. However, after 60 min, the concentration of oxalic acid reached a plateau, which suggests there is some deactivation of the catalyst. The HM_CNF catalyst showed slightly worse performance than CNF_CF in the first 45 min, but considerably surpassed it in the latter stages of reaction. The MWCNT packed bed showed the worst performance among the carbon nanomaterials in the first 90 minutes of reaction. However, it surpassed catalyst SMF_CF in the latter stages of reaction. The ACF sample practically did not show any activity in this case, achieving similar

results to those in the single ozonation experiment. Nevertheless, when comparing the different structured reactors, and even the granulated materials in packed bed, it is important to consider that there are important differences between them, such as mass of carbon nanofibers, the porosity, the hydraulic regimes and the height of the catalyst bed. In an effort to compare the performance of the various catalysts in the ozonation of oxalic acid, the initial zero-order kinetic constants were calculated. The obtained constants per gram of catalyst are presented in Figure 2.6.

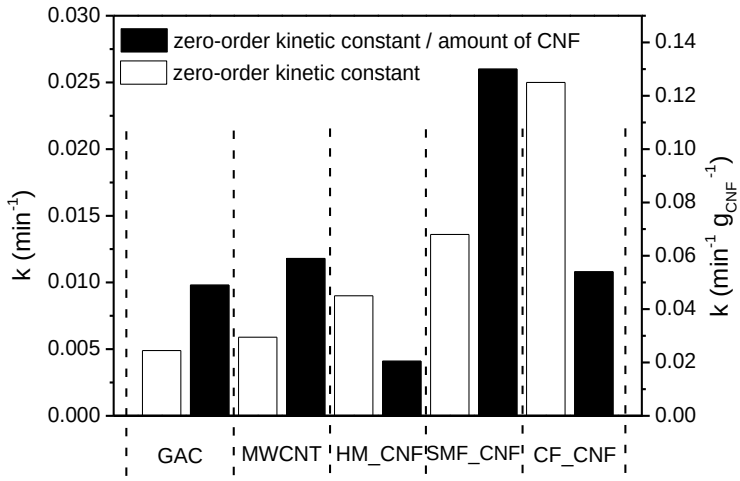

Figure 2.6 – Zero-order kinetic rate constants (calculated for 30 min of reaction) for the removal of oxalic acid during experiments using the integral structured catalysts in the bubble column reactor as a semi-batch system in two-phase configuration.

It is interesting to observe that, when considering the performance obtained taking into account the mass of CNF, the HM_CNF catalyst is less efficient than the activated carbon and multiwalled carbon nanotubes in a packed bed. The most efficient catalyst, considering the amount of CNF, is, clearly, the SMF_CNF catalyst. Nevertheless, Figure 2.5 showed that this catalyst was not active during the whole reaction time (180 min).

2.3 CONTINUOUS OZONATION OF OXALIC ACID

Finally, continuous catalytic ozonation experiments were performed in order to compare the activity of the structured catalysts with that of the granulated carbon materials, activated carbon and multiwalled carbon nanotubes, in a packed bed. The bubble column reactor with a, internal loop was used to these experiments, in a two-phase configuration (detailed in *Methods and materials*).

The removal of oxalic acid as measured when steady-state was reached is presented in Figure 2.7.

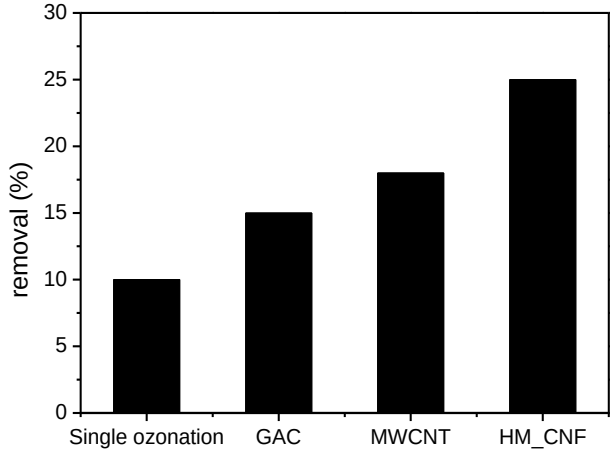

Figure 2.7 – Removal of oxalic acid measured at steady-state during continuous ozonation experiments using grounded catalysts as packed bed and an integral structured catalyst.

A similar behaviour of the catalysts is observed in continuous catalytic ozonation experiments as what was observed when the same materials were tested in a semi-batch system.

Nevertheless, an important feature of the utilization of structured catalysts in this reaction is the expected improvement in performance when the system is used in a three-phase configuration (as explored in detail in section *Operation conditions*) [26-29]. The HM, SMF and CF structures

were tested in a three-phase configuration. However, the SMF and CF supports were observed to not be suitable for this type of applications. A large concentration of gas was observed in the inferior part of the catalysts. When a sufficient large enough amount of gas became accumulated, it was released through the sides to the catalyst, completely bypassing the interior of the catalyst. The pressure drop was shown to be too high to efficiently operate these catalysts in our bubble column system. Thus, the HM structure was selected for further testing in the catalytic ozonation reactions.

2.4 PARTIAL CONCLUSIONS

Several different structured catalysts were tested as catalysts for the ozonation of organic pollutants, and compared with other conventional carbon-based catalysts used in powder form.

On a first approach, the structured catalysts were ground to controlled particle size, when possible, and used in ozonation reactions carried out in a semi-batch stirred tank reactor. Afterwards, the structured catalysts were used in experiments carried out in a bubble column reactor with a closed internal loop, in their integral form, in semi-batch operation and two-phase configuration. Finally, the structured catalysts were used in the continuous catalytic ozonation reaction in their integral form, using the same bubble column reactor with an internal loop, in two-phase configuration. It was found that the structured catalysts showed activity comparable to that of activated carbon and multiwalled carbon nanotubes, even outperforming these in some situations.

The structured catalysts were then used in a three-phase system, to take advantage of the possibility of development of hydrodynamic regimes that enhance the mass transfer between the gas, liquid and solid phases. It was found that structures of type CF and SMF did not perform well in this configuration, due to high pressure drop and consequent coalescence of the gas on the bottom of the catalysts, which eventually lead to bypass of the gas-phase through the sides of the catalyst.

REFERENCES

[1] H. Cao, L. Xing, G. Wu, Y. Xie, S. Shi, Y. Zhang, D. Minakata, J.C. Crittenden, Applied Catalysis B: Environmental, 146 (2014) 169-176.
[2] Z.-Q. Liu, J. Ma, Y.-H. Cui, L. Zhao, B.-P. Zhang, Separation and Purification Technology, 78 (2011) 147-153.
[3] Z.-Q. Liu, J. Ma, Y.-H. Cui, L. Zhao, B.-P. Zhang, Applied Catalysis B: Environmental, 101 (2010) 74-80.
[4] Z.-Q. Liu, J. Ma, Y.-H. Cui, B.-P. Zhang, Applied Catalysis B: Environmental, 92 (2009) 301-306.
[5] C.A. Orge, J.P.S. Sousa, F. Gonçalves, C. Freire, J.J.M. Órfão, M.F.R. Pereira, Catalysis Letters, 132 (2009) 1-9.
[6] Z.Q. Liu, Carbon, 46 (2008) 890.
[7] P.C.C. Faria, J.J.M. Órfão, P. M.F.R., Applied Catalysis B, Environmental, 79 (2008) 237.
[8] F.J. Beltrán, F.J. Rivas, R. Montero-de-Espinosa, Water Research, 39 (2005) 3553-3564.
[9] R. Andreozzi, Applied catalysis. A, General, 138 (1996) 75.
[10] X. Fan, J. Restivo, J.J.M. Órfão, M.F.R. Pereira, A.A. Lapkin, Chemical Engineering Journal, 241 (2014) 66-76.
[11] A. Gonçalves, J.J.M. Órfão, M.F.R. Pereira, Applied Catalysis B: Environmental, 140–141 (2013) 82-91.
[12] A.G. Gonçalves, J.J.M. Órfão, M.F.R. Pereira, Catalysis Communications, 35 (2013) 82-87.
[13] J. Restivo, J.J.M. Órfão, S. Armenise, E. Garcia-Bordejé, M.F.R. Pereira, Journal of Hazardous Materials, 239–240 (2012) 249-256.
[14] A.G. Gonçalves, J.J.M. Órfão, M.F.R. Pereira, Journal of Hazardous Materials, 239–240 (2012) 167-174.
[15] A.G. Gonçalves, J.L. Figueiredo, J.J.M. Órfão, M.F.R. Pereira, Carbon, 48 (2010) 4369-4381.
[16] C.A. Orge, Catalysis Letters, 132 (2009) 1.
[17] P.C.C. Faria, M.F.R. Pereira, J.J.d.M. Orfão, E. Universidade do Porto. Faculdade de, Catalytic ozonation of effluents from the textile industry, [s. n.], 2008.
[18] P.C.C. Faria, J.J.M. Órfão, M.F.R. Pereira, Applied Catalysis B: Environmental, 83 (2008) 150-159.
[19] O.S.G.P. Soares, P.C.C. Faria, J.J.M. Orfao, M.F.R. Pereira, Separation Science & Technology, 42 (2007) 1477-1492.
[20] P.C.C. Faria, J.J.M. Órfão, M.F.R. Pereira, Chemosphere, 67 (2007) 809-815.
[21] C.A. Guzman-Perez, J. Soltan, J. Robertson, Journal of Environmental Science and Health. Part B: Pesticides, Food Contaminants, and Agricultural Wastes, 47 (2012) 544-552.
[22] A. Ikhlaq, D.R. Brown, B. Kasprzyk-Hordern, Applied Catalysis B: Environmental, 123–124 (2012) 94-106.
[23] X. Wang, J. Guan, R.M. Stuetz, Water Sci Technol, 66 (2012) 1781-1786.

[24] Z.L. Chen, F. Qi, B.B. Xu, J.M. Shen, Y. Ben, M.M. Ye, Huan Jing Ke Xue, 28 (2007) 563-568.
[25] J. Restivo, J.J.M. Órfão, M.F.R. Pereira, E. Vanhaecke, M. Rönning, T. Iouranova, L. Kiwi-Minsker, S. Armenise, E. Garcia-Bordejé, Water Science and Technology, 65 (2012) 1854.
[26] T.A. Nijhuis, M.T. Kreutzer, A.C.J. Romijn, F. Kapteijn, J.A. Moulijn, Catalysis Today, 66 (2001) 157-165.
[27] T.A. Nijhuis, M.T. Kreutzer, A.C.J. Romijn, F. Kapteijn, J.A. Moulijn, Chemical Engineering Science, 56 (2001) 823-829.
[28] M.T. Kreutzer, Catalysis Today, 105 (2005) 421.
[29] M.T. Kreutzer, F. Kapteijn, J.A. Moulijn, J.J. Heiszwolf, Chemical Engineering Science, 60 (2005) 5895-5916.

3. OZONATION OF EMERGING ORGANIC MICROPOLLUTANTS

3.1 DESCRIPTION

In this chapter, the ozonation of three selected organic emerging micropollutants is assessed: atrazine, metolachlor and nonylphenol. These compounds were selected as models, among a wide variety of possibilities, due to the interest associated with the development of the MONACAT project, part of the 7th framework program of the European Commission, in which part of the research here presented was included.

On a first approach, semi-batch ozonation experiments were performed to study the reaction mechanism and degradation pathways of the selected pollutants, specifically the differences between the non-catalytic and the catalytic pathway. Afterwards, the same pollutants were used as model pollutants in the continuous ozonation process, to which a structured catalyst was applied, consisting in a CNF-covered honeycomb monolith.

In addition to the study of reaction mechanism taking place, the focus of this chapter was mainly on the improvement of the mineralization degree, and also in the reduction of the potential toxicity of the resulting effluent, since the degradation of these pollutants may result in more toxic effluents, which is undesirable. These types of toxic effluents may not be suitable for discharge, biological treatment, or human consumption.

It was found that the catalytic process leads, in general, to an improved mineralization degree, mostly due to the actions of radical species generated from the action of the catalyst in ozone decomposition, either on the surface of the catalyst or in the liquid bulk. However, since changes in the product distribution take place when a catalyst is used, the toxicity level may not always be improved. Nevertheless, it was found that the resulting product distribution, and thus the toxicity level, may be controlled

through modifications to the operation conditions of the catalytic ozonation process, i.e. residence and contact time.

The structured catalysts used in this section were prepared and made available by the group of E. Garcia-Bordejé at the Instituto de Carboquímica, part of the Consejo Superior de Investigación Científica, in the context of the European Commission financed project MONACAT. Part of the work described in this section has been published in the following references:

J. Restivo, J.J.M. Órfão, S. Armenise, E. Garcia-Bordejé, M.F.R. Pereira, J. Hazard. Mater., 239–240 (2012) 249.

S. Derrouiche, D. Bourdin, P. Roche, B. Houssais, C. Machinal, M. Coste, J. Restivo, J.J.M. Orfao, M.F.R. Pereira, Y. Marco, E. Garcia-Bordeje, Water Sci. Technol., 68 (2013) 1377.

J. Restivo, J.J.M. Órfão, M.F.R. Pereira, E. Garcia-Bordejé, P. Roche, D. Bourdin, B. Houssais, M. Coste, S. Derrouiche, Chem. Eng. J., 230 (2013) 115.

X. Fan, J. Restivo, J.J.M. Órfão, M.F.R. Pereira, A.A. Lapkin, Chem. Eng. J., 241 (2014) 66.

3.2 OZONATION OF ATRAZINE

3.2.1 REACTION PATHWAY AND MECHANISM

On a first approach, experiments of ozonation of atrazine were carried out in a semi-batch completely stirred tank reactor. These experiments were carried out to help understand the behaviour of the organic pollutant when exposed to ozonation, the reaction pathways and the reaction mechanism. Since the main goal of the ozonation and the catalytic ozonation processes is the mineralization of the organic pollutant, experiments were performed using a high concentration of atrazine that allowed following the mineralization degree by TOC, since the identification and quantification of all the degradation products was not

possible. Mineralization of the organic pollutants is of interest since it is known that the oxidation might lead to the formation of more harmful by-products [1-3].

The dimensionless concentration of atrazine during ozonation experiments is presented in Figure 3.1.

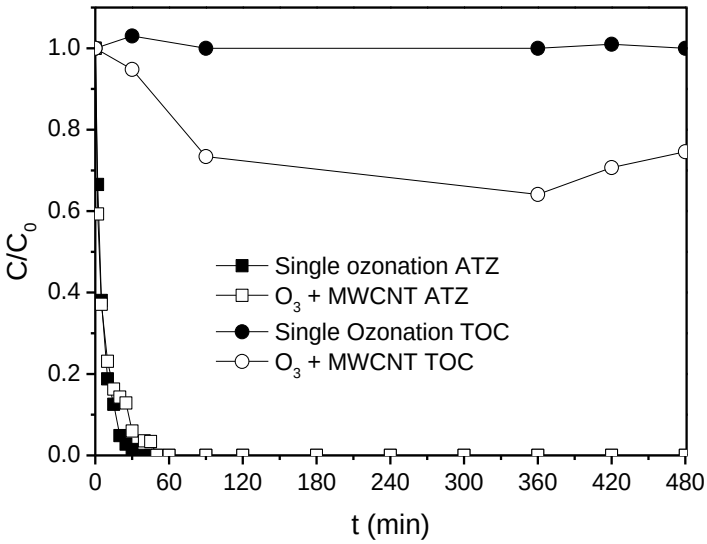

Figure 3.1 – Dimensionless concentration of atrazine and of TOC during semi-batch ozonation experiments.

Atrazine is quickly oxidized under our reaction conditions, even when no catalyst was present in the system. When multiwalled carbon nanotubes (MWCNT) were used as catalyst, the ozonation of atrazine was slightly delayed, probably due to competition of MWCNT in the reaction with dissolved ozone. Nevertheless, in both cases, atrazine is completely removed from the system in under 60 min. In fact, ozone is known to promptly react with atrazine, mainly through dealkylation on a first immediate step [4-8]. The main effect of the presence of the MWCNT catalyst in the system is seen in the increase of the mineralization achieved, as measured by the removal of TOC. Some of the intermediates which are formed during the ozonation of atrazine are known to show very slow reaction rates with molecular ozone [8].

Nevertheless, after 360 min, almost 40 %of TOC has been removed from solution. The small increase in the final stages are attributed to the contribution of the grinding of the carbon materials by the magnetic stirring, which contributes to the TOC value of the solution, which was observed in blank experiments using only water and the carbon material.

When the atrazine molecule is considered, the ratio between the organic carbon that is present in the s-triazine ring with the total organic carbon found in the molecule is $^{3}/_{8}$. This suggests that the TOC removal that was observed in the catalytic ozonation experiment in Figure 3.1 might be attributed to mineralization of the compounds released from the alkyl groups, rather than the s-triazine ring, since it is smaller than the amount of carbon found outside the ring. The formation of the organic intermediates was followed during ozonation experiments. The generation of several products was observed; however, it was only possible to identify three of these compounds: desisoropylatrazine (DIA, $C_5H_8ClN_5$, 173.604 g mol^{-1}), desethylatrazine (DEA, $C_6H_{10}ClN_5$, 187.630 g mol^{-1}) and desisopropylethylatrazine (DEIA, $C_3H_4ClN_5$, 145.55 g mol^{-1}). Several other expected intermediates [1, 5, 9-12] were compared with the products found during analysis, but no correspondence was found: ammelide, cyanuric acid, and the dechlorinated versions of DIA, DEA and DEIA. Furthermore, the formation of several organic acids was also observed. However, only oxalic acid corresponded to our tested standards, which included oxamic, acetic, pyruvic, glycolic, sulfanilic, salicylic, oxaloacetic, lactic, fumaric, gyoxilic and benzenossulfonic acids. Some of the observed organic acids that were formed presented very low concentrations, and thus their unquestionable identification was not possible. The concentrations of DEA, DIA and DEIA during the ozonation experiments, with or without MWCNT catalyst, are presented in Figure 3.2.

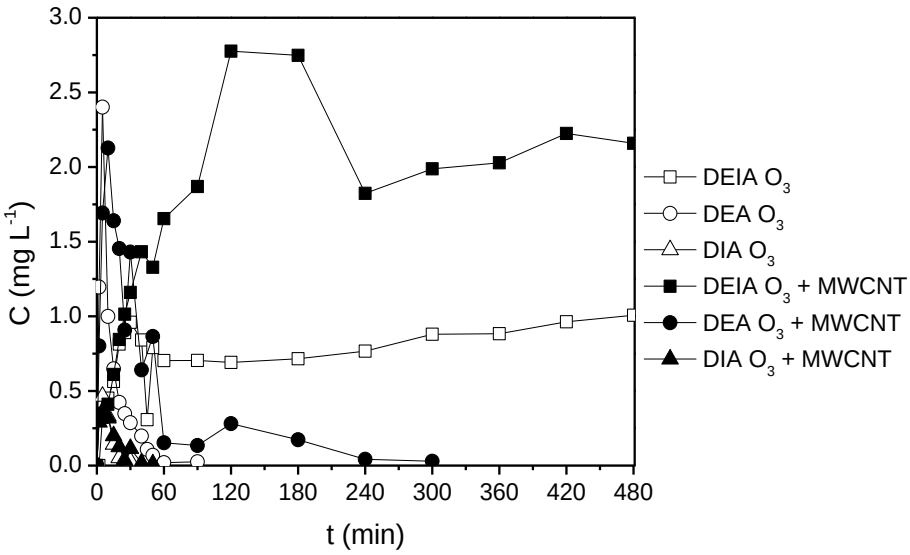

Figure 3.2 – Concentration of intermediates of atrazine degradation during semi-batch ozonation experiments.

The concentration of the identified intermediates varies between the non-catalytic and the catalyst ozonation experiments. While the behaviour of DIA was similar in both experiments, with formation of less than 0.25 mg L^{-1}, which were removed from solution in under 30 min, the concentrations of DEA and DEIA were higher in the catalytic ozonation experiments. Nevertheless, DEA is removed from solution in 60 min in the single ozonation case, and in 300 min in the catalytic ozonation case. DEIA is accumulated in solution during both experiments, reaching around 1.0 mg L^{-1} and 2.5 mg L^{-1} in single and catalytic ozonation experiments respectively, at the end of reaction. To further understand the changes in product distribution, the relative amount of the observed unquantified compounds is presented in Figures 3.3. The relative amounts were obtained through comparison of the peak areas found in HPLC chromatograms. The maximum for each peak was found throughout the compared experiments. Then, the areas found for each peak in each sample are presented as a ratio of that maximum peak area. The values taken into account to find the maximum for each compounds included the non-catalytic and catalytic experiments performed with and without a

radical scavenger (discussed ahead). Thus, it is possible to compare the behaviour of each compound between the experiments, but not to compare the amounts found for different compounds.

The observed behaviour of the intermediate compounds on Figure 3.3 between the non-catalytic and the catalyst experiments was widely different. UOC1 was seen to be formed and removed from solution in 15 min during single ozonation, and in 45 min during catalytic ozonation. The maximum was reached during catalytic ozonation. UOC2 was formed in similar amounts in both systems, and was not removed in 480 min. However, the catalytic system was clearly starting to remove UOC2 in the latter stages of reaction, which did not happen in the single ozonation system. UOC3 and UOC4 behaved similarly to UOC2; however, the amounts formed during catalytic ozonation are smaller than those formed during single ozonation. UOC5 was formed and completely removed from solution in 180 min during single ozonation and in 360 min during catalytic ozonation. UOC6 was not removed from solution in 480 min in both reaction systems; nevertheless, the amount found during catalytic ozonation was smaller than during single ozonation, and a slight removal in the latter stages of reaction could be observed during the catalytic experiment. UOC7, UOC8 and UOC9 are formed and removed from solution, similarly in both experiments, in 10, 180 and 240 min. The maximum value for these compounds was found in the single ozonation experiments.

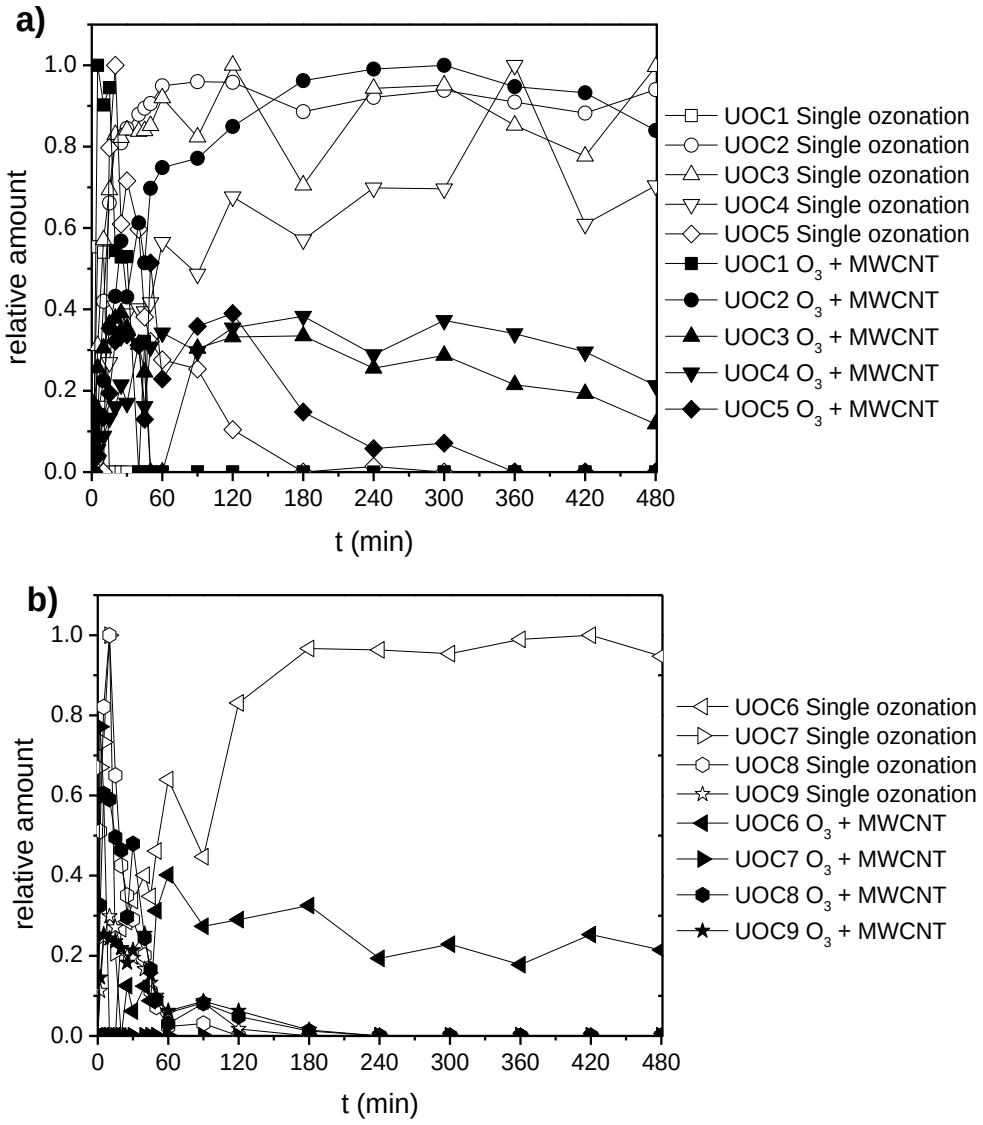

Figure 3.3 – Relative amount of unquantified organic intermediates of atrazine degradation during semi-batch ozonation experiments: a) compounds UOC1 to UOC5; b) compounds UOC6 to UOC9.

In general, the compounds which were formed and completely removed in under 480 min in both experiments were degraded faster during the single ozonation experiment. These compounds are likely being oxidized by molecular ozone. Thus, during the catalytic experiments, the competition

caused by the presence of MWCNT slows down the removal of these products. The compounds which were not completely removed during the experiments in under 480 min, in general, were observed to be slowly oxidized by the catalytic system, while they were observed to accumulate in solution in the single ozonation system. Thus, molecular ozone is not able to degrade these compounds, due to its selective nature in oxidation reactions, while the catalytic system is able to produce ozone-derived species, in surface or in solution, which are less selective and more reactive, and are able to oxidize such accumulating compounds. The larger accumulation of DEIA in the catalytic system can be attributed to the unselective degradation of the compounds which the single ozonation system was not able to oxidize. The larger removal of TOC found in the catalytic experiment may also be attributed to the same effect. Nevertheless, changes in the final distribution of the products of solution show that there are mechanistic differences between the non-catalytic and the catalytic system.

Ozonation experiments were performed in order to understand the degradation pathways of atrazine in our reaction system, using DEA, DIA and DEIA as the initial compound in solution. Several pathways have already been proposed in the literature [1, 5, 9-11]. In general, atrazine degradation leads to the formation of DEA and DIA through dealkylation (or oxidation of alkyl groups [13]), which through further oxidation yields DEIA. DEIA may then be dechlorinated, forming the equivalent Cl-substituted compound with an OH group. Further substitution with OH leads to formation of ammelide, and finally cyanuric acid. The degradation of cyanuric acid and eventual mineralization may proceed after the opening of the s-triazine ring. The C-N bonds which constitute this ring are remarkably difficult to break, as seen in the catalytic ozonation of oxamic acid [14]. The direct substitution of the Cl atom in atrazine, DEA or DIA is also possible. However, dechlorinated atrazine, DEA, DIA, DEIA, cyanuric acid or ammelide were not found during the reactions here described when compared with standards. Since our experiments showed several

compounds which were not identified/quantified, and that did not correspond to dechlorinated versions of the identified compounds, it is interesting to understand where they are originating. While DEIA did not originate any other compound, as expected, DEA originated DEIA, UOC1 and UOC2. DIA originated DEIA, UOC3, UOC4 and UOC6. Thus, UOC7, UOC8 and UOC9 are formed directly from atrazine, or they may originate from the oxidation of one of these three compounds. UOC7, UOC8 and UOC9 are detected in solution after as little as 2 min of reaction. UOC3, UOC5 and UOC6 are only detected in solution after 10 min of reaction minimum, or up to 20 min in the case of UOC6, which suggests that they are not formed directly from atrazine.

The concentration of oxalic acid during ozonation of atrazine is presented in Figure 3.4.

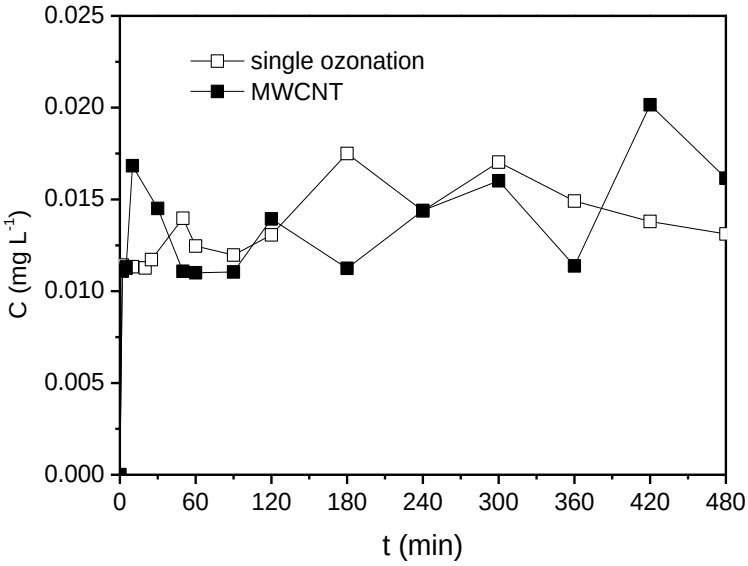

Figure 3.4 – Concentration of oxalic acid measured during atrazine ozonation experiments in semi-batch.

There are no major differences in oxalic acid concentration between the two systems. After an initial increase, the concentration of oxalic acid oscillates around a steady value, if slightly increases. While oxalic acid, and other organic acids, are likely formed from side-chain reactions of the

alkyl groups of the atrazine molecule, the formation of volatile organic compounds should not be discarded, since it is possible that instead of mineralization, the removal of TOC might be due to the release of such products through the gas outlet [15]. However, efforts to measure the formation of CO_2 in the gas outlet as a product of mineralization were not met with useful results, due to the very low concentrations expected.

The release of inorganic ionic compounds into solution during ozonation of atrazine was also measured, and the observed concentrations are presented in Figure 3.5.

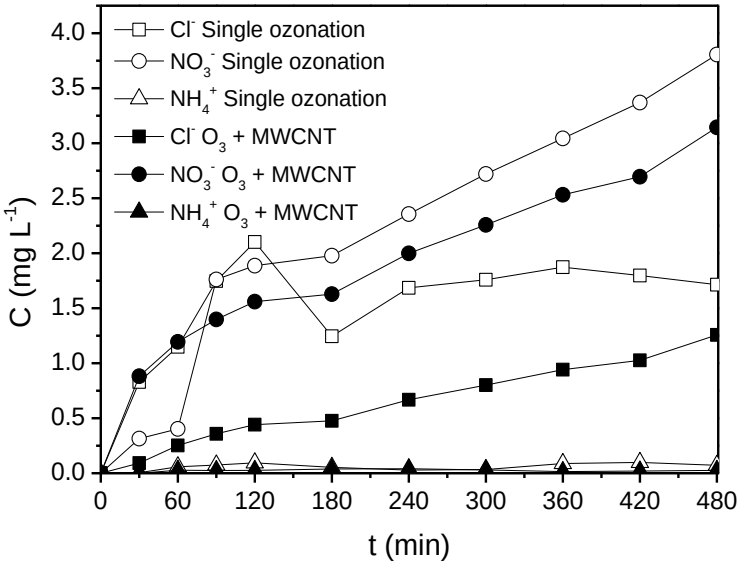

Figure 3.5 – Concentration of inorganic ionic compounds measured during atrazine ozonation experiments in semi-batch.

The experiments carried out without catalyst have resulted in a larger release of inorganic compounds, both anionic and cationic in nature, to the solution. Regarding chlorine, in the case of the single ozonation experiments, the concentration rises quickly after 60 min, and reaches a plateau close to 1.5 mg L^{-1}. Considering the initial atrazine concentration, the maximum amount of chlorine that may be released from atrazine is 0.0315 mM. Considering the maximum concentration of DEIA found during single ozonation experiments, 1.0 mg L^{-1}, it is possible to determine

that the amount of chlorine in this molecule corresponds, in its maximum, to 0.00413 mM. Thus, it is possible to conclude that the remaining accumulated products during single ozonation experiments must be dechlorinated compounds. During the catalytic experiments, the value of chlorine does not reach the maximum value in 480 min of reaction. Regarding nitrogen released in inorganic ionic compounds, the amount of nitrogen contained in the atrazine molecule, considering its initial concentration, is 0.23 mmol. The maximum amount of nitrogen measured in nitrate and ammonium in solution corresponds to 0.059 mmol. Thus, a large percentage of nitrogen is still contained in the organic compounds accumulated in solution, in the s-triazine ring or in alkyl groups. The amount of nitrogen in the s-triazine ring is 0.138 mmol. Thus, the accumulated products must have nitrogen present in the remaining structures of their molecule, approximately 0.033 mmol of nitrogen.

The evolution of toxicity during semi-batch ozonation of atrazine was also evaluated through standard Microtox tests of bacterial activity inhibition [16, 17], and is presented in Figure 3.6.

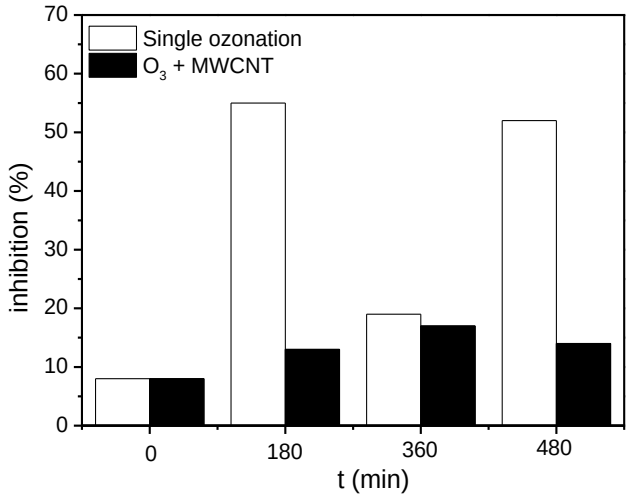

Figure 3.6 – Inhibition of bacterial activity during *Microtox* tests of bacteria exposed to effluent samples obtained during semi-batch ozonation of atrazine.

The toxic potential of the resulting effluents was seen to increase when the initial solution was exposed to ozone, regardless of the presence of the MWCNT catalyst. The products resulting from the degradation of atrazine present a larger toxic potential, individually or in combination, than the parent compound. On the other hand, it has been found that the degradation of atrazine by natural sunlight results in a decrease of its toxicity [2]. Similarly, it has also been reported that, when using phototrophic organisms as models, the degradation products of atrazine are less toxic than the parent compound [3]. It has been suggested that the dechlorination of atrazine and of its intermediates is responsible for the decrease of the toxic activity of the species [1]. The diaminated form of atrazine (DEIA) has also been reported to be considerably less toxic than atrazine, DEA and DIA [3]. However, the results here obtained differ from those reported in the literature. The decomposition of atrazine resulted in more toxic effluent. Since the individual compounds have been reported to be less toxic, the observed values must be attributed to the potential toxicity of the different mixtures that are obtained. During single ozonation experiments, a great increase in the inhibition of bacterial activity was observed after 180 min of reaction, from 8% to 55%. However, after 360 min, the measured toxicity of the resulting effluent was much smaller, but still above that of the initial solution, at 19%. After 480 min, the inhibition value raised up to almost 52%. After 180 min of reaction, the dechlorination process was seen to be practically complete (Figure 3.5). Thus, the changes observed throughout the reaction cannot be attributed to this reaction. However, there is a constant increase in the amount of nitrate in solution, which may indicate that some dealkylation reactions still taking place might be changing the distribution of products in solution, which in turn may result in different levels of toxicity. In the case of the catalytic ozonation experiment, the increased registered after 180 min of reaction is much slighter than in the case of single ozonation, from 8% to 14%. At 360 min, the toxicity value peaked at 17%, but was lowered to 13% at 480 min. At 180 min, DIA and UOC5 are still found in solution, unlike in the case of the single ozonation system. Their

disappearance may lead to the formation of more toxic products, which could explain the higher toxicity found at 360 min, or a more toxic mixture of pollutants. Nevertheless, the toxicity decreases as the accumulated products in solution also decrease in concentration (UOC2, UOC3 and UOC4), as seen at 480 min.

While it is clear that the presence of the MWCNT catalyst, besides leading to a more extensive mineralization of atrazine and its degradation products, results in a wide change of the distribution of the accumulated products in solution after long reaction times, it is important to notice that the catalytic process resulted in much less toxic effluents when compared with the single ozonation process.

To shed light on the effects of the catalytic route in the degradation of atrazine, and what reactions are taking place to lead to a change in the product distribution observed, experiments were performed using *t*-BuOH as a radical scavenger in solution. The presence of a radical scavenger during the catalytic experiments is meant to stop the action of radicalar species which are being generated in solution through the decomposition of ozone [18]. The measured concentrations of atrazine and TOC during experiments using t-BuOH are presented in Figure 3.7.

Regarding the degradation of atrazine, no significant differences were observed when compared with the experiments carried out without radical scavenger in solution (Figure 3.1). The slightly slower removal of atrazine in the case of the experiment with catalyst is analogous to what was observed in the experiments without radical scavenger. The competition for ozone of the MWCNT results in less dissolved ozone available to react with atrazine. The mineralization degree observed in experiments with radical scavenger, in the case of single ozonation, did not significantly change. However, the removal of TOC observed in the catalytic experiment was widely different, which suggests that the catalytic mineralization of atrazine and of its degradation products occurs partially through reactions occurring on the liquid phase, due to the action of radicalar species resulting from the decomposition of ozone.

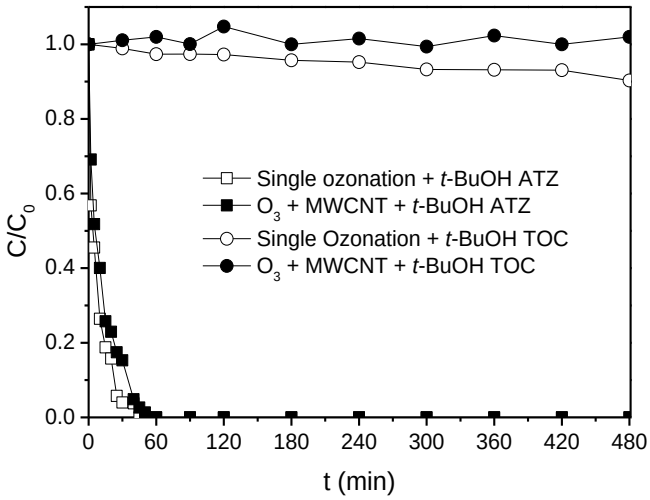

Figure 3.7 – Dimensionless concentration of atrazine and of TOC during semi-batch ozonation experiments with a radical scavenger in solution.

Changes in the distribution of the degradation products of atrazine are expected. Also, the prevalence of reactions involving radical species is expected to lead to a different product distribution, since ozone is known to selectively attack specific bonds in the atrazine molecule [19]. The measured concentrations of the quantifiable intermediate organic degradation products (DEIA, DEA and DIA) during ozonation of atrazine in the presence of a radical scavenger are presented in Figure 3.8.

The behaviour of DIA in the ozonation experiments with and without radical scavenger did not differ significantly. In fact, it is expected that DIA reacts promptly with ozone [8]. A very large increase in the measured concentration of DEA is observed when compared with the experiments without a radical scavenger, for both reaction systems. Unlike observed in the previous experiments, the concentration of DEA was larger when single ozonation was applied, and this compounds was not completely removed in 480 min. In the catalytic system, a smaller amount of DEA was measured in solution, and complete removal was achieved after 420 min. The reaction of DEA with radicalar hydroxyl species is expected to be much faster than the direct reaction with ozone [8]. The experiments with radical scavenger showed a slower decay of DEA, which fits well with the

expected behaviour. Nevertheless, the much higher amounts formed during radical scavenger experiments shows that the presence of the scavenger shifted the degradation pathways of atrazine, producing larger amounts of this compound. The concentrations of DEIA found in solution are slightly higher in the experiments with radical scavenger in the case of single ozonation. However, the catalytic ozonation experiment yielded smaller amounts of DEIA. The smaller amounts may be related with the slower degradation of intermediate products with originate DEIA, such as DEA, due to the scavenging of radicals in solution. The relative amounts of the unidentified organic intermediate products of the degradation of atrazine are presented in Figure 3.9. The values presented were calculated in relation to the maximum value for each compound found in the catalytic and non-catalytic experiments, with and without a radical scavenger.

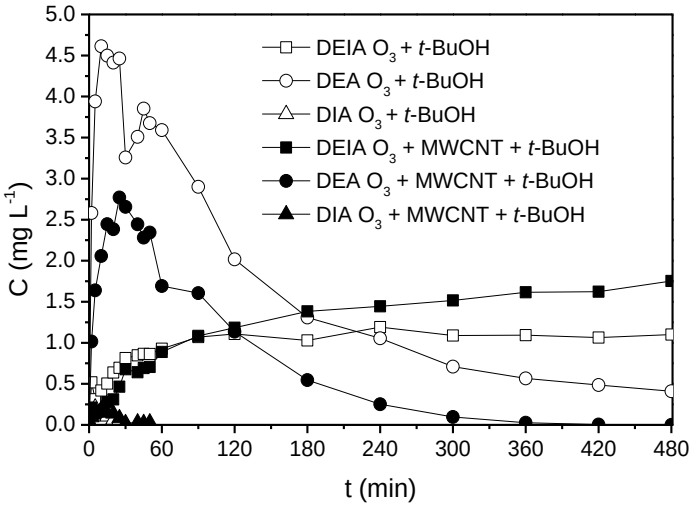

Figure 3.8 – Concentration of intermediates of atrazine degradation during semi-batch ozonation experiments in the presence of a radical scavenger.

The most evident difference between the experiments with and without radical scavenger is that the addition of *t*-BuOH, in general, resulted in smaller amounts of these intermediates, with the exception of UOC9

which peaked in the early stages of the single ozonation experiment. UOC1, UOC6 and UOC7 were not formed during the single ozonation experiment, and were formed in small concentrations during catalytic ozonation. Their formation is thus linked to reactions with radicalar species in solution. UOC2, in both radical scavenger experiments, accumulates through the reaction. In the case of single ozonation, an increase in the amount found in solution is noticeable throughout the whole experiment, while in catalytic ozonation the amount reaches a plateau after 180 min, with a slight decrease in the latter stages. A similar behaviour was observed in the experiments without radical scavenger. Since the four experiments yielded similar results, it is likely that the formation of UOC2 is related to direct ozonation mechanisms. The removal of this compound in the catalytic ozonation system, albeit small, seems to be related to reactions occurring on the surface of the catalyst.

UOC3 appears in much smaller amounts in both radical scavenger experiments. Since it appears to be accumulated during reactions, the smaller amounts probably show that solution radicalar reactions are involved in its formation. UOC4 and UOC5 accumulated throughout the single ozonation experiment. In the catalytic ozonation experiment a similar behaviour was observed, albeit at a slightly higher concentration. Nevertheless, a decreasing tend is noticeable in the latter stages of reaction. Similar behaviour was observed in experiments without the radical scavenger, and thus their degradation may be attributed to surface oxidation reactions. UOC8 is seen in smaller amounts in the catalytic ozonation experiment, being completely removed after 180 min, while in the single ozonation experiments its removal was only observed after 360 min. Its formation and removal should be due to action of direct ozonation in solution. UOC9 is accumulated in solution in the single ozonation experiment, which was not observed in the experiment without radical scavenger. However, its removal was complete in the catalytic ozonation experiment, although slower than when no radical scavenger was present. Surface and bulk reactions with radical species may be taking part in its

removal from solution. The formation of other less reactive radicals in solution might also play a role in the oxidation of some intermediates, more selectively than other more active radical species [1].

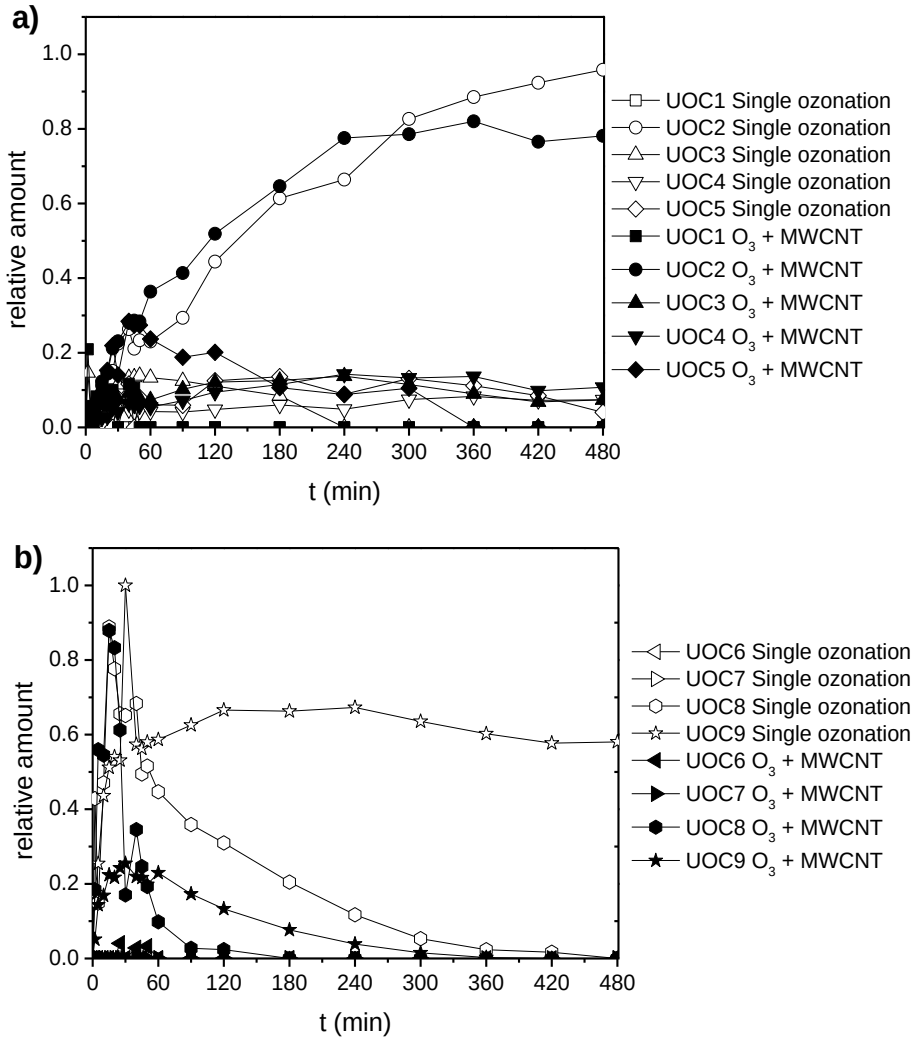

Figure 3.9 – Relative amount of unquantified organic intermediates of atrazine degradation during semi-batch ozonation experiments with a radical scavenger (a) compounds UOC1 to UOC5; b) compounds UOC6 to UOC9).

The concentration of oxalic acid during ozonation of atrazine is presented in Figure 3.10, in experiments using a radical scavenger.

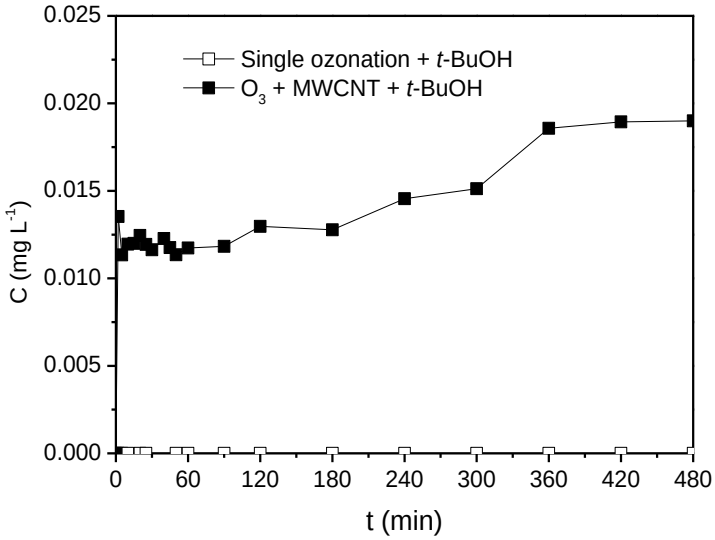

Figure 3.10 – Concentration of oxalic acid measured during atrazine ozonation experiments in semi-batch using a radical scavenger.

The concentration of oxalic acid in the single ozonation experiment carried out in the presence of a radical scavenger was below the limit of quantification, for the whole experiment. Since it is known that oxalic acid is not degraded by direct ozonation [18], the formation may be hindered by the presence of *t*BuOH. This can indicate that oxalic acid is formed through the action of radicalar species in solution, which could be formed by the interaction of ozone with the organic compounds [20]., in the single ozonation experiment. However, no significant differences were observed in the concentration of oxalic acid in the catalytic ozonation experiment carried out in the presence of a radical scavenger when compared with the experiment without radical scavenger, which indicate that surface reactions are responsible for the formation, and removal, of oxalic acid, in this case. However, it is possible that both radicalar surface reactions and radical solution reactions are responsible for the formation of oxalic acid, depending on the reaction system. Nevertheless, the possibility that the difference in the concentrations of oxalic acid is due to changes in the reaction path occurring in earlier stages of reaction cannot be excluded. The products which lead to the formation of oxalic acid may not be

present in solution in the case of the single ozonation experiment carried out in the presence of *t*-BuOH.

The concentrations of inorganic anionic compounds found during experiments carried out in the presence of *t*-BuOH are presented in Figure 3.11.

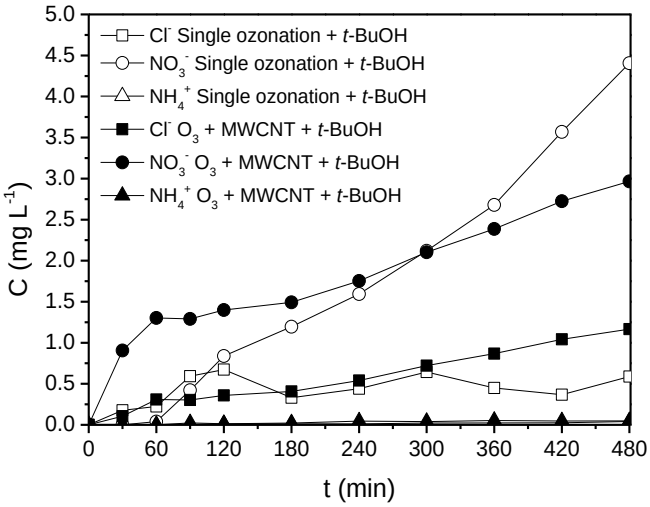

Figure 3.11 – Concentration of inorganic ionic compounds measured during atrazine ozonation experiments in semi-batch with a radical scavenger.

A very interesting change in the evolution of chlorine in solution is noticeable in the experiments in the presence of *t*-BuOH. While in the catalytic ozonation experiment the concentration of chlorine did not significantly change, the single ozonation experiment showed a much smaller amount released into the solution. Furthermore, after around 180 min a steady concentration is reached, after which no increase was observed. The stable value was approximately $^1/_3$ of the amount of chlorine present in atrazine, in the initial solution. Thus, a much lesser degree of dechlorination was observed when the action of radicals in solution was hindered. In fact, the dechlorination of atrazine has been proposed to occur through the action of hydroxyl radical species, in a simultaneous dechlorination-hydroxylation reaction taking place at the C-

Cl position [13]. Nevertheless, the surface reactions taking place in the catalytic ozonation experiments were shown to be the main responsible for the release of chlorine in the catalytic reaction, which suggests that different mechanisms are taking place in the different reaction systems. The release of nitrate in the catalytic ozonation experiment is higher than in the single ozonation experiment in the early stages of reaction, but after 300 min, the tendency is reversed, due to a change in the release rate that happens at around the 60 min mark in the catalytic experiment. However, the increasing trend is kept for both reactions throughout the whole experiment. Similarly to what was observed in the case of chlorine, the evolution observed in the catalytic ozonation experiment did not significantly change, whether the radical scavenger was used or not. On the other hand, during the single ozonation experiment with radical scavenger, the release of nitrate achieved a slightly higher value at the end of the 480 min when compared with the experiment without radical scavenger. The more selective nature of the ozone oxidative action [20] suggests that, when the action of radical species is hindered, the higher release of nitrate is related to the attack of molecular ozone in specific bonds that result in the release of this anion. The release of ammonium was very small when compared with the other anions, which was also observed in the experiments without radical scavenger.

The inhibition of activity of luminescent bacteria, *Vibrio Fischeri*, in the standard *Microtox* test, was evaluated using samples obtained from the ozonation reactions carried out in the presence of *t*-BuOH (Figure 3.12).

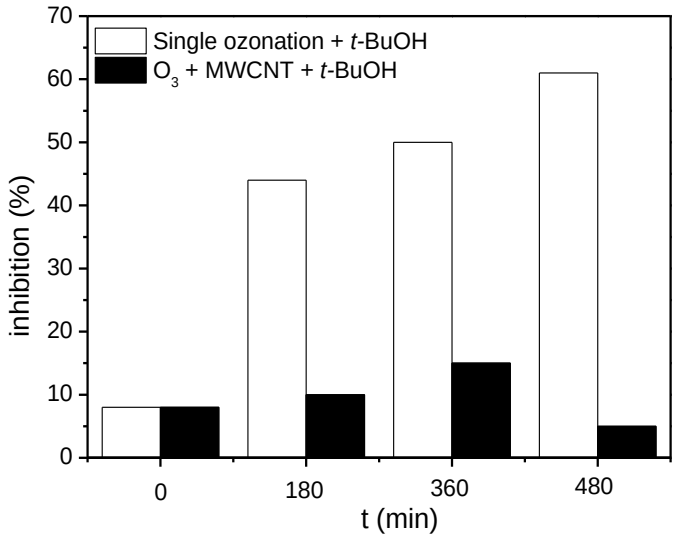

Figure 3.12 – Inhibition of bacterial activity during *Microtox* tests of bacteria exposed to effluent samples obtained during semi-batch ozonation of atrazine in the presence of a radical scavenger.

The measured toxicity of the initial atrazine solution was not altered due to the inclusion of *t*-BuOH, which indicates that the evaluation of the toxicity in these experiments may be compared with that of the experiments without a radical scavenger. It is evident that, as before, the single ozonation process leads to a more toxic effluent than its catalytic counterpart. In the single ozonation experiment, a constant increase was observed, reaching over 60% of inhibition at 480 min. In the experiment without *t*-BuOH, drastic variations were observed throughout the experiment, which were not present in this case, suggesting that the changes in the product distribution result in changes in the toxicity of the effluent. The catalytic experiment resulted in a similar trend throughout the experiment, whether radical scavenger was or not used. However, the former reached slightly lower levels of toxicity at 480 min. The surface reactions taking place clearly have a major role in the reduction of the toxicity of the effluent.

A detailed discussion of the role of adsorption of atrazine on the surface of MWCNT and of the kinetics of the catalytic ozonation of atrazine is presented in Appendix A.

In summary, the presence of a catalyst in the ozonation of atrazine does not significantly affect the degradation of the pollutant. However, the mineralization degree is widely improved, through the action of radical species. The presence of the catalyst also affects the distribution of the products of degradation found in solution, through both surface and bulk reactions. The changes in the distribution of the products by the MWCNT lead to the production of a less toxic effluent.

3.2.2 Continuous catalytic ozonation of Atrazine

After an intensive study of the reaction mechanisms of the catalytic ozonation of atrazine performed in semi-batch, the catalytic ozonation process was studied as a potential application for the removal and mineralization of atrazine in continuous operation. For these experiments, a bubble column reactor with an internal loop was used (detailed experimental conditions in section *Materials and methods*). The reaction was first carried out without any catalyst, and afterwards in the presence of one CNF-covered honeycomb monolith, with CNF loading ~10.2 wt.%.

In Figure 3.13, the removal of atrazine and the mineralization degree, represented by TOC removal, are presented, for the single ozonation and catalytic ozonation carried out in continuous operation, using a structured catalyst in the latter.

While the removal of atrazine was slightly worse in the catalytic experiment, which was expected taking into account what was observed in semi-batch experiments, the mineralization degree achieved was slightly better when a catalyst was used. Nevertheless, the TOC removal was still small, while single ozonation did not lead to mineralization of atrazine at all. The concentration of the quantified organic intermediates did not vary greatly between the non-catalytic and the catalytic

experiments. The concentration of DEA and DEIA were slightly lower in the catalytic ozonation experiment, while the concentration of DIA was slightly higher. For short contact times during the semi-batch ozonation experiments, similar distribution of the products was observed. The considerations regarding the mineralization mechanisms of atrazine made for the semi-batch process should be still valid in the case of the continuous ozonation experiments.

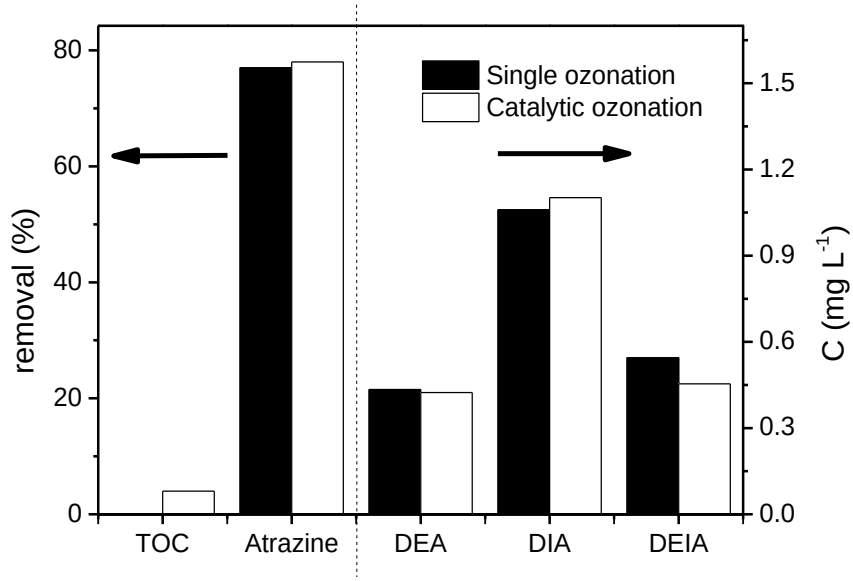

Figure 3.13 – Removal of atrazine and TOC during continuous ozonation experiments (left axis) and concentration of the quantifiable organic intermediates (right axis) measured at steady-state.

The concentration of oxalic acid was also measured in the continuous ozonation experiments, and is presented in Figure 3.14, together with the measured concentrations of inorganic ions found in solution.

The concentrations of the inorganic anionic compounds measured in solution at steady state follow what was observed during the semi-batch experiments at short reaction time; i.e., the concentration of chlorine is slightly higher in the catalytic ozonation experiment, the concentration of nitrate is lower in the catalytic ozonation experiment, and the concentration of ammonium is very small in both experiments. The

observed differences in oxalic acid between the non-catalytic and the catalytic ozonation experiments were not observed in the semi-batch experiments. In fact, the measured concentration of oxalic acid was much higher in this case, which suggests differences in the mechanisms taking place. It is possible that in this system, different reaction pathways are taking place, and thus increasing the production of oxalic acid. On the other hand, the catalytic system is expected to actively remove oxalic acid from solution.

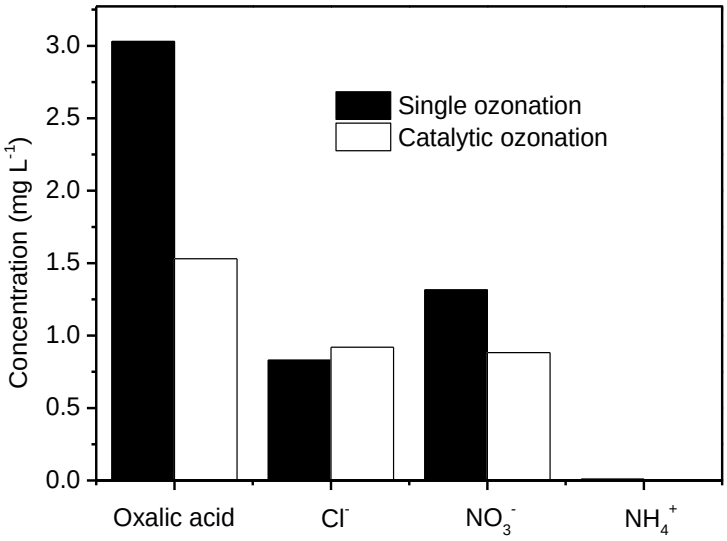

Figure 3.14 – Concentration of oxalic acid and inorganic anionic compounds measured at steady-state during continuous ozonation experiments.

The relative distribution of the unquantified organic compounds in continuous ozonation, as measured at steady state, is presented in Figure 3.15.

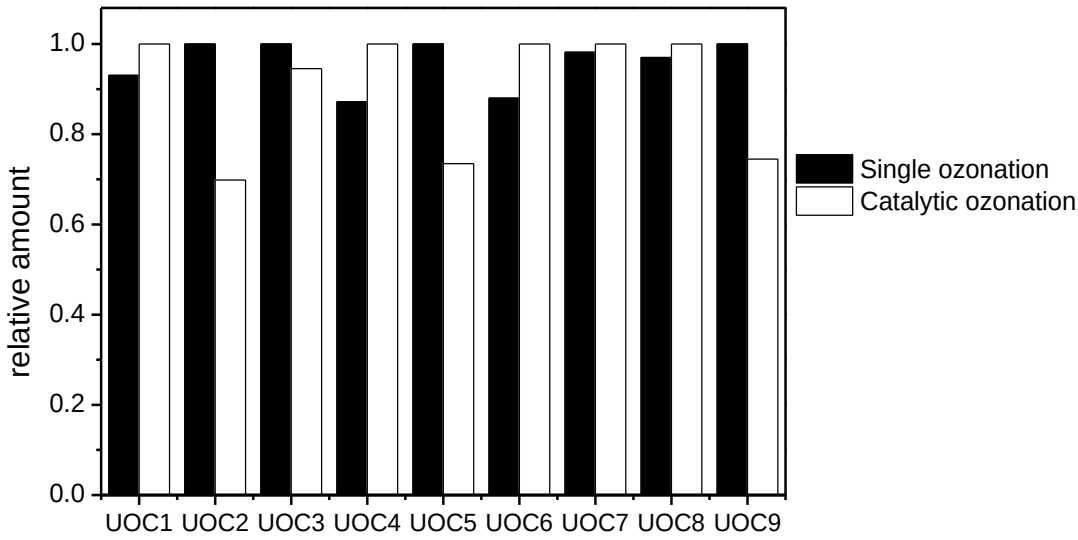

Figure 3.15 – Relative amount of unquantified organic compounds during continuous ozonation experiments, as measured at steady state.

In Figure 3.15, the organic compounds are sorted by polarity, which decreases from UOC1 to UOC9. It is known that the degradation of atrazine successively generates more polar compounds with lower molecular weights [4]. Moreover, from the preliminary semi-batch experiments mentioned above, it is known that the products that tend to accumulate during ozonation are the following: DEIA, UOC2, UOC3, UOC4 and UOC6. The inclusion of a catalyst decreases the accumulation of the products with lower molecular weight (UOC2, UOC3 and DEIA). However, it also slows down the degradation of the primary intermediates (more polar compounds), which explains why some of these compounds present higher relative peak area during catalytic ozonation experiments. Differences can be attributed to the less selective action of the hydroxyl radicals, when compared to the direct ozonation mechanism [20]. Direct ozonation seems to selectively attack atrazine and its first-step degradation products. Such a mechanism is less effective when the mineralization degree is considered. In addition, DEIA is considered to be the most stable degradation product of atrazine after reaction with ozone or hydroxyl radicals [12]. Thus, the more extensive removal of DEIA for

longer contact times with the catalyst indicates that the catalytic ozonation process has potential to achieve high degrees of mineralization.

The toxicity of the resulting effluent during continuous ozonation experiments was also monitored, using the standard *Microtox* test. The inhibition of activity of luminescent bacteria is presented in Figure 3.16, when exposed to samples resulting from the non-catalytic and the catalytic process.

It is clear that the ozonation process yields a more toxic effluent than the initial solution, containing only atrazine. Moreover, the catalytic ozonation results in an even more toxic effluent. While the increase in toxicity during ozonation was also observed in semi-batch experiments, the catalytic ozonation process was expected to result in less toxic effluents than its non-catalytic counterpart. The observed behaviour must be related to the fact that the retention times used in this experiments are representative of short reaction times in semi-batch, and at these times, changes in the reaction path of atrazine produce a more toxic combination of intermediate compounds, together with atrazine, in solution.

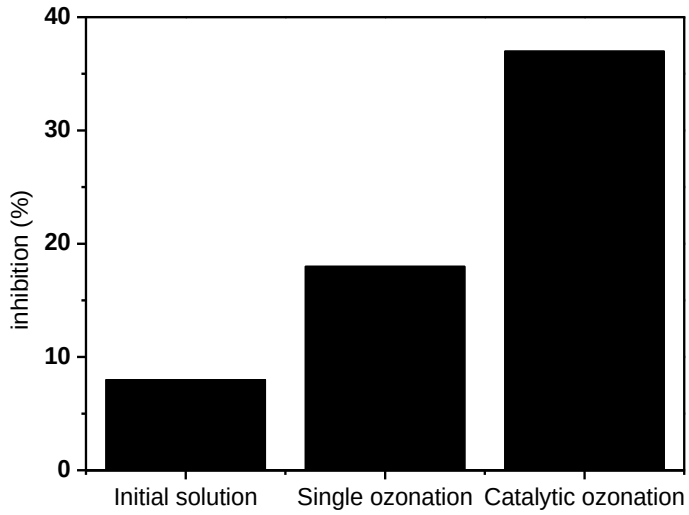

Figure 3.16 – Toxicity levels measured as inhibition of activity of luminescent bacteria when exposed to samples taken from the continuous ozonation experiments at steady-state.

In summary, it was shown that the application of a structured catalyst during continuous ozonation has the potential to further improve the mineralization of atrazine. Furthermore, the distribution of the intermediate products generated during the process was shown to be altered in the presence of a catalyst. In general, the distribution followed what was expected, after the observation made in semi-batch experiments. Nevertheless, some differences were observed, which suggest that different reaction paths may be taking place, most likely due to the difference in the reactors used for the semi-batch and the continuous experiments.

3.3 Ozonation of metolachlor

3.3.1 Reaction pathway and mechanism

The study of the ozonation of metolachlor was initiated, similarly to what was done with atrazine, with experiments carried out in a semi-batch completely stirred tank reactor, in order to understand the behaviour of the organic pollutant when exposed to ozone, and the effect of the catalyst in the reaction. High concentrations of metolachlor were used, which allowed the determination of the mineralization degree through analysis of TOC. The mineralization of metolachlor, rather than just its removal from solution, is of interest since it is known that the oxidation of the pollutant might yield a more toxic effluent [2, 21, 22].

In Figure 3.17 the evolution of the dimensionless concentration of MTLC during the semi-batch catalytic ozonation experiment are presented, together with the results obtained for the blank test (single ozonation). In addition, the adsorption of metolachlor on the surface of MWCNT in also presented in Figure 3.17, as well as the dimensionless concentration of metolachlor during ozonation experiment carried out in the presence of a radical scavenger, *tert*-BuOH.

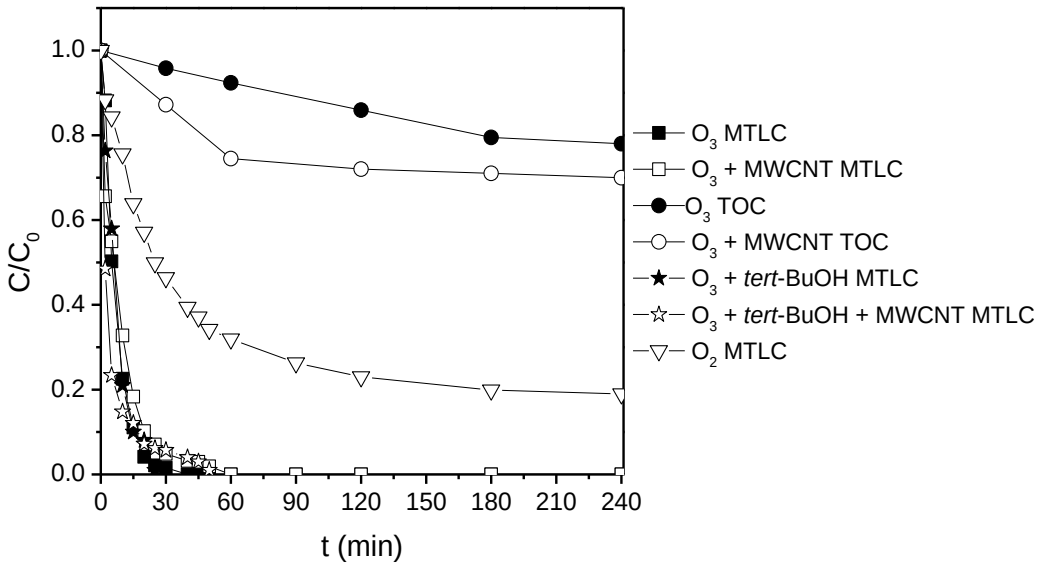

Figure 3.17 – Dimensionless concentration of metolachlor and of TOC during semi-batch ozonation experiments.

It is noticeable that the addition of MWCNT did not accelerate the decomposition of the pesticide when compared with single ozonation, which suggests that the degradation of MTLC is mainly due to the direct reaction with ozone. The formation of non-selective hydroxyl radicals might have a negative effect on the degradation of the parent pollutant, since less ozone is available to directly react with MTLC. However, the difference between the two experiments is negligible when only the parent compound is considered. The addition of the radical scavenger *tert*-BuOH did not significantly alter the rate of MTLC degradation, whether there was or was not a catalyst present. This suggests that under the current experimental conditions MTLC is reacting mainly with ozone. Although adsorption on MWCNT is rather extensive, as seen in the experiment with no ozone, the main mechanism for the catalytic ozonation of metolachlor is by oxidation.

Although MTLC is easily degraded, total mineralization is not readily achieved. The influence of the presence of MWCNT in solution during the ozonation experiments is easily noticeable. Further mineralization of the organic carbon in solution is attributed to hydroxyl radicals or surface

radical species, which production is enhanced by the presence of the catalyst. However, it is visible that the degradation of the organic matter slows down after 60 minutes of reaction. This occurs because the by-products of the oxidation of MTLC are less reactive than MTLC. On the other hand, there is also a contribution of the powder material to TOC concentration that cannot be disregarded [23]. Additional tests (without pollutant) were carried out, but this contribution was found to be dependent on the composition of the solution. Then, it was not possible to unmistakably discount the mentioned effect on TOC values.

The concentration evolution of 2-ethyl-6-methylaniline during the ozonation experiments of metolachlor is presented in Figure 3.18.

The intermediate compound 2-ethyl-6-methylaniline is a known by-product of the oxidation of metolachlor and presents very high values of toxicity [21, 22]. This intermediate is formed almost immediately in the beginning of the ozonation reaction, and seems to be easily degraded, being completely removed after 45 minutes during the single ozonation experiment, and after 30 minutes during the catalytic ozonation experiment.

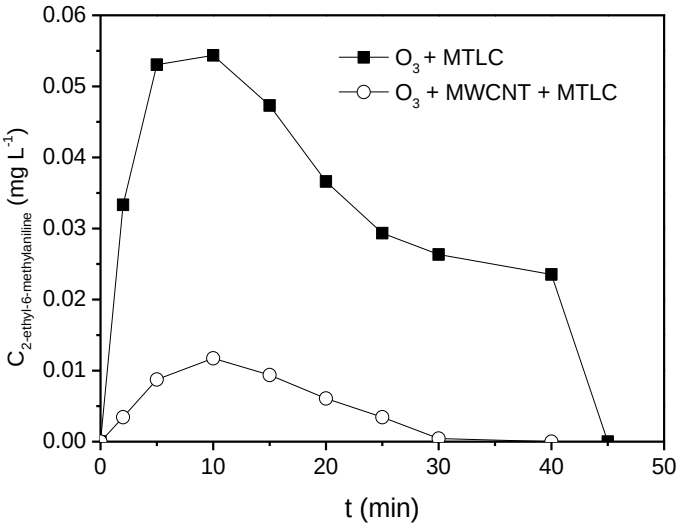

Figure 3.18 – Concentration of 2-ethyl-6-methylaniline during semi-batch ozonation experiments of metolachlor.

To assess the role of molecular ozone and of the highly-reactive radicals in the degradation of this compound, semi-batch ozonation experiments were made using 2-ethyl-6-methylaniline as the starting pollutant (Figure 3.19).

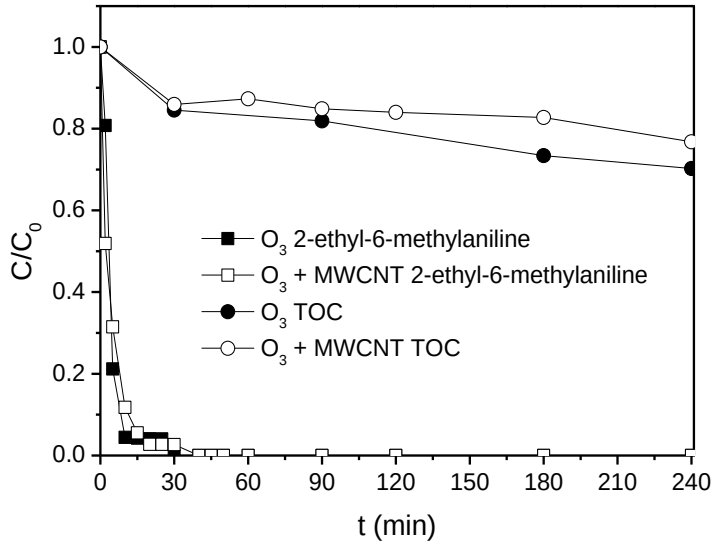

Figure 3.19 – Dimensionless concentration of 2-etyl-6-methylaniline and of TOC during semi-batch ozonation experiments.

A similar behaviour to MTLC was found during these experiments, i.e. the addition of the catalyst did not improve the degradation rate. Thus, the decrease in the amount formed during the ozonation of MTLC with a catalyst can be attributed to the less selective nature of the radicals in the oxidation of organic matter when compared to molecular ozone. The presence of the catalyst did improve the mineralization degree, which again suggests that the more recalcitrant by-products are to be found further in the degradation chain.

The evolution of three identified organic acids (oxalic, pyruvic and oxamic acids) is presented in Figure 3.20, for ozonation and catalytic ozonation.

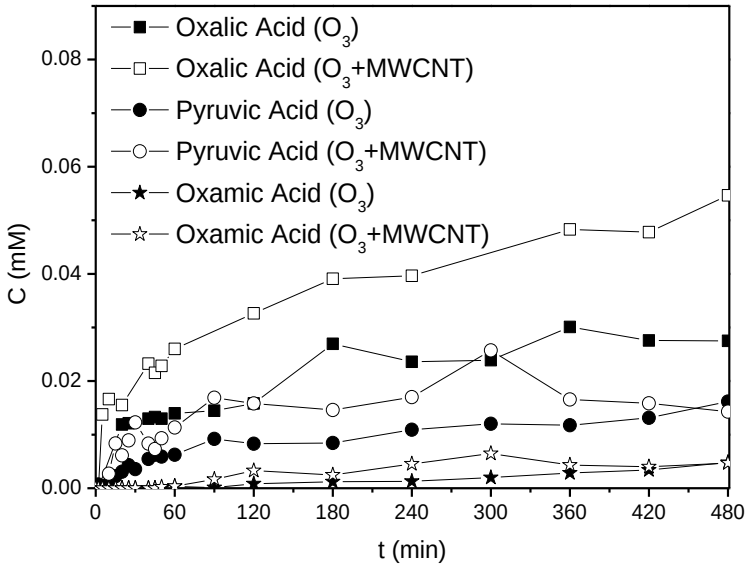

Figure 3.20 – Concentration of oxalic, pyruvic and oxamic cids during semi-batch ozonation experiments of metolachlor.

It is known that the catalytic ozonation process, using carbon materials, greatly improves the oxidation of oxalic acid when compared to single ozonation [14, 18]. In Figure 3.20 there seems to be a constant increase in the concentration of oxalic acid in both experiments. Furthermore, the concentration of this acid was higher for the catalytic ozonation experiment. This indicates that the accumulated TOC during the ozonation experiments is due to more complex organic compounds, which are formed between the primary degradation of MTLC and the appearance of low molecular weight organic acids. The more extensive degradation of these products during catalytic ozonation increases the amount of oxalic acid found in solution [22, 24-27]. Oxalic acid is probably accumulated due to a combination of its continual formation with the competition with the several other organic compounds present in solution. Since the pH of solution decreases during the semi-batch experiments (from ~6 to ~4 in 3 hours), the production of hydroxyl radicals due to the natural decomposition of ozone in water also decreases [25]. Thus, the degradation of the formed intermediates during single ozonation is slowed down.

The evolution of pyruvic acid is in accordance with what is proposed above for oxalic acid. In this case, after 6 hours of reaction, a decrease in the concentration during the catalytic ozonation experiment is observed. For the single ozonation experiment the acid accumulated continuously during the test (8 hours), as mentioned above for oxalic acid.

Oxamic acid is also recalcitrant to direct ozonation. However, the reaction with the highly-reactive radicals produced during the catalytic ozonation experiment is not as fast as for oxalic and pyruvic acids [18], which explains the accumulation in solution during single and catalytic ozonation. The amount detected in solution is far smaller when compared to the other quantified acids.

The mass balance of the carbon measured in the quantified organic compounds in relation to the measured TOC value is presented in Table 3.1. The values of inorganic carbon in solution were residual and are negligible in this case. The identified TOC was calculated following equation 3.1. Mineralized carbon ($TOC_{mineralized}$) was calculated from the removal of TOC from solution.

$$TOC_{identified} = TOC_{MTLC} + TOC_{2-ethyl-6-methylaniline} + TOC_{organic\ acids} + TOC_{mineralized} \quad (3.1)$$

Table 3.1 – Carbon mass balance in quantified organic compounds during semi-batch ozonation of metolachlor.

t (min)	TOC_{MTLC} (mg L^{-1})		$TOC_{2\text{-ethyl-6-methylaniline}}$ (mg L^{-1})		$TOC_{organic\ acids}$ (mg L^{-1})		$TOC_{identified}/TOC_0$	
	O_3	O_3+MWCNT	O_3	O_3+MWCNT	O_3	O_3+MWCNT	O_3	O_3+MWCNT
0	9.2	9.1	0	0	0	0	-	-
30	0.14	0.44	0.02	0.0003	0.0049	0.013	0.05	0.18
60	0	0	0	0	0.0063	0.011	0.07	0.25
120	0	0	0	0	0.0076	0.020	0.14	0.28

Observing Table 3.1, it is evident that there is a large percentage of organic carbon not detected. In fact, it is expected that large amounts of organic compounds, which are not quantified here, are still present in solution, even after 8 hours of reaction [22, 24-27]. In addition, other peaks were detected in the chromatogram resulting from the analysis by HPLC-UV. However, since it was not possible to unmistakably identify the corresponding compounds, they were not quantified in this study. It is, however, important to notice in Table 3.2 that the contribution of unidentified TOC to what is measured in solution is decreasing after the first minutes, when the parent compound is completely degraded. This suggests that, for longer reaction times, a larger amount of the total organic carbon is present in the end-of-chain degradation products [22, 24]. A slightly larger increase in the fraction of identified TOC is seen in the catalytic ozonation experiment. This difference between the two experiments indicates that the catalytic ozonation experiment is degrading the top-of-chain formed intermediates at a faster rate, yielding a larger amount of carbon containing organic acids. This, combined with a larger portion of the initial TOC mineralized, justifies the more extensive increase in identified TOC in the case of the catalytic ozonation experiments.

Figure 3.21 and Figure 3.22 present the concentration of inorganic ions found during semi-batch ozonation experiments.

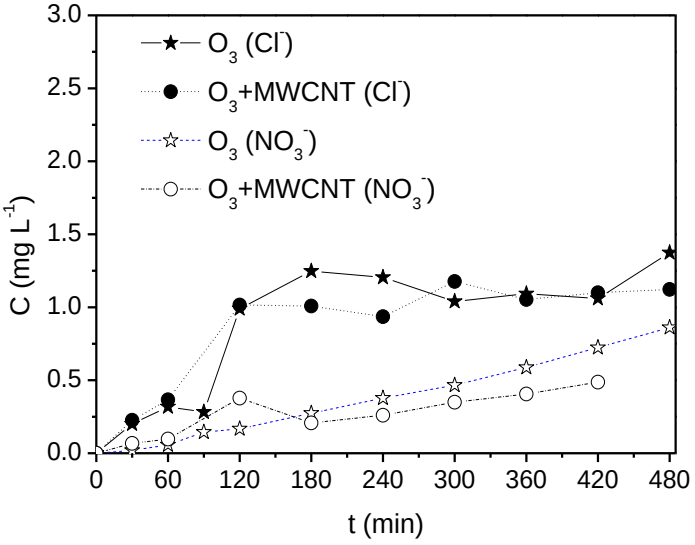

Figure 3.21 – Concentration of chloride and nitrate ions during semi-batch ozonation experiments of metolachlor.

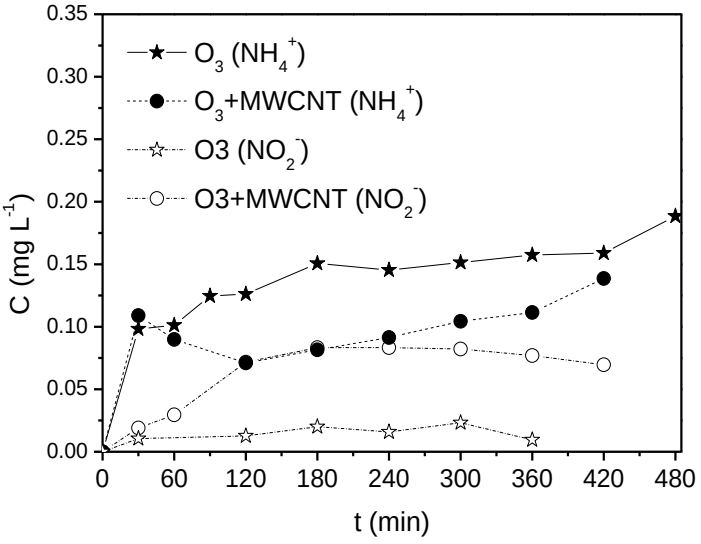

Figure 3.22 – Concentration of ammonium and nitrite ions during semi-batch ozonation experiments of metolachlor.

The release of chloride and nitrate ions during the experiments is very similar whether the catalyst is present or not. The main difference regards the production of ammonium and nitrite. A larger amount of nitrite is

produced in the catalytic ozonation experiment, while the amount of released ammonium decreases. This may be due to the different reaction pathways followed by ozone and hydroxyl radicals to degrade organic compounds.

Mass balances of chlorine and nitrogen quantified during the semi-batch ozonation experiments are presented in Figure 3.23. The concentration of chlorine was calculated by adding the mass of chlorine in the measured MTLC and what was found in solution by ion chromatography. The concentration of nitrogen was calculated by adding the mass of nitrogen in the measured MTLC and that found in solution by ion chromatography as nitrite, nitrate and ammonium, and also the mass of nitrogen in the measured oxamic acid.

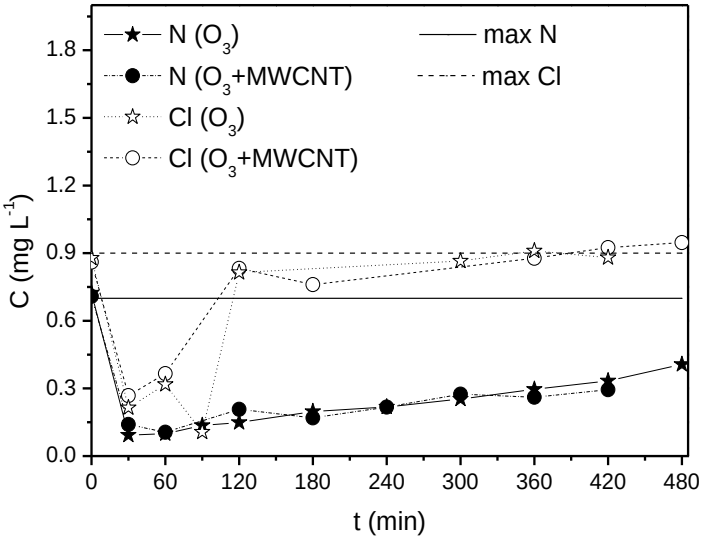

Figure 3.23 – Mass balances of chlorine and nitrogen quantified during semi-batch ozonation experiments of metolachlor.

It is noticeable that all chlorine initially present in MTLC is very quickly released to the solution. The initial decrease indicates that the primary degradation of MTLC does not involve dechlorination. In fact, a large part of chlorine is present in the intermediates formed in the beginning of the degradation of MTLC. These chlorine containing compounds are oxidized

directly by ozone, since this appears to occur similarly in both experiments [22]. After 120 minutes, the chlorine contained in MTLC was completely released into solution. Nitrogen presents a similar behaviour to chlorine, suddenly decreasing in the beginning of the reaction, due to the degradation of MTLC, and then gradually increasing during the experiments. This suggests that intermediate nitrogen containing by-products are being formed and slowly being mineralized. Contrary to chlorine, nitrogen increases much slower throughout the experiments. In fact, a great part of the expected by-products formed contain nitrogen in their structure [22, 24].

The measurements of acute toxicity in terms of inhibition of the luminescent activity of the bacteria are presented in Figure 3.24.

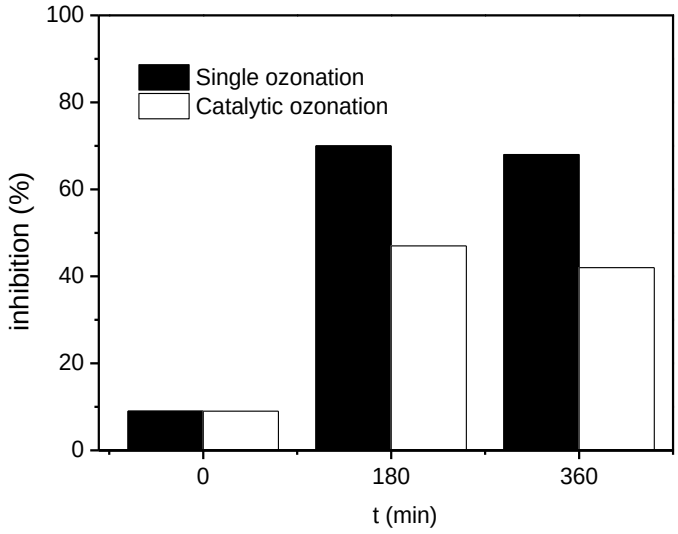

Figure 3.24 – Inhibition of luminescent activity of bacteria exposed to samples taken during semi-batch ozonation of metolachlor.

The oxidation of the parent compound results in by-products which are more toxic for *Vibrio Fischeri* than MTLC itself. The possibility of a synergistic effect among the by-products cannot be excluded [2, 21, 22]. Nevertheless, the presence of the catalyst diminishes the effect of ozonation on toxicity. This may be due to a smaller amount of compounds

toxic to these bacteria presented in solution due to a more complete and less selective oxidation of MTLC [22].

In summary, the degradation of metolachlor was easily achieved with or without the application of a catalyst. However, it was shown that this was not the case for the mineralization of the pollutant. In fact, large amounts of organic matter are still present in solution even after 8 hours of reaction in the semi-batch reactor. The presence of MWCNT in solution catalysed the oxidation of the organic matter. The mineralization degree achieved in semi-batch reactions was higher, and the reaction was shown to reach further down on the degradation chain of the herbicide when compared with single ozonation experiments.

3.3.2 CONTINUOUS OZONATION OF METOLACHLOR

The continuous catalytic ozonation process was used in the removal of metolachlor from water. For these experiments, a bubble column reactor equipped with an internal loop was used, as detailed in section *Methods and materials*. The structured catalysts used for these reactions consisted on CNF-covered honeycomb monolith, with 22 mm diameter and CNF loading of approximately 10.2%.

Since the system is being operated continuously, several samples were taken at steady state (after 2 hours) and the average values are presented. These include the removal of MTLC and TOC, the concentrations of the released inorganic ions and organic acids in the liquid phase, as well as the concentration of 2-ethyl-6-methyaniline.

In Figure 3.25 the removals of metolachlor and of TOC, as a measure of the mineralization degree achieved, are presented, together with the measured concentration of 2-ethyl-6-methylaniline at steady state.

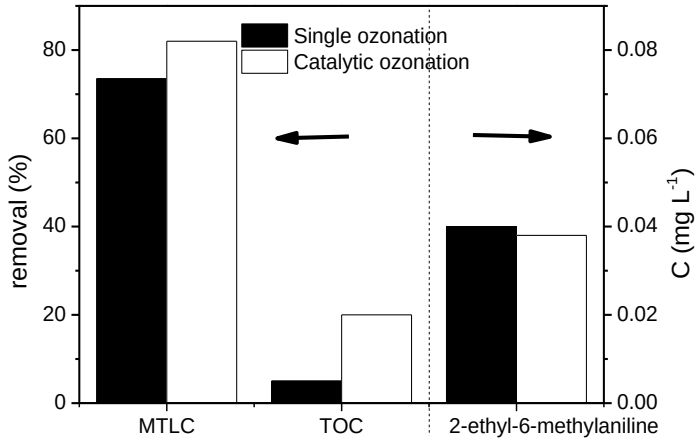

Figure 3.25 – Removal of metolachlor and TOC, and concentration of 2-ethyl-6-methylaniline, during continuous ozonation experiments, measured at steady state.

In Figure 3.25 a trend similar to that found during the semi-batch ozonation experiments is observed for the removal of MTLC and its mineralization. In this case, since the carbon material is well fixed to the structured support (previously tested by ultra-sonication), the TOC measurements were not affected by the release of carbon material to the solution. Thus, the difference between the single ozonation and the catalytic ozonation experiments, regarding the TOC values, is wider, when compared to the semi-batch experiments. The percentage of TOC removal clearly rises with the inclusion of the monolithic catalyst. This agrees with the trend that was found during the semi-batch experiments. Furthermore, the formation of 2-ethyl-6-methylaniline decreased with the presence of the catalyst, and also with longer contact times. This agrees with the trend found during the semi-batch experiments. To assess the role of the hydroxyl radicals and of molecular ozone in the degradation of this intermediate, continuous experiments were made using this compound as the starting pollutant (Figure 3.26).

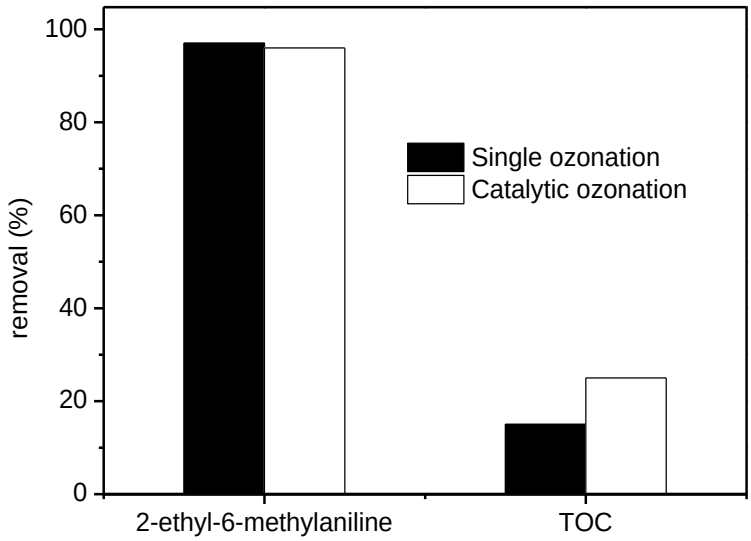

Figure 3.26 – Removal of 2-ethyl-6-methylanilineand TOC during continuous ozonation experiments, measured at steady state.

Although the inclusion of the catalyst did not enhance the degradation of 2-ethyl-6-methylaniline, the mineralization degree is improved. This agrees with the trend found during the semi-batch experiments.

An important difference is found in the organic acids and inorganic ions released into solution when compared to those found in the semi-batch ozonation experiments. The concentration of the organic acids at steady state is presented in Figure 3.27, together with the concentration of the inorganic ions at steady state.

It is likely that, given the residence (~20 minutes) and contact (~1.9 minutes) times at which the system is being operated, the mineralization of MTLC is still in its early stages, as can be attested by the values of the parent compound still present in the effluent. It is known that the hydroxyl radicals produced during catalytic ozonation are less selective than ozone [23]. It is probable that ozone is attacking specific locations of the molecule, which would explain the larger amounts of oxalic acid and chloride released into solution during the single ozonation experiment. Nevertheless, the high relative errors associated with the measurement of

chloride suggest that the observed variability in the concentrations of this ion might be due to experimental errors.

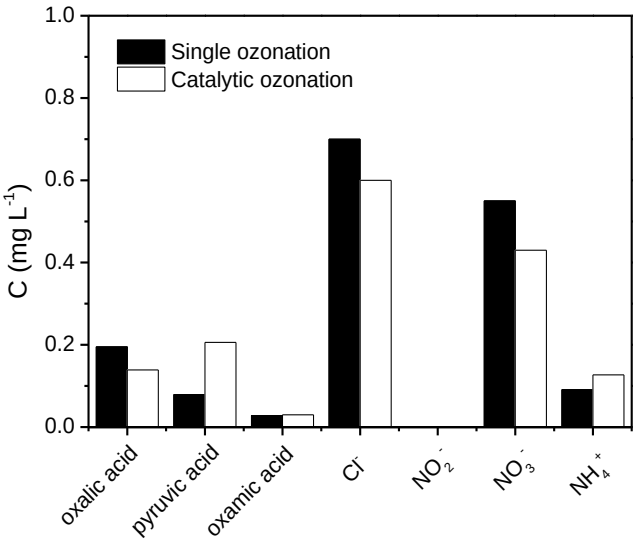

Figure 3.27 – Concentration of organic acids and inorganic ions during continuous ozonation experiments, measured at steady state.

The toxicity values obtained at steady state (Figure 3.28) corroborate the suggestion that the compounds formed present higher toxicity for Vibrio Fischeri than the parent compound [21, 22].The presence of the monolithic catalyst during the reaction reduced the toxicity values when compared to the single ozonation experiment. Longer contact times with the catalyst produced further reduced toxicity levels.

In summary, the application of a structured catalyst in the continuous ozonation experiments was shown to have potential as a solution for practical applications. The presence of the catalyst enhanced the mineralization of the organic matter in solution. The increase of the contact time with the catalyst further increased the mineralization of the organic matter in solution. The ozonation of MTLC was shown to increase the toxicity to the bacteria used to simulate the effect of the effluents produced in this study on an aquatic environment. However, it was shown

that the addition of a catalyst to the system reduces the impact of the ozonation process.

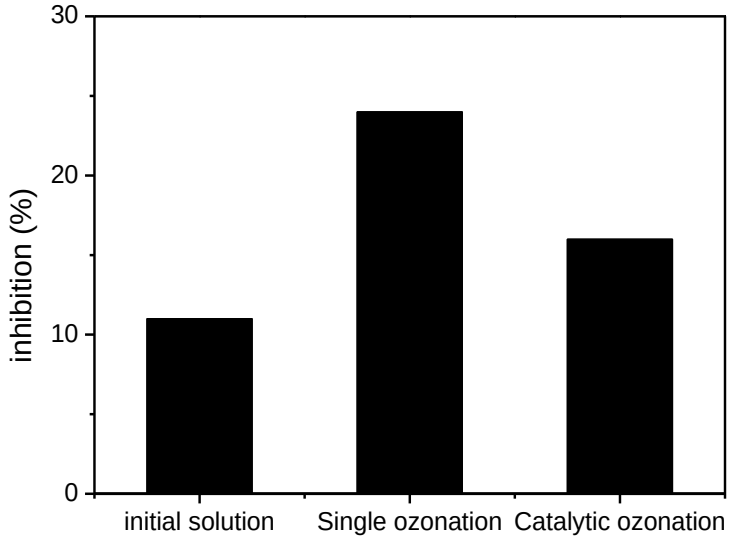

Figure 3.28 – Toxicity of the resulting effluent of continuous ozonation of metolachlor, as measured at steady state.

3.4 OZONATION OF NONYLPHENOL

3.4.1 REACTION PATHWAY AND MECHANISM

The same approach that was carried out for the other emerging organic pollutants was applied to the ozonation of nonylphenol, which was first studied using a semi-batch completely stirred reactor. It was observed that this pollutant reacted very quickly with ozone, and no nonylphenol was detected in solution after as little as 2 min of contact with ozone. For large ozone doses, the oxidation of nonylphenol has been observed to be quick [28, 29]. Nevertheless, the formation of several intermediate by-products is expected [28-34]. Even though it was not possible, in this case, to quantify the intermediates formed, the TOC content was monitored as a tool to assess the degree of mineralization achieved

during the ozonation experiments. The dimensionless TOC concentration is presented in Figure 3.29.

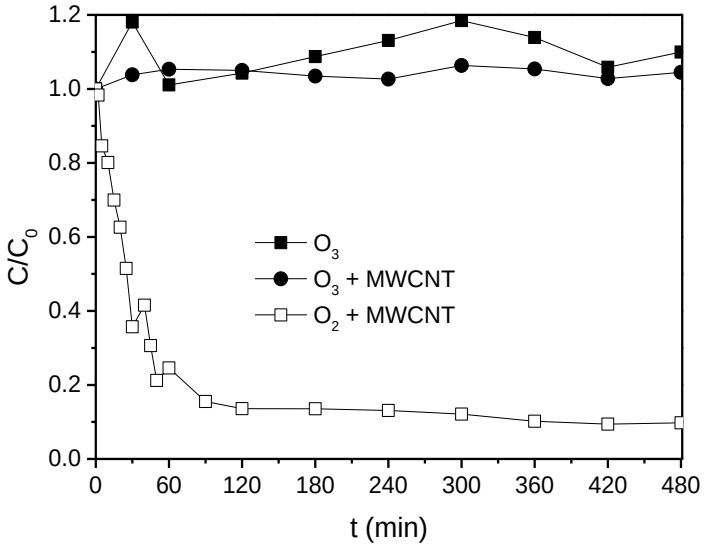

Figure 3.29 – Dimensionless TOC concentration in ozonation experiments of nonylphenol carried out in semi-batch reactor.

It is clear that, while nonylphenol is being removed by ozone, the TOC content is accumulated in solution, even for very long reaction times. Also, while adsorption experiment showed potential for a wide removal of the pollutant, such was not observed in the catalytic ozonation experiment, suggesting that the by-products of the ozonation reaction are not easily adsorbed on MWCNT.

Even though mineralization was not achieved in the ozonation experiments [29], it is likely that changes in the reaction pathway of nonylphenol are taking place due to the presence of the MWCNT catalyst. In fact, the reaction of ozone and of hydroxyl radicals with nonylphenol has been extensively studied and the product distribution is expected to be different, due to different reaction mechanisms [29, 34]. Thus, the resulting toxicity of the effluent is likely to vary with the use of a catalyst in the ozonation process [35-37]. The measured toxicity level as inhibition of

activity of luminescent bacteria throughout the ozonation experiments of nonylphenol is presented in Figure 3.30.

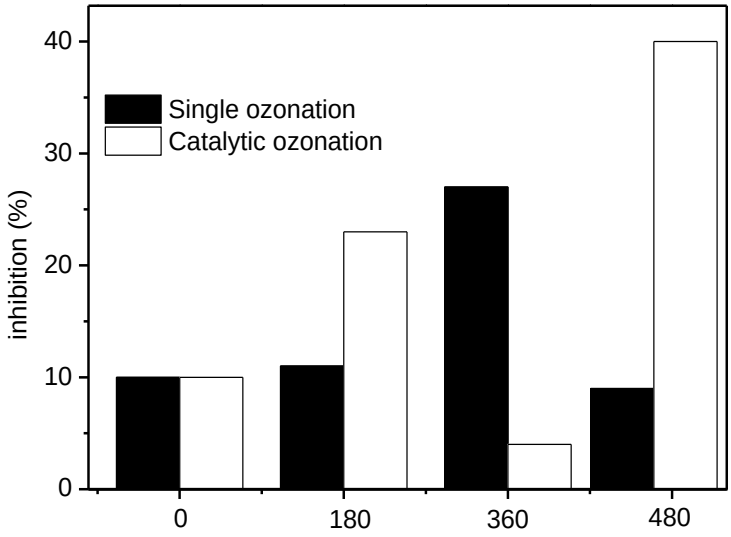

Figure 3.30 – Measured toxicity during semi-batch ozonation experiments of nonylphenol.

As expected, the measured toxicity suffered great variations throughout the ozonation experiments.

3.4.2 CONTINUOUS OZONATION OF NONYLPHENOL

The continuous ozonation process was afterwards applied to the removal of nonylphenol from water. The removals of nonylphenol and of TOC, as a measure of the degree of the achieved mineralization, observed at steady state, are presented in Figure 3.31. For these experiments, a bubble column reactor equipped with an internal loop was used, as detailed in section *Methods and materials*. The structured catalysts used for these reactions consisted on CNF-covered honeycomb monolith, with 22 mm diameter and CNF loading of approximately 10.2%.

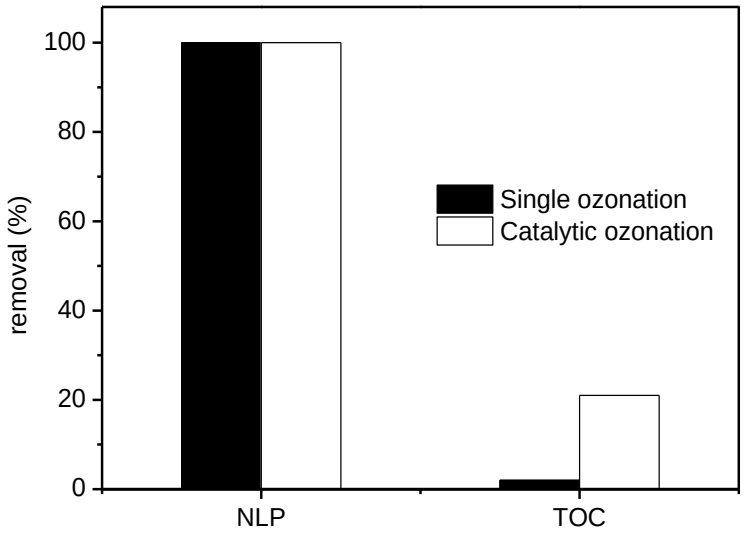

Figure 3.31 – Removal of nonylphenol and TOC during continuous ozonation experiments, measured at steady state.

As was observed in the semi-batch experiments, the removal of nonylphenol was complete during the non-catalytic and the catalytic experiment. However, it is interesting to notice that an increase in the TOC removal is observed. The removal in the catalytic experiment reaches 21%, which is a wide improvement when compared with the 2% obtained during the non-catalytic experiment. However, this observation differs greatly from what was observed in semi-batch experiments, likely due to the greater mass of CNF available for reaction, and no contribution of the carbon materials to the measured TOC value.

The toxicity measured at steady state during the continuous ozonation experiments is presented in Figure 3.32.

Much slighter variations of the measured toxicity were observed in the continuous experiments, when compared with what was observed in semi-batch. However, since the mineralization degree was very improved during the catalytic ozonation experiment, it is not expected that similar products distributions are present in solution, but rather that the small variations are coincidental.

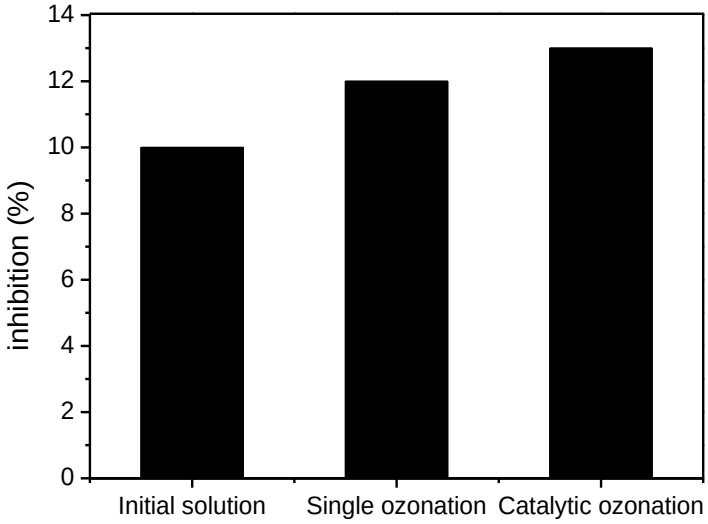

Figure 3.32 – Measured toxicity during continuous ozonation experiments of nonylphenol.

In summary, it was observed that while nonylphenol is quickly removed from solution during the ozonation process, its mineralization is not readily achieved. The changes in the product distribution have a drastic impact in the observed toxicity of the effluent. Nevertheless, mineralization was improved during catalytic continuous experiments, while the toxicity level did not increase much in these experiments.

3.5 PARTIAL CONCLUSIONS

The ozonation of three selected emerging organic micropollutants was studied. It was observed, in general, that while single ozonation was sufficient to remove readily the pollutants from water, their mineralization was not fully achieved. The application of carbon based catalysts was shown to improve mineralization, through the promoting of reactions involving radical species, taking place on the surface of the catalyst and in the solution bulk. Moreover, it was observed that the application of a catalyst has a wide impact in the distribution of the accumulated products in solution, mostly due to this promoting effect, which alters the

mechanism of degradation of the organic pollutants. Furthermore, the variation of the experimental conditions was observed to alter the predominant mechanisms taking place, and also the adsorption of the pollutants on the surface of the catalysts. The larger mineralization degree and the changes in the product distribution eventually led to changes in the toxicity of the effluents. Finally, it was also shown that the continuous ozonation process applied using a structured honeycomb monolith as a support for the carbon active phase is viable, mainly due to the improvement of the mineralization degree when compared with the conventional ozonation process.

REFERENCES

[1] K.H. Chan, W. Chu, Applied Catalysis B: Environmental, 58 (2005) 165-174.
[2] Y.-J. Lin, M. Karuppiah, A. Shaw, G. Gupta, Ecotoxicology and Environmental Safety, 43 (1999) 35-37.
[3] G.W. Stratton, Archives of Environmental Contamination and Toxicology, 13 (1984) 35-42.
[4] Y.M. Vera, R.J.d. Carvalho, M.L. Torem, B.A. Calfa, Chemical Engineering Journal, 155 (2009) 691-697.
[5] C.L. Bianchi, C. Pirola, V. Ragaini, E. Selli, Applied Catalysis B, Environmental, 64 (2006) 131-138.
[6] J. Ma, N.J.D. Graham, Water Research, 34 (2000) 3822-3828.
[7] J. Ma, N.J.D. Graham, Water Research, 33 (1999) 785-793.
[8] F.J. Beltrán, M. González, B. Acedo, F.J. Rivas, Journal of Hazardous Materials, 80 (2000) 189-206.
[9] C.S. Castro, M.C. Guerreiro, M. Gonçalves, L.C.A. Oliveira, A.S. Anastácio, Journal of Hazardous Materials, 164 (2009) 609-614.
[10] K.H. Chan, W. Chu, Applied Catalysis B: Environmental, 58 (2005) 157-163.
[11] B. Balci, N. Oturan, R. Cherrier, M.A. Oturan, Water Research, 43 (2009) 1924-1934.
[12] S. Nélieu, L. Kerhoas, J. Einhorn, Environmental Science & Technology, 34 (1999) 430-437.
[13] K.H. Chan, W. Chu, Journal of Hazardous Materials, 118 (2005) 227-237.
[14] A.G. Gonçalves, J.L. Figueiredo, J.J.M. Órfão, M.F.R. Pereira, Carbon, 48 (2010) 4369-4381.
[15] S.A. Carr, R.B. Baird, Water Research, 34 (2000) 4036-4048.
[16] A. Environmental, Microtox Manual (1—4), 1997.
[17] I.O.f. Standardization—ISO, Water Quality—Determination of the Inhibitory Effect of Water Samples on the Light Emission of Vibrio Fischeri (Luminescent bacteria test)—Part 3: Method using Freeze-Dried Bacteria, Zurich, Switzerland, 2007.
[18] P.C.C. Faria, J.J.M. Órfão, P. M.F.R., Applied Catalysis B, Environmental, 79 (2008) 237.
[19] C.J. Hapeman-Somich, G. Zong, W.R. Lusby, M.T. Muldoon, R. Waters, Journal of Agricultural and Food Chemistry, 40 (1992) 2294-2298.
[20] C. Gottschalk, J.A. Libra, A. Saupe, Ozonation of water and waste water a practical guide to understanding ozone and its application, Wiley-VCH, 2000.
[21] O. Osano, W. Admiraal, H.J.C. Klamer, D. Pastor, E.A.J. Bleeker, Environmental Pollution, 119 (2002) 195-202.
[22] V.A. Sakkas, I.M. Arabatzis, I.K. Konstantinou, A.D. Dimou, T.A. Albanis, P. Falaras, Applied Catalysis B, 49 (2004) 195-205.
[23] F.J. Beltrán, J.P. Pocostales, P.M. Alvarez, J. Jaramillo, Journal of Hazardous Materials, 169 (2009) 532-538.
[24] J.J. Pignatello, Y. Sun, Water Research, 29 (1995) 1837-1844.

[25] H.-y. Li, J.-h. Qu, H.-j. Liu, Journal of Environmental Sciences, 19 (2007) 769-775.
[26] M.L. Hladik, A.L. Roberts, E.J. Bouwer, Water Research, 39 (2005) 5033-5044.
[27] Z. Qiang, C. Liu, B. Dong, Y. Zhang, Chemosphere, 78 (2010) 517-526.
[28] J. Kim, G.V. Korshin, A.B. Velichenko, Water Research, 39 (2005) 2527-2534.
[29] B. Ning, N.J.D. Graham, Y. Zhang, Chemosphere, 68 (2007) 1163-1172.
[30] A.A. Babaei, A.R. Mesdaghiniai, N.J. Haghighi, R. Nabizadeh, A.H. Mahvi, Journal of Hazardous Materials, 185 (2011) 1273-1279.
[31] N.H. Ince, I. Gültekin, G. Tezcanli-Güyer, Journal of Hazardous Materials, 172 (2009) 739-743.
[32] M. Martínez, C. Aristizábal, G. Peñuela, Journal of Photochemistry and Photobiology A: Chemistry, in press.
[33] M. Neamtu, F.H. Frimmel, Sci Total Environ, 369 (2006) 295-306.
[34] B. Ning, N.J.D. Graham, Y. Zhang, Chemosphere, 68 (2007) 1173-1179.
[35] H. Kuramitz, J. Saitoh, T. Hattori, S. Tanaka, Water Research, 36 (2002) 3323-3329.
[36] S. Kohtani, M. Koshiko, A. Kudo, K. Tokumura, Y. Ishigaki, A. Toriba, K. Hayakawa, R. Nakagaki, Applied Catalysis B: Environmental, 46 (2003) 573-586.
[37] R. Goto, T. Kubota, Y. Ibuki, K. Kaji, A. Goto, Toxicology, 202 (2004) 237-247.

4. INFLUENCE OF OPERATION CONDITIONS

4.1 DESCRIPTION

In this chapter, the influence of several parameters in the continuous catalytic ozonation of organic pollutants, using CNF-covered structured catalysts, is assessed. The experimental set-up was hydraulically characterized, and the detailed characteristics of the hydraulic regimes developing inside the monolith channels in three-phase operation were calculated.

The role of the calculated parameters in the ozonation of organic pollutants was then evaluated. To this end, the conversion of dissolved ozone, the degradation of oxalic acid and the degradation of three selected emerging organic micropollutants were followed during several experiments. The organic pollutants used were atrazine (ATZ), metolachlor (MTLC) and nonylphenol (NLP). The performances observed were then related to the changes caused in the hydraulic regimes by the different operation conditions, when possible. On a first approach, the advantages of operating the system by placing simultaneously in contact the three-phases, gas (ozone), liquid (effluent) and solid (catalyst), were discussed. Afterwards, the influence of the size of the bubbles in the gas feed, and their relation with the channel size of the monoliths was analysed. The performance of the system at different flow rates was also evaluated. The increase of the contact area of the catalyst with the gas and liquid phases as a mean to increase the potential of the system was tested. Furthermore, the behaviour of the system when using a simulated natural water matrix, and the role of its individual components were assessed. Finally, the effect of the increase in the carbon loading of the catalysts was also analysed.

The detailed experimental methods are described in section *Methods and materials.* The experiments here performed were carried out using

catalysts that were prepared by the team of Professor Enrique Garcia-Bordejé at the Instituto de Carboquímica, in Zaragoza, part of the Consejo Superior de Investigácion Científica, in the context of projects MONACAT and FREECATS, part of the European Commission's 7th Framework program. Detailed description of these catalysts is presented in section *Methods and materials*.

The work described in this chapter has partly been published in the following references:

J. Restivo, J.J.M. Órfão, S. Armenise, E. Garcia-Bordejé, M.F.R. Pereira, Catalytic ozonation of metolachlor under continuous operation using nanocarbon materials grown on a ceramic monolith, J. Hazard. Mater., 239–240 (2012) 249-256.

S. Derrouiche, D. Bourdin, P. Roche, B. Houssais, C. Machinal, M. Coste, J. Restivo, J.J.M. Orfao, M.F.R. Pereira, Y. Marco, E. Garcia-Bordeje, Process design for wastewater treatment: catalytic ozonation of organic pollutants, Water Sci. Technol., 68 (2013) 1377-1383.

J. Restivo, J.J.M. Órfão, M.F.R. Pereira, E. Garcia-Bordejé, P. Roche, D. Bourdin, B. Houssais, M. Coste, S. Derrouiche, Catalytic ozonation of organic micropollutants using carbon nanofibers supported on monoliths, Chem. Eng. J., 230 (2013) 115-123.

4.2 HYDRAULIC CHARACTERIZATION OF THE REACTION SYSTEM

On a first approach, experiments were conducted to determine the residence time distribution (RTD) of the liquid inside the monoliths, and how the different channel density affected the distribution of the flow. The E(t) curves for the 64 and 400 cpsi monoliths are presented in Figure 4.1. These were obtained by derivation of the dimensionless profile of the tracer at the output of the reactor, which is presented in Figure 4.2. These

experiments were carried out fitting the monolith inside a column with no gas being bubbled and minimal dead volume.

The E(t) and F(t) profiles present a rough appearance which is attributed to the fact that the retrieval of each sample for analysis at the outlet took around 30 seconds, and thus the values obtained do not represent points, but rather a diffuse interval for which the average value is measured.

The mean residence times obtained by integration of the *E(t)* curves [1] were 4.3 and 6.8 min for the systems using the 64 cpsi monolith, and the 400 cpsi monolith, respectively . Blank experiment (without catalytic monolith) resulted in a residence time of 3.4 min. It is noticeable from Figure 4.1 that the 64 cpsi monolith presents a profile closer to that of a plug flow reactor, while its counterpart tends towards a flow reaction with axial dispersion of the liquid. To assess this, the tanks in series model (equation 4.1) was applied [1]:

$$F\ (\theta) = 1 - e^{-N\theta}\left[\sum_{i=1}^{N}\frac{(N\theta)^{i-1}}{(i-1)!}\right] \quad \textbf{(4.1)}$$

where *F* is the dimensionless tracer response at the outlet, *Θ* is the ratio between the time and the mean residence time, *N* is the number of tanks and *i* is an auxiliary variable. Following this procedure, it was determined that the number of tanks-in-series for which equation 1 fitted the experimental data was 2.0 and 100.0, for the 400 and 64 cpsi monoliths, respectively. Such values imply that the 400 cpsi monolith behaves much closer to a perfectly agitated stirred tank due to axial dispersion, while the 64 cpsi monolith behaves much closer to a plug reactor. The blank experimental data converged with equation 1 for 8.3 tanks in series, being placed in between the two experiments with the monoliths. While these experiments were conducted using only liquid flowing through the channels, it is expected that similar trends are observed for three-phase flow. However, it is known that such system would result in wider *E(t)* profiles, indicating a stronger axial dispersion [2].

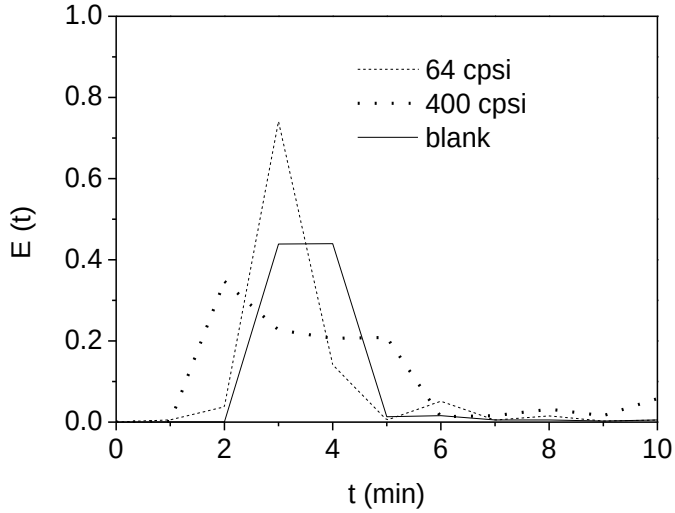

Figure 4.1 – Evolution of the derivative of the residence time distribution of the 64 and the 400 cpsi monoliths.

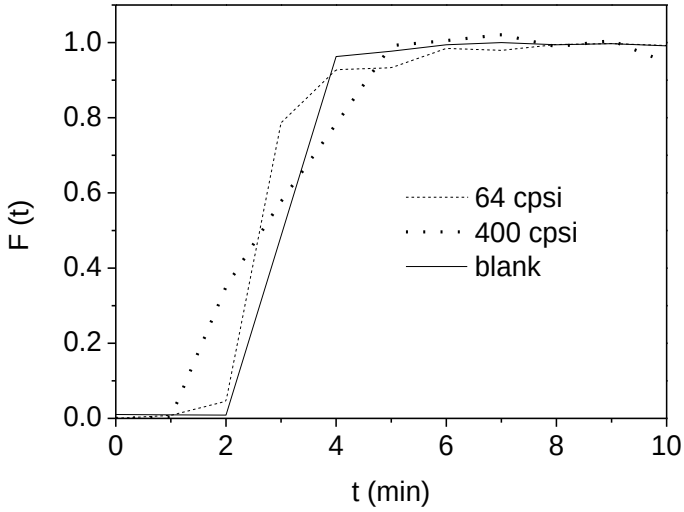

Figure 4.2 – Evolution of the adimensional tracer output on residence time experiments using the 64 and the 400 cpsi monoliths.

Several aspects of Taylor flow inside the monolith's channels are affected by variations in the operating conditions of the system, such as slug length and shape, bubble length and shape, gas hold-up, pressure drop, recirculation inside the slugs and film thickness [3-23]. These parameters control the mass transfer rate between the phases. Thus, a

characterization of the flow is essential to understand the phenomena going on inside the structured catalyst. Several parameters that characterize the hydrodynamics of the system for the whole range of operation are put together in Table 4.1 and Table 4.2, for 64 cpsi and 400 cpsi monoliths, respectively (Two-phase mean velocity (U_{tp}), liquid phase superficial velocity (U_l), gas-phase bubble velocity inside the monolith's channels (U_b), Capillary number (Ca), Reynolds number (Re), Webber number (We), adimensional film thickness (δ/R), slip ratio, gas bubble length (L_{bubble}) and liquid slug length (L_{slug})). Figure 4.3 schematically represents the characteristic physical parameters of Taylor flow.

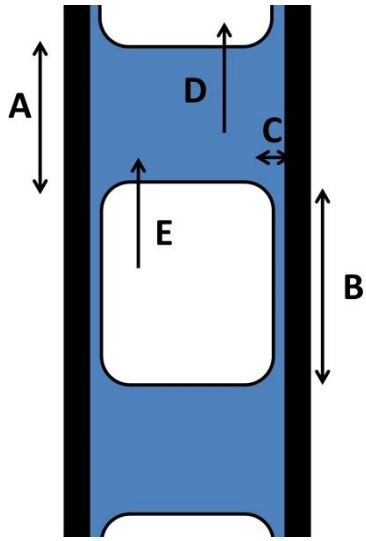

Figure 4.3 – Hydraulic parameters of interest in Taylor flow: a) liquid slug length; b) gas bubble length; c) film thickness; d) liquid slug velocity; e) gas bubble velocity.

Table 4.1 – Hydrodynamic characteristic parameters obtained for the 400 cpsi monolith.

U_{tp} (m s^{-1})	U_l (m s^{-1})	U_b (m s^{-1})	Ca	Re	We	δ/R	Slip ratio	L_{slug} (m)	L_{bubble} (m)
0.16	0.00022	0.16	2.2×10^{-5}	1.6×10^{2}	0.003	1.04 x 10^{-3}E-03	717	0.045	0.0111
0.24	0.00044	0.24	3.3×10^{-5}	2.4×10^{2}	0.008	1.37×10^{-3}	542	0.044	0.0090
0.30	0.00066	0.30	4.2×10^{-5}	3.0×10^{2}	0.013	1.62×10^{-3}	459	0.043	0.0079
0.46	0.00132	0.46	6.3×10^{-5}	4.6×10^{2}	0.029	2.13×10^{-3}	346	0.041	0.0064
0.62	0.00219	0.61	8.5×10^{-5}	6.2×10^{2}	0.052	2.61×10^{-3}	280	0.040	0.0055
0.69	0.00263	0.68	9.4×10^{-5}	6.9×10^{2}	0.065	2.81×10^{-3}	260	0.040	0.0052
0.75	0.00307	0.75	1.0×10^{-4}	7.5×10^{2}	0.077	2.99×10^{-3}	244	0.040	0.0050
0.90	0.00417	0.89	1.2×10^{-4}	9.0×10^{2}	0.110	3.38×10^{-3}	214	0.039	0.0046
0.98	0.00482	0.97	1.3×10^{-4}	9.8×10^{2}	0.131	3.58×10^{-3}	201	0.039	0.0044
1.07	0.00570	1.07	1.5×10^{-4}	1.1×10^{3}	0.158	3.83×10^{-3}	187	0.038	0.0041
1.17	0.00658	1.16	1.6E x 10^{-4}	1.2×10^{3}	0.186	4.05×10^{-3}	176	0.038	0.0040

Table 4.2 – Hydrodynamic characteristic parameters obtained for the 64 cpsi monolith.

U_{tp} (m s^{-1})	U_l (m s^{-1})	U_b (m s^{-1})	Ca	Re	We	δ/R	Slip ratio	L_{slug} (m)	L_{bubble} (m)
0.16	0.00022	0.16	2.1×10^{-5}	6.3×10^{2}	0.013	1.04×10^{-3}	712	0.0036	0.0442
0.24	0.00044	0.23	3.2×10^{-5}	9.4×10^{2}	0.030	1.37×10^{-3}	536	0.0035	0.0357
0.30	0.00066	0.30	4.1×10^{-5}	1.2×10^{3}	0.049	1.61×10^{-3}	453	0.0034	0.0314
0.45	0.00132	0.44	6.1×10^{-5}	1.8×10^{3}	0.109	2.13×10^{-3}	338	0.0033	0.0253
0.60	0.00219	0.59	8.2×10^{-5}	2.4×10^{3}	0.195	2.61×10^{-3}	271	0.0032	0.0216
0.66	0.00263	0.66	9.1×10^{-5}	2.6×10^{3}	0.239	2.80×10^{-3}	250	0.0031	0.0203
0.72	0.00307	0.72	9.9×10^{-5}	2.9×10^{3}	0.284	2.98×10^{-3}	233	0.0031	0.0194
0.85	0.00417	0.85	1.2×10^{-4}	3.4×10^{3}	0.396	3.36×10^{-3}	203	0.0030	0.0175
0.92	0.00482	0.91	1.3×10^{-4}	3.7×10^{3}	0.464	3.56×10^{-3}	190	0.0030	0.0167
1.00	0.00570	1.00	1.4×10^{-4}	4.0×10^{3}	0.555	3.81×10^{-3}	175	0.0030	0.0158
1.08	0.00658	1.08	1.5×10^{-4}	4.3×10^{3}	0.645	4.03×10^{-3}	164	0.0029	0.0151

In this work, the hydrodynamic parameters were estimated from the modelling works found in the literature, regarding three-phase flow inside capillary channels. The film thickness is a function of the velocity of the

gas and liquid phases throughout the channels. However, the gas bubble velocity inside the channels is also dependent on the film thickness, since this factor alters the gas hold-up inside the channels [24]. Thus, for a given system and liquid flow rate, it is necessary to follow a numerical approach to determine these two parameters. The iterative method proposed by Howard and Walsh [16] was followed. The iterative method consists in the following steps:

- approximation of bubble velocity,
- calculation of hydrodynamic related adimensional numbers Ca, Re and We (equations 4.2, 4.3 and 4.4, respectively),
- determination of relative film thickness (equation 4.6),
- determination of gas-phase bubble velocity inside the monolith's channels (equation 4.7),
- correction of first approximation of bubble velocity.

The adimensional parameters Ca, Re and We are widely used in the description of flows inside capillary tubes, and are described in equations 4.2, 4.3 and 4.4, respectively [25]:

$$Ca_{TP} = \frac{\mu . U_{TP}}{\sigma} \quad (\mathbf{4.2})$$

$$Re_{TP} = \frac{\rho . U_{TP} . D}{\mu} \quad (\mathbf{4.3})$$

$$We_{TP} = \frac{\rho . U_{TP}^2 . D}{\sigma} \quad (\mathbf{4.4})$$

where μ is the viscosity (Pa.s), U_{TP} (m/s) is the two-phase mean velocity, defined as $U_{TP}=U_l+U_b$, D (m) is the channel hydraulic diameter, ρ (kg/m^3) is the density and σ (N/m) is the surface tension. The hydraulic diameter of a square channel is defined in equation 4.5:

$$D_h = \frac{4A}{P} \quad (\mathbf{4.5})$$

where A is the cross section area and P is the wet perimeter.

Han and Shikazono [25] have developed an expression to estimate the adimensional film thickness that is formed around the gas bubble inside

the monolith channels, as a function of the above defined hydrodynamic parameters, described by equation 4.6:

$$\frac{\delta}{R} = \frac{1.34Ca^{2/3}}{1+3.13Ca+0.54Ca^{0.672}Re^{0.589}-0.352We^{0.629}} \quad (\mathbf{4.6})$$

where δ is the thickness of the film (m) and R (m) is the radius of the channels. This equation was built upon previous works by Taylor [26], Liu et al. [6] and Aussillous and Quéré [27]. The velocity of the gas bubbles inside the monolith's channel can be predicted through equation 4.7, as described by Howard and Walsh [16]:

$$\frac{U_b}{U_{TP}} = \frac{\left[\frac{R_b^2}{R^2}\left(\frac{\mu_f}{\mu_b}-2\right)+2\right]}{\left[\frac{R_b^4}{R^4}\left(\frac{\mu_f}{\mu_b}-1\right)+1\right]} \quad (\mathbf{4.7})$$

where U_b is the velocity of the bubble inside the monolith's channels, μ_f is the viscosity of the film and μ_b is the viscosity of the bubble.

Liquid slug length can be estimated using equation 4.8, developed by Liu et al. [6]:

$$\frac{U_{TP}}{\sqrt{L_{slug}}} = 0.088Re_g^{0.72}Re_l^{0.19} \quad (\mathbf{4.8})$$

where Re_g and Re_l correspond to the Reynolds number for the gas and the liquid phase, respectively.

Similarly, gas bubble length can be estimated directly through equation 4.9, presented by Kreutzer et al. [12, 28]:

$$\frac{L_{bubble}}{d_{channel}} = \left(\frac{\varepsilon_g}{-0.00141-1.556(\varepsilon_l)^2\ln(\varepsilon_l)}\right)\left(\frac{\varepsilon_g}{1-\varepsilon_g}\right) \quad (\mathbf{4.9})$$

where ε_g and ε_l refer to the gas and liquid hold-ups. For characteristic lengths below 250 mm, the gas hold-up can be determined from equation **4.10** and **4.11** [12, 29]:

$$\varepsilon_g = \frac{0.03{\beta_g}^{0.5}}{1-0.97{\beta_g}^{0.5}} \quad (\mathbf{4.10})$$

$$\beta_g = \frac{U_g}{U_g+U_l} \quad (\mathbf{4.11})$$

Observation of Table 4.2 and Table 4.3 leads to several readings. First of all, the values for *Ca* are very low, due to the fact that the system is being operated at low flow rate, using fluids of low viscosity. Accordingly, the Reynolds number sits firmly in the laminar region for one-phase flows. Nevertheless, both parameters raise almost one order of magnitude during the experiments varying the liquid flow rate, never overpassing the limits for application of equation 4.5, *Ca*<0.3 and *Re*<2000, except for the higher velocities in the 64 cpsi monolith [25]. The Weber number experiences a larger increase since it is related to the square of the mean superficial velocity. The values for liquid and gas velocity inside the monolith channels sit the regime inside the region for Taylor or slug flow [30], while the bubble velocity is higher than that of the liquid phase, as expected [24].

Very important in order to understand the behavior of our system are the variations in the film thickness and in the slip ratio, the latter defined as the ratio between bubble velocity and liquid phase velocity, which are represented in Figure 4.3 as a function of the superficial liquid velocity.

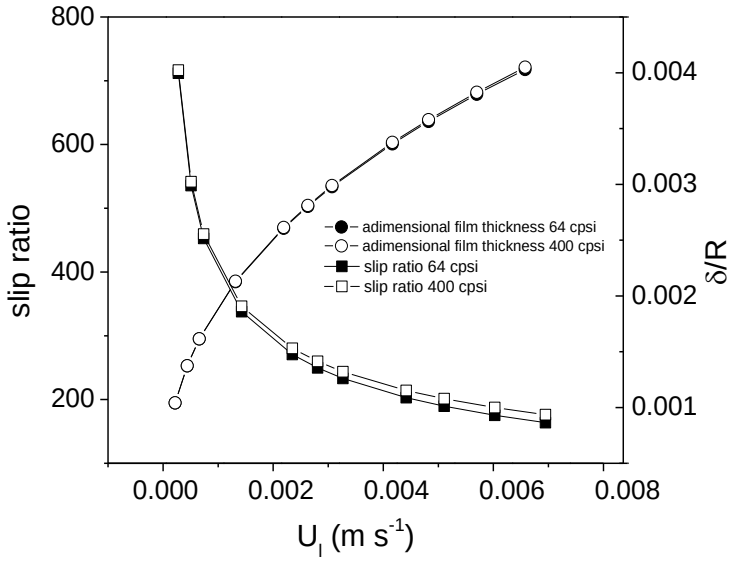

Figure 4.4 – Evolution of the slip ratio and adimensional film thickness for the 64 and 400 cpsi monoliths as function of the liquid superficial velocity.

The adimensional film thickness is seen to increase with the liquid flow rate, and consequently with the gas bubble velocity, as was expected. Such behavior has been previously observed experimentally or determined by simulation in several works [3, 9, 15, 16, 25]. The thickness of the liquid film is known to be controlled by the viscous and the surface tension forces; viscous forces are dominant at higher velocities, making the film thickness increase, while surface tension forces are more important for thinner channels, resulting on a thinner film [25]. The latter is observable in Figure 4.4; when the monolith with higher channel density was used, the calculated film thickness is slightly smaller.

The expression used for the determination of the film thickness above was determined using measurements obtained from experiments carried out using a circular capillary. Kreutzer et al. [4] note that this expressions correctly predict the thickness of the film around the corners of a square capillary that has been coated with a catalytic layer, as is the case in this work, since this results in the rounding of the corners. However, some deviation for the regions away from the corners has been observed [15]. Thus, using data from previously published experimental works [31-33], Kreutzer et al. [4] observe that the adimensional film thickness (δ/R) at low *Ca* (<0.04) is practically independent from the *Ca* value, varying between 0.95 and 0.99.

The slip ratio is diminishing with the increase of the liquid flow rate. This phenomenon is more drastic for lower values of liquid flow rate, but it is still valid for the region of higher values. Abiev et al. [5] defined a convenient relation to evaluate, through the slip ratio, the flow mode between the gas and liquid phase. This relation is presented in equation 4.12:

$$J = 2 - \frac{U_b}{U_l} \quad (\mathbf{4.12})$$

where the fraction between bubble velocity and liquid velocity corresponds to the slip ratio. For values of *J* above 0, it is expected that circulation occurs inside the liquid slugs. For values of *J* below 0, bypass of the liquid

around the bubbles is predicted, with no circulation inside the liquid flows [5]. Since the system studied in this work is operating at U_b/U_l>>>2, the flow mode taking place should undoubtedly the bypass of the liquid around the gas bubbles.

The liquid slug and gas bubble lengths for the 64 cpsi and 400 cpsi monoliths at various liquid flow rates are plotted in Figure 4.5.

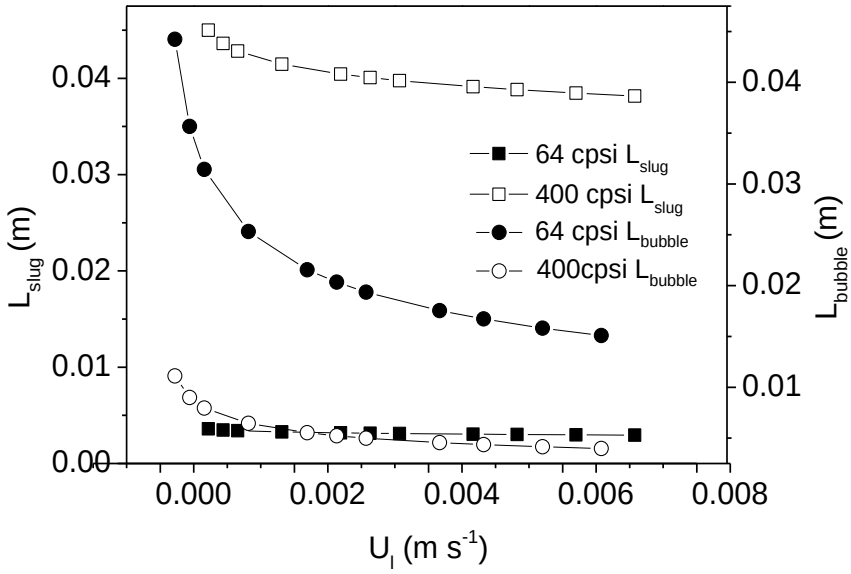

Figure 4.5 – Liquid slug and gas bubble lengths inside the 64 and 400 cpsi monoliths for different liquid superficial velocities.

For both cases the slug length and the bubble length decrease, and consequently the unit cell length as well, when the liquid flow increases. Yet, each present different proportions for the different channel densities. For the 64 cpsi monolith, the bubble length is much larger than the slug length. The opposite occurs in the case of the 400 cpsi monolith. In larger channels, the viscous forces assume a less important role in the behavior of the flow, while the dynamic forces can predominate. In smaller channels, the reverse should occur, as the different behavior of this parameter suggests. Nevertheless, the absolute values are greatly influenced by the configuration of the inlet of the fluids into the monolith [12, 13]. Such effects have yet not been properly studied but, in any case,

the trends found here seem to fit the experimental data [6]. It has been shown that liquid slug lengths can influence greatly the recirculation vortex inside the slugs. Such a vortex has been observed even for very small slugs, with its size decreasing with the increase of $L_{slug}/d_{channel}$ [20].

In the region before the gas and liquid phases come in contact with the monolith inside the bubble column, some ozone is transferred from the gas to the liquid phase. In the system used in this work, both phases are inserted into the bottom of a bubble column, travelling around 15 cm before reaching the catalytic monolith. The amount of ozone transferred to the liquid phase during this path can affect the mass transfer process inside the monolith, since the concentration in the liquid slugs and in the liquid films will differ, which can lead to saturation of the films and of the liquid slugs [34]. Similarly, the mass transfer coefficients can give some insight into what is happening inside the channels in regard of which parameters are influencing the catalytic activity of the coated monolith. Accordingly, the mass transfer coefficients were determined for the system using different bubble sizes and flow rates, using the values obtained for ozone consumption in the gas phase and dissolved ozone concentration in the liquid phase, through equation 4.13:

$$K_l a = \frac{r}{(C^* - C)} \quad \textbf{(4.13)}$$

where $K_l a$ is the mass transfer coefficient, r is the observed mass transfer rate, C is the concentration of ozone in the liquid phase and C^* concentration of ozone in the liquid phase in equilibrium with the partial pressure of ozone in the gas phase [1].

The values obtained for the mass transfer coefficient for the experiments where no catalyst was present are represented in Figure 4.6.

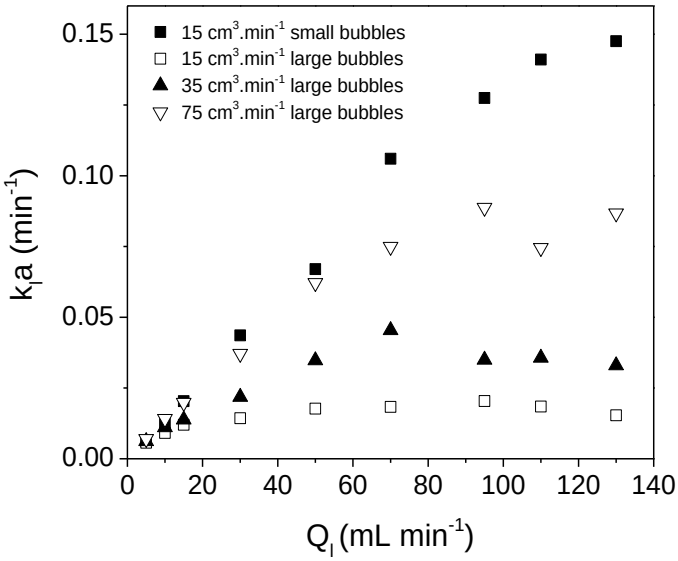

Figure 4.6 – Calculated mass transfer coefficients for the system with catalyst present at varying bubble sizes, gas and liquid flow rates.

As expected, the mass transfer coefficient is higher when smaller bubbles are used, since the interfacial area between the two phases is much higher. Furthermore, the increase in the gas flow when large bubbles were used also resulted in an increased mass transfer coefficient. While generally the increase in the liquid flow rate resulted in an increase of the mass transfer coefficient [35], for high values of Q_l when the system using larger bubbles was used, a plateau is reached after around 80 mL min^{-1}.

4.3 TWO-PHASE AND THREE-PHASE SYSTEM

To better understand and study the advantages brought by the application of a structured honeycomb catalyst to the process, some experiments were conducted in which the system was operated either as a two-phase or a three-phase system. As detailed in the *Methods and materials* section, the experimental set-up used for catalytic reactions allows the experiments to be carried out as a two-phase or a three-phase system, when considering the contact of the liquid and gas phase with the structured catalyst. In the former, the catalyst is placed inside a smaller

column that is connected to the main bubble column, inside a recirculation loop. Thus, the gas phase contacts with the liquid phase in the bubble column, and the ozonized solution contacts with the solid catalyst inside the recirculation loop. In the latter, the structured catalyst is placed inside the main bubble column, where there is a direct contact between the gas, liquid and solid phases. The recirculation loop is kept working in the same conditions as in the two-phase experiments to replicate the hydraulic conditions.

Experiments using oxalic acid as a model compound were performed, in which a CNF-covered honeycomb monolith with a CNF weight loading of ~6.04% was used as catalyst. The removals obtained at steady state are presented in Figure 4.7, where the removal obtained without catalyst (single ozonation) is also presented.

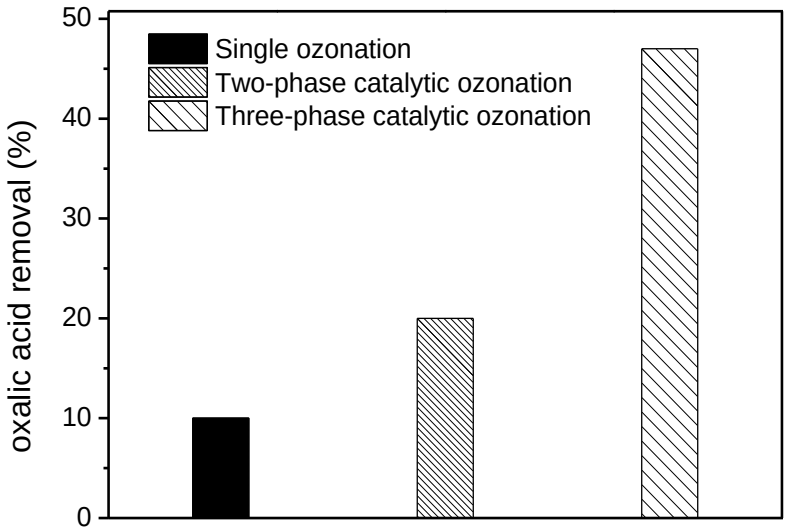

Figure 4.7 – Comparison between the steady-state removals of oxalic acid obtained under continuous operation by single ozonation, and biphasic and triphasic catalytic ozonation experiments.

It is clear that the presence of a catalyst in the system greatly improves the removal of oxalic acid from the solution due to the increased production of highly reactive species, as expected. The most interesting

aspect is the improvement of the performance when the catalytic ozonation experiment was carried out with simultaneous contact between the three phases, more than doubling the removal at steady state. The increase in removal due to the use of a catalyst was already expected, since the refractory nature of oxalic acid to direct oxidation through reaction with dissolved molecular ozone is well known [36-44]. Furthermore, at the used value of solution pH (natural pH, 3), the decomposition of ozone into more reactive compounds is known to be very slow [45].

Similarly, the same comparison was made using three model organic pollutants (atrazine, metolachlor and nonylphenol, detailed description of their oxidation in section *Ozonation of emerging organic micropollutants)*. The removal of the parent pollutants, and their mineralization degree, as measured by TOC removal, is presented in Figure 4.8.

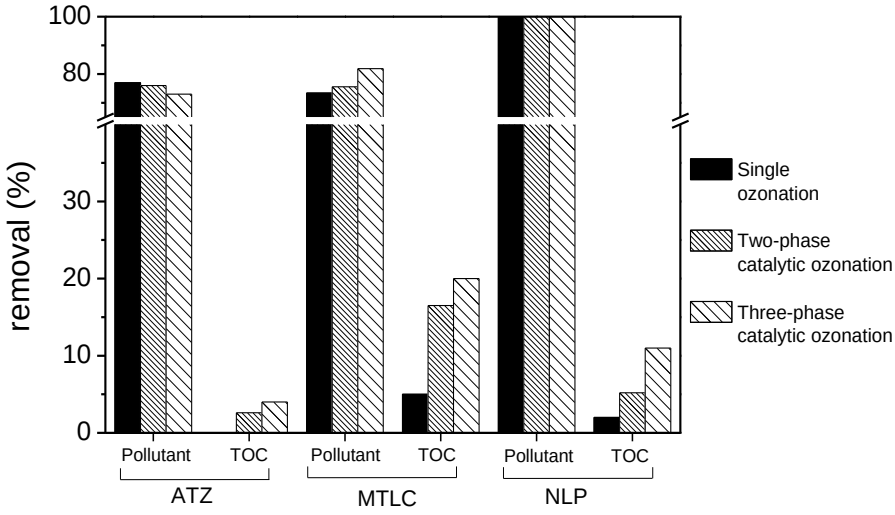

Figure 4.8 – Removal of selected emerging organic pollutants and respective mineralization degrees during continuous ozonation experiments; comparison between non-catalytic, two-phase and three-phase catalytic systems.

Concerning the removal of the selected pollutants, no clear trend was observed regarding the operation of the system in its different configurations. In fact, these pollutants are known to be easily oxidized during the single ozonation process, as reported for atrazine [46-49], metolachlor [47, 50] and nonylphenol [47, 51, 52]. Therefore, the main objective of the application of a catalyst during the ozonation process is to increase the mineralization degree. As was observed previously for the semi-batch ozonation of the selected pollutants, the catalytic system achieves a larger mineralization degree than the non-catalytic system. It is interesting to notice that, in a similar manner to what was observed with oxalic acid, the TOC removal was increased when the system was operated in its three-phase configuration. This observation is confirmed when the behaviour of the oxidation by-products is analysed, as seen in Appendix B.

While it is clear that the application of the system in a three-phase configuration, with the gas, liquid and solid phases in simultaneous contact, improves the mineralization of the selected pollutant when compared with the two-phase system, the resulting toxicity may not decrease accordingly. Since the product distribution may change between the two systems, it is possible that the three-phase system, while converting a larger amount of organic products into inorganic compounds, may alter the distribution of the compounds present in the water in a way that yields a more toxic effluent, which has been reported in some cases [46, 50, 53], and can also be observed in section *Ozonation of emerging organic micropollutants*. Thus, the resulting toxicity as measured by Microtox, in terms of inhibition of activity of the bacteria used for the test, for the continuous ozonation experiments using the three selected organic pollutants, is presented in Figure 4.9.

The toxicity exhibited by the resulting effluent from the different systems showed different behaviours for the different pollutants. In the case of atrazine, independently of the system used, the inhibition of the bacteria

increases relative to the initial solution, due to the production of intermediate products which are more toxic than the parent pollutant [54].

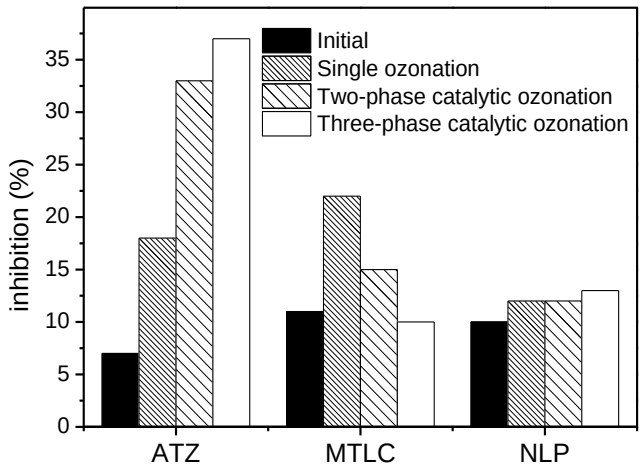

Figure 4.9 – Inhibition of bacterial activity determined by Microtox after exposure to the effluent resulting from the continuous ozonation of the selected organic pollutants using a two-phase and a three-phase configuration of the catalytic system, at steady-state.

The catalytic systems result in an even more toxic effluent, with the three-phase system reaching a maximum of 37% inhibition. Even though the mineralization degree increases when the three-phase configuration was applied, the toxicity of the resulting effluent increases due to changes in the distribution of the accumulated products, resulting on an increased production of those that have a wider contribution to this factor. In the case of metolachlor, while the oxidation of the pollutant resulted in increased toxicity in the effluent, the catalytic process efficiently reduced this factor. In fact, for the three-phase configuration, which also corresponded to the wider mineralization degree observed, the toxicity reaches levels lower than those of the initial solution. Thus, in this case, the catalytic process in the current conditions is degrading the toxic by-products being formed on a sufficient extent to lower the toxicity of the

resulting effluent. In the case of nonylphenol, very small changes were observed, which do not assume relevant significance when the associated measurement error is considered.

When the two-phase system and the three-phase system were compared, it is clear that the operation of the system with the gas, liquid and solid phases in simultaneous contact enhances the oxidative potential of the reaction system, increasing the removal of oxalic acid, and the mineralization degree of the three selected pollutants. However, in the case of the emerging organic pollutants, the increase in their mineralization does not always lead to a less toxic effluent due to changes in the distribution of the accumulated products found in the resulting effluent. The large increase in the removal of oxalic acid, and of the selected organic pollutants, when the structured catalyst was placed in direct contact with the gas and the liquid phases simultaneously, shows that there is a beneficial effect to the performance of the catalytic process in this configuration. It is well known that the formation of specific hydraulic regimes in multiphase flows inside capillary channels, such as Taylor flow, will lead to lessened resistances to mass transfer between the phases [4, 5, 8-10, 14, 15, 17, 21, 23, 55-61]. This phenomenon can be attributed to different factors, such as liquid slug and gas bubble lengths [4, 12, 14, 21, 23, 28, 61-64], recirculation vortexes formed inside the liquid slugs [5, 17, 20, 23, 62, 63] and formation of a thin liquid film around the gas bubbles inside the channel [25, 28, 57, 62, 65]. While the positive influence exerted by this configuration is clear for the catalytic reaction here studied, the influence of these factors on the performance of the structured catalyst is to be discussed in further detail below.

4.4 GAS FEED BUBBLE SIZE

Some experiments were performed to assert whether the size of the bubbles being flown from the bottom of the bubble column had any influence in the performance of the catalytic system, when the honeycomb monolith's channel size was kept constant. An example picture of the

bubbles inside the column that was used to calculate their dimension, as detailed in the *Methods and materials* section, is presented in Figure 4.10.

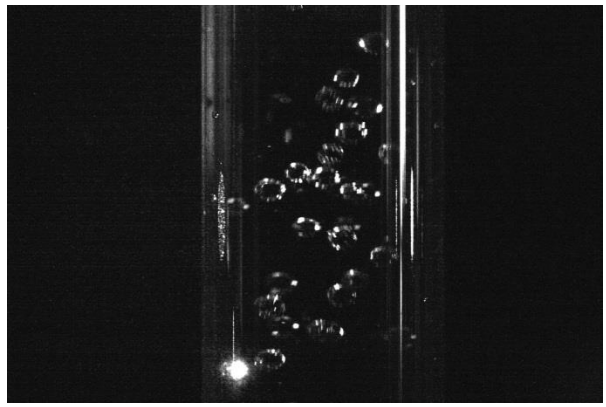

Figure 4.10 – Bubbles inside the bubble column using the glass diffuser with larger pores captured for measurements of bubble sizes.

The distributions of bubble sizes obtained from pictures of the bubbles using two different glass diffusers are shown in Figure 4.11 (glass diffuser with smaller pores) and Figure 4.12 (glass diffuser with larger pores).

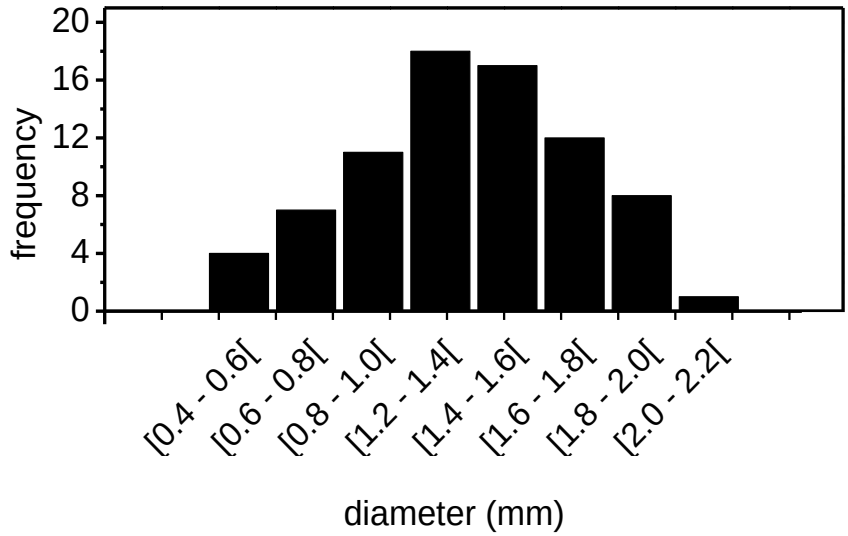

Figure 4.11 – Size distribution of the bubbles inside the bubble column using the glass diffuser with smaller pores.

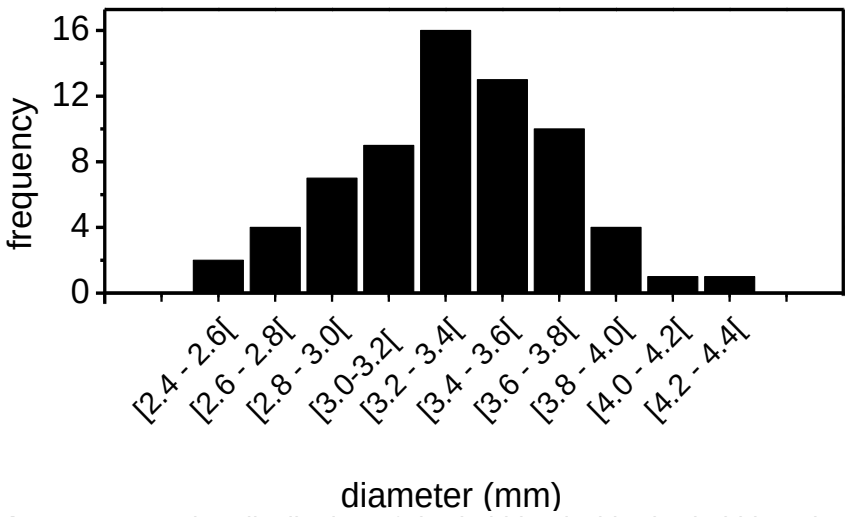

Figure 4.12 – Size distribution of the bubbles inside the bubble column using the glass diffuser with larger pores.

From Figures 4.11 and 4.12 it is clear that the use of glass diffusers with varying pore sizes result in distinctive bubble size distributions. The statistical analysis of the distributions show that the mean bubble size observed for the glass diffuser with smaller pores was of ~1.1 mm, and for the glass diffuser with larger pores was of ~3.2 mm. Standard deviation was calculated for both cases, and a value of 0.60 mm was obtained for the former, and a value of 0.39 mm was obtained for the latter.

For the two configurations of honeycomb monoliths used in this study, the square channels inner diameter was measured directly. For the 64 cpsi monoliths, the inner channel diameter was found to be 2.9 mm, and for the 400 cpsi monolith of 0.9 mm.

Experiments made using the 400 cpsi monolith showed that, for this configuration, the use of the diffuser that produced the larger bubbles resulted in coalescence of the gas at the bottom of the monolith. The gas was released only after a build-up large enough to defeat the pressure loss inside one of the capillaries was formed beneath the monolith, resulting in a deficient horizontal distribution of the gas-phase across the monolith channels. Thus, in this case, it was only possible to use the

diffuser which produced smaller bubbles in the bubble column. For the 64 cpsi monolith, which has much larger channels, this phenomenon was not observed. Therefore, it was possible to conduct experiments using the different bubble sizes with this monolith, keeping the other parameters constant (gas-phase and liquid-phase flows and ozone concentration). To assess the performance of the catalyst, the concentration of dissolved ozone was followed in experiments with no pollutant present in the water matrix. Thus, it is expected that for better performing catalytic systems, the conversion of dissolved ozone should be higher due to the decomposition of ozone into other compounds, namely hydroxyl radicals, for the more efficient operation conditions. The comparisons were made taking into account the dissolved ozone concentrations obtained in blank experiments, i.e. with no catalyst nor any pollutant present in the system, and the residence time calculated for each of the different liquid flow rates used. The improvement in mass transfer to the catalytic wall should be more important than the improvement in the transfer of ozone from the gas to the liquid phase, since the concentration in the liquid phase is already quite high when the gas and liquid phases enter the monolith channels in our reaction system. Thus, an eventual increase in liquid phase ozone concentration should not be important enough to mask an increase in the conversion of ozone at the catalytic wall, for more efficient operation conditions. In order to understand the role of the various operation parameters in the efficiency of the catalytic system, experiments were carried out to assert the behavior of the decomposition of ozone by the employed catalysts. The mass transfer inside the monolith's channels between the gas-phase and the catalytic wall occurs in a two-step process, i.e. gas to liquid film, and liquid film to wall. Furthermore, mass transfer between the caps of the gas bubbles and the liquid slugs, and subsequent transfer of dissolved gas from the liquid slug to the catalyst wall must also be considered. It has been proposed in the literature [4] that the last two steps could be considered resistances in series, and in parallel to the first step. However, each step of the mass transfer process is not perfectly independent inside the monolith, and thus it is impossible

to measure the contribution of each term to the overall mass transfer rate. The general approach for evaluation of mass transfer, with or without reaction, was to estimate the rates in function of the hydrodynamics of the flow inside the monolith's channels. In Figure 4.13, the conversion of dissolved ozone, obtained for different liquid flow rates (Q_l), for experiments using varying bubble sizes fed at the bottom of the bubble column and a 64 cpsi monolith (N-CNF 7.9 wt.%) are presented. To remove the influence of the internal loop in the concentration of dissolved ozone, and to provide wider flexibility in the liquid flow rates used, in these experiments, the bubble column was operated without the internal loop, as seen in section *Methods and materials*. The liquid flow rate was varied between 5 and 130 mL min^{-1}.

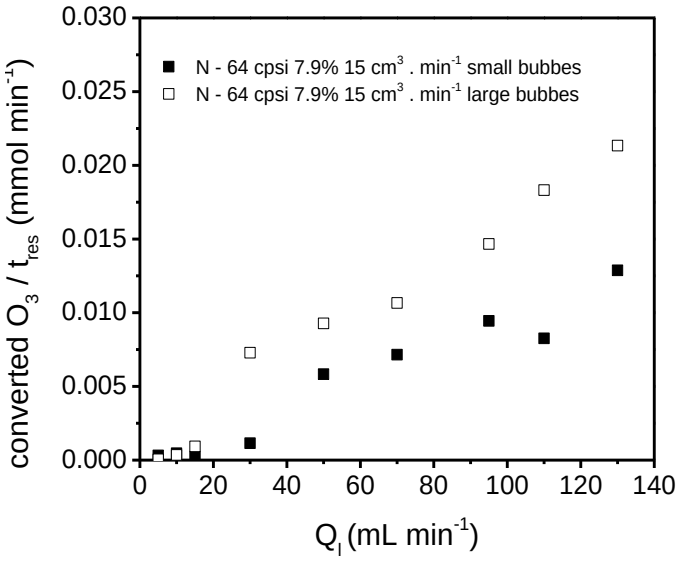

Figure 4.13 – Conversion of dissolved ozone obtained at varying liquid flow rates, using different bubble sizes fed at the bottom of the bubble column and a 64 cpsi monolith.

Analysis of Figure 4.13 shows that the application of the larger bubbles in the system with larger channel diameter results in an increase in the conversion of dissolved molecular ozone into other species, measured by the comparison between the decrease in the concentration of dissolved molecular ozone with the concentration of ozone during experiments with

no catalyst nor pollutant in solution. Such behaviour can be explained by the large distances between the gas bubbles and the monolith walls inside the channels, in the case of the smaller bubbles. In fact, while the $d_{bubble}/d_{channel}$ ratio is close to 1 for the larger bubbles, its value decreases to ~1/3 for the smaller bubbles. Such a ratio should be too small for formation of Taylor flow inside the channels of the monolith, since the gas hold-up inside the channels would be very small, resulting in the development of the regime characterized by small bubbles flowing inside the channels without interaction with the monolith walls (bubbly flow) [4].

Thus, it was concluded that for optimal operation of the system, the appropriate diffuser has to be selected for each channel density; i.e. production of smaller bubbles at the feed on the bottom of the bubble column for the 400 cpsi monoliths, and larger bubbles for the 64 cpsi monoliths.

4.5 FLOW RATES

The influence of the flow rates employed, liquid and gas, through the structured catalysts, using different monoliths and pollutants, was studied for the catalytic ozonation reaction. The observed catalytic performances were then related to the hydraulic conditions inside the monolith channels. These hydraulic conditions were estimated using experimental data obtained during the experiments and information found in the literature, namely correlations between the most important parameters and the experimental conditions used in the operation of multiphasic honeycomb reactors in catalysis. The description of these parameters and the methods used for their calculation can be found in the *Hydraulic characterization of the reaction system* section, included in this chapter.

On a first step, the influence of the gas flow rate fed into the bottom of the bubble column was asserted in experiments using a 64 cpsi monolith (CNF 11.4 wt.%), for three gas flow rates, ranging from 15 to 75 cm^3 min^{-1}. The liquid flow rate was varied between 5 and 130 mL min^{-1}. The modification of the liquid flow rate results in several hydrodynamic

changes in the system, which has various consequences in the observed behavior. First off, there will be a change in the mass transfer between the gas and the liquid phase during the column length before the catalytic monolith. The changes in dissolved ozone for the various liquid flow rates, with gas flow rate kept at 15, 35 and 75 cm^3/min and bubble size at 3.1 mm is shown in Figure 4.14. The ozone concentration in this figure is normalized by the residence time. The observed amounts of dissolved molecular ozone converted by the catalyst for each experiment are presented in Figure 4.15. The comparisons were made taking into account the dissolved ozone concentrations obtained in blank experiments, i.e. with no catalyst nor any pollutant present in the system, and the residence time calculated for each of the different liquid flow rates used.

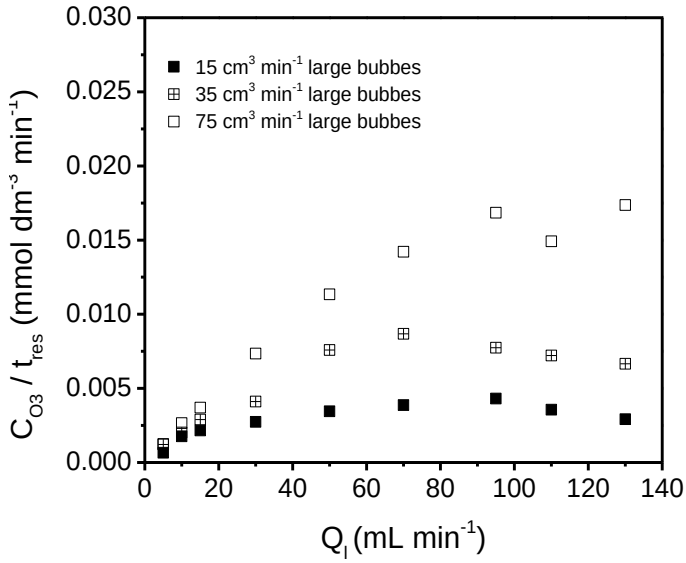

Figure 4.14 - Concentration of dissolved ozone obtained at varying liquid and gas flow rates, in experiment without catalyst.

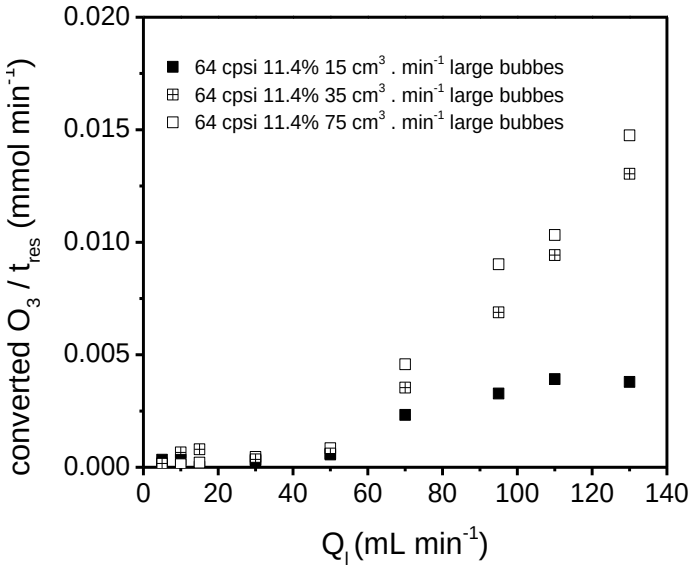

Figure 4.15 - Conversion of dissolved ozone obtained at varying liquid and gas flow rates, using a 64 cpsi monolith.

As expected, the increase in the liquid flow rate from 5 to 135 mL.min^{-1} resulted in the increase of the ozone transferred from the gas phase to the liquid phase (Figure 4.14). Also, higher values of the gas flow rate, between 15 and 75 cm^3.min^{-1} result in the increase of the dissolved ozone concentration. Furthermore, the increase of the liquid flow rate led to a more noticeable conversion of the dissolved ozone when the monolith was used (Figure 4.15).

Analysis of Figure 4.15 leads to two main observations regarding the decomposition of ozone by the studied catalysts. In one hand, the increase of the liquid superficial velocity (u_{sl}) results in a wider conversion of dissolved ozone for the catalytic experiments. On the other hand, the increase of the gas flow similarly results in an increase of this phenomenon. The latter is most likely related to the distribution of the gas bubbles throughout the several channels of the monolith, as observed during operation and as schematized in Figure 4.16. In fact, the velocity of the gas bubble inside the monolith is not necessarily connected to the gas flow used, since the gas phase is not being directly fed inside the monolith channels, but into the column containing the liquid phase before reaching

the monolith. Furthermore, the velocity of the bubbles that reach the monolith is only dependent of their own characteristics, namely their size [66], and is not related to the flow rate. The results in Figure 4.15 suggest that between the 35 and 75 $cm^3.min^{-1}$ experiments, the horizontal distribution of the gas bubbles should be similar.

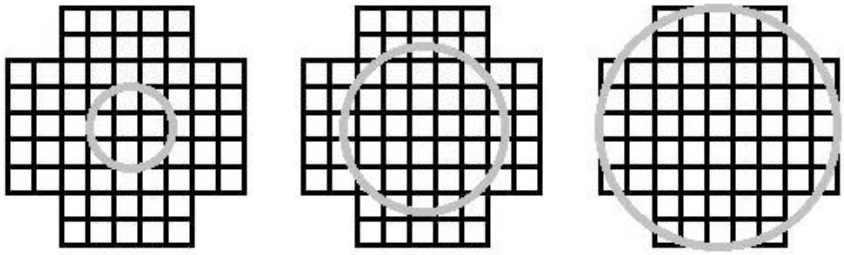

Figure 4.16 – Changes to horizontal distribution of the gas bubbles throughout the monolith channels at 15, 35 and 75 cm^3/min gas flow rate (area inside the grey circle corresponds to the channels through which the gas bubbles passed at the different flow rates).

The changes to ozone conversion observed in Figure 4.15 with the increase of the liquid flow rate may be attributed to the hydrodynamics of the flow inside the channels of the monoliths. The hydrodynamic behavior of the three phase flow inside the channels is dependent on several operation conditions, such as the channel morphology, channel diameter and phase velocities [31, 67]. Accordingly, Figure 4.17 presents the changes in dissolved ozone for various liquid flow rates, with gas flow rate kept at 15 $cm^3.min^{-1}$ and bubble size at 1.1 mm, using two monoliths with 400 cpsi and 0.9 mm square channels.

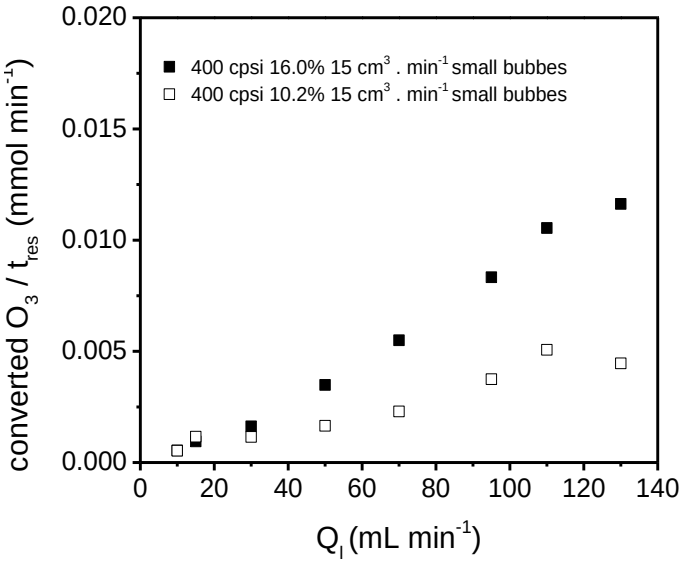

Figure 4.17 – Conversion of dissolved ozone obtained at varying liquid flow rates, using two 400 cpsi monolith.

Similarly to what was observed during the experiments using the 64 cpsi monolith, the increase of the liquid flow rate results in a wider difference in the dissolved ozone between the experiments with or without a catalyst. This difference is accentuated when a monolith with a higher loading of carbon is used, as discussed in section *Carbon loading.*

To better understand the increase on the dissolved ozone conversion for higher liquid flow rates that was observed for experiments with different gas flow rates and different monoliths, the data was compared with the calculated hydraulic parameters for the experimental conditions used, as described in section *Hydraulic characterization of the reaction system.*

On a first approach, the converted dissolved ozone values observed for the experiments at varying gas and liquid flow rates, using both the 64 and 400 cpsi monoliths, were compared with the values obtained for the slip ratio, which was calculated taking into account the different flow rates and channel diameters. The resulting curves for the 64 cpsi monolith are plotted in Figure 4.18, and for the 400 cpsi monoliths in Figure 4.19.

Analysis of Figures 4.18 and 4.19 shows that, in both configurations, the conversion of molecular dissolved ozone is maximized for lower slip ratios. Such behaviour is related to the bypass regime occurring inside the monolith channels, which is known to be prevalent for high values of slip ratio [5]. In bypass regime, there is no recirculation in the gas bubbles, which is a main factor in the improvement of the mass transfer between the gas and the liquid phase inside the monolith channels [4, 5]. The differences in the behaviour observed for the varying gas flow rates using the 64 cpsi monolith, as seen in Figure 4.18, are similar to those observed in Figure 4.15, already discussed in this section.

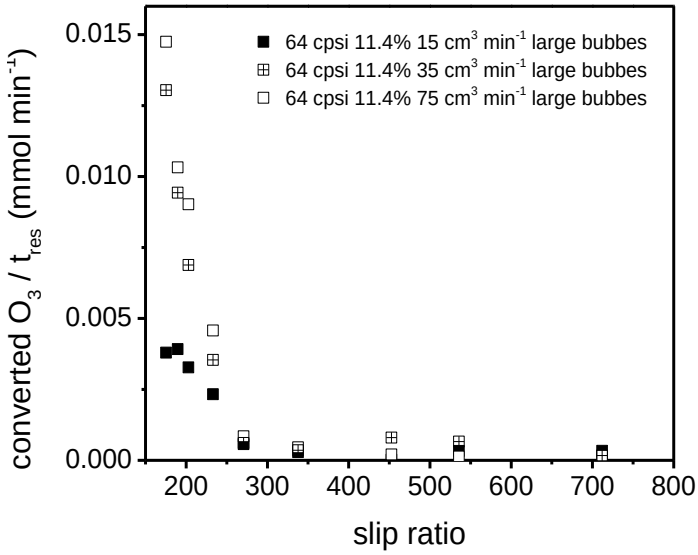

Figure 4.18 - Conversion of dissolved ozone obtained at varying liquid and gas flow rates, using a 64 cpsi monolith, as a function of the slip ratio.

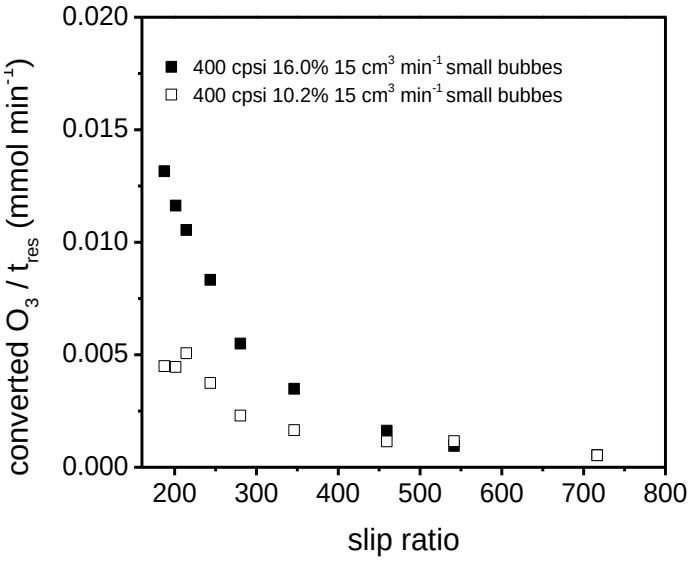

Figure 4.19 - Conversion of dissolved ozone obtained at varying liquid and gas flow rates, using two 400 cpsi monoliths, as a function of the slip ratio.

Another important hydraulic parameter is the slug length inside the monolith channels. For analysis of its effect on the conversion of dissolved molecular ozone, these values, obtained for the 64 and 400 cpsi monolith configurations, are plotted in function of the varying slug length in Figures 4.20 and 4.21.

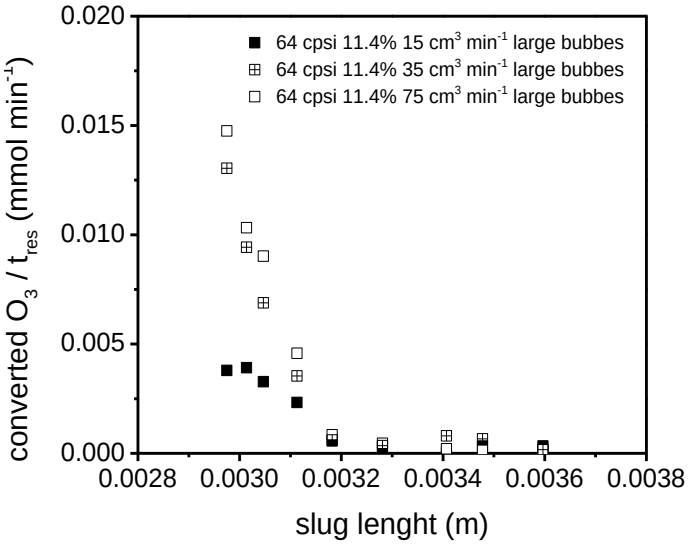

Figure 4.20 - Conversion of dissolved ozone obtained at varying liquid and gas flow rates, using a 64 cpsi monolith, as a function of the slug length.

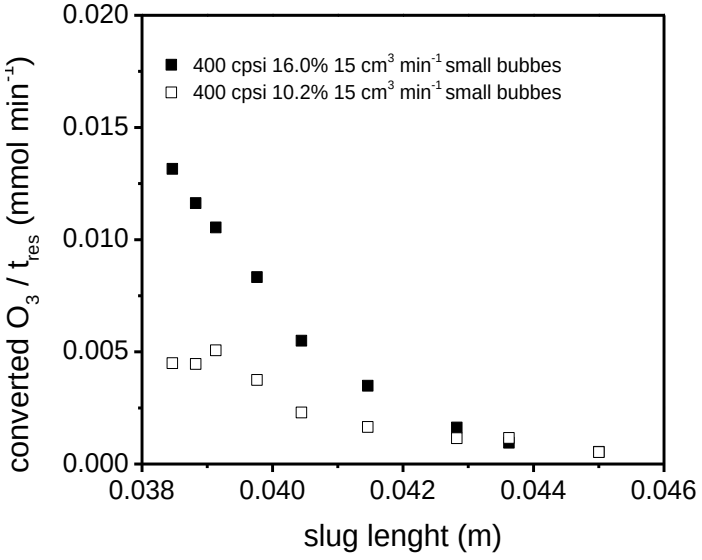

Figure 4.21 - Conversion of dissolved ozone obtained at varying liquid and gas flow rates, using two 400 cpsi monoliths, as a function of the slug length.

It is clear that the maximum dissolved ozone conversion is obtained, in all cases, for the smaller slug lengths calculated for both monolith configurations. Similarly, the gas bubble length is also an important parameter in the mass transfer between the phases inside the monolith channels. The conversion of dissolved ozone obtained for the 64 cpsi monolith, at varying gas and liquid flow rates, is presented in Figure 4.22.

The conversion of dissolved ozone obtained for two 400 cpsi monolith, at varying liquid flow rates, is presented in Figure 4.23.

Similarly to what was observed when the liquid slug length was considered, in Figures 4.20 and 4.21, the highest values for ozone conversion were obtained for the smaller calculated gas bubble lengths.

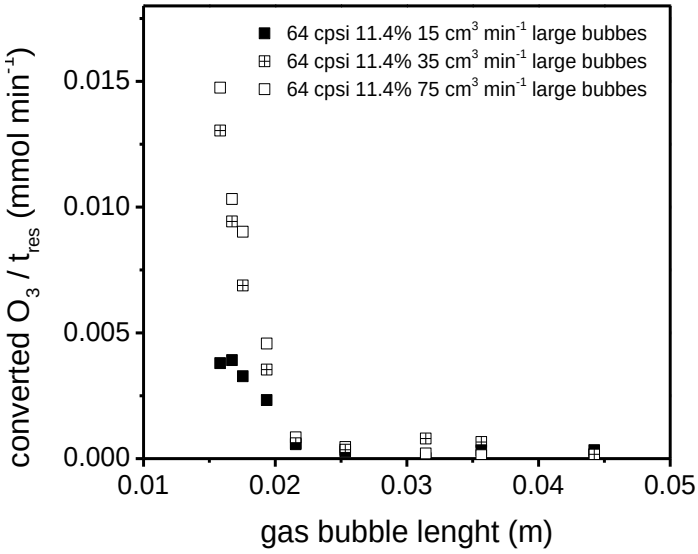

Figure 4.22 - Conversion of dissolved ozone obtained at varying liquid and gas flow rates, using a 64 cpsi monolith, as a function of the gas bubble length.

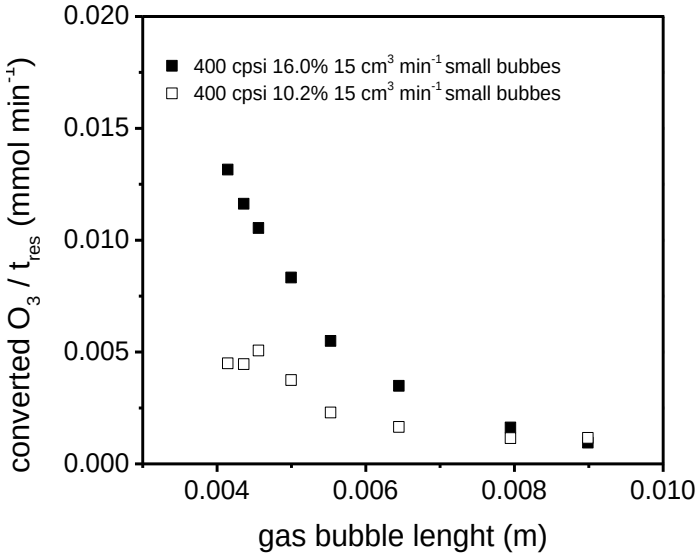

Figure 4.23 - Conversion of dissolved ozone obtained at varying liquid and gas flow rates, using two 400 cpsi monoliths, as a function of the gas bubble length.

It is known that the slug length has a large impact on the mass transfer from the liquid phase to the catalytic walls, which is the most important interface for mass transfer to the catalytic wall and is particularly evident in cases where the surface of the catalyst does not become saturated with the reactants, and when the liquid-phase has a high concentration of the gas component [14]. A similar behaviour to what is presented here was observed by Bercic and Pintar [14] for the hydrogenation of nitrite, where the conversion obtained was higher when smaller slug lengths were utilized. Furthermore, longer slugs were shown by the authors to lead to a lowered mass transfer to and from the catalyst wall and also between the gas and the liquid phase, both by mathematical prediction and by experimental measurements. Kreutzer et al. have also observed that short slug lengths are important to ensure good mass transfer from the gas to the liquid [21]. Tsoligkas et al. [63] have found that the length of the liquid slugs plays a controlling role in the mass transfer between the phases, since the recirculation time of the liquid inside the liquid slugs (number of times the slug travels its own length before a particle travels from one end

of the slug to the other) is strongly dependent on the length of the liquid slugs. Van Baten and Krishna [9] reported that the increase in mass transfer to the catalytic wall due to shorter slug lengths occurs due to an increase in the length of the liquid film around the gas bubbles, since they measured a contribution of these films to the mass transfer between 60 and 80% of the total. A similar observation is made by Ganapathy et al. [11]. On a later work, Van Baten and Krishna [55] observed that shorter liquid slugs resulted in higher values of Sherwood number, and that the wall-film interface presented poorer mass transfer values than the wall-slug interface, contrary to what was reported beforehand [9]. In fact, Kreutzer et al. [59] suggest that longer films, i.e. long gas bubbles, result in their saturation, in cases where the gas presents high diffusivity on the liquid phase. Thus, longer contact times between the gas bubbles and the films do not improve mass transfer, with predominance of the mass transfer from the liquid slugs to the monolith walls, which was also observed by Nijhuis et al. [65]. The authors go on to attribute the improvement of the mass transfer between the phases in Taylor flow to the short distances between the vortex inside the liquid slugs and the interfaces with the solid and gas phases, and to the recirculation inside the liquid slugs which results in convection of all the liquid to the channel walls, with similar residence time for all the particles [59]. The dependence of the toroidal vortex inside the liquid slugs on the slug length was also observed by Abiev [20]. Shao et al. [64] also agree that the recirculation inside the liquid slugs is responsible for the increase in mass transfer and that long gas bubbles lead to saturation of the films, and thus a decrease in the mass transfer between the phases. However, while the authors agree that short slugs improve the observed mass transfer, they argue that this is mostly due to an increase in the specific contact area, rather than due to changes in the recirculation time. A similar view was reported by Onea et al. [61].

Thus, in general, the slug and gas bubble length seems to play a pivotal role in controlling the mass transfer between the phases inside the

monolith. Short slug lengths seem to favour the process due to promotion of the liquid recirculation inside the slugs, and also due to a stronger contribution to the transfer of the reactants to the catalytic wall when compared with the liquid films surrounding the gas bubbles. For long gas bubbles, the contact time between the gas bubbles and the films increases, leading to saturation of the films, thus hindering the mass transfer through this interface. The most important path for transport between the gas and the liquid phase is from the end-caps of the gas bubbles to the liquid slugs, when the film is saturated. When saturation does not occur, the most important path between the gas and liquid phases is from the bubbles to the liquid films that surround them. Shorter liquid slugs and gas bubbles also result in larger interfacial area for mass transfer between these two phases, which may also contribute to the increase in efficiency of the catalytic process. However, since a high concentration of ozone in the liquid-phase is reached before the phases come into contact with the monolithic catalyst, this factor may not be playing a major role in the improvement of the efficiency of the system.

Consequently, it is to be expected that the maximum value for converted molecular dissolved ozone, observed for both monolith configurations, was obtained for the calculated shorter liquid slug length and gas bubble length. Nevertheless, it should be noticed that this region coincides with the region where the slip ratio was also the most appropriate for the maximum efficiency of the process (Figures 4.18 and 4.19). However, the slip ratio is particularly important when the transfer between the gas and liquid phases is the controlling step of the overall performance, which may not be the case.

Another important hydraulic parameter is the thickness of the liquid film that is being formed around the gas bubbles inside the channels of the monoliths. The observed values of converted molecular dissolved ozone at varying liquid flow rates using a 64 cpsi monolith are presented in Figure 4.24, and those obtained using two 400 cpsi monoliths are presented in Figure 4.25.

It is clear that, in both cases, the conversion of dissolved molecular ozone is increasing with the adimensional film thickness. However, this behaviour is contrary to what was expected, if considering this parameter alone. Kreutzer et al. [21] observed that mass transfer increased with the decrease of the film thickness. Van Baten and Kirshna [55] observed a similar effect, but argue that the improvement in mass transfer for thin liquid films is related to the faster saturation of the films. This leads to smaller contribution of the mass transfer through the film, which the authors have found to be less favourable than the slug-wall interface for the mass transfer process. Kreutzer et al. [34], on a later work, also state that the thinning of film only brings visible positive effects if saturation does not occur. Thus, whether due to shorter diffusional path or due to saturation of the film, the mass transfer between the three phases should improve with the thinning of the liquid film around the gas bubbles. The fact that, according to Figures 4.24 and 4.25, the conversion of molecular dissolved ozone does not improve, in your system, with the thinning of this film, suggests that this factor is not playing an important role in controlling the efficiency of the process, probably since the transfer of ozone from the gas phase to the liquid phase is not playing a major role in the control of the process efficiency in our operation conditions. It should also be taken into account that for small values of Ca, the variation of the film thickness might be too small to have a measurable impact on the observed mass transfer [4].

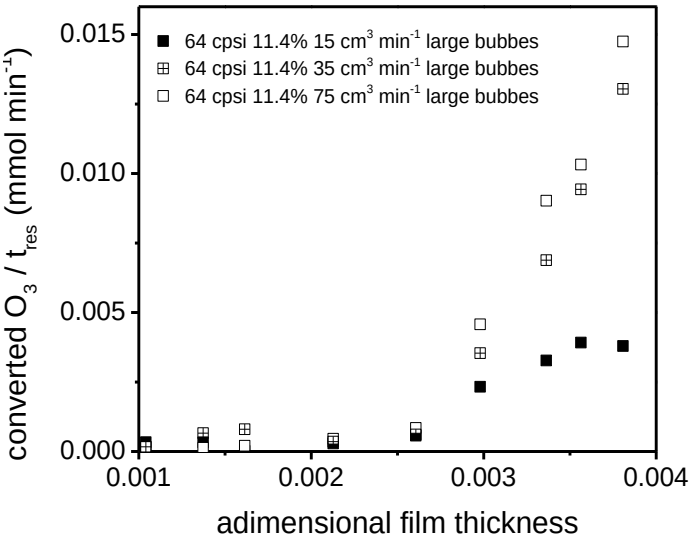

Figure 4.24 - Conversion of dissolved ozone obtained at varying liquid and gas flow rates, using a 64 cpsi monolith, as a function of the adimensional film thickness

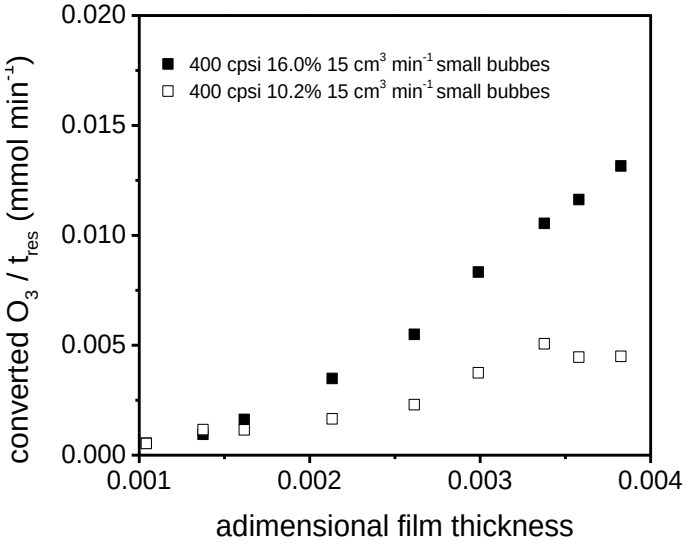

Figure 4.25 - Conversion of dissolved ozone obtained at varying liquid flow rates, using two 400 cpsi monoliths, as a function of the adimensional film thickness.

Similar experiments were performed using oxalic acid as a model compound for the efficiency of the catalytic ozonation process in the removal of recalcitrant organic pollutants from water, as detailed in the *Methods and materials* section. The conversion of oxalic acid obtained, normalized by the residence time of the liquid phase in the system, is presented in Figure 4.26, for experiments using a 64 cpsi monolith at different liquid and gas flow rates.

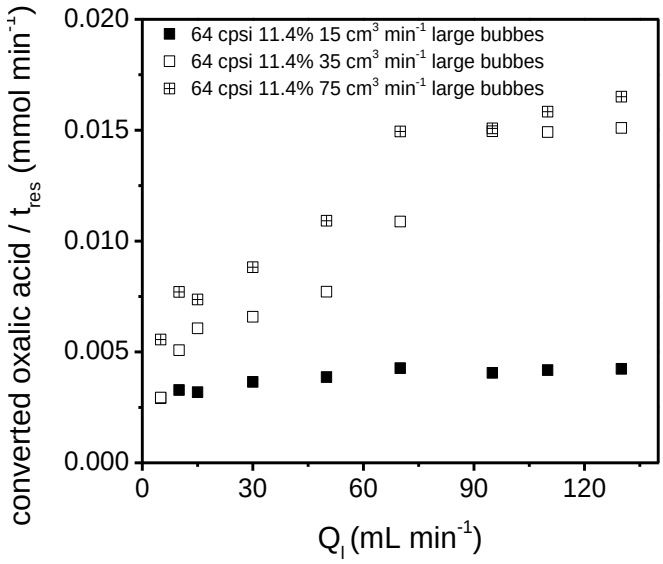

Figure 4.26 - Conversion of oxalic acid obtained at varying liquid and gas flow rates, using a 64 cpsi monolith.

As expected, the conversion of oxalic acid obtained at steady state follows the trend observed for the conversion of the dissolved molecular ozone in the experiment in the same conditions, but without the model organic pollutant (Figure 4.15). In fact, it is well known that oxalic acid is refractory to direct ozonation by molecular dissolved ozone, but, on the other hand, it is very reactive with compounds which are formed from the decomposition of ozone in water [39]. Among these compounds, it is thought that the most reactive ones are the hydroxyl radicals $OH^{\bullet}$ formed in solution. However, in the case of carbon-based catalysts, at least, it is known that the formation of surface radical species is also an important

factor in the catalytic ozonation of organic pollutants [50, 68]. The main species that are contributing for the enhancement of the degradation of the model organic pollutant are further discussed in section *Ozonation of emerging organic micropollutants*. In any case, the formation of these species is directly related to the conversion of dissolved molecular ozone, which is also here observed to be correlated with the removal of oxalic acid from solution.

It is also clear in Figure 4.26 that the larger improvement in the observed removal of oxalic acid is more noteworthy in the cases when the gas flow rate was higher. This is probably related to the phenomenon presented in Figure 4.16. For lower gas flow rates, there is a smaller horizontal cross-section of the monolith that is being used for multiphasic flow, thus the improved mass transfer between the phases due to Taylor flow effects should only take place in this area. Logically, since this area is smaller in this case, the visible effect in the degradation of oxalic acid is smaller.

It is also important to mention that the conversion of oxalic acid from solution is due to mineralization, as was observed by TOC measurements, and that no adsorption is being observed at steady-state. The monoliths were previously subject to long-term exposure to both ozone and the organic pollutants used in this work, to ensure that the measured concentration values at steady-state were not affected by adsorption phenomena. The stability and deactivation of the monoliths in catalytic ozonation is discussed in section *Stability and deactivation of the catalyst*.

Oxalic acid removal experiments were also performed at varying liquid flow rates using two 400 cpsi monoliths. The obtained removals measured at steady-state are presented in Figure 4.27.

Analysis of Figure 4.27 suggests that a very similar behaviour occurs when the 400 cpsi monoliths were applied in the catalytic ozonation of oxalic acid in continuous operation, when compared with the case of the 64 cpsi monoliths. The increase of the liquid flow rate fed into the system

lead to an increase in the amount of removed oxalic acid at steady-state. Once more, this behaviour correlates well with the conversion of dissolved molecular ozone in the same experimental conditions, without oxalic acid in solution, as presented in Figure 4.17.

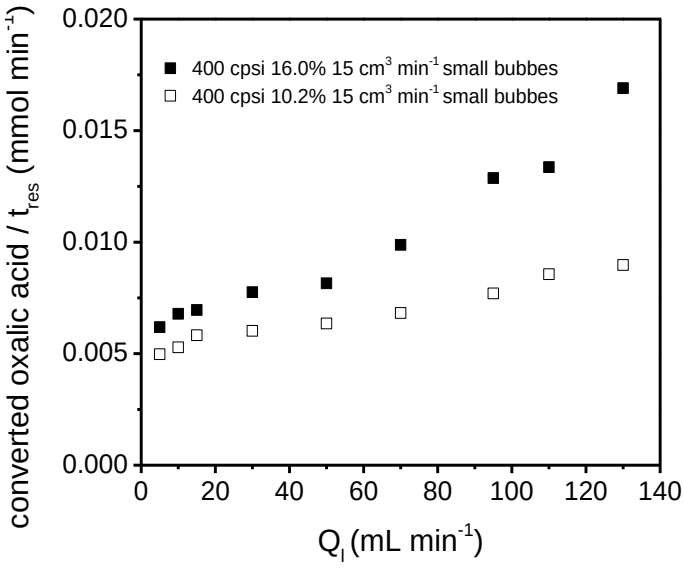

Figure 4.27 - Conversion of oxalic acid obtained at varying liquid and gas flow rates, using a 400 cpsi monolith.

The removals of oxalic acid in the different cases in function of the calculated hydraulic characteristics of the flow regime developed inside the monolith channels are not pictured here to avoid redundancy, since they follow the exact same trends observed for the conversion of ozone.

Three pathways for mass transfer in the three-phase system can be identified, as seen in Figure 4.28: a) between the gas bubbles and the liquid slug; b) between the gas bubble and the catalytic wall, through the liquid film; and c) between the liquid slug and the catalytic wall [9, 55].

Considering the possible mechanisms for catalytic ozonation using carbon as catalyst, the transfer of the organic pollutants from the liquid phase to the solid phase, the catalytic wall, is seen to assume an important role. This situation could happen if the surface reactions assume a more

prominent part when compared with the reactions taking place in the liquid bulk, between the highly reactive radicals being formed and the organic pollutant. To assess what is the contribution of the improved liquid-solid transfer of the organic pollutants in Taylor flow for higher flow rates, where the oxalic acid degradation was observed to increase, in comparison with the contribution of the liquid-solid transfer of ozone, relative increases of the observed conversion with the increase in the liquid flow rate were calculated.

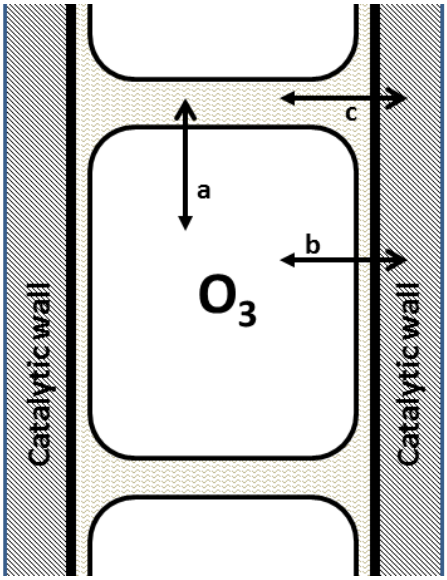

Figure 4.28 – Possible pathways of mass transfer between the three-phases involved in the reaction taking place inside the monolith channels.

The relative increases are presented in Table 4.3. These were calculated as the relative increase between consecutive points, after which the average value of these values was taken.

Table 4.3 – Increase in the conversion of dissolved ozone and of oxalic acid with the increase of the liquid flow rate during continuous ozonation experiments using 64 and 400 cpsi monoliths.

Experiment	64 cpsi 11.4% 15 $cm^3.min^{-1}$	64 cpsi 11.4% 35 $cm^3.min^{-1}$	64 cpsi 11.4% 75 $cm^3.min^{-1}$	400 cpsi 16.0%	400 cpsi 10.2%
conversion of dissolved ozone	34%	49%	47%	23%	16%
removal of oxalic acid	2%	14%	13%	14%	7%

It is clear that, for all cases, the increase of the conversion of dissolved ozone is larger than that of the removal of oxalic acid when the liquid flow rate is increased. This suggests that the transfer of oxalic acid from the liquid phase to the catalytic wall, where it may react with highly-reactive surface species, is the limiting step in the three-phase configuration of the continuous ozonation system. The transfer of ozone from the gas-phase to the liquid-phase, through the bubble endcaps, or from the gas bubbles to the catalytic wall, through the liquid film, should not be playing an important role due to saturation of the liquid phase, attributed to the contact of the gas and liquid phases before reaching the catalyst placed in the bubble column. In cases when the liquid-phase is close to saturation when concerning the compounds present in the gas phase, it is expected that the interface between the liquid slugs and the catalytic wall (Figure4.28, c)) is the major pathway for mass transfer to and from the catalytic wall [34, 55, 59, 61, 64]. In fact, the catalytic wall in contact with the liquid phase has been suggested to be the most important interface for reactions taking place on the surface of the solid catalyst [14]. Thus, the improvement in the conversion of oxalic acid can be attributed to the

enhanced mass transfer of oxalic acid and ozone to the catalytic wall, which can be attributed to the improved recirculation inside the liquid slugs [5, 34, 59, 61, 63, 64], which is seen to be highly dependent on the length of the liquid slugs [5, 23, 63] and the bubble velocity [5]. Similarly to the ozone conversion, the removal of oxalic acid improved with the decrease in slug length for all the cases. The expected contribution of the increase in the film thickness to hindering the mass transfer between the phases is not observed, since it is less important than the other factors at play.

The role of the gas and liquid flow rates in the catalytic ozonation process was also assessed using three emerging organic micropollutants: atrazine, metolachlor and nonylphenol. The detailed ozonation of these pollutants is discussed in the section *Ozonation of emerging organic micropollutants.* For these experiments, the experimental set-up was operated using the internal loop, as opposed to the experiments carried out without any pollutant or with oxalic acid. The flow of the internal loop was varied between two flow rates, 60 and 150 cm^3 min^{-1}. The feed flow rate was kept at 12 cm^3 min^{-1} for all the experiments. The gas flow rate was kept at 15 cm^3 min^{-1} for the experiments with the 400 cpsi monoliths, and at 75 cm^3 min^{-1} for the experiments with the 64 cpsi monolith. Initial concentrations of the selected pollutants were of 20 mg L^{-1} for atrazine, 10 mg L^{-1} for metolachlor and 6 mg L^{-1} for nonylphenol. The behaviour of the ozonation by-products is described in Appendix B.

The removals of the three selected pollutants, obtained using the 64 cpsi monolith, at different loop flow rates, and the amount of TOC removed during the same experiments, are presented in Figure 4.29.

The larger loop flow rate leads to a slight increment in the removal of the parent pollutant, which is not particularly relevant here. However, it is noticeable that the mineralization degree is considerably improved with the increase of the loop flow rate, for all the three pollutants studied here. The improved mineralization degree is consistent with what was observed when several liquid flow rates were assessed using oxalic acid as a model

compound. While the organic pollutants used in these reactions are easily degraded by molecular ozone in solution, the mineralization is improved by reactions occurring at the surface of the catalyst between the pollutants and highly-active surface species [46, 47, 50, 53] (see section *Ozonation of organic emerging micropollutants*).

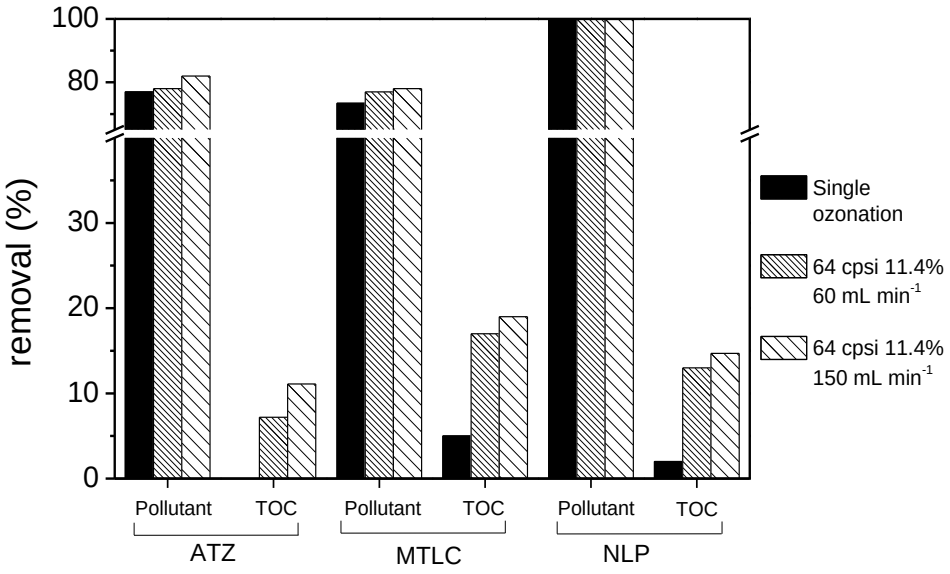

Figure 4.29 - Removal of selected emerging organic pollutants and respective mineralization degrees during continuous ozonation experiments; comparison between non-catalytic and catalytic systems at different loop flow rates, using 64 cpsi 11.4% monolith.

Similar experiments were conducted using the 400 cpsi 16.0% monolith, using the same three model organic pollutants and the same variations to the loop flow rate. The achieved removal of the pollutants and their mineralization degree as measured by TOC removal are presented in Figure 4.30. The behaviour of the by-products of ozonation is detailed in Appendix B.

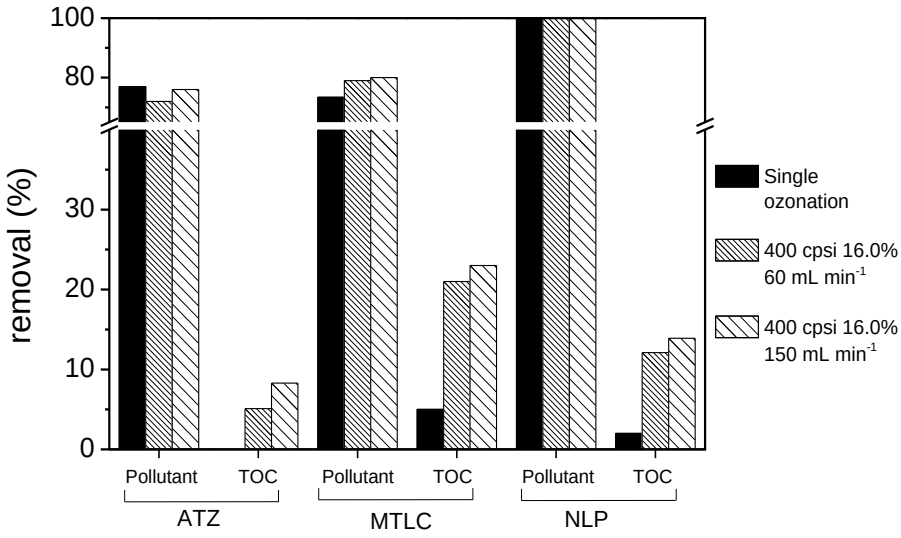

Figure 4.30 - Removal of selected emerging organic pollutants and respective mineralization degrees during continuous ozonation experiments; comparison between non-catalytic and catalytic systems at different loop flow rates, using 400 cpsi 16.0% monolith.

Similarly to what was observed in the case of the 64 cpsi monolith, the increase in the loop flow rate lead to a higher mineralization degree, while no significant changes were observed in the removal of the parent organic pollutants. Such behaviour reinforces the idea that a promotion of the reactions occurring at the surface of the catalyst is being promoted when the liquid flow through the channels of the monoliths is increased.

The toxicity of the resulting effluents, as measured by the inhibition in the luminescent activity of a bacteria medium subject to samples taken at steady-state following the Microtox procedure, is presented in Figure 4.31 for the three selected pollutants, using the 64 and 400 cpsi monolith at different liquid loop flow rates.

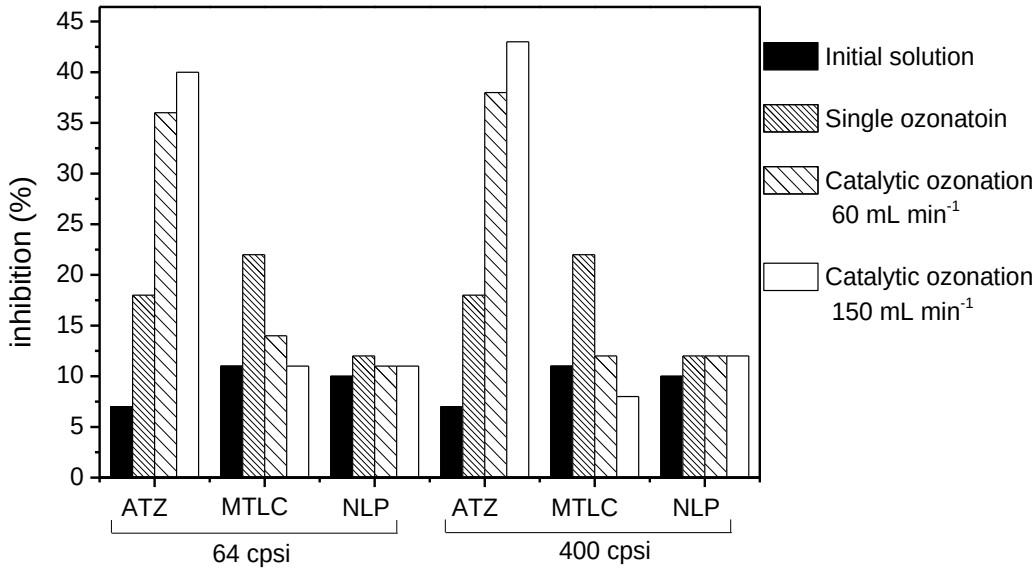

Figure 4.31 – Inhibition of bacterial activity determined by Microtox after exposure to the effluent resulting from the continuous ozonation of the selected organic pollutants using 64 and 400 cpsi monoliths at different liquid loop flow rates.

The observed toxicity of the resulting effluents presented a behaviour in accordance with the mineralization degree achieved in these experiments, following the trends that were observed for the ozonation of these pollutants in semi-batch operation, considering the retention times in question (see section *Ozonation of emerging organic micropollutants*). While the further mineralization degree of atrazine corresponded to a more toxic effluent, due to changes in the product distribution, the toxicity of the effluent resulting from the ozonation of MTLC decreased as the loop flow rate increased. The toxicity of the effluent resulting from the ozonation of nonylphenol remained approximately constant.

In summary, changes to the flow rate of the liquid and gas phases are able to alter the performance of the catalytic ozonation system. The increase in the gas flow rate affected mostly the horizontal bubble

distribution throughout the monoliths' channels. Thus, a larger gas flow rate, besides contributing to an increased mass transfer between the gas and liquid phases in the bubble column, below the monolith, also contributes to the establishment of a three-phase system in a larger number of channels. Changes to the liquid flow rate lead to changes in the flow regime that is established inside the monolith channels in three-phase operation, which were shown to have an impact in the performance of the system. In general, the mass transfer from the gas-phase to the liquid-phase inside the monolith channels should be improved due to changes in the slip ratio between the two phases. A large slip ratio will lead to bypass regime, which does not favour the process. On the other hand, large concentrations of ozone in the liquid-phase inside the monolith channels, due to prior contact between the phases, will diminish the role played by the transfers occurring in this interface. Then, the increase in the liquid flow rate may play a larger role regarding the enhancement of the recirculation inside the liquid slugs formed inside the channels, and thus facilitating the transfer of the organic pollutants and of ozone to the catalytic wall, improving the rate of reactions occurring preferably on the surface of the solid catalyst. In this case, the main pathway for mass transfer to and from the catalytic wall would be from the liquid slugs to the wall, rather than through the film formed around the gas-bubbles. The results obtained suggest that the increase in the liquid flow rate is important to enhance the rate of the reactions occurring on the catalytic wall, while contributing to a larger concentration of ozone in the liquid phase.

4.6 CONTACT AREA

The influence of the contact area available for reaction, i.e. the surface area of the monolithic catalyst, was assessed in the catalytic ozonation of, on a first approach, oxalic acid, and later using the three selected emerging organic micropollutants, atrazine, metolachlor and nonylphenol.

The contact area was varied through the addition of several identically prepared monoliths in series inside the bubble column. By placing four monoliths in series instead of one, the area available for reaction increases four times. The monoliths used in these experiments consisted in 400 cpsi monoliths with a CNF loading between 10 and 11 wt.%. The experiments were carried out using a loop flow rate of 60 mL min^{-1} and a feed flow rate of 12 mL min^{-1}.

The removals of the organic pollutants during ozonation experiments obtained using the configuration with one monolith and with four monoliths are presented in Figure 4.32, together with the mineralization degree achieved. Behaviour of the formed intermediates is discussed in Appendix B.

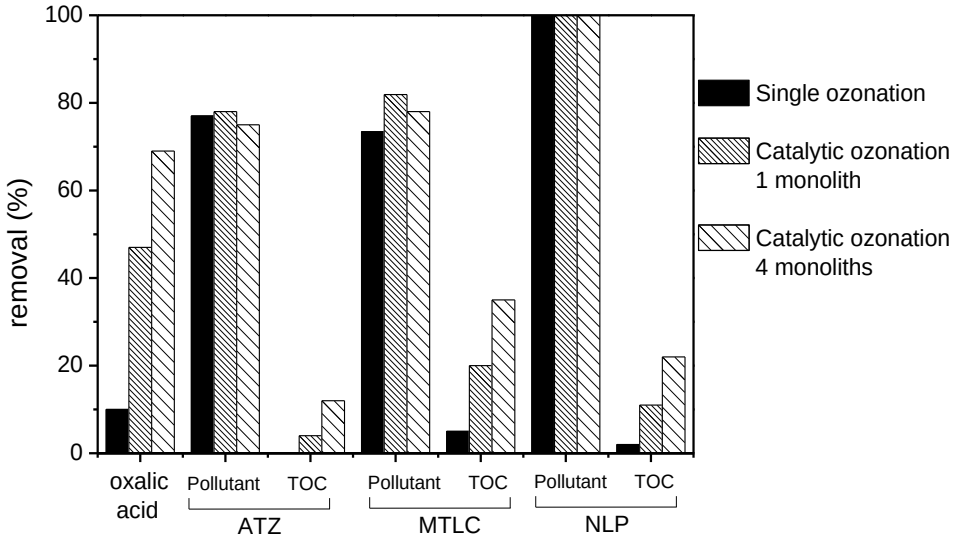

Figure 4.32 - Removal of oxalic acid and selected emerging organic pollutants and respective mineralization degrees during continuous ozonation experiment with different catalyst contact areas available for reaction.

The larger contact area available when the configuration using four monoliths in series is used promoted larger degradation of oxalic acid, for which the reactions occurring on the surface of the catalyst are known to

play an important role [39]. Regarding the three organic pollutants, the increment in contact area does not seem to play an important role in the removal of these pollutants from solution. These are known to react promptly with molecular ozone, and thus the decomposition of ozone by action of the catalyst, or the reaction of the pollutants on the surface of the catalyst, does not play a major role here [46, 47, 50, 53] (see section *Ozonation of emerging organic micropollutants*). On the other hand, the mineralization degree was remarkably improved with the increase in contact area. Surface reactions are shown to be playing a major role in improving the mineralization degree.

The toxicity of the resulting effluents was also measured by the standard Microtox test. The measured inhibition of bacterial activity caused by the resulting effluents is presented in Figure 4.33.

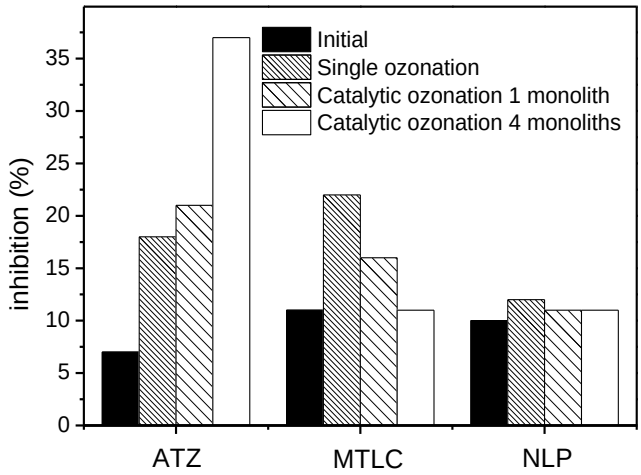

Figure 4.33 – Inhibition of bacterial activity determined by Microtox after exposure to the effluent resulting from the continuous ozonation experiment with different catalyst contact areas available for reaction.

While the increase in contact area lead to reduced toxicity of the effluent after ozonation in the cases of metolachlor and nonylphenol, the same did not happen in the case of atrazine. The production of more toxic

intermediates was still occurring, even when considering the wider extent of mineralization observed.

In summary, the increase in the contact area of the catalyst with the gas and liquid phases improves the potential of the ozonation system to further mineralize emerging organic micropollutants. The toxicity of the resulting effluents is still widely affected by the distribution of the accumulated intermediates in solution.

4.7 WATER MATRIX

In order to assess the potential of the catalytic ozonation process using monolithic structured catalysts to be applied to a real effluent, experiments were carried out using a simulated natural water matrix. The components of the matrix are described in detail in the *Methods and materials* section.

On a first approach, experiments were carried out using atrazine, metolachlor and nonylphenol. The catalytic ozonation experiments were carried out using a three-phase configuration with four monoliths in series, using a loop flow rate of 60 mL min^{-1}. The removals of the organic pollutants and their corresponding mineralization degree obtained in experiments using ultrapure water (UP) and natural water (NW) are presented in Figure 4.34. The behaviour of the main identified intermediates is discussed in Appendix B.

It is observable that the catalytic system increases the mineralization degree at steady state, from 0 to 12%. Blank experiments were made where no ozone was fed into the system. In these cases, no significant removal of the pollutants were witnessed, and thus adsorption does not seem to play a major role in the TOC removal accounted for in this section. The removal of the parent pollutant seems to be improved by using the natural water matrix, when compared with the ultrapure water matrix. Since the HCO_3^- present in the natural water matrix acts as a radical scavenger [45], it is likely that more ozone is available in solution to react directly with atrazine, in this case. However, no difference was

observed in the mineralization degree, which suggests that the reactions of the oxygenated radicals, necessary for the mineralization of atrazine, occur mainly on the catalyst surface [39]. Considering metolachlor, performances are similar to what was observed in the case of atrazine. However, there is a decrease in the mineralization degree during the catalytic experiment using natural water in comparison to ultrapure water. Contrary to the case of atrazine, this suggests that there was some inhibition caused by the inorganic compounds in the water matrix. In the case of nonylphenol, complete removal of nonylphenol was achieved in all experiments. However, the mineralization degree was greatly improved when the catalytic process was used. Similarly to atrazine, the different water matrices did not alter the mineralization degree, which indicates that the reactions of the intermediates with hydroxyl radicals occur mainly on the catalyst surface.

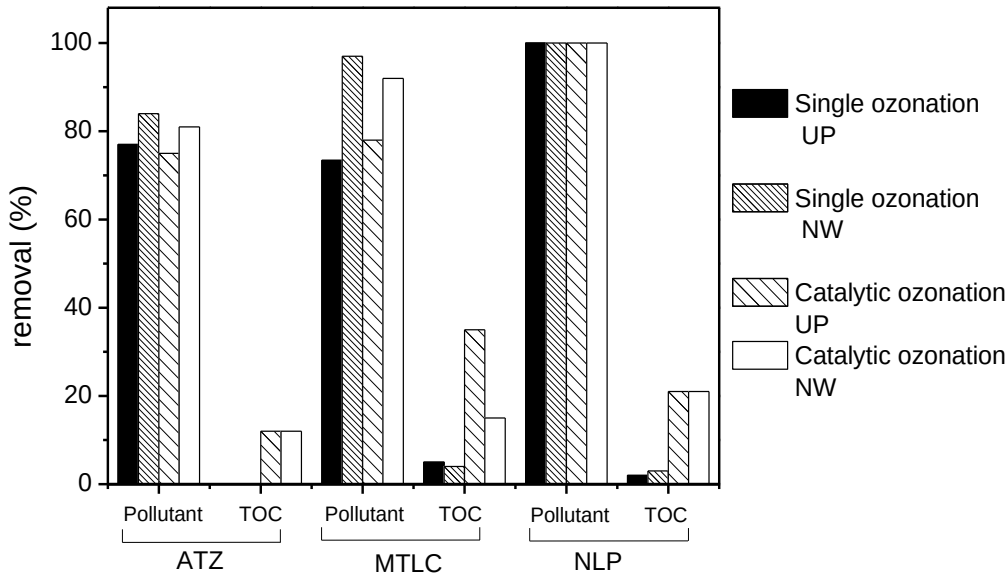

Figure 4.34 - Removal of the selected emerging organic pollutants and respective mineralization degrees during continuous ozonation experiment with different water matrices.

Another important parameter to evaluate the final effluent is the acute toxicity, which is presented in Figure 4.35, as the inhibition of the

luminescent activity of standard bacteria when exposed to each effluent for 30 min.

Observing the experiments with atrazine, the single ozonation process in ultrapure water resulted in a more toxic effluent than the initial solution for the *Vibrio Fischeri* bacteria. Additionally, the catalytic process caused an even larger increase in toxicity. It is thus clear that the intermediates formed during the degradation of atrazine are more toxic than the parent compound. When the natural water matrix was used, the toxicity remained almost constant, even decreasing slightly for the catalytic ozonation process. This most likely results from the different degradation pathways for each process, as can be seen by the differences in concentration of the quantified intermediates, resulting in degradation products with variable toxicity levels [69]. Considering the metolachlor experiments, the single ozonation process results in intermediate products that are more toxic than the parent compound. The natural water matrix leads to a more toxic effluent, which is probably related to the inhibition in the mineralization that was observed. The presence of a catalyst considerably reduces the toxicity of the effluent. This can be related in part to the production of 2-ethyl-6-methylaniline, which is known to be one of the major contributors to the toxicity value [70]. However, since the difference between concentration are somewhat subtle, this effect is probably not the unique responsible for the variation of toxicities, but is an indicator of a difference in the degradation pathways of the two processes (single and catalytic ozonation). The toxicity of the resulting effluents from the ozonation of nonylphenol was very similar to that of the initial solution.

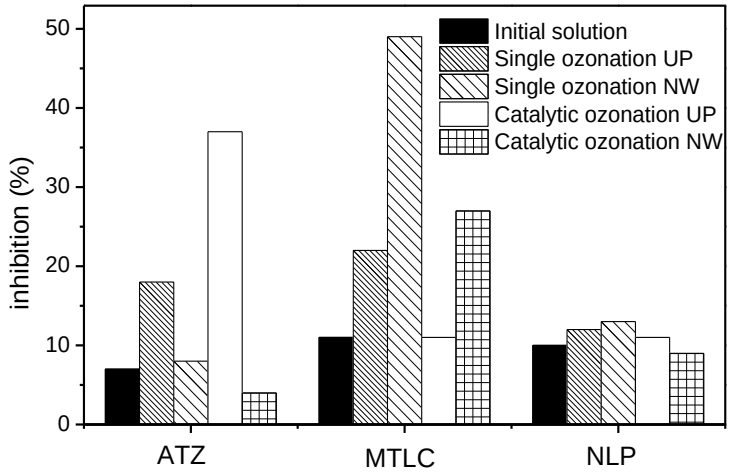

Figure 4.35 – Inhibition of bacterial activity determined by Microtox after exposure to the effluent resulting from the continuous ozonation experiment with different water matrices.

Since it was clear that the constituents of the natural water matrix had an effect on the performance of the catalyst, further catalytic ozonation experiments were performed, systematically removing each component from the matrix. The selected pollutant for this series of experiments was metolachlor, and the results obtained are presented in Figure 4.36. The pH value of the natural water solution is strongly buffered by HCO_3^- (at around 7), and thus the natural decomposition of ozone into radicals is minimized.

The removal of the parent pollutant was not importantly affected by the removal of each constituent from the natural water matrix, since the reaction with molecular dissolved ozone seems to play the major role in its degradation. However, significant differences were observed regarding the mineralization degree achieved. The main inhibitors of the catalytic ozonation process were ions HCO_3^-, SO_4^{2-} and Ca^{2+}. The effect of the first as a radical scavenger, as mentioned before, justifies the improvement of the mineralization degree attained upon its removal. Rosal et al. suggest that sulfate may affect the dissolution of ozone in water, which is lower for

higher concentrations of the inorganic ion [71]. Furthermore, sulfate ion has also been reported to react with hydroxyl radicals but not with molecular ozone [72], which may inhibit the degradation of organic matter and also the ozone degradation chain that results in the further production of more highly reactive radicals. Regarding the effect of Ca^{2+}, it was observed that, when this ion is not present in the water matrix, the TOC removal increased from 15 to 35%. This shows that calcium is greatly disrupting the process of conversion of the organic pollutant and of its degradation products. In fact, without calcium, the TOC removal is close to that obtained during experiments using milliQ ultrapure water (without inorganic ions). The reaction of degradation compounds with calcium in solution is known to form precipitates, which may block the access to the surface of the catalyst, and it was also postulated that Ca^{2+} may bind to carboxylic groups in high molecular weight intermediates of metolachlor ozonation [73], thus hindering their degradation by catalytic ozonation. The removal of humic acid from solution had a negative effect on the mineralization degree. Humic acid has a very high organic carbon loading, which could be one of the reasons why this occurs, since when monitoring the mineralization degree, the organic carbon present in the humic acid, and its possible degradation, is also being accounted for. Low concentrations of humic acid have been found to enhance the performance of ozone by initiating its decomposition into more reactive compounds [74, 75]. The combination of these two factors should account for the decrease in the efficiency of mineralization when humic acid was removed from the natural water matrix.

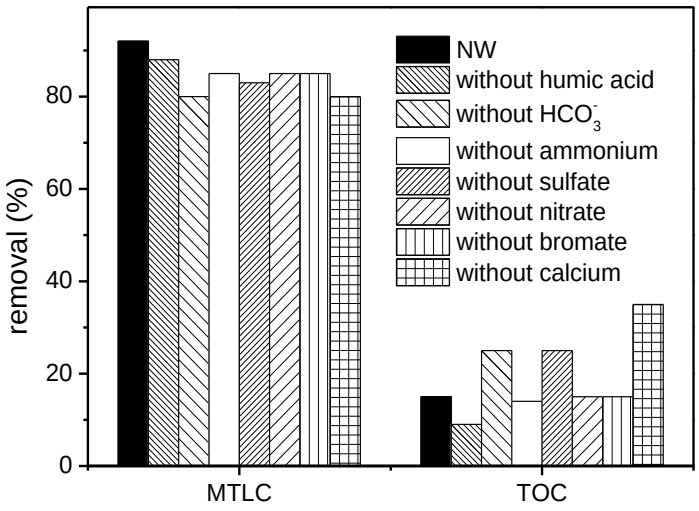

Figure 4.36 - Removal of metolachlor and respective mineralization degrees during continuous ozonation experiment with natural water matrix from which the components were sequentially removed.

The resulting effluents from the catalytic ozonation experiments using natural water from which the constituents were systematically removed also had their toxicity level monitored, as can be seen in Figure 4.37.

There seems to be a trend connecting the mineralization degree with the toxicity level found. It seems that while the oxidation reaction goes further in the degradation path of the parent compound, more toxic products are being produced. In fact, the highest values found correspond to the experiments without HCO_3^- and without calcium present in the matrix. However, after the reaction without sulfate, the toxicity level was very low. The production of less toxic intermediates could be the cause. However, the variation in 2-ethyl-6-methylaniline concentration was almost insignificant and thus this seems unlikely. It is possible that sulfate, or the products of the reaction between hydroxyl radicals and sulfate, has an inhibitory effect in the luminescent activity of *Vibrio Fischeri*.

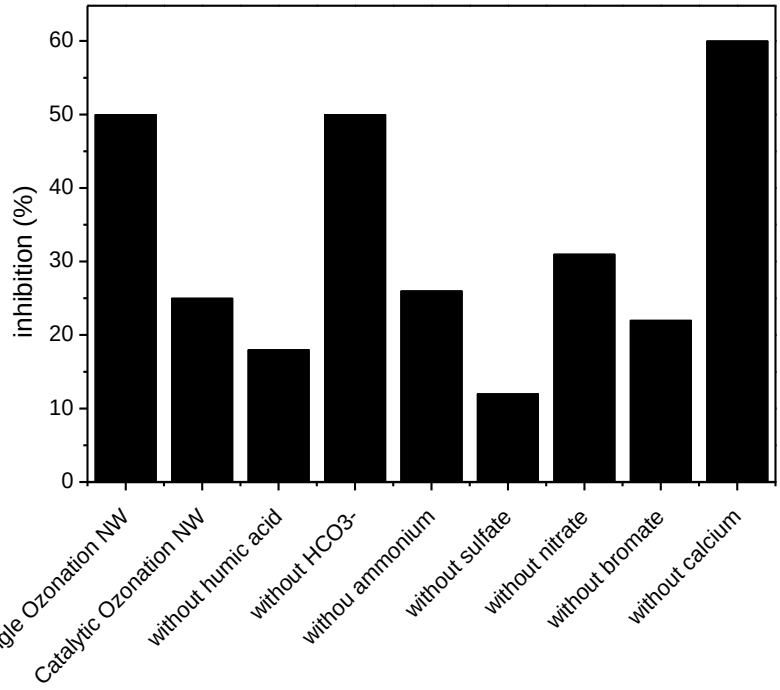

Figure 4.37 - Inhibition of bacterial activity determined by Microtox after exposure to the effluent resulting from continuous catalytic ozonation experiment with natural water matrix from which the components were sequentially removed.

In summary, the catalytic ozonation process, using structured catalysts constituted by honeycomb monoliths covered by carbon nanofibers, was demonstrated to, notwithstanding some changes to the performance of the system, have potential for application with real effluents.

4.8 CARBON LOADING

The increase of the carbon loading of the structured catalysts may have an influence in the performance of the catalyst, since there will be a larger number of active sites available for reaction [76]. The increase in catalyst loading in semi-batch ozonation reactions has already been demonstrated to enhance the oxidative potential [46] (see *Ozonation of emerging organic micropollutants*).

In Figure 4.17 the conversion of dissolved ozone as a function of the liquid flow rate is compared for two 400 cpsi monoliths with different loading of CNF (10.2 and 16 wt.%). The higher loading of CNF is shown to result in a larger conversion of ozone. A similar behaviour was observed when the same monoliths were applied to the ozonation of oxalic acid, as seen in Figure 4.27. Once more, the monolith with a higher loading of CNF was able to degrade a larger amount of oxalic acid.

While an increase in the amount of CNF grown on the structured catalysts results in a larger number of active sites, the increase in the thickness of the CNF layer should also be taken into consideration [77]. It is possible that a too thick CNF layer may block access of the reactants to the carbon material that is closer to the support, and thus buried beneath additional layers of CNF.

Experiments were performed using structured catalysts with a large variance of CNF loading as catalysts for the ozonation of oxalic acid. These experiments were run in a closed loop two-phase setup, since the structured catalysts used had a smaller diameter (10 mm) and thus did not fit properly inside the bubble column, without bypass of the liquid and gas phases. The calculated first-order kinetic constants are shown in Figure 4.38 as a function of the mass of CNF grown on the structured catalysts.

It is noticeable in Figure 4.38 that, in spite of the increase in the reaction rate with the CNF mass, for high mass, the effect of the mass increase is lower than for lower masses of CNF. The relation between the removal rate and the CNF mass seems to follow approximately a logarithmic increase, suggesting that it is not efficient to increase the CNF mass from a certain point. This is likely due to the increase in the thickness of the CNF layer, which reduces the accessibility of the reactants to the layers closer to the support, which are not then able to catalyse the reaction.

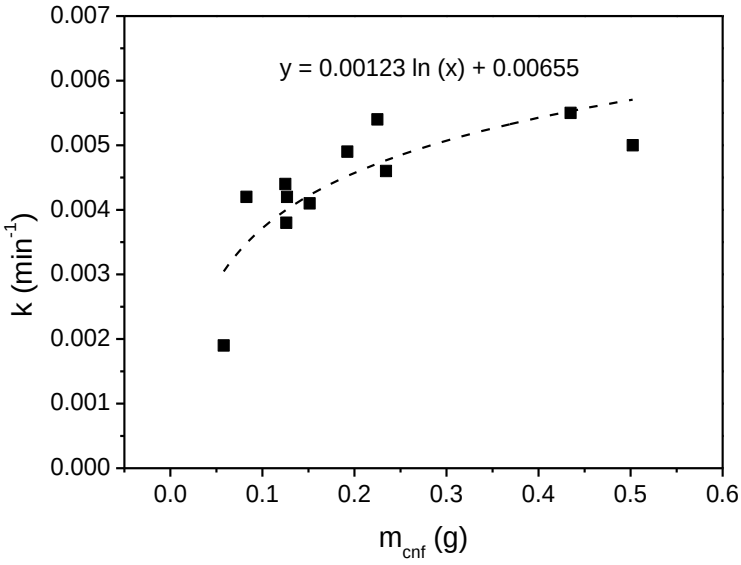

Figure 4.38 – First-order rate constant of the removal of oxalic acid in ozonation experiments using structured catalysts with different loadings of carbon nanofibers, represented as a function of the mass of carbon nanofibers on the surface of the structured catalysts.

4.9 PARTIAL CONCLUSIONS

In this chapter, the influence of various operation parameters was evaluated in the catalytic ozonation of organic pollutants.

On a first approach, the hydraulic features of the experimental setup were characterized. The detailed behaviour of the hydraulic regime developed inside the monolith channels was then also characterized through application of the relations found in the literature. Afterwards, these parameters were related to the performance of the catalysts in the ozonation of organic pollutants. After showing that the application of a three-phase system was advantageous, it was found that the relative size of the bubbles and the monolith channels are important, since they affect the distribution of the gas-phase inside the monolith, as well as its contact with the catalytic wall. Furthermore, the efficiency of the process was suggested to be dependent, under our operating conditions, on the

transfer of the organic pollutants from the solution to the channel walls, where a major part of the degradation reaction of the pollutants is taking place. This factor seems to be strongly related to the length of the slugs inside the monolith channels, which is, on the other hand, linked with the liquid flow rate used. Another factor which seems to be important is the relation of the velocities of the slugs and bubbles inside the channels; however, since there is already a high concentration of ozone in the liquid phase inside the monolith, it was suggested that this phenomenon might not be as important in this case.

In addition, the effect of several components of natural waters in the process was evaluated, as well as the influence of the loading of carbon on the structured catalysts. It was found that, despite showing an influence in the process, the use of natural water matrices does not hinder significantly the efficiency of the catalytic ozonation process. It was observed that its influence varies when different pollutants are used. The increase in the loading of carbon on the structured catalysts was shown to enhance the performance of the system, up to a certain point, since a CNF layer that is too thick will decrease the accessibility of the reactants to the layers closer to the support.

REFERENCES

[1] O. Levenspiel, Chemical reaction engineering, John Wiley & Sons, 1972.
[2] R.H. Patrick, T. Klindera, L.L. Crynes, R.L. Cerro, M.A. Abraham, AIChE Journal, 41 (1995) 649-657.
[3] D. Ito, M. Damsohn, H.-M. Prasser, M. Aritomi, Experiments in Fluids, 51 (2011) 821-833.
[4] M.T. Kreutzer, Chemical Engineering Science, 60 (2005) 5895.
[5] R.S. Abiev, I.V. Lavretsov, Chemical Engineering Science, 74 (2012) 59-68.
[6] H. Liu, C.O. Vandu, R. Krishna, Industrial & engineering chemistry research, 44 (2004) 4884-4897.
[7] C.O. Vandu, J. Ellenberger, R. Krishna, Chemical Engineering and Processing: Process Intensification, 44 (2005) 363-374.
[8] C.O. Vandu, H. Liu, R. Krishna, Chemical Engineering Science, 60 (2005) 6430-6437.
[9] J.M. van Baten, R. Krishna, Chemical Engineering Science, 59 (2004) 2535-2545.
[10] P. Sobieszuk, R. Pohorecki, P. Cygański, J. Grzelka, Chemical Engineering Science, 66 (2011) 6048-6056.
[11] H. Ganapathy, E. Al-Hajri, M. Ohadi, Chemical Engineering Science, in press.
[12] H. Ganapathy, E. Al-Hajri, M.M. Ohadi, Chemical Engineering Science, 94 (2013) 156-165.
[13] H. Ganapathy, E. Al-Hajri, M.M. Ohadi, Chemical Engineering Science, 94 (2013) 138-149.
[14] G. Berčič, A. Pintar, Chemical Engineering Science, 52 (1997) 3709-3719.
[15] D. Liu, S. Wang, Chemical Engineering and Processing: Process Intensification, 47 (2008) 2098-2106.
[16] J.A. Howard, P.A. Walsh, International Journal of Multiphase Flow, 55 (2013) 32-42.
[17] S. Kececi, M. Wörner, A. Onea, H.S. Soyhan, Catalysis Today, 147, Supplement (2009) S125-S131.
[18] P. Sobieszuk, P. Cygański, R. Pohorecki, Chemical Engineering Research and Design, 88 (2010) 263-269.
[19] T. Abadie, C. Xuereb, D. Legendre, J. Aubin, Chemical Engineering Research and Design, in press.
[20] R.S. Abiev, Chemical Engineering Journal, 227 (2013) 66-79.
[21] M.T. Kreutzer, P. Du, J.J. Heiszwolf, F. Kapteijn, J.A. Moulijn, Chemical Engineering Science, 56 (2001) 6015-6023.
[22] R.M. de Deugd, R.B. Chougule, M.T. Kreutzer, F.M. Meeuse, J. Grievink, F. Kapteijn, J.A. Moulijn, Chemical Engineering Science, 58 (2003) 583-591.
[23] A.N. Tsoligkas, M.J.H. Simmons, J. Wood, C.G. Frost, Catalysis Today, 128 (2007) 36-46.

[24] M.J.F. Warnier, E.V. Rebrov, M.H.J.M. de Croon, V. Hessel, J.C. Schouten, Chemical Engineering Journal, 135, Supplement 1 (2008) S153-S158.
[25] Y. Han, N. Shikazono, International Journal of Heat and fluid flow, 30 (2009) 842-853.
[26] G.I. Taylor, Journal of Fluid Mechanics, 10 (1961) 161-165.
[27] P. Aussillous, D. Quere, Physics of Fluids, 12 (2000) 2367-2371.
[28] M.T. Kreutzer, Hydrodynamics of Taylor Flow in Capillaries and Monolith Reactors Delft University Press, 2003.
[29] A. Kawahara, P.M.Y. Chung, M. Kawaji, International Journal of Multiphase Flow, 28 (2002) 1411-1435.
[30] K. Mishima, T. Hibiki, International Journal of Multiphase Flow, 22 (1996) 703-712.
[31] T.C. Thulasidas, M.A. Abraham, R.L. Cerro, Chemical Engineering Science, 50 (1995) 183-199.
[32] W.B. Kolb, R.L. Cerro, Physics of Fluids A, 5 (1993) 1549.
[33] A.L. Hazel, M. Heil, Journal of Fluid Mechanics, 470 (2002) 91-114.
[34] M.T. Kreutzer, F. Kapteijn, J.A. Moulijn, J.J. Heiszwolf, Chemical Engineering Science, 60 (2005) 5895-5916.
[35] H. Chaumat, A. Billet-Duquenne, F. Augier, C. Mathieu, H. Delmas, Chemical Engineering Science, 60 (2005) 5930-5936.
[36] R. Andreozzi, Applied catalysis. A, General, 138 (1996) 75.
[37] F.J. Beltrán, F.J. Rivas, R. Montero-de-Espinosa, Water Research, 39 (2005) 3553-3564.
[38] Z.Q. Liu, Carbon, 46 (2008) 890.
[39] P.C.C. Faria, J.J.M. Órfão, P. M.F.R., Applied Catalysis B, Environmental, 79 (2008) 237.
[40] Z.-Q. Liu, J. Ma, Y.-H. Cui, B.-P. Zhang, Applied Catalysis B: Environmental, 92 (2009) 301-306.
[41] Z.-Q. Liu, J. Ma, Y.-H. Cui, L. Zhao, B.-P. Zhang, Applied Catalysis B: Environmental, 101 (2010) 74-80.
[42] Z.-Q. Liu, J. Ma, Y.-H. Cui, L. Zhao, B.-P. Zhang, Separation and Purification Technology, 78 (2011) 147-153.
[43] C.A. Orge, J.J.M. Órfão, M.F.R. Pereira, Applied Catalysis B: Environmental, 126 (2012) 22-28.
[44] A.G. Gonçalves, J.L. Figueiredo, J.J.M. Órfão, M.F.R. Pereira, Carbon, 48 (2010) 4369-4381.
[45] C. Gottschalk, J.A. Libra, A. Saupe, Ozonation of water and waste water a practical guide to understanding ozone and its application, Wiley-VCH, 2000.
[46] X. Fan, J. Restivo, J.J.M. Órfão, M.F.R. Pereira, A.A. Lapkin, Chemical Engineering Journal, 241 (2014) 66-76.
[47] S. Derrouiche, D. Bourdin, P. Roche, B. Houssais, C. Machinal, M. Coste, J. Restivo, J.J.M. Orfao, M.F.R. Pereira, Y. Marco, E. Garcia-Bordeje, Water Sci Technol, 68 (2013) 1377-1383.
[48] C.A. Guzman-Perez, J. Soltan, J. Robertson, Separation and Purification Technology, 79 (2011) 8-14.
[49] Y.M. Vera, R.J.d. Carvalho, M.L. Torem, B.A. Calfa, Chemical Engineering Journal, 155 (2009) 691-697.

[50] J. Restivo, J.J.M. Órfão, S. Armenise, E. Garcia-Bordejé, M.F.R. Pereira, Journal of Hazardous Materials, 239–240 (2012) 249-256.
[51] B. Ning, N.J.D. Graham, Y. Zhang, Chemosphere, 68 (2007) 1163-1172.
[52] J. Kim, G.V. Korshin, A.B. Velichenko, Water Research, 39 (2005) 2527-2534.
[53] J. Restivo, J.J.M. Órfão, M.F.R. Pereira, E. Garcia-Bordejé, P. Roche, D. Bourdin, B. Houssais, M. Coste, S. Derrouiche, Chemical Engineering Journal, 230 (2013) 115-123.
[54] Y.-J. Lin, M. Karuppiah, A. Shaw, G. Gupta, Ecotoxicology and Environmental Safety, 43 (1999) 35-37.
[55] J.M. van Baten, R. Krishna, Chemical Engineering Science, 60 (2005) 1117-1126.
[56] F. Kapteijn, T.A. Nijhuis, J.J. Heiszwolf, J.A. Moulijn, Catalysis Today, 66 (2001) 133-144.
[57] T.A. Nijhuis, M.T. Kreutzer, A.C.J. Romijn, F. Kapteijn, J.A. Moulijn, Chemical Engineering Science, 56 (2001) 823-829.
[58] S. Roy, American Institute of Chemical Engineers. AIChE Journal, 50 (2004) 2918.
[59] M.T. Kreutzer, F. Kapteijn, J.A. Moulijn, Catalysis Today, 105 (2005) 421-428.
[60] M.N. Kashid, L. Kiwi-Minsker, Industrial & engineering chemistry research, 48 (2009) 6465-6485.
[61] A. Onea, M. Wörner, D.G. Cacuci, Chemical Engineering Science, 64 (2009) 1416-1435.
[62] M.T. Kreutzer, Catalysis Today, 105 (2005) 421.
[63] A.N. Tsoligkas, M.J.H. Simmons, J. Wood, Chemical Engineering Science, 62 (2007) 4365-4378.
[64] N. Shao, A. Gavriilidis, P. Angeli, Chemical Engineering Journal, 160 (2010) 873-881.
[65] T.A. Nijhuis, M.T. Kreutzer, A.C.J. Romijn, F. Kapteijn, J.A. Moulijn, Catalysis Today, 66 (2001) 157-165.
[66] M.A.R. Talaia, World Academy of Science, Engineering and Technology, 28 (2007).
[67] T.C. Thulasidas, M.A. Abraham, R.L. Cerro, Chemical Engineering Science, 52 (1997) 2947-2962.
[68] P.C.C. Faria, J.J.M. Órfão, M.F.R. Pereira, Applied Catalysis B: Environmental, 79 (2008) 237-243.
[69] G.W. Stratton, Archives of Environmental Contamination and Toxicology, 13 (1984) 35-42.
[70] V.A. Sakkas, I.M. Arabatzis, I.K. Konstantinou, A.D. Dimou, T.A. Albanis, P. Falaras, Applied Catalysis B, 49 (2004) 195-205.
[71] R. Rosal, A. Rodríguez, J.A. Perdigón-Melón, A. Petre, E. García-Calvo, Chemical Engineering Journal, 149 (2009) 311-318.
[72] C. Tizaoui, L. Bouselmi, L. Mansouri, A. Ghrabi, Journal of Hazardous Materials, 140 (2007) 316-324.
[73] M.S. Chandrakanth, B.D. Honeyman, G.L. Amy, Colloids and Surfaces A: Physicochemical and Engineering Aspects, 107 (1996) 321-342.

[74] K. Okawa, Y. Nakano, W. Nishijima, M. Okada, Chemosphere, 57 (2004) 1231-1235.
[75] S.J. Masten, M.J. Galbraith, S.H.R. Davies, Ozone Science and Engineering, 18 (1996) 535-547.
[76] J.L. Figueiredo, F.R. Ribeiro, Catálise Heterogénea, Calouste Gulbenkian.
[77] E. García-Bordejé, I. Kvande, D. Chen, M. Rønning, Carbon, 45 (2007) 1828-1838.

5. MODIFICATION OF THE CARBON SURFACE

5.1 DESCRIPTION

In this chapter, the influence of the doping of carbon materials with different heteroatoms in the catalytic ozonation process was assessed.

On a first approach, a screening of elements of interest was made using multiwalled carbon nanotubes, and nitrogen was selected as the most able to enhance the catalytic activity of the materials.

On a second step, the nitrogen doping was evaluated using carbon nanofibers, both in powder form and as structured catalysts. In these experiments, three selected emerging organic micropollutants were used, and the activity of the pristine and N-doped carbon nanofibers was evaluated.

Finally, the influence of the amount and of the type of the nitrogen functionalities on the surface of carbon materials was evaluated, using carbon xerogels. A positive correlation between the amount of nitrogen and the catalytic activity of the materials on the ozonation of oxalic acid was found.

The materials used in this chapter were prepared and kindly made available by: doped MWCNT, by Raquel P. Rocha, prepared at Laboratório de Catálise e Materiais, Universidade do Porto; pristine and doped CX, by Dr. Juliana P. S. Sousa, prepared at Laboratório de Catálise e Materiais, Universidade do Porto; and pristine and doped CNF by the group of Prof. Enrique Garcia-Bordejé, at Instituto de Carboquímica, part of the Consejo Superior de Investigación Científica, in the context of the European Commission financed project MONACAT. The work presented in this chapter has been partially published in the following references:

R.P. Rocha, J. Restivo, J.P.S. Sousa, J.J.M. Órfão, M.F.R. Pereira, J.L. Figueiredo, Nitrogen-doped carbon xerogels as catalysts for advanced oxidation processes, in press, Catalysis today, (2014),

J. Restivo, R.P. Rocha, A.M. Silva, J.J. Órfão, M.F. Pereira, J.L. Figueiredo, Catalytic performance of heteroatom-modified carbon nanotubes in advanced oxidation processes, 35 (2014) 896-905.

5.2 INTRODUCTION OF SURFACE HETEROATOMS

5.2.1 SEMI-BATCH OZONATION

An initial approach was made to assess the influence of the introduction of different elements on the surface of carbon nanotubes (MWCNT). The detailed characterization of the materials used in these experiments is presented in section *Materials and methods*. The MWCNT used in this study present on their surface oxygen-containing species (CNT-N, treated with nitric acid), nitrogen containing species (CNT-NUT, treated with urea) and sulphur-containing species (CNT-S and CNT-NS, treated with sulphuric acid and with nitric and sulphuric acid, respectively).

The catalytic performance of the pristine and modified CNT samples was studied using oxalic acid (Figure 5.1) and phenol (Figure 5.2) as model pollutants in ozonation.

A clear influence of the surface chemistry of the carbon samples in the catalytic performance can be observed. The acidic samples CNT-N, CNT-NS and CNT-S (which present low pH_{pzc}) underperform compared with the samples with neutral or slightly basic nature (CNT-O and CNT-NUT). Almost complete degradation of oxalic acid can be achieved in 60 min using the pristine CNTs and the N-modified CNT sample, while the oxalic acid conversions are in the range 50-75% with the S-containing samples (CNT-S and CNT-NS) and CNT-N.

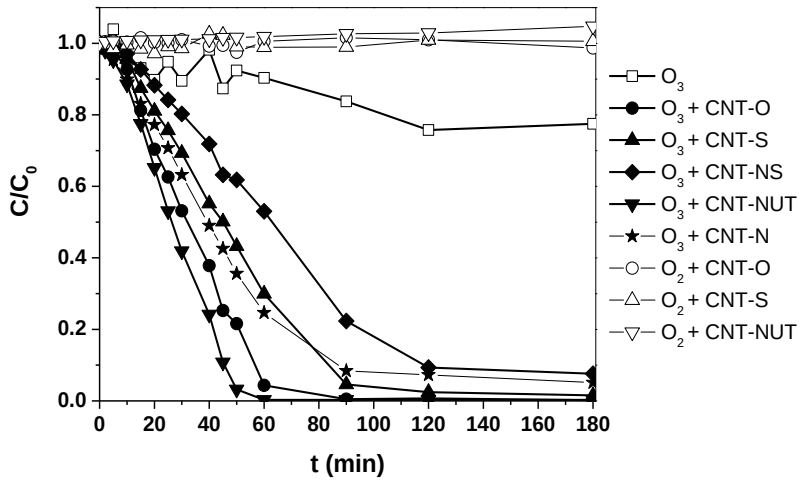

Figure 5.1 – Dimensionless concentration of oxalic acid during semi-batch ozonation experiments carried out in the presence of MWCNT with different surface functionalities.

Due to the large amount of O-containing groups (carboxylic acids and anhydrides, and phenols) on the CNT-N sample, the poor catalytic performance was expected. In fact, the presence of acidic surface groups in the CNTs has a negative influence in the decomposition of ozone, which is directly related with the efficiency of the catalyst to improve the degradation of refractory organic compounds by ozonation [1, 2]. Furthermore, the positive effect of basicity in liquid-phase oxidations with carbon materials is commonly accepted [3], including the degradation of organic compounds by ozonation [4] [5, 6] [2, 7-14].

The absence of acidic groups (O-containing or S-containing) lead to a faster degradation of oxalic acid, as observed with samples CNT-O and CNT-NUT. The good performance of the pristine CNTs (CNT-O) in catalytic ozonation can be explained by the presence of π electrons on the surface, which are known to be active sites for ozone decomposition and formation of radicals [15], but also by the absence of acidic surface species that can hinder the formation of radicals or restrain the surface reaction mechanisms [1, 10]. Concerning the CNT-NUT sample, which shows the best catalytic performance for oxalic acid degradation, it seems

that the N-functionalities introduced are responsible for the improved catalytic activity observed. The results obtained in the catalytic ozonation of oxalic acid support the idea that the increase in electronic density on the surface, promoted by the N-functionalities, favours the reduction of ozone, as recently proposed [6, 8, 11, 14, 16].

Comparison with published results for oxalic acid degradation by catalytic ozonation shows that the CNT-NUT sample performs better than N-doped carbon xerogels [11] and activated carbon [2], which did not allow complete oxalic acid degradation after 120 min, but reveals only a small improvement in performance when compared with other modified commercial CNTs [1], which led to 100 % conversion of oxalic acid in less than 60 min, under similar conditions.

Figure 5.2 shows the catalytic activity of the pristine and modified CNT samples in the removal of phenol by ozonation

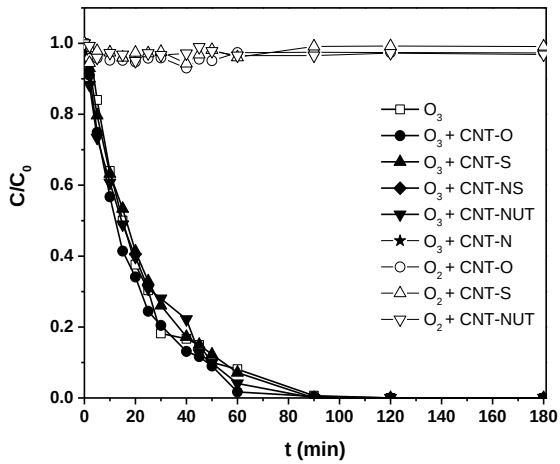

Figure 5.2 – Dimensionless concentration of phenol during semi-batch ozonation experiments carried out in the presence of MWCNT with different surface functionalities.

Regarding the ozonation process, phenol reacts promptly with dissolved molecular ozone, and no significant differences are observed in the presence of any of the CNT samples; in addition, adsorption was

negligible. However, slight differences were observed regarding the mineralization, determined by TOC analysis (Figure 5.3).

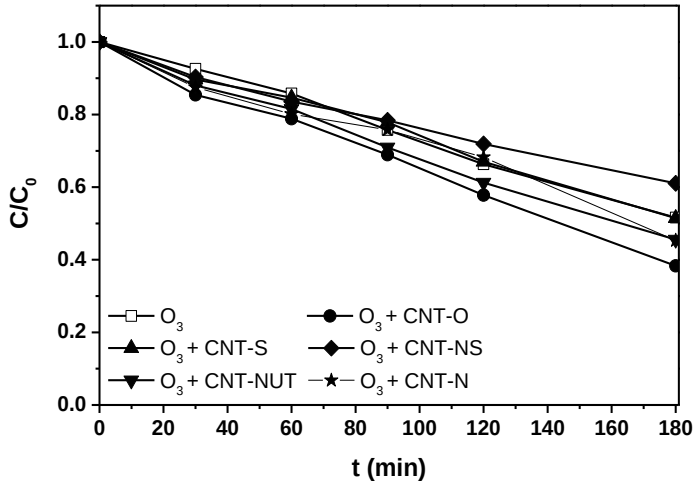

Figure 5.3 – Dimensionless concentration of TOC during semi-batch ozonation of phenol experiments carried out in the presence of MWCNT with different surface functionalities.

Complete mineralization of phenol degradation products by ozone requires higher dosages of oxidant and longer contact times when compared with the parent pollutant [17], and may be aided by the addition of a carbon catalyst [18]. In spite of the fast phenol conversion by reaction with ozone, the TOC removals were low, a maximum of 60 % being obtained with the pristine CNTs after 180 min. Analysis of the main aromatic intermediates identified, namely hydroquinone and benzoquinone, did not reveal any significant differences between the catalytic and non-catalytic experiments, as seen in Figure 5.4. and Figure 5.5.

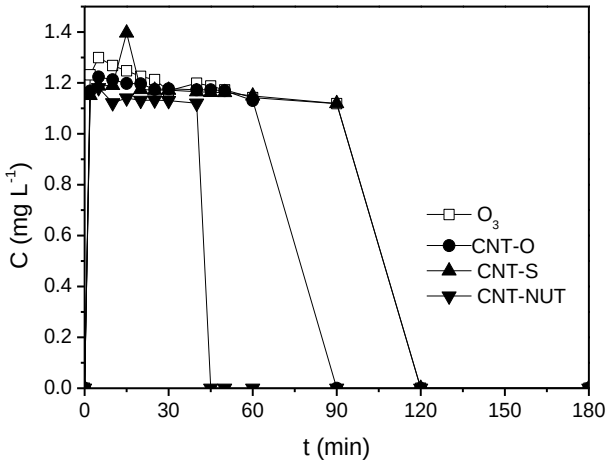

Figure 5.4 – Concentration of benzoquinone during semi-batch ozonation of phenol experiments carried out in the presence of MWCNT with different surface functionalities.

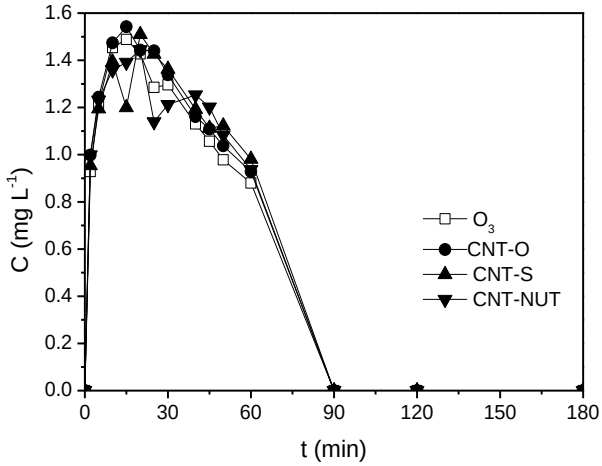

Figure 5.5 – Concentration of hydroquinone during semi-batch ozonation of phenol experiments carried out in the presence of MWCNT with different surface functionalities.

Both compounds are formed as soon as the oxidation of phenol begins, and are removed from solution in under 90 min. Organic acids are final by-products of the oxidation of phenol, in particular oxalic acid [17]. The concentrations of oxalic acid accumulated after 180 min (Figure 5.6) are in complete agreement with what was observed during the ozonation

experiments using oxalic acid as a model compound; i.e., the catalysts which showed better performance in the removal of oxalic acid were those that led to a lower concentration of oxalic acid in the experiments with phenol.

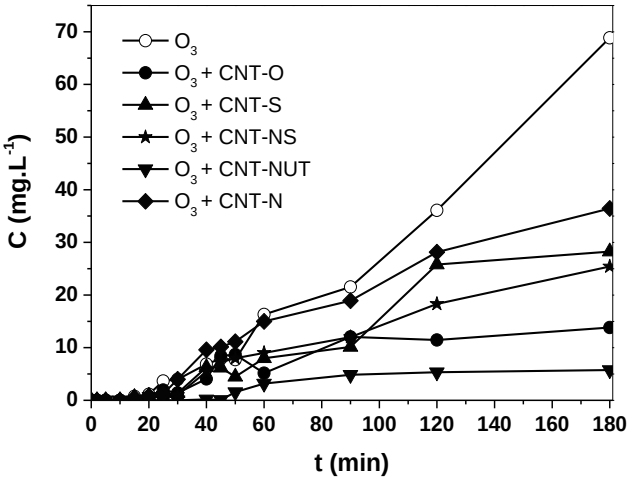

Figure 5.6 – Concentration of oxalic acid during semi-batch ozonation of phenol experiments carried out in the presence of MWCNT with different surface functionalities.

However, while oxalic acid in the final solution contributed to a major part of the final TOC (35% in the case of the single ozonation experiment, 5-25% in the case of the catalytic ozonation experiments), there was still a large contribution from other organic compounds, which were not identified, as seen in Figure 5.7.

While the CNT-NUT sample yielded the least amount of oxalic acid accumulated in solution, the contribution of other organic compounds is clearly larger than what was observed in the experiments carried out with the remaining MWCNT samples. This may indicate that the inclusion of different catalysts in solution, besides enhancing the removal of compounds refractory to direct ozonation, may change the reaction path, favouring the formation of specific by-products over others, which may differ in their reactivity with ozone, or ozone derived oxidants [19]. This explains why the CNT-O sample conducted to a greater mineralization

than the CNT-NUT sample, even though the latter was shown to perform better in the ozonation of oxalic acid. The samples containing acidic S-containing groups on the surface, as was observed when oxalic acid was used as a model compound, were the least active catalysts where the mineralization of phenol was concerned.

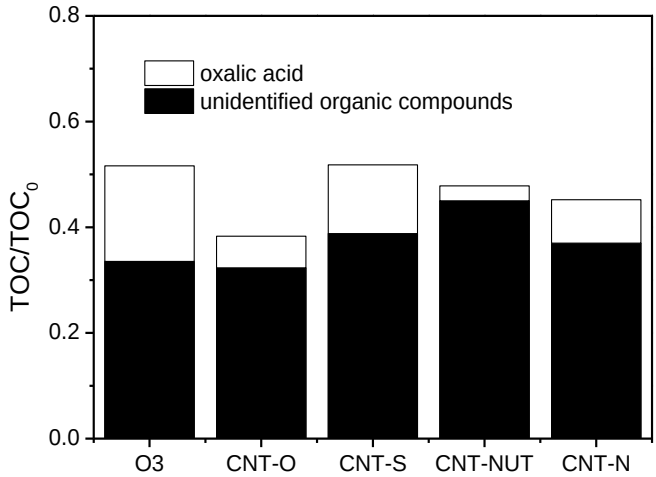

Figure 5.7 – Dimensionless concentration of TOC, with the contribution of oxalic acid and of other organic compounds identified, after 180 minutes, during the semi-batch ozonation of phenol experiments carried out in the presence of MWCNT with different surface functionalities.

The improvement in the removal of phenol by addition of activated carbon to the ozonation process has been reported by other authors; however, these results were obtained with a very high loading of catalyst in one case [20], or have been attributed to adsorption in another case [21]. An activated carbon modified by plasma treatment has also been reported to enhance the removal of phenol from water, its activity being ascribed to the increase in the amount of surface oxygenated groups; however, mineralization was not reported in that case [22]. The application of activated carbon as catalyst for the ozonation process to achieve mineralization has resulted in similar observations to what is reported here [18].

While the low activity of sample CNT-S can be attributed to its acid character, its activity in the catalytic wet air oxidation of phenol has been shown to be remarkable, possibly due to the formation of S-containing radical species, such as persulfate radicals [23-25]. Some experiments were performed in order to understand if, and why, such behaviour was not observed in the ozonation process. For this end, sodium persulfate was used as a precursor to the formation of sulfate-containing radicals, and *tert*-BuOH was used as a radical scavenger. The dimensionless concentration of oxalic acid during semi-batch experiments performed to give insight into the role of the S-containing surface functionalities is presented in Figure 5.8.

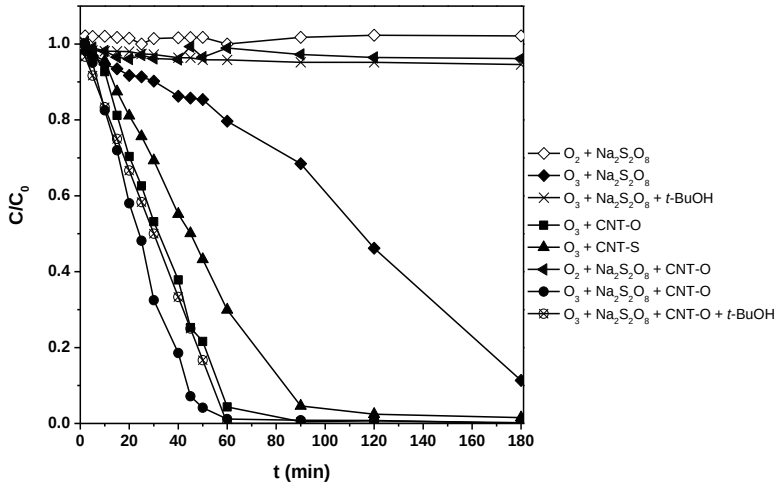

Figure 5.8 – Dimensionless concentration of oxalic acid during the semi-batch ozonation experiments carried out in the presence of MWCNT with different surface functionalities, using sodium persulfate and *tert*-BuOH.

The amount of sodium persulfate added to each system was determined by considering the mass of catalyst (100 mg) and the amount of SO_2 released by sample CNT-S in TPD (see section *Materials and methods*). Therefore, the reactions were performed using equivalent S molar concentrations.

The addition of persulfate ion to the ozonation reaction system enhances the degradation of oxalic acid. Since the experiment without ozone in the

gas feed showed no removal of the pollutant, it is clear that the interaction of ozone, or ozone-derived species, with persulfate, or derived species, is responsible for this positive effect [26, 27]. While the reaction of hydroxyl radicals with the persulfate ion is reported to be responsible for the generation of sulfate radicals when AOPs are concerned [26-28], the spontaneous homogeneous generation of hydroxyl radicals does not occur at the pH (3.0) of the initial oxalic acid solution [13]. Thus, it is likely that ozone, or ozone-derived species, activate the persulfate ions, thus forming more active radical species which enhance the degradation of oxalic acid. In fact, no degradation of oxalic acid was observed when *tert*-butanol (*t*-BuOH, a known radical scavenger [2]) was added to this reaction system, therefore suggesting the intervention of radical species in the $O_3/Na_2S_2O_8$ system.

A positive effect in the degradation of oxalic acid was observed when $Na_2S_2O_8$ was added to the O_3+CNT-O experiment. This enhanced performance was eliminated in the presence of the radical scavenger, confirming the role of radicals in solution. When the same experiment was carried without ozone in the gas feed (O_2+CNT-O+$Na_2S_2O_8$), no removal of oxalic acid was observed. It has been suggested that carbon materials can promote the formation of active radicals from persulfate [29, 30], but this was not observed in our working conditions (most likely due to the lower concentration of persulfate in solution).

These experiments suggest that the species resulting from the decomposition of S-containing groups during ozonation are not activated by ozone in the same way as persulfate. This seems to be the main difference between catalytic wet air oxidation and catalytic ozonation, in regard to the mechanism when the S-containing sample is used. This was confirmed when t-BuOH was added to the catalytic ozonation of oxalic acid carried out with sample CNT-S (Figure 5.9), where no difference in the removal was observed.

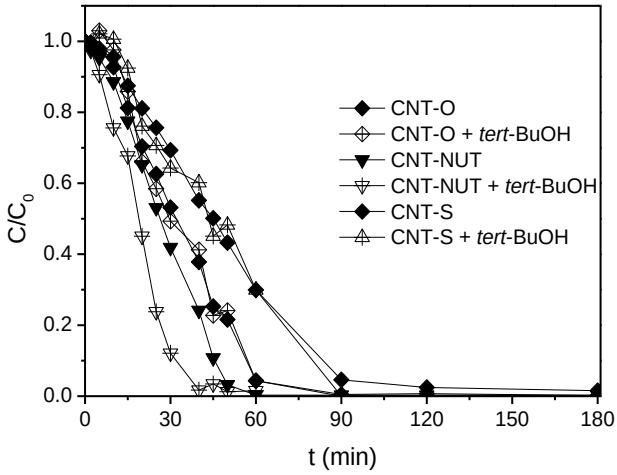

Figure 5.9 – Dimensionless concentration of oxalic acid during the semi-batch ozonation experiments carried out in the presence of MWCNT with different surface functionalities, using *tert*-BuOH.

Similarly, the removal of oxalic acid when a radical scavenger was applied during experiments using samples CNT-O and CNT-NUT was not hindered, when compared with the catalytic experiments without *tert*-BuOH. Thus, it is expected that the reaction is occurring on the surface of the catalysts, at this working conditions.

The recycling of these catalysts and their stability in the ozonation reaction is further assessed in section *Stability and deactivation of the catalysts.*

Finally, semi-batch ozonation experiments were performed using carbon nanofibers in powder form, similar to those that are found in the honeycomb monolith catalysts, as described in section *Materials and methods.* The activity of the carbon nanofibers (CNF) was assessed using pristine and N-doped samples as catalysts in the ozonation of oxalic acid and phenol. The characterization of the pristine and N-doped CNF samples is presented in section *Materials and methods.*

The dimensionless removal of oxalic acid during catalytic ozonation using CNF samples in semi-batch is presented in Figure 5.10.

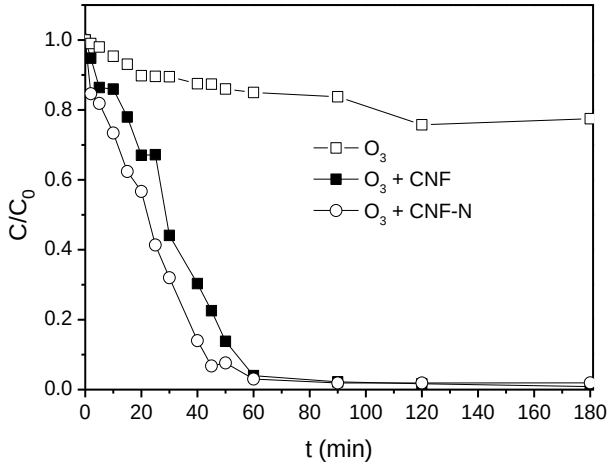

Figure 5.10 – Dimensionless concentration of oxalic acid during the semi-batch ozonation experiment carried out in the presence of pristine and N-doped carbon nanofibers.

Similarly to what was observed with MWCNT samples, the N-doped CNF showed better activity in the removal of oxalic acid during ozonation. The results obtained in the catalytic ozonation of oxalic acid support the idea that the increase in electronic density on the surface, promoted by the N-functionalities, favours the reduction of ozone, as recently proposed [6, 8, 11, 14, 16]. It is interesting to notice that the activity observed for the CNF samples is very close to that observed for the MWCNT samples, for the pristine and also for the N-doped CNF. Thus, it is expected that the behaviour of CNF is similar to that of MWCNT in the catalytic ozonation process.

The same samples were also used in the catalytic ozonation of phenol. The dimensionless concentration of phenol is presented in Figure 5.11.

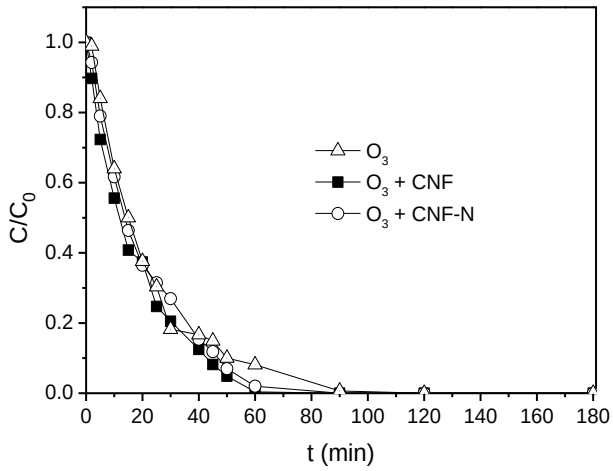

Figure 5.11 – Dimensionless concentration of phenol during the semi-batch ozonation experiments carried out in the presence of pristine and N-doped carbon nanofibers.

As was observed with the MWCNT samples, the presence of a catalyst in the ozonation of phenol does not significantly alter its removal from solution, likely due to its fast reaction with molecular ozone [17, 18]. The dimensionless concentration of TOC during ozonation experiments using CNF catalysts is presented in Figure 5.12, as a measure of the mineralization degree.

As expected, the differences in the production of benzoquinone and hydroquinone are not significant between the pristine and the N-doped samples. Moreover, the concentration of these compounds in the catalyst and the non-catalytic ozonation experiments was very similar, regardless of the catalyst used (CNF or MWCNT).

While the mineralization degree was improved from the single ozonation experiment, there was not much difference between the pristine and the N-doped CNF; the pristine sample is slightly more active than the N-doped sample. Since the distribution of the accumulated products was observed to change with the catalysts when MWCNT catalysts were used in this reaction, the formation of benzoquinone and hydroquinone is presented in Figure 5.13 and Figure 5.14 respectively.

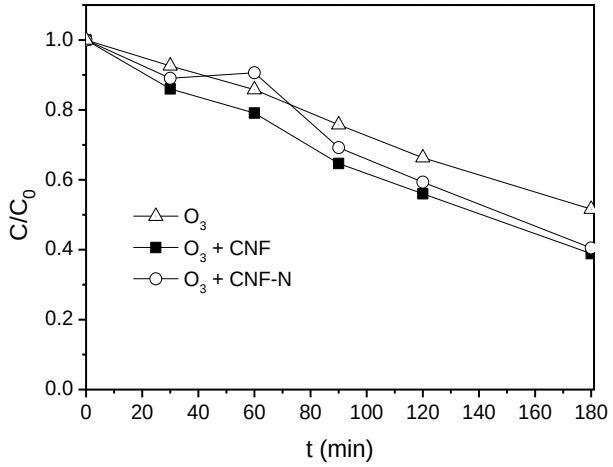

Figure 5.12 – Dimensionless concentration of TOC during the semi-batch ozonation of phenol experiments carried out in the presence of pristine and N-doped carbon nanofibers.

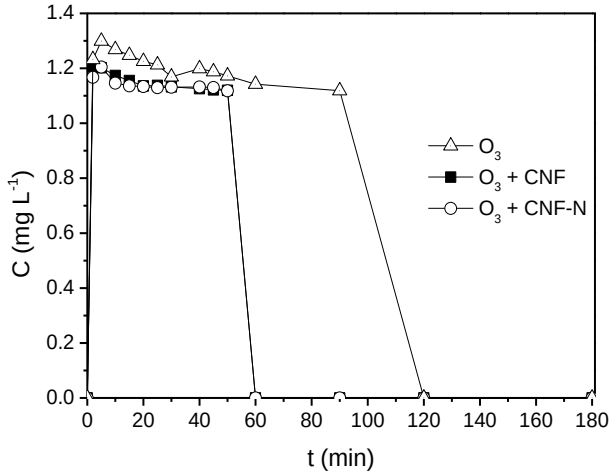

Figure 5.13 – Concentration of benzoquinone during semi-batch ozonation of phenol experiments carried out in the presence of pristine and N-doped carbon nanofibers.

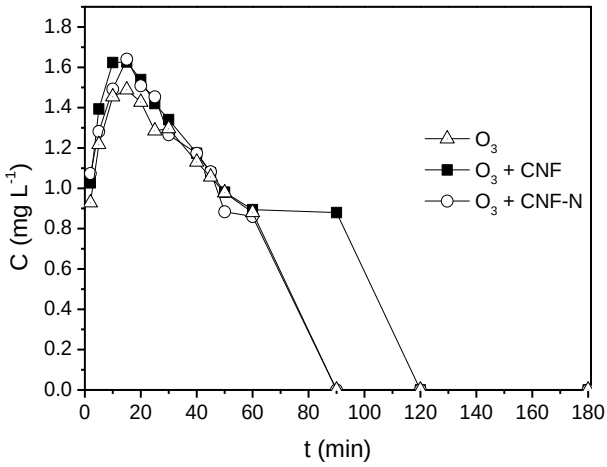

Figure 5.14 – Concentration of hydroquinone during semi-batch ozonation of phenol experiments carried out in the presence of pristine and N-doped carbon nanofibers.

However, the same was not observed in the formation of oxalic acid, presented in Figure 5.15.

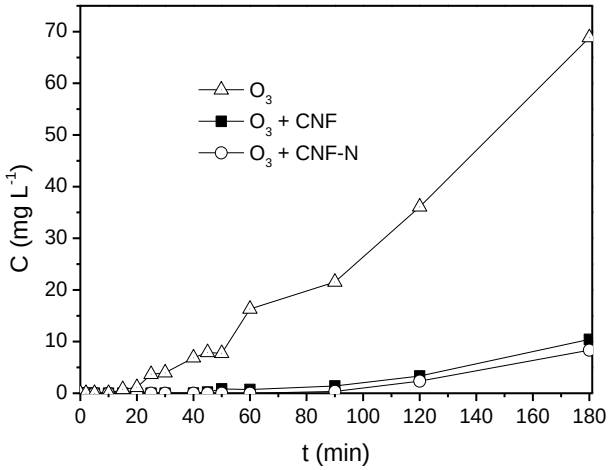

Figure 5.15 – Concentration of oxalic acid during semi-batch ozonation of phenol experiments carried out in the presence of pristine and N-doped carbon nanofibers.

While the concentration of oxalic acid in the catalytic experiments was much lower than that of the non-catalytic experiment, the difference

between the pristine and the N-doped CNF samples is not so evident. Nevertheless, the final accumulated TOC values obtained in these experiments are presented in Figure 5.16, where the contribution of oxalic acid and of other unidentified organic compounds is discriminated.

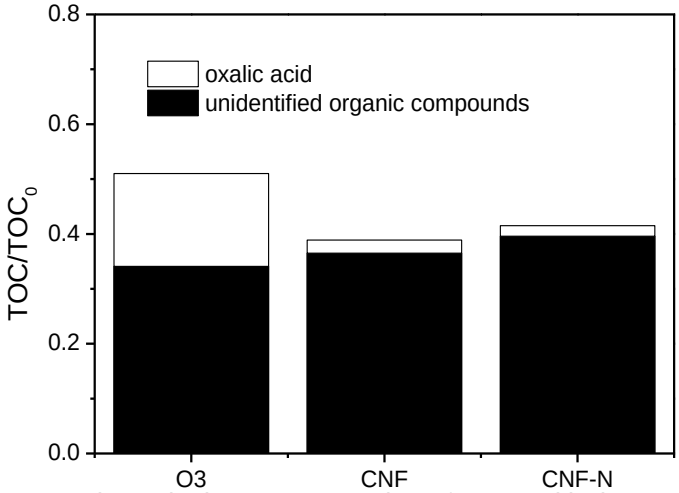

Figure 5.16 – Dimensionless concentration of TOC, with the contribution of oxalic acid and of other organic compounds identified, after 180 minutes, during the semi-batch ozonation of phenol experiments carried out in the presence of pristine and N-doped carbon nanofibers.

Observation of Figure 5.20 clearly indicates that the main contribution for the lower TOC removal during experiments with CNF-N were due to the increase in the amount of other organic intermediates other than oxalic acid. As in MWCNT, this indicates that these compounds, which are likely harder to degrade than oxalic acid, tend to be the preferred path of degradation. The amount of nitrogen on the CNF seems to play a determinant role in the ozonation of phenol, likely due to changes in the electronic density on the surface of the material [31]. Nevertheless, changes to the degradation mechanism, i.e. whether the reaction is occurring on the catalyst surface or on the liquid bulk through direct ozonation or interaction with radical species, should not be disregarded. In fact, it has been reported that different types of nitrogen species may lead to different reaction mechanisms [6, 8, 14].

5.2.2 CONTINUOUS OZONATION

After the semi-batch experiments using powder catalysts, experiments were performed in continuous operation using structured catalysts in ozonation. The catalysts consisted in CNF-covered honeycomb cordierite monoliths. Two different catalysts were used: one CNF covered monolith with carbon loading 11.4 wt.% and one N-doped CNF-covered monolith with carbon loading 7.9 wt.%. Both catalysts were 60 mm x 22 mm, with channel density 64 cpsi. Further description of the catalysts can be found in section *Materials and methods*. The experiments were performed in a bubble column reactor using an internal recirculation loop, in three-phase operation, as described in detail in section *Materials and methods.*

First off, the unmodified CNF and the N-doped CNF monoliths were used as catalysts in the continuous ozonation of oxalic acid. The removals as measured at steady state are presented in Figure 5.17.

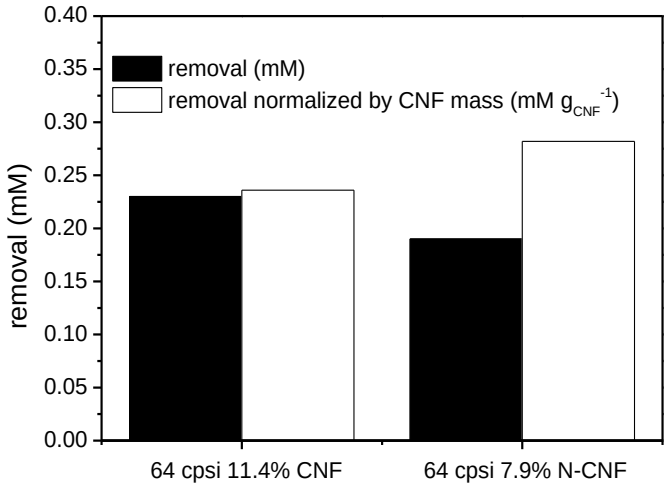

Figure 5.17 – Removal of oxalic acid during continuous ozonation experiments using unmodified and N-doped CNF covered monoliths: absolute values and normalized by CNF mass values.

While the removal of oxalic acid was less extensive when the N-CNF monolith was used, the normalization of the measured removal of oxalic acid by the loading of carbon materials on the structured catalysts inverts

this trend. In fact, if the removal per mass of CNF is considered, the N-CNF structured catalyst removed approximately 5 mM of oxalic acid more than its CNF counterpart, per gram of CNF. This observation agrees with what was observed in semi-batch experiments, where the amount of catalyst used was the same for the experiments with the different samples. Thus, while the efficiency of the catalyst is smaller, the doping of the CNF with nitrogen improves the activity of the CNF in the catalytic ozonation of oxalic acid.

Further experiments were carried out using selected emerging organic micropollutants: atrazine, metolachlor and nonylphenol. The detailed description of the ozonation of these pollutants is presented in section *Ozonation of emerging organic micropollutants.*

The removal of the three pollutants during the continuous ozonation experiments is presented in Figure 5.18.

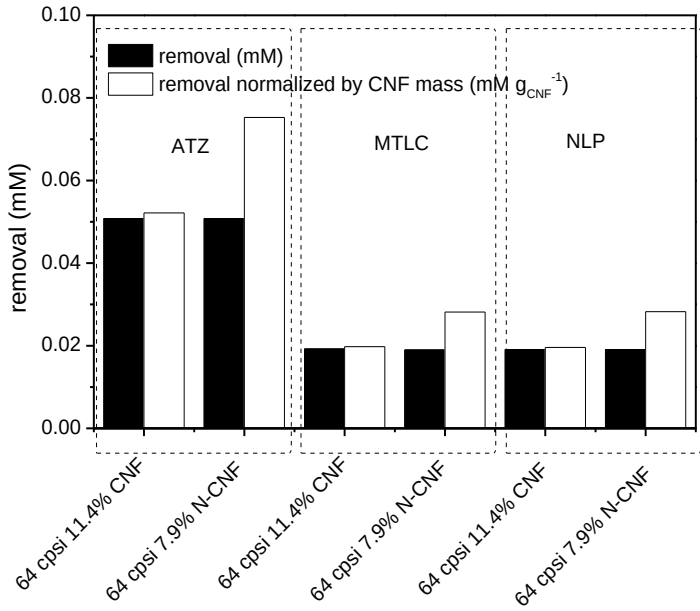

Figure 5.18 – Removal of atrazine, metolachlor and nonylphenol during continuous ozonation experiments using unmodified and N-doped CNF covered monoliths: absolute values and normalized by CNF mass values.

Observing the values for removal of the pollutants, it is clear that there is not much of a difference when the either of the structured catalysts was used. Furthermore, when compared with the values obtained during single ozonation experiments, not shown here (section *Ozonation of emerging organic micropollutants)*, it is clear that the addition of the catalysts does not improve the oxidation of these pollutants. In fact, all the three pollutants have been demonstrated to quickly react with ozone, as depicted in section *Ozonation of emerging organic micropollutants* [32-41]. Thus, while a similar calculation of the removal per CNF loading as made for oxalic acid is presented in Figure 5.18, its significance should be observed with caution. In fact, there is no evidence to support that surface reactions might be improving the oxidation of these pollutants; kinetic experiments performed with atrazine have shown an increase in its removal when the catalyst loading was increased in semi-batch experiments using MWCNT in powder form, but this was attributed to adsorption rather than oxidation; since the measured values are presented at steady state, adsorption should not be playing an important role due to saturation of the CNF surface [19]. In the case of oxalic acid, it is known that surface reactions are contributing to the oxidation of the pollutant during ozonation, at similar conditions to those used here [2]. The mineralization degree, as measured through TOC removal, is a better measure of the efficiency of the catalysts, and is much more closely related with surface reactions, or radical reactions in the liquid bulk, than the oxidation of the parent pollutant [19, 32, 33, 39]. The mineralization degree of the three organic pollutants obtained during continuous ozonation experiments using CNF and N-CNF structured catalysts is presented in Figure 5.19.

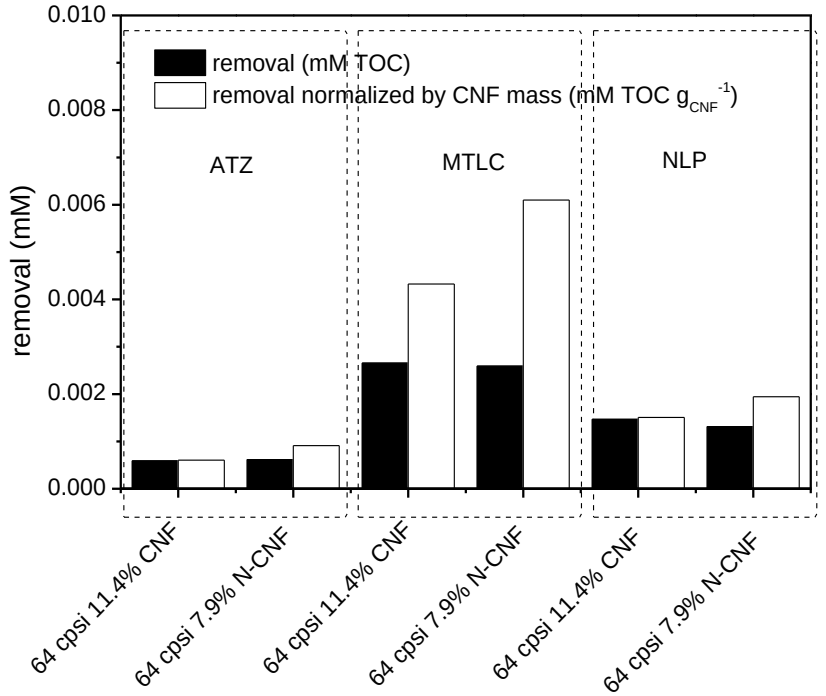

Figure 5.19 – Removal of TOC from atrazine, metolachlor and nonylphenol during continuous ozonation experiments using unmodified and N-doped CNF covered monoliths: absolute values and normalized by CNF mass values.

The mineralization degree achieved by the CNF and N-CNF structured catalysts was higher than what was observed in the case of the non-catalytic experiments. Moreover, only a slight difference was observed between the two catalysts; the CNF catalyst showed a somewhat improved activity when compared with the N-doped catalyst. However, similarly to what was observed in the experiments with oxalic acid, the removal of the TOC normalized by the amount of CNF is higher when the N-CNF structure is considered. As seen in section *Ozonation of emerging organic micropollutants*, the TOC removal is improved in the presence of a carbon based catalyst, either due to surface reactions or through the generation of hydroxyl radicals in solution. Behaviour of the ozonation by-products is discussed in Appendix B.

The toxicity of the resulting effluents was also evaluated, using CNF and N-CNF structured catalysts in the catalytic ozonation of the selected organic micropollutants. However, since the toxicity is not inherent to a single parameter, but rather due to the interaction between all the components in the water sample, it is not possible to normalize the obtained inhibitions levels by the mass of CNF on the catalyst. Thus, only the absolute values are presented in Figure 5.20.

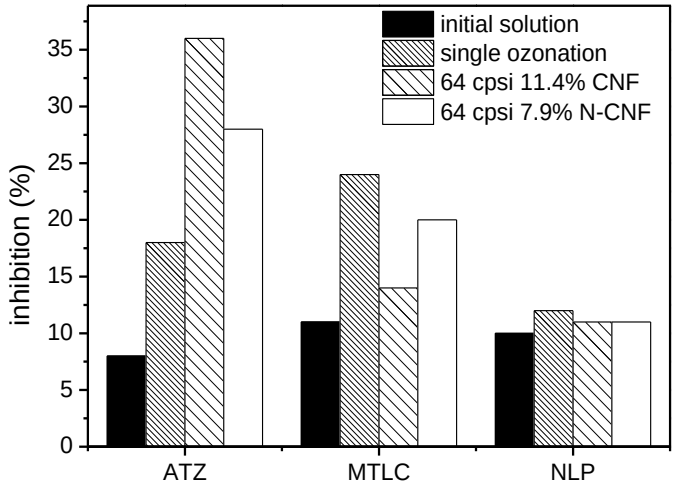

Figure 5.20 – Inhibition of luminescent activity of *Vibrio Fischeri* bacteria during Microtox tests, after exposure to samples taken at steady-state during continuous ozonation experiments of atrazine, metolachlor and nonylphenol using CNF and N-CNF structured catalysts.

Observing atrazine, it is clear that the application of a catalyst to the ozonation system results in more toxic effluents, as had been observed in section *Ozonation of emerging organic micropollutants*. Nevertheless, the N-CNF structured catalyst lead to a less toxic effluent, probably due to a lesser extent in the degradation of the products of atrazine ozonation. In fact, when the contact area of the effluent with the catalyst was increased, in section *Operation conditions*, it was observed that further degradation of atrazine lead to more toxic effluents. In this case, the smaller loading of CNF on the structured catalyst resulted in a less toxic mixture of components; however, one should notice that this is not necessarily a sign

of a better catalyst, but most probably simply a consequence of the reaction conditions. In the case of metolachlor, the trend follows closely what was observed in sections section *Ozonation of emerging organic micropollutants* and *Operation conditions*. The more extensive TOC removal resulted in a less toxic effluent, which means that N-CNF produced a more toxic sample than CNF, despite improving the toxicity of the effluent subject to the non-catalytic process. Finally, nonylphenol, has had been observed in section *Ozonation of emerging organic micropollutants*, did not present significant variations of the toxicity measured at steady state.

In summary, it has been observed that the modification of the surface of nanocarbon materials with different heteroatoms results in different catalytic activities in the catalytic ozonation process. The introduction of N-containing functionalities was shown to be the most interesting of those studied here, since they were observed to improve the performance of the catalysts. Furthermore, a similar effect was observed whether carbon nanotubes or carbon nanofibers were used. The application of N-doped carbon nanofibers as a structured catalyst was shown to, in fact, presents a better activity in the catalytic ozonation process. However, the production of these N-CNF materials yields a smaller loading of carbon on the structured catalyst, which is detrimental to the overall performance of the system. Besides enhancing the catalytic activity of the carbon materials, the N-containing functionalities were also observed to lead to changes in the degradation path of organic emerging micropollutants.

5.3 Influence of amount and type of nitrogen content

Since the samples with N-containing surface groups showed good activity as catalysts for the catalytic ozonation process, experiments were performed in order to study how the amount, and the type, of nitrogen included on the surface of carbon catalysts influences their performance.

For this end, several N-doped carbon xerogels were used in the ozonation of oxalic acid. These materials were selected due to their wide spectra of nitrogen content on the surface, both in amount and in type, which is obtained through changes in their preparation method. The characterization of these materials is detailed in section *Materials and methods.*

The concentration profiles of oxalic acid during ozonation experiments using the selected samples of N-doped carbon xerogels are presented in Figure 5.21.

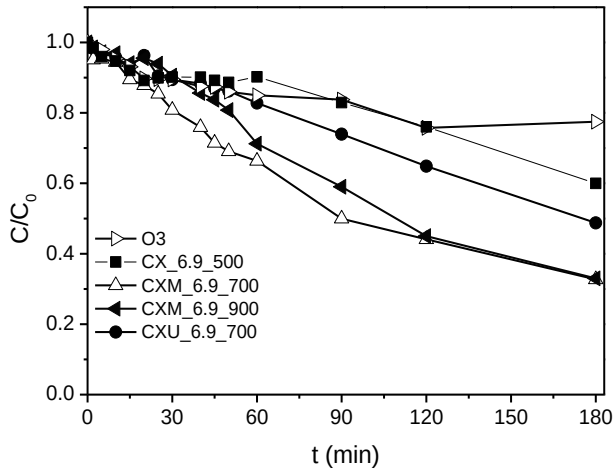

Figure 5.21 – Dimensionless concentration of oxalic acid during the semi-batch ozonation experiments carried out in the presence of carbon xerogels with different amounts and types of nitrogen on the surface.

Figure 5.21 shows that inclusion of a catalyst improves the removal of oxalic acid from solution when compared with the single ozonation experiment. The removal increased from 20% (without catalyst) to around 55% with the best catalysts, after 120 min of reaction. The results show that carbon xerogels promote the formation of more reactive species from ozone, either in solution or on the surface of the catalyst [42]. Nevertheless, complete conversion of oxalic acid was never achieved up to the limit of the experiments (120 min). It is clear that these carbon xerogels do not perform as well as other carbon catalysts which have

been previously tested in the same system: complete removal of oxalic acid was achieved after approximately 60 minutes of reaction with multi walled carbon nanotubes, using the same reaction system and operating conditions [1]; with activated carbons, the removal of oxalic acid was close to 70 % after 120 minutes [2].

The apparent first-order reaction rate constants in ozonation of oxalic acid are listed in Table 5.1.

Table 5.1 – Apparent constant of reaction calculated for the catalytic ozonation of oxalic acid using N-doped carbon xerogel samples.

Sample	k (min^{-1})
CX_6.9_500	0.0026
CXM_6.9_700	0.0084
CXM_6.9_900	0.0053
CXU_6.9_700	0.0034

It is interesting to note that the performance of the catalysts is not significantly affected by the surface area. In fact, the sample which presents the largest surface area (sample CXU_6.9_700) performs worse than the remaining; while the sample with the smallest value of S_{BET} shows the best performance (sample CXM_6.9_700). In principle, the surface area should affect the amount of ozone decomposed [1, 5, 43-45], but in the present case the chemical properties are more important. A positive correlation was found between the first order reaction rate constant and the N content, as shown in Figure 5.22.

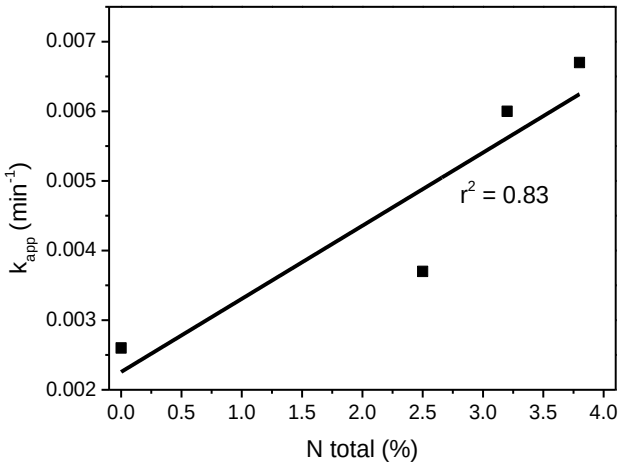

Figure 5.22 – Apparent constant of reaction calculated for the catalytic ozonation of oxalic acid versus the amount of N contained on the carbon xerogels, determined by XPS.

Correlations with the pH_{pzc} or with the surface oxygen content have been previously reported [1, 2, 4, 7, 13, 46]. However, one should note that the changes in the pH at the point of zero charge are not very drastic in the present case, and thus its influence is probably not noticeable. Nevertheless, the effect of the nitrogen functionalities is quite significant. These groups contribute with electrons to the π-electron system, increasing the electron density on the surface of the material, which favours the reduction of ozone due to its electrophilic properties [1, 47-49]. Furthermore, it has been suggested that ozone may attack pyrrolic groups on the carbon surface, yielding the hydroperoxide radical, which would lead to the formation of other highly reactive species which greatly contribute to increase the removal rate of oxalic acid during ozonation [14, 50]. However, attempts to correlate specific nitrogen functionalities with the activity did not yield good correlations, which suggest that the positive effect might be due to the compound action of the various species.

Further experiments were performed with *tert*-BuOH as a radical scavenger using the most active sample as catalyst, in order to provide further insights into the reaction mechanism. *tert*-BuOH is a well-known

hydroxyl radical scavenger [51], reacting rapidly with hydroxyl radicals in the liquid phase [52]. The performance of the catalyst is shown in Figure 5.23, together with the corresponding adsorption experiment, using the same carbon xerogel sample.

It is clear that the extent of adsorption of oxalic acid on the catalyst is not significant when compared with the removals obtained during the catalytic ozonation experiments. A decrease in the removal of oxalic acid of approximately 15 % after 120 min is observed when *tert*-BuOH is used as a radical scavenger. Such behaviour suggests that the production of radicals in the liquid phase plays only a secondary role in the catalytic ozonation using N-containing carbon xerogels.

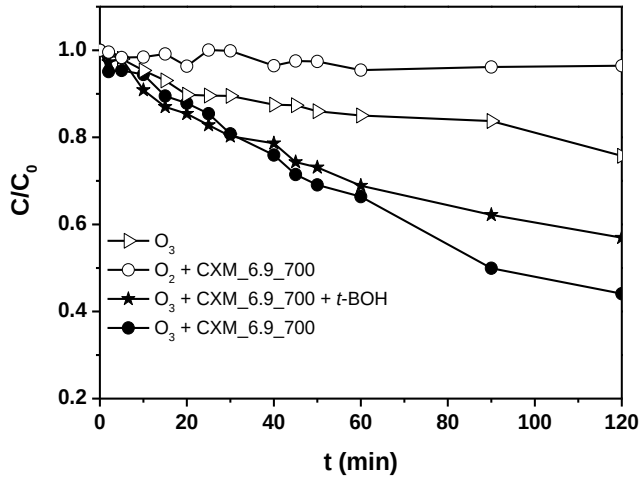

Figure 5.23 – Dimensionless concentration of oxalic acid during the semi-batch ozonation experiment carried out in the presence of carbon xerogel using a radical scavenger, and in experiment carried out without ozone.

Recycling experiments performed with the CXM_6.9_700 sample are presented in Figure 5.24. A slightly worse performance was observed when compared to the fresh sample; deactivation may be due to the oxidation of the carbon surface, as reported previously [1, 44, 48].

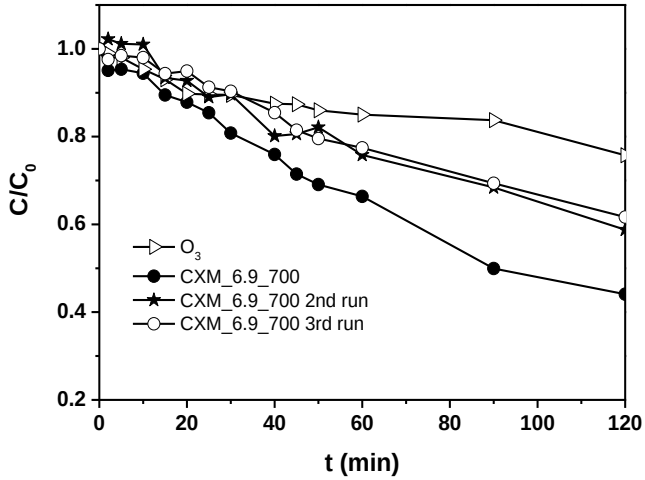

Figure 5.24 – Dimensionless concentration of oxalic acid during the recycling semi-batch ozonation experiments carried out in the presence of carbon xerogel.

Post-reaction analysis of the CXM_6.9_700 sample by XPS, as detailed in section *Stability and deactivation of the catalysts*, showed a new peak, when compared with the fresh sample, with binding energy around 402.8 eV, which may be attributed to oxidized nitrogen species [31]. In addition, a large decrease was observed in the area of the N6 peak, corresponding to pyridine functionalities. In reactions with ozone with activated carbons, it has been observed that the surface pyridine groups were stable [6, 8, 14]. However, it is clear that the stability of the N6 group is lower in carbon xerogels. Nevertheless, rigorous quantification of the species found in the post-reaction samples was not possible, due to the interference of the support used for XPS analysis of granulated samples, which did not form a uniform piece when mechanical pressure was applied. The results support the idea that the enhanced catalytic ozonation with N-treated carbon xerogels is mostly due to the increase of the electronic density on the surface.

In summary, the effect of the N-doping of carbon xerogels on the catalytic performance of the materials was evaluated. In the ozonation experiments, despite the basic nature of their surface, the CXs

underperformed when compared with other carbon based catalysts. In fact, complete conversion of oxalic acid was never achieved in the reaction times employed (120 min). However, a positive correlation was found between the removal rate and the surface nitrogen content. Attempts to correlate the activity with the type of nitrogen functionalities did not provide good correlations. Therefore, N-doping improves the catalytic performance of the carbon xerogels in this liquid phase oxidation process. Moreover, experiments with a radical scavenger suggest that a surface reaction mechanism is the main pathway for the degradation of oxalic acid by ozonation, but there seems to be some contribution of the reactions carried out by hydroxyl radicals in the liquid bulk.

5.4 PARTIAL CONCLUSIONS

The influence of surface heteroatoms on the activity of carbon materials in the catalytic ozonation of organic pollutants was evaluated.

On a first approach, carbon nanotubes which were subject to doping with several different elements were used as catalysts in the catalytic ozonation process. The introduction of these elements lead to the formation of oxygen-containing, sulphur-containing and nitrogen-containing functionalities, which lead to materials with different surface acidities and electronic densities. To evaluate the catalytic activity of the materials, oxalic acid was used as a model compound. It was observed that the most active materials were those that presented a more basic character, with the N-containing MWCNT sample being the most active. Afterwards, the same materials were tested in the ozonation of phenol. In this case, the modifications of the surface of the MWCNT did not lead to improved mineralization of phenol, but rather to changes in the distribution of the products accumulated in solution.

After experiments with MWCNT, the same procedure was used to evaluate the influence of N-doping on carbon nanofibers. Similar observations were made during ozonation of oxalic acid and phenol. The

activity of the CNF was similar to that of MWCNT, with sample N-CNF proving to be the most active sample.

On a next step, the doping of CNF with nitrogen was evaluated in the continuous ozonation of organic pollutants using structured catalysts, consisting on honeycomb cordierite monoliths covered with CNF. These materials were tested using oxalic acid as a model compound, but also three different emerging organic micropollutants. It was observed that the N-CNF catalyst performed better than the CNF catalyst, when the mass of CNF on the structure was considered. In fact, the N-CNF presented a smaller amount of carbon due to constrictions during its preparation. Thus, in absolute values, the CNF structured catalyst achieved better results than the N-CNF catalyst.

Finally, the influence of the amount and type of nitrogen on the catalytic activity of carbon materials in the ozonation process was assessed. For this, different carbon xerogels were used due to the vast array of varying amounts and types of N-containing functionalities that can be introduced. It was possible to positively correlate the amount of nitrogen with the activity of the materials, using oxalic acid as a model compound. However, attempts to correlate the activity with specific types of functionalities were not successful.

REFERENCES

[1] A.G. Gonçalves, J.L. Figueiredo, J.J.M. Órfão, M.F.R. Pereira, Carbon, 48 (2010) 4369-4381.
[2] P.C.C. Faria, J.J.M. Órfão, P. M.F.R., Applied Catalysis B, Environmental, 79 (2008) 237.
[3] J.L. Figueiredo, M.F.R. Pereira, Catalysis Today, 150 (2010) 2-7.
[4] Z.-Q. Liu, J. Ma, Y.-H. Cui, L. Zhao, B.-P. Zhang, Separation and Purification Technology, 78 (2011) 147-153.
[5] C.A. Orge, Catalysis Letters, 132 (2009) 1.
[6] H. Cao, L. Xing, G. Wu, Y. Xie, S. Shi, Y. Zhang, D. Minakata, J.C. Crittenden, Applied Catalysis B: Environmental, 146 (2014) 169-176.
[7] Z.Q. Liu, Applied catalysis. B, Environmental, 92 (2009) 301.
[8] L. Xing, Y. Xie, H. Cao, D. Minakata, Y. Zhang, J.C. Crittenden, Chemical Engineering Journal, 245 (2014) 71-79.
[9] Z.-Q. Liu, J. Ma, Y.-H. Cui, L. Zhao, B.-P. Zhang, Applied Catalysis B: Environmental, 101 (2010) 74-80.
[10] F.J. Beltrán, J.F. García-Araya, I. Giráldez, Applied Catalysis B: Environmental, 63 (2006) 249-259.
[11] R.P. Rocha, J. Restivo, J.P.S. Sousa, J.J.M. Órfão, M.F.R. Pereira, J.L. Figueiredo, in press, Catalysis today, in press(2014).
[12] S. Yang, X. Li, W. Zhu, J. Wang, C. Descorme, Carbon, 46 (2008) 445-452.
[13] P.C.C. Faria, J.J.M. Órfão, M.F.R. Pereira, Chemosphere, 67 (2007) 809-815.
[14] M. Sanchez-Polo, U. von Gunten, J. Rivera-Utrilla, Water Res, 39 (2005) 3189-3198.
[15] P.C.C. Faria, J.J.M. Órfão, M.F.R. Pereira, Applied Catalysis B: Environmental, 79 (2008) 237-243.
[16] Z.-Q. Liu, J. Ma, Y.-H. Cui, B.-P. Zhang, Applied Catalysis B: Environmental, 92 (2009) 301-306.
[17] K. Turhan, S. Uzman, Desalination, 229 (2008) 257-263.
[18] F.J. Beltrán, F.J. Rivas, R. Montero-de-Espinosa, Journal of Chemical Technology and Biotechnology, 78 (2003) 1225-1233.
[19] X. Fan, J. Restivo, J.J.M. Órfão, M.F.R. Pereira, A.A. Lapkin, Chemical Engineering Journal, 241 (2014) 66-76.
[20] J.W. Choi, H.S. Lee, Applied Chemistry for Engineering, 23 (2012) 490-495.
[21] W. Pratarn, T. Pornsiri, S. Thanit, C. Tawatchai, T. Wiwut, Chinese Journal of Chemical Engineering, 19 (2011) 76-82.
[22] P. Limsuwan, S. Kumagai, M. Nonaka, K. Sasaki, W. Tanthapanichakoon, T. Hirajima, Advanced Materials Research, 701 (2013) 305-309.
[23] R.P. Rocha, A.M.T. Silva, S.M.M. Romero, M.F.R. Pereira, J.L. Figueiredo, Applied Catalysis B: Environmental, 147 (2014) 314-321.
[24] H.T. Gomes, S.M. Miranda, M.J. Sampaio, J.L. Figueiredo, A.M.T. Silva, J.L. Faria, Applied Catalysis B: Environmental, 106 (2011) 390-397.

[25] H.T. Gomes, S.M. Miranda, M.J. Sampaio, A.M.T. Silva, J.L. Faria, Catalysis Today, 151 (2010) 153-158.
[26] S.S. Abu Amr, H.A. Aziz, M.N. Adlan, Waste Management, 33 (2013) 1434-1441.
[27] S.S. Abu Amr, H.A. Aziz, M.N. Adlan, M.J.K. Bashir, Chemical Engineering Journal, 221 (2013) 492-499.
[28] J. Criquet, N.K.V. Leitner, Chemosphere, 77 (2009) 194-200.
[29] X.-Y. Xu, G.-M. Zeng, Y.-R. Peng, Z. Zeng, Chemical Engineering Journal, 200–202 (2012) 25-31.
[30] H. Sun, C. Kwan, A. Suvorova, H.M. Ang, M.O. Tadé, S. Wang, Applied Catalysis B: Environmental, 154-155 (2014) 134-141.
[31] H.-P. Boehm, Catalytic Properties of Nitrogen-Containing Carbons, Carbon Materials for Catalysis, John Wiley & Sons, Inc.2008, pp. 219-265.
[32] S. Derrouiche, D. Bourdin, P. Roche, B. Houssais, C. Machinal, M. Coste, J. Restivo, J.J.M. Orfao, M.F.R. Pereira, Y. Marco, E. Garcia-Bordeje, Water Sci Technol, 68 (2013) 1377-1383.
[33] C.A. Guzman-Perez, J. Soltan, J. Robertson, Separation and Purification Technology, 79 (2011) 8-14.
[34] J. Ma, N.J.D. Graham, Water Research, 33 (1999) 785-793.
[35] J. Ma, N.J.D. Graham, Water Research, 34 (2000) 3822-3828.
[36] S. Nélieu, L. Kerhoas, J. Einhorn, Environmental Science & Technology, 34 (1999) 430-437.
[37] Y.M. Vera, R.J.d. Carvalho, M.L. Torem, B.A. Calfa, Chemical Engineering Journal, 155 (2009) 691-697.
[38] M.L. Hladik, A.L. Roberts, E.J. Bouwer, Water Research, 39 (2005) 5033-5044.
[39] J. Restivo, J.J.M. Órfão, S. Armenise, E. Garcia-Bordejé, M.F.R. Pereira, Journal of Hazardous Materials, 239–240 (2012) 249-256.
[40] B. Ning, N.J.D. Graham, Y. Zhang, Chemosphere, 68 (2007) 1163-1172.
[41] B. Ning, N.J.D. Graham, Y. Zhang, Chemosphere, 68 (2007) 1173-1179.
[42] B. Legube, Catalysis Today, 53 (1999) 61.
[43] M. Sanchez-Polo, Water Research, 39 (2005) 3189.
[44] C.A. Orge, J.J.M. Órfão, M.F.R. Pereira, Applied Catalysis B: Environmental, 126 (2012) 22-28.
[45] J. Rivera-Utrilla, M. Sánchez -Polo, Applied catalysis. B, Environmental, 39 (2002) 319.
[46] F.J. Beltrán, Applied Catalysis B, Environmental, 63 (2006) 249.
[47] J.P.S. Sousa, M.F.R. Pereira, J.L. Figueiredo, Applied Catalysis B: Environmental, 125 (2012) 398-408.
[48] P.C.C. Faria, J.J.M. Órfão, M.F.R. Pereira, Industrial & engineering chemistry research, 45 (2006) 2715-2721.
[49] C.A. Leon y Leon, J.M. Solar, V. Calemma, L.R. Radovic, Carbon, 30 (1992) 797-811.
[50] C. Gottschalk, J.A. Libra, A. Saupe, Ozonation of water and waste water a practical guide to understanding ozone and its application, Wiley-VCH, 2000.

[51] F.J. Beltrán, F.J. Rivas, L.A. Fernández, P.M. Álvarez, R. Montero-de-Espinosa, Industrial & engineering chemistry research, 41 (2002) 6510-6517.
[52] J. Hoigné, Water Science and Technology, 35 (1997) 1-8.

6. STABILITY AND DEACTIVATION OF THE CATALYSTS

6.1 DESCRIPTION

In this chapter the stability of the nanocarbon based materials was assessed during the ozonation reaction.

On a first approach, the activity of pristine and modified MWNT in powder form was assessed during recycling experiments. The modification of the surface properties of the materials were monitored, and were related to the observed behaviour during recycling experiments. Similar observations were made for other types of carbons, i.e. carbon xerogels and carbon nanofibers.

Afterwards, CNF covered honeycomb monoliths were used in long term continuous ozonation experiments. A similar approach to what was carried out with the catalysts in powder form was taken, and the deactivation of the structured catalysts was related to the modification of the surface chemistry due to the action of ozone.

The materials used in this chapter were prepared and kindly made available by: doped MWCNT, by Raquel P. Rocha, prepared at Laboratório de Catálise e Materiais, Universidade do Porto; pristine and doped CX, by Dr. Juliana P. S. Sousa, prepared at Laboratório de Catálise e Materiais, Universidade do Porto; and pristine and doped CNF by the group of Prof. Enrique Garcia-Bordejé, at Instituto de Carboquímica, part of the Consejo Superior de Investigación Científica, in the context of the European Commission financed project MONACAT.

The work presented in this chapter has been partially published in the following references:

R.P. Rocha, J. Restivo, J.P.S. Sousa, J.J.M. Órfão, M.F.R. Pereira, J.L. Figueiredo, Nitrogen-doped carbon xerogels as catalysts for advanced oxidation processes, in press, Catalysis today, (2014).

J. Restivo, R.P. Rocha, A.M. Silva, J.J. Órfão, M.F. Pereira, J.L. Figueiredo, Catalytic performance of heteroatom-modified carbon nanotubes in advanced oxidation processes, 35 (2014) 896-905.

J. Restivo, J.J.M. Órfão, M.F.R. Pereira, E. Garcia-Bordejé, P. Roche, D. Bourdin, B. Houssais, M. Coste, S. Derrouiche, Catalytic ozonation of organic micropollutants using carbon nanofibers supported on monoliths, Chem. Eng. J., 230 (2013) 115-123.

6.2 Recycling of catalysts in semi-batch

6.2.1 Catalytic activity

On a first approach to the assessment of the stability of the catalysts during the catalytic ozonation reactions, recycling experiments were performed using several catalysts in powder form, in a semi-batch completely stirred tank reactor. For these experiments, pristine and modified MWCNT and N-doped carbon xerogels were used. Their characterization is detailed in section *Materials and methods*, and their activity in the catalytic ozonation process was assessed in section *Modification of the carbon surface*.

The dimensionless concentration of oxalic acid during the reutilization of the pristine MWCNT in the ozonation of oxalic acid, used as a model compound, is presented in Figure 6.1. The performance of the fresh pristine MWCNT is also included, as seen in section *Modification of the carbon surface.*

The activity of the reused pristine MWCNT was observed to decrease when it was reutilized. The reaction of ozone with MWCNT has been observed to increase the amount of acidic oxygen-containing surface groups [1], as shown in the *Post-reaction characterization* below. The introduction of such functionalities on the surface of carbon materials has been shown to hinder their activity in this reaction, due to the delocalization of π-electrons on the surface of the catalyst [1-8]. However,

a 3rd reutilization cycle showed that the activity is stabilized after sufficient time, due to a stabilization of the amount of acidic O-containing groups on the surface of the catalyst [1, 9].

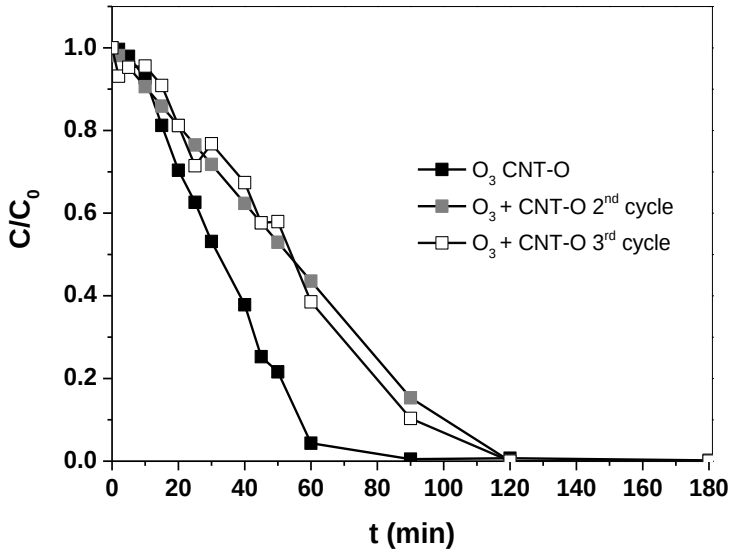

Figure 6.1 – Dimensionsless concentration of oxalic acid during semi-batch ozonation experiments using fresh and recycled pristine MWCNT.

Similar experiments were performed using the S-modified MWCNT samples, as presented in Figure 6.2.

The activity of the recycled CNT-S sample was similar to what was observed with the pristine MWCNT, in that a decrease in the removal of oxalic acid was observed when compared with the fresh catalyst. Even though the fresh CNT-S sample presents a low pH_{pzc}, the amount of acidic O-containing groups was observed to increase with the use in the ozonation reaction. While TPD of the CNT-S sample showed a large release of S-containing groups from the surface, as shown further below in SO_2 spectra, these groups do not seem to play a role in the ozonation reaction (section *Modification of the carbon surface).*

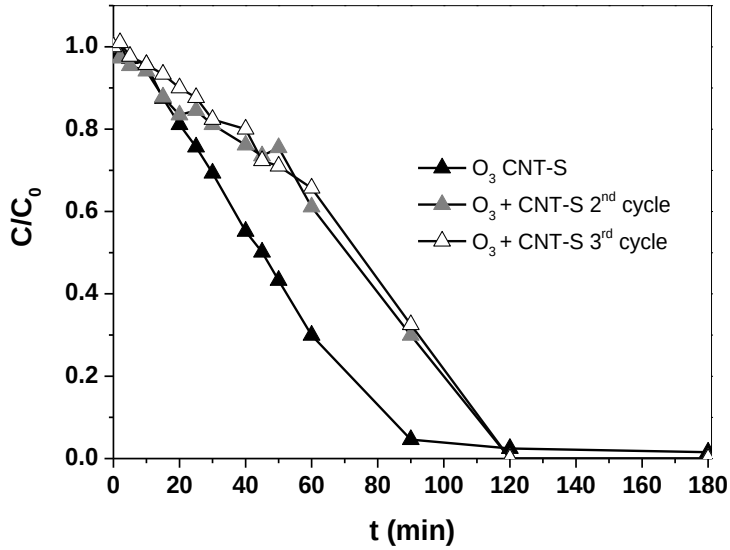

Figure 6.2 – Dimensionsless concentration of oxalic acid during semi-batch ozonation experiments using fresh and recycled S-doped MWCNT.

The reutilization of the N-treated MWCNT was also performed in the ozonation of oxalic acid, as presented in Figure 6.3.

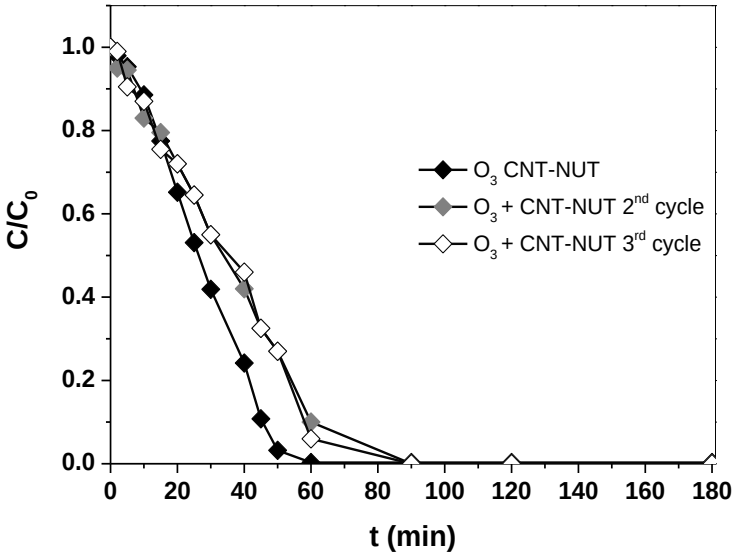

Figure 6.3 – Dimensionsless concentration of oxalic acid during semi-batch ozonation experiments using fresh and recycled N-doped MWCNT.

The recycling of the CNT-NUT samples also lead to a decrease in their catalytic activity. After the third reutilization cycle, the activity stabilized, as was observed in the cases of the pristine and S-doped MWCNT. While an increase in the amount of surface oxygenated functionalities was observed for CNT-NUT samples used in the ozonation reaction, some modifications of the nitrogen functionalities was observed. Thus, both factors might be taking part in the deactivation of the MWCNT, since the N-containing functionalities have been shown to be important for the improved activity of the CNT-NUT sample [3] (*Modification of the carbon surface)*. XPS analysis performed before and after the reaction are analysed further below.

Recycling experiments were also performed using N-doped carbon xerogel in the catalytic ozonation of oxalic acid, presented in Figure 6.4. The performance of the fresh carbon xerogel sample is also presented, as seen in section *Modification of the carbon surface*.

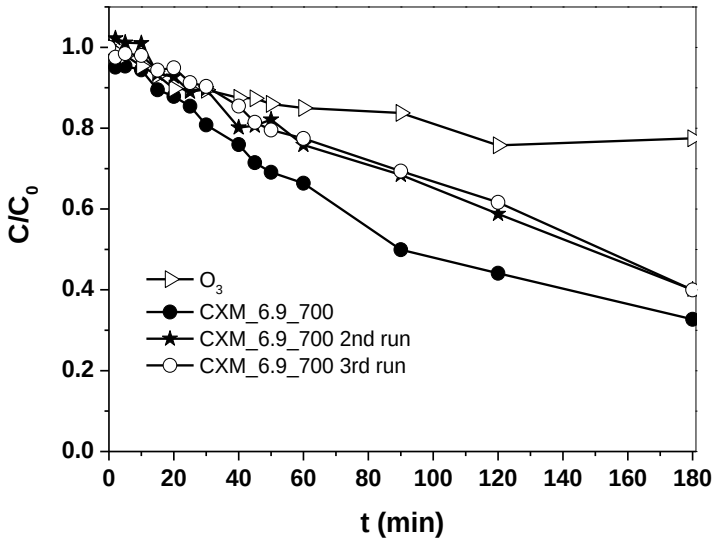

Figure 6.3 – Dimensionsless concentration of oxalic acid during semi-batch ozonation experiments using fresh and recycled N-doped carbon xerogel.

The reutilization of the N-doped carbon xerogel in the catalytic ozonation results lead to results similar to what was observed in the case of pristine and treated MWCNT. After the 1st utilization, the activity of the catalyst dropped, but became stable after the 2nd cycle. The deactivation of the catalyst is related with the introduction of acidic oxygen-containing functionalities on the surface of the carbon material. Nevertheless, it was observed by XPS that modifications of the N-containing functionalities took place during the ozonation process, which may be also playing a part in the observed decreased in catalytic activity. The changes in the carbon surface during the catalytic ozonation of oxalic acid are discussed further below.

In summary, it was observed that the reutilization of pristine and modified carbon materials, such as MWCNT and carbon xerogels, results in a loss of activity after the 1st run. However, the activity was observed to become stable after the 2nd reutilization. The modification of the carbon materials through the introduction of heteroatoms on the surface did not seem to alter the observed pattern. Nevertheless, different phenomena may be taking place on the surface of the material, depending on the element used in the modification of the surface.

6.2.2 Post-reaction characterization

Characterization of the catalyst samples was performed post-reaction, in order to relate the observed changes in the activity of the recycled catalysts with changes to the catalytic surface.

Temperature programed desorption (TPD) was carried out, on a first approach, on the pristine and modified MWCNT samples after ozonation with oxalic acid (see section *Modification of the carbon surface*). The obtained spectra for the release of CO and CO_2 during ozonation experiments are presented in Figure 6.4. The spectra for the fresh samples are also presented in Figure 6.4. The spectra for samples CNT-NUT and CNT-S were obtained from the papers by Rocha et al [10, 11].

Furthermore, the amount of CO and CO_2 released during the TPD experiments shown in Figure 6.4 are presented in Table 6.1.

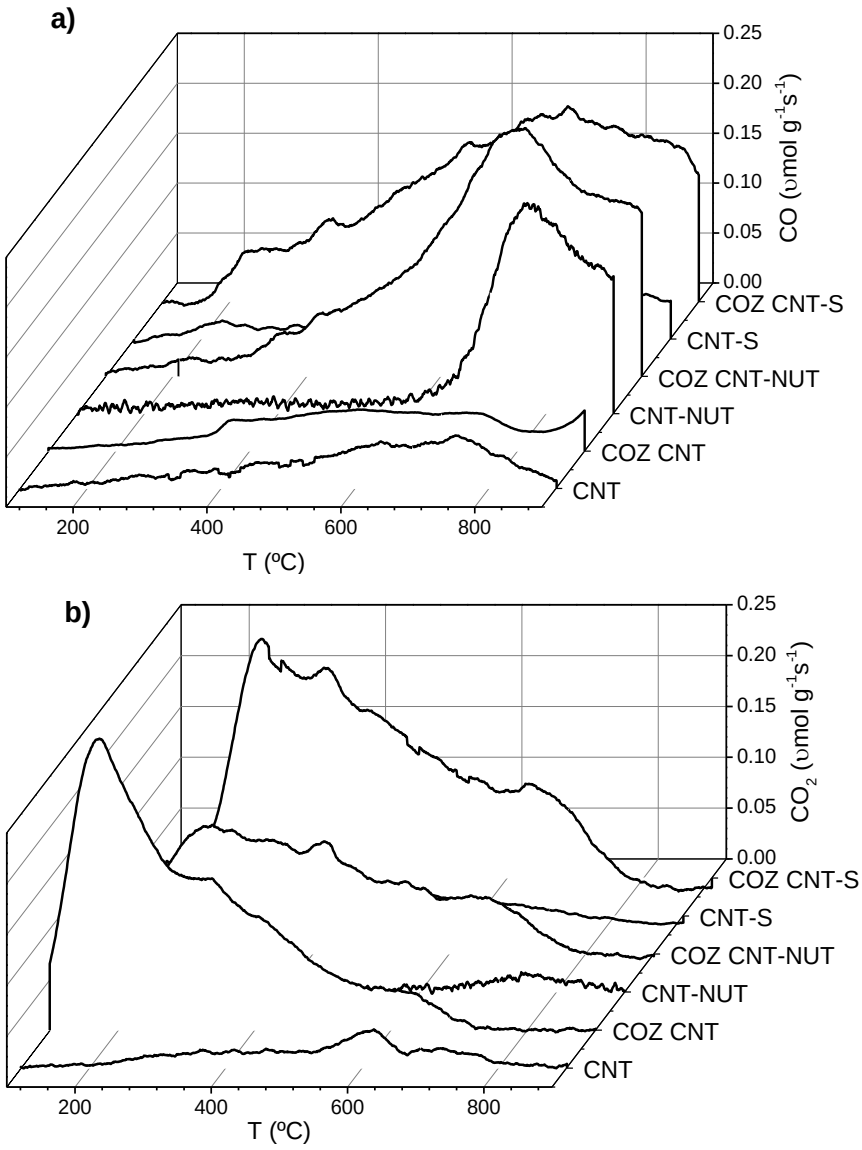

Figure 6.4 – Release of CO (a) and CO_2 (b) during TPD experiments carried out using the pristine and modified MWCNT samples before and after catalytic ozonation.

For all the MWCNT samples, either pristine or modified, the catalytic ozonation process resulted on an increase of the oxygenated species on

the surface released during TPD experiments as CO or CO_2. In the case of the CNT sample, the ozonation reaction lead mostly to the formation of groups released as CO_2 at low temperatures (from 150^{o}C to 600 ^{o}C). Typically, these correspond to carboxylic groups on the surface of the catalyst [12]. Furthermore, a small shoulder at 600 ^{o}C may be attributed to carboxylic anhydrides or lactones [12]; however, the quantity found here is very small and does not seem to change during the ozonation reaction. The CO spectra of the fresh and used CNT sample are very similar, with only a very slight increase in the mid-temperature region (400-600 ^{o}C) and in the high-temperature region (> 800 ^{o}C), which may correspond to the formation of quinones, phenol or carbonyl groups [12]. In the case of CNT-NUT, a smaller increase in the CO_2 released during TPD was observed, showing that the modification of the surface must change the interaction with ozone during reaction. Nevertheless, the increase that was observed was in similar regions to what was observed with the pristine CNT sample. The CNT-NUT sample already presented a large peak at high temperatures released as CO. Nevertheless, there was an increase in the amount released, mostly in the over 600 ^{o}C region. Regarding sample CNT-S, a similar behaviour was observed where the CO_2 is concerned. However, there was a large increase in the amount of groups released as CO when compared with the fresh CTN-S sample. Nevertheless, for all the samples, the formation of groups at low temperatures as CO_2 and at high temperatures as CO correspond to the expected formation of surface acidic oxygenated groups during ozonation, which then results on the observed decrease of activity during the recycling experiments [1, 2, 5-7, 12-14].

Table 6.1 – Amounts of CO and CO_2 released during TPD experiments of fresh and used pristine and modified MWCNT samples.

Sample	CO (μmol g^{-1})	CO_2 (μmol g^{-1})
CNT	200	128
COZ CNT	297	855
CNT-NUT	703	76
COZ CNT-NUT	1203	586
CNT-S	381	195
COZ CNT-S	936	1134

For the CNT-NUT sample, XPS analyses were carried out in order to assess the modification of the N-containing surface functionalities during the ozonation treatment. The deconvoluted N1s XPS peak of sample CNT-NUT before and after ozonation reaction is presented in Figure 6.5. The characterization of the fresh catalyst is here presented for the sake of comparison, as presented in section *Materials and methods*.

A decrease in the intensity of the peak attributed to N6 (pyridine) was observed. It has been suggested that ozone may attack pyrrolic groups on the surface of carbon materials, yielding the hydroperoxide radical, which would enhance the formation of other highly reactive species which greatly contribute to the increase in the removal rate of oxalic acid during ozonation, while the pyridinic groups remained stable [8, 15, 16]. The disparity in observations suggests that the stability of the N-functionalities on the surface of carbon might depend on the carbon matrix used, or on the preparation method employed.

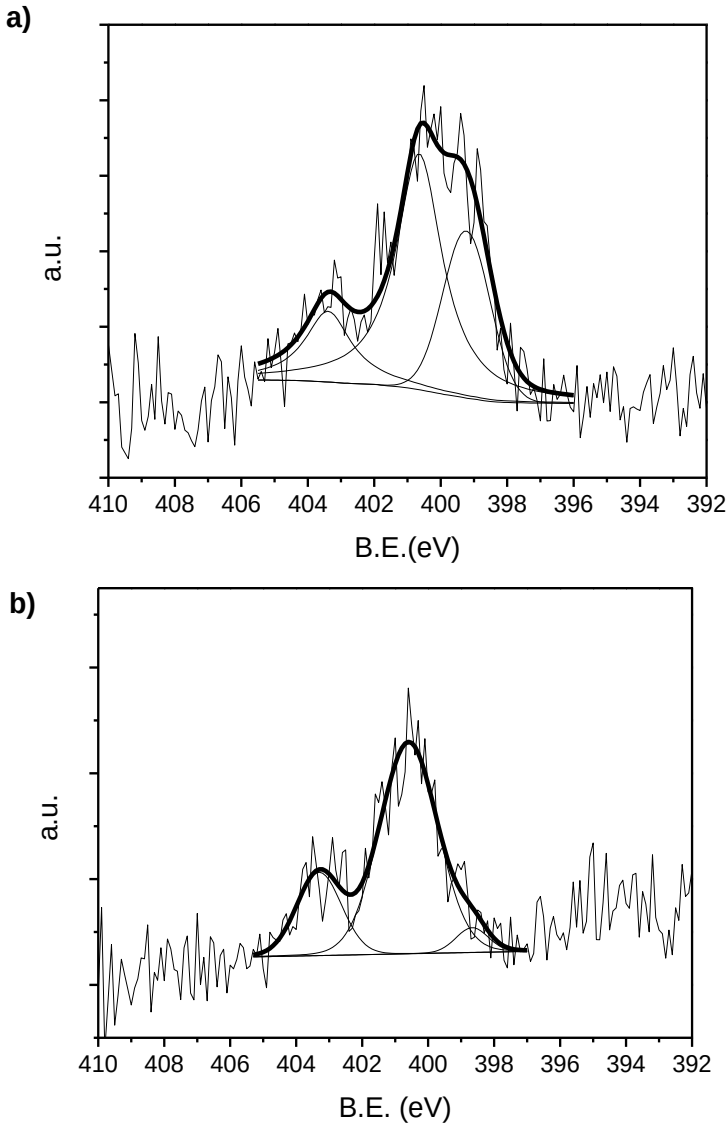

Figure 6.5 – Deconvoluted N1s peak obtained by XPS of sample CNT-NUT before (a) and after (b) the catalytic ozonation reaction.

Regarding the CNT-S sample, the SO_2 signal was also followed during TPD experiments of fresh and used catalyst. The obtained spectra are presented in Figure 6.6.

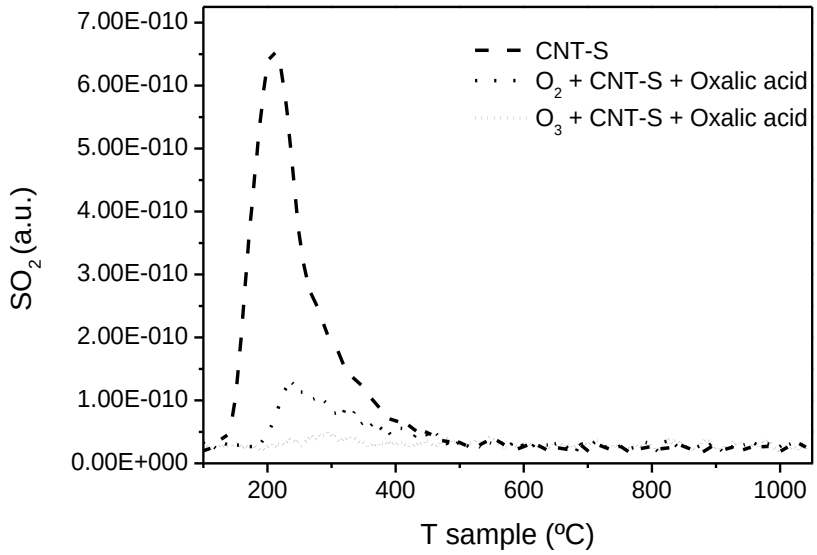

Figure 6.6 – Spectra of released SO_2 during TPD experiments of fresh and used CNT-S.

It is clear that the amount of S-containing groups on the surface of the CNT-S sample released as SO_2 decreased drastically during the ozonation reaction. In fact, even during adsorption experiment in the presence of oxygen, a large decrease in the amount of released SO_2 took place. Thus, it is clear that a large release of sulphur species occurs during these reactions. The role of these compounds in the ozonation reaction with sample CNT-S is discussed in section *Modification of the carbon surface*. Furthermore, XPS analyses of the S2p were carried out before and after catalytic ozonation reaction, and the resulting deconvoluted spectra are presented in Figure 6.7.

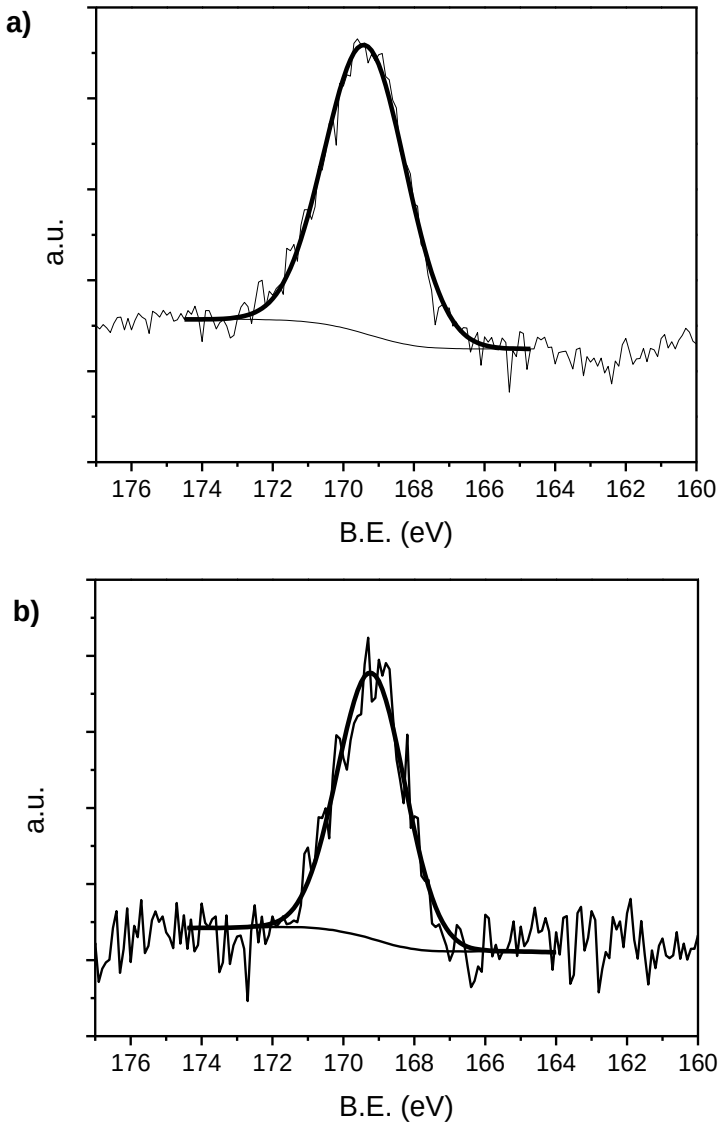

Figure 6.7 - Deconvoluted S2p peak obtained by XPS of sample CNT-S before (a) and after (b) the catalytic ozonation reaction.

Despite the release of S-containing functionalities during the catalytic ozonation experiment, the nature of these surface groups was not observed to change during the reaction process.

Similarly to what was done in the case of the pristine and modified MWCNT samples, the best performing N-doped carbon xerogel was also subject to post-reaction characterization by XPS.

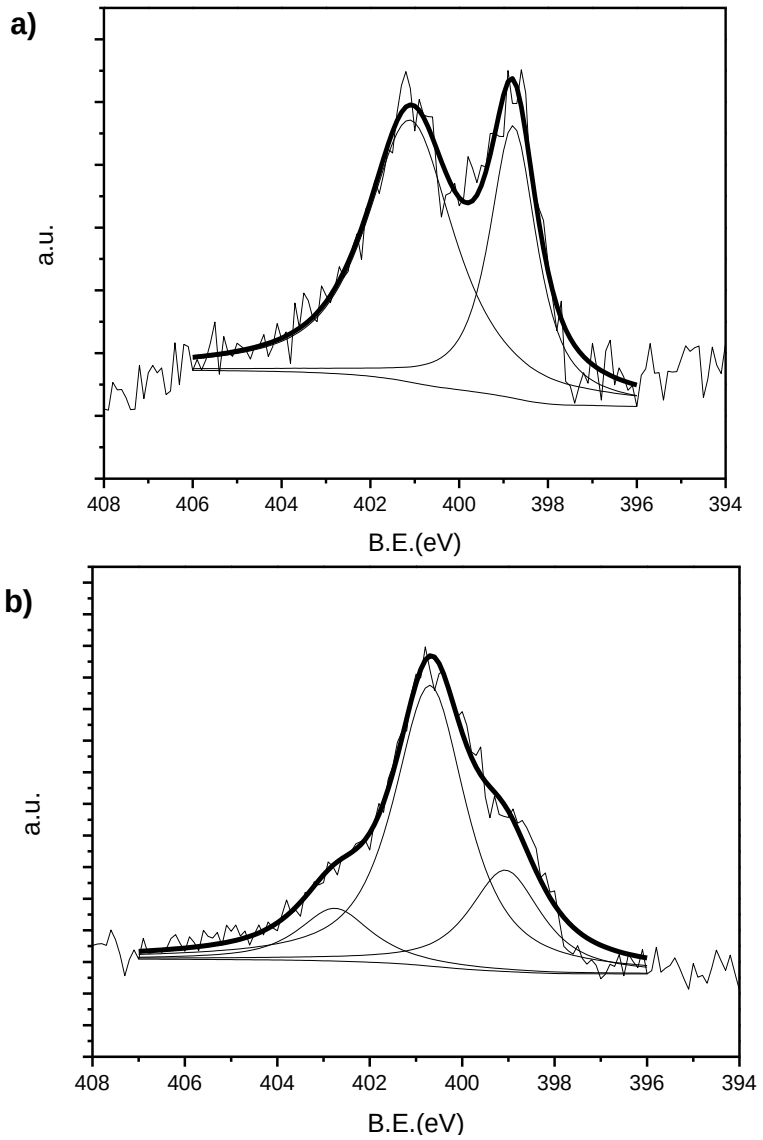

Figure 6.8 - Deconvoluted N1s peak obtained by XPS of sample CXM_6.9_700 before (a) and after (b) the catalytic ozonation reaction.

Post-reaction analysis of the CXM_6.9_700 sample by XPS showed a new peak, when compared with the fresh sample, with binding energy

around 402.8 eV, which may be attributed to oxidized nitrogen species [17]. In addition, a large decrease was observed in the area of the N6 peak, corresponding to pyridine functionalities. In their work with ozone on activated carbons, Sánchez-Polo et al. observed that the surface pyridine groups were stable [18]. However, it is clear that the stability of the N6 group is lower in carbon xerogels. Nevertheless, rigorous quantification of the species found in the post-reaction samples was not possible, due to the interference of the support used for XPS analysis of granulated samples, which did not form a uniform piece when mechanical pressure was applied.

Regarding the carbon nanofibers in powder form that were also used in the catalytic ozonation process (*Modification of the carbon surface*), the deconvoluted N1s peak obtained by XPS analysis of the post-reaction sample is presented in Figure 6.9.

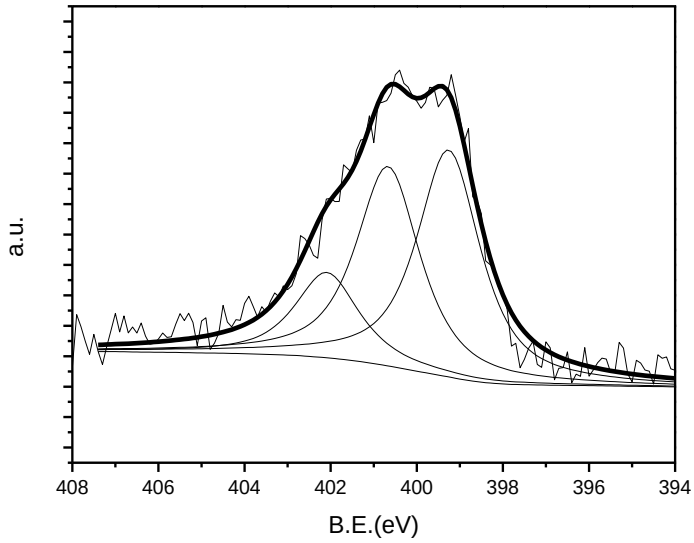

Figure 6.9 - Deconvoluted N1s peak obtained by XPS of sample N-CNF after the catalytic ozonation reaction.

The XPS analysis of CNF after ozonation showed a similar behaviour to what was observed in the case of the CNT-NUT samples, with a decrease in the contribution of the peak corresponding to pyridinic functionalities to

the N1s XPS peak, when compared with the fresh material (shown in [19]).

Finally, post-reaction characterization of the MWCNT used in the ozonation of emerging organic micropollutants (section *Ozonation of emerging organic micropollutants*) was also performed, to further understand the influence of the presence of large molecules during the ozonation reaction. On a first approach nitrogen adsorption isotherms were performed, to characterize the textural properties of the post-reaction MWCNT. The profile of the adsorption isotherms is presented in Figure 6.10.

The adsorption profile of nitrogen on the sample that was subject to ozonation without any pollutant is very similar to what was found for the samples that were used in the ozonation reactions with the selected pollutants. Also, these were similar among themselves, being characteristic of a Type II isotherm, corresponding to non-porous solids [20, 21]. The hysteresis during desorption was also observed to be very similar among the analysed samples. The specific surface area calculated using the BET ($0.05< p/p_0<0.30$) method [20] is presented in Table 6.2.

Table 6.2 – Specific surface area of post-ozonation MWCNT samples.

sample	S_{BET} ($m^2 g^{-1}$)
O_3 + MWCNT	374
O_3 + MWCNT + ATZ	359
O_3 + MWCNT + MTLC	392
O_3 + MWCNT + NLP	325

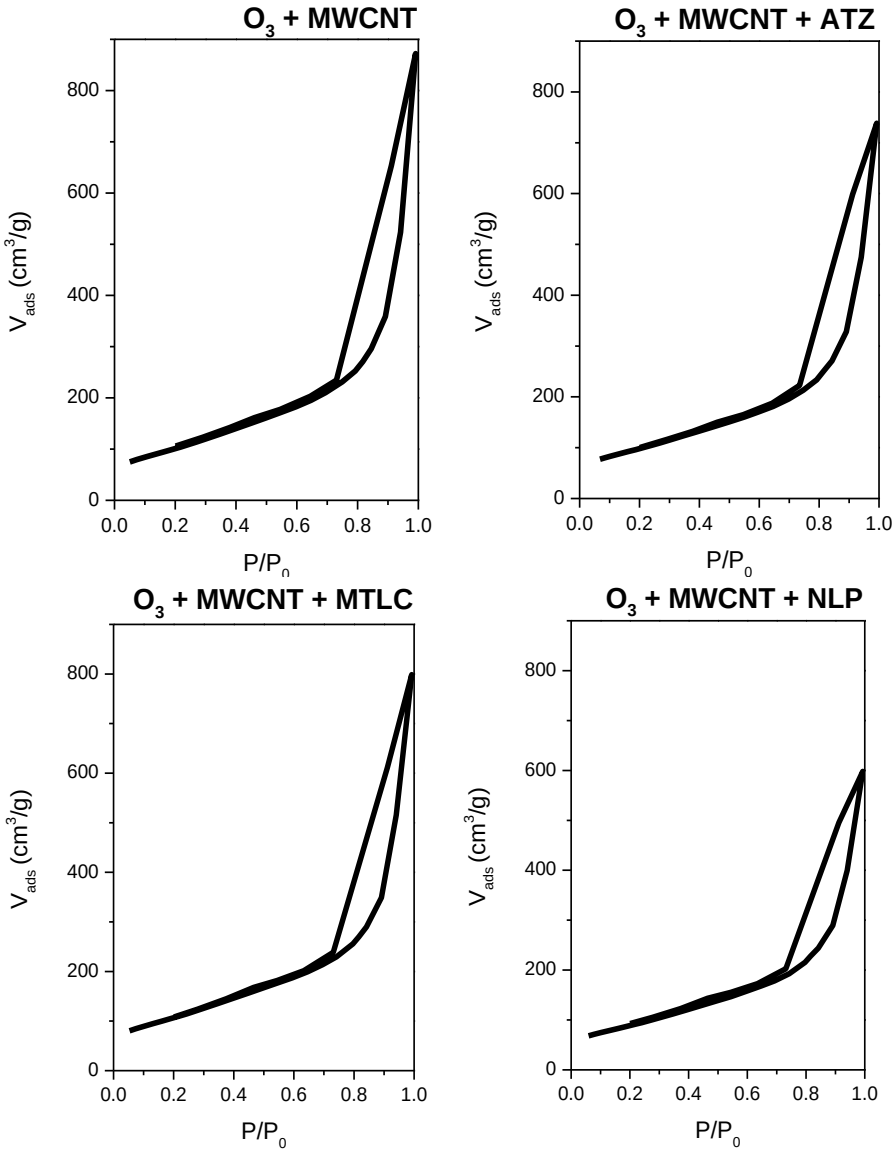

Figure 6.10 – Nitrogen adsorption isotherms on recovered MWCNT post-reaction used in the ozonation of emerging organic micropollutants.

The changes in the specific surface area due to the action of ozone, with or without pollutant, were not very drastic (original material is in the range 300-350 m^2/g [1, 11, 22]). Nevertheless, a small increase was observed which may attributed to the opening of the MWCNT endcaps during reaction with ozone [1]. On the other hand, a decrease in the total pore

volume was registered, which was even more drastic when the pollutants were present, and may be related blocking of the pores.

The post-reaction MWCNT samples were also analysed by TPD, and the registered CO and CO_2 released amounts are presented in Figure 6.11.

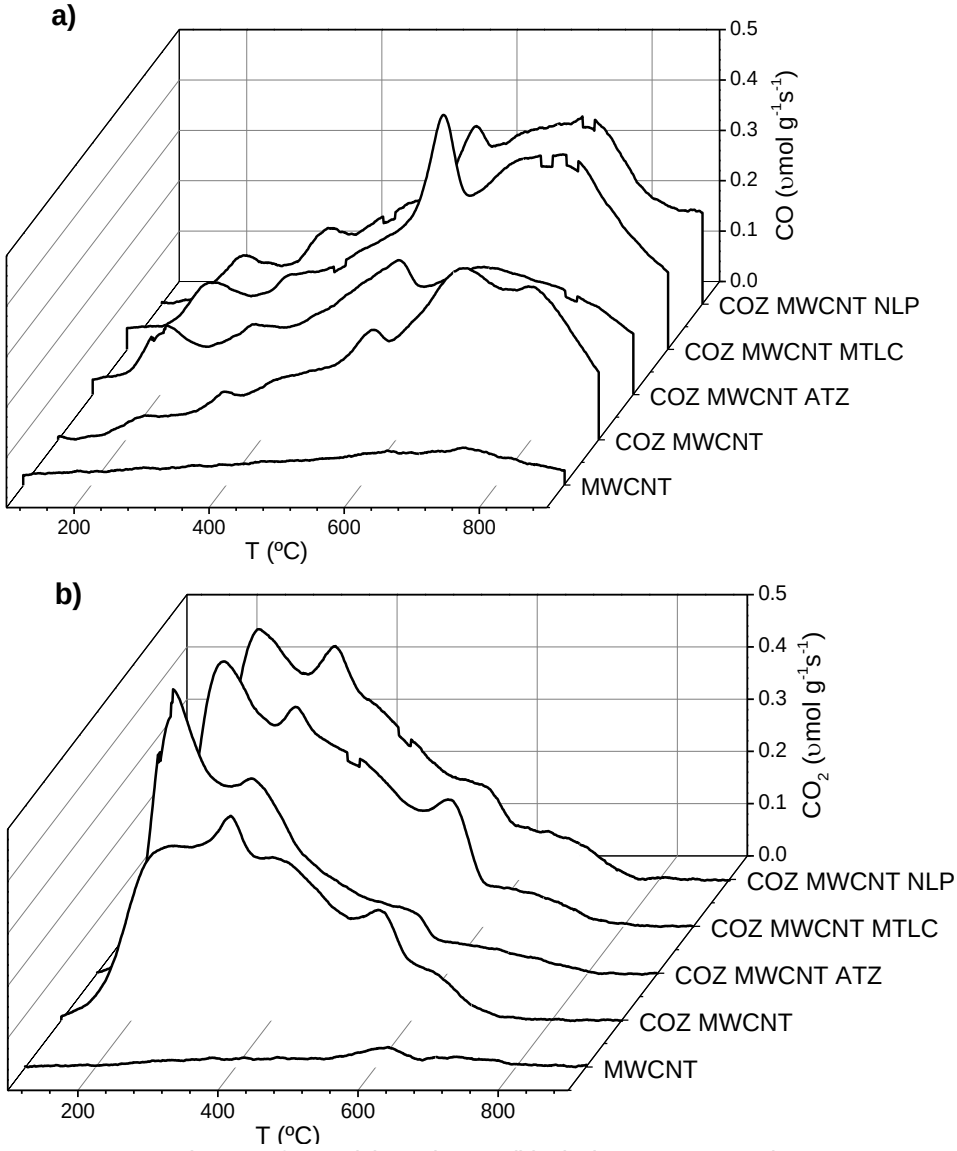

Figure 6.11 – Release of CO (a) and CO_2 (b) during TPD experiments carried out using the MWCNT samples before and after catalytic ozonation of emerging organic micropollutants.

The obtained total amounts of released CO and CO_2 during these same experiments are presented in Table 6.3.

First off, it is clear that the ozonation process increases the amount of oxygen-containing groups released as CO and CO_2, as was observed in the experiments carried out using pristine and modified CNT in the ozonation of oxalic acid and phenol. However, since the experiments using emerging organic micropollutants were longer (8h), the amount that is introduced on the surface of the carbon nanomaterials is much higher. Nevertheless, the nature of the introduced functionalities seems to be similar, since the temperatures of decomposition of CO and CO_2 is the same for the 3h and the 8h long reactions. However, when comparing the profiles of the MWCNT subject only to ozonation with those used in reaction with the selected pollutants, an increase in the amount of CO and CO_2 released is detected. Specifically, both as CO and as CO_2, peaks at 200 and 550 ^{o}C are observed, which may be due to the adsorption of the pollutants, or intermediates formed during their degradation [23, 24].

Table 6.3. - Amounts of CO and CO_2 released during TPD experiments of MWCNT samples before and after catalytic ozonation of emerging organic micropollutants.

Sample	CO (μmol g^{-1})	CO_2 (μmol g^{-1})
MWCNT	200	128
COZ MWCNT	1664	1501
COZ MWCNT ATZ	1700	1653
COZ MWCNT MTLC	1994	1796
COZ MWCNT NLP	2021	1713

In summary, it was observed that the main changes on the surface of the carbon materials is related with the introduction of surface oxygenated functionalities, which confer a more acidic character to the material. A

large release of the S-containing functionalities was also observed in the case of S-doped MWCNT. However, no changes to the nature of the remaining surface functionalities were observed. On the other hand, when N-doped carbon materials were concerned, some modification of the N-containing surface groups was observed, mostly in the disappearance of the pyridinic groups.

6.3 LONG-TERM CONTINUOUS OZONATION

6.3.1 CATALYTIC ACTIVITY

The long term catalytic activity of the CNF-covered honeycomb monoliths was tested in the continuous ozonation of oxalic acid, in their structured form. The dimensionless removal of oxalic acid during 100h long experiments is presented in Figure 6.12. These experiments were conducted using various honeycomb-type monoliths, as described in section *Materials and methods.* The 400 cpsi monoliths were tested in two-phase mode, and the 64 cpsi monoliths in three-phase mode, so the achieved removals should be regarded with care.

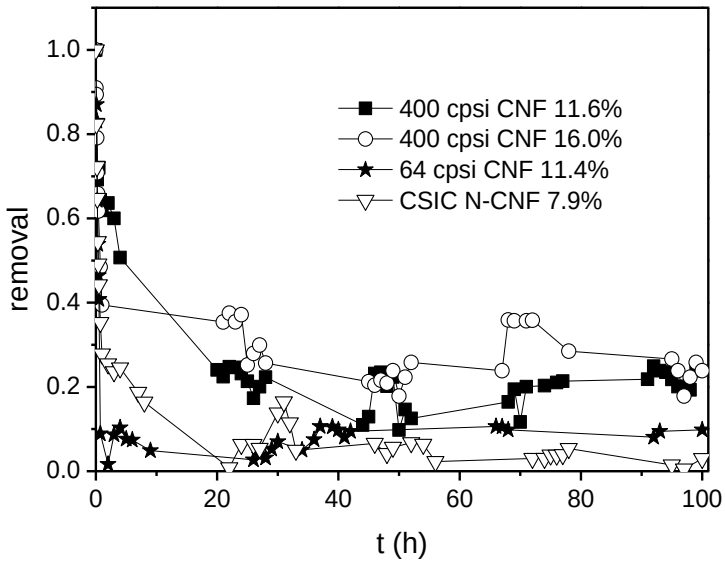

Figure 6.12 – Dimensionless oxalic acid removal during long term continuous catalytic ozonation experiments using several different honeycomb monoliths.

During the first stage of the experiment (until 2 h) there is a drastic drop in the efficiency of the oxalic acid removal. This is simply due to the fact that, prior to starting the feed of oxalic acid solution, water is flowing through the system, and thus around 2-3 retention times are needed to achieve steady state. However, even after this period, a loss of activity is observed during the first 30 h, after which the removal of oxalic acid remains relatively stable until the end of the experiment. Slight variations are related to the fluctuations of ozone concentration in the gas phase, which is affected by the room temperature.

In Figure 6.13 a comparison between semi-batch catalytic ozonation experiments carried out before and after the long-term experiment is presented. It is clear that some deactivation of the catalyst occurred after the long term experiment.

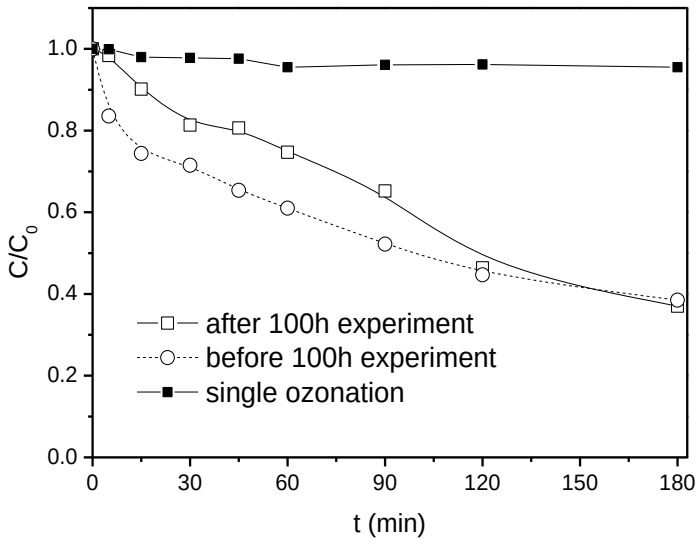

Figure 6.13 – Dimensionless oxalic acid concentration during semi-batch experiments (closed loop) using a honeycomb monolith before and after the long term continuous ozonation experiments.

It is known that exposure of nanocarbon materials to ozone will introduce oxygenated surface groups which diminish their catalytic activity, until the point where no more oxygenated groups can be introduced onto the surface of the materials; after that the activity becomes stable [1]. In addition, some adsorption of oxalic acid is expected to occur in the fresh catalyst, in the beginning of the experiments. The behaviour of the nanofibers grown on a ceramic support is considered to be analogous to that of carbon nanotubes in powder form when used in the ozonation of organic pollutants [25]. Thus, the initial deactivation and stabilization of the catalytic activity observed corresponds to what was expected.

6.3.2 Post-reaction characterization

The contact angle of water on a specially prepared sample of nanocarbon materials grown on a flat ceramic support was measured after different exposure times to ozone, and the evolution of the ratio between the spread rate and the initial contact angle is presented in Figure 6.14, together with the evolution of the contact angle measured for each flat CNF covered ceramic sample.

It is shown that for ozone exposure times as long as 3 h, the contact angle and the spreading rate of water on the surface of the sample changes drastically. After 28 h, the difference is much less significant. This shows that the oxidized nanomaterials become more hydrophilic, as it is expected when the surface of carbon becomes oxidized [26]. The presence of oxygen containing surface groups is known to decrease the performance of carbon materials to decompose O_3 [16].

Furthermore, the evolution of surface oxygenated groups was followed by XPS, and the corresponding oxygen fraction, is shown in Table 6.4, for peak O1s. Four functional groups were considered: C=O groups at 531.1 eV (I), carbonyl oxygen atoms in ester, amides, anhydrides and oxygen atoms in hydroxyls or ethers at 532.3 eV (II), ether oxygen atoms in esters and anhydrides at 533.2 eV (III) and oxygen atoms in carboxyl groups at 534.2 eV (IV) [27]. The intensity at 536.1 eV, corresponding to oxygen in

adsorbed water was also followed, but the areas obtained were negligible, and thus are not shown. The deconvoluted XPS spectra of O1s peak are presented in Figure 6.15.

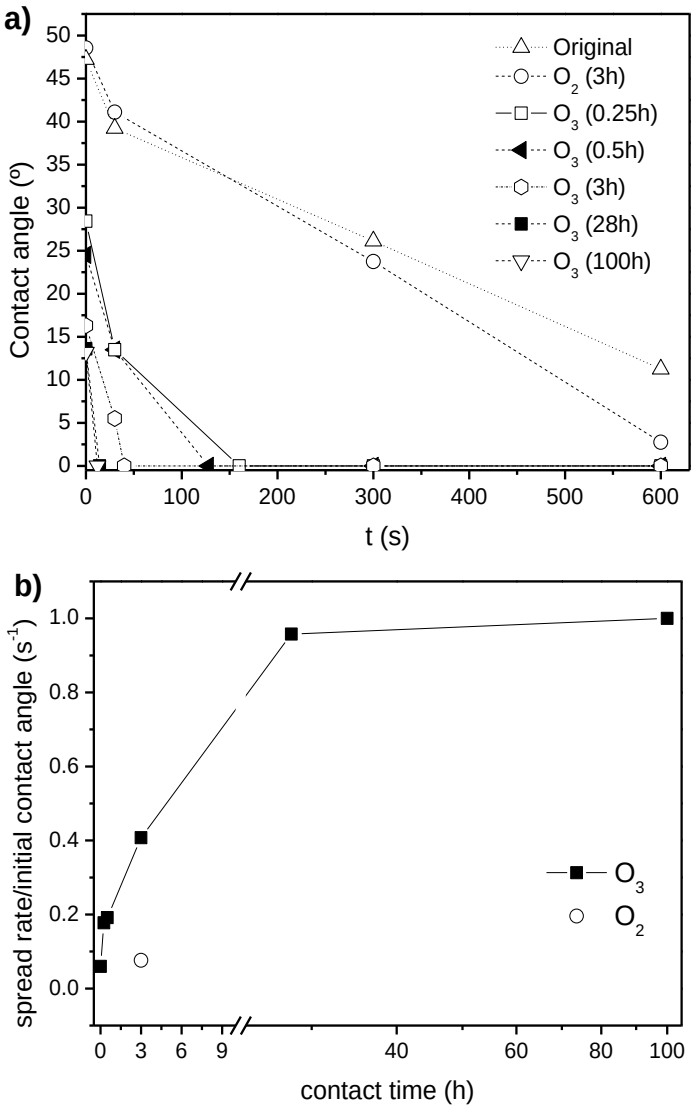

Figure 6.14 – Evolution of the contact angle for flat CNF covered ceramic pieces exposed to different ozonation times (a) and the evolution of the spread rate with the ozonation time (b).

After 3 hours of ozonation, the oxygen content on the surface increases mostly due to peaks III and IV, which correspond to anhydrides and carboxyl surface functionalities. In fact, it has been reported that MWCNT used as catalysts for ozonation of organic matter present an increase in the amount of surface oxygenated groups, released as CO_2 during temperature programed desorption (TPD) mostly in the 200-400 ºC range, corresponding to a loss of activity of the materials in the catalytic ozonation of oxalic acid [1]. It is known that surface oxygenated groups released as CO_2 at this temperature range during TPD correspond to carboxyl groups [12]. Such results are compatible with the ones here obtained. After 100 hours of contact time with ozone, a very large increase in groups II and III was found, which does not seem to affect the performance of the material, nor the contact angle. It is likely that this results from an experimental artefact, since from 3 to 28 h, practically no changes were observed.

Table 6.4 - Results obtained by XPS analyses of the samples subject to different ozonation times.

Peak	Binding Energy (eV)	Weight fraction (%)			
		0h O_3	3h O_3	8h O_3	100h O_3
I	531.1	0.29	1.70	1.56	1.51
II	532.3	1.99	3.57	4.05	2.01
III	533.3	1.84	4.60	5.25	30.23
IV	534.2	2.08	8.12	9.71	10.48
total		6.21	17.99	20.57	64.24

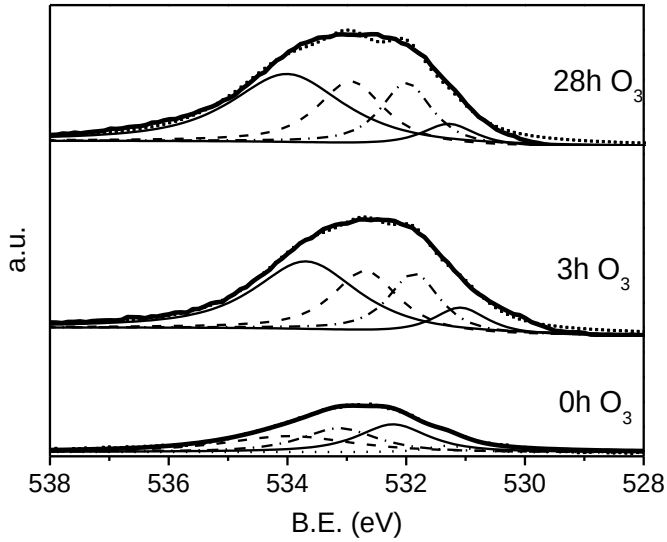

Figure 6.15 - Deconvoluted O1s peak obtained by XPS of CNF covered flat ceramic pieces subject to different contact times with ozone.

The spectra of CO and CO_2 released during TPD experiments carried out using the CNF covered ceramic pieces at different ozone contact times are presented in Figure 6.16.

Table 6.5 - Amounts of CO and CO_2 released during TPD experiments of CNF covered flat ceramic pieces subject to different contact times with ozone.

Ozone contact time	CO (μmol g^{-1})	CO_2 (μmol g^{-1})
0h	289	36
3h	297	49
28h	383	71
100h	418	69

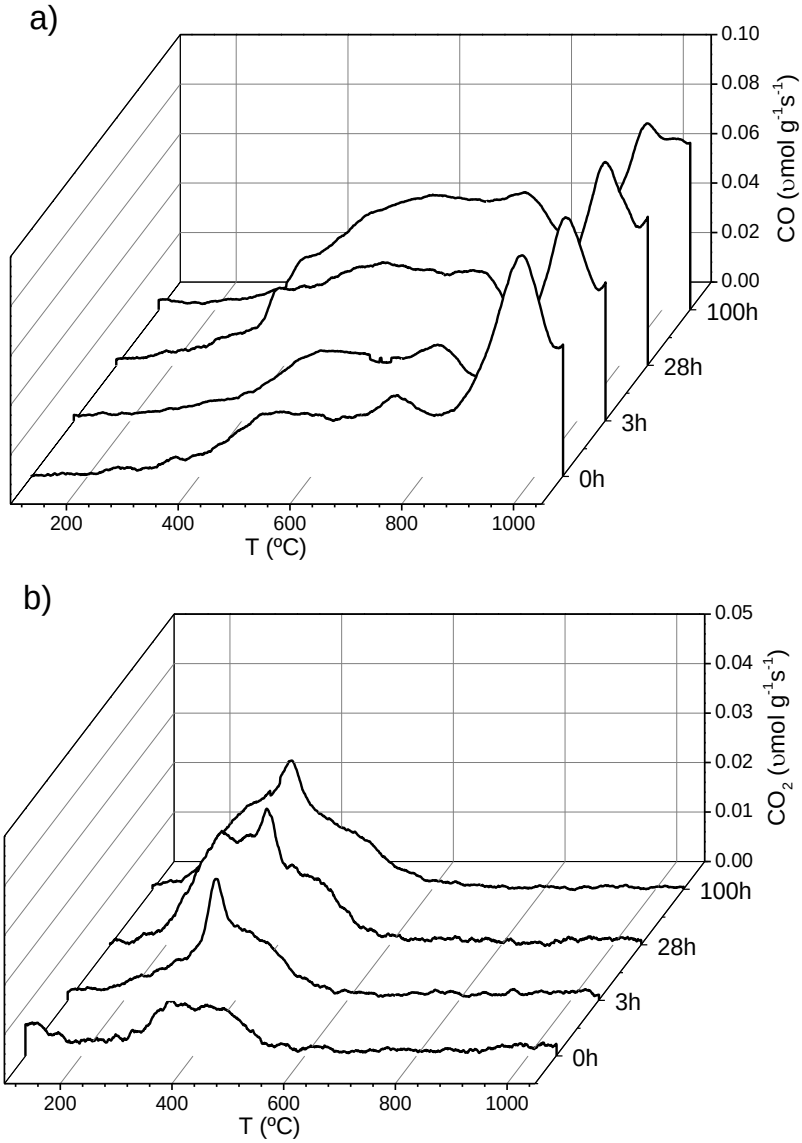

Figure 6.16 – Release of CO (a) and CO_2 (b) during TPD experiments carried out using the CNF covered flat ceramic pieces subject to different contact times with ozone.

The total amount of CO and CO_2 released during these TPD experiments is presented in Table 6.5.

In accordance with what was observed during the XPS analyses of the CNF covered flat ceramic pieces, the amount of oxygen-containing groups

on the surface of the carbon materials is increasing with the ozone contact time. However, after 28h, the amount of CO_2 seems to become stable, and the increase of CO is also smaller than what was observed for smaller contact times. Thus, the observed stabilization of the catalytic activity of the monoliths after 30h of reaction may in fact be related with the introduction of acidic functionalities during this period of time.

In addition, the specific surface area of the CNF covered ceramic slabs was calculated from the corresponding N_2 adsorption isotherms at - 196 ºC. The results are presented in Table 6.6, which are related to specific surface area of the complete sample. Thus, since the ceramic support is known to have a low surface area, these values are lower than what is typical for carbon nanomaterials (around 200 m^2/g) [25].

The specific surface area was not significantly altered by the ozonation procedure, decreasing from 28 to 23 m^2/g after 100 hours of contact time with ozone, which is within the experimental error.

Table 6.6 - Specific surface area of the CNF covered flat ceramic pieces subject to different contact times with ozone.

Sample	Specific surface area (m^2/g)
0h O_3	28
3h O_3	26
28h O_3	24
100h O_3	23

Finally, thermogravimetric analyses were performed with the CNF covered ceramic pieces after exposure to different ozone contact times. The derivative weight loss profiles are presented in Figure 6.17.

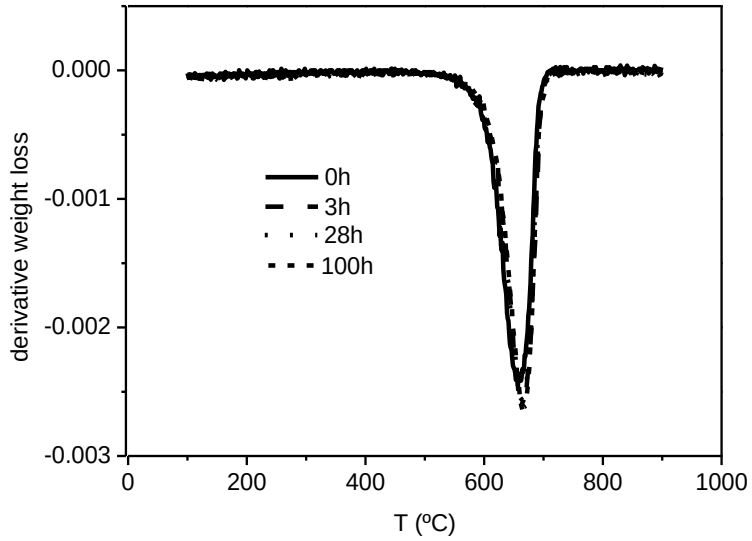

Figure 6.17 – Derivative weight loss during thermogravimetric analyses of the CNF covered flat ceramic pieces subject to different contact times with ozone and derivative.

The derivative of the weight loss for the different CNF covered pieces did not vary with the increase of the ozone contact time. The temperature of the peak found in the derivative of the weight loss curves is typical of graphitic carbon [28].

6.4 PARTIAL CONCLUSIONS

The deactivation of pristine and modified multiwalled carbon nanotubes was assessed in the catalytic ozonation of oxalic acid. It was found that, independently of the treatment applied to the catalyst, the introduction of acidic oxygen-containing surface groups lead to a loss of activity. Nevertheless, further reutilization suggested that the amount of O-containing groups reaches a plateau, after which the catalysts show stable activity. It was also observed that while there is a loss of S-containing functionalities when S-doped MWCNT samples were studied, the nature of these groups did not change during the reaction; besides, the loss of activity of the catalyst did not seem to be related with this

phenomenon. In the case of the N-doped MWCNT and CNF, it was observed that the N-containing surface groups suffer some changes during the ozonation procedure, mostly related with the decrease of the amount of pyridinic groups.

Furthermore, structured catalysts consisting of CNF covered honeycomb monoliths were used in long term continuous ozonation experiments. It was observed that, after an initial period of deactivation, the catalyst were stable in the reaction, maintaining a constant removal of oxalic acid throughout the experiments. The loss of activity was shown to be related to the introduction of O-containing surface functionalities through reaction with ozone.

REFERENCES

[1] A.G. Gonçalves, J.L. Figueiredo, J.J.M. Órfão, M.F.R. Pereira, Carbon, 48 (2010) 4369-4381.
[2] P.C.C. Faria, J.J.M. Órfão, P. M.F.R., Applied Catalysis B, Environmental, 79 (2008) 237.
[3] J. Restivo, R.P. Rocha, A.M. Silva, J.J. Órfão, M.F. Pereira, J.L. Figueiredo, Chinese Journal of Catalysis, 35 (2014) 896-905.
[4] F.J. Beltrán, Applied Catalysis B, Environmental, 63 (2006) 249.
[5] Z.Q. Liu, Applied catalysis. B, Environmental, 92 (2009) 301.
[6] Z.-Q. Liu, J. Ma, Y.-H. Cui, L. Zhao, B.-P. Zhang, Separation and Purification Technology, 78 (2011) 147-153.
[7] Z.-Q. Liu, J. Ma, Y.-H. Cui, L. Zhao, B.-P. Zhang, Applied Catalysis B: Environmental, 101 (2010) 74-80.
[8] M. Sanchez-Polo, U. von Gunten, J. Rivera-Utrilla, Water Res, 39 (2005) 3189-3198.
[9] J. Restivo, J.J.M. Órfão, M.F.R. Pereira, E. Garcia-Bordejé, P. Roche, D. Bourdin, B. Houssais, M. Coste, S. Derrouiche, Chemical Engineering Journal, 230 (2013) 115-123.
[10] R.P. Rocha, A.M.T. Silva, S.M.M. Romero, M.F.R. Pereira, J.L. Figueiredo, Applied Catalysis B: Environmental, 147 (2014) 314-321.
[11] R.P. Rocha, J.P.S. Sousa, A.M.T. Silva, M.F.R. Pereira, J.L. Figueiredo, Applied Catalysis B: Environmental, 104 (2011) 330-336.
[12] J.L. Figueiredo, M.F.R. Pereira, M.M.A. Freitas, J.J.M. Órfão, Carbon, 37 (1999) 1379-1389.
[13] P.C.C. Faria, J.J.M. Órfão, M.F.R. Pereira, Industrial & engineering chemistry research, 45 (2006) 2715-2721.
[14] J.L. Figueiredo, M.F.R. Pereira, Catalysis Today, In Press, Corrected Proof (2009).
[15] H. Cao, L. Xing, G. Wu, Y. Xie, S. Shi, Y. Zhang, D. Minakata, J.C. Crittenden, Applied Catalysis B: Environmental, 146 (2014) 169-176.
[16] L. Xing, Y. Xie, H. Cao, D. Minakata, Y. Zhang, J.C. Crittenden, Chemical Engineering Journal, 245 (2014) 71-79.
[17] H.-P. Boehm, Catalytic Properties of Nitrogen-Containing Carbons, Carbon Materials for Catalysis, John Wiley & Sons, Inc.2008, pp. 219-265.
[18] M. Sánchez-Polo, U. von Gunten, J. Rivera-Utrilla, Water Research, 39 (2005) 3189-3198.
[19] L. Roldán, S. Armenise, Y. Marco, E. García-Bordejé, Physical Chemistry Chemical Physics, 14 (2012) 3568-3575.
[20] J.L. Figueiredo, F.R. Ribeiro, Catálise Heterogénea, Calouste Gulbenkian.
[21] K.S.W. Sing, D.H. Everett, R.A.W. Haul, L. Moscou, R.A. Pierotti, J. Rouquerol, T. Siemieniewska, Reporting Physisorption Data for Gas/Solid Systems, Handbook of Heterogeneous Catalysis, Wiley-VCH Verlag GmbH & Co. KGaA2008.
[22] J.P. Tessonnier, Carbon, 47 (2009) 1779.

[23] A. Gonçalves, J.J.M. Órfão, M.F.R. Pereira, Applied Catalysis B: Environmental, 140–141 (2013) 82-91.
[24] A.G. Gonçalves, J.J.M. Órfão, M.F.R. Pereira, Chemical Engineering Journal, 250 (2014) 366-376.
[25] J. Restivo, J.J.M. Órfão, M.F.R. Pereira, E. Vanhaecke, M. Rönning, T. Iouranova, L. Kiwi-Minsker, S. Armenise, E. Garcia-Bordejé, Water Science and Technology, 65 (2012) 1854.
[26] P. Delhaes, Graphite and Precursors, Taylor & Francis, 2000.
[27] U. Zielke, K.J. Hüttinger, W.P. Hoffman, Carbon, 34 (1996) 983-998.
[28] E. García-Bordejé, I. Kvande, D. Chen, M. Rønning, Carbon, 45 (2007) 1828-1838.

Part III

Reduction

1. MATERIALS AND METHODS

1.1 DESCRIPTION

In this chapter, the catalysts used in the reduction of bromate under hydrogen are described, as well as the methods used for their preparation, characterization and evaluation when applicable.

Two types of catalysts are described in this section: mono and bimetallic powder catalysts using different supports, and monometallic structured catalysts. Thus, two types of reaction systems are also here described, used for the semi-batch and continuous reduction of bromate under hydrogen.

The described catalysts include those that were previously prepared in our laboratory and made available by Dr. Salomé Soares for the present study, and those which were prepared during the development of this project.

1.2 CATALYSTS

The catalysts that were used in the hydrogen reduction of bromate in water are divided in two major groups: powder catalysts, which were used in the semi-batch reduction of bromate; and structured catalysts, which were used in the continuous reduction of bromate.

1.2.1 POWDER CATALYSTS

The supported metallic catalysts in powder form that were used in the semi-batch hydrogen reduction of bromate, using different supports (activated carbon, AC; multiwalled carbon nanotubes, MWCNT; titanium dioxide, TiO_2) already existed in the laboratory, as they were prepared in the context of other on-going projects, by Dr. Salomé Soares, who kindly

made them available to be applied to the study of the reduction of bromate under hydrogen over supported metallic catalysts.

The detailed preparation methods, by incipient impregnation, are described elsewhere [1-7]. In short, the catalysts were prepared by the incipient wetness impregnation method, followed by heat treatment under nitrogen and reduction under hydrogen. The characterization of the prepared catalysts was found in the relevant literature [1-7], or was performed during the work here presented. The relevant characterization of prepared monometallic and bimetallic catalysts is described below.

1.2.1.1. MONOMETALLIC CATALYISTS ON ACTIVATED CARBON

Textural characterization of the activated carbon support and of selected metallic catalysts was performed. The activated carbon support shows a high surface area (869 $m^2 g^{-1}$), mainly due to the presence of micropores. The BET surface areas of the supported catalysts are similar to that of the support (e.g. 829 and 872 m^2 g^{-1} for 1%Pt/AC and 1%Rh/AC, respectively). A slight decrease was observed for the Pt catalyst, which can be attributed to the blockage of some of the micropores of the activated carbon.

The dispersion and average particle size of some of the prepared catalysts, obtained by H_2 chemisorption, are presented in Table 1.1.

Table 1.1 – Characterization of the impregnated metallic phases on the activated carbon supports.

Catalyst	Dispersion (%)	Average particle size (nm)
1% Pt/AC	20	5.6
1% Pd/AC	39	2.9
1%Ir/AC	50	2.2
1% Ru/AC	16	7.0
1%Rh/AC	15	7.1

The monometallic catalysts showed good dispersions and average particle sizes in the nanometric range. TEM results (Figure 1.1) also reveal small metal particles in all the catalysts. As the metal particle size is small, good metal-support interaction is expected, due to large interfacial contact area.

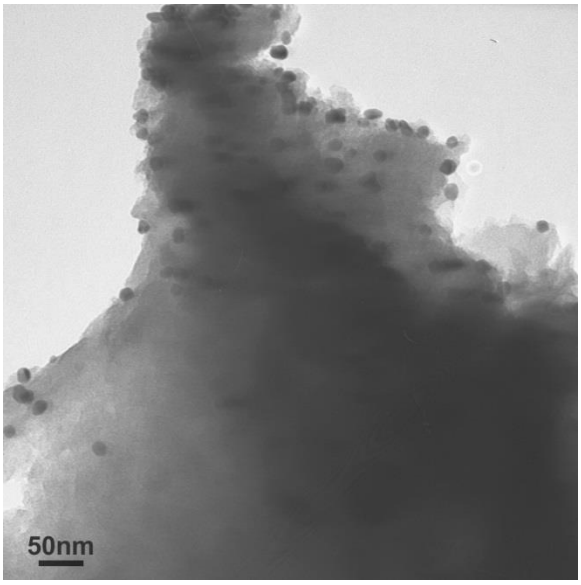

Figure 1.1 - TEM micrograph of 1%Pd/AC monometallic catalyst.

1.2.1.2. BIMETALLIC CATALYSTS ON ACTIVATED CARBON

From H_2 chemisorption experiments it was possible to obtain the metal dispersion of the monometallic catalyst, but for the bimetallic catalysts no H_2 chemisorption was noticed. This may be an indication that some interaction exists between the noble metal, Pd, Pt, Ru, Rh or Ir, and promoter metal, Cu, Sn, Ni, Zn and Fe (forming an alloy) or/and the promoter metal is covering most of the noble metal, strongly limiting H_2 chemisorption.

Table 1.2 shows that the BET surface area of the support is 869 $m^2\ g^{-1}$ and it can be observed that for the supported bimetallic catalysts the textural parameters remained practically unchanged compared to the unloaded carbon. Therefore, it was assumed that the textural properties of

the supported metallic catalysts are not significantly different from those of the original activated carbon.

Selected catalysts were analysed by TEM. In general, the metal particles are well dispersed on the support, most of the catalysts present a metal particles diameter between 3 and 7 nm, but in some cases few larger particles are also observed.

Table 1.2 - Textural characterization of the activated carbon (ACo) and some of the bimetallic catalysts.

Sample	S_{BET} ($m^2 g^{-1}$)	S_{meso} [a] ($m^2 g^{-1}$)	V_{micro} [a] ($cm^3 g^{-1}$)
AC	869	97	0.318
2%Pd-1%Cu/AC	870	90	0.330
1%Pt-1%Cu/AC	876	168	0.275
1%Rh-1%Cu/AC	862	104	0.280

[a] Micropore volume (V_{micro}) and mesopore surface area (S_{meso}) calculated by the t-method.

Figure 1.2 shows a representative TEM image of 1%Pd-1%Cu (%wt) catalyst supported on activated carbon. It was also observed that there are no significant differences in the metal particle size varying the amounts of Pd or Cu in the Pd-Cu bimetallic catalysts.

Scanning electron microscopy pictures of selected samples are presented in Figure 1.3, in which both the secondary (SE) and backscattered electrons (BSE) images obtained are represented.

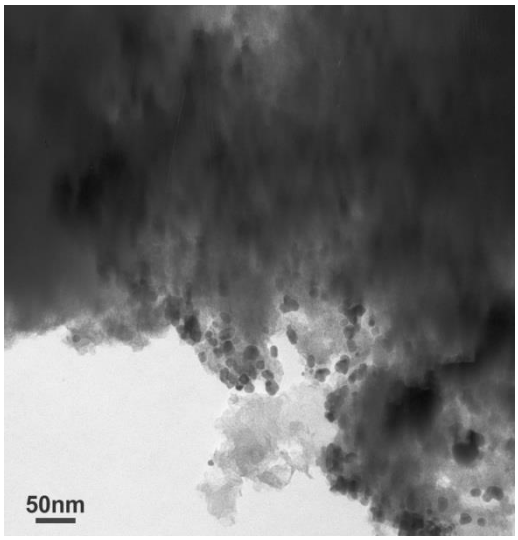

Figure 1.2 - TEM micrograph of 1%Pd-1%Cu/AC bimetallic catalyst.

It is clear from Figure 1.2 that the metallic particles on the surface of the activated carbon are well dispersed and present throughout the surface fairly homogeneously.

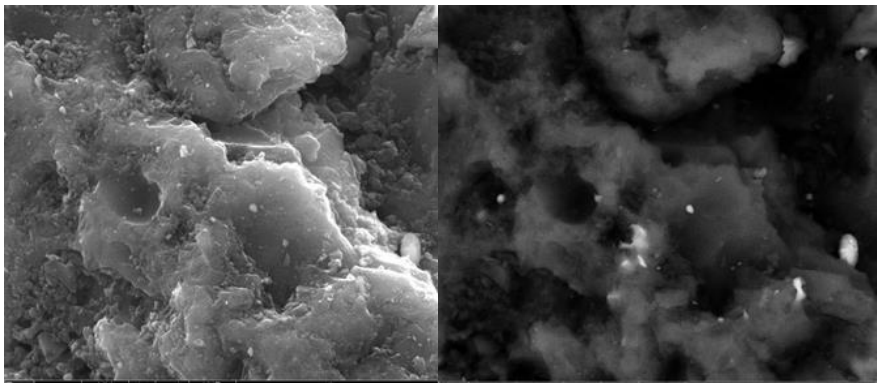

Figure 1.3 – SEM pictures of bimetallic catalysts supported on activated carbon: SE images of bimetallic Pd-Cu catalyst supported on activated carbon (left) and BSE images of bimetallic Pd-Cu catalyst supported on activated carbon (right).

1.2.1.3. MONOMETALLIC CATALYSTS ON MWCNT

Textural characterization of the multiwalled carbon support was performed. The MWCNT support presented a specific surface area of 320

m^2g^{-1}. It is not expected that there are significant changes to the textural properties of the catalysts after the impregnation of the metallic phase [4, 6].

The prepared catalysts using MWCNT as support were analysed by TEM. Good homogeneous dispersions were observed in general. The TEM images obtained and the corresponding observed particle size distribution are presented in Figure 1.4 for Pd, Pt, Rh and Ru supported catalysts.

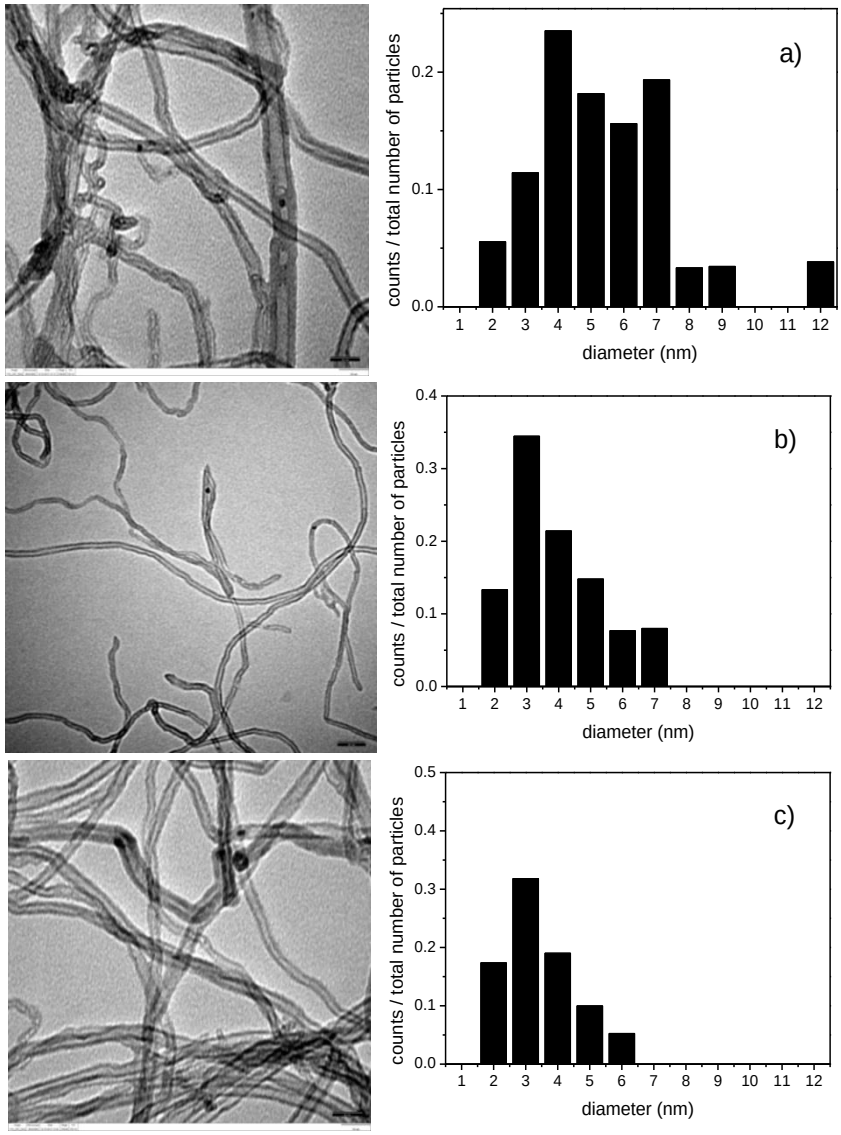

(cont.)

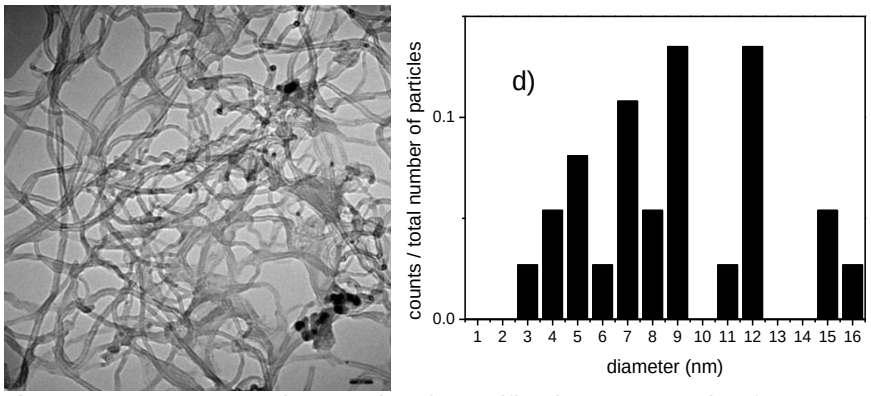

Figure 1.4 – TEM micrographs (magnification 278400x) of MWCNT supported metallic catalyst with particle size distribution (a) Pd, b) Pt, c) Rh and d) Ru).

Mean particle sizes for the MWCNT supported catalysts were calculated: 5.2 nm for Pd, 4.0 nm for Pt, 3.5 nm for Rh and 11.7 nm for Ru.

1.2.1.3. MONOMETALLIC CATALYSTS ON TiO_2

Textural characterization of the TiO_2 supported catalysts was carried out. The specific surface area of TiO_2 as calculated by the BET method was 50 m^2g^{-1}, mostly attributed to its mesoporosity, and the metallic catalysts are not expected to significantly change this value [6].

The prepared catalysts using TiO_2 as support were analysed by TEM. Good homogeneous dispersions were observed in general. The TEM images obtained and the corresponding observed particle size distribution are presented in Figure 1.5 for Pd, Pt, Rh and Ru supported catalysts.

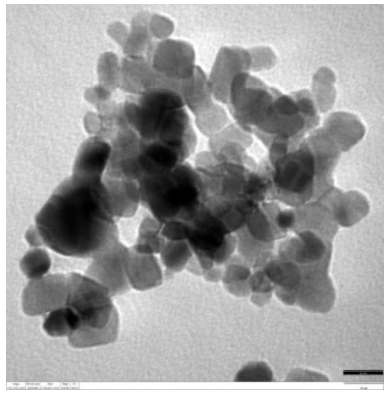

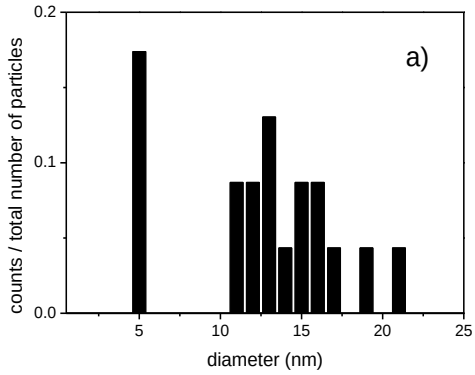
a)
counts / total number of particles
diameter (nm)
0.0
0.1
0.2
5
10
15
20
25

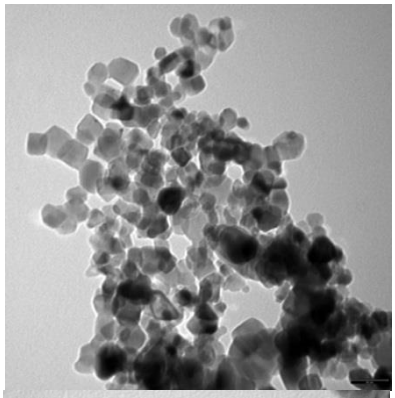

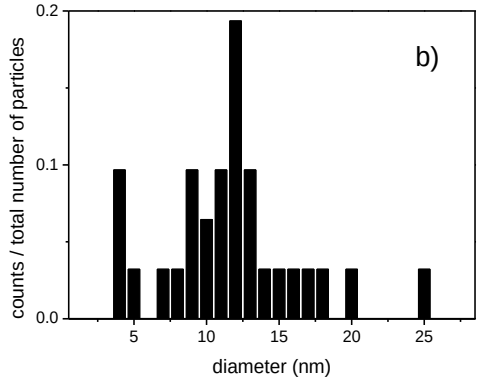
b)
counts / total number of particles
diameter (nm)
0.0
0.1
0.2
5
10
15
20
25

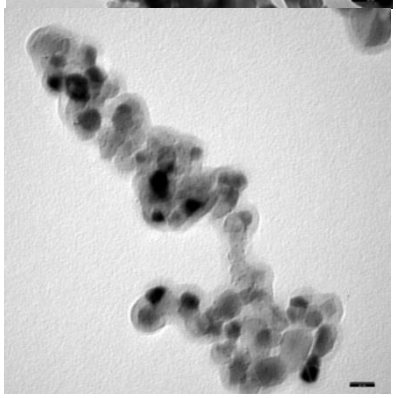

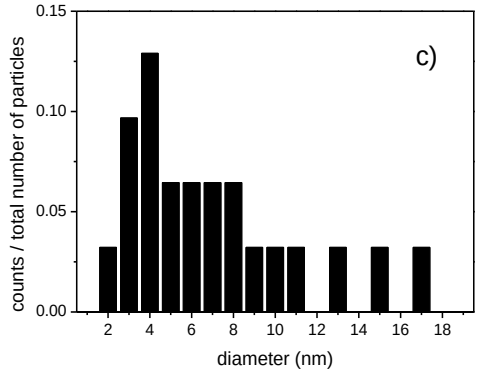
c)
counts / total number of particles
diameter (nm)
0.00
0.05
0.10
0.15
2
4
6
8
10
12
14
16
18

(cont.)

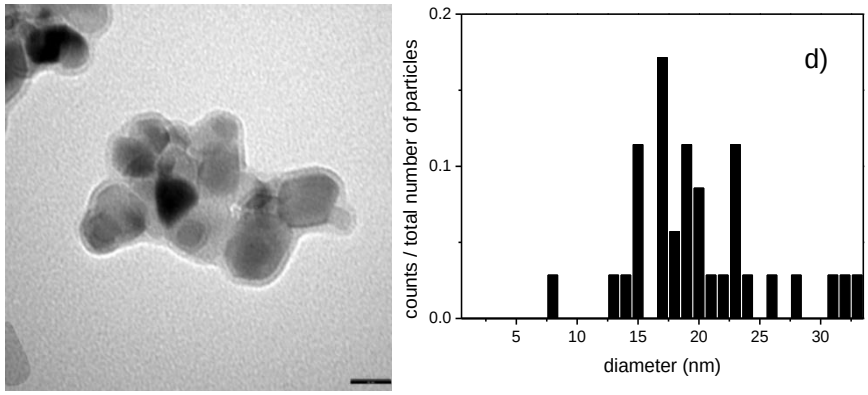

Figure 1.5 – TEM micrographs (magnification 278400x) of TiO_2 supported metallic catalyst with particle size distribution (a) Pd, b) Pt, c) Rh and d) Ru).

Mean particle sizes for the TiO_2 supported catalysts were calculated: 14.0 nm for Pd, 12.0 nm for Pt, 6.9 nm for Rh and 20.4 nm for Ru.

Additional TEM analyses were performed in the Ru catalyst supported on TiO_2 with smaller metal loadings, as presented in Figure 1.6.

Mean particle sizes, for the Ru/TiO_2 catalysts with different metal loadings, were calculated: 18.4 nm for 0.5% Ru/TIO_2 and 21.2 nm for 0.1% Ru/TIO_2.

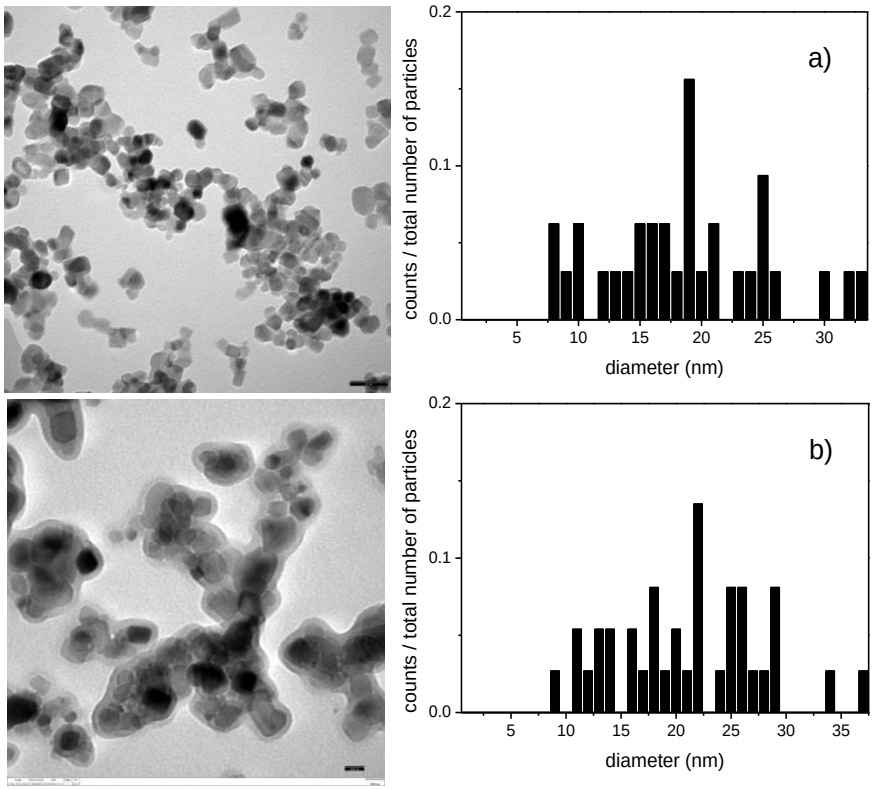

Figure 1.6 – TEM micrographs (magnification 278400x) of Ru/TiO_2 supported metallic catalyst with particle size distribution (a) 0.5% Ru/TIO_2, b) 0.1% Ru/TIO_2).

TPR experiments were conducted in order to evaluate the effect of the different supports on selected catalysts, as presented in Figure 1.7.

The TPR profiles of the Ru catalyst supported on different materials present some evident differences between them, despite all being reduced at 200 ^{o}C. The H_2 consumption peak, observed by changes in the TCD signal, in the case of the titanium dioxide supported catalyst, presented a shoulder at a lower temperature. It has been reported that reduction at low temperatures of Ru on different supports lead to almost complete reduction of oxide species into metallic ruthenium [8, 9]. However, the 1% Ru/AC catalyst showed two reduction peaks. While the second peak could correspond to the reduction of salts left from the impregnation from a precursor, it is also possible that the separate peaks

may correspond to the step by step reduction of the ruthenium species on the surface of the catalyst [10]. In any case, it is generally considered that the interaction of noble metals and the different supports studied here decreases in the order MWCNT>TiO_2>>>AC [8, 9, 11, 12].

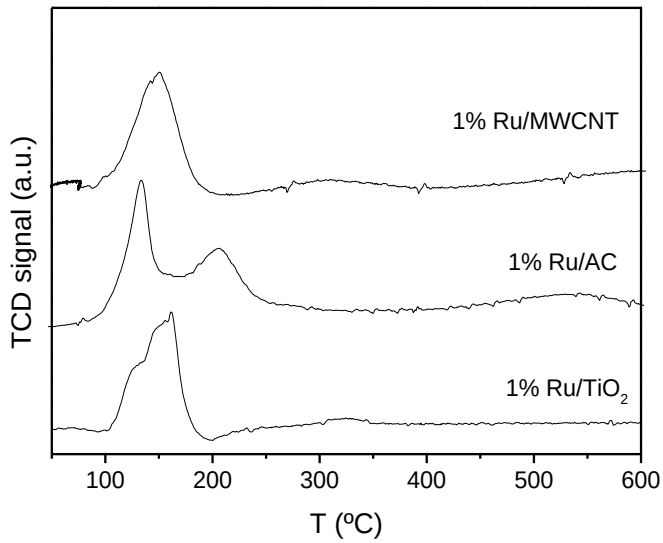

Figure 1.7 – TPR profiles of the Ru supported catalysts.

1.2.2 STRUCTURED CATALYSTS

A series of structured catalysts were prepared to be applied to the continuous reduction of bromate in water under hydrogen. The catalysts were prepared using honeycomb cordierite monoliths, and may be divided in two groups: Pd/CNT (60mm x 22mm) and Pd/TiO_2 (40 mm x 22mm). The former consisted in CNT covered honeycomb monoliths upon which the metallic phase was impregnated using palladium as the active metal. The latter consisted on honeycomb monoliths upon which titanium dioxide was layered, and were afterwards impregnated with the active metal catalyst.

The CNT monoliths were prepared following a procedure adapted from the literature [13-17]. The honeycomb cordierite monoliths were initially heat treated at 900 ^{o}C under air (50 cm^3 $min^{-}1$; 1 h ,10 ^{o}C min^{-1}) to remove

impurities. Afterwards, the monoliths were dipped into a nyacol alumina suspension (25% nyacol in water; 30mm min^{-1} dip speed; 1 min dipped in suspension). The alumina washcoated monoliths were then rinsed with distilled water and dried overnight at room temperature; followed by a final drying stage at 110 ^{o}C in air for 1h. The dried alumina washcoated monoliths were then heat treated under air at 450 ^{o}C (50 cm^3 min^{-1}; 1 ^{o}C min^{-1}), in order to achieve a γ-alumina coating [13, 18], using a low heating rate to avoid cracking of the alumina layer [17]. The CNT growth catalyst, nickel, was then impregnated on the surface of the monoliths, by adsorption from a pH neutral nickel solution. The Ni solution was prepared using 29 g $Ni(NO_3)_2 \cdot 6H_2O$ as precursor on 1L of water, together with 80 g NH_4NO_3 and 4 mL ammonia solution (25%). The monoliths were kept overnight in this solution (12h) and the liquid was continuously flowed through the channels, which was achieved by keeping the solution stirred while the monolith was fixed on a horizontal position, oriented in the direction of the flow. The monoliths were then rinsed with distilled water and dried overnight at room temperature, followed by drying at 110 ^{o}C in air for 1h. Afterwards, the monoliths were calcined under nitrogen at 450^{o}C for 2h (50 cm^3 min^{-1}; 1 ^{o}C min^{-1}). Finally, the growth of the CNT was carried out under a C_2H_6:H_2 mixture (0.6:0.4) at 600 ^{o}C for 210 min. The temperature and growth times were selected after optimization of the process to obtain a high carbon loading, while avoiding excessive growth of the CNT that would result in blocking of the channels and in fracture to the cordierite structure. The growth of CNT followed the scheme found in Figure 1.8.

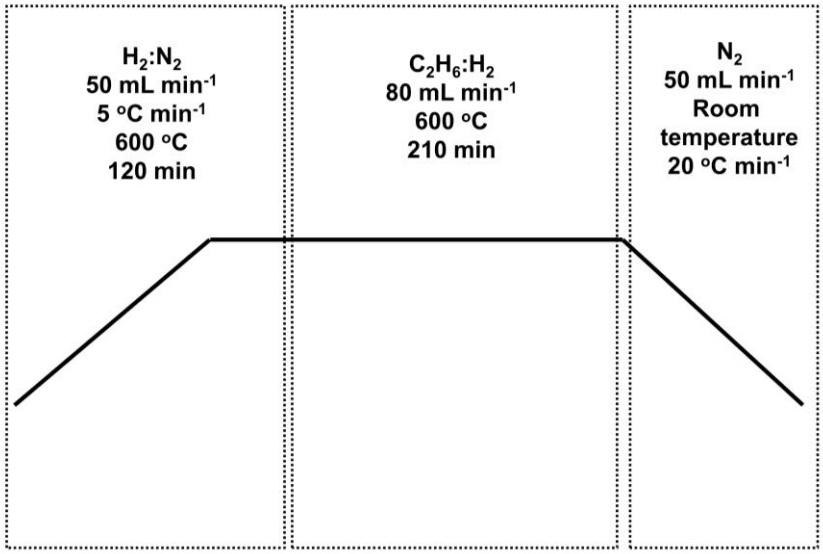

Figure 1.8 – Scheme of method for growth of CNT over Ni impregnated monoliths under ethane.

In Figure 1.9 a CNT monolith after growth is shown, together with a fractured CNT monolith due to excessive growth of the CNT.

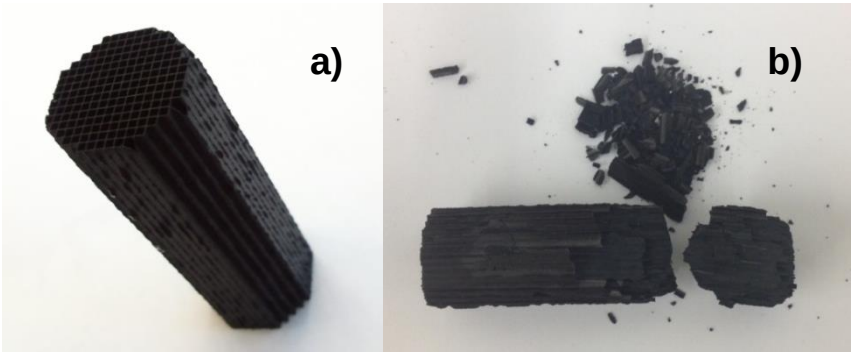

Figure 1.9 – CNT monolith after growth (a) and fractured CNT monolith due to excessive growth of CNT (b).

The loadings of alumina, nickel and CNT that were obtained during the preparation of the CNT monolith to be used as support for the metal phase to be applied to the continuous reduction of bromate are presented in Table 1.3

Table 1.3 – Loading of alumina, nickel and CNT during the preparation of the CNT monoliths, prior to impregnation of the active metallic catalyst.

Sample	Initial weight (g)	Weight gain after alumina washcoat (wt.%)	Weight gain after nickel impregnation (wt.%)	CNT loading (wt.%)
CNT4	7.2559	3.36	0.013	6.27
CNT9	7.6805	3.35	0.012	6.35
CNT10	7.3480	3.35	0.014	6.46

Similar weight gains after the different treatment procedures were obtained, which suggests that the preparation methodology is reproducible and, thus, adequate for the purpose of this study.

The carbon layer grown on the surface of the monoliths was scraped off and analysed by TEM, to give insight to what kind of structures resulted from the preparation methodology. These images are presented in Figure 1.10.

The carbon structures that were identified in the TEM pictures were clearly identified as multiwalled carbon nanotubes, with around 5-10 nm of thickness, which was expected from the growth temperature and the carbon source employed [13]. Nevertheless, the carbon nanofibers in platelet or fishbone fashion that were expected from the growth procedure no Ni were not found [13], which is likely due to the use of a colloidal alumina solution (nyacol) instead of pseudoboehmite in the preparation of the suspension used for the deposition of alumina.

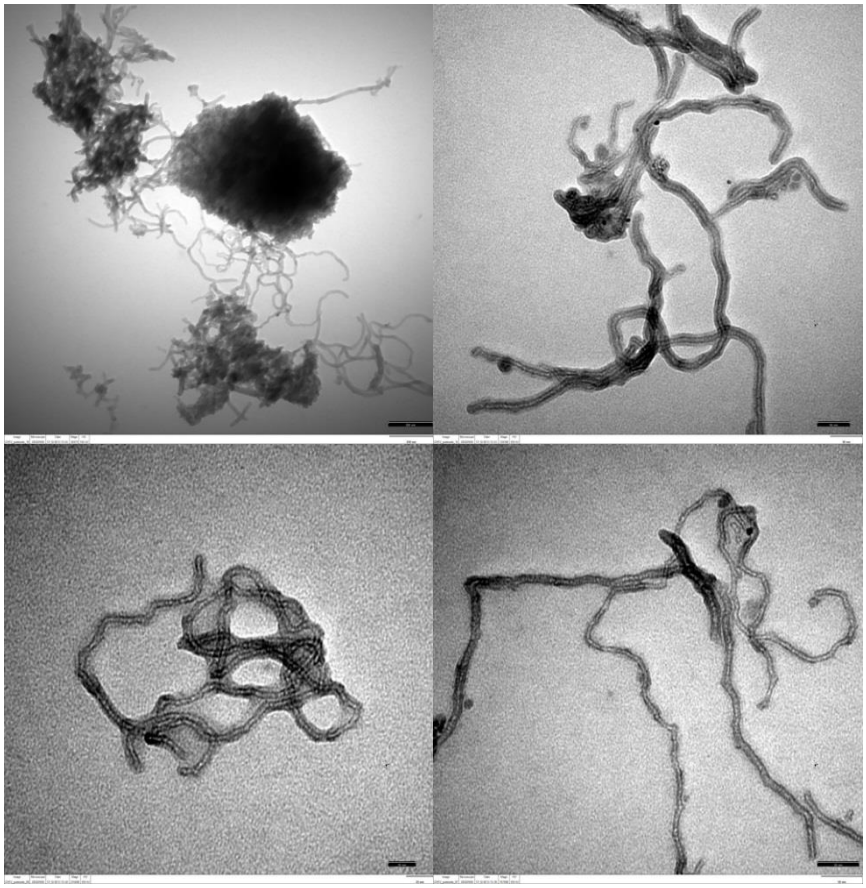

Figure 1.10 – TEM micrographs (magnification 215600x) of the CNT layer as grown on the honeycomb monoliths.

Temperature programed desorption (TPD) was carried out using a piece of a CNT covered monolith. The measured amounts of CO and CO_2 released during the experiment are presented in Figure 1.11.

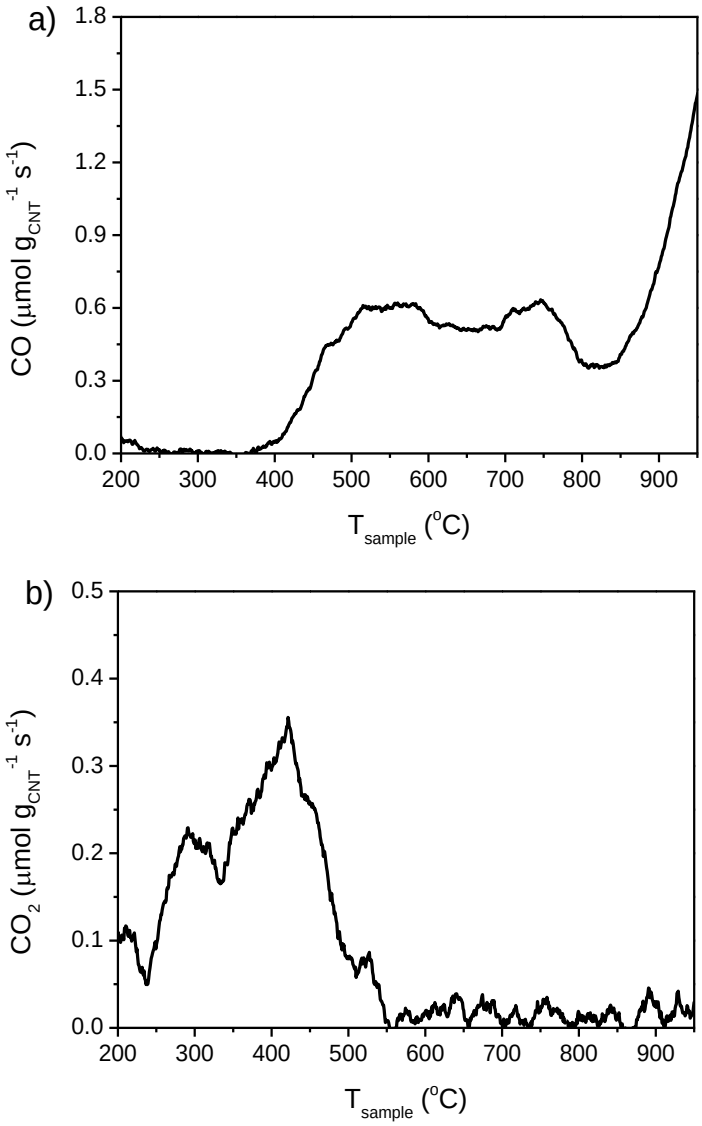

Figure 1.11 – Amounts of CO and CO_2 released during TPD experiments using a CNT covered monolith (per amount of CNT).

It is clear that the produced CNT using the methodology here described have some acidic oxygenated groups on the surface [19].

The textural properties of the grown CNT were also assessed through the isothermal adsorption of N_2. The adsorption/desorption isotherm obtained is presented in Figure 1.12.

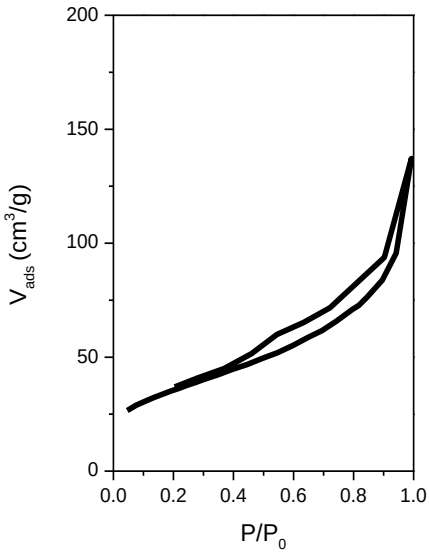

Figure 1.12 – Nitrogen adsorption isotherm obtained using the CNT covered monolith (per amount of CNT).

The isotherms obtained are characteristic of a Type II isotherm, corresponding to non-microporous solids [20, 21]. The calculated specific surface area is 125 m^2 g^{-1}, as calculated using the BET method for partial pressures between 0.05 and 0.3 [20].

Finally, TPO experiments were also performed using a thermogravimetric (TG) apparatus and the CNT covered monolith. The derivative of the weight loss observed during TPO experiments of the CNT monolith is presented in Figure 1.13.

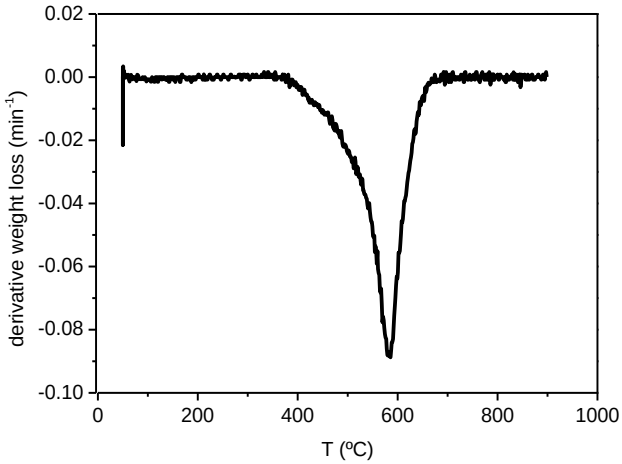

Figure 1.13 – Derivative weight loss of the CNT covered monolith during TPO experiment.

The temperature of the peak found in the derivative of the weight loss curves is typical of graphitic carbon [14].

The metallic catalyst was then impregnated on the CNT covered monoliths. Palladium was chosen due to the high activity observed during metal assessment experiments. The impregnation was performed using a similar method to that of the nickel impregnation; a solution was prepared using a $PdCl_2$ precursor, and the monoliths were put into this solution overnight (12h) while the liquid was flown through the channels continuously. The different methods for the preparation of the Pd solution are detailed in Table 1.4, and the obtained palladium loadings, calculated by concentration difference on the impregnation solution, on the different CNT monolith are presented in Figure 1.14.

It was clear that the method used during the impregnation of palladium influenced the amount that was impregnated onto the CNT monoliths. Furthermore, the use of polyvinyl alcohol (PVA) as a stabilizer helped the more extensive adsorption of palladium, likely due to linking promoted by PVA, which is known to form colloids with palladium in solution [22, 23]. On the other hand, the increase in the pH value of the impregnation

solution also increased the amount of adsorbed Pd, due to an increase in the interaction between the metal and the carbon surface due to electrostatic forces [12, 24-28].

Table 1.4 – Methods employed during the impregnation of palladium on the CNT monoliths.

Sample	Method
CNT4	2 wt.% Pd/CNT; 0.1M NaCl in water; pH 10
CNT9	2 wt.% Pd/CNT; 2% PVA + 0.1M NaCl in water; pH 3
CNT10	2 wt.% Pd/CNT; 2% PVA + 0.1M NaCl in water; pH 10

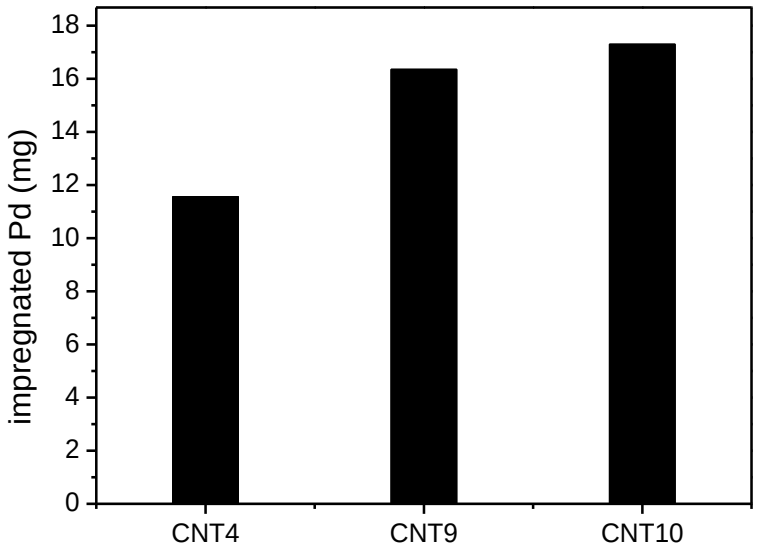

Figure 1.14 – Amount of palladium impregnated onto the surface of the CNT monoliths.

SEM-EDS images of the Pd/CNT monoliths were acquired, in order to identify differences in the distribution of the metal on the surface of the CNT. These images are presented in Figure 1.15, together with the respective EDS spectra obtained.

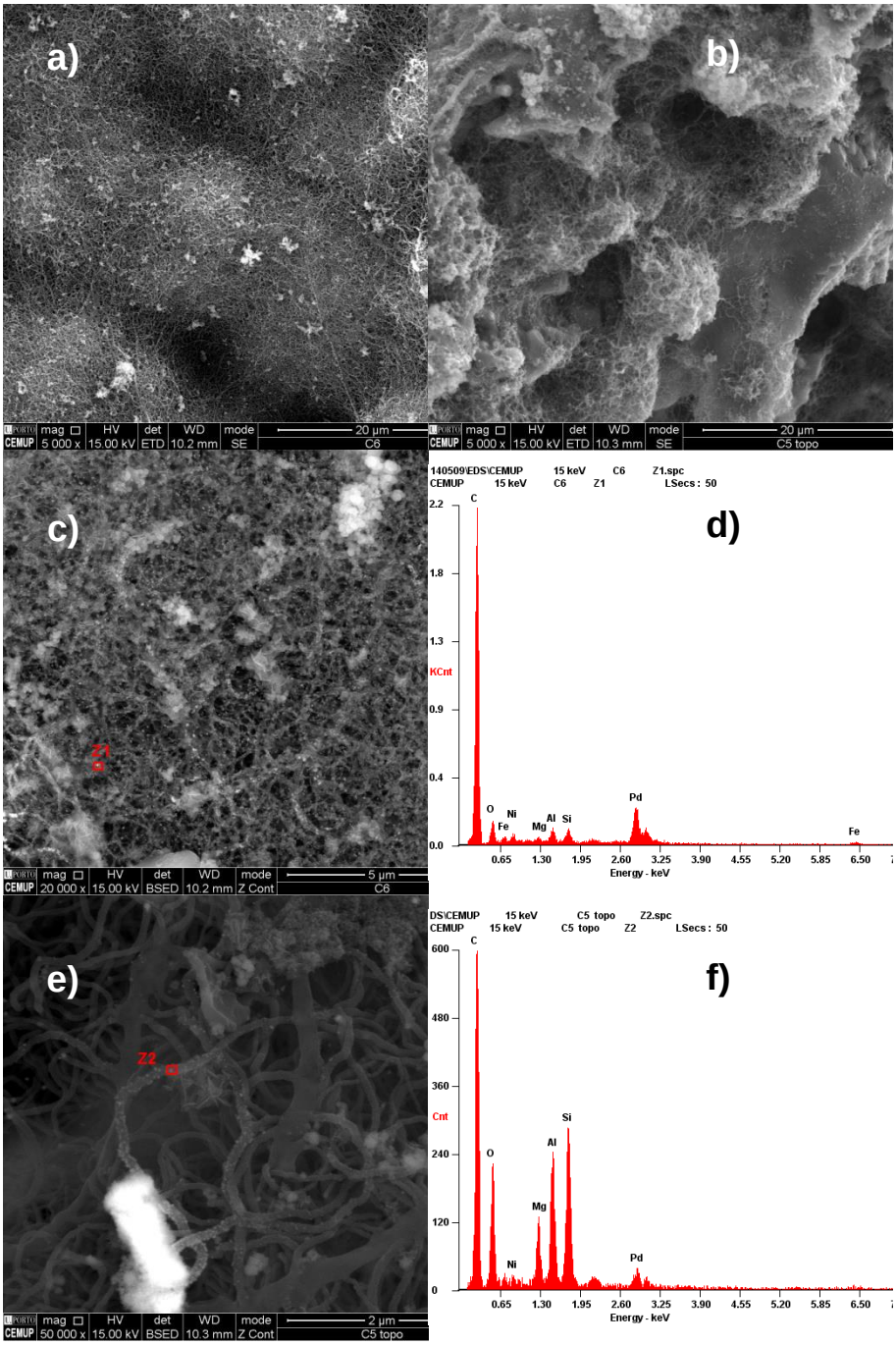

Figure 1.15 – SEM images and respective EDS spectra of the CNT monoliths: a) channel side view; b) top view; c) channel side view with

highlighted particle analysed by EDS (d); e) top view with highlighted particle analysed by EDS (f).

A homogeneous layer of CNT was achieved on the channel walls of the monoliths. However, on the top, a more heterogeneous dispersion was observed. The Pd particles on the channel walls and on the top of the monoliths seem to be homogeneously present throughout the CNT layer. Figure 1.15 e) and f) show, in particular, the presence of palladium particles on the walls of the individual carbon nanotubes, together with a large agglomerate of smaller particles. No significant differences between the monoliths were observed during SEM-EDS analysis.

The Pd/TiO_2 monoliths were prepared following several different methods for the sequential layering of the different components: alumina, titania and palladium. In general, the alumina and titania deposition were performed by dip coating, while the palladium impregnation was made by adsorption from solution, which was kept flowing through the channels of the monoliths during a period of time. The detailed methods used for each monolith are presented in Table 1.5.

Table 1.5 – Preparation methods used for the different Pd/TiO_2 structured catalysts.

Sample	Alumina deposition (18 mm min^{-1}, 1 min dipped)	Titania deposition (18 mm min^{-1}, 1 min dipped)	Palladium impregnation (12h impregnation with continuously flown solution)
TiO2 1	2 x 10% nyacol in ethanol	2 x 20% TiO_2 in ethanol	2% Pd for 100 mg TiO_2 in water:acetonitrilie 1:1 pH 3
TiO2 2	-	2 x 20% TiO_2 in ethanol	2% Pd for 100 mg TiO_2 in water:acetonitrilie 1:1 pH 3
TiO2 3	2 x 20% TiO_2 + 10% nyacol in ethanol		2% Pd for 100 mg TiO_2 in water:acetonitrilie 1:1 pH 3
TiO2 4	2 x 10% nyacol in ethanol	2 x 20% TiO_2 + 10% nyacol in ethanol	2% Pd for 100 mg TiO_2 in water:acetonitrilie 1:1 pH 3
TiO2 5	2 x 1:4 nyacol in water	2 x 20%TiO_2 + 6% nyacol in water	2% Pd for 100 mg TiO_2 in 0.5M NaCl in water pH 3
TiO2 6	2 x 1:4 nyacol in water	2 x 20%TiO_2 + 6% nyacol in water	2% Pd for 100 mg TiO_2 in 0.5M NaCl in water pH 10
TiO2 14	2 x 1:4 nyacol in water	2 x 20% 1%Pd/TiO_2 + 2% PVA in water pH 3	
TiO2 15	2 x 1:4 nyacol in water	2 x 20% 1%Pd/TiO_2 + 6% nyacol in water pH 3	
TiO2 16	2 x 1:4 nyacol in water	2 x 20%TiO_2 + 6% nyacol in water	2% Pd for 100 mg TiO_2 in 2% PVA + 0.5M NaCl in water pH 10
TiO2 17	2 x 1:4 nyacol in water	2 x 20% TiO_2 + 10% nyacol in ethanol	2% Pd for 100 mg TiO_2 in 0.5M NaCl in water pH 10
TiO2 18	2 x 1:4 nyacol in water	2 x 20% 1%Pd/TiO_2 + 1.68% nyacol + 1.68% PVA pH 3	
TiO2 19	2 x 1:4 nyacol in water	2 x 20%TiO_2 + 6% nyacol in water	2% Pd for 100 mg TiO_2 in 2% PVA + 0.5M NaCl in water pH 3

The relative weight gain after the deposition of alumina by dip coating for each monolith is presented in Figure 1.16

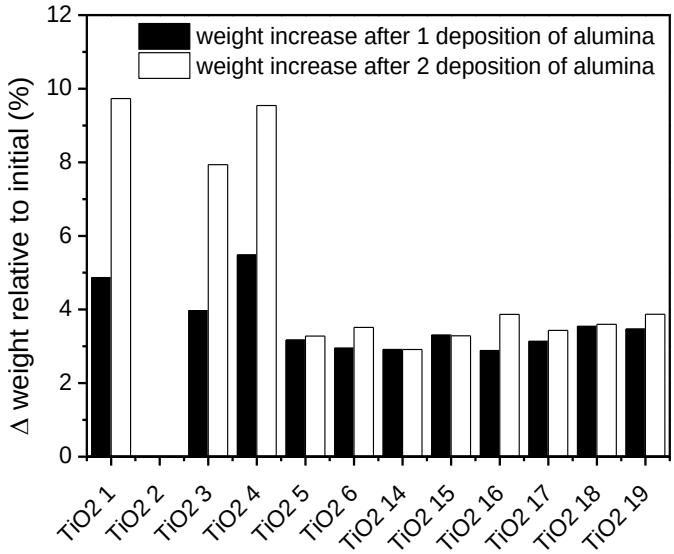

Figure 1.16 – Weight increase of the monoliths after alumina deposition in relation to the initial weight.

It is clear that the suspensions in ethanol lead to a more pronounced increase in the amount of alumina deposited through dip coating. Furthermore, the ethanol suspensions almost doubled the alumina loading when a second dip was performed, while the water suspensions barely increased the weight after the first dip. The sample TiO2 3, which was dipped in a combined nyacol/TiO_2 suspension, registered a slightly smaller increase in weight when compared with the other samples dipped in ethanol. This suggests that the presence of titania in the suspension slightly decreased the capacity for layering, probably due to changes in the physical properties of the slurry, which could also explain the smaller loadings obtained with water [17, 29].

The relative weight gain after the deposition of titania by dip coating for each monolith is presented in Figure 1.17.

The TiO2 3 structured catalyst is represented as zero since the titania was included in the slurry with the alumina, and the combined weight

increased was considered in Figure 1.16. In general, the catalysts which were dipped in a titania suspension in ethanol yielded a smaller loading, most likely due to changes in the properties of the slurry [29]. Furthermore, the catalysts which were coated with alumina using an ethanol suspension, which resulted on a higher loading of alumina, were observed to have a decreased capacity for layering with titania, which could be related to different textural properties of alumina when the weight loading increases [30, 31]. Nevertheless, it should be noticed that the increase in weight during impregnation with titania could be also attributed to further deposition of the alumina that is used as a stabilizer in the slurry.

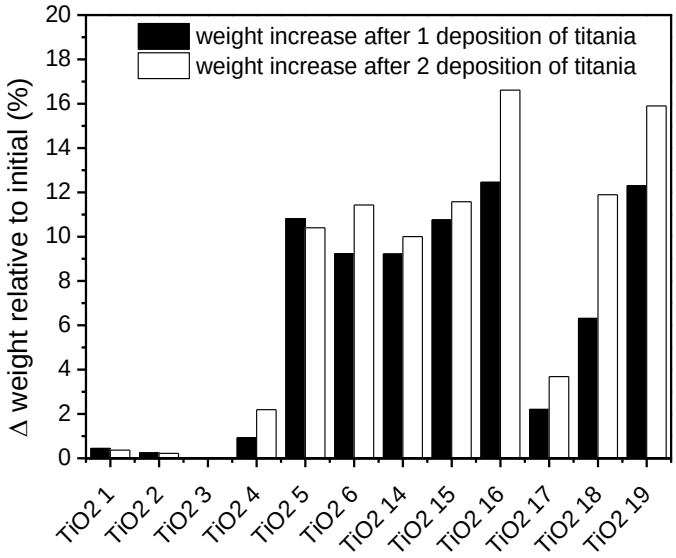

Figure 1.17 – Weight increase of the monoliths after titania deposition in relation to the weight after alumina deposition.

The amount of palladium adsorbed by the TiO_2 structured catalysts was also measured, as is presented in Figure 1.18.

The impregnation of palladium from a solution containing acetonitrile resulted in the lowest amount incorporated on the structured catalysts. The complex formed by the reaction between the palladium precursor and acetonitrile likely reduced the impregnation of palladium on the structured

catalyst [32]. In fact, the catalyst TiO2 17 was prepared using the same technique as TiO2 4 for the deposition of alumina and titanium dioxide. However, in this case, NaCl was used to help the dissolution of palladium in water, and a higher pH value was used. As expected, a higher loading of Pd on the catalyst was obtained.

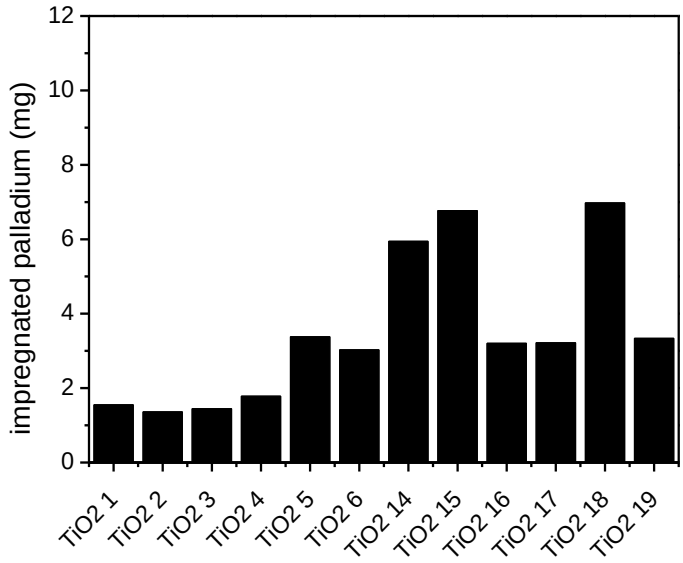

Figure 1.18 – Amount of palladium impregnated on the TiO_2 structured catalysts.

The structured catalysts with higher loadings were those that were prepared using a ball milled 1% Pd/TiO_2 powder catalyst in the slurry used for dip coating (TiO2 14, TiO2 15 and TiO2 18). The remaining catalysts were observed to have very similar palladium loadings among themselves, despite having been prepared using very different techniques.

SEM-EDS analyses were carried out using the Pd/TiO_2 in order to understand the differences in the structures due to the different preparation techniques, as presented in Figure 1.19.

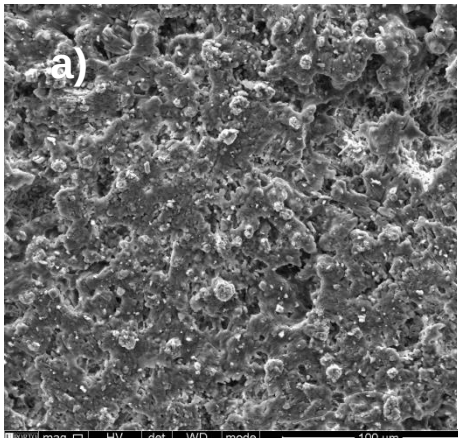
a)
mag
HV
det
WD
mode
1 000 x
15.00 kV
ETD
9.8 mm
SE
100 µm
C0

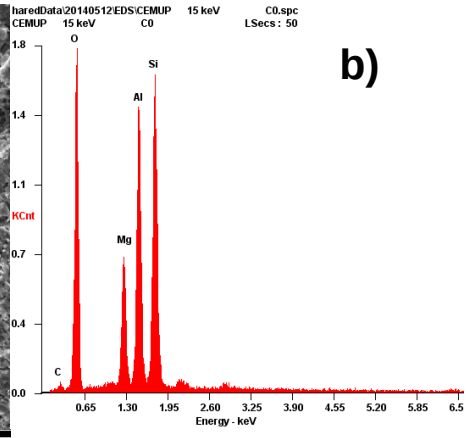
haredData\20140512\EDS\CEMUP 15 keV C0.spc
CEMUP 15 keV C0 LSecs : 50
b)
O
Si
Al
Mg
C
KCnt
Energy - keV

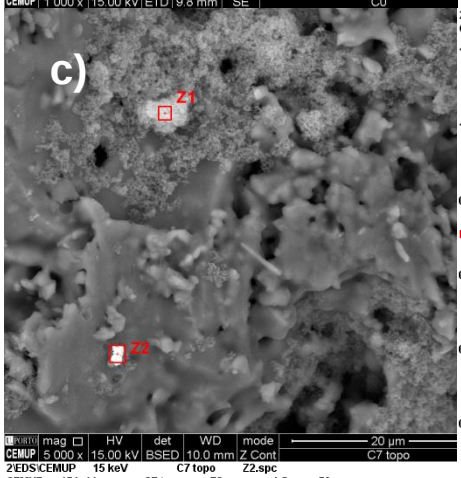
c)
Z1
Z2
mag
HV
det
WD
mode
5 000 x
15.00 kV
BSED
10.0 mm
Z Cont
20 µm
C7 topo

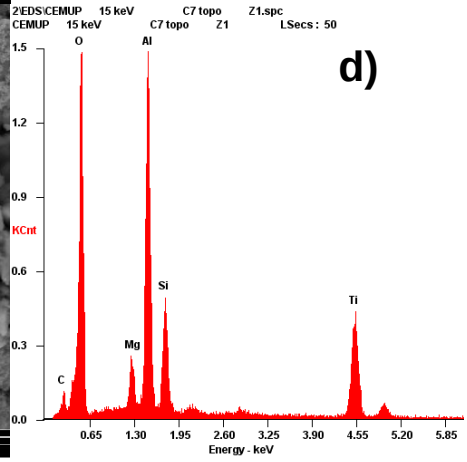
2\EDS\CEMUP 15 keV C7 topo Z1.spc
CEMUP 15 keV C7 topo Z1 LSecs : 50
d)
O
Al
Si
Ti
Mg
C
KCnt
Energy - keV

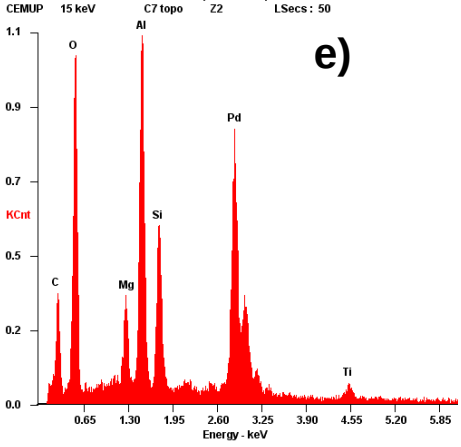
2\EDS\CEMUP 15 keV C7 topo Z2.spc
CEMUP 15 keV C7 topo Z2 LSecs : 50
e)
Al
O
Pd
Si
Mg
C
Ti
KCnt
Energy - keV

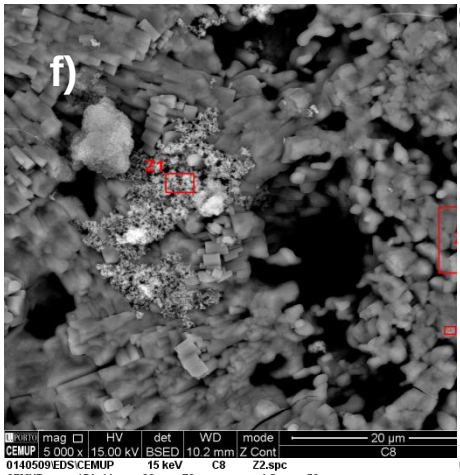
f)
Z1
mag HV det WD mode
5 000 x 15.00 kV BSED 10.2 mm Z Cont
20 µm
C8

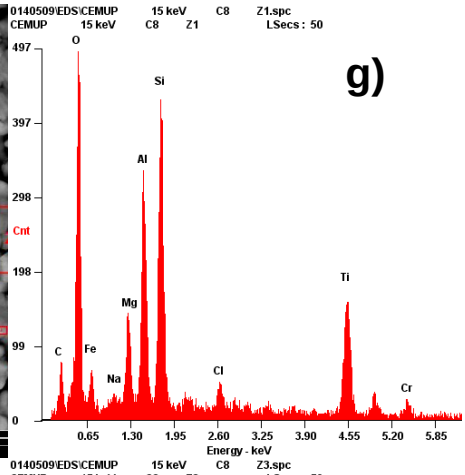
0140509\EDS\CEMUP 15 keV C8 Z1.spc
CEMUP 15 keV C8 Z1 LSecs : 50
g)
Cnt
O
Si
Al
Ti
Mg
C
Fe
Na
Cl
Cr
Energy - keV

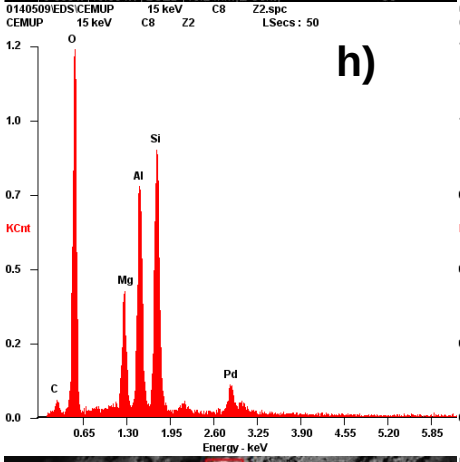
0140509\EDS\CEMUP 15 keV C8 Z2.spc
CEMUP 15 keV C8 Z2 LSecs : 50
h)
KCnt
O
Si
Al
Mg
C
Pd
Energy - keV

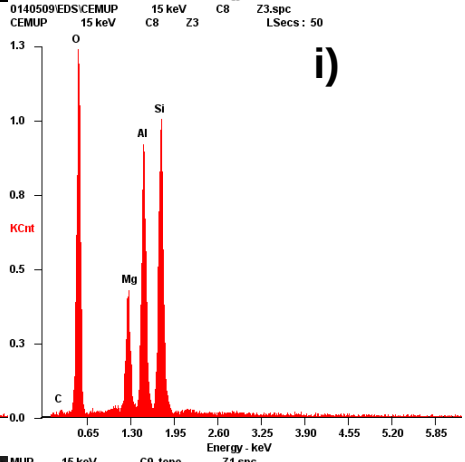
0140509\EDS\CEMUP 15 keV C8 Z3.spc
CEMUP 15 keV C8 Z3 LSecs : 50
i)
KCnt
O
Si
Al
Mg
C
Energy - keV

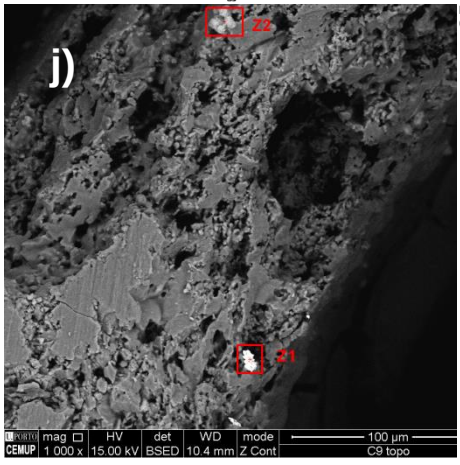
j)
Z2
Z1
mag HV det WD mode
1 000 x 15.00 kV BSED 10.4 mm Z Cont
100 µm
C9 topo

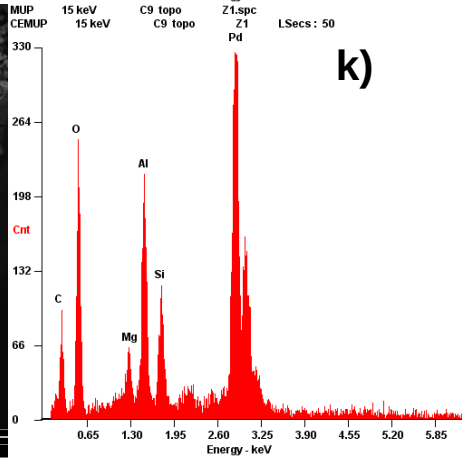
MUP 15 keV C9 topo Z1.spc
CEMUP 15 keV C9 topo Z1 LSecs : 50
k)
Cnt
Pd
O
Al
Si
C
Mg
Energy - keV

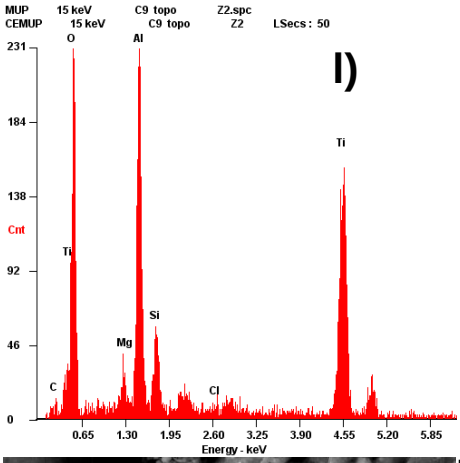
MUP 15 keV C9 topo Z2.spc
CEMUP 15 keV C9 topo Z2 LSecs : 50
l)
O
Al
Ti
Ti
Si
Mg
C
Cl
Cnt
231
184
138
92
46
0
0.65 1.30 1.95 2.60 3.25 3.90 4.55 5.20 5.85
Energy - keV

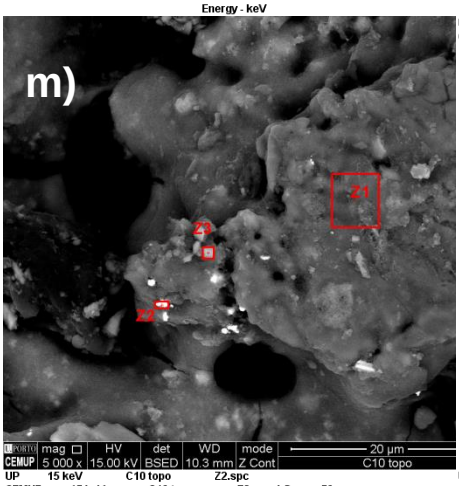
m)
Z1
Z2
Z3
mag HV det WD mode
5 000 x 15.00 kV BSED 10.3 mm Z Cont
20 µm
C10 topo

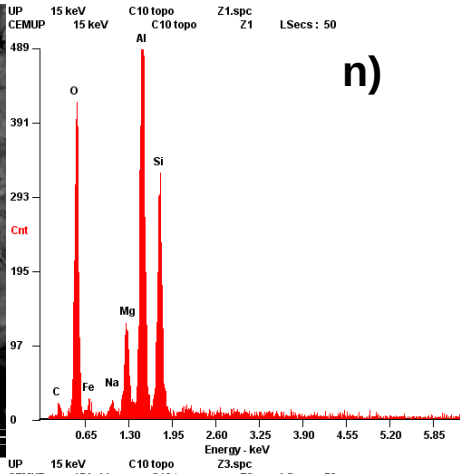
UP 15 keV C10 topo Z1.spc
CEMUP 15 keV C10 topo Z1 LSecs : 50
n)
Al
O
Si
Mg
C
Fe
Na
Cnt
489
391
293
195
97
0
0.65 1.30 1.95 2.60 3.25 3.90 4.55 5.20 5.85
Energy - keV

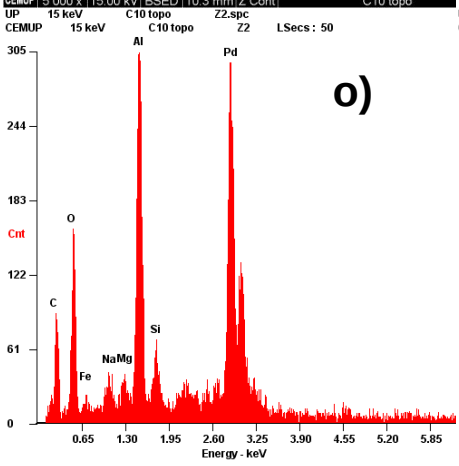
UP 15 keV C10 topo Z2.spc
CEMUP 15 keV C10 topo Z2 LSecs : 50
o)
Al
Pd
O
C
Si
Fe
Na
Mg
Cnt
305
244
183
122
61
0
0.65 1.30 1.95 2.60 3.25 3.90 4.55 5.20 5.85
Energy - keV

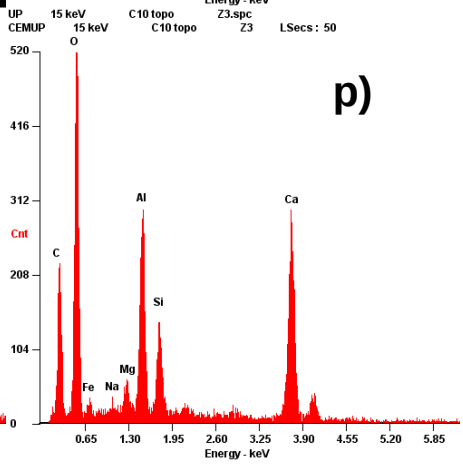
UP 15 keV C10 topo Z3.spc
CEMUP 15 keV C10 topo Z3 LSecs : 50
p)
O
Al
Ca
C
Si
Mg
Fe
Na
Cnt
520
416
312
208
104
0
0.65 1.30 1.95 2.60 3.25 3.90 4.55 5.20 5.85
Energy - keV

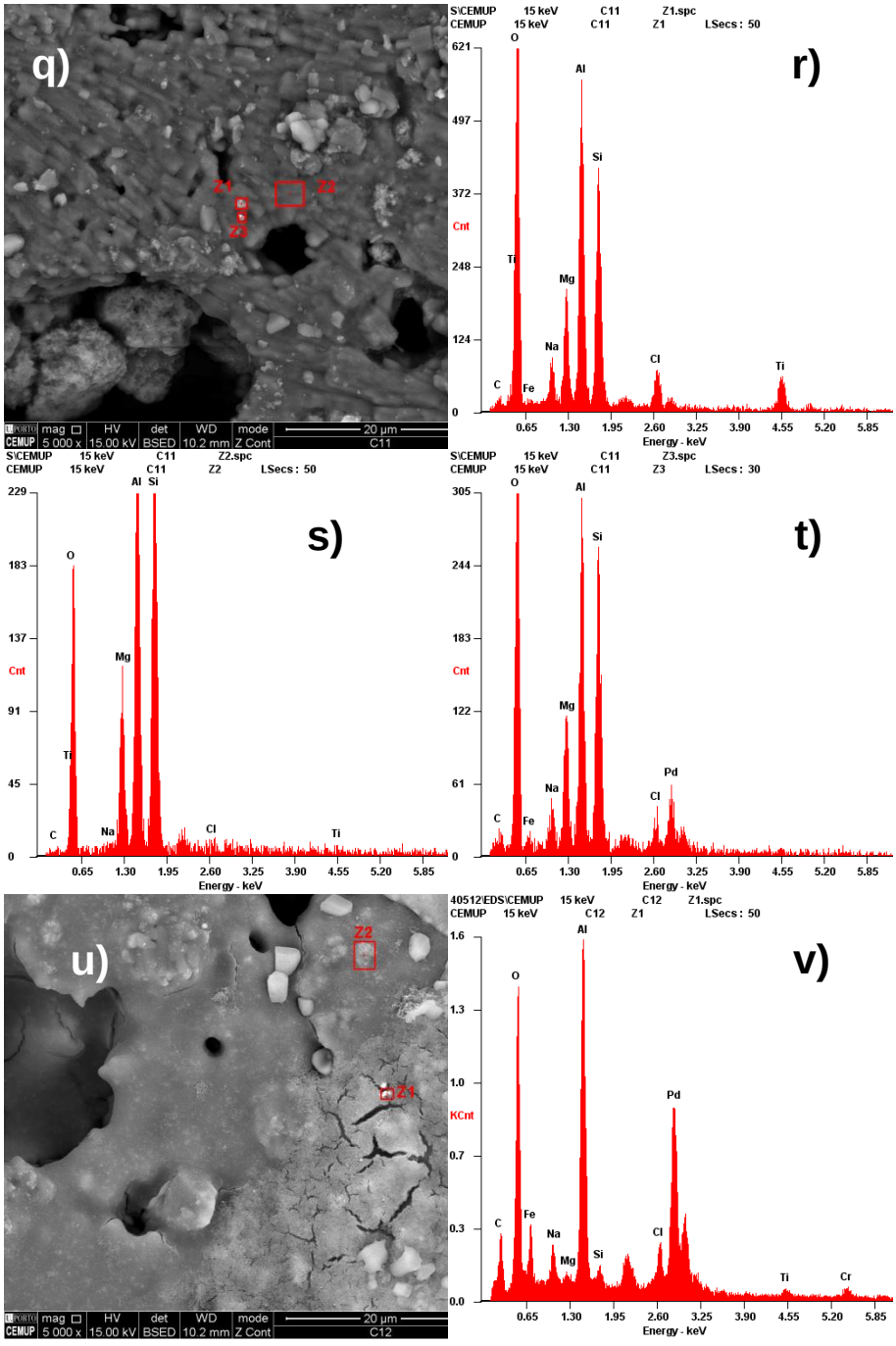
q)
Z1
Z2
Z3
mag HV det WD mode
CEMUP 5 000 x 15.00 kV BSED 10.2 mm Z Cont
20 µm
C11
r)
S\CEMUP 15 keV C11 Z1.spc
CEMUP 15 keV C11 Z1 LSecs : 50
621
497
372
Cnt
248
124
0
O
Al
Si
Ti
Mg
Na
Cl
C
Fe
Ti
0.65 1.30 1.95 2.60 3.25 3.90 4.55 5.20 5.85
Energy - keV
s)
S\CEMUP 15 keV C11 Z2.spc
CEMUP 15 keV C11 Z2 LSecs : 50
229
183
137
Cnt
91
45
0
Al Si
O
Mg
Ti
C
Na
Cl
Ti
0.65 1.30 1.95 2.60 3.25 3.90 4.55 5.20 5.85
Energy - keV
t)
S\CEMUP 15 keV C11 Z3.spc
CEMUP 15 keV C11 Z3 LSecs : 30
305
244
183
Cnt
122
61
0
O
Al
Si
Mg
Pd
Na
Cl
C
Fe
0.65 1.30 1.95 2.60 3.25 3.90 4.55 5.20 5.85
Energy - keV
u)
Z2
Z1
mag HV det WD mode
CEMUP 5 000 x 15.00 kV BSED 10.2 mm Z Cont
20 µm
C12
v)
40512\EDS\CEMUP 15 keV C12 Z1.spc
CEMUP 15 keV C12 Z1 LSecs : 50
1.6
1.3
1.0
KCnt
0.7
0.3
0.0
Al
O
Pd
C
Fe
Na
Mg
Si
Cl
Ti
Cr
0.65 1.30 1.95 2.60 3.25 3.90 4.55 5.20 5.85
Energy - keV

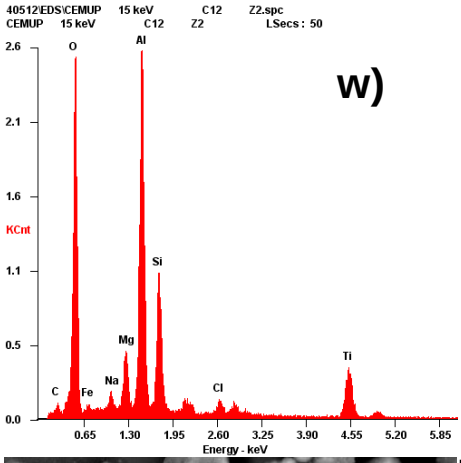
40512\EDS\CEMUP 15 keV C12 Z2.spc
CEMUP 15 keV C12 Z2 LSecs : 50
w)
KCnt
O
Al
Si
Mg
Na
Fe
C
Cl
Ti
Energy - keV

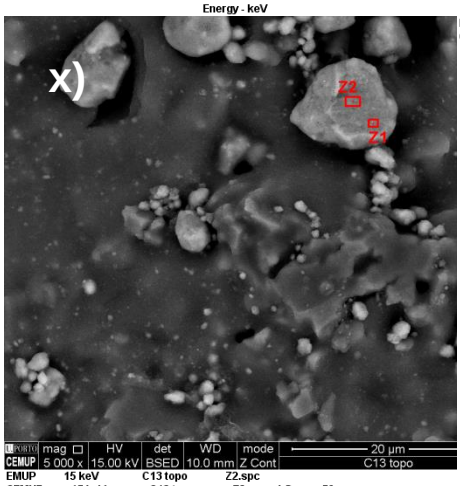
x)
Z1
Z1
mag HV det WD mode
5 000 x 15.00 kV BSED 10.0 mm Z Cont
20 µm
C13 topo

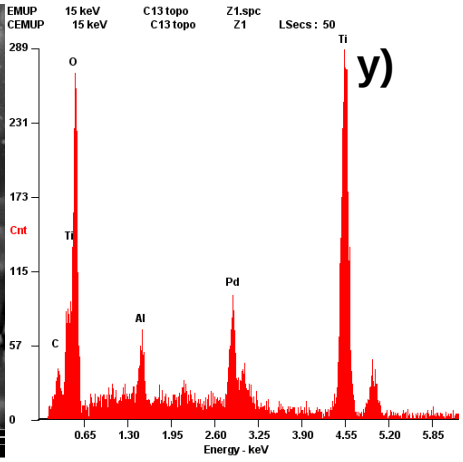
EMUP 15 keV C13 topo Z1.spc
CEMUP 15 keV C13 topo Z1 LSecs : 50
y)
Cnt
O
Ti
Al
Pd
C
Ti
Energy - keV

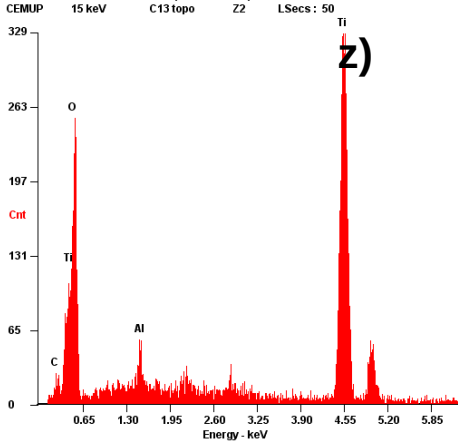
EMUP 15 keV C13 topo Z2.spc
CEMUP 15 keV C13 topo Z2 LSecs : 50
z)
Cnt
O
Ti
Al
C
Ti
Energy - keV

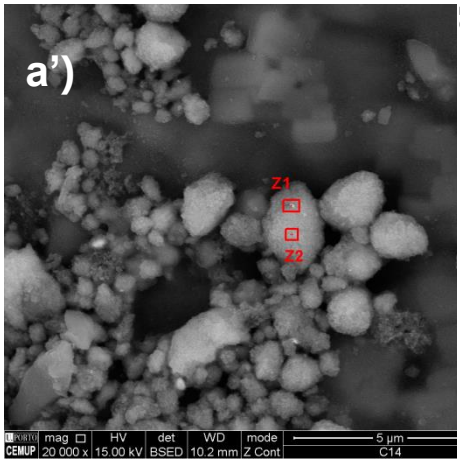
a')
Z1
Z2
mag
HV
det
WD
mode
20 000 x
15.00 kV
BSED
10.2 mm
Z Cont
5 µm
CEMUP
C14

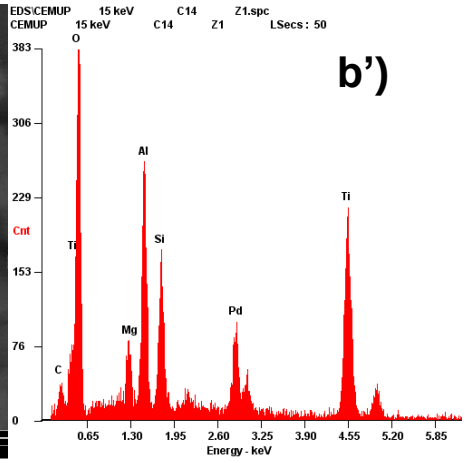
EDS\CEMUP 15 keV C14 Z1.spc
CEMUP 15 keV C14 Z1 LSecs : 50
b')
O
Al
Ti
Si
Pd
Mg
C
Cnt
383
306
229
153
76
0
0.65 1.30 1.95 2.60 3.25 3.90 4.55 5.20 5.85
Energy - keV

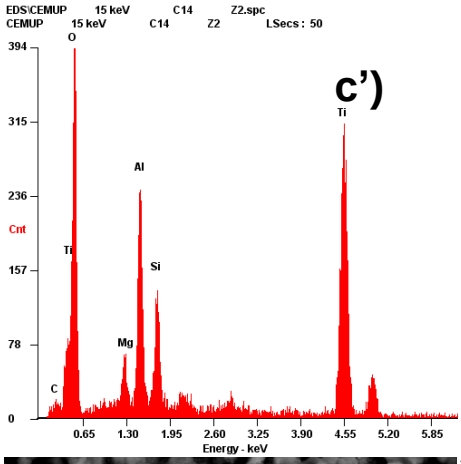
EDS\CEMUP 15 keV C14 Z2.spc
CEMUP 15 keV C14 Z2 LSecs : 50
c')
O
Ti
Al
Si
Mg
C
Cnt
394
315
236
157
78
0
0.65 1.30 1.95 2.60 3.25 3.90 4.55 5.20 5.85
Energy - keV

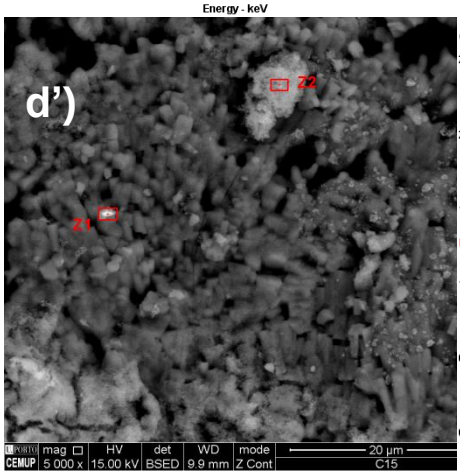
d')
Z2
Z1
mag
HV
det
WD
mode
5 000 x
15.00 kV
BSED
9.9 mm
Z Cont
20 µm
CEMUP
C15

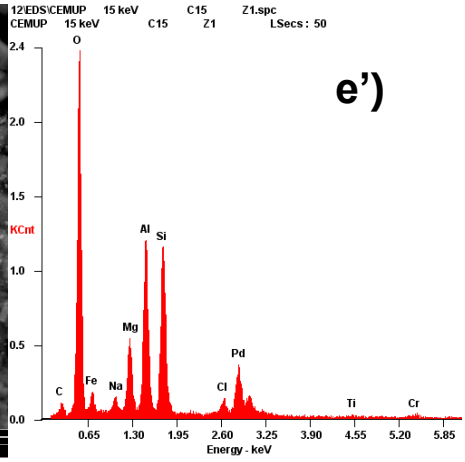
12\EDS\CEMUP 15 keV C15 Z1.spc
CEMUP 15 keV C15 Z1 LSecs : 50
e')
O
Al
Si
Mg
Pd
C
Fe
Na
Cl
Ti
Cr
KCnt
2.4
2.0
1.5
1.0
0.5
0.0
0.65 1.30 1.95 2.60 3.25 3.90 4.55 5.20 5.85
Energy - keV

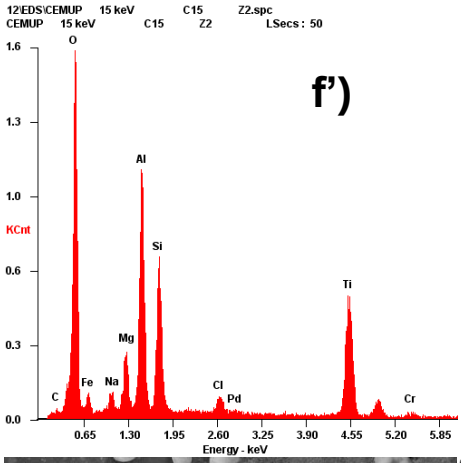
12\EDS\CEMUP 15 keV C15 Z2.spc
CEMUP 15 keV C15 Z2 LSecs : 50
f')
O
Al
Si
Ti
Mg
C
Fe
Na
Cl
Pd
Cr
KCnt
Energy - keV

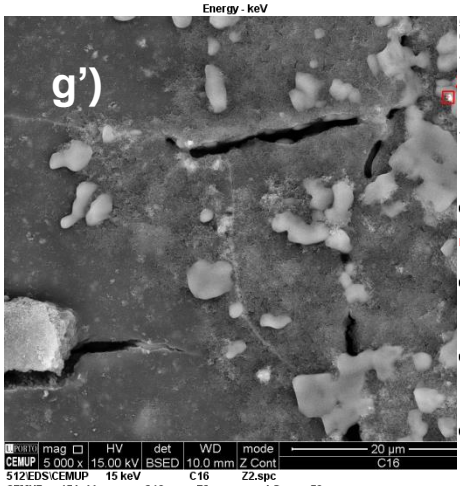
g')
mag HV det WD mode
5 000 x 15.00 kV BSED 10.0 mm Z Cont
20 µm
C16

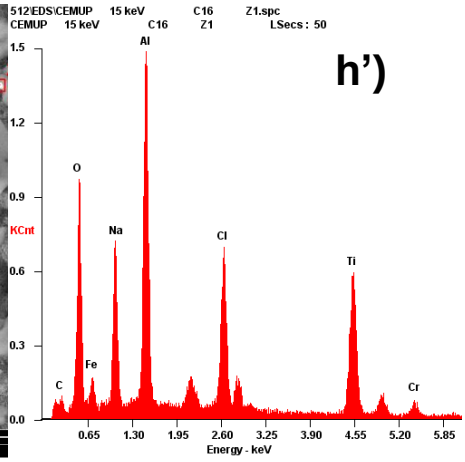
512\EDS\CEMUP 15 keV C16 Z1.spc
CEMUP 15 keV C16 Z1 LSecs : 50
h')
Al
O
Na
Cl
Ti
Fe
C
Cr
KCnt
Energy - keV

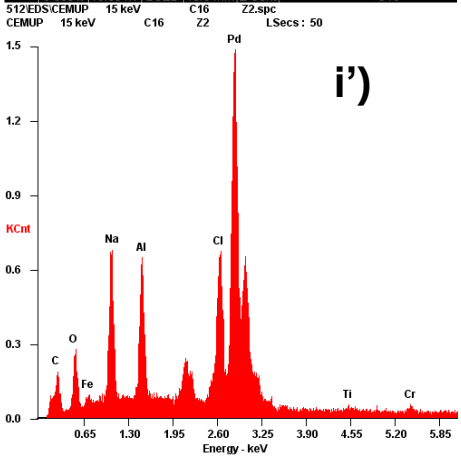
512\EDS\CEMUP 15 keV C16 Z2.spc
CEMUP 15 keV C16 Z2 LSecs : 50
i')
Pd
Na
Al
Cl
O
C
Fe
Ti
Cr
KCnt
Energy - keV

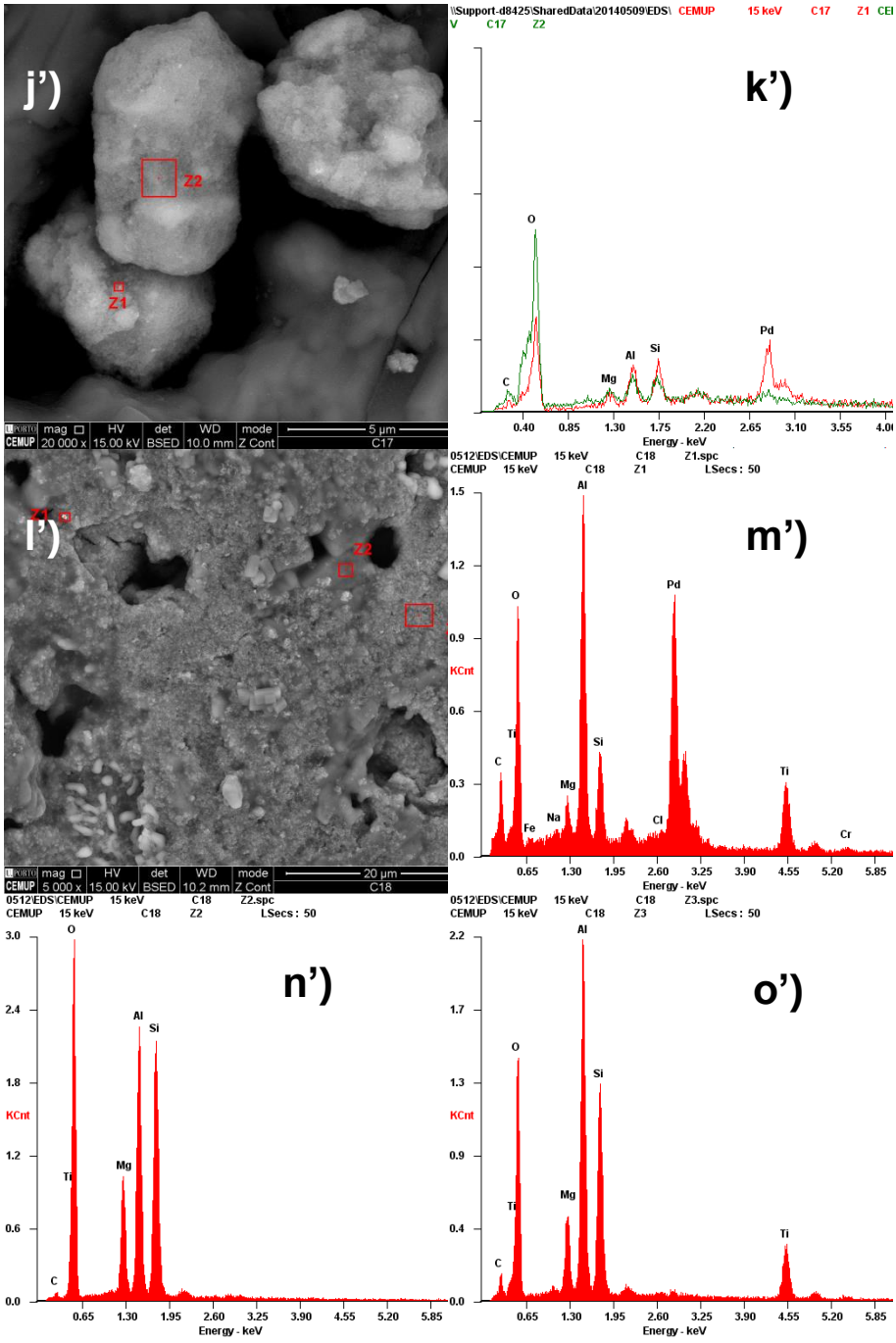
j')
Z2
Z1
mag HV det WD mode
CEMUP 20 000 x 15.00 kV BSED 10.0 mm Z Cont
5 µm
C17
\\Support-d8425\SharedData\20140509\EDS\ CEMUP 15 keV C17 Z1 CEI
V C17 Z2
k')
O
C
Mg
Al
Si
Pd
Energy - keV
0512\EDS\CEMUP 15 keV C18 Z1.spc
CEMUP 15 keV C18 Z1 LSecs : 50
l')
Z1
Z2
mag HV det WD mode
CEMUP 5 000 x 15.00 kV BSED 10.2 mm Z Cont
20 µm
C18
m')
KCnt
Al
O
Pd
Ti
C
Si
Mg
Fe
Na
Cl
Cr
Energy - keV
0512\EDS\CEMUP 15 keV C18 Z2.spc
CEMUP 15 keV C18 Z2 LSecs : 50
n')
O
Al
Si
Ti
Mg
C
KCnt
Energy - keV
0512\EDS\CEMUP 15 keV C18 Z3.spc
CEMUP 15 keV C18 Z3 LSecs : 50
o')
Al
O
Si
Ti
Mg
C
KCnt
Energy - keV

Figure 1.19 – SEM images of the prepared Pd/TiO_2 structured catalysts, presented together with EDS data obtained at the highlighted areas: a) cordierite support (EDS: b); c) TiO2 1 (EDS: d and e); f) TiO2 2 (EDS: g, h and i); j) TiO2 3(EDS: k and l); m) TiO2 4 (EDS: n, o and p); q) TiO2 5 (EDS: r, s and t); u) TiO2 6(EDS: v and w); x) TiO2 14 (EDS: y and z); a') TiO2 15 (EDS: b' and c'); d')TiO2 16 (EDS: e' and f'); g') TiO2 17 (EDS: h' and i'); j') TiO2 18 (EDS: k') and l') TiO2 19 (EDS: m', n' and o').

It is clear that the uniform layering of titania was not well achieved using the current preparation method. In fact, in most cases, aggregates were found either layered upon the alumina washcoat, or blended with it (depending on the preparation method, i.e. if nyacol was used in the titania slurry as stabilizer/dispersant or not). Also, the dispersion of palladium did not seem to have a preference for the titania containing regions, as it was found homogeneously and randomly distributed through the surface of the materials [29]. Nevertheless, the catalysts where a previously Pd impregnated titanium dioxide powder was layered presented, as expected, close contact of palladium and titanium dioxide. There were some differences observed related to the availability of the deposited powder particles, mostly due to where they were found on the surface of the materials: either deeper into pores or laying on the alumina surface. The amount of titanium present on the surface was also visibly different among the catalysts, either because less was deposited on the surface, or because most of it was covered by alumina that was deposited simultaneously, in the case of the structured catalysts that were prepared using nyacol in the titania slurry used for dip coating. It was also observed that, in the cases where a larger amount of alumina was deposited onto the catalysts, some fractures of the surface were observed, due to accumulation of alumina slurry [18]. Some iron and chromium was detected in small quantities in some cases, most likely originated from the stainless steel supports used during the palladium impregnation step.

Textural characterization of the prepared structured catalysts was performed by isothermal adsorption of N_2 at -196 ^{o}C. The calculated

specific surface areas, as determined by the BET method for partial pressures between 0.05 and 0.30, are presented in Table 1.6.

It is clear that layering of alumina on the surface of the catalyst contributes to the increase of the specific surface area of the catalysts, when compared with the case where no alumina was used (TiO2 2) [18].

Table 1.6 – Specific surface area of the prepared $Pd/TiO_2/Al_2O_3$ structured catalysts.

Sample	S_{BET} (m^2 g^{-1})
TiO2 1	230
TiO2 2	101
TiO2 3	212
TiO2 4	218
TiO2 5	267
TiO2 16	235
TiO2 17	203
TiO2 18	216
TiO2 19	188

1.3 CHEMICALS

Bromate (≥99%) and bromine (≥99%) sodium salts were acquired as standard for the evaluation of the catalytic activity of the prepared materials. Metallic precursors H_2PtCl_6, $PdCl_2$, $Cu(NO_3)_2$, $SnCl_2$, $RhCl_3$, $RuCl_3$, $Ni(NO_3)_2$, $(NH_4)_3IrCl_6$, $Fe(NO_3)_3$, $ZnCl_2$ were used for the impregnation of the catalysts. Norit GAC 1240 Plus activated carbon, P25 Degussa titanium dioxide and Nanocyl 3100 multiwalled carbon nanotubes were used as supports for the metallic catalysts. Honeycomb cordierite monoliths produced commercially by Corning. Nyacol colloidal alumina was used for the alumina washcoating.

1.4 CHARACTERIZATION TECHNIQUES

Selected catalysts were characterized using different techniques: hydrogen chemisorption, temperature programmed reduction (TPR), N_2 adsorption at – 196 ^{o}C, transmission electron microscopy (TEM) and scanning electron microscopy coupled with energy-dispersive X-ray spectroscopy (SEM-EDS).

The chemisorption of H_2 was carried out at 35 ^{o}C and atmospheric pressure in an Altamira Instruments AMI-200 apparatus, using the pulse method. Pulses of 58 μL (from a calibrated loop) were successively injected in the carrier gas (25 Ncm^3 min^{-1} of Ar), which passes through a catalyst bed (150 mg), until saturation of the catalyst surface. The non-adsorbed hydrogen is measured with an online thermal conductivity detector.

TPR experiments were carried out in an Altamira Instruments AMI-200 apparatus, by heating approximately 150 mg of the sample at 5 ^{o}C min^{-1} up to 600 ^{o}C under a flow of 5% (v/v) hydrogen diluted in argon (30 Ncm^3 min^{-1}). The consumption of hydrogen was measured using a thermal conductivity detector (TCD).

Textural characterization of the support and of the supported catalysts was based on the analysis of N_2 adsorption isotherms, measured at -196 ^{o}C with a Nova 4200e (Quantachrome Instruments) equipment.

TEM analyses were obtained using a LEO 906E microscope operating at a 120 kV accelerating voltage.

SEM-EDS analyses were performed using a FEI QUANTA 400 FEG ESEM/EDAX PEGASUS X4M apparatus.

The amount of metals in solution during impregnation of the structured catalysts, and the eventual leaching of the metals, were measured by atomic absorption spectroscopy (AAS) using a UNICAM 939/959 apparatus.

1.5 ANALYTICAL METHODS

Bromate ions concentrations were determined by HPLC using a Hitachi Elite Lachrom apparatus equipped with a diode array detector. The stationary phase was a Hamilton PRP-X100 column (150 mm x 4.1 mm) working at room temperature, under isocratic conditions. The mobile phase was a solution of 0.1 M NaCl:CH_3OH (45:55). Bromide ion concentrations were followed using a MetrOHM 881 Compact Pro ion chromatography apparatus coupled with a 863 Compact Autosampler. An appropriate MetrOHM chromatography column for anions was used with a 3.6 mM Na_2CO_3 stationary phase.

1.6 CATALYSTS EVALUATION

For the sake of brevity, the experimental set-ups that were used for the reduction of bromate under hydrogen are not pictured here, only described, since they were in all similar to those used during the ozonation reactions discussed elsewhere in this work.

1.6.1 SEMI-BATCH

Bromate reduction was carried out in a semi-batch reactor, equipped with a magnetic stirrer and a thermostatic jacket, at room temperature and atmospheric pressure, and using hydrogen as reducing agent. Initially, 180 mL of deionised water and the necessary amount of catalyst (400 mg for activated carbons, 50 mg for TiO_2 and MWCNT catalysts) were fed into the reactor, the magnetic stirrer was adjusted to 700 rpm and hydrogen was fed to the reactor at 100 $Ncm^3\ min^{-1}$ during 15 min to remove oxygen. After that period, 20 mL of a bromate solution, prepared from $NaBrO_3$, were added to the reactor, in order to obtain an initial BrO_3^- concentration equal to 10 mg L^{-1}.

1.6.2 CONTINUOUS

Continuous bromate reduction was carried out in a bubble column reactor, which was equipped with an internal loop (same as in Part II). The bromate solution at 10 mg L^{-1} was fed into the bottom of the bubble column using a peristaltic pump at 5 mL min^{-1}, while the recirculation in the internal loop was kept at 40 mL min^{-1}. The volume inside the reactor was 300 mL. Pure hydrogen was bubbled through a gas diffuser at the bottom of the bubble column at 100 cm^3 min^{-1}. The monolithic catalysts were lodged inside the bubble column, thus contacting with the gas and liquid phase simultaneously. Characterization of the resulting effluents was made from samples taken at the outlet of the reactor after the necessary time for steady state was reached.

REFERENCES

[1] O.S.G.P. Soares, J.J.M. Órfão, M.F.R. Pereira, Catalysis Letters, 126 (2008) 253-260.
[2] O.S.G.P. Soares, J.J.M. Órfão, M.F.R. Pereira, Desalination, 279 (2011) 367-374.
[3] O.S.G.P. Soares, J.J.M. Órfão, M.F.R. Pereira, Applied Catalysis B: Environmental, 102 (2011) 424-432.
[4] O.S.G.P. Soares, J.J.M. Órfão, M.F.R. Pereira, Catalysis Letters, 139 (2010) 97-104.
[5] O.S.G.P. Soares, J.J.M. Órfão, M.F.R. Pereira, Industrial and Engineering Chemistry Research, 49 (2010) 7183-7192.
[6] O.S.G.P. Soares, J.J.M. Órfão, M.F.R. Pereira, Applied Catalysis B: Environmental, 91 (2009) 441-448.
[7] O.S.G.P. Soares, J.J.M. Órfo, E. Gallegos-Suarez, E. Castillejos, I. Rodríguez-Ramos, M.F.R. Pereira, Environmental Technology, 33 (2012) 2353-2358.
[8] J. Kang, S. Zhang, Q. Zhang, Y. Wang, Angewandte Chemie, 121 (2009) 2603-2606.
[9] S.F. Yin, B.Q. Xu, W.X. Zhu, C.F. Ng, X.P. Zhou, C.T. Au, Catalysis Today, 93–95 (2004) 27-38.
[10] N.W. Hurst, S.J. Gentry, A. Jones, B.D. McNicol, Catalysis Reviews, 24 (1982) 233-309.
[11] T.C. Chang, J.J. Chen, C.T. Yeh, Journal of Catalysis, 96 (1985) 51-57.
[12] J. Zhu, J. Zhou, T. Zhao, X. Zhou, D. Chen, W. Yuan, Applied Catalysis A: General, 352 (2009) 243-250.
[13] E. Garcia-Bordeje, I. Kvande, D. Chen, M. Ronning, Advanced Materials, 18 (2006) 1589.
[14] E. García-Bordejé, I. Kvande, D. Chen, M. Rønning, Carbon, 45 (2007) 1828-1838.
[15] N. Jarrah, J.G. van Ommen, L. Lefferts, Catalysis Today, 79-80 (2003) 29-33.
[16] N.A. Jarrah, Journal of materials chemistry, 14 (2004) 1590.
[17] T.A. Nijhuis, A.E. Beers, T. Vergunst, I. Hoek, F. Kapteijn, J.A. Moulijn, Catalysis Reviews, 43 (2001) 345-380.
[18] P.A.R. Cebollada, E. Garcia-Bordejé, Chemical Engineering Journal, 149 (2009) 447-454.
[19] J.L. Figueiredo, M.F.R. Pereira, M.M.A. Freitas, J.J.M. Órfão, Carbon, 37 (1999) 1379-1389.
[20] J.L. Figueiredo, F.R. Ribeiro, Catálise Heterogénea, Calouste Gulbenkian.
[21] K.S.W. Sing, D.H. Everett, R.A.W. Haul, L. Moscou, R.A. Pierotti, J. Rouquerol, T. Siemieniewska, Reporting Physisorption Data for Gas/Solid Systems, Handbook of Heterogeneous Catalysis, Wiley-VCH Verlag GmbH & Co. KGaA2008.
[22] Z. CSUROS, A. LENGYEL, PERIODICA POLYTECHNICA-CHEMICAL ENGINEERING, 18 (1974) 155-165.

[23] J.K. Chinthaginjala, A. Villa, D.S. Su, B.L. Mojet, L. Lefferts, Catalysis Today, 183 (2012) 119-123.
[24] S. Morales-Torres, A.F. Pérez-Cadenas, F. Kapteijn, F. Carrasco-Marín, F.J. Maldonado-Hódar, J.A. Moulijn, Applied Catalysis B: Environmental, 89 (2009) 411-419.
[25] C. Pham-Huu, Journal of molecular catalysis. A, Chemical, 170 (2001) 155.
[26] G. Strukul, Catalysis Today, 55 (2000) 139.
[27] J.-P. Tessonnier, L. Pesant, G. Ehret, M.J. Ledoux, C. Pham-Huu, Applied Catalysis A: General, 288 (2005) 203-210.
[28] P. Tribolet, L. Kiwi-Minsker, Catalysis Today, 105 (2005) 337.
[29] P. Avila, M. Montes, E.E. Miró, Chemical Engineering Journal, 109 (2005) 11-36.
[30] L. Martínez-Latorre, S. Armenise, E. Garcia-Bordejé, Carbon, 48 (2010) 2047-2056.
[31] L. Martínez-Latorre, P. Ruiz-Cebollada, A. Monzón, E. García-Bordejé, Catalysis Today, 147, Supplement (2009) S87-S93.
[32] B.P. Barbero, L. Costa-Almeida, O. Sanz, M.R. Morales, L.E. Cadus, M. Montes, Chemical Engineering Journal, 139 (2008) 430-435.

2. METAL ASSESSMENT

2.1. DESCRIPTION

In this chapter, different metals (Pd, Pt, Ir, Rh, Ru, Fe, Sn, Cu, Zu and Ni) supported on activated carbon were assessed for the catalytic reduction of bromate under hydrogen at room temperature and pressure.

A mechanism for the reduction of bromate was proposed, involving reactions in the liquid phase, on the surface of the activated carbon support, and on the surface of the supported metal particles. It is proposed that the reaction mechanism on the surface of the metal catalysts comprises the decomposition of hydrogen and subsequent reaction with bromate.

The catalysts that were studied in this chapter were prepared in the Laboratory of Catalysis and Materials, by Dr. Salomé Soares in the context of her doctoral thesis, who kindly made them available for the study of their application in the reduction of bromate.

2.2. CATALYTIC TESTS

Blank tests using only hydrogen or using activated carbon (AC) with hydrogen or nitrogen were carried out to evaluate the role of the reducing agent (hydrogen) and of adsorption on the support (AC). Nitrogen was used to understand the role of adsorption while maintaining similar mixing conditions in the reactor. The results obtained are presented in Figure 2.1.

Hydrogen by itself allows obtaining a bromate removal of approximately 90% after 120 min of reaction. Activated carbon, on its own, is a fairly good adsorbent of the bromate ion, removing over 80% when experiments were done using only nitrogen in the gas phase. Similar removals are reported in the literature for adsorption of bromate using a granulated activated carbon (GAC) filter and distilled water as solvent [1]. However,

whereas in the aforementioned work the reduction of bromate using only GAC, without hydrogen, is reported, such a result was not observed in this study, as discussed below. When AC is coupled with hydrogen, the concentration curve has an evolution very similar to that observed with only AC, suggesting that adsorption is playing the major role in the removal of bromate when only the activated carbon is present. In addition, in the presence of AC, there was a drastic reduction of bromate concentration in solution for short reaction times, whereas in the presence of only hydrogen it decreased much more slowly.

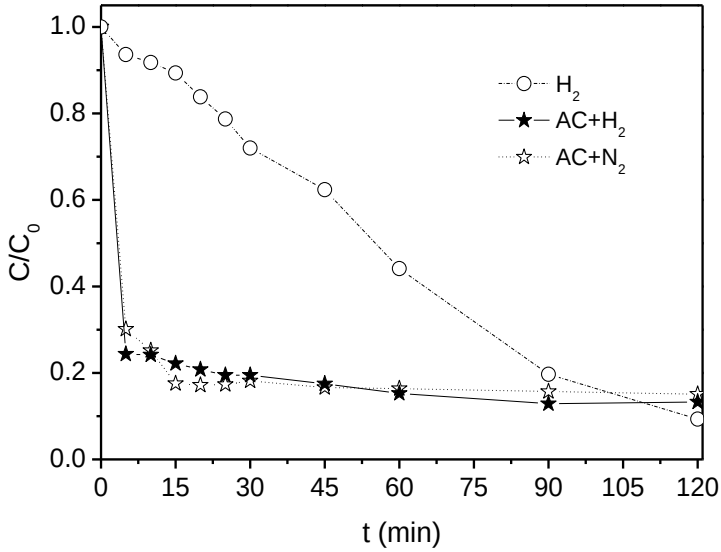

Figure 2.1 - Dimensionless concentration of bromate during experiments using activated carbon together with hydrogen ($AC+H_2$) and with nitrogen ($AC+N_2$) or only hydrogen (H_2).

Figure 2.2 shows concentrations of bromate and bromide ions after 120 min in the experimental conditions mentioned before. The experiment using activated carbon coupled with hydrogen resulted in a small reduction of bromate into bromide, which, on the other hand, was not detected when no hydrogen was introduced into the solution. Most of the removal of bromate from water during experiments with activated carbon was due to adsorption on the activated carbon surface, even when hydrogen was present. A small amount of bromide was detected in

solution during the experiments using activated carbon coupled with hydrogen, which suggests that some reduction of bromate is occurring either on the surface of the support, probably due to interaction with hydrogen, or by direct interaction with hydrogen in solution. The reduction of bromate to bromide on the surface of activated carbon has been previously reported to occur due to the interaction with surface oxygenated groups [2-4]. In our study, when no hydrogen was present, the release of bromide to the solution was not observed. It was also not possible to identify the species adsorbed on the AC surface, due to their small amount. However, the commercial activated carbon used in this study is known to have a small concentration of surface oxygenated groups [5], which explains why it is possible to identify a small amount of bromide released into solution only when hydrogen is present in solution. Moreover, activated carbon has been reported to have low capacity for the adsorption of bromide [6].

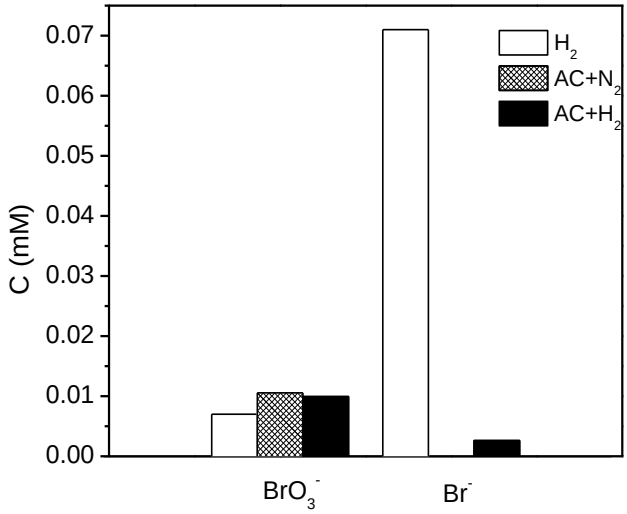

Figure 2.2 - Final concentrations of bromate and bromide after 120 minutes experiments using activated carbon together with hydrogen ($AC+H_2$) and with nitrogen ($AC+N_2$) or only hydrogen (H_2). (C_o=0.078 mM)

The first approach to the catalytic reduction of bromate consisted in the assessment of the activity of various metals. The dimensionless

concentration of bromate during reduction experiments using hydrogen over monometallic catalysts supported on activated carbon is presented in Figure 2.3.

The inclusion of a monometallic catalyst during the hydrogen reduction of bromate in water clearly improves the removal rate. In fact, the most efficient metals (Pd, Rh, Ru and Pt) completely convert bromate in 30 min or less. It has also been observed that bromate is being completely converted into bromide in all cases, which rules out the possibility of removal by adsorption on the AC support.

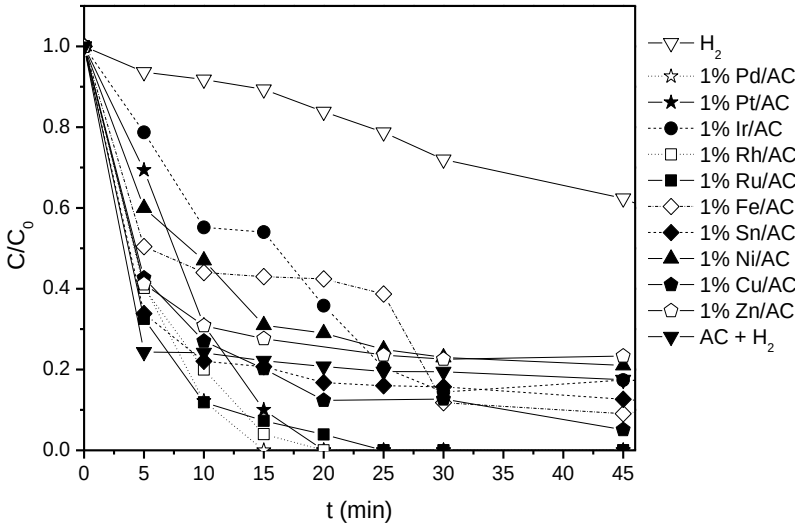

Figure 2.3 - Dimensionless concentration of bromate during reduction experiments using hydrogen in the presence of monometallic catalysts supported on activated carbon.

The distributions of bromate and bromide after 120 min of reaction over the metallic catalysts are presented in Figure 2.4, together with the evolution of the total bromine concentration in solution during selected experiments. It is shown that the removal of bromate from solution over the metallic catalysts completely corresponds to conversion to bromide. Complete bromate conversion is not achieved in the presence of some catalysts, even after 120 min. The most efficient metal was found to be

Pd, completely converting bromate in just 15 min, although Rh, Pt and Ru also showed good performances (see Figure 2.3). The different performances observed must be related with the chemical nature of the metals, as well as with the metallic dispersion, since all the catalysts present the same amount of metal. Nevertheless, the results clearly show that bromates can be easily reduced over selected metals supported on activated carbon in the presence of hydrogen.

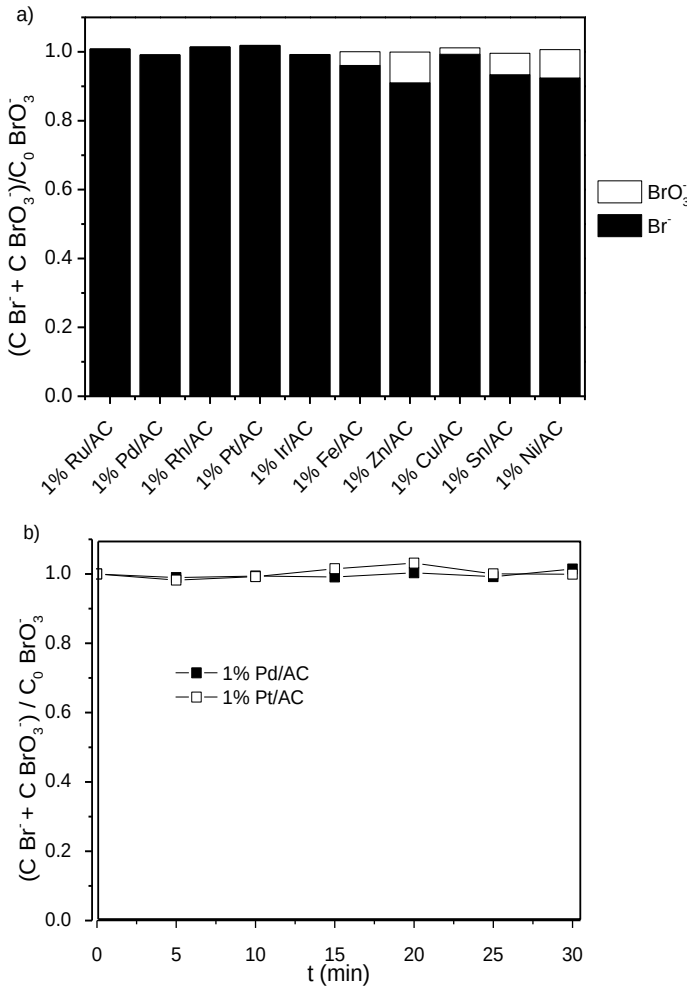

Figure 2.4 - Dimensionless concentration of bromate and bromide after 120 min (a) and evolution of molar balance of bromine during experiments with selected catalysts (b).

Assuming that the bromate reduction mechanism involves hydrogen chemisorption on the metal surface, it was expected that the most active catalysts were those that form a medium-strength bond with hydrogen, according to the Sabatier principle [7]. The turn over number (TON) after 10 minutes of reaction is plotted in Figure 2.5 as a function of the hydrogen dissociative chemisorption energy per atom of some metals tested in the experiments [8]. TON was calculated as the number of moles converted divided by the accessible moles of metal atoms, which take dispersion into account. The trend observed approximates that of a typical volcano curve [9].

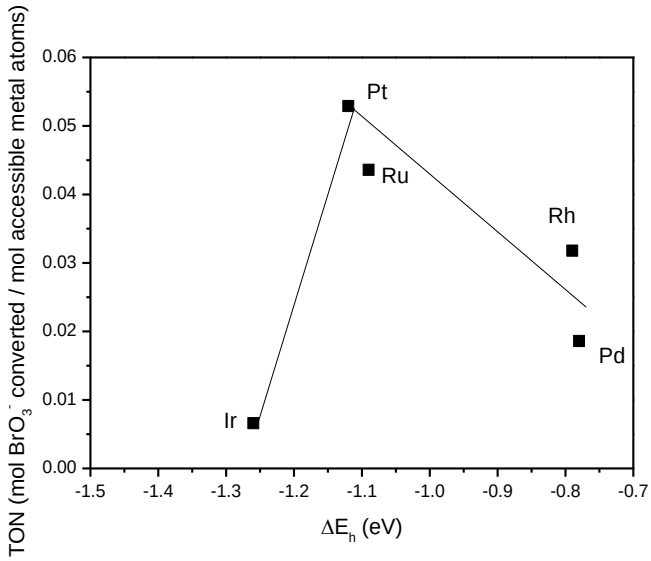

Figure 2.5 - Turn over number (TON) after 10 min of reaction vs. hydrogen chemisorption energy per metal atom.

Metals with a moderate hydrogen chemisorption energy are shown to be more active in the reduction of bromate, as was reported for the reduction of nitrite using supported metallic catalysts [10]. Platinum seems to be the most active metal for bromate reduction with hydrogen.

In the catalytic reduction of bromate over metal catalysts, two different reaction schemes have been proposed. On one hand, the addition of a reducing agent to the system would lead to the restoration of the metal to

its original oxidation state, which was modified after interaction with bromate. Thus, the metal particles would then be in the necessary oxidation state (i.e. reduced) to be able to further interact with bromate [11]. On the other hand, the reduction of bromate on the surface of a metallic catalyst is due to reaction with hydrogen atoms, which could originate from the hydrolysis of water or from the decomposition of an added reducing agent, such as hydrogen or an alcohol [12, 13]. To clear out ambiguities regarding the reaction mechanism and to understand the role of hydrogen in the reaction, experiments using the supported palladium metal catalyst were carried out using nitrogen instead of hydrogen, in order to retain similar hydrodynamic conditions in the reactor. The pre-reduction stage under hydrogen was still performed, after which the whole system was purged with nitrogen before the introduction of the bromate solution. Afterwards, this catalyst sample was recovered and tested in a second experiment using only nitrogen, this time skipping the pre-reduction with hydrogen. Tests were repeated until no change in the performance of the catalyst was observed. Afterwards, the same catalyst was reused in an experiment with hydrogen. The removal of bromate during these experiments is presented in Figure 2.6.

Analysis of the curves presented in Figure 6.a leads to several conclusions. Comparison between the reaction with hydrogen in the presence of the fresh catalyst and the reaction using nitrogen shows a loss of conversion, as expected. Comparing the later reutilization cycles to the 2^{nd} cycle of reutilization, a much larger loss is observed. Thus, the pre-reduction step in the first case increased the availability of metal in the necessary oxidation state (reduced) for reaction, while in the following experiment much less is present. Without hydrogen in solution, the reduction of the metal by hydrolysis is much slower, as is the case for the reduction of bromate, and thus a large drop in performance was expected. It is also possible that some dissolved hydrogen was still present in the case of the experiment with pre-reduction under hydrogen. Further reutilization of the catalyst led to a point, after the third reutilization under

the conditions tested, in which the reduction of the metal and the dissociation of hydrogen for reaction with bromate were solely from hydrogen in water, and thus the performance did not drop further. Reutilization of this catalyst using hydrogen (5th cycle) led to a similar result to that observed in the experiments using the fresh catalyst.

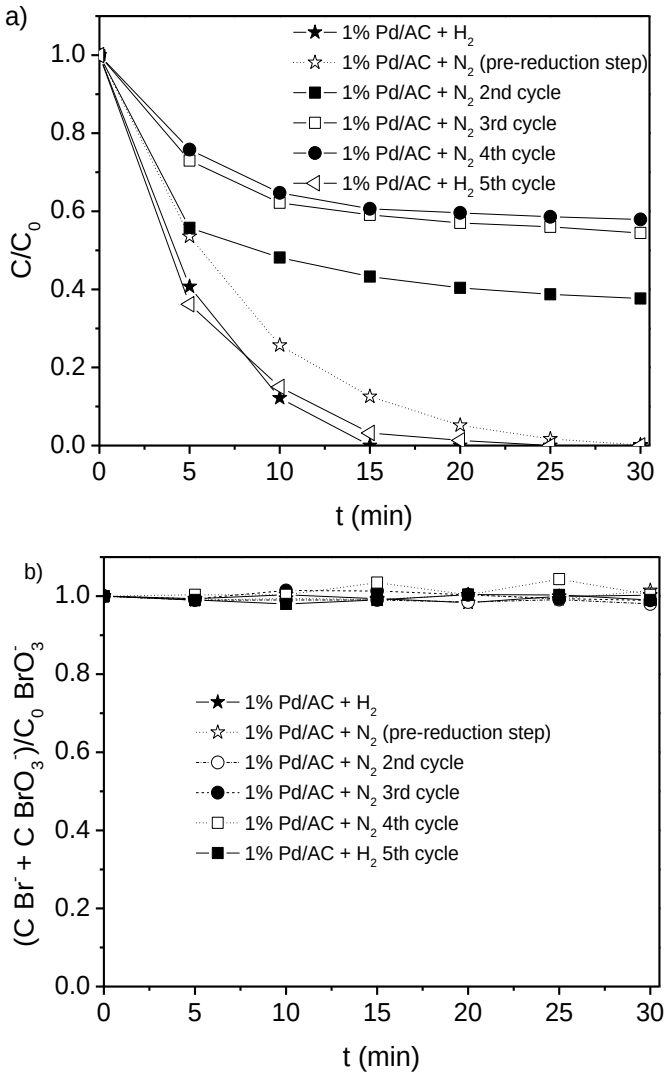

Figure 2.6 - Dimensionless concentration of bromate (a) and molar balance of bromine (b) during successive experiments with and without hydrogen, using a Pd monometallic catalyst supported on activated carbon.

The results obtained are in accordance with the reaction mechanism proposed by Chen et al. [12] and by Mills and Meadows [13]. In all these experiments, bromate was always stoichiometricly reduced to bromide (Figure 2.6.b).

Thus, four reaction steps for the reduction of bromate can be proposed when metal catalysts supported on activated carbon are used (Figure 2.7): direct reaction with hydrogen in solution, as observed in the experiments where no support nor metal catalyst were present (a); adsorption and reduction by hydrogen on the surface of activated carbon, as observed in the reactions using activated carbon without a metal phase (b); adsorption of bromate on the surface of the activated carbon, when no hydrogen was present in solution (c); adsorption and reduction on the surface of the metallic particles (d).

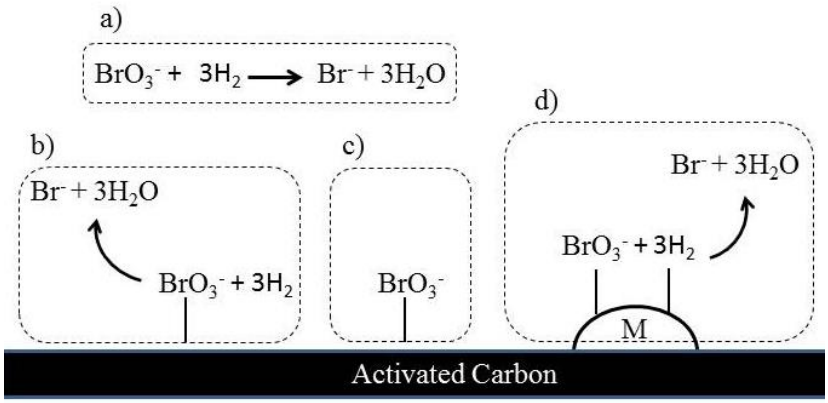

Figure 2.7 - Bromate removal pathways.

The most important reaction pathway identified in this work is undoubtedly the reduction on the surface of the metal catalyst. This is a process that comprises several steps, as shown in Figure 2.8.

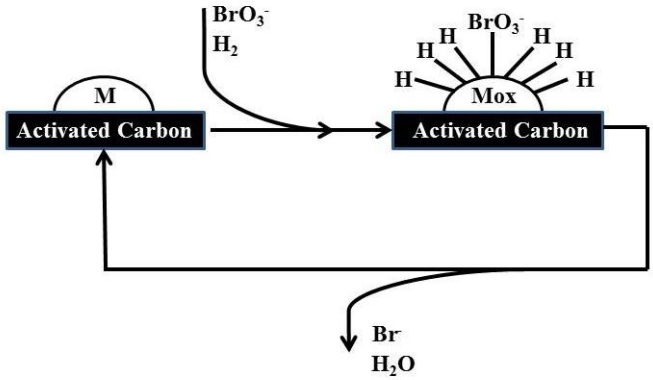

Figure 2.8 - Scheme of bromate reduction with hydrogen taking place in the presence of metal catalysts (as seen in Figure 7– path d).

As suggested in the literature, the mechanism involves the dissociative adsorption of hydrogen on the surface of the metal, and the reaction between adsorbed bromate ion and hydrogen atoms [12, 13]. Such mechanism agrees with what was presented in Figure 5, where the catalytic activities of the different metals are plotted as a function of the dissociative adsorption energies of hydrogen. The cyclic experiments using only nitrogen in the gas phase have shown that hydrogen plays a role not only on the reduction of bromate ions, but also on the reduction of the metal. Thus, the reaction mechanism here proposed involves the adsorption of bromate ions on the surface of the catalyst, and their reduction by adsorbed and dissociated hydrogen. Bromide is consequently released into the bulk of the solution, while the metal becomes oxidized. Then, hydrogen converts it to the original reduced form, thus becoming available to further interact with bromate and hydrogen [11, 14]. While Pd is known to be able to store hydrogen due to the formation of β-PdH [15], it does not explain by itself the reduction of bromate when the stoichiometry is considered, since only 0.0146 mmol of Pd are reacting in the catalyst used in the present experiments. Further experiments using the Pd catalyst prior to calcination and/or reduction ($N_{cal}N_{red}$ and N_{red}) were carried out in order to clarify the reaction mechanism proposed in Figures 2.7 and 2.8. Figure 2.9 contains the

obtained bromate removal profiles using these samples, where a comparison of the performance obtained with or without in-situ pre-reduction is also presented.

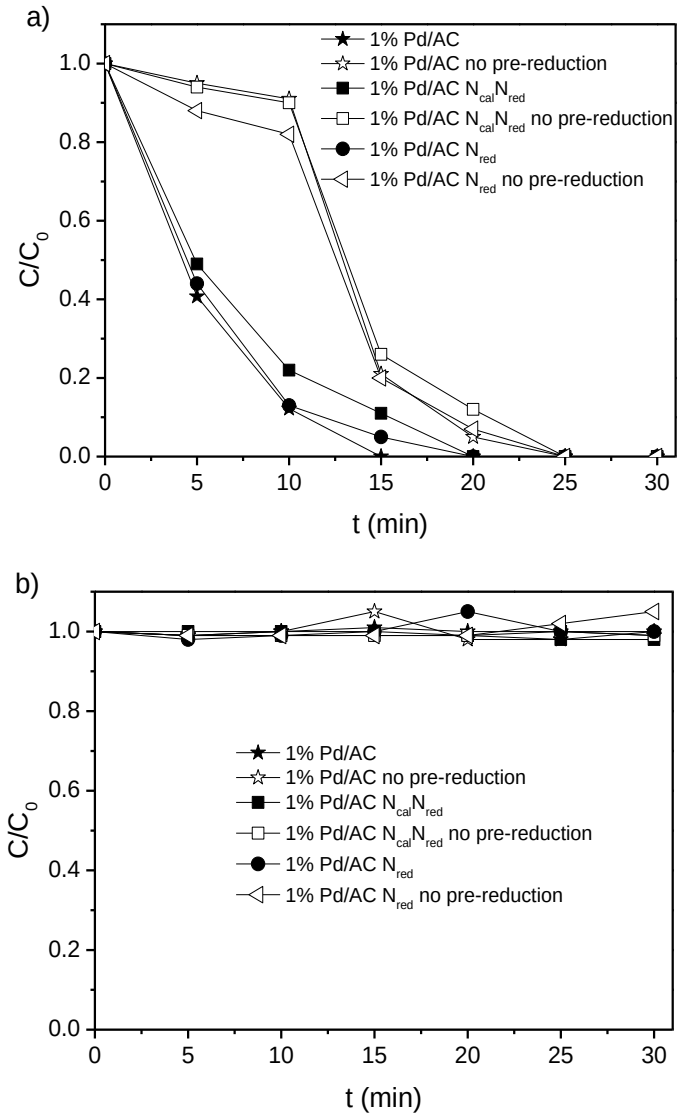

Figure 2.9 - Dimensionless concentration of bromate (a) and molar balance of bromine (b) during experiments using a Pd monometallic catalyst supported on activated carbon before and after calcination and reduction.

The calcination of the catalyst during its preparation contributes to an increased activity likely due to the formation of palladium particles on the surface of the support, due to migration and sintering, to which the thermal decomposition of the oxygenated groups present on the surface of the activated carbon might contribute [16-18]**.** The activity of the $N_{cal}N_{red}$ and N_{red} catalysts shows that the contact with hydrogen in water is sufficient to achieve a reduced state of the metallic phase, thus supporting the reaction mechanism proposed. The delay in the activation of the three catalysts during experiments carried out without the pre-reduction step (15 min of contact with hydrogen in water prior to the introduction of the bromate solution) agrees with what is here proposed.

The characterization carried out by XPS of the catalysts during the various reaction steps only revealed the presence of the oxidized forms of the metals; handling of the samples and contact with air do not allow the rigorous determination of the oxidation states, since the XPS analysis were performed ex-situ [16]**.**The mechanism of reaction was additionally studied in the case of non-noble metals.

Consecutive experiments carried out using the Cu/AC catalyst, both under nitrogen and hydrogen, are presented in Figure 2.10.

The observed bromate removals during consecutive experiments using the Cu/AC catalyst were similar to those observed when the same experiments were carried out using the Pd/AC catalyst (Figure 2.6). The activity of the catalyst is reduced during consecutive experiments carried out under nitrogen (after an initial pre-reduction with hydrogen in the first experiment of the series), until it becomes stable after three runs. The initial activity of the fresh catalyst was restored when the reused catalyst was reapplied under standard conditions (Figure 2.10, 5^{th} cycle). These observations suggest that the mechanism for bromate removal is similar whether noble or non-noble metals are used. Non-noble metals have been observed to be able to participate in reduction reactions under hydrogen, albeit with smaller activities than noble metals [10].

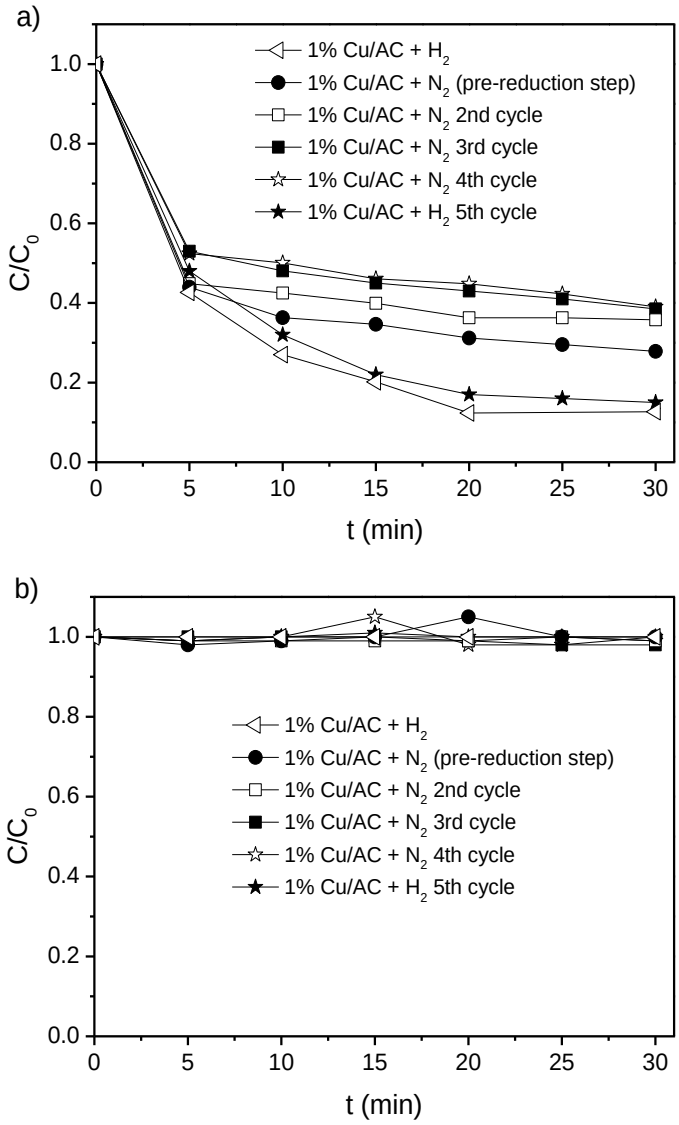

Figure 2.10 - Dimensionless concentration of bromate (a) and molar balance of bromine (b) during successive experiments with and without hydrogen, using a Cu monometallic catalyst supported on activated carbon.

2.3 PARTIAL CONCLUSIONS

Noble metal catalysts (Pd, Pt, Ru, Rh) supported on activated carbon efficiently catalyze the conversion of bromate into bromide ion under hydrogen at room temperature and pressure. An extensive adsorption on activated carbon was observed when no hydrogen was present in the system. However, complete conversion into bromide was obtained only when a metal catalyst was present.

Among the several catalysts tested, the palladium catalyst was shown to be the most efficient in terms of bromate conversion. However, when the available metal surface for reaction is considered, it was clear that platinum has the highest intrinsic activity. A simplified mechanism for the reduction of bromate was proposed, which takes into account reactions in the liquid phase, on the surface of the support, and on the surface of the supported metal particles. The roles of the metal and of the reducing agent were assessed, and it was proposed that the reaction mechanism on the surface of the metal comprised the dissociative adsorption of hydrogen and subsequent reaction with adsorbed bromate. This results in the release of bromide ion and water. The oxidized metal is then reduced by hydrogen, thus being available for further interaction with bromate and hydrogen.

REFERENCES

[1] M.J. Kirisits, V.L. Snoeyink, J.C. Kruithof, Water Research, 34 (2000) 4250-4260.
[2] M. Siddiqui, W. Zhai, G. Amy, C. Mysore, Water Research, 30 (1996) 1651-1660.
[3] M. Asami, T. Aizawa, T. Morioka, W. Nishijima, T. Akihisa, Y. Magara, Water Research, 33 (1999) 2797-2804.
[4] W.J. Huang, Y.L. Cheng, Separation and Purification Technology, 59 (2008) 101-107.
[5] P.C.C. Faria, J.J.M. Órfão, M.F.R. Pereira, Chemosphere, 67 (2007) 809-815.
[6] E.A. Sigworth, S.B. Smith, Journal of the American Water Works Association, 64 (1972) 386-391.
[7] P. Sabatier, European Journal of Inorganic Chemistry, 44 (1911) 1984-2001.
[8] T. Bligaard, J.K. Nørskov, S. Dahl, J. Matthiesen, C.H. Christensen, J. Sehested, Journal of Catalysis, 224 (2004) 206-217.
[9] J. Cheng, P. Hu, P. Ellis, S. French, G. Kelly, C.M. Lok, Journal of Physical Chemistry C, 112 (2008) 1308-1311.
[10] O.S.G.P. Soares, J.J.M. Órfão, M.F.R. Pereira, Catalysis Letters, 126 (2008) 253-260.
[11] D.B. Thakur, R.M. Tiggelaar, Y. Weber, J.G.E. Gardeniers, L. Lefferts, K. Seshan, Applied Catalysis B: Environmental, 102 (2011) 243-250.
[12] H. Chen, Z. Xu, H. Wan, J. Zheng, D. Yin, S. Zheng, Applied Catalysis B: Environmental, 96 (2010) 307-313.
[13] A. Mills, G. Meadows, Water Research, 29 (1995) 2181-2185.
[14] D. Duonghong, W. Erbs, L. Shuben, M. Grätzel, Chemical Physics Letters, 95 (1983) 266-268.
[15] D.G. Narehood, S. Kishore, H. Goto, J.H. Adair, J.A. Nelson, H.R. Gutiérrez, P.C. Eklund, International Journal of Hydrogen Energy, 34 (2009) 952-960.
[16] O.S.G.P. Soares, J.J.M. Órfão, J. Ruiz-Martínez, J. Silvestre-Albero, A. Sepúlveda-Escribano, M.F.R. Pereira, Chemical Engineering Journal, 165 (2010) 78-88.
[17] A. Sepulveda-Escribano, F. Coloma, F. Rodrıguez-Reinoso, Applied Catalysis A: General, 173 (1998) 247-257.
[18] F. Coloma, A. Sepúlveda-Escribano, J. Fierro, F. Rodríguez-Reinoso, Applied Catalysis A: General, 136 (1996) 231-248.

3. BIMETALLIC CATALYSTS

3.1 DESCRIPTION

In this chapter, the coupling of a noble metal with a promoter metal supported on activated carbon has been studied for this reaction. Several metals were used for this goal, resulting in a wide array of combinations of noble and promoter metals.

The role played by the promoter metal was extensively studied, for which several experiments were conducted using physical mixtures of the corresponding monometallic catalysts and also different metal amounts on the supported bimetallic catalysts.

The catalysts that were studied in this chapter were prepared in the Laboratory of Catalysis and Materials, by Dr. Salomé Soares in the context of her doctoral thesis, who kindly made them available for the study of their application in the reduction of bromate.

3.2 CATALYTIC EXPERIMENTS

3.2.1 BIMETALLIC CATALYSTS

The bromate reduction in the presence of hydrogen was evaluated using several different metallic catalysts. To assess this effect, the same activated carbon support was used for all the metal pairs.

On a first approach, palladium was coupled with different metals. The corresponding bromate removals are shown in Figure 3.1.

The coupling of Pd with Cu shows to be the more efficient combination among those tested. All the other combinations present similar or lower performance than the Pd monometallic catalyst. A similar trend was observed for the second metal alone, as presented elsewhere: Cu > Sn > Fe > Zn [1].

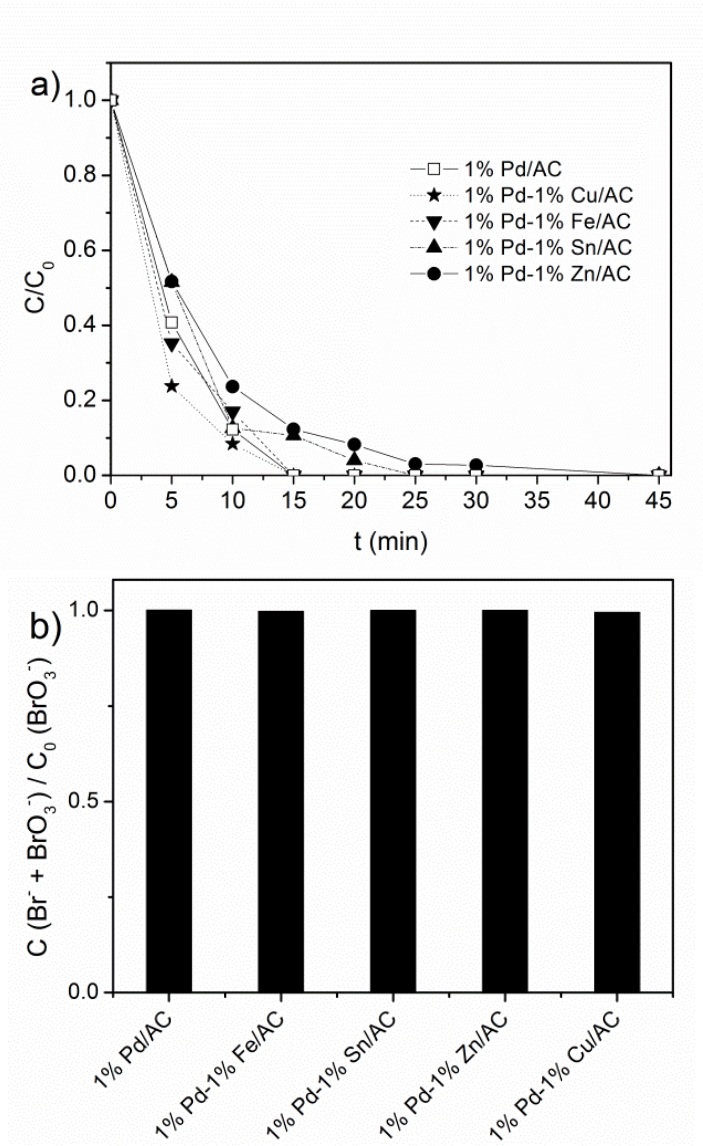

Figure 3.1 - Evolution of the dimensionless concentration of bromate (a) and total mass balance of bromine after 45 min (b) for reduction experiments using H_2 and bimetallic palladium catalysts supported on activated carbon.

Among the metals tested, the Cu monometallic catalyst shows the best activity both alone [1] and also paired with Pd. Therefore, bimetallic catalysts containing Cu and different noble metals (Pd, Ir, Pt, Ru)

supported on activated carbon were tested in the bromate reduction in the presence of hydrogen, as seen in Figure 3.2.

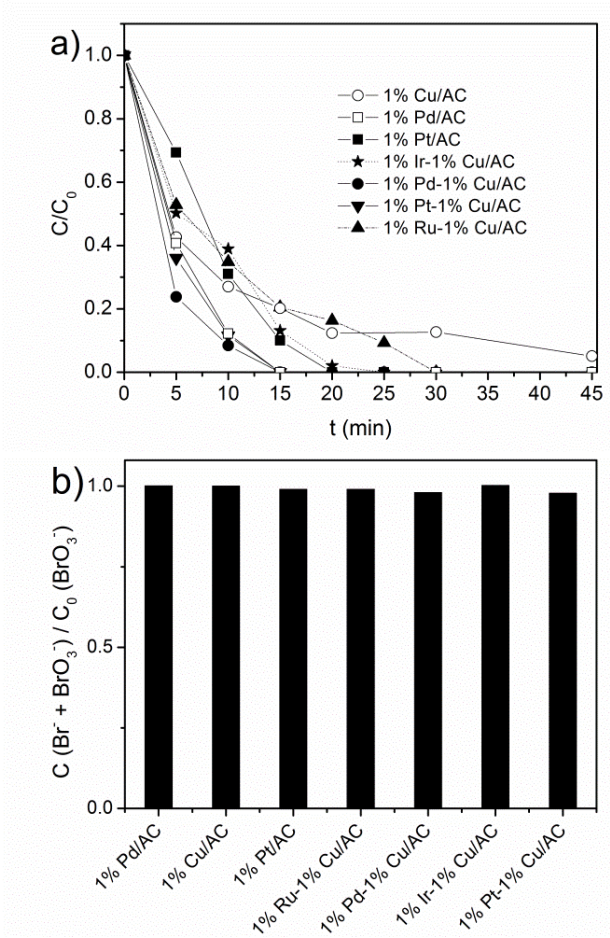

Figure 3.2 - Evolution of the dimensionless concentration of bromate (a) and total mass balance of bromine after 45 min (b) for reduction experiments using H_2 and bimetallic catalysts containing Cu, supported on activated carbon.

Once again, the Pd-Cu catalyst showed the best performance of those tested, closely followed by the Pt-Cu catalyst. Ir-Cu and Ru-Cu catalysts are outperformed by the Cu monometallic catalyst in the first 10 and 15 min, respectively, but eventually overpass it, promoting 100% bromate conversion after 25 and 30 minutes respectively; with the Cu monometallic catalyst total bromate reduction was only achieved after 60

min of reaction. Overall, the performance of every Cu-containing bimetallic catalyst tested here is between that of the Pd-Cu and the Cu monometallic catalyst.

To assess the performance of different noble metals in the reduction of bromate using bimetallic catalysts, some noble metals (Pd, Pt or Rh) were paired with tin and evaluated in the reaction (Figure 3.3).

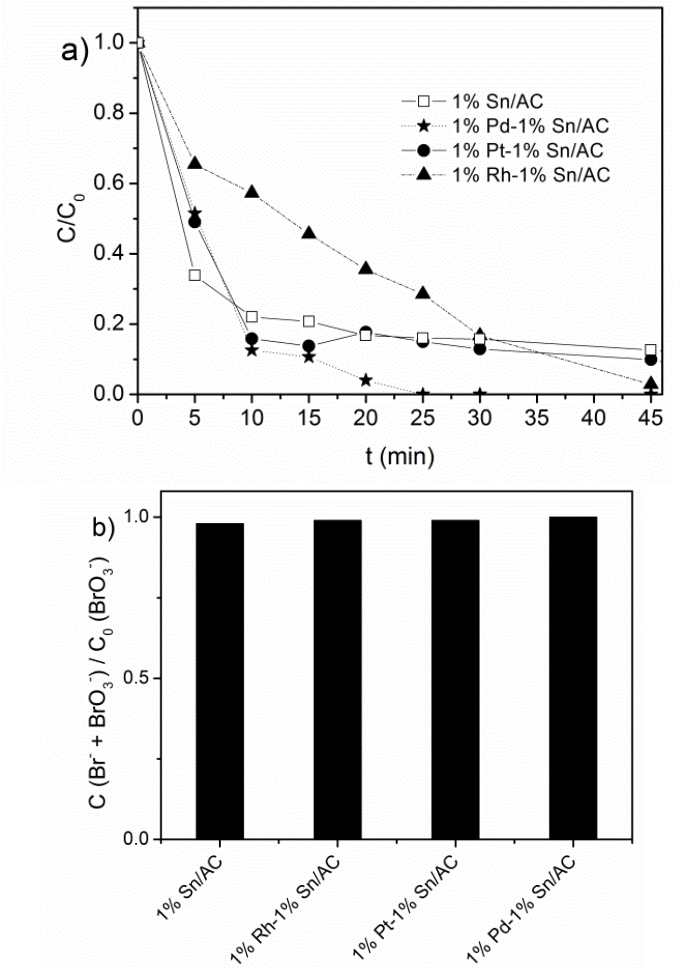

Figure 3.3 - Evolution of the dimensionless concentration of bromate (a) and total mass balance of bromine after 45 min (b) for reduction experiments using H_2 over bimetallic catalysts containing Sn, supported on activated carbon.

As can be seen in Figure 3.3, the Pd-Sn catalyst shows the best catalytic activity. Nevertheless, the performance of this catalyst is inferior to that observed with the pair Pd-Cu and also with the Pd monometallic catalyst (Figure 3.2).

3.2.2 PHYSICAL MIXTURES

Since the monometallic catalysts supported on activated carbon have shown good activities in the hydrogen reduction of bromate in water [1], it is necessary to compare the performance of the monometallic and bimetallic catalysts to understand if there is a synergic effect in the coupling of two different metals, or if the increase in the performance, when observed, is merely due to the higher metal loading available. Therefore, to understand why some bimetallic catalysts are outperformed by the monometallic catalysts, and also to evaluate if there is a synergic effect in the other cases, experiments were made using physical mixtures of monometallic catalysts supported on activated carbon. As already mentioned (Figures 3.1 to 3.3), the bimetallic catalyst does not always perform better than the monometallic catalyst. When other metals were coupled with Pd, only Cu managed to improve the removal of bromate from water. In a different case, the Rh-Sn pair was outperformed by both Sn and Rh monometallic catalysts [1]. Three different metal pairs (Pd-Cu, Ru-Ni and Pt-Sn) were selected for this study.

The SEM-EDS spectra obtained for the post-reaction recovered catalysts are presented in Figure 3.4. This analysis was made for recovered catalysts from the experiments using bimetallic catalysts and physical mixtures of monometallic catalysts. The observations shown here were compared with the SEM-EDS spectra obtained with fresh catalysts, as well as those for the corresponding monometallic catalysts [2].

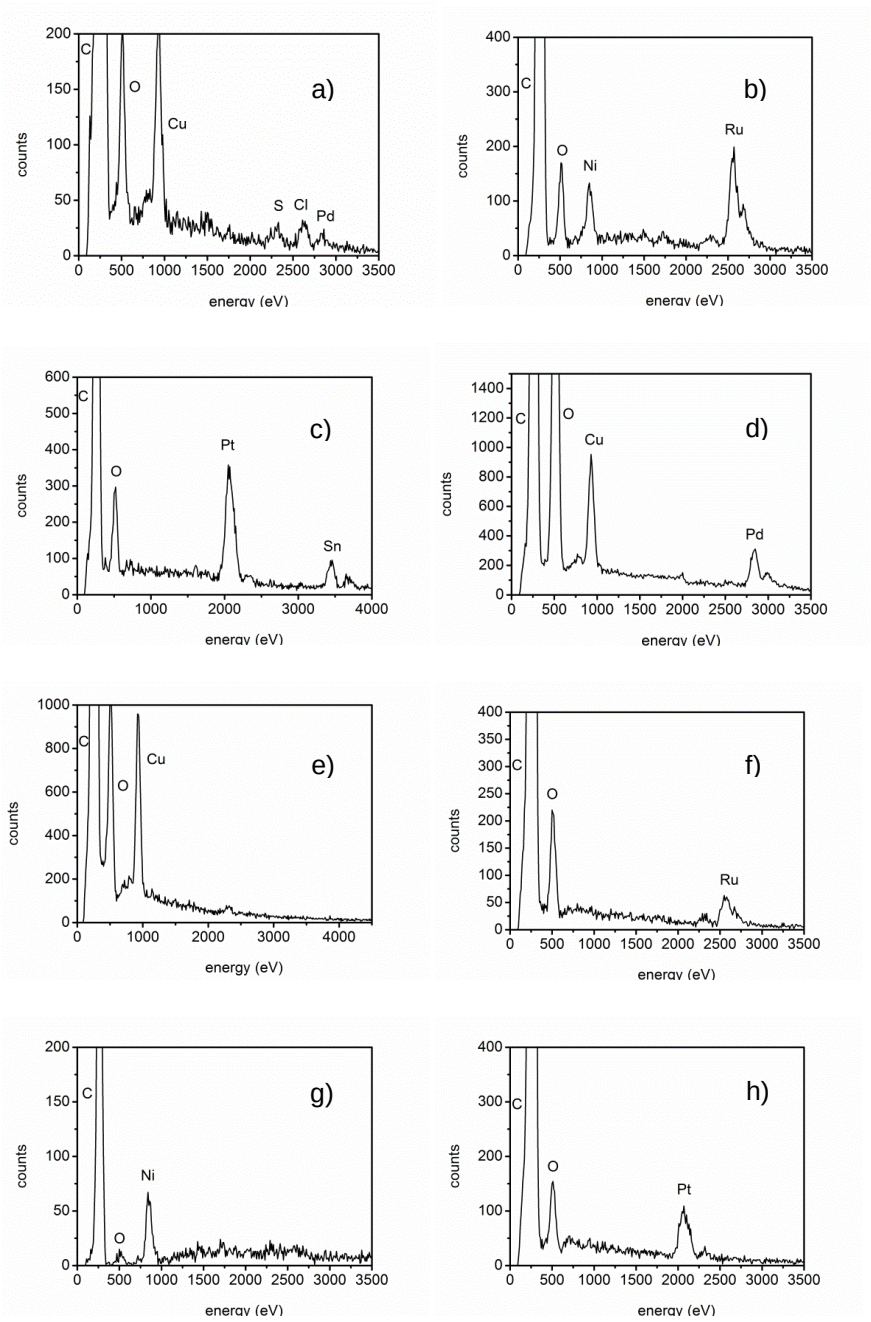
a)
C
O
Cu
S
Cl
Pd
counts
energy (eV)
b)
C
O
Ni
Ru
counts
energy (eV)
c)
C
O
Pt
Sn
counts
energy (eV)
d)
C
O
Cu
Pd
counts
energy (eV)
e)
C
O
Cu
counts
energy (eV)
f)
C
O
Ru
counts
energy (eV)
g)
C
Ni
O
counts
energy (eV)
h)
C
O
Pt
counts
energy (eV)

(cont.)

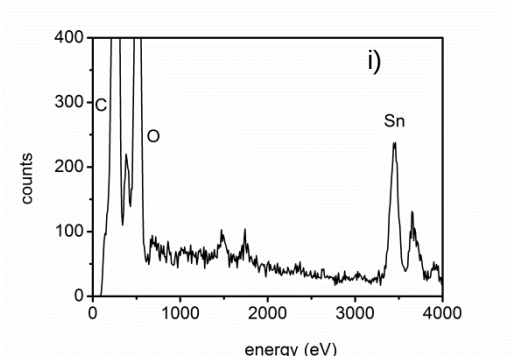

Figure 3.4 – EDS spectra of metallic particles found in the surface of the catalysts after reaction: a) 1% Pd - 1% Cu/AC; b) 1% Ru - 1%Ni/AC; c) 1%Pt - 1%Sn/AC; d) 1%Pd/AC + 1%Cu/AC; e) 1%Pd/AC + 1%Cu/AC (copper particle) f) 1%Ru/AC + 1%Ni/AC (ruthenium particle); g) 1%Ru/AC + 1%Ni/AC (nickel particle); h) 1%Pt/AC + 1%Sn/AC (platinum particle); i) 1%Pt/AC + 1%Sn/AC (tin particle).

It is observable from the EDS data in Figure 3.4 that, for the bimetallic catalysts, both metals were identified in close contact. This was observed for all the bimetallic catalysts tested: 1%Pd – 1%Cu/AC catalyst (Figure 3.4-a), the 1%Ru – 1%Ni/AC catalyst (Figure 3.4-b) and the 1%Pt-1%Sn/AC catalyst (Figure 3.4-c). Similar spectra were obtained for the fresh bimetallic catalysts, as reported elsewhere [2], This suggests that no changes, such as metal leaching or migration, occur during the bromate reduction reactions in the conditions used in the present work.

The EDS spectra of the recovered materials after bromate reduction experiments using physical mixtures of monometallic catalysts show that there was no leaching of the metallic phases which could lead to the in-situ formation of bimetallic particles, in the case of the 1%Ru/AC + 1%Ni/AC pair (Figures 3.4-f and 3.4-g) and the 1% 1%Pt/AC + 1%Sn/AC pair (Figures 3.4-h and 3.4-i) [2]; for each particle analysed on the AC support, only one metal was detected. The spectra obtained were similar to those of the fresh monometallic catalysts [2]. On the contrary, for the physical mixture of 1%Pd/AC and 1%Cu/AC, both metals were identified in the metal particles where Pd was observed on the surface of the

support (Figure 3.4-d). Only individual Cu particles were observed (Figure 3.4-e). This is due to the leaching of Cu, which has also been witnessed when similar experiments were carried out for the hydrogen reduction of nitrates in water [2]. In fact, the leaching of copper in similar supports has been observed by several authors, which leads to the conclusion that in the case of the Pd/Cu physical mixture, a bimetallic catalyst is formed in-situ under the reaction conditions used [2, 3].

In Figure 3.5 the bromate conversions obtained using the Pd and Cu system as monometallic catalysts, as a bimetallic catalyst and as a physical mixture of the two monometallic catalysts are compared.

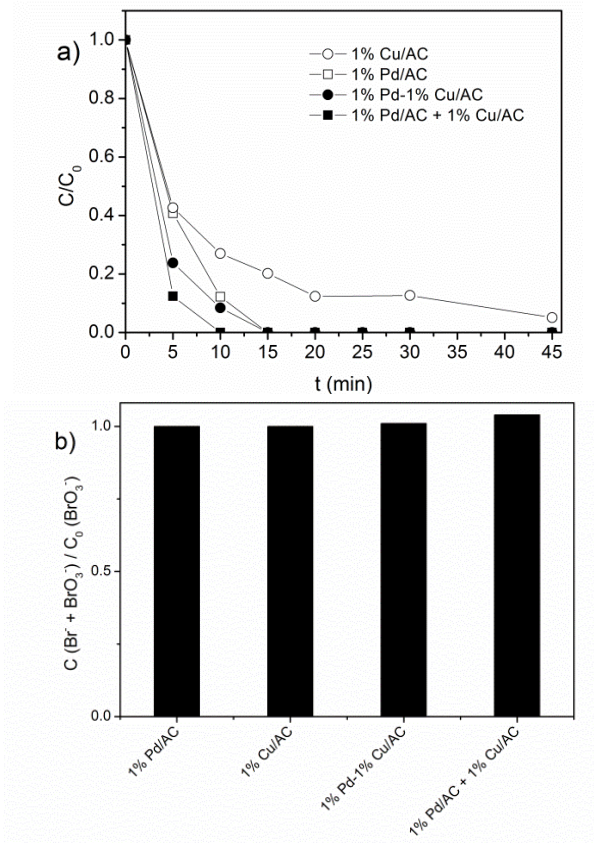

Figure 3.5 - Evolution of the dimensionless concentration of bromate (a) and total mass balance of bromine after 45 min (b) for reduction experiments using H_2 over the bimetallic Pd-Cu catalyst and physical mixture of the corresponding monometallic catalysts.

From Figure 3.5 it is possible to see that the bimetallic catalyst shows better performance than the corresponding monometallic catalysts, as was already stated. Most importantly, the physical mixture of Pd and Cu monometallic catalysts presents even higher performance in the bromate reduction than the bimetallic catalyst. This must be related with the disposition of the metals on the support. When a mixture of monometallic catalysts is used, all the metal active sites are accessible on the catalyst surface for the bromate reduction, whereas the same may not occur when bimetallic catalysts are used [2], since the most active metal could be covered by the other metal. In fact, during the hydrogen chemisorption analyses no H_2 chemisorption was observed on the Cu and Pd-Cu catalysts, as was expected since Cu does not chemisorb H_2 [4]. This may indicate that some interaction between the noble metal and Cu occurs, forming an alloy, and/or that Cu is covering most of the noble metal, which may result in a strong limitation in the amount of H_2 chemisorbed in the bimetallic catalyst. In addition, it has been reported [5] that the heat of adsorption during CO adsorption microcalorimetry experiments using a 1%Pd-0.3%Cu catalyst supported on an activated carbon (similar to that used in this work) decreases when compared to the Pd monometallic catalyst. This behavior was observed for catalysts heat treated at or above 200 ^{o}C, which was explained by the formation of alloys. Such observations have also been confirmed by XRD [6]. Thus, since the catalysts used in this study were heat treated at 200 ^{o}C, the different activities obtained in the experiments with the physical mixtures and bimetallic catalysts could be related with some alloy formation in the bimetallic catalyst leading to a decrease in the bromate reduction, which is known to involve the dissociation of hydrogen on the surface of the noble metal [1, 7]. SEM/EDS data show that the particles on the surface of the activated carbon contain both metals. This was observed for the bimetallic catalysts and for the physical mixtures of monometallic catalysts after reaction. Similar results were reported for the same type of catalysts when physical mixtures where used in the nitrate reduction [2], where the physical mixture of Pd and Cu catalysts performs equal or even better

than the corresponding bimetallic catalyst. Thus, it is possible to conclude that for the Pd-Cu pair, while there is an improvement in the bromate reduction when compared with the Pd monometallic catalyst, the activity of the bimetallic catalyst could be partially hindered by the interaction between the Cu and Pd on the surface of the activated carbon support. An additional experiment was made using homogeneous Cu^{2+} as catalyst, where an amount equal to that present on the corresponding activated carbon supported catalysts was used. Only a residual improvement of the performance was achieved when compared with the experiment only with H_2. Thus, the leaching of Cu into solution should not contribute significantly to the reduction of bromate in the case of the physical mixtures of monometallic Pd and Cu catalysts.

Figure 3.6 presents the results obtained with the monometallic Ru and Ni catalysts, the bimetallic Ru-Ni catalyst and the corresponding physical mixture of monometallic catalysts supported on activated carbon.

In the case of the Ru-Ni pair, the use of a Ru-Ni bimetallic catalyst decreases the system's overall catalytic performance when compared to the Ru monometallic catalyst. This phenomenon also occurs when a mixture of Ru and Ni monometallic catalysts is used. In fact, the physical mixture shows even less efficiency than the bimetallic catalyst. It has been reported that the coupling of Ru and Ni reduces the total adsorption capacity for CO in microcalorimetry experiments, approaching that of Ni alone, probably due to alloy formation [8]. So, the decrease in the bromate reduction when comparing the Ru monometallic catalyst with the Ru-Ni bimetallic catalyst must be related with the interaction of the two metals on the surface of the support, which agrees with what was observed in SEM-EDS analysis, since both metals are present in close contact. In addition, it is known that H_2 chemisorption on Ni is strong [9]. Thus, Ni might be competing with Ru for H_2 chemisorption. For nitrite reduction, it has been shown that strong absorption of H_2 results in lower catalytic activity, with Ni catalysts supported on activated carbon showing no activity [10]. Since, in the case of the bimetallic catalysts, Ni was found in close contact with

Ru, it is expected that this effect might be reduced when compared with the experiments with the physical mixtures, where individual Ni particles are present. It is worth mentioning that in the case of the monometallic Ni catalyst, and in the case of the experiment using a physical mixture with this catalyst, bromate was not completely removed from solution. However, the amount of bromate that was removed was due to conversion into bromide, and not due to adsorption on the activated carbon surface, even though the kinetics could suggest otherwise [1].

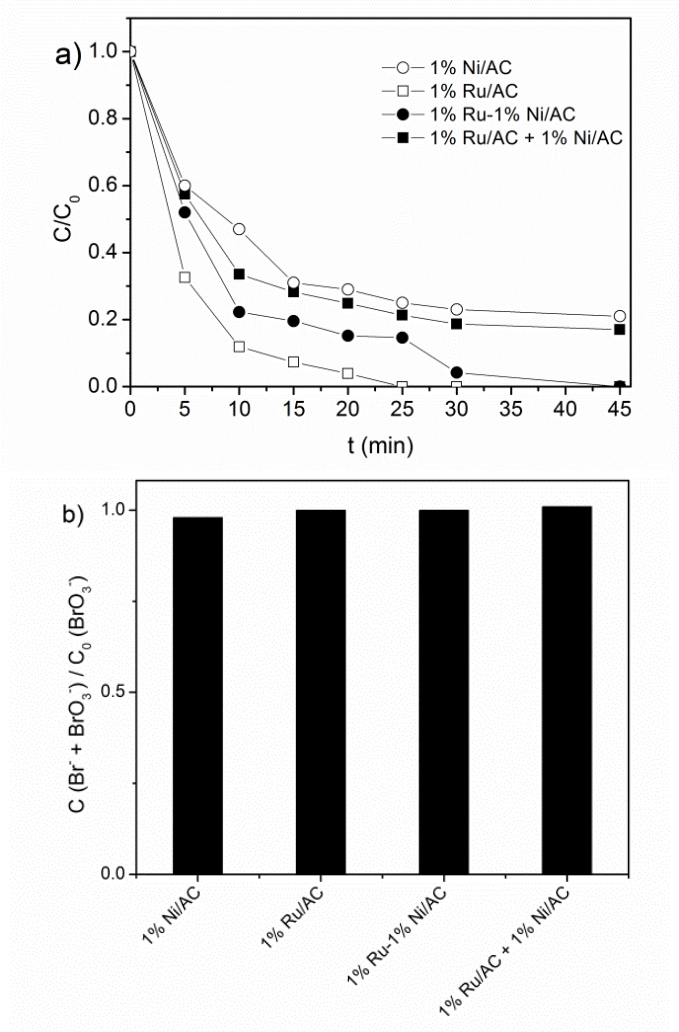

Figure 3.6 - Evolution of the dimensionless concentration of bromate (a) and total mass balance of bromine after 45 min (b) for reduction

experiments using H_2 over the bimetallic Ru-Ni catalyst and physical mixture of the corresponding monometallic catalysts.

Figure 3.7 presents the catalytic bromate reduction activity of supported mono and bimetallic, and the corresponding physical mixture of the Pt-Sn system.

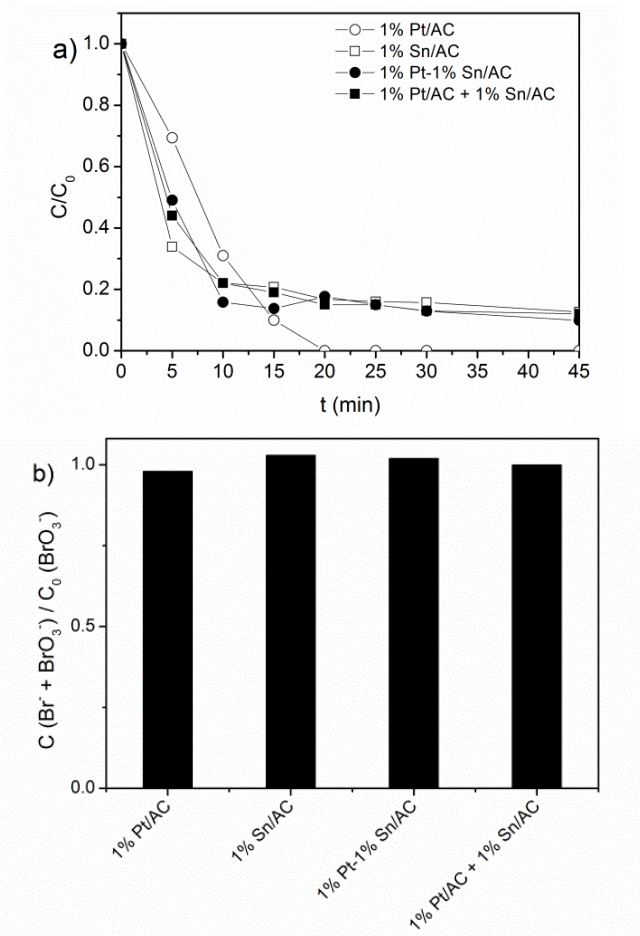

Figure 3.7 - Evolution of the dimensionless concentration of bromate (a) and total mass balance of bromine after 45 min (b) for reduction experiments using H_2 over the bimetallic Pt-Sn catalyst and physical mixture of the corresponding monometallic catalysts.

The monometallic Pt catalyst in Figure 3.7 shows better performance than the Sn monometallic catalyst, the bimetallic Pt-Sn catalyst and the

corresponding physical mixture. With the exception of the Pt monometallic catalyst, all the others show very similar efficiencies. The coupling of Pt with Sn in a bimetallic catalyst supported on alumina and prepared at low reduction temperatures has been observed to result in a loss of activity in the hydrogenation of crotonaldehyde, mostly due to the partial blocking of Pt active sites by Sn [11]. The same effect was observed for the conversion of isobutene when the Sn content was higher than 0.5% [12]. A similar reason can explain why the addition of Sn reduces the activity of Pt in our case. However, such phenomenon does not account for the loss of activity of the physical mixture of the monometallic catalysts. Metallic Sn is known to have no capacity for H_2 chemisorption [10] and no leaching of Sn to the Pt support was found by SEM-EDS, since both metals were isolated in the corresponding support particles. Thus, the presence of Sn likely hinders the process by competing with Pt for the adsorption of bromate. Additionally, in accordance with the proposed reaction mechanism [1], deactivation of the Sn monometallic catalyst for this reaction should be occurring, since this metal does not have the capability to chemisorb H_2, and thus is not able to return to the reduced state after reduction of bromate. When in close contact with Pt, as in the bimetallic catalyst, such a phenomenon should not take place, since Pt is able to dissociatively chemisorb H_2.

Taking in account the results obtained, only the Pd-Cu metal pair seems to have potential as efficient bimetallic catalyst. Therefore, different proportions of the pair Pd-Cu as a bimetallic catalyst were tested in the catalytic reduction of bromate, and the removals obtained after 10 minutes of reaction are depicted in Figure 3.8 as a function of the atomic percentage of copper. Since the removal of bromate was complete after 30 minutes of reaction for all the proportions, an intermediate stage of reaction was selected to allow the comparison between the catalysts.

The performance of the bimetallic Pd-Cu catalysts with different loadings of both metals can be arranged in the following order: 1% Pd-2% Cu > 1% Pd-1%Cu ≈ 1% Pd-0.6% Cu > 1%Pd ≈ 2% Pd-1%Cu > 1% Pd-0.3% Cu >

1% Pd-5% Cu ≈ 1% Pd-0.1% Cu. When considering the atomic compositions presented, it is clear that a fraction of Cu at least equal to 0.5 is needed to improve the performance of the bimetallic catalyst relatively to the monometallic palladium catalyst. However, a large atomic fraction was shown to actually hinder the reduction rate of bromate (see 1% Pd-5% Cu/AC).

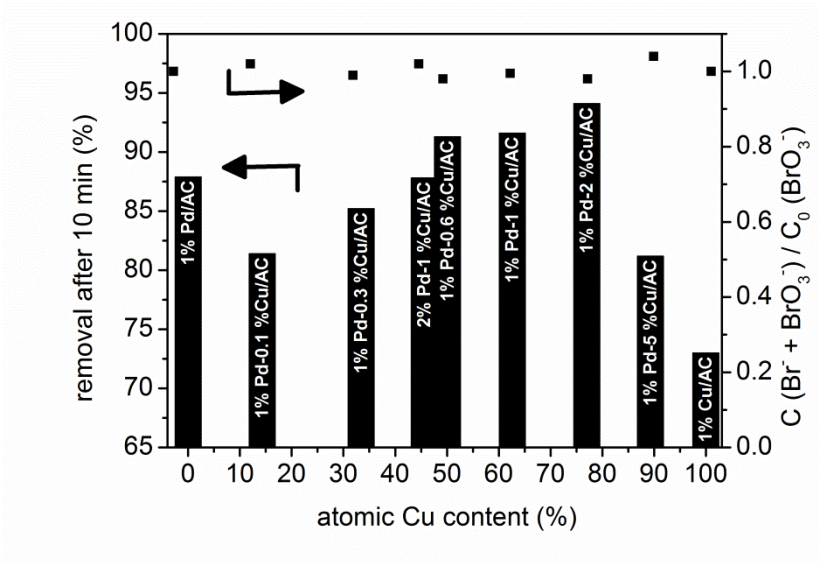

Figure 3.8 - Removal of bromate after 10 min during reduction experiments using H_2 over different bimetallic Pd-Cu catalysts vs. atomic copper content.

It has been suggested for the Pd-Cu bimetallic catalysts supported on activated carbon that the increase in the relative amount of the promoter metal decreases the availability of isolated noble metal particles [6]. Additionally, it has been observed than on a Pd-Cu catalyst, applied to the catalytic hydrogenation of nitrite, the Pd promotes the dissociation of H_2 to react with nitrite ions, while also reducing oxidized Cu, which is then able to participate in the reaction, thus increasing the reaction rate by providing two active centers for reaction [13]. In regard of the textural characterization of the catalysts, particularly the information relative to metal particle size, significant changes have not been detected [6, 14].

Therefore, the presence of the promoter metal increases the reactivity of the system on a certain range of atomic ratios; outside this interval the available noble metal surface necessary to interact with hydrogen and bromate ion decreases [5, 6]. It has been observed that the addition of Cu to supported Pd catalysts reduces the availability of high coordination sites for reaction [15]. The low coordination sites, which become more predominant on the Pd surface with the addition of Cu, are known to have higher activity in hydrogenation reactions [16, 17]. This behavior has been observed in the reduction of nitrates over Pd-Cu bimetallic catalysts, where the selectivity to the desired product (nitrogen) is hurt due to over hydrogenation [18]. In the case of bromate reduction, the conversion into bromide is always complete; so there is an improvement on the reaction rate when Cu is coupled with Pd. However, when the ratio of Cu to Pd is too high, the performance of the catalyst decreases, probably because the low coordination sites on the Pd surface become blocked by the added Cu.

The comparison of the performance of the bimetallic catalyst with different loadings (Figure 3.8) with the performance of the physical mixtures of the same pair (Figure 3.5) is useful to better understand the role of the bimetallic catalysts in the reduction of bromate in water using hydrogen. The performance of the physical mixture of the pair Pd-Cu is noticeably better than that of the corresponding bimetallic catalyst, regardless of the Pd/Cu ratio chosen (results not shown). It is also important to remark that the only case in which the physical mixtures show better catalytic activity than the corresponding bimetallic catalyst was for the Pd-Cu pair, which was also the only case in which the in-situ formation of bimetallic particles were observed for the physical mixture, under the reaction conditions used. It has been shown that for the remaining pairs tested, the addition of other metal did not improve the removal of bromate obtained with the noble metal monometallic catalyst. Thus, it seems that the utilization of a bimetallic catalyst is only beneficial for this reaction in specific cases. Accordingly, for the Pd-Cu pair, the addition of Cu as promoter metal to

the Pd catalyst improves the reaction rate due to interaction between the metals, when they are found in a specific range of atomic ratios; this was not observed for the remaining metal pairs studied.

3.3 PARTIAL CONCLUSIONS

Several bimetallic pairs supported on activated carbon were studied as catalysts for the hydrogen reduction of bromate in water. All the tested catalysts showed remarkable activity on the reduction of bromate under hydrogen. Furthermore, the conversion of bromate into bromide was observed to be complete for all the cases, without formation or accumulation of by-products in solution.

The Pd-Cu pair was shown to be the most promising catalyst, completely converting bromate in less than 10 minutes of reaction. Most of the other pairs resulted in reduced activity when compared to the corresponding monometallic noble metal catalysts.

Experiments using physical mixtures were carried out, and it was observed that the presence of a second metal, in most cases, can decrease the available surface of the noble metal for reaction, or can decrease the capacity of the most active metal to adsorb hydrogen. However, for the Pd-Cu pair, the experiment carried out using the corresponding physical mixture outperformed the bimetallic catalyst; nevertheless, during the physical mixtures experiments, in-situ formation of bimetallic catalyst was observed. This suggests that the interaction between the two metals improved the removal of bromate.

The influence of the composition in Pd-Cu catalysts was investigated, and it was shown that some improvement can be obtained regarding the reduction of bromate ion in water, when this pair was compared with the Pd monometallic catalyst. The improved performance of the Pd-Cu catalyst was observed to only occur in a specific range of atomic ratios.

REFERENCES

[1] J. Restivo, O.S.G.P. Soares, J.J.M. Órfão, M.F.R. Pereira, in press(2014) submitted.
[2] O.S.G.P. Soares, J.J.M. Órfão, M.F.R. Pereira, Applied Catalysis B: Environmental, 102 (2011) 424-432.
[3] L. Calvo, M.A. Gilarranz, J.A. Casas, A.F. Mohedano, J.J. Rodriguez, Industrial & engineering chemistry research, 49 (2010) 5603-5609.
[4] C. Crisafulli, S. Galvagno, R. Maggiore, S. Scirè, A. Saeli, Catalysis Letters, 6 (1990) 77-83.
[5] O.S.G.P. Soares, J.J.M. Órfão, J. Ruiz-Martínez, J. Silvestre-Albero, A. Sepúlveda-Escribano, M.F.R. Pereira, Chemical Engineering Journal, 165 (2010) 78-88.
[6] O.S.G.P. Soares, J.J.M. Órfão, M.F.R. Pereira, Applied Catalysis B: Environmental, 91 (2009) 441-448.
[7] H. Chen, Z. Xu, H. Wan, J. Zheng, D. Yin, S. Zheng, Applied Catalysis B: Environmental, 96 (2010) 307-313.
[8] M. Cerro-Alarcón, A. Maroto-Valiente, I. Rodríguez-Ramos, A. Guerrero-Ruiz, Applied Catalysis A: General, 275 (2004) 257-269.
[9] W. Yi, T. Kasuga, I. Mikami, Y. Kamiya, T. Okuhara, Chemistry Letters, 36 (2007) 994-995.
[10] O.S.G.P. Soares, J.J.M. Órfão, M.F.R. Pereira, Catalysis Letters, 126 (2008) 253-260.
[11] J.C. Serrano-Ruiz, G.W. Huber, M.A. Sánchez-Castillo, J.A. Dumesic, F. Rodríguez-Reinoso, A. Sepúlveda-Escribano, Journal of Catalysis, 241 (2006) 378-388.
[12] J.C. Serrano-Ruiz, A. Sepúlveda-Escribano, F. Rodríguez-Reinoso, Journal of Catalysis, 246 (2007) 158-165.
[13] W. Gao, J. Chen, X. Guan, R. Jin, F. Zhang, N. Guan, Catalysis Today, 93–95 (2004) 333-339.
[14] N. Barrabes, J. Just, A. Dafinov, F. Medina, J.L.G. Fierro, J.E. Sueiras, P. Salagre, Y. Cesteros, Applied Catalysis B: Environmental, 62 (2006) 77-85.
[15] F. Gauthard, F. Epron, J. Barbier, Journal of Catalysis, 220 (2003) 182-191.
[16] J.K. Chinthaginjala, A. Villa, D.S. Su, B.L. Mojet, L. Lefferts, Catalysis Today, 183 (2012) 119-123.
[17] Y. Yoshinaga, T. Akita, M. Ikko, O. Toshio, Journal of Catalysis, 207 (2002) 37-45.
[18] F. Epron, F. Gauthard, C. Pinéda, J. Barbier, Journal of Catalysis, 198 (2001) 309-318.

4. DIFFERENT SUPPORTS FOR METAL CATALYSTS

4.1 DESCRIPTION

In this chapter, the activity of four selected metallic catalysts (Pd, Pt, Rh and Ru) for the reduction of bromate in water was assessed using three different supports: activated carbon (AC), multiwalled carbon nanotubes (MWCNT) and titanium dioxide (TiO_2).

On a first approach, the activity of the bare supports was assessed, both under an inert atmosphere (nitrogen) and under a reducing agent (hydrogen). Secondly, the activity of the metallic catalysts supported on the different materials was evaluated. The activity was assessed taking into account the distribution of the metallic particles on the surface of the supports, and some considerations about the contribution of the support to the reduction of bromate were made.

The catalysts that were studied in this chapter were prepared in the Laboratory of Catalysis and Materials, by Dr. Salomé Soares in the context of her doctoral thesis, who kindly made them available for this study.

4.2 ACTIVITY OF THE SUPPORTS

The supports AC, MWCNT and TiO_2 were selected for this study because they presented very promising results for the reduction of nitrate in water under hydrogen [1], as well as for other hydrogenation reactions; the reduction using AC has been discussed previously in section *Metal assessment*, while several works on the use of TiO_2 [2-10] and MWCNT [1, 11-21] may be found in the literature. Figure 4.1 presents the observed bromate removal during experiments using the three different supports, both under hydrogen and under nitrogen.

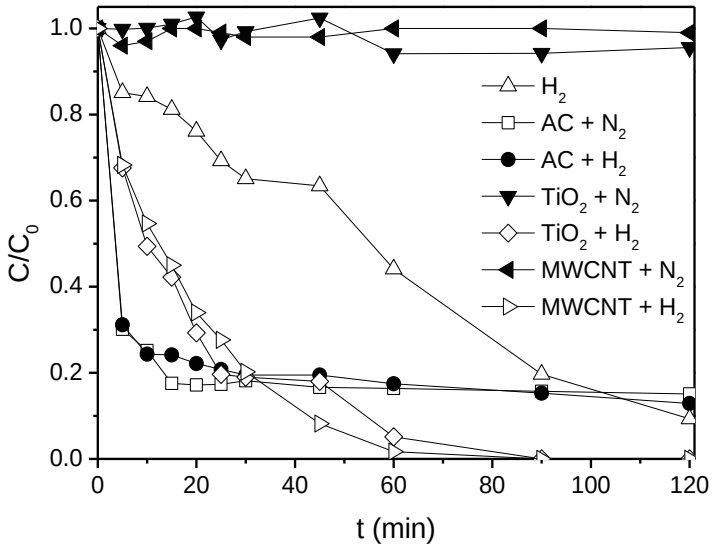

Figure 4.1 – Dimensionless concentration of bromate during experiments using the bare supports under hydrogen and under nitrogen.

Different behaviours were observed for the different supports. While the activated carbon extensively adsorbs bromate, as seen during the experiment using nitrogen, the same was not observed for TiO_2 or MWCNT. In these cases, the bromate concentration remained stable throughout the reaction when no hydrogen was present. However, when hydrogen was used, while in the case of AC the removal profile of bromate was similar to that observed for adsorption, using TiO_2 and MWCNT it was greatly improved. The mass balance of bromine at the end of the reaction, Figure 4.2, was performed in order to assess whether the bromates removal during the experiments using the bare supports corresponded to conversion to bromide in water, or whether it was due to adsorption on the surface of the different materials.

The activated carbon support has a different behaviour from the other two supports. In this case, adsorption plays an important role in the observed removal of bromate, whether hydrogen or nitrogen was used. In the case of MWCNT or TiO_2 no adsorption was observed. Furthermore, complete conversion of bromate into bromide was observed in the experiments under hydrogen, after 120 min. Thus, these two supports are observed to

be capable of reducing bromate on their own, under hydrogen. In fact, the application of monometallic titanium dioxide supported catalysts have been shown to be active in the reduction of nitrate, which typically requires a bimetallic catalyst system [9]. It has been speculated that the formation of Ti^{3+} centres by trapping of excess electrons might be responsible for the catalytic activity of the support [9]. On the other hand, the presence of electron enriched partially reduced species on the surface of the titanium dioxide, which may form during reduction of the support, may also contribute for the reduction of anionic species [1, 4, 22]. Adsorption of anionic species, necessary for the reduction of the bromate, may occur at acid sites through electrostatic interactions [9, 23].

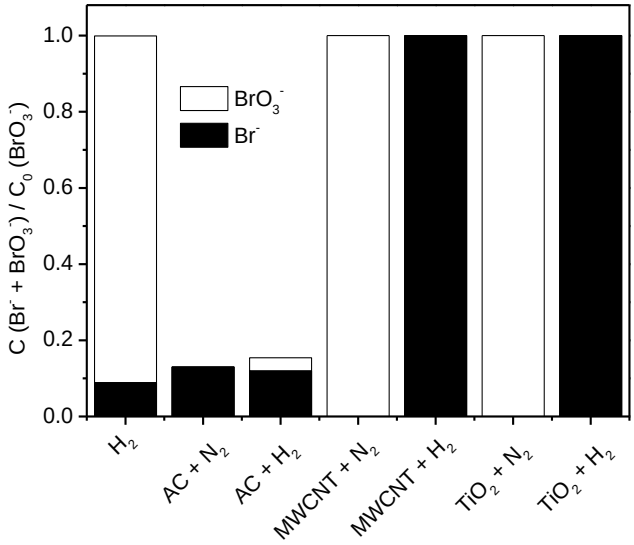

Figure 4.2 – Dimensionless concentration of bromate and bromide at the end of the experiments (120 min) using the bare supports under hydrogen and under nitrogen.

In the case of the MWCNT, the improved reduction of bromate when compared with the reaction with hydrogen alone is likely related to the electronic properties of the support material, which may be enhancing the reactions occurring between bromate and hydrogen.

4.3 METALLIC CATALYSTS ON DIFFERENT SUPPORTS

In order to compare the activity of the metallic catalysts supported on different materials, the most active metals were selected for this effect: Pt, Pd, Rh and Ru. On a first approach, the catalysts supported on AC, TiO_2 and MWCNT were tested in the reduction of bromate under hydrogen, using a 1 g L^{-1} catalyst loading (see section *Metal assessment*). The obtained removal profiles for the AC supported catalysts are presented in Figure 4.3.

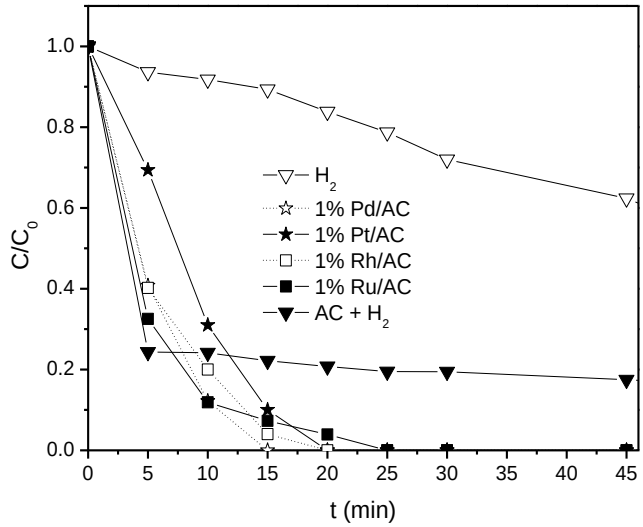

Figure 4.3 – Dimensionless concentration of bromate during experiments using the selected metallic catalysts supported on activated carbon.

As observed before, the addition of a metallic catalyst improves the reduction of bromate to bromide in the presence of AC; in fact, conversion to bromide is complete, while when only the support was used, there was no conversion observed (Figure 4.2). However, it was observed that when the metallic catalysts supported on MWCNT and on TiO_2 were used in these experiments, using the same catalyst loading as in the experiments with AC, the removal of bromate was too fast to be measureable. In between the introduction of the bromate solution onto the reactor, where the catalyst has been stirred under hydrogen, and the collection of the

initial sample (the process takes a few seconds), bromate was already completely converted into bromide. Thus, experiments were carried out using a smaller catalyst loading (0.25 g L^{-1}), to allow the comparison of the activity of the metallic catalysts.

The removal of bromate during experiments using the Pd catalysts supported on the different materials, with a catalyst loading of 0.25 g L^{-1}, is presented in Figure 4.4.

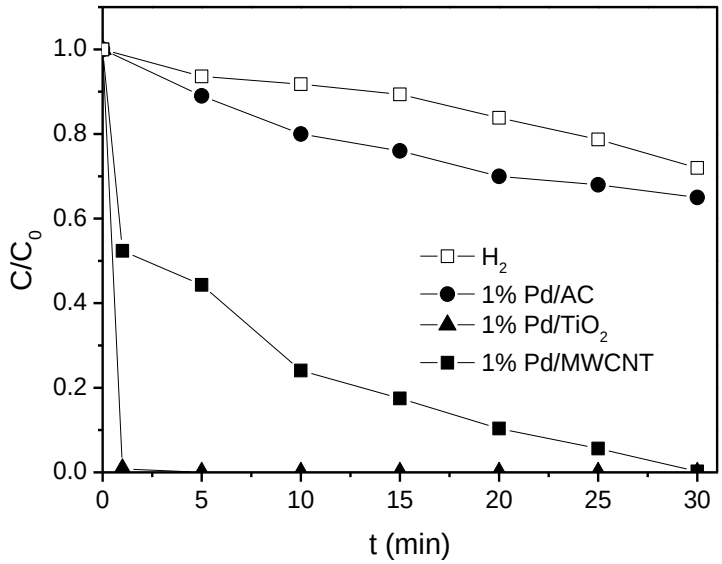

Figure 4.4 – Dimensionless concentration of bromate during experiments using the Pd metallic catalysts supported on the different materials.

The removal of bromate during experiments using the Pt catalysts supported on the different materials, with a catalyst loading of 0.25 g L^{-1}, is presented in Figure 4.5.

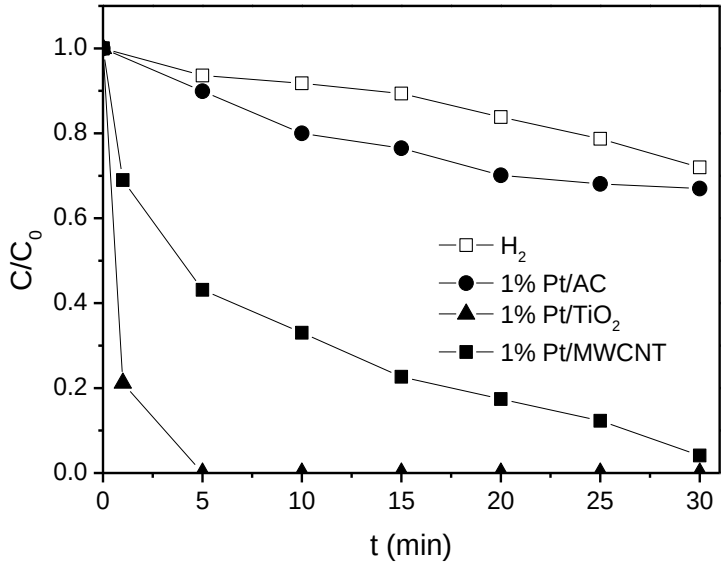

Figure 4.5 – Dimensionless concentration of bromate during experiments using the Pt metallic catalysts supported on the different materials.

The removal of bromate during experiments using the Ru catalysts supported on the different materials, with a catalyst loading of 0.25 g L^{-1}, is presented in Figure 4.6.

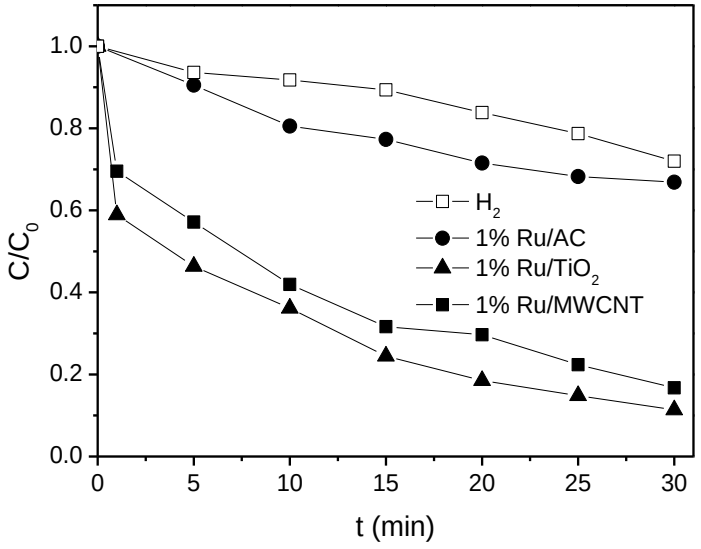

Figure 4.6 – Dimensionless concentration of bromate during experiments using the Ru metallic catalysts supported on the different materials.

The removal of bromate during experiments using the Rh catalysts supported on the different materials, with a catalyst loading of 0.25 g L^{-1}, is presented in Figure 4.7.

In all cases, the metal catalysts supported on MWCNT and TiO_2 showed a widely better performance in the removal of bromate from solution, when compared with those supported on activated carbon.

The titanium dioxide supports were observed to be the best performing catalysts. Since the surface area or the particle sizes do not seem to severely affect the activity of the catalysts, the chemical nature of the support must be the responsible for the increase in the activity observed [1, 24]. This high activity may be attributed to the electron transfer from the Ti^{3+} centres on the support lattice, otherwise inaccessible for reaction, either directly to the adsorbed anion or through the metallic particles [1, 9]. A strong metal-support interaction (SMSI) state could result in the transfer of the electrons to the metallic particles [3, 7, 9, 25, 26]. Such state has been observed when titanium dioxide was used as support for metallic catalysts [27], and changes in the temperatures of reduction observed by TPR on the different supports suggest that a SMSI state is achieved in the case of the titanium dioxide supported catalysts (see *Materials and methods*) [9, 10]. Furthermore, the presence of a metallic catalyst might increase the formation and stability of Lewis acid sites, where anionic species might adsorb through exchange with hydroxyl species, for future reduction [22, 28]. Nevertheless, presence of electron enriched surface species have been detected in metal loaded titanium dioxide supports, even at low reduction temperatures, which play a role in the reduction mechanism [5, 22, 29]. The use of titanium dioxide as support for the metallic phase facilitates the reduction to its metallic form, which is known to facilitate the reduction of nitrites. This reaction has a similar reduction mechanism using metallic catalysts under hydrogen as bromate [8, 30, 31].

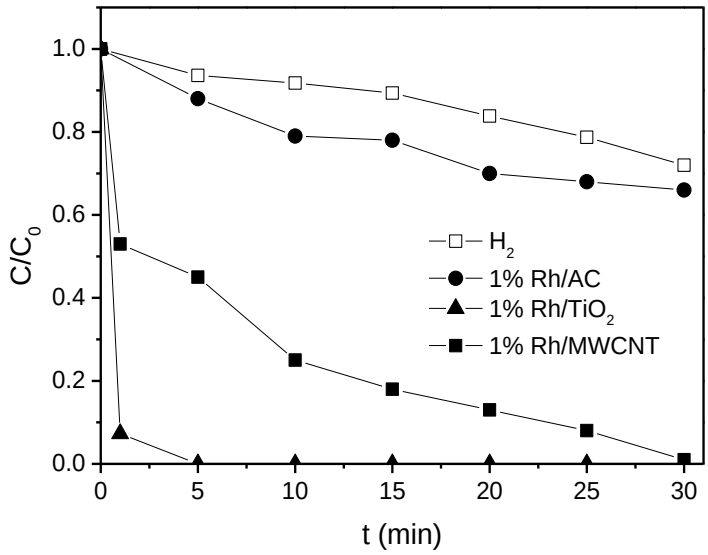

Figure 4.7 – Dimensionless concentration of bromate during experiments using the Rh metallic catalysts supported on the different materials.

Nevertheless, the MWCNT supported metal catalysts also showed remarkable activity when compared with the activated carbon support. The mesoporous nature of the MWCNT support might contribute to the increased activity by reducing diffusional limitations [32-38]. In addition, it has been suggested that despite contributions of the porosity and low tortuosity of CNF layers, the intrinsic activity of supported metallic catalysts on nanocarbon materials for the hydrogenation of nitrite is still higher than that observed in other carbon and alumina supports [15]. Thus, it is likely that, as what was observed for titanium dioxide, the physical and chemical properties of the material are positively influencing its performance in the reduction of bromate under hydrogen. Due to the size of the metallic particle, and due to low activity observed with AC in the hydrogenation of nitrite over supported metallic catalysts, it has been proposed that the influence of the support on the shape or the electronic structure of the metallic catalysts or any possible charge effects are not likely to occur [15]. It has been suggested that the adsorption of anionic compounds on the graphitic support, and reaction with spilled-over

hydrogen from the metallic particles, might be contributing to the increased activity of these catalysts [16, 33, 39-41].

In Figure 4.8 the dimensionless distribution of bromate and bromide after 30 min of reaction obtained during experiments under hydrogen using the selected metals supported on different materials is presented.

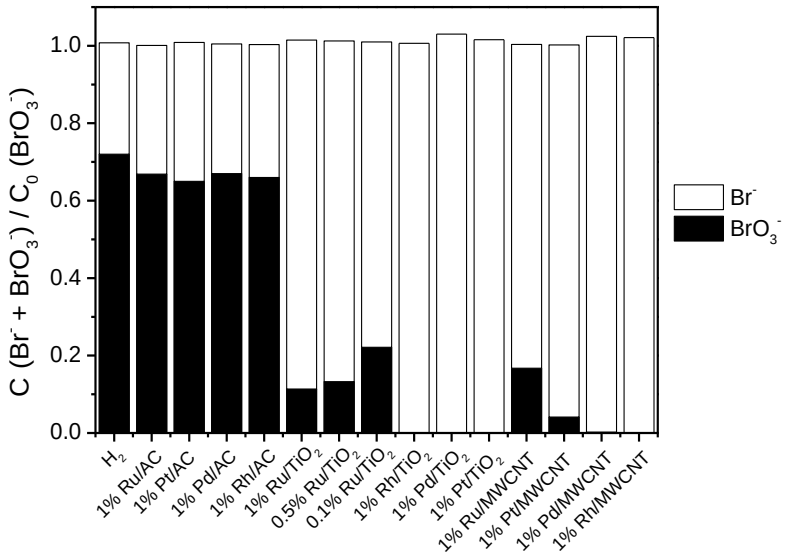

Figure 4.8 – Dimensionless concentration of bromate and bromide at the end of the experiments (30 min) using the metallic catalysts on different supports under hydrogen.

As was observed in section *Metal assessment*, the removal of bromate from solution corresponds to conversion to bromide, with no formation of intermediates detected, and with no contribution of adsorbed products.

Due to the high activity observed for the TiO_2 support, Ru supported catalysts were prepared using smaller metal loadings. This metal was selected, despite its lower activity, since it was the best suited for comparison of the activities, due to the very fast kinetics of the remaining catalysts. The dimensionless removal is presented in Figure 4.9.

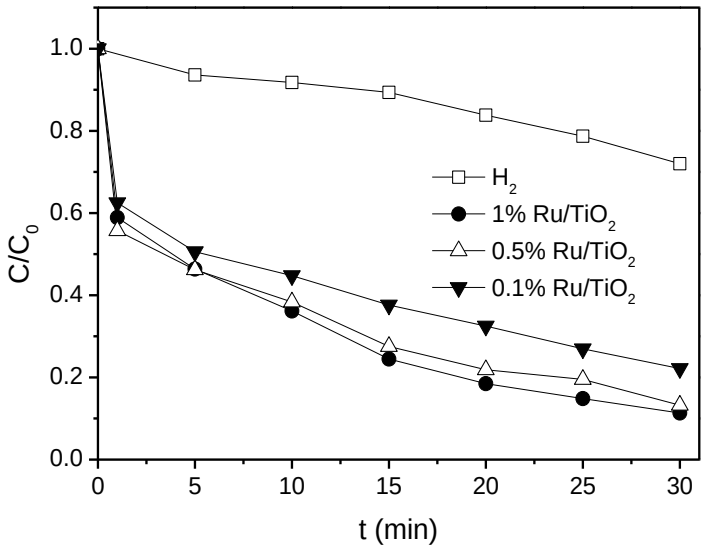

Figure 4.9 – Dimensionless concentration of bromate during experiments using the Ru metallic catalysts supported on titanium dioxide with varying metal loadings.

The smaller loadings of Ru used, while resulting in a slight decrease of the activity of the catalyst, still showed remarkable activity when compared with the AC supported counterpart.

In order to better assess the activity of the supported metals used, the turn-over frequencies (TOF) obtained for each catalysts were calculated as the rate of conversion of bromate per area unit of accessible metal surface [42]. The obtained TOF for the TiO_2 and MWCNT supported catalysts is present in Figure 4.10.

It is clear that the TiO_2 supported metallic catalysts achieved much higher values of TOF than the MWCNT counterparts. The influence of the support is more evident in the former. The Ru/TiO_2 catalyst, despite performing worse than its titanium dioxide supported counterparts (Figure 4.6), still achieves a comparable value of TOF. Since the mean particle size that was observed was larger than for the other metallic catalysts (*Materials and methods*), the available metal surface for reaction is

smaller. Its intrinsic activity was observed to be quite high, which was also observed when the AC and MWCNT supports were used.

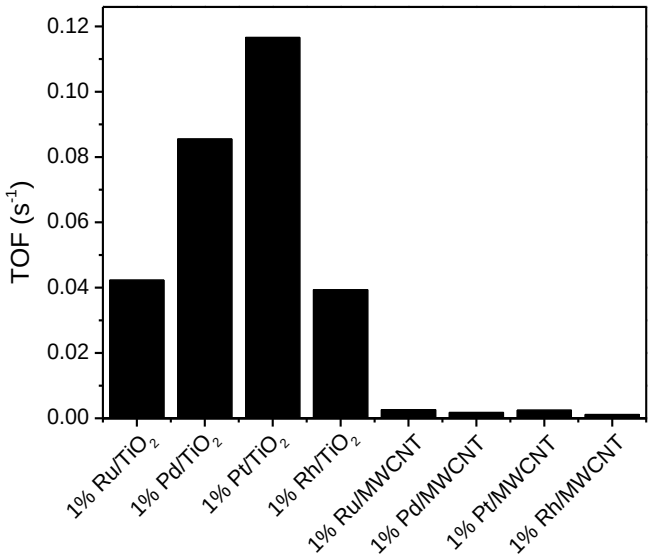

Figure 4.10 – Turn-over frequencies of bromate observed during experiments using catalysts supported on TiO_2 and MWCNT under hydrogen.

Nevertheless, regardless of the support used, Pt was observed to be the most efficient catalyst in the removal of bromate. However, if the available surface area of the metal for reaction is not considered, the Pd catalyst over performed when compared with the Pt catalyst.

Similarly, the TOF obtained during experiments performed using lower metal loadings of Ru on titanium dioxide are presented in Figure 4.11.

Since the mean particle size does not significantly change when the loading of Ru is decreased, and no significant changes in the interaction of the support and the metal are expected (section *Materials and methods*), the increase in TOF for lower metal loadings is an evidence for the important role the TiO_2 support plays in the reduction of bromate under hydrogen.

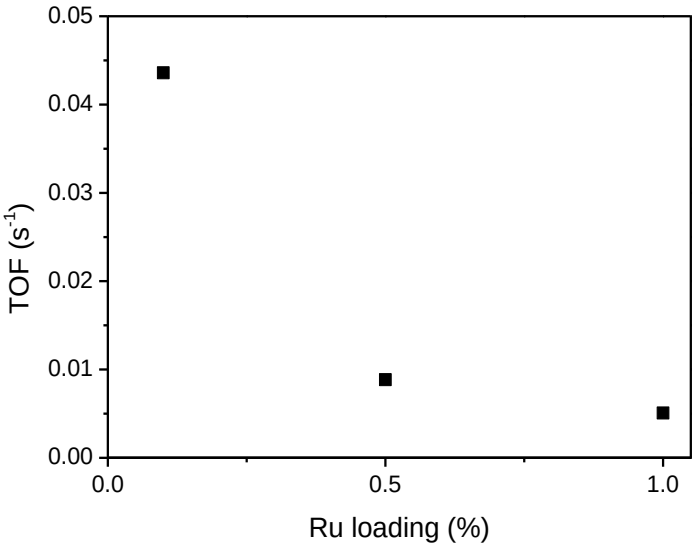

Figure 4.11 – Turn-over frequencies of bromate observed during experiments using Ru catalysts supported on TiO_2 with varying metal loadings under hydrogen.

4.4 PARTIAL CONCLUSIONS

Three different materials (activated carbon, titanium dioxide and multiwalled carbon nanotubes) were used as supports for four metallic catalysts (Pd, Pt, Rh and Ru) in the reduction of bromate under hydrogen in water. The activity of the bare supports was assessed, and it was observed that while activated carbon mostly contributed with adsorption of bromate, the other two supports were active in the reduction of bromate.

The activity of the supported metallic catalysts followed the trend TiO_2>MWCNT>AC. The activity of the support and the interaction of the support with the metallic catalyst were postulated to be responsible for the differences in activity.

The platinum catalysts were observed to be the most active catalysts for the removal of bromate, when the available surface area was considered. However, in terms of efficiency considering the mass of catalyst, the supported palladium catalysts were shown to be the most promising.

REFERENCES

[1] O.S.G.P. Soares, J.J.M. Órfão, M.F.R. Pereira, Desalination, 279 (2011) 367-374.
[2] Y.-n. Guo, J.-h. Cheng, Y.-y. Hu, D.-h. Li, Applied Catalysis B: Environmental, 125 (2012) 21-27.
[3] W.J. Kim, J.H. Kang, I.Y. Ahn, S.H. Moon, Applied Catalysis A: General, 268 (2004) 77-82.
[4] O.S.G.P. Soares, E.O. Jardim, Á. Reyes-Carmona, J. Ruiz-Martínez, J. Silvestre-Albero, E. Rodríguez-Castellón, J.J.M. Órfão, A. Sepúlveda-Escribano, M.F.R. Pereira, Journal of Colloid and Interface Science, 369 (2012) 294-301.
[5] H. Chen, Y. Shao, Z. Xu, H. Wan, Y. Wan, S. Zheng, D. Zhu, Applied Catalysis B: Environmental, 105 (2011) 255-262.
[6] W. Gao, J. Chen, X. Guan, R. Jin, F. Zhang, N. Guan, Catalysis Today, 93–95 (2004) 333-339.
[7] M.-S. Kim, S.-H. Chung, C.-J. Yoo, M.S. Lee, I.-H. Cho, D.-W. Lee, K.-Y. Lee, Applied Catalysis B: Environmental, 142–143 (2013) 354-361.
[8] J. Ruiz-Martínez, F. Coloma, A. Sepúlveda-Escribano, J.A. Anderson, F. Rodríguez-Reinoso, Catalysis Today, 133–135 (2008) 35-41.
[9] J. Sá, T. Berger, K. Föttinger, A. Riss, J.A. Anderson, H. Vinek, Journal of Catalysis, 234 (2005) 282.
[10] A.A. Wismeijer, A.P.G. Kieboom, H. Van Bekkum, Applied Catalysis, 25 (1986) 181-189.
[11] O.S.G.P. Soares, X. Fan, J.J.M. Órfão, A.A. Lapkin, M.F.R. Pereira, Industrial and Engineering Chemistry Research, 51 (2012) 4854-4860.
[12] O.S.G.P. Soares, J.J.M. Órfão, M.F.R. Pereira, Industrial and Engineering Chemistry Research, 49 (2010) 7183-7192.
[13] O.S.G.P. Soares, J.J.M. Órfo, E. Gallegos-Suarez, E. Castillejos, I. Rodríguez-Ramos, M.F.R. Pereira, Environmental Technology, 33 (2012) 2353-2358.
[14] H.C. Aran, S. Pacheco Benito, M.W.J. Luiten-Olieman, S. Er, M. Wessling, L. Lefferts, N.E. Benes, R.G.H. Lammertink, Journal of Membrane Science, 381 (2011) 244-250.
[15] J.K. Chinthaginjala, J.H. Bitter, L. Lefferts, Applied Catalysis A: General, 383 (2010) 24-32.
[16] J.K. Chinthaginjala, L. Lefferts, Applied Catalysis B: Environmental, 101 (2010) 144-149.
[17] Y. Marco, E. García-Bordejé, C. Franch, A.E. Palomares, T. Yuranova, L. Kiwi-Minsker, Chemical Engineering Journal, 230 (2013) 605-611.
[18] A.E. Palomares, C. Franch, T. Yuranova, L. Kiwi-Minsker, E. García-Bordeje, S. Derrouiche, Applied Catalysis B: Environmental, 146 (2014) 186-191.
[19] D.B. Thakur, R.M. Tiggelaar, J.G.E. Gardeniers, L. Lefferts, K. Seshan, Chemical Engineering Journal, 227 (2013) 128-136.

[20] D.B. Thakur, R.M. Tiggelaar, Y. Weber, J.G.E. Gardeniers, L. Lefferts, K. Seshan, Applied Catalysis B: Environmental, 102 (2011) 243-250.
[21] P. Yaseneva, C.F. Marti, E. Palomares, X. Fan, T. Morgan, P.S. Perez, M. Ronning, F. Huang, T. Yuranova, L. Kiwi-Minsker, Chemical Engineering Journal, 248 (2014) 230-241.
[22] J. Sá, J.A. Anderson, Applied Catalysis B: Environmental, 77 (2008) 409-417.
[23] F. Epron, F. Gauthard, J. Barbier, Journal of Catalysis, 206 (2002) 363-367.
[24] C.L. Constantinou, C.N. Costa, A.M. Efstathiou, Environmental Science & Technology, 41 (2007) 950-956.
[25] R. Green, P. Morrall, M. Bowker, Catalysis Letters, 98 (2004) 129-133.
[26] P. Weerachawanasak, P. Praserthdam, M. Arai, J. Panpranot, Journal of Molecular Catalysis A: Chemical, 279 (2008) 133-139.
[27] T.C. Chang, J.J. Chen, C.T. Yeh, Journal of Catalysis, 96 (1985) 51-57.
[28] W. Gao, N. Guan, J. Chen, X. Guan, R. Jin, H. Zeng, L. Zhiguang, F. Zhang, Applied Catalysis B: Environmental, 46 (2003) 341-351.
[29] O.S.G.P. Soares, E.O. Jardim, Á. Reyes-Carmona, J. Ruiz-Martínez, J. Silvestre-Albero, E. Rodríguez-Castellón, J.J.M. Órfão, A. Sepúlveda-Escribano, M.F.R. Pereira, Journal of Colloid and Interface Science, 369 (2012) 294-301.
[30] K. Wada, T. Hirata, S. Hosokawa, S. Iwamoto, M. Inoue, Catalysis Today, 185 (2012) 81-87.
[31] C.-B. Wang, H.-K. Lin, C.-M. Ho, Journal of Molecular Catalysis A: Chemical, 180 (2002) 285-291.
[32] T. Onoe, S. Iwamoto, M. Inoue, Catalysis Communications, 8 (2007) 701-706.
[33] L. Chen, A.C. Cooper, G.P. Pez, H. Cheng, The Journal of Physical Chemistry C, 111 (2007) 18995-19000.
[34] C. Pham-Huu, Journal of molecular catalysis. A, Chemical, 170 (2001) 155.
[35] J.-P. Tessonnier, L. Pesant, G. Ehret, M.J. Ledoux, C. Pham-Huu, Applied Catalysis A: General, 288 (2005) 203-210.
[36] H. Vu, F. Gonçalves, R. Philippe, E. Lamouroux, M. Corrias, Y. Kihn, D. Plee, P. Kalck, P. Serp, Journal of Catalysis, 240 (2006) 18-22.
[37] F. Qin, W. Shen, C. Wang, H. Xu, Catalysis Communications, 9 (2008) 2095-2098.
[38] C.-H. Li, Z.-X. Yu, K.-F. Yao, S.-f. Ji, J. Liang, Journal of Molecular Catalysis A: Chemical, 226 (2005) 101-105.
[39] S.D. Ebbesen, B.L. Mojet, L. Lefferts, Langmuir, 24 (2008) 869-879.
[40] A. Miyazaki, T. Asakawa, I. Balint, Applied Catalysis A: General, 363 (2009) 81-85.
[41] D.J. Browning, M.L. Gerrard, J.B. Lakeman, I.M. Mellor, R.J. Mortimer, M.C. Turpin, Nano Letters, 2 (2002) 201-205.
[42] J.L. Figueiredo, F.R. Ribeiro, Catálise Heterogénea, Calouste Gulbenkian.

5. STRUCTURED CATALYSTS

5.1 DESCRIPTION

In this chapter, several prepared structured catalysts were used in the continuous catalytic hydrogen reduction of bromate in water. Two types of structured catalysts were used, upon which the active metallic catalyst was deposited: CNT covered honeycomb cordierite monoliths and TiO_2 covered honeycomb cordierite monoliths. Their detailed preparation methods are described in section *Materials and methods*.

The performance of the structured catalysts was evaluated taking into account their characteristics, in order to understand how the efficiency of these catalysts may be improved. Recyling experiments were conducted with the most active catalyst in order to assess its stability in water.

5.2 CARBON BASED STRUCTURED CATALYSTS

The prepared carbon nanotubes (CNT) covered structured catalysts, which were used as support for palladium particles as described in the *Materials and methods* section, were used in the catalytic hydrogen reduction of bromate, under continuous operation, due to the high activity observed during experiments carried out using MWCNT as support for the metal phase. The experimental conditions employed are detailed in section *Materials and methods.*

The measured removals of bromate at steady state are presented in Figure 5.1.

At the applied operating conditions, it is clear that hydrogen by itself, with no catalyst present in the system, is not able to remove bromate from solution. The addition of the Pd/CNT structured catalysts was observed to drastically improve the achieved removal at steady state. The use of Pd supported on different carbon materials applied to the hydrogen reduction

of bromate removal has already been demonstrated, as seen in the previous sections [1-6]. In the system here presented, in which the Pd/CNT structured catalysts were used, removals of up to 91.9% were obtained.

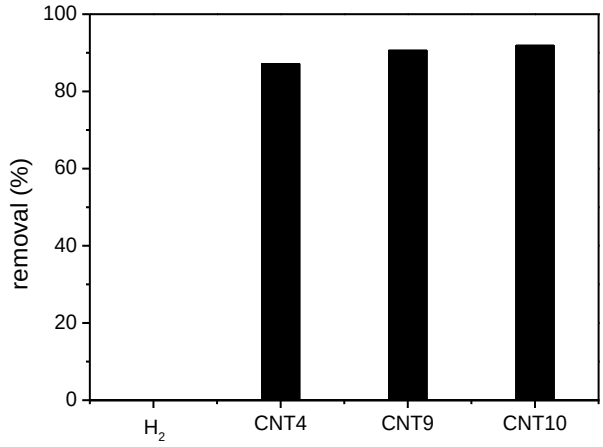

Figure 5.1- Removal of bromate during continuous catalytic hydrogen reduction using Pd supported on CNT covered honeycomb monoliths.

The removal of bromate was observed to correspond completely to conversion to bromide, as shown in Figure 5.2.

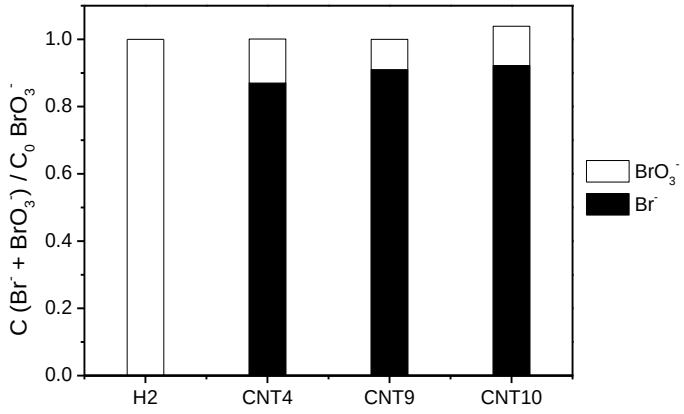

Figure 5.2- Dimensionless mass balance of bromine during continuous catalytic hydrogen reduction of bromate using Pd supported on CNT covered honeycomb monoliths.

Regarding the utilization of the different Pd/CNT structured catalysts, their performance in the catalytic reduction of bromate under hydrogen did not differ much between them. The range of measured removals was 87.2 to 91.9%. Nevertheless, since the CNT supports were all prepared using the same method, it is expected that the differences in removal are due to differences in the characteristics of the metallic phase. When the amount of palladium that was adsorbed by the monoliths during the deposition step is considered, the bromate converted at steady state increased with the amount of adsorbed Pd. The amount of dissolved Pd used to impregnate the CNT was calculated to achieve a 1%Pd/CNT wt.%. Since the mass of carbon in the different catalysts was similar, the amount of dissolved Pd did not greatly differ and did not affect the impregnation of the structured catalysts with different amounts of palladium. The Pd/CNT structured catalysts prepared using a mixture of NaCl and polyvinyl alcohol (PVA) as stabilizer/dispersant (CNT9 and CNT10) were observed to result on a more efficient catalyst. Moreover, when the deposition was carried out at pH 10, the adsorbed amount, and consequently the activity of the catalyst, was improved. The effect of pH is likely related with the promotion of the electrostatic interaction between the surface of the carbon and the metallic salts [7-9]. Nevertheless, the use of a stabilizer (PVA) was also shown to increase the amount of Pd impregnated onto the structured catalysts, likely due to linking with Pd at the surface of the carbon [10].

During the experiments performed using the structured catalysts prepared using PVA during the palladium impregnation, some leaching was visibly observed. Atomic absorption spectroscopy experiments, however, did not show any trace amount of palladium in solution. This is likely due to the visible deposition of the Pd on other components of the experimental set-up used, or due to the low concentrations that would be found in solution, considering the amounts of metal in the catalyst and the volume of solution used during the reaction. In order to assess how the leaching of palladium affected the performance of the catalysts, the CNT9 structured

catalyst was repeatedly used in consecutive experiments, between which it was rinsed with distilled water and dried, while the reaction system was thoroughly washed to remove any traces of deposited palladium that might be enhancing the conversion of bromate. The removals observed during these consecutive experiments are presented in Figure 5.3.

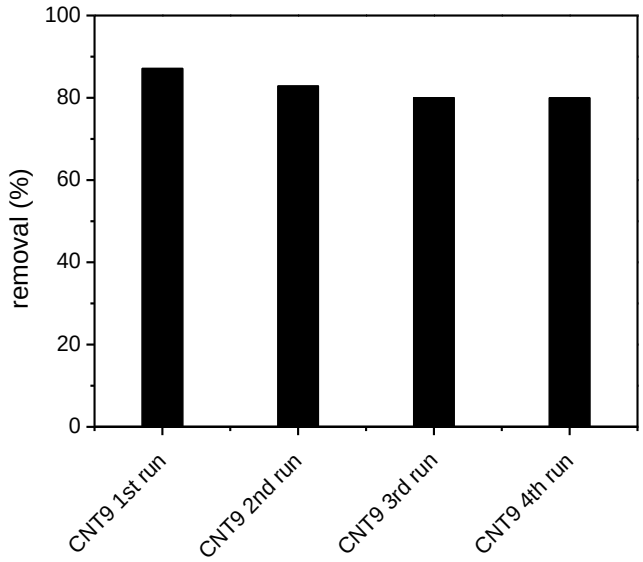

Figure 5.3- Removal of bromate during sequential continuous catalytic hydrogen reduction reusing a selected Pd/CNF supported catalyst.

While a slight loss of activity was detected after the first three runs, further reutilization of the CNT9 catalyst lead to similar removals of bromate, suggesting that no more leaching of Pd took place.

In summary, the activity of Pd/CNF structured catalysts was shown to be related with the palladium content on the surface of the carbon. Furthermore, the use of a stabilizer during the impregnation step was observed to increase the content of palladium, and consequently the performance of the catalyst. A similar effect was observed when basic pH was used during the impregnation step.

5.3 TITANIUM DIOXIDE BASED STRUCTURED CATALYSTS

Due to the remarkably high activity observed during the experiments using TiO_2 as support for metallic catalysts in power form for the hydrogen reduction of bromate, structured catalysts prepared using titanium dioxide and palladium supported on alumina washcoated honeycomb cordierite monoliths (section *Materials and methods,* where a detailed description of the preparation methods and characterization of the materials is included) were used in the continuous catalytic reduction of bromate. The experimental conditions employed are detailed in section *Materials and methods.*

The removal of bromate as measured at steady state during the experiments using Pd/TiO_2 structured catalysts is presented in Figure 5.4.

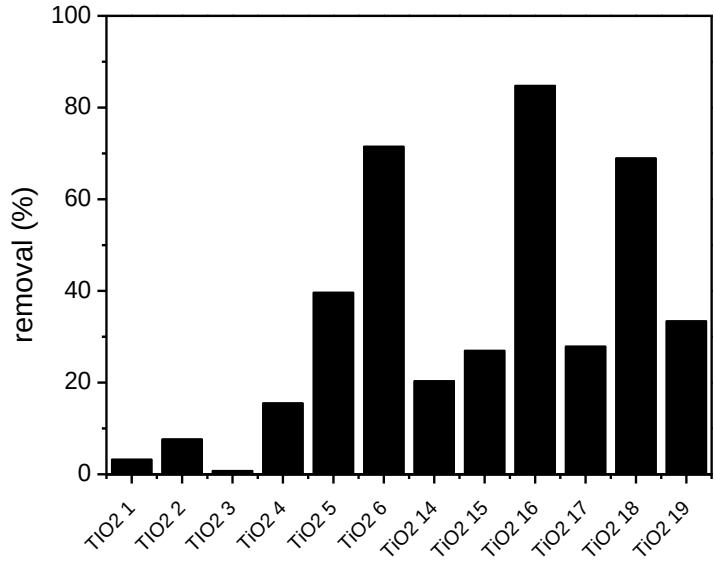

Figure 5.4- Removal of bromate during continuous catalytic hydrogen reduction using Pd supported on TiO_2 covered honeycomb monoliths.

It is clear that the addition of a Pd/TiO_2 structured catalyst increases the removal rate of bromate from water. In Figure 5.5 the mass balance of the bromine in the effluent at steady state is presented, where it is clearly seen that the removed bromate was completely converted into bromide.

Widely different activities for the different Pd/TiO_2 structured catalysts were observed. The activity of the catalysts here presented might be divided in three categories: below 20% (TiO2 1, TiO2 2, TiO2 3 and TiO2 4), between 20 and 40% (TiO2 5, TiO2 14, TiO2 15, TiO2 17 and TiO2 19), and finally above 40% (TiO2 6, TiO2 16 and TiO2 18).

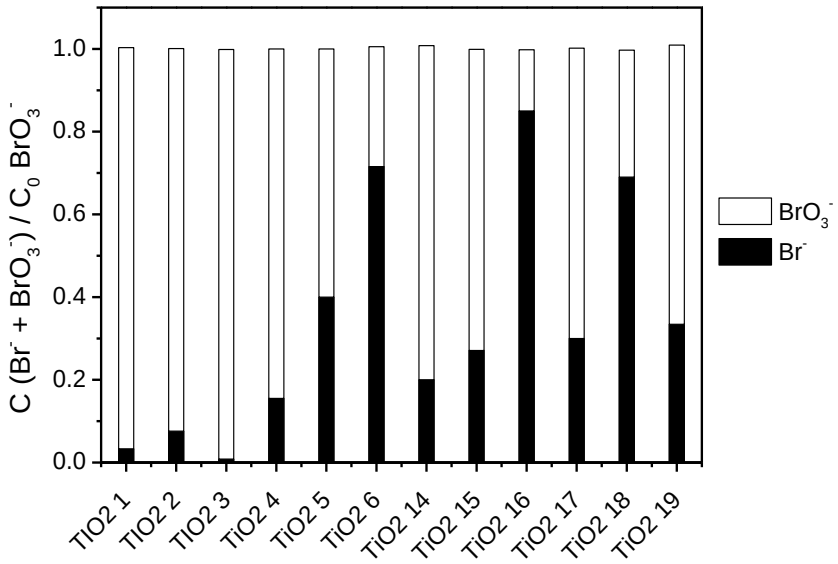

Figure 5.5- Dimensionless mass balance of bromine during continuous catalytic hydrogen reduction of bromate using Pd supported on TiO_2/Al_2O_3 covered honeycomb monoliths.

The first group of catalysts clearly has a much lower loading of palladium when compared with the remaining, even though the amount of palladium dissolved in the impregnation solution was similar for all the TiO_2 structured catalysts (2%Pd/TiO_2 wt.%, considering 100 mg of TiO_2), as seen in section *Materials and methods*. These four catalysts were prepared using a mixture of acetonitrile:water meant to help in the dissolution of the palladium precursor during the impregnation step [2]. However, this technique resulted in lower amounts of adsorbed Pd (section *Materials and methods)*, which contributed to the low removals observed. The complex formed by the reaction between the palladium precursor and acetonitrile likely reduced the impregnation of palladium on the structured catalyst. In fact, the catalyst TiO2 17 was prepared using

the same technique as TiO2 4 for the deposition of alumina and titanium dioxide. However, in this case, NaCl was used to help the dissolution of palladium in water, and a higher pH value was used. As expected, a higher loading of Pd on the catalyst was obtained (section *Materials and methods*), which corresponded to a higher removal.

Nevertheless, it was observed that TiO2 4, which was prepared with a previous alumina washcoat, followed by the deposition of titanium dioxide through dip coating on a ethanol suspension that also had alumina (nyacol) present to aid in the dispersion and stability of the suspension [11], presented the higher activity. However, it was observed that TiO2 3, which was prepared using a similar TiO_2/nyacol ethanol suspension, resulted in the lowest catalytic activity, which suggests that a previous washcoat with alumina improved the catalytic performance. In fact, SEM/EDS pictures presented in section *Materials and methods* suggested that a higher content of titanium dioxide was present on the surface of the catalyst in the case of TiO2 4, while in TiO2 3 either less TiO_2 was present, or it was covered by the alumina layer, which was deposited simultaneously with the titanium dioxide layer. In fact, TiO2 2, which was prepared without any alumina, with direct deposition of a titanium dioxide suspension by dip coating, was more active than TiO2 3, likely because all the titanium that was deposited on the cordierite surface was available for reaction.

TiO2 6 was prepared to assess the role of ethanol in the alumina/titania suspension; in this case, water was the only solvent used. The Pd impregnation technique was the same as in the case of TiO2 17. It was observed that a large increase in the removal of bromate from water was achieved, but the amounts of adsorbed palladium were similar in both cases, as seen in section *Materials and methods*. The SEM/EDS (*Materials and methods)* images suggest that TiO2 17 has much larger available amounts of titanium dioxide on the surface, which likely resulted on an enhancement of the removal of bromate.

The role of pH on the impregnation of palladium was assessed by comparison of TiO2 5 and TiO2 6, which followed the same preparation methods, except the palladium solution for impregnation had pH 3 in the former and pH 10 in the latter. While similar loadings of palladium were observed (section *Materials and methods*), widely different activities were obtained. The catalyst prepared with pH 10 removed 30% more bromate than its pH 3 counterpart. While SEM/EDS pictures are not conclusive, it is likely that either the acidic pH caused some changes to the catalytic surface during the impregnation step, or the Pd is distributed differently on the surface of the catalyst, in closer contact with the available titanium dioxide [9, 12-14].

A dispersant/stabilizer (PVA) was also used in the preparation of the Pd/TiO_2 catalysts. To assess its role, the catalyst TiO2 16 was prepared adding PVA to the Pd solution prior to impregnation. The catalyst TiO2 17 was prepared using the same technique as TiO2 16, at basic pH, except no PVA was used in the latter. It was observed that a much higher removal was obtained in the case using PVA, which was in fact the highest removal obtained using the titanium dioxide based structured catalysts, despite not achieving higher loadings of palladium when compared with the TiO2 17 catalyst with no PVA used in the impregnation step. However, it is also expected that the use of PVA might result on a finer dispersion of palladium, which is likely to affect the removal rate of bromate due to the higher available metallic area for reaction [10, 15].

Different results were obtained when TiO2 5 and TiO2 19, prepared at acidic pH, are compared: the first did not include PVA in the preparation methods, while the latter did. In this case, similar removals were obtained at steady state, with a slightly higher removal obtained for the catalyst without PVA. Thus, basic pH with PVA using water/NaCl suspension yielded the best results, while the addition of PVA to the impregnation solution at acidic conditions lead to worse performance when compared with the technique without PVA.

Finally, a different technique was used in the preparation of the monoliths which consisted in the use of a pre-prepared 1%/TiO_2 powder catalyst, which was then finely grounded by ball milling, put in a suspension and deposited onto the surface of the structured catalysts through dip coating (TiO2 14, TiO2 15 and TiO2 18). While TiO2 14 and TiO2 15 yielded poor results, even though the loading of Pd was much higher than the catalyst prepared by impregnation of Pd in solution upon the already TiO_2-containing catalysts, TiO2 18 reached considerably high bromate removals at steady state. In the preparation of TiO2 14 and TiO2 15, PVA and nyacol were used in the impregnation step to help achieve good dispersion of the catalyst particles in suspension, respectively. In TiO2 18, a combination of the two was used, in order to reduce the viscosity while maintaining load and adherence of the materials to the monolith. The differences in the behaviour seem to be related to where the catalyst particles were deposited, since on the TiO2 18 structured catalyst, these seem to be found on the alumina surface, while in the remaining two cases, the particles seem to be lodged inside pores in the alumina layer, as observed in SEM pictures in section *Materials and methods*, which may hinder the access of the reactants due to limitations to the diffusion. Capillary forces during the drying process may lead to the deposition of the particles in macropores, and the use of different binders may lead to configurations which may hinder or favour the reaction [9, 16, 17].

5.4 PARTIAL CONCLUSIONS

Several structured catalysts were prepared, using palladium as the active metallic phase, and using carbon nanotubes or titanium dioxide as the substrate for palladium support. These catalysts were applied to the continuous catalytic hydrogen reduction of bromate in water. It was found that, in the case of the CNT structured catalysts, the loading of Pd was directly related with the catalytic performance. In the case of the TiO_2 structured catalysts, while the Pd loading affected the performance of the catalyst, other factors were proposed to play a major role, such as the

relation of the dispersed Pd with the TiO_2 on the surface of the catalyst, the dispersion of Pd and the availability of the active phases for reaction.

REFERENCES

[1] Y. Marco, E. García-Bordejé, C. Franch, A.E. Palomares, T. Yuranova, L. Kiwi-Minsker, Chemical Engineering Journal, 230 (2013) 605-611.
[2] A.E. Palomares, C. Franch, T. Yuranova, L. Kiwi-Minsker, E. García-Bordeje, S. Derrouiche, Applied Catalysis B: Environmental, 146 (2014) 186-191.
[3] D.B. Thakur, R.M. Tiggelaar, Y. Weber, J.G.E. Gardeniers, L. Lefferts, K. Seshan, Applied Catalysis B: Environmental, 102 (2011) 243-250.
[4] P. Yaseneva, C.F. Marti, E. Palomares, X. Fan, T. Morgan, P.S. Perez, M. Ronning, F. Huang, T. Yuranova, L. Kiwi-Minsker, Chemical Engineering Journal, 248 (2014) 230-241.
[5] T. Yuranova, L. Kiwi-Minsker, C. Franch, A.E. Palomares, S. Armenise, E. García-Bordejé, Industrial & engineering chemistry research, 52 (2013) 13930-13937.
[6] P. Zhang, F. Jiang, H. Chen, Chemical Engineering Journal, 234 (2013) 195-202.
[7] S. Morales-Torres, A.F. Pérez-Cadenas, F. Kapteijn, F. Carrasco-Marín, F.J. Maldonado-Hódar, J.A. Moulijn, Applied Catalysis B: Environmental, 89 (2009) 411-419.
[8] A.F. Pérez-Cadenas, F. Kapteijn, J.A. Moulijn, F.J. Maldonado-Hódar, F. Carrasco-Marín, C. Moreno-Castilla, Carbon, 44 (2006) 2463-2468.
[9] P. Avila, M. Montes, E.E. Miró, Chemical Engineering Journal, 109 (2005) 11-36.
[10] Z. Csuros, A. Lengyel, Periodia polytechnica - Chemical engineering, 18 (1974) 155-165.
[11] B.P. Barbero, L. Costa-Almeida, O. Sanz, M.R. Morales, L.E. Cadus, M. Montes, Chemical Engineering Journal, 139 (2008) 430-435.
[12] C. Perego, P. Villa, Catalysis Today, 34 (1997) 281-305.
[13] M. Komiyama, Catalysis Reviews Science and Engineering, 27 (1985) 341-372.
[14] W.A. Spieker, J.R. Regalbuto, Chemical Engineering Science, 56 (2001) 3491-3504.
[15] J.K. Chinthaginjala, A. Villa, D.S. Su, B.L. Mojet, L. Lefferts, Catalysis Today, 183 (2012) 119-123.
[16] T.A. Nijhuis, A.E. Beers, T. Vergunst, I. Hoek, F. Kapteijn, J.A. Moulijn, Catalysis Reviews, 43 (2001) 345-380.
[17] A.V. Boix, E.E. Miró, E.A. Lombardo, R. Mariscal, J.L.G. Fierro, Applied Catalysis A: General, 276 (2004) 197-205.

Part IV

Conclusions

CONCLUSIONS

In general, structured catalysts were developed and applied to the continuous catalytic ozonation of emerging organic pollutants and to the continuous catalytic reduction of bromate. Promising results were obtained regarding their application in real cases, and some progress was made in the understanding of the related fundamental science.

Several different structured catalysts were tested for the ozonation of organic pollutants, and compared with other conventional carbon-based catalysts used in powder form. On a first approach, the structured catalysts were ground to controlled particle size, when possible, and used in ozonation reactions carried out in a semi-batch stirred tank reactor. Afterwards, the structured catalysts, in their integral form, were used in experiments carried out in a bubble column reactor with a closed internal loop, in semi-batch operation and two-phase configuration. Later, the structured catalysts were used in the continuous catalytic ozonation reaction, using the same bubble column reactor with an internal loop, in two-phase configuration. It was found that the structured catalysts showed activity comparable to that of activated carbon and multiwalled carbon nanotubes, even outperforming these in some situations. Finally, the structured catalysts were then used in a three-phase system, to take advantage of the possibility of development of hydrodynamic regimes that enhance the mass transfer between the gas, liquid and solid phases. It was found that structured of the type carbon felts (CF) and sintered metal fibers (SMF) did not perform well in this configuration, due to high pressure drop and consequent coagulation of the gas on the bottom of the catalysts, which eventually lead to bypass of the gas-phase through the sides of the catalyst.

The ozonation of three selected emerging organic pollutants was studied in detail. In general, it was observed that while single ozonation was sufficient to remove readily the parent pollutants from water, their

mineralization was not fully achieved. The application of carbon based catalysts was shown to improve mineralization, by promotion of the reactions involving radical species, taking place on the surface of the catalyst and in the solution bulk. Moreover, it was observed that the application of a catalyst has a wide impact in the distribution of the accumulated products in solution, mostly due to this promoting effect, which alters the pathway of degradation of the organic pollutants. Furthermore, the variation of the experimental conditions was observed to modify the predominant pathways taking place, and also the adsorption of the pollutants on the surface of the catalysts. The larger mineralization degree and the changes in the product distribution eventually led to changes in the toxicity of the effluents. Finally, it was also shown that the continuous ozonation process applied using a structured honeycomb monolith as a support for the carbon active phase is viable, mainly due to the improvement of the mineralization degree when compared with the conventional ozonation process.

The influence of various operation parameters was evaluated in the catalytic ozonation of organic pollutants. Initially, the hydraulic features of the experimental setup were characterized. The detailed behaviour of the hydraulic regime developed inside the monolith channels was then also characterized through application of the equations found in the literature. Afterwards, the corresponding parameters were related to the performance of the catalysts in the ozonation of organic pollutants. After showing that the application of a three-phase system was advantageous, it was found that the relative size of the bubbles and the monolith channels are important, since they affect the distribution of the gas-phase inside the monolith, as well as its contact with the catalytic wall. Furthermore, the efficiency of the process was suggested to be dependent, under our operating conditions, on the transfer of the organic pollutants from the solution to the channel walls, where a major part of the degradation reaction of the pollutants is taking place. This factor seems to be strongly related to the length of the slugs inside the monolith channels,

which is, on the other hand, linked with the liquid flow rate used. Another factor which seems to be important is the relation of the velocities of the slugs and bubbles inside the channels; however, since there is already a high concentration of ozone in the liquid phase inside the monolith, it was suggested that this phenomenon might not be as important in this case. In addition, the effect of several components of natural waters in the process was evaluated, as well as the influence of the carbon loading on the structured catalysts. It was found that, despite showing an influence in the process, the use of natural water matrices does not hinder significantly the efficiency of the catalytic ozonation process. It was observed that its influence varies when different pollutants are used. The increase in the loading of carbon on the structured catalysts was shown to enhance the performance of the system, up to a certain point, since a CNF layer that is too thick will decrease the accessibility of the reactants to the layers closer to the support.

The influence of surface heteroatoms on the activity of carbon materials in the catalytic ozonation of organic pollutants was evaluated. For this purpose, carbon nanotubes (MWCNT) that were subject to doping with several different elements were used as catalysts. The introduction of these elements lead to the formation of oxygen-containing, sulphur-containing and nitrogen-containing functionalities, which lead to materials with different surface acidities and electronic densities. To evaluate the catalytic activity of the materials, oxalic acid was used as a model compound. It was observed that the most active materials were those that presented a more basic character, with the N-containing MWCNT sample being the most active. Afterwards, the same materials were tested in the ozonation of phenol. In this case, the modifications of the MWCNT surface did not lead to improved mineralization of phenol, but rather to changes in the distribution of the products accumulated in solution. After experiments with MWCNT, the same procedure was used to evaluate the influence of N-doping on carbon nanofibers (CNF). Similar observations were made during ozonation of oxalic acid and phenol. The activity of the CNF was

similar to that of MWCNT, with the N-containing sample proving to be the most active sample. On a next step, the doping of CNF with nitrogen was evaluated in the continuous ozonation of organic pollutants using structured catalysts, consisting on honeycomb cordierite monoliths covered with CNF. These materials were tested using oxalic acid as a model compound, but also three different emerging organic pollutants. It was observed that the N-CNF catalyst performed better than the CNF catalyst, when the mass of CNF on the structure was considered. Finally, the influence of the amount and type of nitrogen functionality on the catalytic activity of carbon materials in the ozonation process was assessed. For this, different carbon xerogels were used due to the vast array of varying amounts and types of N-containing functionalities that can be introduced. It was possible to positively correlate the amount of nitrogen with the activity of the materials, using oxalic acid as a model compound. However, attempts to correlate the activity with specific types of functionalities were not successful.

The deactivation of pristine and modified multiwalled carbon nanotubes was assessed in the catalytic ozonation of oxalic acid. It was found that, independently of the treatment applied to the catalyst, the introduction of acidic oxygen-containing surface groups lead to a loss of activity. Nevertheless, further reutilization suggested that the amount of O-containing groups reaches a plateau, after which the catalysts show stable activity. It was also observed that, although there is a loss of S-containing functionalities when S-doped MWCNT samples were studied, the nature of these groups did not change during the reaction; besides, the loss of activity of the catalyst did not seem to be related to this phenomenon. In the case of the N-doped MWCNT and CNF, it was observed that the N-containing surface groups suffer some changes during the ozonation procedure, mostly related to the decrease of the amount of pyridinic groups.

Furthermore, structured catalysts consisting of CNF covered honeycomb monoliths were used in long term continuous ozonation experiments. It

was observed that, after an initial period of deactivation, the catalyst were stable in the reaction, maintaining a constant removal of oxalic acid throughout the experiments. The loss of activity was shown to be related to the introduction of acidic O-containing surface functionalities through reaction with ozone.

Several different metals supported on activated carbon were tested in the catalytic reduction of bromate under hydrogen. Noble metal catalysts (Pd, Pt, Ru, Rh) supported on activated carbon efficiently catalyze the conversion of bromate into bromide ion under hydrogen at room temperature and pressure. An extensive adsorption on activated carbon was observed when no hydrogen was present in the system. However, complete conversion into bromide was obtained only when a metal catalyst was present. Among the several catalysts tested, the palladium catalyst was shown to be the most efficient in terms of bromate conversion. However, when the available metal surface for reaction is considered, it was clear that platinum has the highest intrinsic activity. A simplified mechanism for the reduction of bromate was proposed, which takes into account reactions in the liquid phase, on the surface of the support, and on the surface of the supported metal particles. The roles of the metal and of the reducing agent were assessed, and it was proposed that the reaction mechanism on the surface of the metal comprised the dissociative adsorption of hydrogen and subsequent reaction with adsorbed bromate. This results in the release of bromide ion and water. The oxidized metal is then reduced by hydrogen, thus being available for further interaction with bromate and hydrogen.

Several bimetallic pairs supported on activated carbon were studied as catalysts for the hydrogen reduction of bromate in water. All the tested catalysts showed remarkable activity on the reduction of bromate under hydrogen. Furthermore, the conversion of bromate into bromide was observed to be complete for all the cases, without formation or accumulation of by-products in solution. The Pd-Cu pair was shown to be the most promising catalyst, completely converting bromate in less than

10 minutes of reaction. Most of the other pairs resulted in reduced activity when compared to the corresponding monometallic noble metal catalysts. Experiments using physical mixtures were carried out, and it was observed that the presence of a second metal, in most cases, can decrease the available surface of the noble metal for reaction, or can decrease the capacity of the most active metal to adsorb hydrogen. However, for the Pd-Cu pair, the experiment carried out using the corresponding physical mixture outperformed the bimetallic catalyst; nevertheless, during the physical mixtures experiments, in-situ formation of bimetallic catalyst was observed. This suggests that the interaction between the two metals improved the removal of bromate. The influence of the composition in Pd-Cu catalysts was investigated, and it was shown that some improvement can be obtained, in a specific range of atomic ratios, regarding the reduction of bromate ion in water, when this pair was compared with the Pd monometallic catalyst.

Three different supports (activated carbon, titanium dioxide and multiwalled carbon nanotubes) were used as supports for four metallic catalysts (Pd, Pt, Rh and Ru) in the reduction of bromate under hydrogen in water. The activity of the bare supports was assessed, and it was observed that while activated carbon mostly contributed with adsorption of bromate, the other two supports were active in the reduction of bromate. The activity of the supported metallic catalysts followed the trend TiO_2>MWCNT>AC. The activity of the support and the interaction of the support with the metallic phase were postulated to be responsible for the differences in activity. The platinum catalysts were observed to be the most active catalysts for the removal of bromate. However, when the mass of catalysts was considered, the supported palladium catalysts were shown to be the most efficient.

Several structured catalysts were prepared, using palladium as the active metallic phase, and using carbon nanotubes or titanium dioxide as support. These catalysts were applied to the continuous catalytic hydrogen reduction of bromate in water. It was found that, in the case of

the CNT structured catalysts, the loading of Pd was directly related to the catalytic performance. In the case of the TiO_2 structured catalysts, while the Pd loading affected the performance of the catalyst, other factors were proposed to play a major role, such as the placement of the dispersed Pd with the TiO_2 on the surface of the catalyst, the dispersion of Pd and the availability of the active phases for reaction.

FUTURE WORK

Several avenues for continuation of the developments of the work presented here are open to be explored in the near future.

The most immediate one would concern the application of the best performing catalysts in a larger scale pilot plant that would evaluate the behaviour of the system using real conditions in terms of water matrix, pollutants, and hydrodynamic regimes. Besides the dimensioning of such a pilot plant that could approximate the needs of the real life cases, the biggest challenge concerns the development of preparation methods of the catalysts of adequate size.

Regarding the ozonation reaction, the testing of different carbon based structured catalysts is also a possibility that may be explored. In particular, the development of methods of preparation of structured catalysts containing other forms of carbons that may show better activity in powder form, but have not yet been prepared supported on a macrostructure, is an interesting path to achieve better performing systems. Similarly, the preparation of structured catalysts using carbon-metal oxides composites, or other similar materials, might be one path to achieve better performing catalysts. The combination of the catalytic ozonation system using structured catalysts with other emerging technologies should also be considered regarding the application of the system in the context of a water treatment plant.

Regarding the reduction reaction, several other catalytic systems might be prepared under the form of structured catalysts, using a large array of techniques that may be explored in the near future. The preparation of bimetallic structured catalysts that could be applied to the reduction of nitrate is one concern that could be easily addressed. The development of catalysts to achieve efficient removal of highly refractory pollutants such as perchlorates presents a bigger challenge that may still be achieved in the future. The testing of the structured catalysts in the reduction of inorganic pollutants using other cheaper and more accessible reducing

agents is interesting, considering the sustainability of the application of this process in real life water or wastewater treatment plants.

APPENDIX A

ADSORPTION OF ATRAZINE ON MWCNT

The extent of adsorption of atrazine on the surface of MWCNT was also assessed, since it may be contributing to the removal of TOC that was observed during the catalytic ozonation experiments, as well as to the changes observed in the distribution of the intermediate products and the resulting toxicity [1-5]. On a first approach, the time needed for the concentration of atrazine in solution to reach equilibrium with the adsorbed amount was assessed, as seen in Figure1.

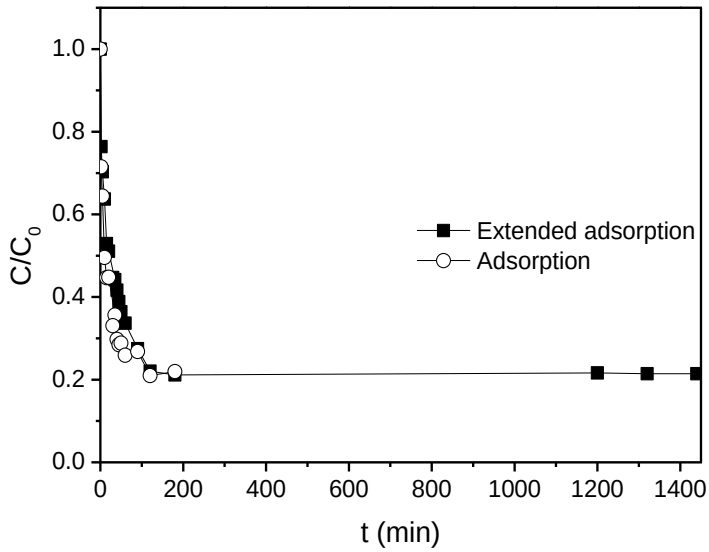

Figure1 - Dimensionless concentration of atrazine during experiment of extended adsorption on MWCNT compared with short-term adsorption experiment.

It is clear that at 180 min, the extent of adsorption of atrazine is the same as what was observed after 1440 min. Thus, for the experiments performed to evaluate the contribution of adsorption in the removal of atrazine and degradation products during ozonation experiments, 180 min was selected as the length of the experiments.

Adsorption isotherms of atrazine, DEIA, DIA and DEA were experimentally obtained, using MWCNT as adsorbent, in order to acquire information about the contribution of adsorption in the removal of these products during catalytic ozonation reactions, particularly during kinetic experiments described further ahead. The obtained adsorption isotherms for atrazine are presented in Figure2.

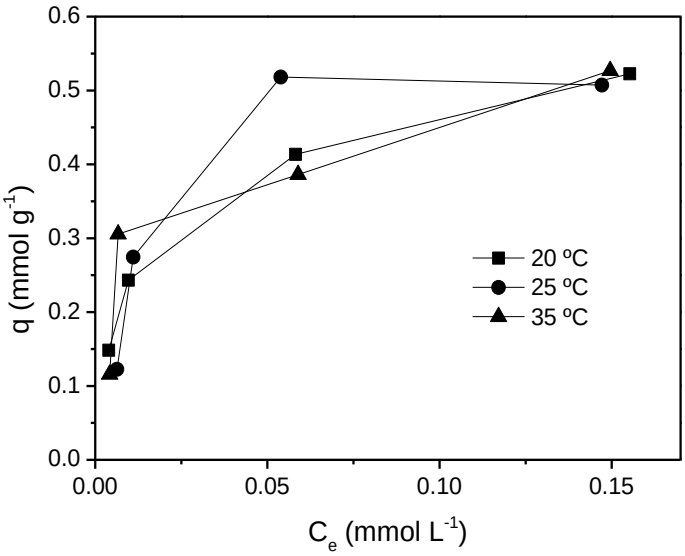

Figure2 – Amount of atrazine adsorbed as a function of the equilibrium concentration in solution during isothermal experiments using MWCNT as adsorbent.

The obtained adsorption isotherms for DEA are presented in Figure3.

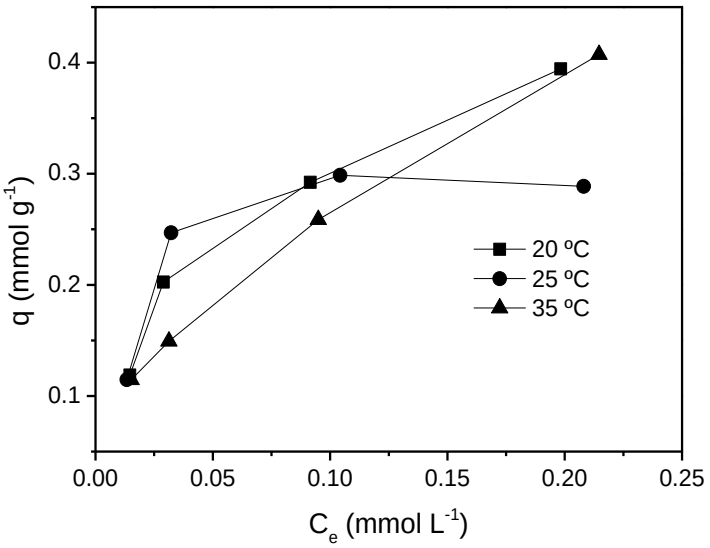

Figure3 – Amount of DEA adsorbed as a function of the equilibrium concentration in solution during isothermal experiments using MWCNT as adsorbent.

The obtained adsorption isotherms for DIA are presented in Figure4.

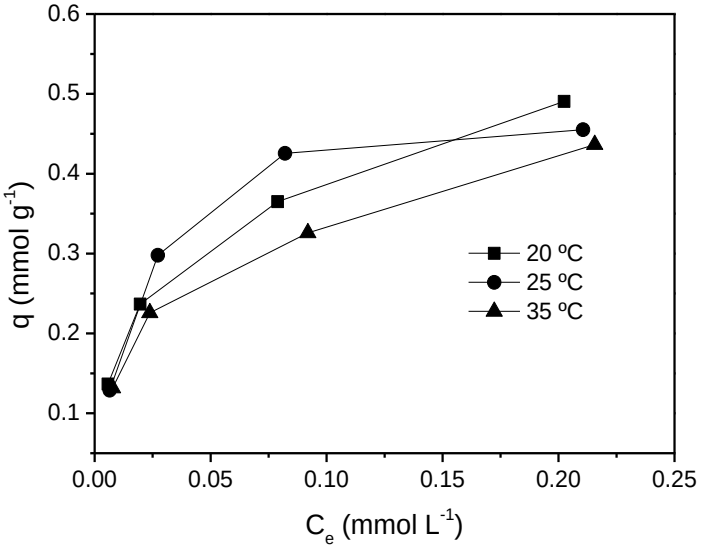

Figure4 – Amount of DIA adsorbed as a function of the equilibrium concentration in solution during isothermal experiments using MWCNT as adsorbent.

Finally, the obtained adsorption isotherms for DEIA are presented in Figure5.

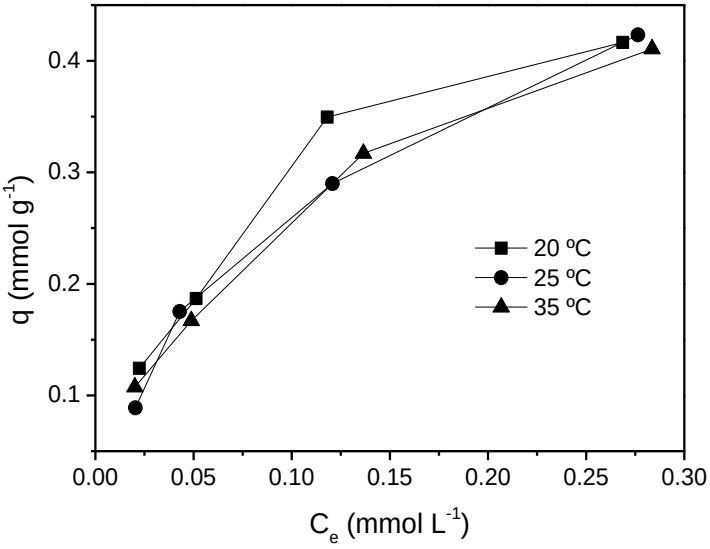

Figure5 – Amount of DEIA adsorbed as a function of the equilibrium concentration in solution during isothermal experiments using MWCNT as adsorbent.

The adsorption data was fit to the Langmuir expression [6] (Equation 1), and the calculated q_{max} and *K,* through linear regression, are presented in Table 1;

$$\frac{C_e}{q} = C_e \frac{1}{q_{max}} + \frac{1}{K.q_{max}} \quad (1)$$

, where C_e is the concentration of the adsorbate in solution, q is the amount adsorbed, q_{max} is the maximum amount adsorbed and K is the adsorption constant.

Table 1 – Values of the characteristic constants obtained by fitting of experimental adsorption data on MWCNT to the Langmuir equation.

ATZ	20^{o} C	25^{o} C	35^{o} C
q_{max} (mmol g^{-1})	0.562	0.568	0.563
K (L $mmol^{-1}$)	22.47	22.44	21.42
DEA			
q_{max} (mmol g^{-1})	0.475	0.314	0.529
K (L $mmol^{-1}$)	4.992	7.048	3.756
DIA			
q_{max} (mmol g^{-1})	0.539	0.496	0.482
K (L $mmol^{-1}$)	11.65	14.41	8.16
DEIA			
q_{max} (mmol g^{-1})	0.551	0.590	0.547
K (L $mmol^{-1}$)	3.664	3.091	3.095

In the case of atrazine, while the q_{max} value did not show a detectable trend with changes in the temperature, the *K* value was observed to decrease with the increase in temperature. Similar results were observed when DEIA was probed as adsorbate. In the case of DEA, while the smallest value of *K* was observed for the highest temperature, the lowest temperature did not corresponded to the higher value. A similar observation was made in the case of DIA. The value of *K* followed the following decreasing order: atrazine>DIA>DEA>DEIA.

An adsorption experiment was carried out using a mixture of atrazine and its three identified main intermediates, in order to understand how the adsorption of the compounds on MWCNT changed in a competitive environment (Figure6).

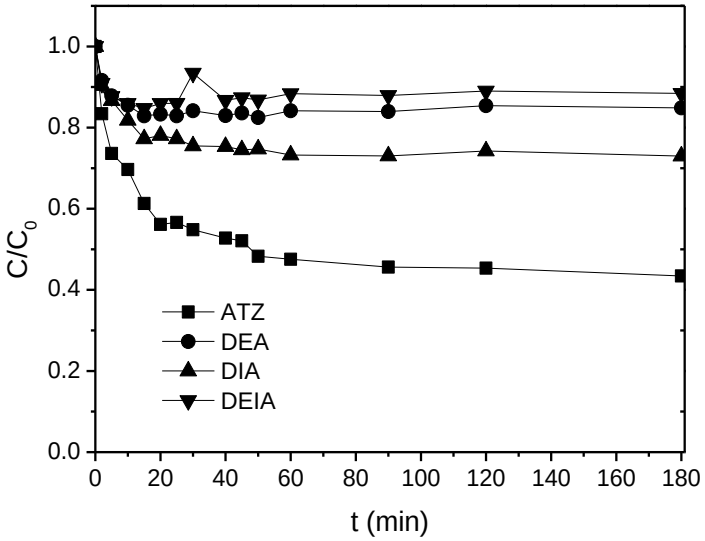

Figure6 – Dimensionless concentration of atrazine, DEA, DIA and DEIA during adsorption experiments on MWCNT at 25 ^{o}C.

The distribution of the organic compounds in solution after 180 min, when equilibrium is reached, follows the order that was found for the values of *K*. The adsorbed amounts of each compound, individually and in mixture, are compared in Figure7, at 25 ^{o}C and 10 mg L^{-1} of each compound in the initial solution.

As expected, the adsorbed amount at equilibrium is smaller when the experiment was carried out using a mixture of the pollutants, which was true for the four compounds analysed. The biggest decrease in the adsorbed amount was observed with DEA, with 76%, followed by DEIA with 63%, DIA with 60% and finally atrazine with 26%. Nevertheless, the removal of atrazine by adsorption still corresponded to 56%, DEA to 15%, DIA to 27% and DEIA to 11%, which are considerable amounts.

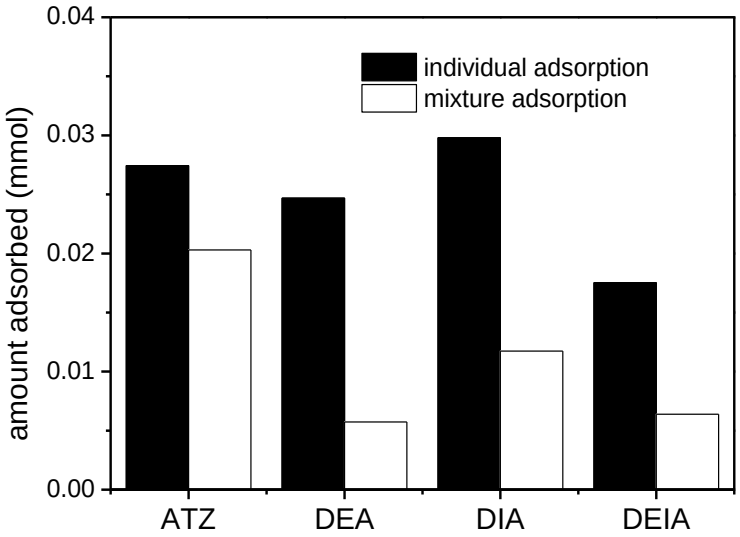

Figure7 – Adsorbed amounts of atrazine, DEA, DIA and DEIA on MWCNT during experiments carried out using the individual compounds or a mixture of the compounds.

Furthermore, an experiment was carried out to assess the extent of adsorption of the unidentified organic compounds generated during the ozonation of atrazine, and of the identified intermediates, on MWCNT, in mixture (Figure8). To this end, a solution of atrazine was exposed to ozone during 180 min, and then MWCNT was introduced after the solution was stripped of ozone, in order to measure the adsorption.

The extent of DEIA adsorption in this case is much larger than in the case of adsorption of the sole compound or when in mixture of pollutants, since those solutions were prepared with 10 mg L^{-1} of the pollutants. The concentration in this case is much smaller at the beginning of reaction, approximately 0.98 mg L^{-1}. Similar behaviour was observed with DIA, which presented a concentration of 0.23 mg L^{-1} at the start of the adsorption experiment. The extent of adsorption of UOC2, UOC3 and UOC4 was similar among them, varying between 80 and 90%. The compound which presented the least adsorbed amount was UCO6, approximately 30%. Since these compounds are not quantified, it is not possible to comment on the influence of the initial concentrations. The

affinity of atrazine and atrazine-derived organic pollutants to MWCNT adsorption is likely related to its polarity, since more polar compounds [7, 8] were observed to be less extensively adsorbed on the surface of the carbon material.

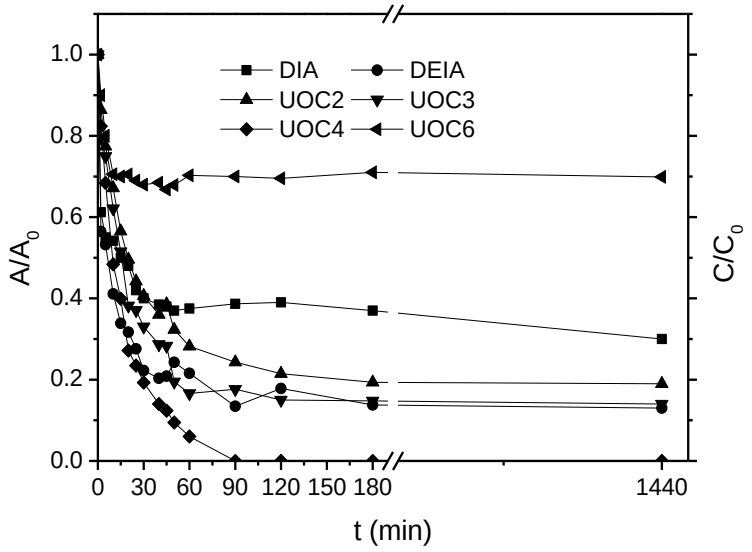

Figure8 – Dimensionless concentration of DIA and DEIA (right axis) and dimensionless chromatogram peak area of UOC2, UOC3, UOC4 and UOC6 (left axis) during adsorption experiments on MWCNT, carried out after single ozonation of atrazine during 180 min.

Finally, changes to the surface of the carbon material during the ozonation procedure should also be considered, since it is likely that the adsorption capacity may be affected [9-11]. For this end, MWCNT were subject to a previous ozonation treatment, which resulted in the introduction of oxygen-containing groups on the surface [12, 13], as discussed in section *Stability and deactivation of the catalysts*. The extent of adsorption of atrazine in fresh MWCNT and in ozonised MWCNT is compared in Figure9.

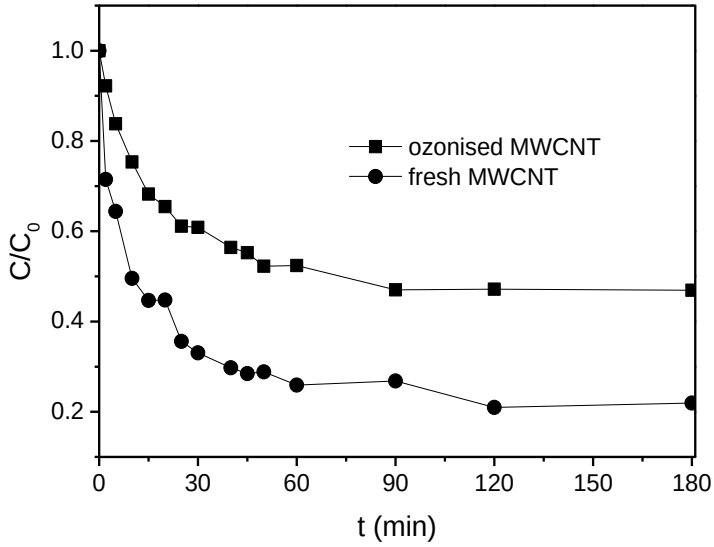

Figure9 – Dimensionless concentration of atrazine during adsorption experiments on fresh and ozonized MWCNT.

It is clear that the introduction of oxygen-containing functionalities on the surface of MWCNT hinders their capacity of adsorption of atrazine, likely due to changes in the electronic density and in the acid-base character of the carbon material [9-11]

In summary, it was shown that the extent of adsorption of atrazine and of its degradation compounds varies with changes in the temperature, with the concentration in which the compounds are present and with the competition with other compounds present in solution. Moreover, it was observed that the capacity of the MWCNT to adsorb atrazine and degradation products depends greatly on the compound, and is modified by the introduction of oxygen-functionalities due to the ozonation process. In any case, the contribution of adsorption of atrazine on MWCNT during catalytic ozonation experiments should not be disregarded [3-5].

KINETICS OF CATALYTIC OZONATION OF ATRAZINE IN THE PRESENCE OF MWCNT

Several catalytic ozonation experiments were carried out at different conditions in order to determine their influence in the removal of atrazine, as well as in the generation of the detected organic intermediates, identified or otherwise.

The disappearance of atrazine from solution during ozonation experiments is seen to follow first-order reaction kinetics [14, 15]. Thus, the apparent rate constant, k_{ATZ}, for each reaction system, was found through fitting of the experimental data to Equation 2,

$$r_{ATZ} = \frac{-dC_{ATZ}}{dt} = k_{ATZ} C_{atz} \quad (2)$$

, where r_{ATZ} is the rate of degradation of atrazine and C_{ATZ} is the concentration of atrazine for a given time, *t*.

The obtained values of k_{ATZ} calculated for different experimental conditions are presented in Figure10. The experiments were performed varying the pH, the ozone concentration in the gas phase, the catalyst loading, the initial concentration of atrazine and the temperature of reaction (experimental conditions detailed in section *Materials and methods*).

The apparent atrazine degradation rate constant varied between 0.05 and 0.52 min^{-1}. The r^2 obtained for the linear fits used to determine the rate constant were always above 0.93, which suggests good fitting of the first-order reaction model. The increase of the initial concentration of atrazine is seen to decrease its removal, with the apparent rate constant varying between 0.0748 and 0.2398. However, this variation was the smallest registered, since the concentration of ozone in the liquid phase is sufficient to extensively react with atrazine, even when its decomposition is enhanced by the presence of a catalyst. The increase in the catalyst loading was seen to result in higher values of k_{ATZ}, which increased from

0.1432 to 0.4768. Interestingly, the apparent removal rate constant slightly decreased when the catalyst loading was varied between 50 mg L^{-1} and 100 mg L^{-1}. This observation could be attributed to the fact that the main role for the removal of atrazine, in this system, is being played by the direct ozonation of the organic pollutant, rather than oxidation by more active species formed from the decomposition of ozone. Thus, for low loadings of MWCNT, the promoted decomposition of ozone might be hindering the degradation of atrazine (k_{ATZ} in single ozonation was calculated to be 0.2328 min^{-1}) Nevertheless, for higher loadings of MWCNT, the contribution of adsorption should be responsible for the large increase in the apparent removal rate constant, which compensates the decrease in the available ozone for reaction with atrazine. The increased decomposition of ozone for higher loadings of MWCNT [16] is seen in Figure11, where the values of dissolved molecular ozone in experiments without any pollutant at varying catalyst loadings are presented. The temperature was shown to increase the degradation of atrazine, which is contrary to what was observed in the adsorption experiments. The main difference that was observed was related to the concentration of dissolved ozone, which decreased with the temperature, thus suggesting that the temperature increase is improving the decomposition of ozone. Notwithstanding, the temperature increase has been reported to affect the ozone reactions much more significantly than the reactions involving hydroxyl radicals, which agrees with the increase in the removal of atrazine with temperature that was observed here [17]. The use of larger ozone concentrations on the gas feed, keeping the gas flow rate constant, thus increasing the ozone dose, resulted in an increment to the removal rate constant of atrazine. The larger dose of ozone leads to a larger amount of ozone that is available for reaction with atrazine, thus enhancing its removal from solution.

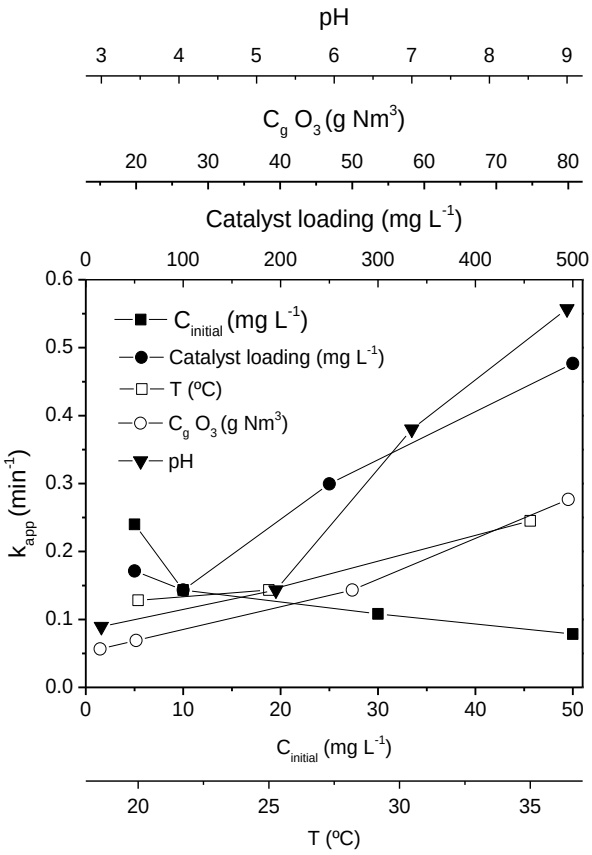

Figure10 – Calculated values of apparent removal rate of atrazine from solution during semi-batch ozonation experiments in which the experimental conditions were systematically varied.

Finally, the rate of removal of atrazine is also increased with the increase of pH; at pH 9, the removal rate constant reaches its maximum observed value. It is well known that the increase of pH promotes the homogeneous decomposition of dissolved molecular ozone [17-19]. When a carbon catalyst is present in solution, at basic pH, the contribution of the heterogeneous decomposition of ozone may be minor when compared with the homogeneous decomposition caused by the presence of OH^- ions in solution [16]. On the other hand, changes in the solution pH may interfere with the adsorption process on the surface of carbon materials, due to changes on its surface charge [20]. The pH_{pzc} of the MWCNT has

been reported to be 7 [12], which means that the change of pH to more basic ones through the addition of a buffer might be changing the adsorption dynamics of atrazine. However, the difference in adsorption of atrazine at varying pH on MWCNT has been found to be negligible [5]. The conversion of ozone into active non-selective hydroxyl radicals in solution at higher pH is probably the main contributor to the degradation of atrazine through reactions occurring on the liquid phase. Such radicals are known to have a very high reaction rate with atrazine [15], and the small values of ozone concentrations in this case might mean that this is the main path for atrazine removal in this case. In fact, reactions carried out at pH 9 showed a decrease of almost 70% in the concentration of dissolved molecular ozone.

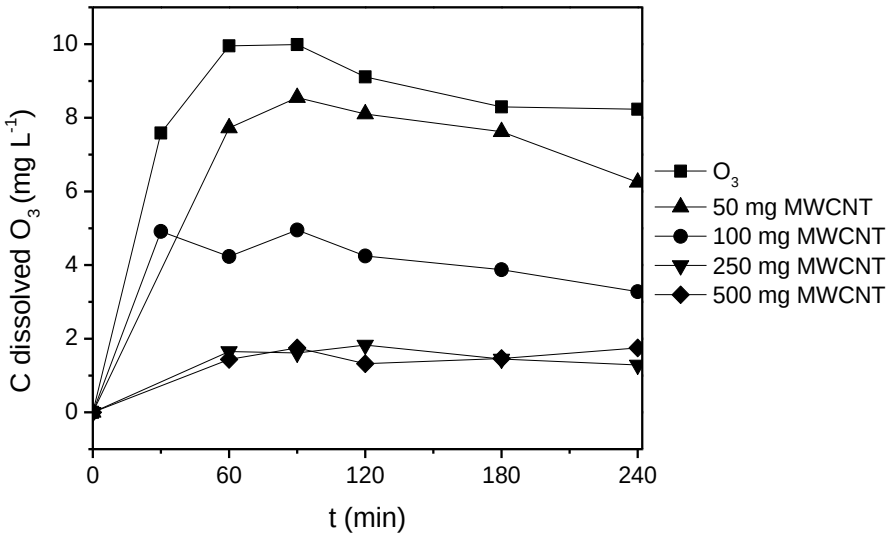

Figure11 – Concentration of dissolved molecular ozone measured in experiments without any pollutant, using different loadings of MWCNT.

To further understand the role of the experimental conditions on the degradation of atrazine during catalytic ozonation, the formation of the intermediate compounds was followed. In the case of DIA and DEA, two of the intermediates formed during ozonation and atrazine, the concentrations found during the experiments are presented in Figure12 and 13 respectively. The reaction rate constants for formation and

removal of these compounds were not calculated, since they did not vary significantly with the experimental conditions, and thus only the concentration profiles throughout the reaction are presented here, for the sake of brevity.

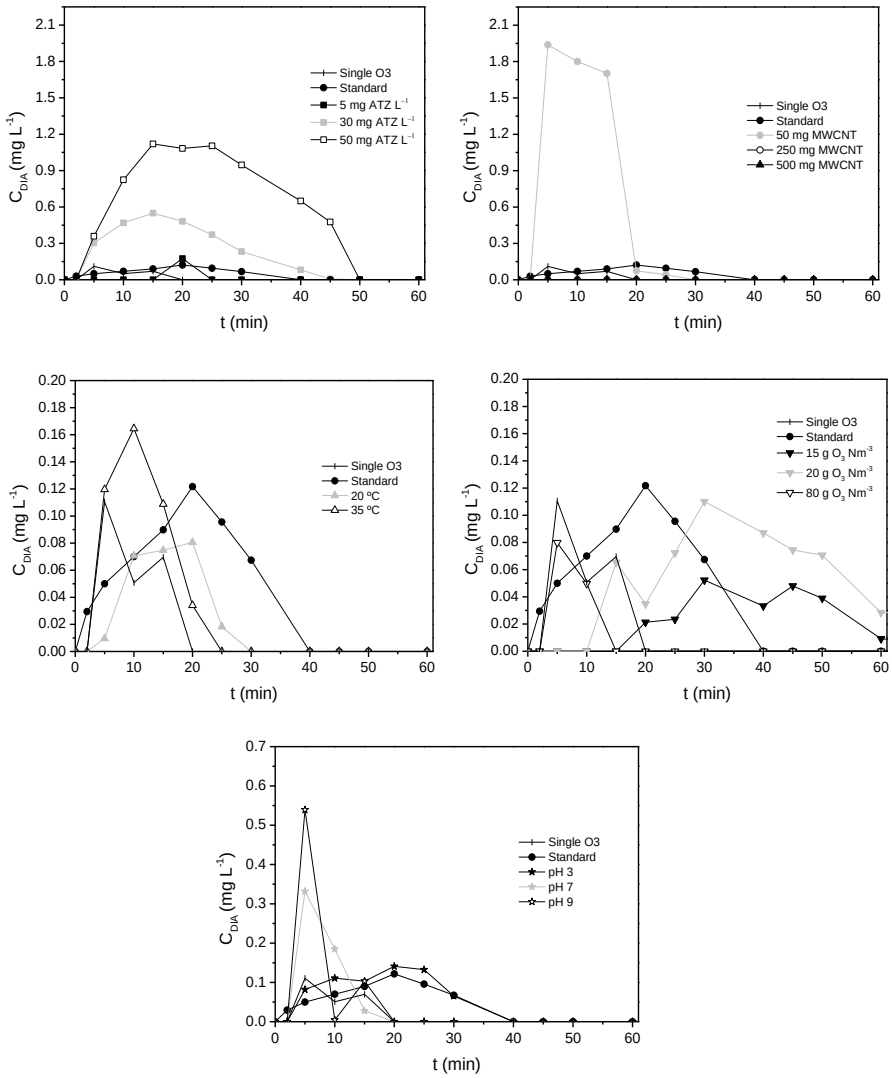

Figure12 – Concentration of DIA during semi-batch ozonation experiments in which the experimental conditions were systematically varied.

The biggest variation in the formation of DIA was observed in the experiment where the initial concentration of atrazine was varied, with a large increase in formation, due to the larger availability of atrazine in solution. Similarly, a large amount of DIA was formed in the experiment where the catalyst loading was reduced to 50 mg L^{-1}. Since no trace of DIA was found in the experiment with larger catalyst loadings, it is clear that a change in the reaction mechanism occurs, either due to a decrease in the formation of DIA when a catalytic route is preferred, or an increase on the removal of DIA that is quick enough to render DIA undetectable in solution. Smaller increases were also observed with the increase of pH, which should also be related to changes in the reaction mechanism. It has been reported that the formation of DIA from oxidation of atrazine by radical action is much faster than that promoted by direct ozonation [15].

Similarly to what was observed in the evolution of DIA during the kinetic ozonation experiments, the concentration of DEA increased largely in the experiments where the initial concentration of atrazine was increased. The decrease of the loading of MWCNT increased the production of DEA, has had been seen in the case of DIA. Since the reaction of DIA with hydroxyl radicals is much faster than with ozone, it is likely that in the cases where the radical mechanism is preferred, the decrease in the concentration of DEA is related to an increase in its removal rate, rather than a decrease in its formation rate [15]. The much higher concentrations of DEA found throughout these experiment are likely related, in part, with the fact that ozone reacts with DIA much faster than with DEA, thus decreasing the removal of the latter from solution [15]. On the other hand, the increase on pH actually decreased the amount of DEA found in solution, likely due to an increase in the homogeneous decomposition of ozone, resulting on a faster removal of DEA from solution. A similar behaviour was observed with the increase of the temperature. The increase of the concentration of ozone in the gas phase resulted, on one hand, on an increase of the production of DEA, and on the other hand, on a faster removal of DEA from solution.

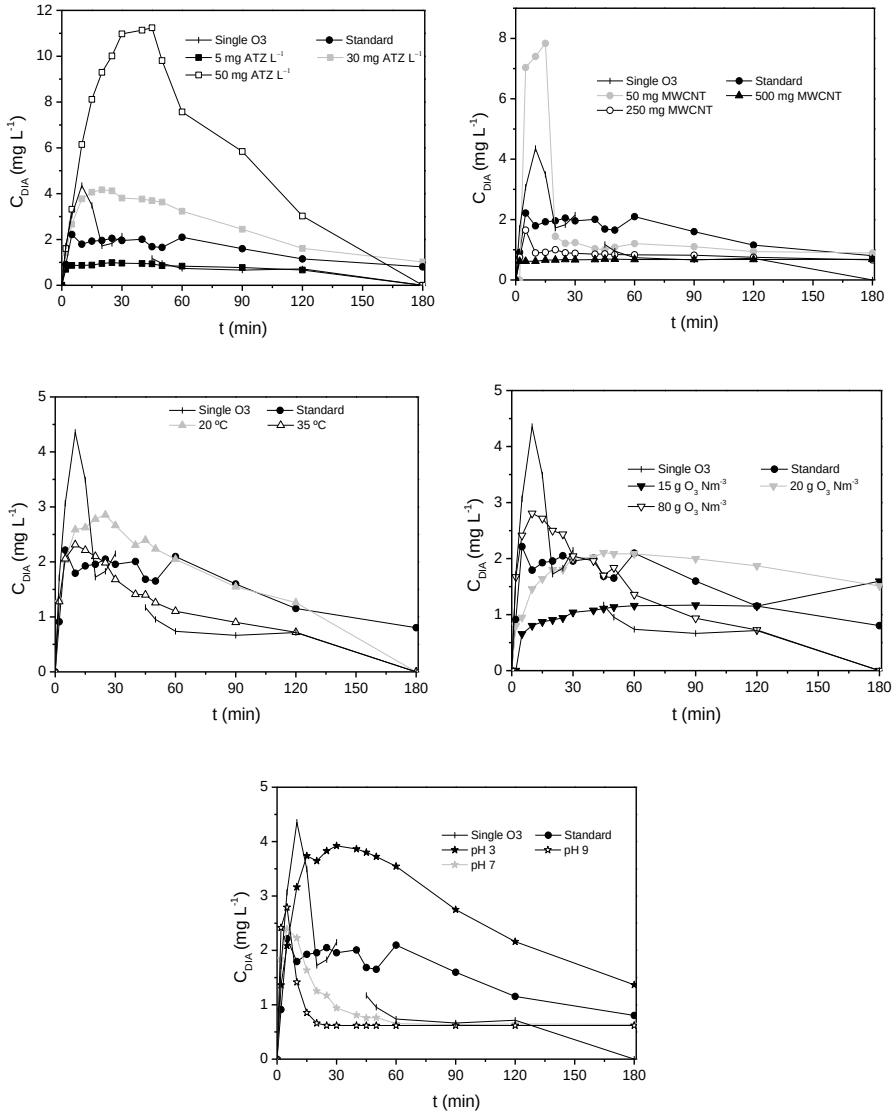

Figure13 – Concentration of DEA during semi-batch ozonation experiments in which the experimental conditions were systematically varied.

The kinetics of the formation of DEIA are very complex, due to its multiple origins, including unquantified organic intermediates [21-25]. Thus, fitting of first or second order reaction model were not satisfactory. Therefore,

the measured concentrations during the experiments at different reaction conditions are presented in Figure14.

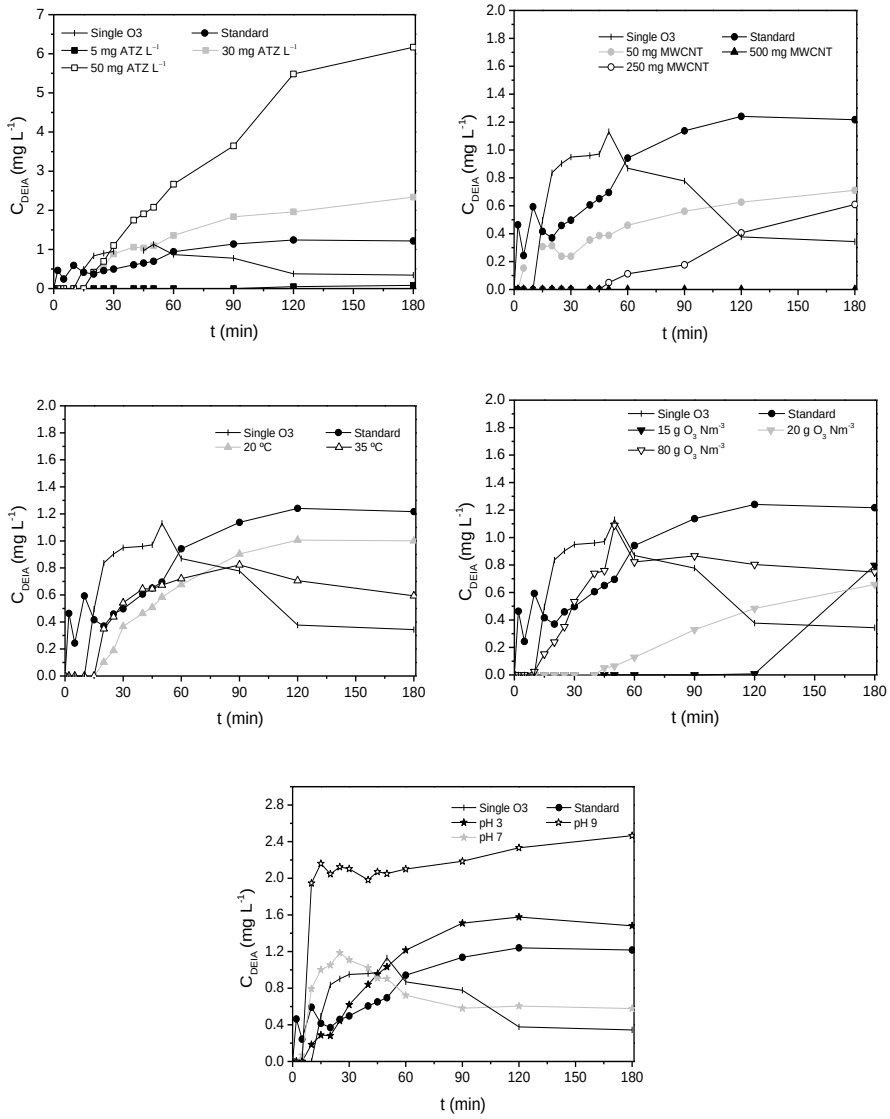

Figure 14 – Concentration of DEIA during semi-batch ozonation experiments in which the experimental conditions were systematically varied.

The increase in the initial concentration of atrazine resulted on an increase in the amount of DEIA accumulated in solution, as was observed

in the case of DIA and DEA. The increase of the catalyst loading, on the other hand, resulted on a decrease of the detected concentration of DEIA. This behaviour could be due to several factors: a decrease in the production of DEIA, an increase in its oxidation or an increase in the adsorbed amount on the MWCNT. DEIA is not extensively adsorbed on the surface of MWCNT. Thus, either the increase of the amount of DEIA results on a decrease in the production of DEIA, due to a shift on the reaction mechanism towards other compounds, or DEIA is being oxidized into other compounds due to the action of the catalyst. The increase in temperature to 35 ^{o}C resulted on a decrease of DEIA in solution, and the same was observed when the temperature was decreased to 20 ^{o}C. However, an increase in the degradation of DEA and DIA was observed at 35 ^{o}C and 20 ^{o}C, and thus an increase in the concentration of DEIA would be expected. The fact that this was not observed means that either an increase in the degradation of DEIA is observed when the temperature was changed or a change in the reaction pathway of these compounds takes place. Lower concentrations of ozone in the gas phase resulted in lower accumulated concentrations of DEIA, most likely due to a decrease on its formation rate, and also of the formation rate of the compounds from which DEIA originates. However, the experiment carried out with 80 g O_3 Nm^{-3} in the gas phase showed less accumulated DEIA than the standard experiment, carried out at 50 g O_3 Nm^{-3} in the gas phase. Thus, since an increase in the formation of DEIA is expected, an increase of its removal rate at the highest ozone concentration in the gas phase may explain this behaviour. In fact, experiments at different pH showed widely different behaviours of the evolution of DEIA concentration throughout the experiments. The experiment carried out at pH 3 showed a slightly higher concentration of DEIA measured in solution, which is likely related to the hampering of the homogeneous decomposition of ozone, thus altering the reaction pathway in the direction of the formation of this intermediate compound. The reaction carried out at pH 7 showed a decrease in the concentration of DEIA, which is in agreement with what was observed for the reactions at pH 3 and at standard conditions (natural pH, 5.25).

However, when the pH was raised to 9, the concentration of DEIA was much higher than in the other experiments. It was expected that, at this pH, the increase in the action of radical species, surface or otherwise, would yield lower concentrations of DEIA, with basis in what was observed during other experiments. Nevertheless, a similar increase was observed in the formation of DEA and DIA at this pH, while at lower pH values, in the acidic range, the concentration of DEA and DIA decreased with its increase. Thus, a change in the reaction mechanism at pH 9 is resulting in a much larger formation of DEA and DIA, which eventually also lead to a higher concentration of DEIA found accumulated in solution.

The formation of other unquantified organic compounds is also relevant in the study of the influence of the reaction conditions in the catalytic ozonation of atrazine. In fact, as seen before, there are four compounds which are accumulated in solution, and which are relevant for this study: UOC2, UOC3, UOC4 and UOC6. The relative peak area was calculated in relation to the maximum area found for each compound in the chromatograms, throughout all the kinetics experiments presented in this section. The relative peak areas of UOC2 found during the experiments at varying reaction conditions are presented in Figure15.

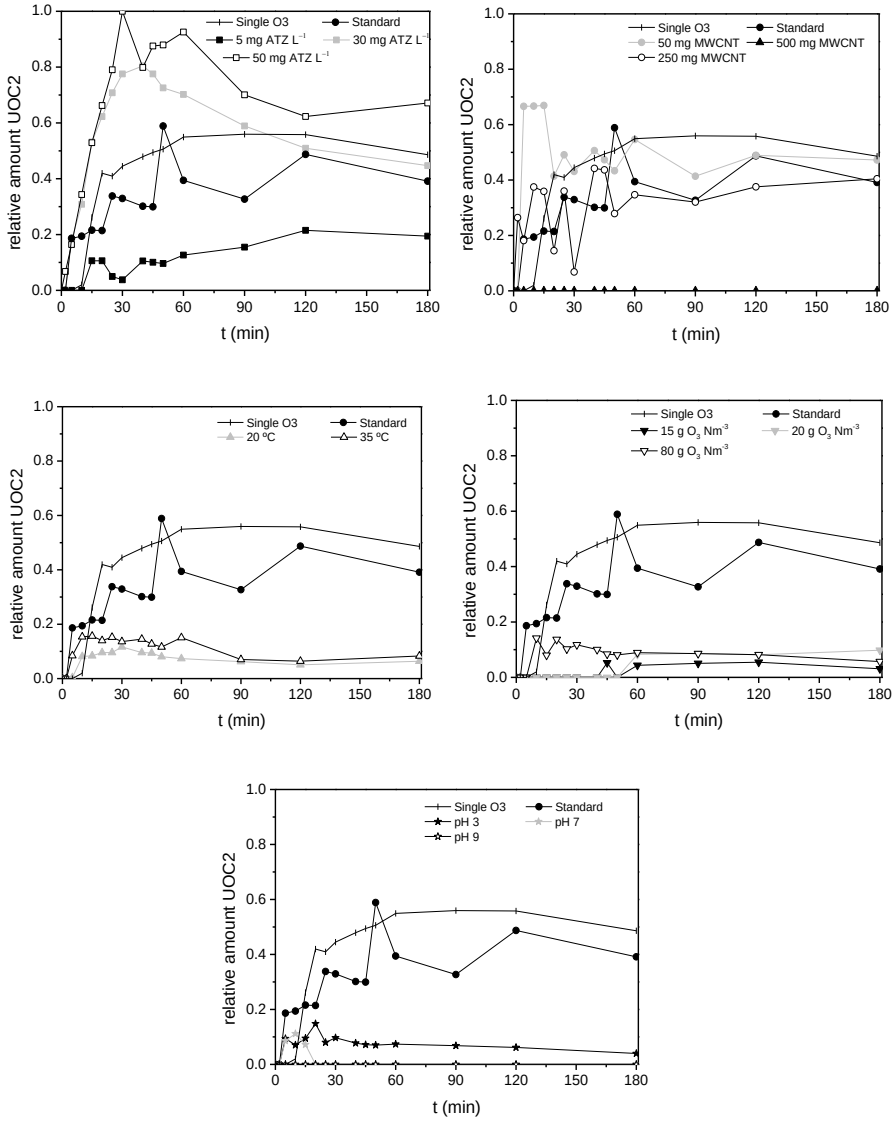

Figure15 – Relative amount of UCO2 during semi-batch ozonation experiments in which the experimental conditions were systematically varied.

The amount of UOC2 found accumulated in solution is higher during single ozonation than in the experiment at standard conditions at 180 min, as seen before. The amount of UOC2 found in solution increases with the initial concentration of atrazine, as witnessed for the other intermediate

organic compounds. When the concentration of MWCNT was varied, the accumulation of UOC2 in solution was smaller for larger values of catalyst loading. It is possible that adsorption, as well as an increase in the oxidation of UOC2, is playing a part, since the removal of UOC2 from solution has been observed to probably be related with surface reactions in experiments carried out to give insight into the reaction mechanism. Regardless of the direction of the variation of temperature, these experiments resulted in less UOC2 in solution than what was found in the case of the experiment at standard conditions. A similar behaviour has been observed for the previously presented organic intermediates. While the decrease in the ozone concentration in the gas phase resulted on much smaller concentrations of UOC2, when compared with the experiment at standard conditions, the increase of the ozone concentration also resulted in small concentrations. In the former case, it is likely that this effect is due to a diminished production of the organic compound during reaction, while the latter should be due to an increase in the removal of UOC2 from solution, since there is more ozone available to react with the pollutant, likely through radical action. A similar behaviour was observed in the experiments at different values of pH. While basic pH may enhance the removal of the compound due to the homogeneous decomposition of ozone, it is likely that at lower values of pH the production is being hindered. However, UOC2 formation has been linked with direct ozonation reactions during experiment carried out in the presence of *tert*-BuOH.

The relative amount of UOC3 found accumulated in solution during the experiments at varied reaction conditions are presented in Figure16.

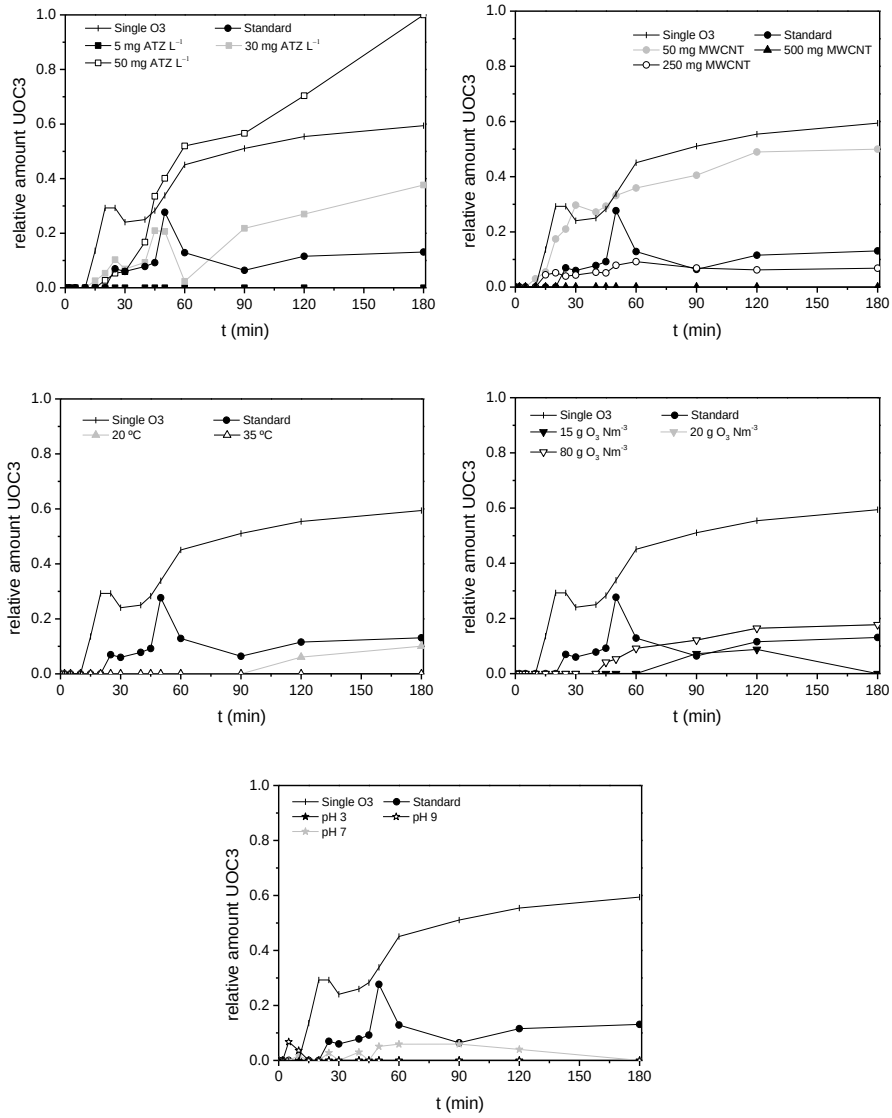

Figure16 – Relative amount of UCO3 during semi-batch ozonation experiments in which the experimental conditions were systematically varied.

The increase of the initial concentration of atrazine, as before, yielded larger concentrations of UOC3 found during the catalytic experiments. Higher loadings of MWCNT resulted in smaller concentrations of UOC3, which may be explained by either adsorption of the compound on the

surface of the catalyst, or by an increase in the oxidative potential of the system. When the temperature was varied, a similar behaviour to what was observed before, was also registered in the case of UOC3; changes in the temperature yielded smaller concentrations when compared with the catalytic experiment at standard conditions. The catalytic experiments, independent of the ozone concentration in the gas phase, resulted in smaller concentrations than the single ozonation experiment, without major differences between them. Changes in the pH of the solution through buffering resulted in similar UOC3 concentrations to those that were observed for UOC2, which suggested that at high pH, the removal of the intermediate compound is being enhanced, and at low pH, the production of the intermediate compound is being hindered. In fact, the formation of UOC3 has been suggested to be linked with reactions with radical species formed in solution, during experiments carried out using a radical scavenger.

The relative amount of UOC4 found accumulated in solution during the experiments at varied reaction conditions are presented in Figure17.

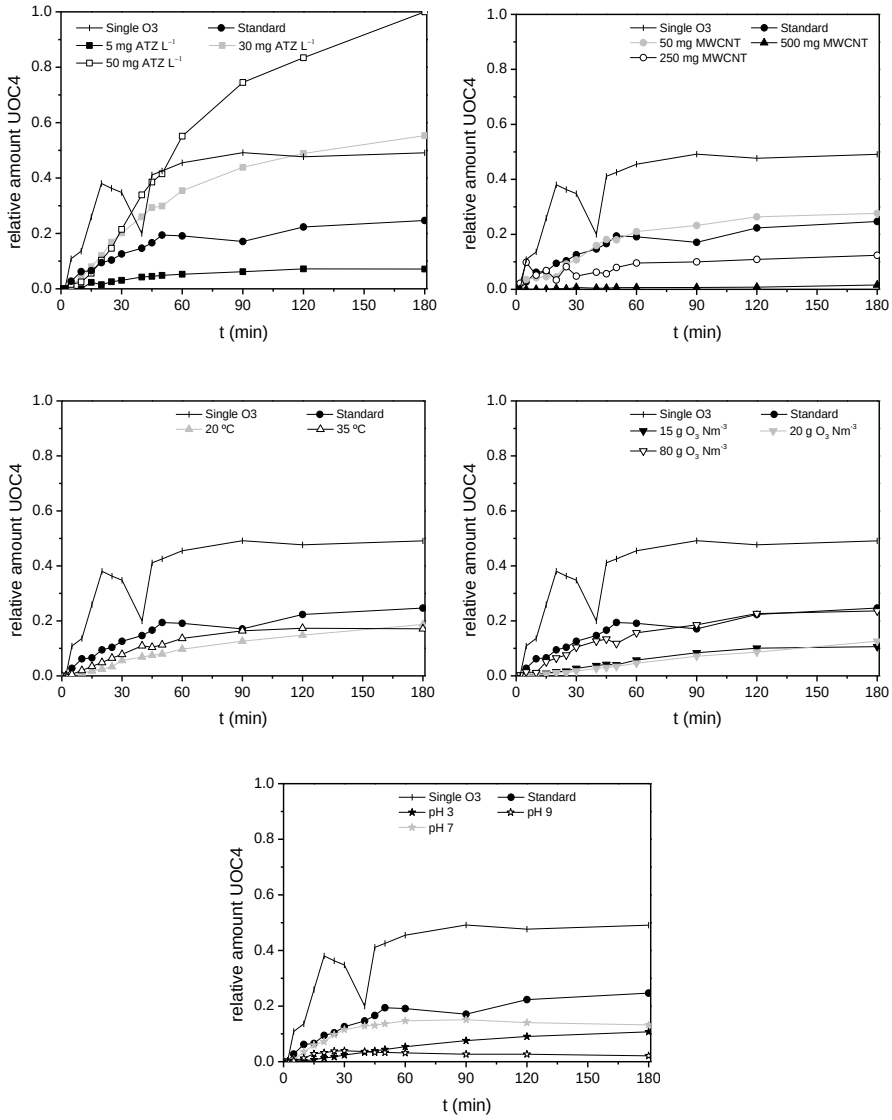

Figure17 – Relative amount of UCO4 during semi-batch ozonation experiments in which the experimental conditions were systematically varied.

In general, the catalytic experiments yielded smaller concentrations of UOC4 in solution throughout the experiments, the exception being the experiment carried out using the highest initial concentration of atrazine. In fact, the increase in this factor resulted in gradually higher

concentration of UOC4 in solution. On the other hand, the larger loadings of MWCNT resulted in smaller concentrations of UOC4, which suggests that either the oxidation of this compound is being enhanced, or its formation is being hindered when catalytic reaction mechanisms are more prominent. The role of surface reactions in the oxidation of UOC4 has been shown to be important during experiments carried out in the presence of a radical scavenger. Nevertheless, the role of adsorption should not be ignored. Changes to the reaction temperature did not alter the concentration of UOC4 during the catalytic ozonation experiments. Low concentrations of ozone in the gas phase decreased the concentration of UOC4 observed in solution, due to a decrease in the production of this compound. The increase from 50 to 80 g O_3 Nm^{-3} did not alter the concentration, which suggests that the removal is not affected by an increase in the ozone dose. However, changes in the pH resulted in very different concentrations of UOC4, which suggest that the oxidation through radical mechanism is important in the formation and/or removal of this organic compound.

Finally, the relative amount of UOC6 found accumulated in solution during the experiments at varied reaction conditions are presented in Figure18.

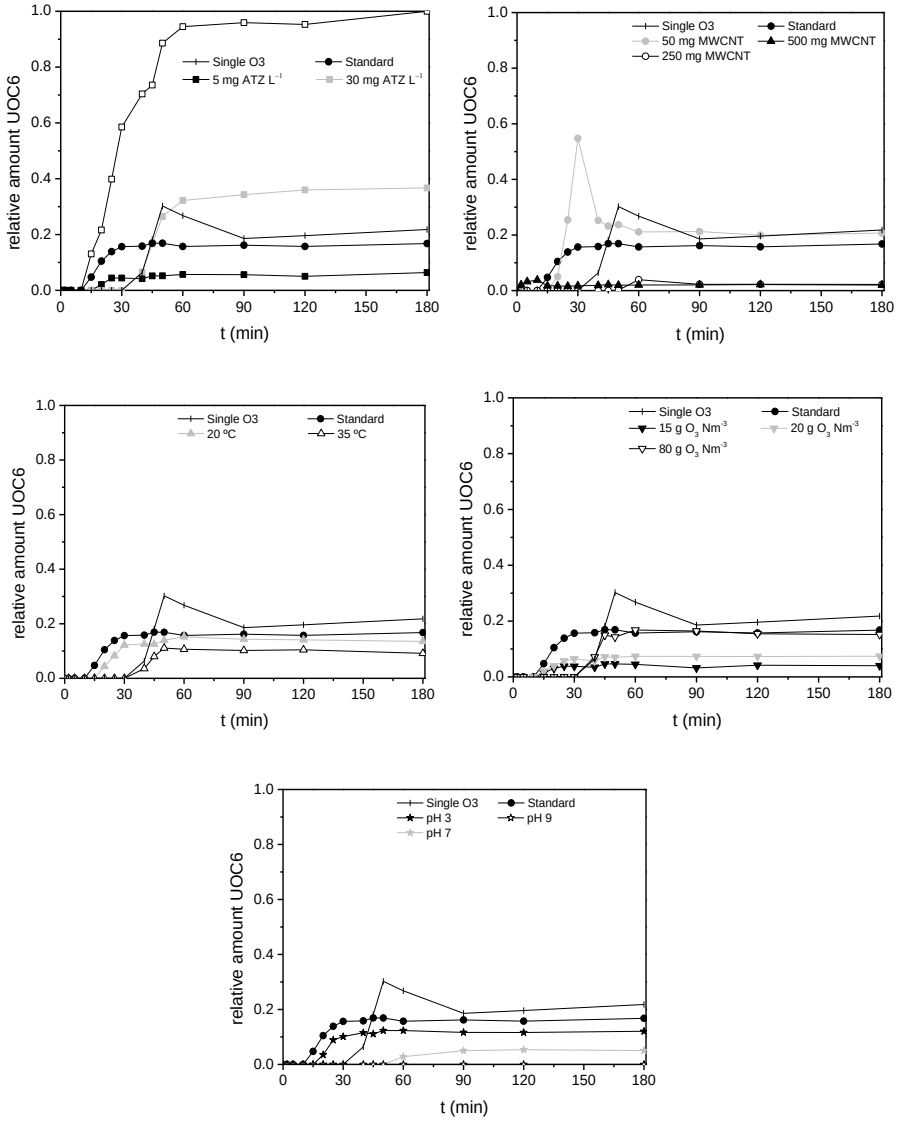

Figure18 – Relative amount of UCO6 during semi-batch ozonation experiments in which the experimental conditions were systematically varied.

Similarly to what has been observed for the other organic intermediates, the concentration of UOC6 increased with the increase in the initial concentration of atrazine. In a similar manner, the increase in the loading of MWCNT yielded smaller concentrations of UOC6, which may be due to

changes in the formation of this compound, the increase in the oxidative potential of the system due to the role of MWCNT as catalyst, or to the contribution of adsorption to the removal of organic compounds from solution. The increase in the temperature to 35 ^{o}C seemed to slightly lower the concentration of UOC6 found in solution, which could be related to an increase in the oxidative potential of the ozonation system. However, the increase in the ozone dose only increased the concentration of UOC6 up to 50 g O_3 Nm^{-3}, which suggests that lower concentrations might be related to the hindering of the formation of this compound. Nevertheless, basic pH values showed smaller concentrations of UOC6, which suggest that the oxidation of the organic compound by radical action in solution is important to its degradation. In the experiments using a radical scavenger, it was suggested that the formation of this product is link with reactions through radical species, either directly, or due to differences in the formation of the products which originate UOC6.

In summary, it was observed that adsorption of atrazine, and of its intermediate degradation products, plays an important role in their removal from solution, during catalytic ozonation experiments. Changes in the experiment conditions were shown to affect the oxidation of atrazine. Moreover, the reaction pathways of atrazine degradation was observed to be widely altered when different experimental conditions were employed, due to changes in the reaction mechanism, i.e. direct ozonation, radical action in solution or on the surface of MWCNT, to changes in the availability of the reactants and due to the contribution of adsorption.

REFERENCES

[1] C.S. Castro, M.C. Guerreiro, M. Gonçalves, L.C.A. Oliveira, A.S. Anastácio, Journal of Hazardous Materials, 164 (2009) 609-614.
[2] C.A. Guzman-Perez, J. Soltan, J. Robertson, Separation and Purification Technology, 79 (2011) 8-14.
[3] S. Jain, R. Yamgar, R.V. Jayaram, Chemical Engineering Journal, 148 (2009) 342-347.
[4] G.-C. Chen, X.-Q. Shan, Y.-Q. Zhou, X.-e. Shen, H.-L. Huang, S.U. Khan, Journal of Hazardous Materials, 169 (2009) 912-918.
[5] X.M. Yan, B.Y. Shi, J.J. Lu, C.H. Feng, D.S. Wang, H.X. Tang, Journal of Colloid and Interface Science, 321 (2008) 30-38.
[6] J. Toth, Adsorption, Taylor & Francis, 2002.
[7] S. Derrouiche, D. Bourdin, P. Roche, B. Houssais, C. Machinal, M. Coste, J. Restivo, J.J.M. Orfao, M.F.R. Pereira, Y. Marco, E. Garcia-Bordeje, Water Sci Technol, 68 (2013) 1377-1383.
[8] Y.M. Vera, R.J.d. Carvalho, M.L. Torem, B.A. Calfa, Chemical Engineering Journal, 155 (2009) 691-697.
[9] J.J.M. Órfão, A.I.M. Silva, J.C.V. Pereira, S.A. Barata, I.M. Fonseca, P.C.C. Faria, M.F.R. Pereira, Journal of Colloid and Interface Science, 296 (2006) 480-489.
[10] P.C.C. Faria, J.J.M. Órfão, M.F.R. Pereira, Water Research, 38 (2004) 2043-2052.
[11] M.F.R. Pereira, S.F. Soares, J.J.M. Órfão, J.L. Figueiredo, Carbon, 41 (2003) 811-821.
[12] A.G. Gonçalves, J.L. Figueiredo, J.J.M. Órfão, M.F.R. Pereira, Carbon, 48 (2010) 4369-4381.
[13] J.L. Figueiredo, M.F.R. Pereira, M.M.A. Freitas, J.J.M. Órfão, Carbon, 37 (1999) 1379-1389.
[14] X. Fan, J. Restivo, J.J.M. Órfão, M.F.R. Pereira, A.A. Lapkin, Chemical Engineering Journal, 241 (2014) 66-76.
[15] F.J. Beltrán, M. González, B. Acedo, F.J. Rivas, Journal of Hazardous Materials, 80 (2000) 189-206.
[16] P.M. Alvarez, Carbon, 44 (2006) 3102.
[17] M.S. Elovitz, U. von Gunten, H.-P. Kaiser, Ozone: Science & Engineering, 22 (2000) 123-150.
[18] C. Gottschalk, J.A. Libra, A. Saupe, Ozonation of water and waste water a practical guide to understanding ozone and its application, Wiley-VCH, 2000.
[19] J. Staehelin, Environmental Science & Technology, 16 (1982) 676.
[20] P.C.C. Faria, J.J.M. Órfão, P. M.F.R., Applied Catalysis B, Environmental, 79 (2008) 237.
[21] B. Balci, N. Oturan, R. Cherrier, M.A. Oturan, Water Research, 43 (2009) 1924-1934.
[22] C.L. Bianchi, C. Pirola, V. Ragaini, E. Selli, Applied Catalysis B, Environmental, 64 (2006) 131-138.
[23] K.H. Chan, W. Chu, Water Research, 37 (2003) 3997-4003.

[24] K.H. Chan, W. Chu, Applied Catalysis B: Environmental, 58 (2005) 165-174.
[25] K.H. Chan, W. Chu, Applied Catalysis B: Environmental, 58 (2005) 157-163.

APPENDIX B

BEHAVIOUR OF BY-PRODUCTS OF OZONATION OF EMERGING ORGANIC MICROPOLLUTANTS DURING OPERATION CONDITION EXPERIMENTS

TWO-PHASE AND THREE-PHASE SYSTEM

The concentration at steady-state of the main quantified intermediates of ATZ degradation during the ozonation experiments is presented in Figure 1.

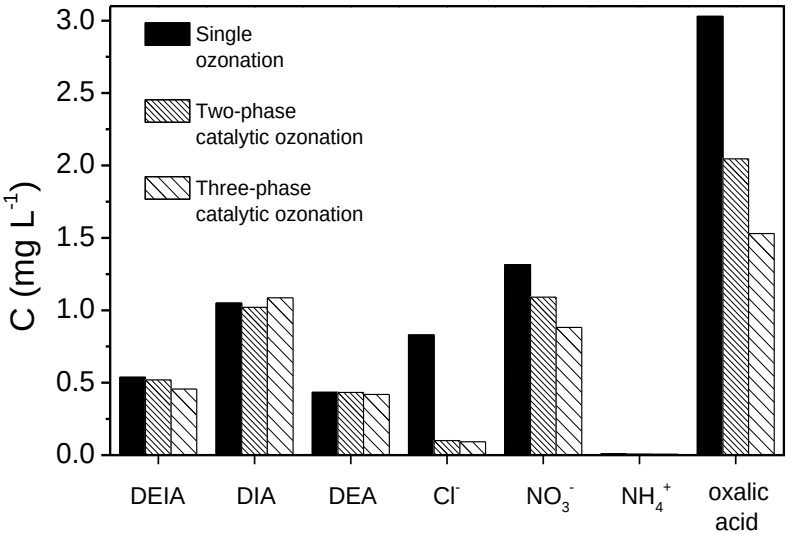

Figure 1 – Concentration of main by-products of atrazine ozonation during continuous experiments using a two-phase and a three-phase configuration of the catalytic system, at steady-state.

The observed concentrations of the intermediates of atrazine ozonation follow a similar trend to what was observed in the detailed study in section *Ozonation of emerging organic micropollutants*; i.e. while DIA and DEA, which are compounds which result directly from atrazine [1], do not

present a clear trend, the secondary degradation products, such as oxalic acid and DEIA were found in lower concentrations as the removal of TOC increased. The concentration of ionic products in solution follows an inverse trend, decreasing when the mineralization degree increases, suggesting changes to the degradation pathway when a catalyst is used in the system [2].

The concentrations of the by-products identified and quantified during experiments using metolachlor at steady-state are presented in Figure 2.

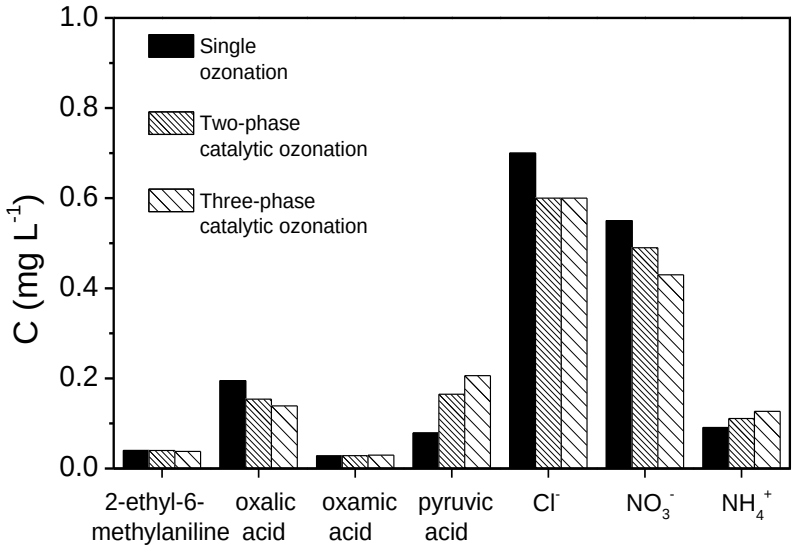

Figure 2 – Concentration of main by-products of metolachlor ozonation during continuous experiments using a two-phase and a three-phase configuration of the catalytic system, at steady-state.

The behaviour of the quantified intermediates of the ozonation of metolachlor followed what was expected when compared with the mineralization degree achieved during each experiment, as was reported during semi-batch experiments [3] (see section *Ozonation of emerging organic micropollutants*). The main aromatic intermediate, 2-ethyl-6-methylaniline, did not present a significant change among the different configurations. In fact, this compound is easily oxidized by ozone alone, and thus the catalytic system does not enhance its removal, as is also

observed for the parent pollutant. On the other hand, oxamic acid also did not present any significant changes in concentration at steady-state. However, this compound is known to be very unreactive to both ozone and ozone-derived radicalar species [4], and thus the catalytic process is likely not enhancing its removal in these conditions. Regarding the increase observed for pyruvic acid, for short semi-batch reaction times, it has been observed that the catalytic process tends to produce more of this compound than single ozonation. However, the situation is inverted as the reaction proceeds to longer contact times. Thus, it is likely that there is an increase in the production of pyruvic acid in the early stages of reaction, due to attack of the radicalar species, during the catalytic process, but it is also being degraded by these same species, which is observed in the latter stages of reaction. Considering the retention time of the continuous system, steady-state is being reached when the reaction is still in the earlier stages in this case. The ionic compounds released into solution are also in accordance to what is expected, when compared to the mineralization degree obtained in the different system configurations. Dechlorination of the organic pollutant is almost total, while the nitrogen content found in ionic form is still far away from the total nitrogen of the feed solution contained in metolachlor. In any case, the trends of nitrate and ammonia formation follow what was expected regarding the mineralization degree, suggesting, once again, changes in the reaction path of ozone or the ozone-derived reactants with the organic compounds in solution. Nitrate levels measured at steady-state decreased with the increase of TOC removal, while ammonia levels increased.

In the case of nonylphenol, the identification and/or quantification of the organic intermediates was not possible, due to no available quantification methods or to very low concentrations in solution; furthermore, no release of ionic species was expected in this case, which was confirmed by analysis in ionic chromatography. Therefore, no analysis in the effect of the system configuration on the distribution of by-products of nonylphenol ozonation in the outlet of the system was made.

LIQUID FLOW RATES

The concentrations of the main identified intermediates, as measured at steady-state, of the ozonation of atrazine during the experiments at different loop flow rates using the 64 cpsi 11.4% monolith are presented in Figure 3.

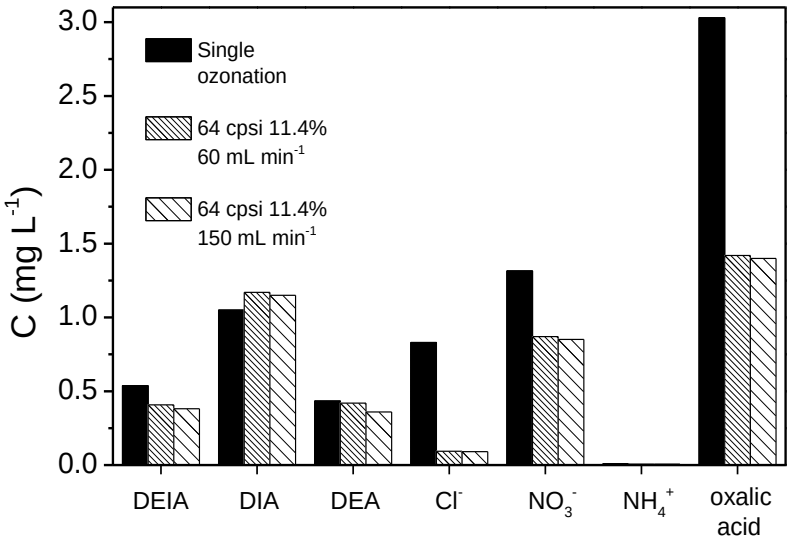

Figure 3 - Concentration of main by-products of atrazine ozonation during continuous experiments; comparison between non-catalytic and catalytic systems at different loop flow rates, using 64 cpsi 11.4% monolith.

The concentration of the main identified intermediates formed during the ozonation of atrazine follow a similar trend to what was observed in section *Ozonation of organic emerging micropollutants*. The improved mineralization achieved by the increase in the loop flow rate resulted in a lower concentration of DEIA and oxalic acid in the effluent at steady-state. These two compounds should be those which are more affected by the reactions occurring at the surface of the catalyst, and thus should benefit more from the added mass transfer potential from the liquid to the solid phase caused by the increase in the flow rate [2, 5].

The concentration of main identified intermediates, as measured at steady-state, of the ozonation of metolachlor during the experiments at different loop flow rates using the 64 cpsi 11.4% monolith are presented in Figure 4.

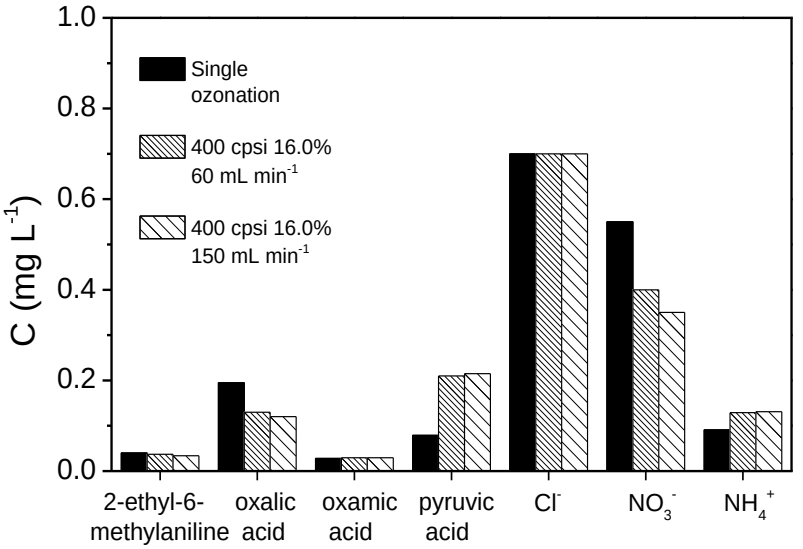

Figure 4 - Concentration of main by-products of metolachlor ozonation during continuous experiments; comparison between non-catalytic and catalytic systems at different loop flow rates, using 64 cpsi 11.4% monolith.

As in the case of atrazine, the concentration of the identified intermediates found at steady-state is in accordance to what was described in section *Ozonation of emerging organic micropollutants*, concerning their distribution when compared with the mineralization degree achieved [3]. The increase in the loop flow rate lead to an increase in the degradation of oxalic acid, which can be attributed to the promotion of surface reactions between this compound and highly reactive surface species formed by ozone. On the other hand, 2-ethyl-6-methylaniline reacts very promptly with molecular ozone, while oxamic acid has a slow reaction rate with both ozone and ozone-derived species, and thus do not show a significant difference. The increase in concentration of pyruvic acid and ammonia,

and decrease in the release of nitrate agree with what is observed in semi-batch experiments, considering the retention times here used, while dechlorination of the organic pollutant is total.

As seen in the case of the 64 cpsi monolith, the role of surface reactions is confirmed where the concentrations of the intermediates of atrazine and metolachlor ozonation using the 400 cpsi monolith are concerned (Figures 5 and 6 respectively), showing almost identical behaviour to what was observed in the case of the 64 cpsi monolith.

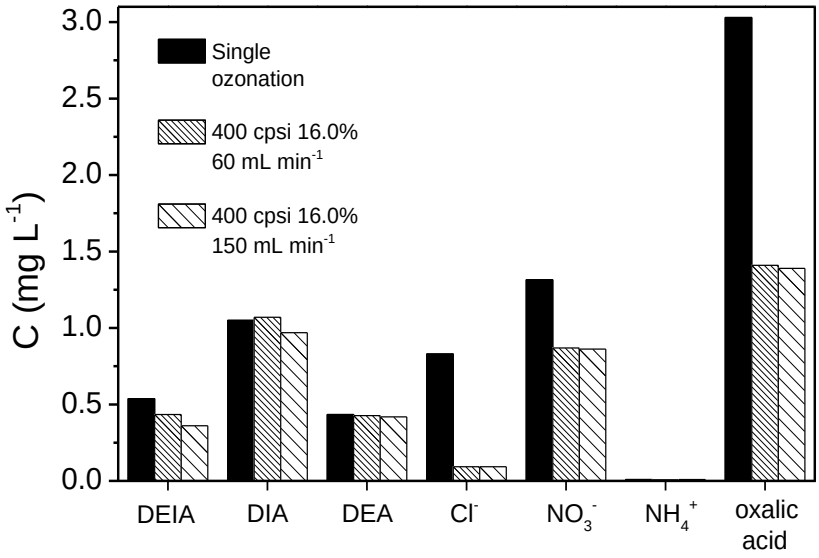

Figure 5 - Concentration of main by-products of atrazine ozonation during continuous experiments; comparison between non-catalytic and catalytic systems at different loop flow rates, using 400 cpsi 16.0% monolith.

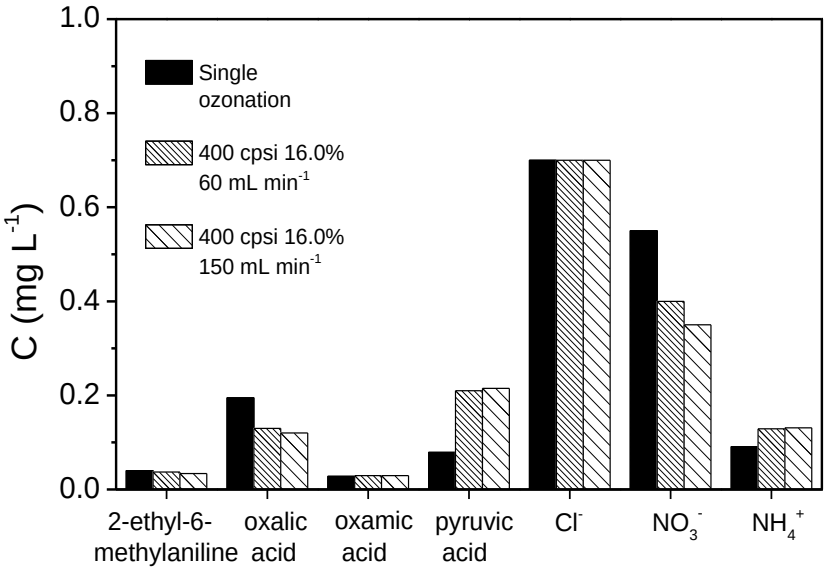

Figure 6 - Concentration of main by-products of metolachlor ozonation during continuous experiments; comparison between non-catalytic and catalytic systems at different loop flow rates, using 400 cpsi 16.0% monolith.

CONTACT AREA

The main identified intermediates found during the ozonation experiments of atrazine and metolachlor are presented in Figures 7 and 8, respectively.

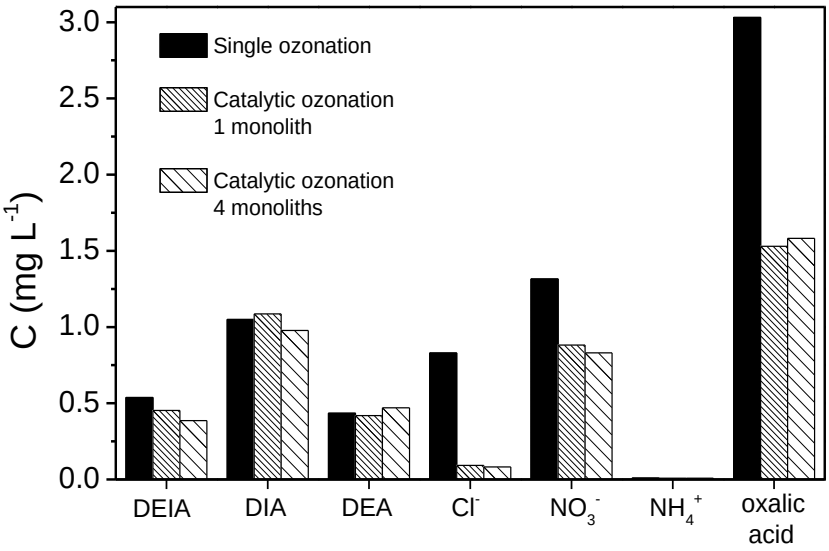

Figure 7 - Concentration of main by-products of atrazine ozonation during continuous ozonation experiment with different catalyst contact areas available for reaction.

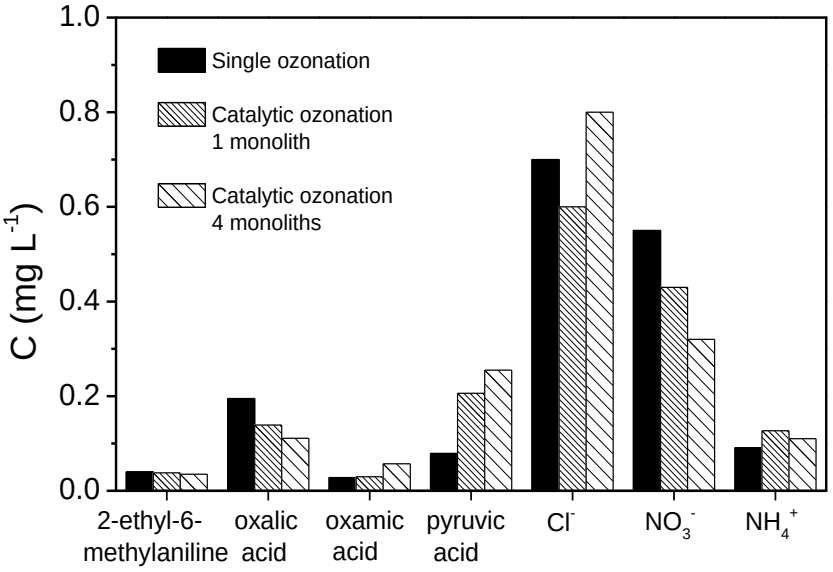

Figure 8 - Concentration of main by-products of metolachlor ozonation during continuous ozonation experiment with different catalyst contact areas available for reaction.

In the case of atrazine, the increase in the available catalyst contact area resulted in a more extended degradation of DEIA, one of the main accumulated by-products of atrazine ozonation [2]. It is interesting to notice that the increase in TOC removal actually corresponded to a slight increase in the accumulated oxalic acid in the effluent. Since oxalic acid has been shown to be removed to a wider extent with the increase of the contact area, it is then clear that this increase results from a larger formation of oxalic acid derived from the degradation of atrazine and its organic by-products [5]. Considering the products of metolachlor, it is observed that the larger contact area resulted in less oxalic acid accumulated in the effluent. The increase in the production of oxamic and pyruvic acid may be related with the more extensive degradation of organic intermediates from the ozonation of the parent pollutant [3].

To assess the role that the increase of the contact area may have in enhancing the mineralization of persistent organic pollutants and in the reduction of the toxicity of the resulting effluents, experiments were performed using DEIA and 2-ethyl-6-methylaniline (not pictured), chosen due to their persistence in solution during catalytic ozonation (in the case of DEIA) and their toxic potential (in the case of 2-ethyl-6-methylaniline). It was observed that, while single ozonation mineralized 15% of 2-ethyl-6-methylaniline, the catalytic ozonation using one monolith increased this value up to 25%, and the use of four monoliths raised the mineralization degree up to 35%. The removal of this compound was approximately 96% for all the cases. In the case of DEIA, the mineralization degree achieved was not as prominent, rising from 0% to 3% when comparing single ozonation to catalytic ozonation using one monolith, and up to 7% using the four monoliths setup. The removal of this organic pollutant was approximately 20% in all the cases.

WATER MATRIX

The concentration of the main intermediates found during the ozonation procedure using different water matrices is presented in Figure 9.

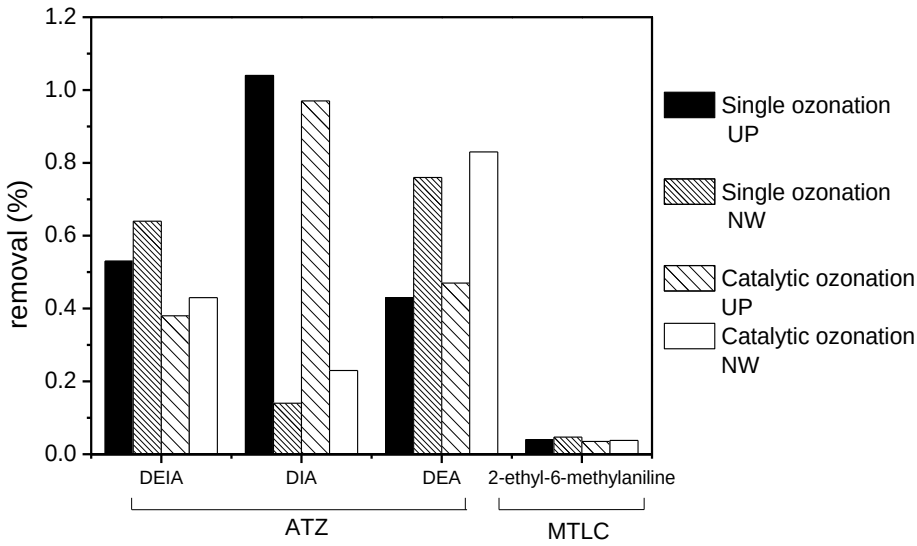

Figure 9 - Concentration of main by-products of atrazine and metolachlor ozonation during continuous ozonation experiment with different water matrices.

MODIFICATION OF THE CARBON SURFACE

When the formation of intermediates during continuous ozonation of atrazine and metolachlor is considered, some care in the analysis of the results is needed. Even though it is possible to normalize the amount formed during reaction, at steady state, by the amount of CNF present on the structured catalysts, the significance of these observations may not be correct. The relevance of reactions which do not involve the catalysts, through direct ozonation, is too large to be ignored [2, 6-11]. The concentration of 2-ethyl-6-methylaniline during ozonation of metolachlor has been observed to decrease in the presence of a catalyst, when compared with the single ozonation process, which may be attributed to

changes in the degradation pathway of metolachlor [3]. Thus, the normalization of the concentration at steady state by the mass of CNF does not reflect what is actually taking place in the reaction system. On the other hand, at similar contact times, the concentration of DEA and DEIA was smaller in the catalytic ozonation experiment, when compared with the non-catalytic counterpart, while the concentration of DIA increased when a catalyst was applied. Since DEIA was observed to be accumulated in solution during semi-batch experiments, it is expected that changes in its concentration at steady state are attributed to changes in the degradation path. Similarly, it has also been observed that differences in the concentration of DEA and DIA are related to similar phenomena. Thus, in order to evaluate the difference in activity of CNF and N-CNF, a different approach has to be made. In Figure 10 the difference in the concentration of the main intermediate products, in relation to the single ozonation experiments, whether positive or negative, is presented.

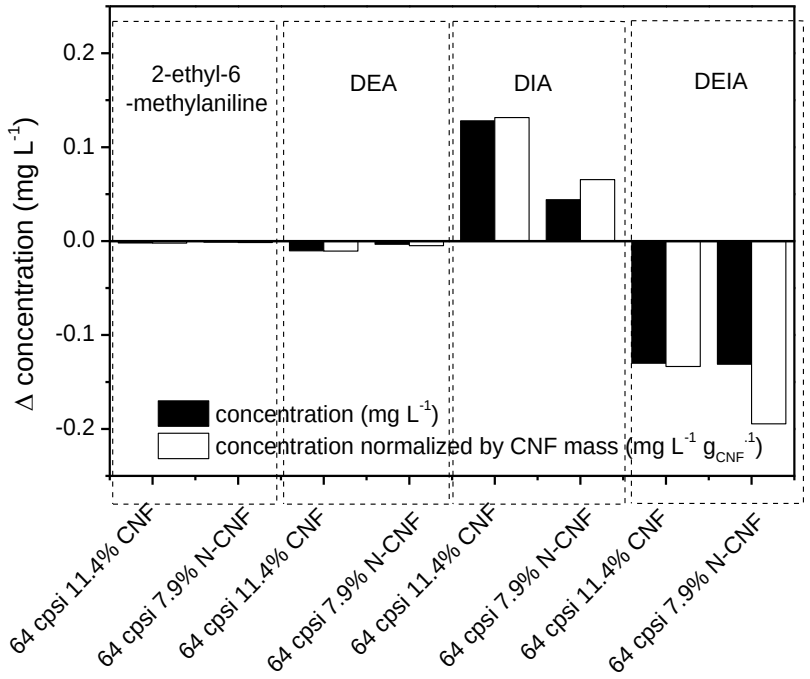

Figure 10 – Difference of the concentration of the main intermediates from atrazine and metolachlor during continuous ozonation experiments

using unmodified and N-doped CNF covered monoliths when compared with single ozonation experiment: absolute values and normalized by CNF mass values.

In the case of 2-ethyl-6-methylaniline, a slightly smaller concentration is produced in the case of catalytic ozonation, which corresponds to the early stages of the product distribution observed in the semi-batch experiment, in section *Ozonation of emerging organic micropollutants* [3]. When the CNF mass was considered, the difference to the concentration measured in single ozonation was slightly larger in the case of the N-CNF. It is important to notice that these differences are likely not related with a larger extent of oxidation of this intermediate product. In fact, during semi-batch ozonation experiments using 2-ethyl-6-methylaniline, it was observed that it was removed from solution similarly in the non-catalytic and in the catalytic system. Therefore, changes in its concentration in solution at steady state should be attributed to changes in the degradation path of metolachlor during the ozonation process in the presence of a catalyst. Thus, the modifications of the surface of the catalyst are then also expected to lead to changes in the concentration of such products. In the case of DEA, a similar behaviour took place, since it was observed that even considering the mass of CNF in the structured catalysts the N-CNF system yielded a smaller concentration of this compound at steady state. It has been observed that reaction with direct ozone result in a larger amount of DEA in solution, in prior experiments with a radical scavenger in semi-batch ozonation. Moreover, the action of the catalysts, through surface and liquid bulk reactions, was observed to yield smaller amounts of DEA, whether through faster degradation of a change in the degradation pathway of atrazine. Thus, in this case, the N-doping of the structured CNF did not seem to enhance the catalytic activity of CNF, when the mass was considered. It is likely that different reaction mechanisms are at play here (i.e., a predominance of surface reactions over liquid bulk reactions or prevalence of some types of radicals over others). An opposing behaviour was observed in the case of DIA; the

concentration of this compound was much larger than in the case of single ozonation, which suggests that the presence of a catalyst is in fact changing the degradation pathway of atrazine. However, similarly to what was observed with DEA, even when the mass of CNF was considered, the yield of this product was still larger when the not-modified CNF structured catalyst was used. This behaviour again suggests that changes in the degradation pathway of atrazine due to changes in the reaction system may be taking place when the N-doped CNF was used. In fact, it has been proposed that, besides improving the ability of the catalyst to enhance the activity of ozone through changes in the electronic density of the catalytic surface [12], some types of N-containing functionalities may lead to a preference for the formation of hydroxyl radicals in solution, thus shifting the reaction pathway taking place [13-15]. In the case of DEIA, however, the N-CNF structured catalyst yielded a larger concentration of this compound per mass of CNF, which indicates that the N-containing functionalities are leading to a larger formation of DEIA. In fact, it has been observed that the catalytic system accumulates a larger amount of DEIA in solution when compared with single ozonation [2].

The difference in the concentration of the main organic acids formed during ozonation of atrazine and metolachlor, in relation to the single ozonation experiments, whether positive or negative, is presented in Figure 11.

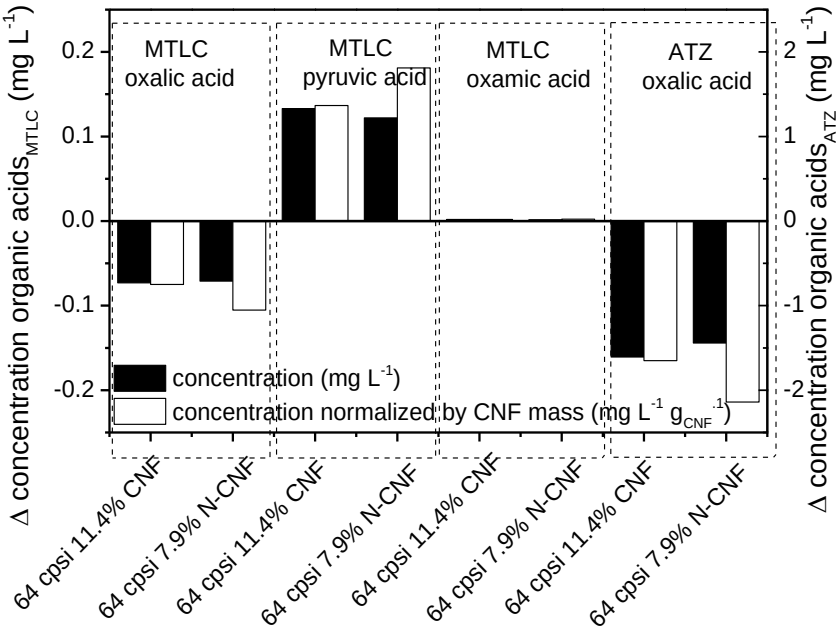

Figure 11 – Difference of the concentration of the main organic acids formed from atrazine and metolachlor during continuous ozonation experiments using unmodified and N-doped CNF covered monoliths when compared with single ozonation experiment: absolute values and normalized by CNF mass values.

When the organic acids are considered, it is clear that, while opposing trends were observed when the concentrations found were compared with the single ozonation experiment, the use of N-CNF catalyst enhances the catalytic effect when the mass of CNF is considered, when the obtained results are compared with what was observed in sections *Ozonation of organic emerging micropollutants* and *Operation conditions*. Thus, what is observed for the formation of organic acids corresponds to the expected enhanced catalytic performance of N-doped CNF [12]. The trends observed, in terms of increase or decrease in the production of the acids, when compared with the single ozonation experiments, correspond to what was observed in section *Ozonation of organic emerging pollutants* [3, 5]. In this case, changes in the reaction mechanism due to the

presence of N-functionalities on the surface of the carbon catalysts did not seem to play a determinant role.

REFERENCES

[1] B. Balci, N. Oturan, R. Cherrier, M.A. Oturan, Water Research, 43 (2009) 1924-1934.
[2] X. Fan, J. Restivo, J.J.M. Órfão, M.F.R. Pereira, A.A. Lapkin, Chemical Engineering Journal, 241 (2014) 66-76.
[3] J. Restivo, J.J.M. Órfão, S. Armenise, E. Garcia-Bordejé, M.F.R. Pereira, Journal of Hazardous Materials, 239–240 (2012) 249-256.
[4] A.G. Gonçalves, J.L. Figueiredo, J.J.M. Órfão, M.F.R. Pereira, Carbon, 48 (2010) 4369-4381.
[5] S. Derrouiche, D. Bourdin, P. Roche, B. Houssais, C. Machinal, M. Coste, J. Restivo, J.J.M. Orfao, M.F.R. Pereira, Y. Marco, E. Garcia-Bordeje, Water Sci Technol, 68 (2013) 1377-1383.
[6] F.J. Beltrán, M. González, B. Acedo, F.J. Rivas, Journal of Hazardous Materials, 80 (2000) 189-206.
[7] K.H. Chan, W. Chu, Water Research, 37 (2003) 3997-4003.
[8] K.H. Chan, W. Chu, Applied Catalysis B: Environmental, 58 (2005) 165-174.
[9] K.H. Chan, W. Chu, Applied Catalysis B: Environmental, 58 (2005) 157-163.
[10] C.A. Guzman-Perez, J. Soltan, J. Robertson, Separation and Purification Technology, 79 (2011) 8-14.
[11] C.J. Hapeman-Somich, G. Zong, W.R. Lusby, M.T. Muldoon, R. Waters, Journal of Agricultural and Food Chemistry, 40 (1992) 2294-2298.
[12] H.-P. Boehm, Catalytic Properties of Nitrogen-Containing Carbons, Carbon Materials for Catalysis, John Wiley & Sons, Inc.2008, pp. 219-265.
[13] H. Cao, L. Xing, G. Wu, Y. Xie, S. Shi, Y. Zhang, D. Minakata, J.C. Crittenden, Applied Catalysis B: Environmental, 146 (2014) 169-176.
[14] L. Xing, Y. Xie, H. Cao, D. Minakata, Y. Zhang, J.C. Crittenden, Chemical Engineering Journal, 245 (2014) 71-79.
[15] M. Sanchez-Polo, U. von Gunten, J. Rivera-Utrilla, Water Res, 39 (2005) 3189-3198.